8708149

Pfaff, Virginia J.

ON FORMS OF FOLDS

University of Cincinnati PH.D. 1986

University
Microfilms
International 300 N. Zeeb Road, Ann Arbor, MI 48106

PLEASE NOTE:

In all cases this material has been filmed in the best possible way from the available copy. Problems encountered with this document have been identified here with a check mark __√__.

1. Glossy photographs or pages __√__
2. Colored illustrations, paper or print ______
3. Photographs with dark background __√__
4. Illustrations are poor copy ______
5. Pages with black marks, not original copy ______
6. Print shows through as there is text on both sides of page ______
7. Indistinct, broken or small print on several pages __√__
8. Print exceeds margin requirements ______
9. Tightly bound copy with print lost in spine ______
10. Computer printout pages with indistinct print ______
11. Page(s) __________ lacking when material received, and not available from school or author.
12. Page(s) __________ seem to be missing in numbering only as text follows.
13. Two pages numbered ______. Text follows.
14. Curling and wrinkled pages ______
15. Dissertation contains pages with print at a slant, filmed as received ________
16. Other ____________________

University
Microfilms
International

ON FORMS OF FOLDS

A dissertation submitted to the

Division of Graduate Studies and Research
of the University of Cincinnati

in partial fulfillment of the
requirements for the degree of

DOCTOR OF PHILOSOPHY

in the Department of Geology
of the College of Arts and Sciences

1986

by

Virginia J. Pfaff

B.A., Swarthmore College, 1972

B.S., Portland State University, 1979

M.S., Portland State University, 1981

UNIVERSITY OF CINCINNATI

September 5 *19* 86

I hereby recommend that the thesis prepared under my supervision by Virginia J. Pfaff

entitled On Forms of Folds

be accepted as fulfilling this part of the requirements for the degree of Doctor of Philosophy

Approved by:

John E. Grover

[illegible]

David M. Johnson

ABSTRACT

A 3rd order theory of folding of viscous multilayers indicates that forms of folds are controlled by the behavior of layer contacts or interbeds, the relative stiffnesses of the multilayer and confining media, and the scale of the folding. A 2nd order analysis shows that asymmetry of folds is determined largely by the behavior of layer contacts and the sense of layer-parallel shear during folding.

Localization or distribution of slip at layer contacts partly determines shapes of folds in multilayers. Kink or box folds form if slip is localized along short segments of layer contacts; slip is localized if interfaces or thin interbeds have adhesional strength or some other nonlinear resistance to slip. Concentric or chevron folds form if slip is distributed all along layer contacts; slip is distributed if interfaces have low adhesional strength or constant resistance to slip.

Relative stiffnesses of the multilayer and media also determine fold shapes. Parallel folds, such as concentric and kink folds, form in finite multilayers confined by soft media, and constrained, internal folds form in multilayers confined by stiff media.

The ratio of fold wavelength to multilayer thickness largely determines whether folds are parallel or similar.

Parallel -- concentric or kink -- folds form if the ratio is one or larger. Similar -- box or chevron -- folds form if the ratio is much smaller than one.

Asymmetric folds form in multilayers subjected to combined layer-parallel compression and shear; compression produces folding and shear produces asymmetry. The theory shows that the sense of asymmetry can be reversed by changing the behavior of layer contacts. If resistance to slip is constant, folds have drag-fold asymmetry. If resistance to slip is variable, folds have monoclinal kink-fold asymmetry.

ACKNOWLEDGMENTS

My advisor, Arvid Johnson, provided guidance, encouragement, and enthusiasm throughout the course of this research -- thanks, Arvid. I thank my committee members Attila Kilinc and John Grover for their suggestions and comments; I especially appreciate John's careful review of the manuscript.

Beccae Chaulot-Talmon and Lyla Messick drafted most of the figures.

John Oggerino and Dan Emerson provided able assistance with the field work.

This research was funded by National Science Foundation Grant No. EAR 8311318. Field work was supported in part by summer research grants from the Geological Society of America and the ARCO Exploration Company.

TABLE OF CONTENTS

LIST OF FIGURES

Figure | Page

Figure | Page

LIST OF TABLES

INTRODUCTION

High above the Juniata River, in the central Appalachians of Pennsylvania, roadcuts through the southeast limb of the New Bloomfield anticline expose a particularly rich assortment of folds: tightly folded chevron folds and more open, concentric-like folds, both with the sense of asymmetry of drag folds; and a kink-like fold with the sense of asymmetry of a monoclinal kink fold.

The spatial associations of folds with different forms and of folds with opposite senses of asymmetry pose the two fundamental questions on which I focus my research:

1. What physical characteristics of this sequence of rocks and what conditions of folding allow kink-like, chevron, and concentric-like folds to develop in such close proximity? Why should styles of folding change so abruptly locally?
2. How can folds with opposite senses of asymmetry form on the same limb of an anticline under the influence of the same sense of shear stress?

I approach these questions from two perspectives: detailed observation of folds in order to determine deformation mechanisms responsible for different folds and asymmetries; and theoretical analyses of folding in order to investigate effects of different rheological and dimensional parameters on fold form and fold asymmetry. The descriptions of field examples are presented in Chapter IV; the theoretical analyses are presented in Chapters I, II, and III.

The theory of folding of viscous multilayers assumes that folds grow from initial, low-amplitude, sinusoidal perturbations in layer interfaces. Distinct, non-sinusoidal forms develop as the folds grow to higher amplitudes. Previous theoretical analyses of single- and multi-layers have been largely restricted to infinitesimal amplitudes and thus can only describe initial, sinusoidal fold forms. In order to study forms of folds, therefore, I first had to extend the theory of folding of viscous multilayers to higher amplitudes. This analysis forms the basis of Chapter I, in which I develop a 3rd order analysis of multilayer folding that can treat relatively high-amplitude folding (maximum slopes of 25-30° in some problems).

My field studies of the folds in Pennsylvania indicate that the slip between layers was an important deformation mechanism in the development of those folds. Furthermore, in some folds, layers slipped along only part of their contacts. Previous analyses could not address localized slip because they were restricted to either bonded contacts, for which no slip takes place at layer contacts, or to free slip at contacts, for which the layers slip everywhere along their contacts. Therefore, I decided to incorporate drag along layer contacts into the 3rd order equations which describe the development of fold form. In Chapter II, I model localized slip between layers by describing contact behavior with a powerlaw rheology.

The 3rd order theoretical analysis of viscous multilayers with various resistances to slip at layer contacts (Chapters I and II) can be used to derive virtually all the basic fold forms: parallel, concentric-like and kink; similar, chevron and box; and constrained. These forms are all the result solely of layer-parallel compression and are symmetric.

Asymmetry of folds is produced by a layer-parallel shear stress acting in conjunction with layer-parallel compression. However, prior to my research, no equations existed that could describe the growth of an asymmetric fold from an initial, symmetric perturbation. By including layer-parallel shearing deformation in my theoretical analysis, I develop a comprehensive theory of asymmetric folding in Chapter III.

On the basis of the theoretical analyses developed in Chapters I, II, and III, I can answer the questions originally posed by the field examples. The theory indicates that properties of contacts or of thin interbeds between layers play a critical role in determining both the form and the sense of asymmetry of a fold. Thus even subtle changes in the lithology of the rock section being folded on the limb of the anticline in central Pennsylvania can produce spectacular changes in the forms and asymmetries of the folds which develop.

CHAPTER I

PARALLEL, SIMILAR, AND CONSTRAINED FOLDS

ABSTRACT

Theoretical analysis of folding of viscous multilayers with free slip or bonding at layer contacts indicates that folds in such multilayers can be described in terms of three end-members: parallel, in which orthogonal thicknesses of layers are largely preserved; similar, in which vertical thicknesses of layers and shapes of successive interfaces are essentially constant; and constrained, in which amplitudes of anticlines and synclines decrease to zero at upper and lower boundaries. Constrained, internal folds form if the multilayer is confined by rigid media; parallel, concentric-like folds form if the multilayer is confined by soft media, provided soft interbeds are sufficiently thin for the stiff layers to fold as an ensemble. Similar, sinusoidal or chevron folds form throughout much of the thickness of a multilayer, for any stiffness of confining media, provided wavelengths of folds are short relative to the thickness of the multilayer or soft interbeds are sufficiently soft and thick for the stiff layers to act independently. The analysis shows that multilayer folds may have the same form regardless of whether the layer contacts are freely slipping or bonded.

The forms of folds in multilayers confined by media with different viscosities above and below depend on the viscosity contrast of the media. For no medium above and a rigid medium below, the forms are concentric-like in the upper part and internal in the lower part of the multilayer. For no medium above and a soft medium below, the folds are concentric-like throughout the multilayer.

The theory indicates that a useful way to analyze forms of folds in rocks or in experiments is in terms of component waveforms, as defined, for example, by Fourier series. The distributions of amplitudes of component waveforms throughout the multilayer appears to be diagnostic, reflecting contrasts in properties of the multilayer and its confining media. Analysis of a large fold in the central Appalachians, Pennsylvania, and of a smaller fold in the Huasna syncline, California, indicates that at least three component waveforms are required to produce the gross forms of those folds.

The theory closely predicts wavelengths and shapes of folds produced in analogous elastic multilayers, indicating that nonlinearities in material behavior, which are inherent in the elastic material but are absent in the viscous material, are less significant than nonlinearities in the boundary conditions, which are the same in elastic and viscous materials.

INTRODUCTION

This chapter investigates systematically how forms of folds in viscous multilayers are controlled by contrasts of interbedded layers, by relative stiffnesses of multilayers and confining media, and by amounts of growth of folds. The multilayers investigated are simple, repetitive stacks of layers, so many of the classical fold forms, including sinusoidal, internal, chevron, and concentric-like, develop. Using the theoretical analysis I can determine the types of conditions responsible for these forms as well as for forms that have yet to be named.

Certain classical fold forms, such as kink and box folds, are conspicuously absent in the multilayers analyzed in this chapter. Kink folding does not develop under the conditions -- linear behavior of layers and freely slipping or bonded contacts between layers -- considered here but will be investigated in Chapter II.

The study reported here focuses on the causes of different fold forms in multilayers. Previous studies are restricted to 1st order accuracy in the maximum slope of layering, and such studies necessarily focus not on fold form but on dominant wavelengths and initial, selective amplification of perturbations. Fold form develops at moderate to high amplitudes, so the theoretical analysis presented here is carried to 3rd order accuracy. The layers are assumed to be viscous because higher-order analysis of folding of viscous layers is simplest.

The 3rd order analysis allows one to follow the initiation and evolution of the classical fold forms, described by complex waveforms, from initial perturbations, described by simple, sinusoidal waveforms.

In conjunction with the 3rd order analysis, I describe a method of transforming arbitrary constants into particular interface stresses. The transformation reduces the number of arbitrary constants that need to be determined from four per layer to one or two per interface and thus considerably reduces the work of solving particular problems. Another new feature I introduce is a remarkably simple method of computing preferred wavelengths from dominant wavelengths for single layers or multilayers.

However, most methods used in my study of multilayer folding were introduced into folding theory by others. The modern, 1st order theory was developed by Fletcher (1974, 1977) and was extended by him to 2nd order to study the shapes of single-layer folds to small, but finite, amplitude (Fletcher, 1979, 1982). Smith (1975, 1977) independently developed the same theory. Ramberg (1970) and Smith (1979) previously used eigenvalues and eigenvectors in folding theory to study initial growth of perturbations. The method of analyzing component waveforms in an interface between layers was previously used by Stabler (1968) and Hudleston (1973).

My investigation is also related to a much broader group of previous studies of infinitesimal-amplitude folding. Biot (1957, 1959, 1961, 1963, 1965a, 1965b) developed folding theory and showed how to determine dominant wavelengths and characteristic initial amplitude distributions for various boundary conditions. His methods are essentially to 1st order accuracy in maximum slopes of elastic or viscous layers (Fletcher, 1977; Johnson, 1977). Biot's analysis of "internal instability" (1963, 1964, 1965a), in which folds develop in a multilayer confined above and below by rigid media, was a major contribution to folding theory; his method of treating multilayers as homogeneous, anisotropic media is still being developed (Latham, 1985a, 1985b). Ramberg (1959, 1962, 1963a, 1963b, 1964, 1970), who initiated folding research at about the same time as Biot, also developed a theory roughly to 1st order accuracy (Fletcher, 1977). Ramberg studied folding of multilayers with various configurations to explain drag folds, the simultaneous growth of folds with different wavelengths, and the parameters that control wavelengths of folds in multilayers. Johnson (1969) used elementary folding theory of multilayers to explain different distributions of fold amplitudes in the Carmel Formation, Utah, and Johnson and Page (1976) used the theory to derive wavelengths and three-dimensional shapes of folds associated with the Huasna syncline in central California. Johnson and Honea (1975) developed 1st order theory for elastic materials to investigate the transition from sinusoidal to concentric-like to chevron forms in elastic multilayers but found that the transitions can be understood only qualitatively in terms of the 1st order analysis.

This chapter is organized unconventionally, so I will mention the sequence of presentation. First I describe the results of my theoretical studies of fold form via representative examples of folds that developed in repetitive multilayers at moderate amplitudes; this is essentially a summary. Then I analyze the fold forms geometrically in terms of variables specified by the theory; this provides a method of studying multilayer folds in general. Only then do I present the essential steps in the 3rd order analysis and explain the methods developed in the course of my research. After the basic solutions have been derived, I discuss the extraction of eigenvalues and eigenvectors which provide dominant wavelengths and shapes of perturbations that grow most rapidly during layer-parallel shortening. Then I show how to compute preferred wavelengths and amplitude vectors; these correspond to wavelengths and shapes of folds that have grown the most after certain amounts of layer-parallel shortening. Finally, I show how fold forms in selected multilayers change during growth of the folds. In the Discussion, I examine two field examples of large folds, one in Pennsylvania and one in California, and deduce some of the conditions of folding from the shapes and wavelengths of the folds. I also compare wavelengths and shapes of small folds produced experimentally in elastic multilayers with wavelengths and shapes of folds produced theoretically in viscous materials.

Thus, those interested primarily in fold forms and how one applies the theory to folds could read the first two sections and then skip to the Discussion. Those interested primarily in the theoretical methods could skip the first two sections and read the central part of the paper.

EXAMPLES OF THEORETICAL FOLD FORMS

Terminology

The simple multilayers I analyze consist of stiff layers and soft interbeds; they are confined above and below by media that may have different stiffnesses (Fig. 1). In all examples I will discuss, the folding is a result of layer-parallel shortening.

Layers are separated from neighbors by viscous films (Fig. 1C). The films are very thin, so they can deform only in simple shear. By specifying the relative viscosity of the films, one can model free slip ($\mu_f \ll \mu_2$), viscous drag ($\mu_f < \mu_2$), or bonded contacts ($\mu_f \geq \mu_2$); the symbols are defined in Fig. 1.

For the example shown in Fig. 1A, the thicknesses of stiff and soft layers are the same, the viscosities of the media and the soft layers are the same, and the viscosity ratio of stiff to soft layers is ten. In other examples each of these parameters may be different.

In all the theoretical folds, each interface is initially perturbed into a <u>first cosine waveform</u>. The folds are a result of the growth of the first waveform as well as of the spontaneous initiation and growth of <u>second</u> and <u>third cosine waveforms</u> which have wavelengths that are

Figure 1. Representative multilayer. A. Simple multilayer, composed of alternating stiff and soft viscous layers, confined above with a halfspace of viscosity μ_U and below with a halfspace of viscosity μ_L. The multilayer, of total thickness H, is subjected to mean horizontal stretch, $\bar{S}_x$, and mean vertical stretch, $\bar{S}_z$. The stretch is defined as the ratio of final to initial lengths of a material line element. For the incompressible materials treated here, $\bar{S}_x = 1/\bar{S}_z$. B. Segment of representative layer, showing relation between horizontal x-coordinate and s- and n-coordinates tangential and normal, respectively, to interfaces. ζ_t is height of top interface; ζ_b is height of bottom interface. C. Representative element including parts of soft layer, with viscosity μ_2 and vertical thickness h_2, and stiff layer (μ_1, h_1), as well as thin interlayer film of viscous material (μ_f, h_f). For the example shown in Fig. 1, $h_1 = h_2$, $\mu_U = \mu_L = \mu_2$, and $\mu_1/\mu_2 = 10$; the viscosity of contact films is so high that the stiff and soft layers are bonded together and the media are bonded to the multilayer.

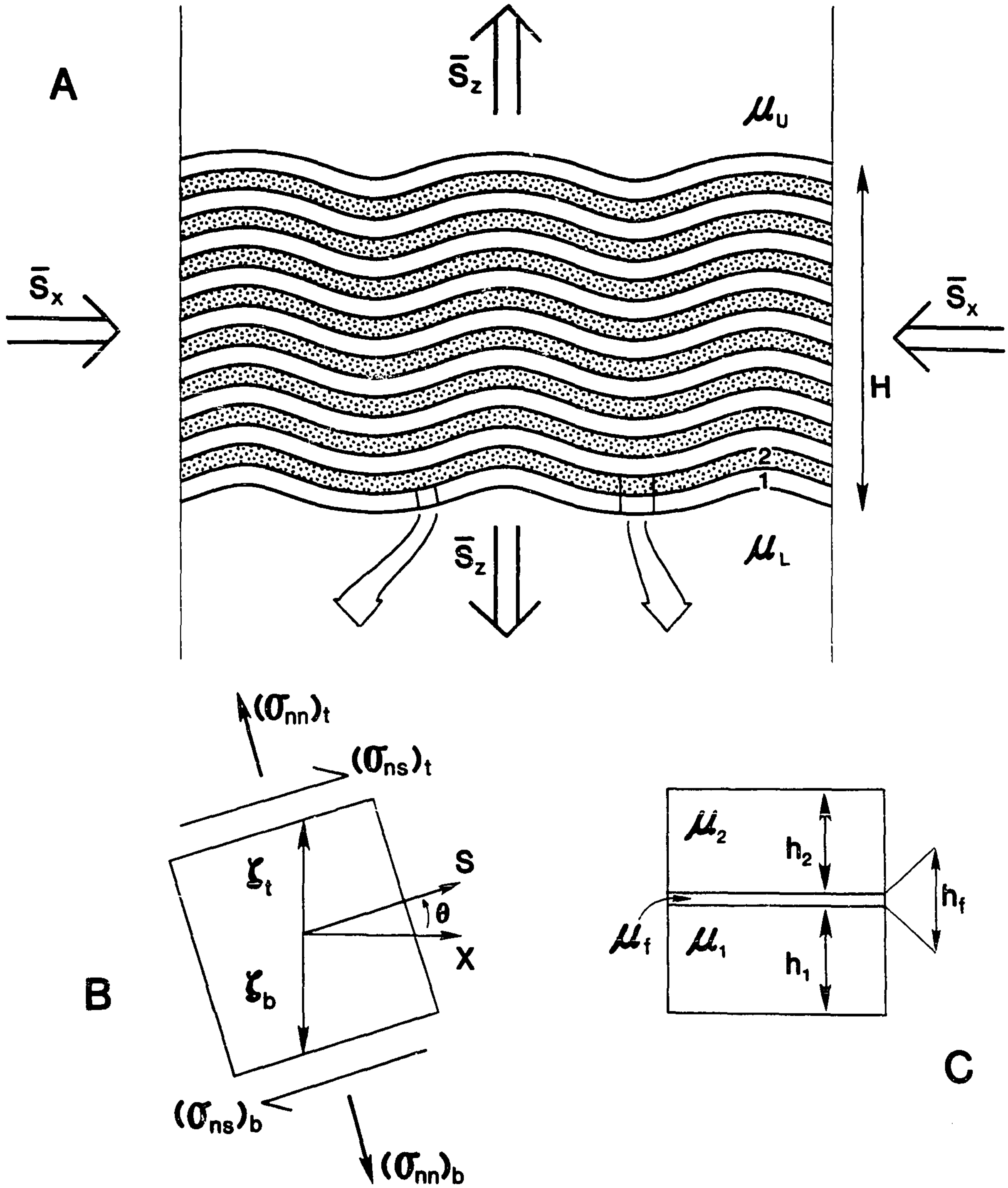
A
S̄z
μU
S̄x
S̄x
H
2
1
S̄z
μL
B
(σnn)t
(σns)t
ζt
S
θ
X
ζb
(σns)b
(σnn)b
C
μ2
h2
hf
μf
μ1
h1

one-half and one-third, respectively, that of the first waveform. The amplitudes of the first cosine waveforms are initially very low; the maximum corresponds to a slope angle of one degree; the others are scaled according to the specification of an eigenvector of amplitudes, which describes the relative amplitude of the first waveform at each interface. For each multilayer there is a dominant wavelength, the wavelength of the first waveform that grows most rapidly. The eigenvector of amplitudes corresponds to the dominant wavelength and thereby defines the multilayer fold form which amplifies most rapidly.

I broadly classify theoretical folds I have studied into parallel, similar, and constrained. In parallel folds (Van Hise, 1896), thicknesses of layers measured normally to layering tend to be preserved. In similar folds (Van Hise, 1896), thicknesses of layers measured parallel to axial planes tend to be preserved, so shapes of successive interfaces can change only slightly. In constrained folds, both normal and vertical thicknesses are variable, and amplitudes die out systematically toward boundaries. Idealized concentric and kink folds are examples of parallel folds; idealized chevron and box folds are examples of similar folds. Constrained folds are generally unnamed. Biot termed one type "internal instability" (1964).

Fold Forms

Two of the broad groups of folds, parallel and constrained, are results of differences in properties of confining media, as can be illustrated by examining fold forms produced in multilayers comprised of identical stiff layers with free slip at contacts (Fig. 2). The multilayers shown in Fig. 2, locations A1, A2, and A3, are confined by identical upper and lower media ($\mu_U = \mu_L$) ranging from soft ($\mu_U/\mu_1 = 0.1$) at loc. A1 to rigid ($\mu_U/\mu_1 \to \infty$) at loc. A3. In each case, the middle interface remains essentially a simple cosine waveform, which was the waveform used to seed the fold, but the other interfaces change shape during folding. For the multilayer confined by soft media (Fig. 2, loc. A1), the top interface has broad crests and narrow troughs whereas the bottom interface has broad troughs and narrow crests, and the ensemble of interface waveforms defines a fold of concentric-like form. Amplitudes of waveforms are nearly constant throughout the stack of layers because the multilayer is weakly constrained by soft media.

The distribution of amplitudes is quite different for the multilayer confined by very stiff media (Fig. 2, loc. A3). The amplitudes are zero at the upper and lower contacts of the multilayer and are maximal at middepth, so the fold is of the broad group of constrained folds. In this particular multilayer, interfaces near the upper boundary define broad, flat crests and narrow, puckered troughs, and the ensemble of interface waveforms defines an internal fold form, which is the high-amplitude analogue of the sinusoidal fold that Biot (1964) terms "internal instability." Finally, for the example where the media have intermediate stiffness (Fig. 2, loc. A2), the fold form is intermediate between the concentric-like and the internal fold forms.

Increasing the number of layers in the multilayer confined by stiff media produces an ensemble of interface waveforms dominated by limbs and

Figure 2. Array of fold forms, according to 3rd order analysis, of multilayers composed of identical stiff layers with free slip at contacts and confined by various media. A. Multilayers confined above and below by identical viscous media, ranging from soft ($\mu_U/\mu_1 = 0.1$), loc. A1, to rigid ($\mu_U/\mu_1 \rightarrow \infty$), loc. A3. Fold form at loc. A1 is parallel, concentric-like; that at loc. A3 is constrained, internal. B. Multilayers unconfined above but confined below by viscous media.

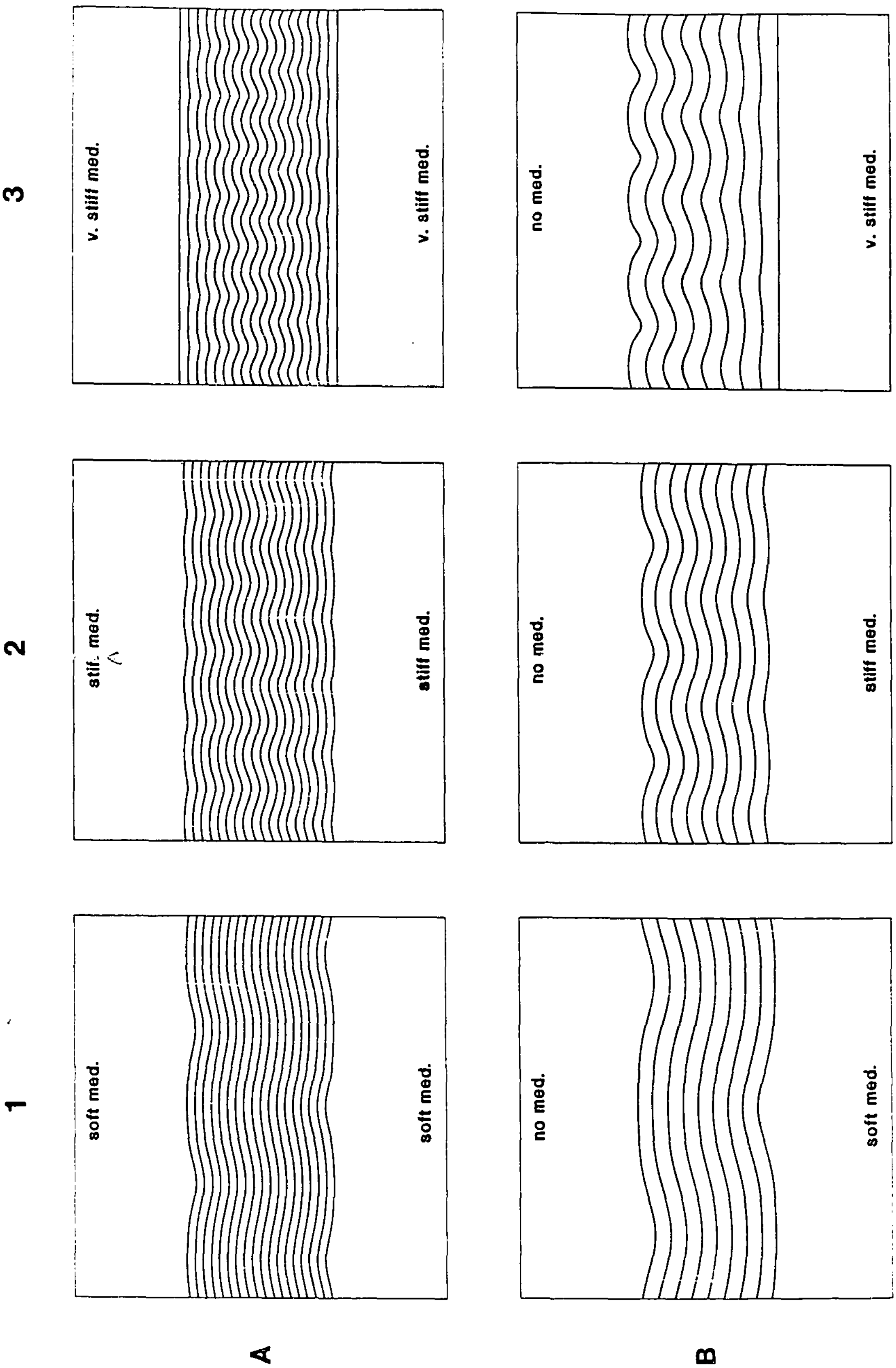
1
2
3
A
B
soft med.
soft med.
stif. med.
stiff med.
v. stiff med.
v. stiff med.
no med.
soft med.
no med.
stiff med.
no med.
v. stiff med.

intervening flats. The multilayer shown in Fig. 3 is composed of 40 identical layers with free slip at contacts. The limbs are shortest at the upper and lower edges of the multilayer and gradually lengthen to a maximum at middepth. The intervening flat at a crest is insignificant in the lower part of the multilayer and broadens to a maximum width near the top of the multilayer.

Elements of both the concentric-like and the internal fold forms may be blended within one fold if a simple multilayer is confined by media of different stiffnesses above and below. The three multilayers shown in Fig. 2, locs. B1, B2, and B3, are composed of identical layers with free slip at contacts and are unconfined above. For the multilayer shown at loc. B1, the medium below is much softer than the layers ($\mu_L/\mu_1 = 0.1$). The ensemble of interface waveforms assumes a concentric-like form, much like that shown at loc. A1. The multilayer shown at loc. B3 is rigidly confined below. The top interface has a well-developed arc-and-cusp structure, with rounded crests and pointed troughs. The lower interfaces have broad, flat-bottomed troughs and narrow pinches as crests. The form of the ensemble of waveforms is a hybrid, the upper few interfaces resembling the concentric-like form and the lower interfaces resembling the internal form. The lower medium for the multilayer shown at loc. B2 has the same viscosity as the layers. The ensemble of interfaces shows a concentric-like form in crests, but the troughs are flattened in the lower part of the multilayer; the anticlines appear to be unconstrained and the synclines relatively highly constrained in this multilayer.

Figure 3. Constrained fold form in thick multilayer composed of identical stiff layers, with free slip at contacts, and confined by very stiff media. Ratio of fold wavelength *L* to total multilayer thickness *H* is $L/H = 0.3$. Constrained form characterized by short limbs, narrow anticlinal hinges, and flat synclinal hinges near bottom of multilayer; nearly sinusoidal form at middepth; and short limbs, narrow synclinal hinges, and flat anticlinal hinges near top.

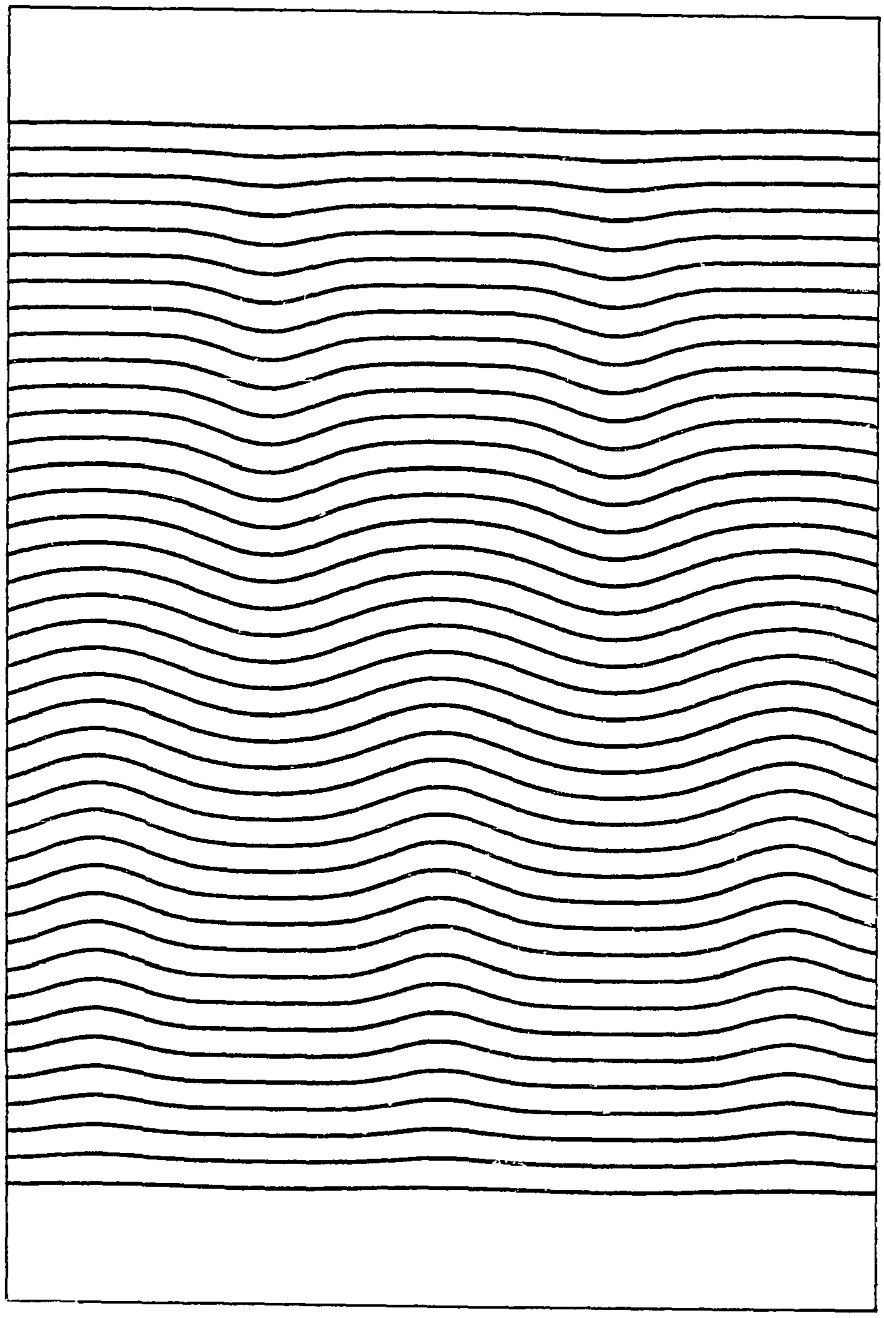

All three of the broad groups of fold forms -- parallel, constrained, and similar -- can be produced in identical multilayers containing many layers and confined by soft (Fig. 4A) or stiff (Fig. 4B) media. The similar form develops near middepth in the multilayer, provided the fold wavelength is short, relative to the total thickness of the multilayer, as will be shown in Chapter II. The fold form in the multilayer confined by soft media (Fig. 4A) consists of essentially similar, sinusoidal folds near middepth and parallel, concentric-like folds near the upper and lower boundaries of the multilayer. These fold forms have been observed experimentally (Currie and others, 1962; Ramberg, 1963b; Johnson and Ellen, 1974). The fold form in the multilayer confined by stiff media (Fig. 4B) consists of essentially similar, chevron folds near middepth but has constrained, internal folds near the upper and lower contacts with the stiff media. These folds also have been observed experimentally (Honea and Johnson, 1976; Latham, 1979).

Interbedding of stiff and soft layers in a multilayer introduces several degrees of freedom in fold form. Even in simple, repetitive multilayers such as those being considered here, shapes of individual stiff layers can be quite different from shapes of soft interbeds, and changes in thicknesses of soft interbeds can significantly affect the multilayer fold forms. If soft interbeds are relatively thin, the stiff layers cooperate and interact to produce parallel or constrained multilayer forms. If soft interbeds are thick, however, the stiff

Figure 4. Parallel, similar, and constrained forms, according to 3rd order analysis, in thick identical multilayers (59 layers) with free slip at contacts and confined by soft ($\mu_u/\mu_l = 0.1$) media (Fig. 4A) or rigid ($\mu_u/\mu_l \to \infty$) media (Fig. 4B). Ratio of fold wavelength *L* to total multilayer thickness *H* is *L/H* = 0.06. Similar, sinusoidal (Fig. 4A) or chevron (Fig. 4B) folds form at middepth. Parallel, concentric-like folds form near boundaries of multilayer and soft media (Fig. 4A); constrained, internal folds form near boundaries of multilayer and rigid media (Fig. 4B).

A

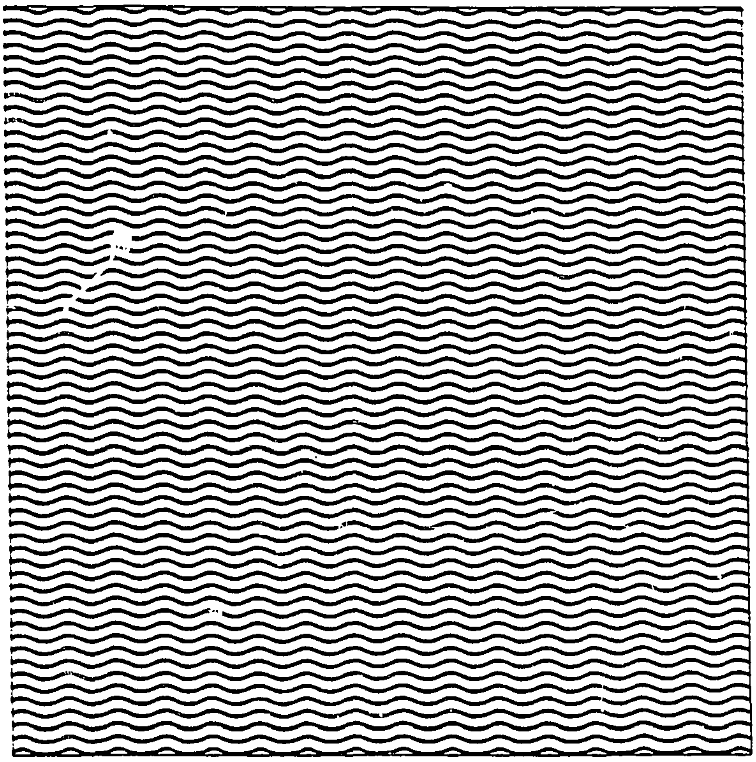

B

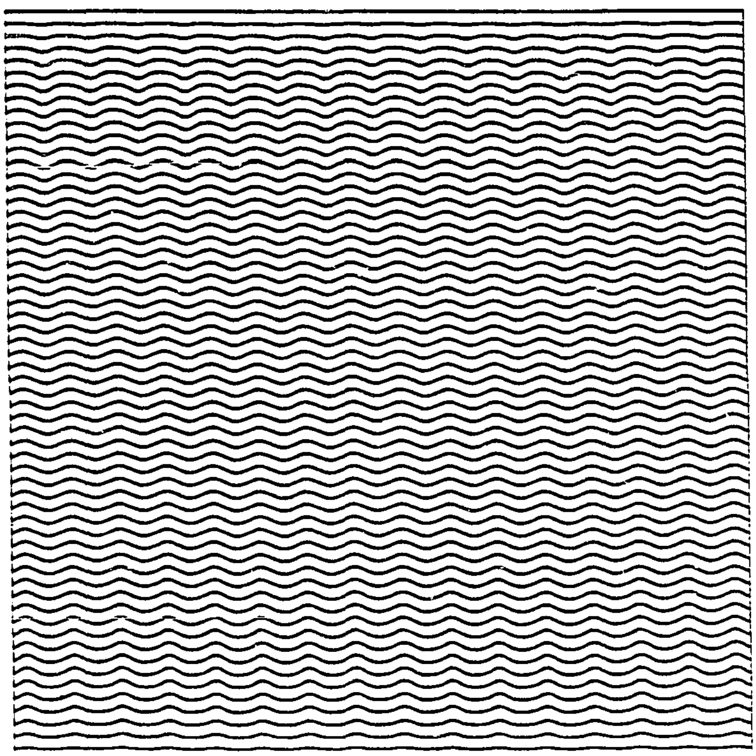

layers act independently and the multilayer fold form defined by the ensemble of stiff layers becomes similar. Johnson (1970, p. 149; 1977, pp. 188, 384) has shown that the critical spacing for marked interaction of stiff layers is on the order of the wavelength $\underline{L}$ of folds in stiff layers, that is, $\underline{h_2}/\underline{L} = 1$. Thus I define the _degree of independence of stiff layers_, $\underline{d}$, of a multilayer as

$$d = (h_2/L)\,(1 - \mu_n/\mu_1) \tag{1a}$$

in which μ_n is the normal viscosity. The _normal viscosity_ of the multilayer is the weighted average viscosity of stiff and soft layers,

$$\mu_n = [1/(h_1 + h_2)]\,(h_1\mu_1 + h_2\mu_2) \tag{1b}$$

in which subscripts $\underline{1}$ and $\underline{2}$ refer to stiff and soft, respectively. If $\underline{d}$ is zero, the stiff layers will behave as an ensemble, whereas if $\underline{d}$ is significantly greater than zero, say on the order of 0.5 or larger, the stiff layers will behave weakly as an ensemble and the folds in stiff layers will be independent.

The form of the ensemble of interfaces in a multilayer with low degree of independence of stiff layers, $\underline{d}$, will closely resemble the form in a multilayer composed entirely of stiff layers ($\underline{d} = 0$) if the ratios of viscosity of media (μ_U or μ_L) to normal viscosity, μ_n, of the multilayer are nearly the same. In all three multilayers of interbedded stiff and soft layers shown in Fig. 5, $\underline{d}$ is low and the normal viscosity is

Figure 5. Fold forms of selected multilayers composed of alternating stiff and soft layers ($\mu_2 = \mu_1/10$). A. Viscosity of soft media same as viscosity of soft interbeds; free slip at contacts. Concentric-like fold form nearly identical to that in same multilayer, but with bonded contacts, shown in Fig. 1 and intermediate between those shown in Fig. 2, locs. A1 and A2. B. Viscosity of stiff media same as viscosity of stiff layers; bonded contacts. Fold form intermediate between constrained form shown in Fig. 2, loc. A3, and that shown at loc. A2. C. Multilayer with free upper surface, stiff lower medium; bonded contacts. Fold form intermediate between those in Fig. 2, locs. B2 and B3.

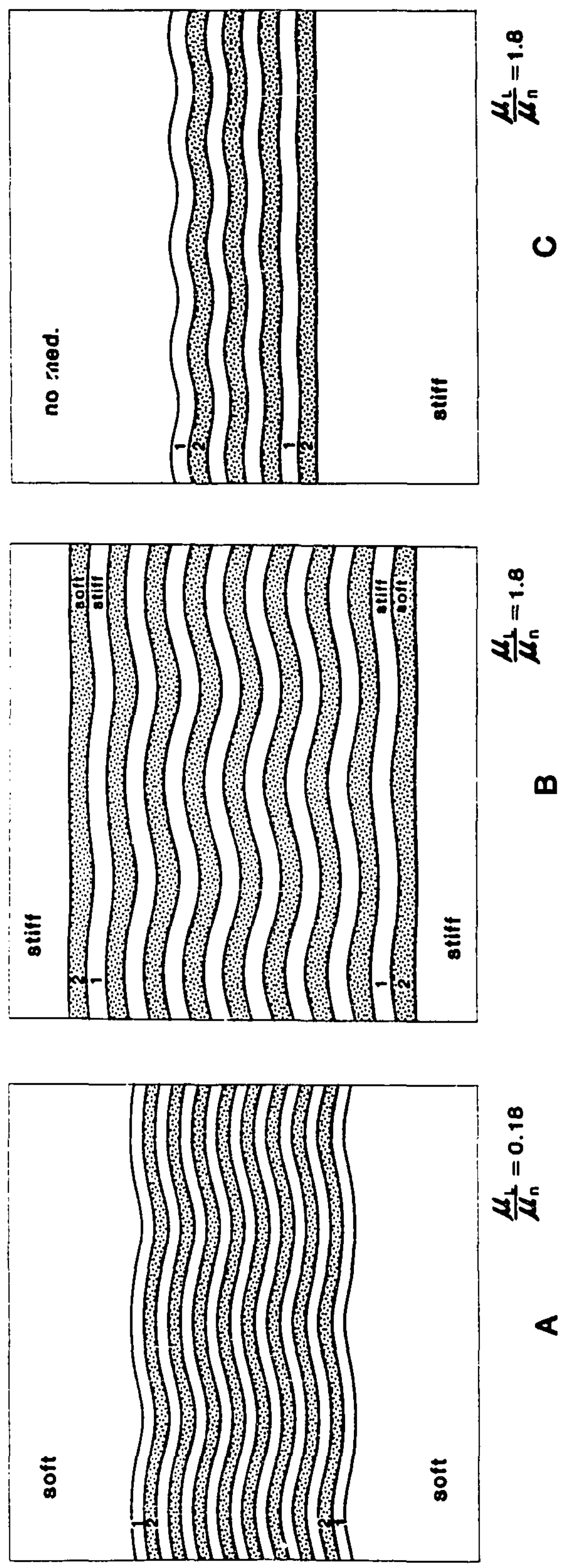

soft
soft
A
$\frac{\mu_L}{\mu_n} = 0.18$
stiff
stiff
soft
stiff
stiff
soft
B
$\frac{\mu_L}{\mu_n} = 1.8$
no med.
stiff
C
$\frac{\mu_L}{\mu_n} = 1.8$

$$\mu_n = (1/2)(\mu_1 + \mu_2) = 0.55\ \mu_1$$

because $\underline{h}_1 = \underline{h}_2$ and $\mu_1 = 10\ \mu_2$

The forms of ensembles of interfaces in multilayers shown in Fig. 5 can be predicted in terms of the six forms shown in Fig. 2 and the viscosity ratio μ_U/μ_n or μ_L/μ_n of the upper or lower medium to the normal viscosity. The multilayer shown in Fig. 5A has a viscosity ratio of $\mu_U/\mu_n = \mu_L/\mu_n = 0.18$, which is intermediate between those for Fig. 2, locs. A1 ($\mu_L/\mu_n = 0.1$) and A2 ($\mu_L/\mu_n = 1.0$). The form of the ensemble of interfaces in the multilayer shown in Fig. 5A is correspondingly intermediate between those shown in Fig. 2, locs. A1 and A2. Similarly, the multilayer shown in Fig. 5B has a viscosity ratio of $\mu_U/\mu_n = \mu_L/\mu_n = 1.8$, which is intermediate between the viscosity ratios for the multilayers shown in Fig. 2, locs. A2 and A3; the multilayer fold form is also intermediate. The multilayer shown in Fig. 5C also has the viscosity ratio $\mu_L/\mu_n = 1.8$, but it is unconfined above. This multilayer has a viscosity ratio and fold form intermediate between those for multilayers shown in Fig. 2, locs. B2 and B3.

The change of multilayer fold form with increasing independence of stiff layers is demonstrated in Fig. 6 by comparison of three 17-layer systems in which the thicknesses of soft interbeds are one, three, and five times that of the stiff beds, and in which $\underline{d} = 0.034$, 0.184, and 0.430, respectively. For the multilayers shown in Fig. 6, the form of the ensemble of interfaces is parallel, concentric-like if $\underline{d}$ is low

Figure 6. Forms of folds in multilayers that differ only in thickness of soft interbeds, illustrating effect of degree of independence of stiff layers, d, eq. (1a). Viscosity of media same as that of soft interbeds ($\mu_2 = \mu_1/10$). A. Closely-spaced layers with low d fold as ensemble into concentric-like form. B. As degree of independence of increases, the stiff layers begin to fold as individual layers rather than as an ensemble. C. For large d, individual layers fold virtually independently, forming an overall similar fold throughout most of the thickness of the multilayer.

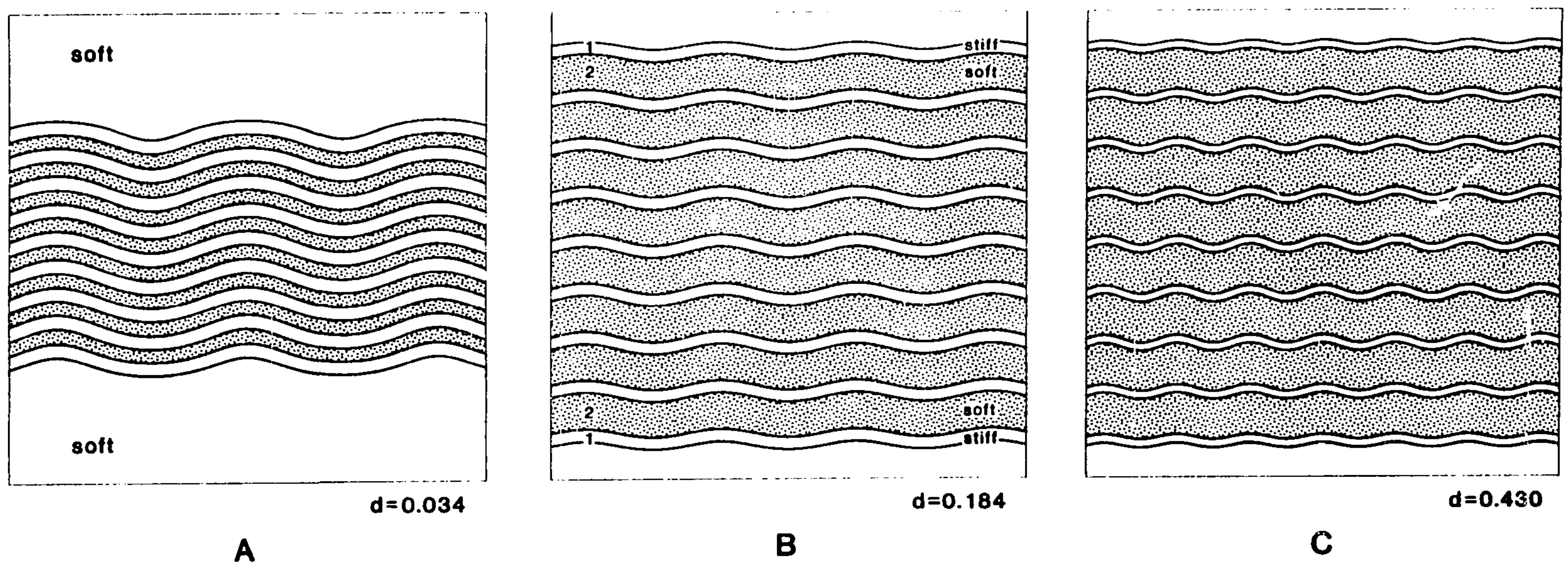
soft
soft
d=0.034
A
1
2
stiff
soft
2
1
soft
stiff
d=0.184
B
d=0.430
C

(Fig. 6A); as <u>d</u> increases, the fold form becomes more nearly <u>similar</u> in form (Fig. 6C).

Thus, three broad, end-member fold shapes can be recognized in simple, viscous multilayers folded to moderate amplitudes. For multilayers composed of identical stiff layers or stiff layers and thin, soft interbeds, in which the wavelength is roughly equal to the multilayer thickness, the multilayer fold shape is a <u>parallel</u>, <u>concentric-like</u> fold if the viscosity ratio μ_L/μ_n (or μ_U/μ_n) is much less than unity (Fig. 2, loc. A1; Fig. 5A; Fig. 6A) and is a <u>constrained</u>, <u>internal</u> fold if the viscosity ratio is greater than unity (Fig. 2, loc. A3; Fig. 3; Fig. 5C). For multilayers composed of thin stiff layers and thick soft interbeds, and for multilayers composed of stiff layers folded at short wavelengths, the multilayer fold shape near middepth tends to be a <u>similar</u>, <u>sinusoidal</u> (Figs. 4A, 6C) or <u>chevron</u> (Fig. 4B) form even to moderate amplitudes, regardless of the relative stiffness of confining media.

If stiff layers interact to fold as an ensemble, multilayer folds may have virtually the same form regardless of whether the layer contacts are freely slipping or bonded. For example, the multilayer shown in Fig. 6A is identical to that shown in Fig. 5A except that contacts are bonded for the former and freely slipping for the latter; the fold forms are both concentric-like. Furthermore, a multilayer composed entirely of stiff layers, with free slip at contacts, and confined by soft media (Fig. 2, loc. A1) also folds into a concentric-like form. However, as will be shown in following pages, folds grow much faster for multilayers with free slip at contacts than for multilayers with bonded contacts, particularly if the viscosity contrast of stiff layers and soft interbeds is low.

GEOMETRIC ANALYSIS OF FOLD SHAPES

Multi-interface fold forms are defined by an ensemble of interface forms: the fold forms depend on the shapes of all the individual interfaces and on the distribution of amplitudes of those shapes. For example, the essential feature of the internal fold (Fig. 2, loc. A3) is that amplitudes of anticlines and synclines decrease to zero at upper and lower boundaries. A concentric-like fold, which can form in a softly confined multilayer in which stiff layers interact (Fig. 2, loc. A1), or in a softly confined single stiff layer, is characterized by an internal transition from wide crests and narrow troughs on the upper interface to narrow crests and wide troughs on the lower interface.

The shape of each interface, according to the 3rd order analysis of folding, results from the summation of first, second, and third component waveforms. Each waveform is characterized by an amplitude and a wavelength; positive amplitudes are shown in Fig. 7. The height of a single interface is described by the function

$$\zeta = {}_1A\cos(\ell x) + {}_2A\cos(2\ell x) + {}_3A\cos(3\ell x) \qquad (2)$$

Figure 7. First, second, and third component waveforms. Each is a pure cosine wave. Wavelength of second component waveform is one-half that of first, and wavelength of third component waveform is one-third that of first. All amplitudes are positive.

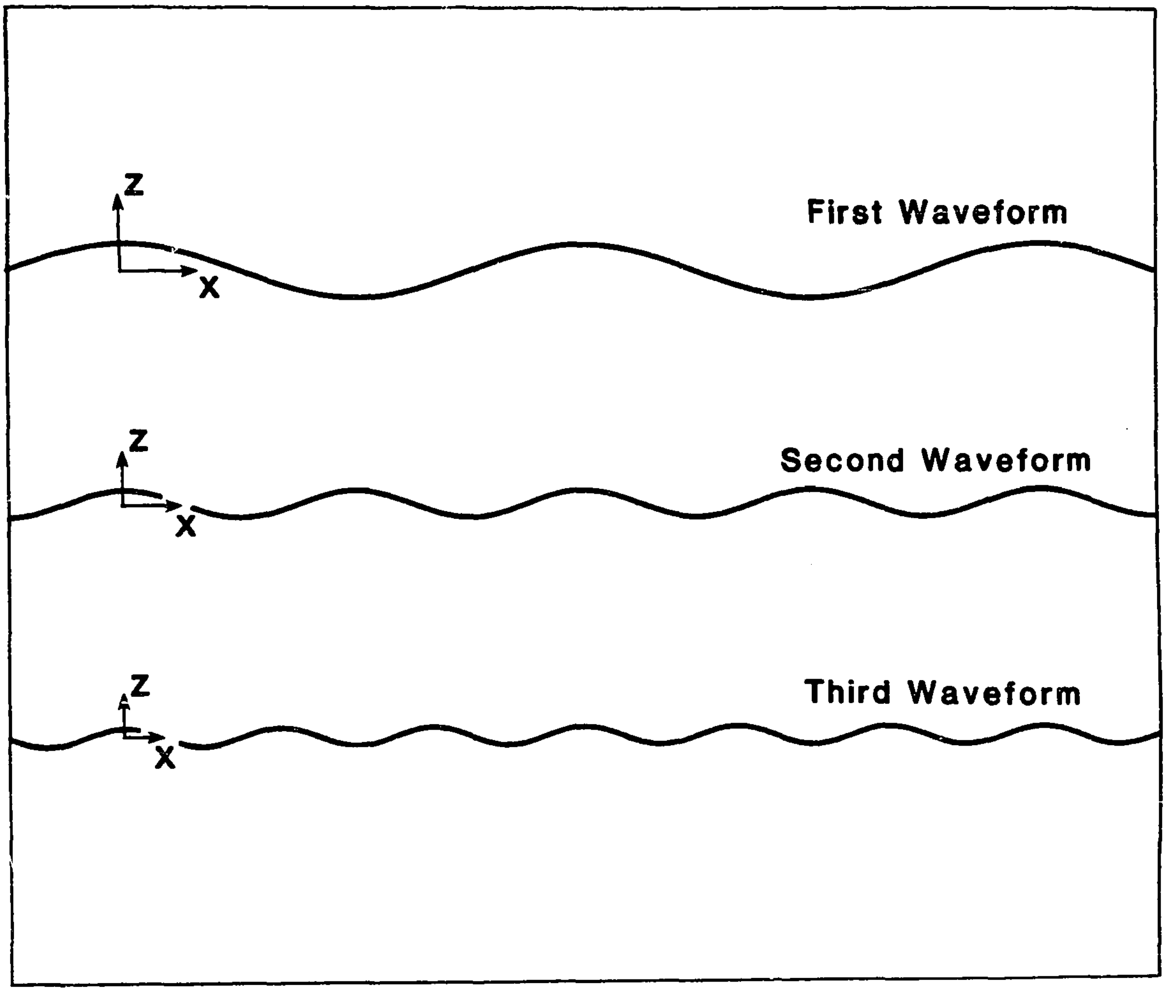
Z
X
First Waveform
Z
X
Second Waveform
Z
X
Third Waveform

in which ℓ is the wavenumber

$$\ell = 2\pi/L$$

$\underline{L}$ is the wavelength of the first waveform, and ${}_i\underline{A}$ are amplitudes of the various component waveforms. The wavelength of the second component waveform is one-half that of the first, and the wavelength of the third component waveform is one-third that of the first. The combination of the first, second, and third component waveforms in eq. (2) produces the resultant waveform of a single interface.

Four illustrations of the addition of two component waveforms to produce a resultant waveform are shown in Fig. 8. Column 1 contains four identical first component waveforms of positive amplitude ${}_1\underline{A}$. Each of these first waveforms is added to a second or third component waveform, of positive or negative amplitude, $\pm{}_2\underline{A}$ or $\pm{}_3\underline{A}$, respectively, shown in column 2. Column 3 shows the resultant waveforms. Comparison of row A and row B, or row C and row D, demonstrates that the nature of the effect of adding a second, or third, component waveform to the first depends on the signs of their amplitudes; however, the magnitude of the effect depends on the relative magnitudes of their amplitudes.

The shape of an individual layer is defined by the shapes of the upper and lower interfaces of the layer; the shapes of the upper and lower interfaces are each determined by three component waveforms. The heights of the top ($\underline{t}$) and bottom ($\underline{b}$) interfaces of a layer are described by the functions,

Figure 8. Shapes of individual interfaces determined by addition of two component waveforms. First component waveforms of positive amplitude in column 1; second and third component waveforms of positive or negative amplitude in column 2. Each row, A-D, illustrates the addition of a waveform in column 1 to a waveform in column 2 to produce a resultant waveform in column 3. A. Second waveform of positive amplitude sharpens crests and broadens troughs. B. Second waveform of negative amplitude sharpens troughs and broadens crests. C. Third waveform of positive amplitude sharpens crests and troughs and decreases slope at inflection points. D. Third waveform of negative amplitude broadens crests and troughs and increases slope at inflection points.

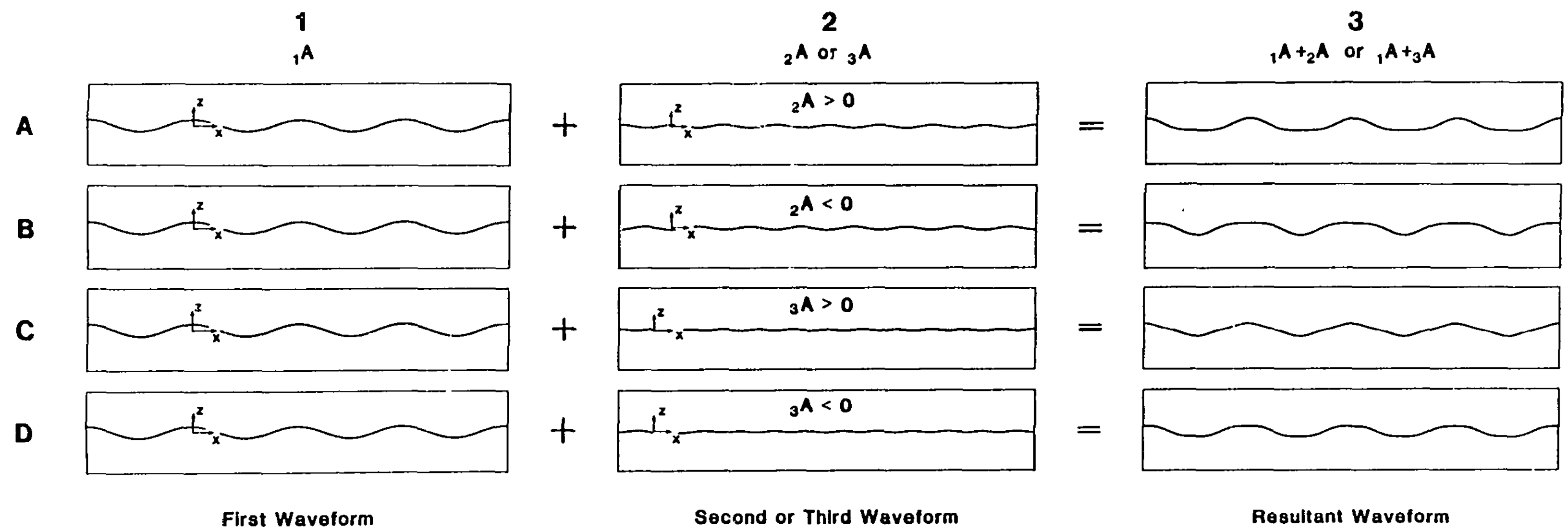
1
$_{1}A$
2
$_{2}A$ or $_{3}A$
3
$_{1}A + _{2}A$ or $_{1}A + _{3}A$
A
B
C
D
$_{2}A > 0$
$_{2}A < 0$
$_{3}A > 0$
$_{3}A < 0$
z
x
+
=
First Waveform
Second or Third Waveform
Resultant Waveform

$$\zeta_t = h/2 + {}_1A_t\cos(\ell x) + {}_2A_t\cos(2\ell x) + {}_3A_t\cos(3\ell x) \tag{3a}$$

$$\zeta_b = -h/2 + {}_1A_b\cos(\ell x) + {}_2A_b\cos(2\ell x) + {}_3A_b\cos(3\ell x) \tag{3b}$$

in which $\underline{h}$ is the mean vertical thickness of the layer and ${}_i\underline{A}_{t,b}$ are amplitudes of various component waveforms.

One way to determine the shape of a layer is in terms of eqs. (3), where, for example, one sums the component waveforms in the bottom interface, eq. (3b), to produce a resultant bottom interface waveform. The pair of resultant interface waveforms, eqs. (3a) and (3b), defines the shape of the layer. Alternatively, the equations for the individual interfaces, eqs. (3), could be added and subtracted to produce two new equations which describe the shape of the layer:

$$(\zeta_t + \zeta_b)/2 = \bar{\zeta} = {}_1A_a\cos(\ell x) + {}_2A_a\cos(2\ell x) + {}_3A_a\cos(3\ell x) \tag{4a}$$

$$(\zeta_t - \zeta_b) = \hat{h} = h + 2{}_1A_s\cos(\ell x) + 2{}_2A_s\cos(2\ell x) + 2{}_3A_s\cos(3\ell x) \tag{4b}$$

in which

$${}_iA_a = ({}_iA_t + {}_iA_b)/2; \qquad {}_iA_s = ({}_iA_t - {}_iA_b)/2 \tag{4c}$$

Equation (4a) describes the variation in average height $\bar{\zeta}$ of the layer with horizontal distance $\underline{x}$ along the layer, and eq. (4b) describes the variation in vertical thickness $\underline{\hat{h}}$ with horizontal distance $\underline{x}$. The pure folding mode is the shape of a layer with only one wavelength and for which $\underline{A}_s$ is zero (Fig. 9A); the pure pinch-and-swell mode results if $\underline{A}_a$ is zero (Fig. 9B).

Various layer shapes are produced by the addition of a pinch-and-swell mode to a folding mode; four examples are shown in Fig. 10. Column 1 contains the folding mode component of the first waveforms, chosen because ${}_1\underline{A}_a$ is almost always the dominant coefficient in eq. (4a). Column 2 contains four possible pinch-and-swell components, positive and negative contributions of the first and second component waveforms, chosen because ${}_1\underline{A}_s$ and ${}_2\underline{A}_s$ tend to be much larger than ${}_3\underline{A}_s$ in eq. (4b). Layer shapes resulting from the addition of the modes shown in columns 1 and 2 are shown in column 3. The folding modes ${}_2\underline{A}_a$ and ${}_3\underline{A}_a$ of the second and third waveforms have the same effects on the shape of a single layer as the amplitudes ${}_2\underline{A}$ and ${}_3\underline{A}$ have on the shape of a single interface (Fig. 8).

The shapes of folds in multilayers analyzed in this chapter are determined primarily by the distributions and relative magnitudes of amplitudes of the first and second waveforms, ${}_1\underline{A}$ and ${}_2\underline{A}$, within the ensemble of interfaces. The distribution and magnitudes of amplitudes within a multilayer depend, in turn, on the stiffness of confinement of the whole multilayer and on $\underline{d}$, the degree to which the stiff layers can act independently.

Each multilayer shown in Fig. 11 consists of all stiff layers ($\underline{d}$ = 0) confined by identical media ($\mu_U = \mu_L$). The stiff layers

Figure 9. Shapes of single layers with only one wavelength. A. Pure folding mode, for which $\underline{A}_a$ is positive and $\underline{A}_s$ is zero. B. Pure pinch-and-swell mode, for which $\underline{A}_a$ is zero and $\underline{A}_s$ is positive. Terms are explained in eq. (4c) and text.

A

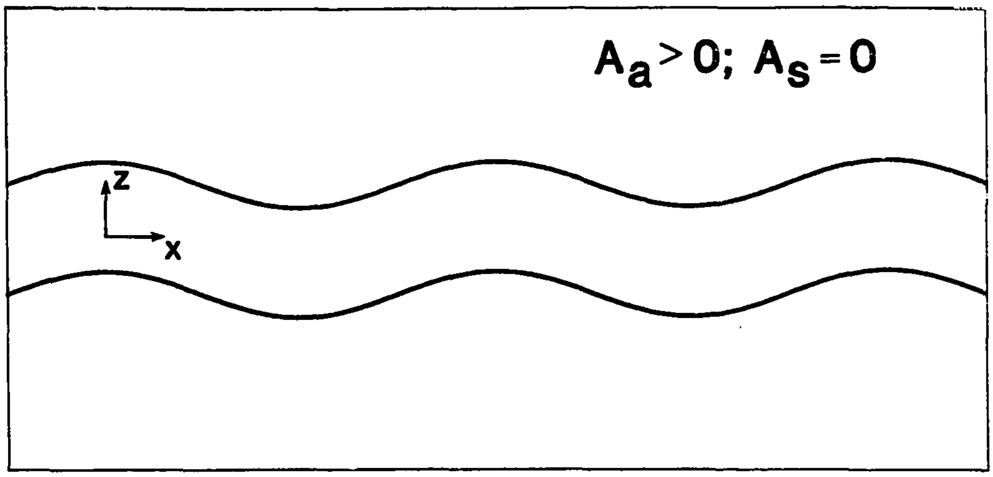

Folding Mode

B

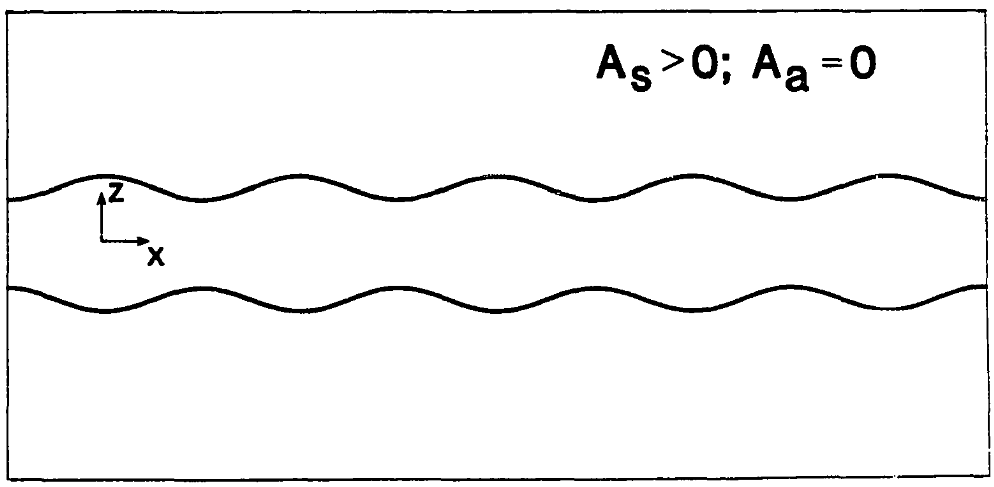

Pinch–and–Swell Mode

Figure 10. Shapes of single layers as determined by addition of a pinch-and-swell mode to a folding mode. Folding mode component of first waveforms in column 1; pinch-and-swell mode components of first or second waveforms of positive or negative amplitudes in column 2. Each row, A-D, illustrates the addition of a folding mode in column 1 to a pinch-and-swell mode in column 2 to produce a layer shape in column 3.

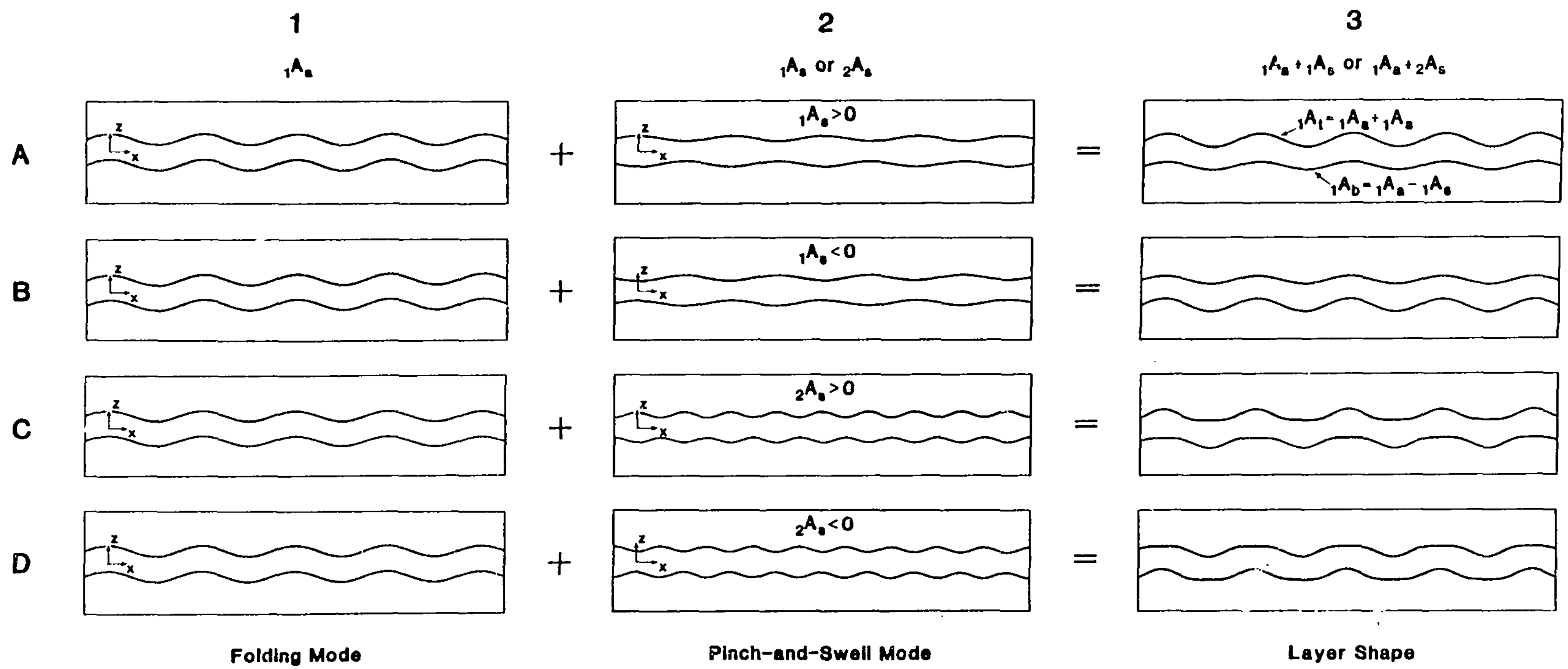
1
${}_1A_a$
2
${}_1A_s$ or ${}_2A_s$
3
${}_1A_a + {}_1A_s$ or ${}_1A_a + {}_2A_s$
A
B
C
D
z
x
${}_1A_s > 0$
${}_1A_s < 0$
${}_2A_s > 0$
${}_2A_s < 0$
${}_1A_t = {}_1A_a + {}_1A_s$
${}_1A_b = {}_1A_a - {}_1A_s$
+
=
Folding Mode
Pinch-and-Swell Mode
Layer Shape

strongly interact, so the distributions of amplitudes depend primarily on the stiffness of confinement of the multilayer. The distribution of first-waveform amplitudes ${}_1\underline{A}$ in column 1 reflects a folding mode of the entire multilayer. Although the magnitudes change from interface to interface as a function of the confinement, the signs of ${}_1\underline{A}_i$ are positive on every interface. For example, the amplitudes are nearly the same for every interface in a multilayer with soft confinement (loc. A1) but die off to zero at the edges of a multilayer with very stiff confinement (loc. C1).

The distribution of second-waveform amplitudes ${}_2\underline{A}$ in column 2 reflects a pinch-and-swell mode of the entire multilayer. In the pinch-and-swell mode, the amplitudes of the second component waveform, ${}_2\underline{A}_i$, are negative in the top half of the multilayer, positive in the bottom half, and zero at middepth. The amplitudes increase to maxima at the edges of the softly confined multilayer (loc. A2) but go through maxima halfway between the edges and middepth of the very stiffly confined multilayer (loc. C2).

The multilayer shapes that result from addition of a folding mode in column 1 to a pinch-and-swell mode in column 2 are shown in column 3. In a softly confined multilayer, the multilayer fold shape is a concentric-like fold (loc. A3); in a very stiffly confined multilayer, the fold shape is an internal fold (loc. C3). The components of a concentric-like fold in a multilayer, Fig. 11, row A, correspond to the components of a concentric-like fold in a single stiff layer, Fig. 10, row D.

Fold forms in column 1 differ from their counterparts in column 3 because of the addition of a pinch-and-swell mode in column 2. The effectiveness of the pinch-and-swell mode in modifying the shape produced by the pure folding mode depends on the <u>strength of the second waveform</u>, measured as the ratio of the amplitude of the second waveform to that of the first on the interface $\underline{i}$ with the maximum amplitude of the second waveform. In column 2, $({}_2A_i)_{max}/{}_1A_i$ is approximately -0.25 for all three modes; in loc. A2, the maximum ${}_2\underline{A}_i$ occurs on the top and bottom interfaces, but in loc. C2, on the two interfaces halfway between the edges and middepth of the multilayer. The fold form shown in column 1 would also be the resultant fold form if the strength of the second waveform in column 2 were equal to zero, that is, $({}_2A_i)_{max}/{}_1A_i = 0$. If the strength of the second waveform were between zero and -0.25, the resultant multilayer fold shapes would be intermediate between those shown in columns 1 and 3.

The differences between the concentric-like and internal multilayer fold forms shown in Fig. 11 are a result of different distributions of amplitudes of first and second waveforms throughout the multilayer. Although the 3rd order analysis of folding determines these amplitude distributions, it reveals very little about which parameters control the distributions. For this purpose, the elementary folding theory of multilayers (e.g., Johnson and Page, 1976; Johnson, 1982) provides significant insights. The elementary folding theory indicates that, to 2nd order, the height of interfaces above middepth in a multilayer confined by media above and below is, approximately,

Figure 11. Shapes of multilayers as determined by addition of a multilayer pinch-and-swell mode to a multilayer folding mode. Multilayer folding mode of first waveforms in column 1; multilayer pinch-and-swell mode of second waveforms in column 2. Confinement ranges from soft ($\mu_u/\mu_1 = 0.1$) in row A to stiff ($\mu_u/\mu_1 = 1.0$) in row B to rigid ($\mu_u/\mu_1 \to \infty$) in row C. Multilayer fold form in loc. A3 is concentric-like; form in loc. C3 is internal; form in loc. B3 is intermediate.

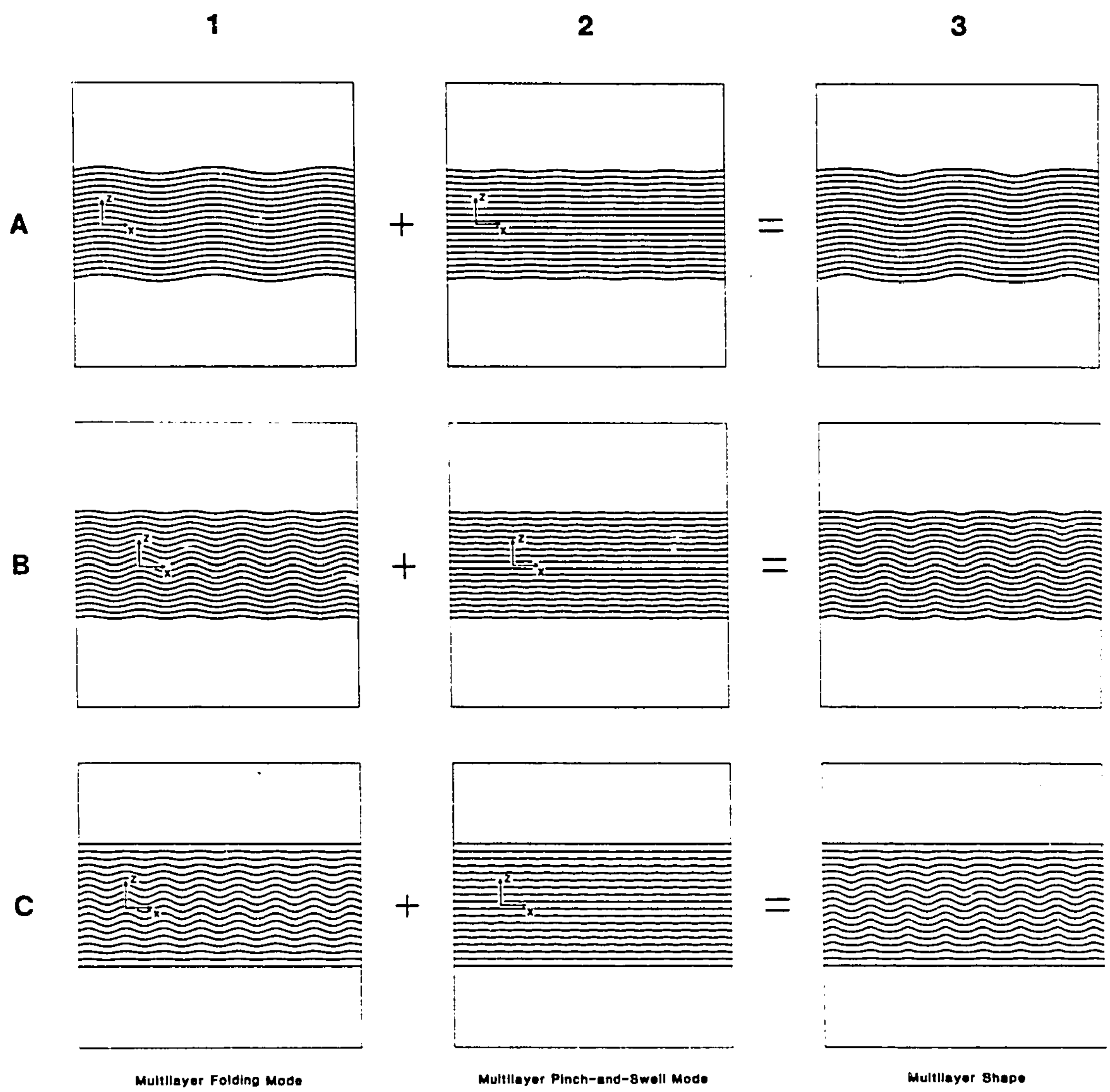
1
2
3
A
B
C
+
=
z
x
Multilayer Folding Mode
Multilayer Pinch-and-Swell Mode
Multilayer Shape

$$\zeta = \bar{z} + {}_1\bar{A}\cos(c\bar{z}\ell L/2H)\cos(\ell x) + {}_2\bar{A}\sin(c\bar{z}\ell L/H)\cos(2\ell x) \tag{5}$$

in which $\bar{z}$ is the distance above middepth, H is the total thickness of the multilayer, and c is constraint.

I define the constraint operationally as

$$c = (2/\pi)\cos^{-1}({}_1A_e/{}_1A_m) \tag{6}$$

where ${}_1A_e$ is the amplitude at the upper or lower edge of the multilayer ($\bar{z} = \pm H/2$) and ${}_1A_m$ is the maximum amplitude. Constraint may be different at the top and bottom of the multilayer if the confining media have different properties.

If ${}_2\bar{A}$ is zero, eq. (5) approximately describes the distribution of amplitudes of first waveforms shown in column 1, Fig. 11, for values of c of nearly zero, 0.5, and 1.0. Similarly, if ${}_1\bar{A}$ is zero, eq. (5) approximately describes the distribution of amplitudes of second waveforms shown in column 2, Fig. 11. However, eq. (5) is based on a theory that approximates the behavior of a multilayer by selecting a representative element consisting of an entire stiff layer with half of a soft layer both above and below. Such approximations allow the distribution of amplitudes of interfaces to be treated as a continuum and expressed by a continuous function such as eq. (5). Because the elementary theory describes the position of a line at middepth in a stiff layer rather than describing the positions of the upper and lower interfaces of each stiff layer, the results cannot be used to determine fold shapes of individual layers.

Constraint, c, will be used as one of the parameters in the description of multilayer fold forms. Constraint ranges from zero to unity, depending on the viscosity of the confining media, μ_m, the normal viscosity of the multilayer, μ_n, eq. (1b), and the wavelength-to-thickness ratio of the folds. The derivation of c is presented by Johnson and Page (1976), where variable n there is the inverse of c here:

$$c \tan(c\pi/2) = (\mu_m/\mu_n)(H/L) \tag{7a}$$

The relation is nonlinear. For small values of c, however,

$$c \simeq \sqrt{(2/\pi)(\mu_m/\mu_n)(H/L)} \quad ; \quad c << 1 \tag{7b}$$

Furthermore, the wavelength-to-thickness ratio, L/H, itself is a function of the constraint (Johnson and Page, 1976). According to elementary multilayer folding theory, the dominant wavelength for soft media depends on N_p, the number of pairs of stiff and soft layers, μ_1/μ_2, the viscosity ratio, and h_1/h_2, the thickness ratio of stiff to soft layers. The functional relation is given by Johnson and Page (1976). Here, the solution is presented graphically (Fig. 12B) by relating the dominant wavelength ratio for soft media to the dominant wavelength ratio for rigid media, which is

$$(L_d/H)_R = 2\pi \sqrt[2]{(1/N_p\pi)} \sqrt[4]{(\mu_1/12\mu_n)\{1/(1+h_2/h_1)^3\}} \tag{7c}$$

The constraint for multilayers confined by soft media can be determined for the dominant wavelength of folds by writing eq. (7a) in the form,

Figure 12. Graphs for determining constraint and dominant wavelengths according to elementary multilayer folding theory. A. Relations between constraint, c, and ratio of dominant wavelength to total thickness of rigidly confined multilayer, $(L_d/H)_R$, for various ratios of viscosity of media, μ_m, to normal viscosity, μ_n, of multilayer. Equations for $(L_d/H)_R$ and μ_n are given in text. Values of $(L_d/H)_R$ for several multilayers composed of identical stiff layers but containing different numbers of stiff layers indicated at top of figure.
B. Relation between dominant wavelength for multilayer confined by soft media, $(L_d/H)_S$, and dominant wavelength for same multilayer confined by rigid media, $(L_d/H)_R$, for various values of μ_m/μ_n.

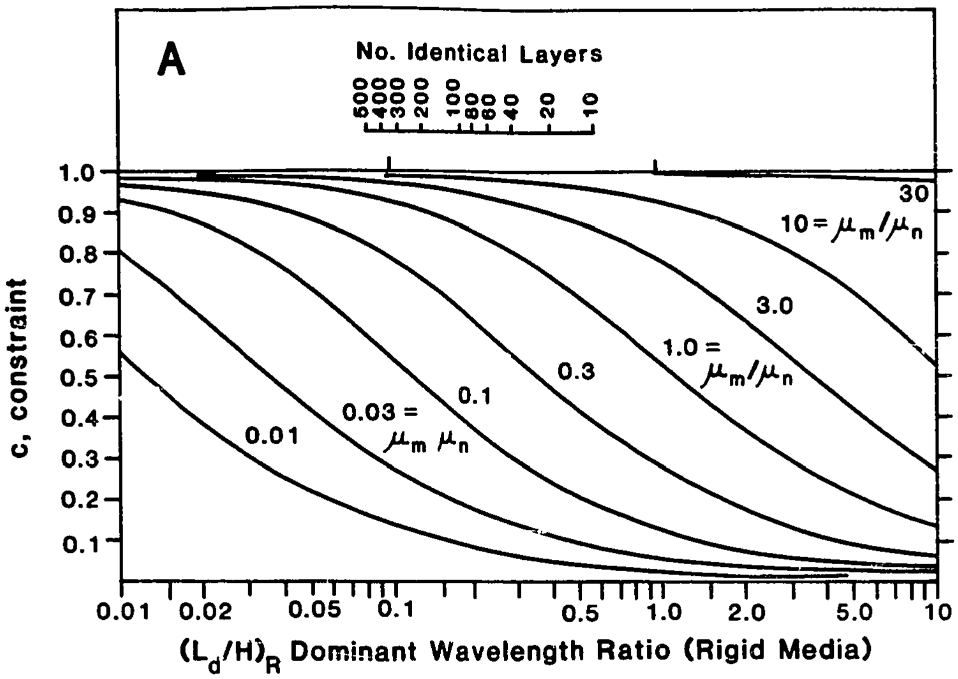
A
No. Identical Layers
500
400
300
200
100
80
60
40
20
10
1.0
0.9
0.8
0.7
0.6
0.5
0.4
0.3
0.2
0.1
c, constraint
30
10 = μ_m/μ_n
3.0
1.0 = μ_m/μ_n
0.3
0.1
0.03 = μ_m μ_n
0.01
0.01
0.02
0.05
0.1
0.5
1.0
2.0
5.0
10
$(L_d/H)_R$ Dominant Wavelength Ratio (Rigid Media)

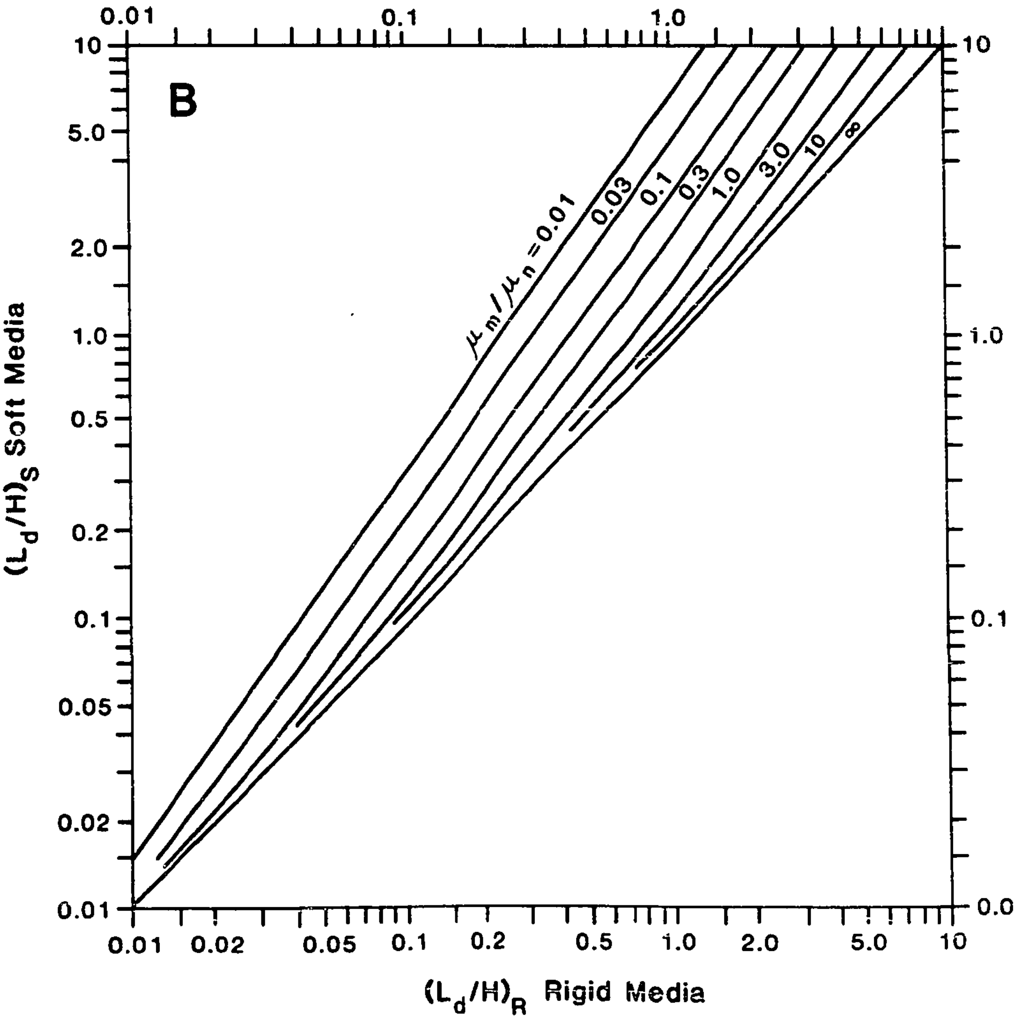
B
0.01
0.1
1.0
10
5.0
2.0
1.0
0.5
0.2
0.1
0.05
0.02
0.01
$(L_d/H)_S$ Soft Media
μ_m/μ_n=0.01
0.03
0.1
0.3
1.0
3.0
10
∞
0.01
0.02
0.05
0.1
0.2
0.5
1.0
2.0
5.0
10
$(L_d/H)_R$ Rigid Media

$$c \tan(c\pi/2) = (\mu_m/\mu_n)/(L_d/H)_S$$

and using Fig. 12B to determine the dominant wavelength ratio for soft media.

Relations between the constraint, c, corresponding to the dominant wavelength for a multilayer confined by soft media, the viscosity ratio μ_m/μ_n, and the dominant wavelength for the same multilayer confined by rigid media, $(L_d/H)_R$, are shown in Fig. 12A. Examination of Fig. 12A and eq. (7c) indicates that constraint will increase if any one of the following happens: the viscosity of the medium, μ_m/μ_n, increases; the number of pairs, N_p, of stiff and soft layers increases; the relative viscosity, μ_1/μ_n, of stiff layers decreases; the relative thickness, h_2/h_1, of soft interbeds increases.

One can use Figs. 12A and 12B as follows. For given properties of a multilayer, one computes the dominant wavelength ratio for rigid media using eq. (7c). Then one uses Fig. 12A to determine c by interpolating between curves of constant relative viscosity of media, μ_m/μ_n. The constant c provides information about fold shape. One uses Fig. 12B to compute the dominant wavelength ratio for soft media, again interpolating between curves of constant relative viscosity of media. The dominant wavelength ratio provides information about the size of the multilayer folds confined by soft media.

The relation for the dominant wavelength ratio for multilayers confined by rigid media, eq. (7c), simplifies markedly if the multilayer is composed solely of stiff layers, with free slip at layer contacts:

$$(L_d/H)_R \approx 1.9 \sqrt[2]{(1/N)} \tag{7d}$$

as Biot (1964) showed. Here N is the number of layers. Wavelength ratios of folds in such multilayers with ten to 500 layers are indicated near the top of Fig. 12A.

The most important insight from the elementary theory is that the shapes of multilayer folds can be expressed, approximately, in terms of the constraint, c. The strength of the second waveform, $({}_2A_i)_{max}/{}_1A_i$, and the degree of independence of stiff layers, d, have already been identified (Fig. 11; eq. 1a) as significant parameters. Simple multilayers with low degree of independence of stiff layers and with the same constraint and strength of the second waveform will have the same shapes, as defined by the ensemble of interfaces, whether the multilayer consists solely of stiff layers or consists of interbedded stiff and soft layers.

Therefore, folds with a wide range of shapes can be classified in terms of constraint and strength of the second waveform (Fig. 13). Each row of fold forms in Fig. 13 is for a certain value of constraint: c = 0.05 for row A, c = 0.50 for row B, and c = 1.0 for row C. Each column of fold forms is for a different strength of the second waveform: $({}_2A_i)_{max}/{}_1A_i = 0$ for column 1, $({}_2A_i)_{max}/{}_1A_i = -0.15$ for column 2, and $({}_2A_i)_{max}/{}_1A_i = -0.25$ for column 3. The fold shown in loc. A1 is virtually similar, whereas that shown at loc. C1 is the constrained form that Biot (1963, 1964, 1965a) termed "internal instability." The fold

Figure 13. Multilayer fold forms corresponding to a range of values of constraint and strength of the second waveform. Constraint, c, ranges from 0.05 in row A to 0.50 in row B to 1.0 in row C; strength of the second waveform, $({}_{2}A_{i})_{max}/{}_{1}A_{i}$, ranges from zero in column 1 to -0.15 in column 2 to -0.25 in column 3. The fold form at loc. A1 is similar; the fold forms at locs. A2 and A3 are concentric-like; the fold forms in row C are constrained.

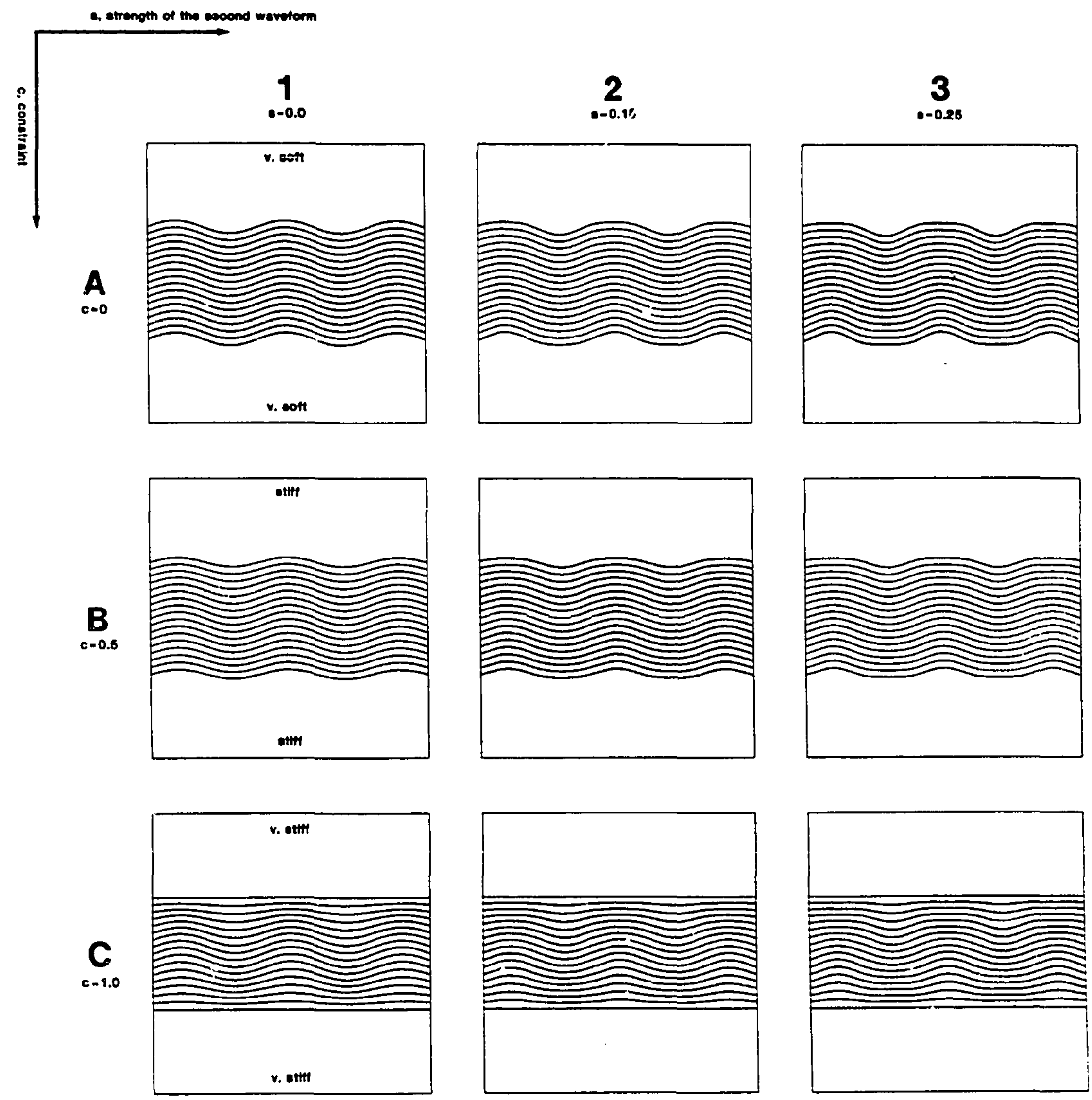

s, strength of the second waveform
c, constraint
1
s=0.0
2
s=0.15
3
s=0.25
A
c=0
v. soft
v. soft
B
c=0.5
stiff
stiff
C
c=1.0
v. stiff
v. stiff

shown at loc. B1 is intermediate. All three examples in column 1 are for zero amplitudes of the second waveform, but the folds would look nearly the same even if the maximum amplitudes of second waveforms were up to five or seven percent of amplitudes of first waveforms; I have found that the effect of the second waveform is visually unrecognizable until $({}_2A_i)_{max}/{}_1A_i$ is at least ± 0.08. The folds shown at locs. A2 and A3 are concentric-like folds, those shown at locs. C2 and C3 are internal folds.

Figure 14 shows fold forms derived to 3rd order accuracy in maximum slopes of interfaces for multilayers unconfined above and confined below by a soft (Fig. 14A), stiff (Fig. 14B), or very stiff (Fig. 14C) medium. The strength of the second waveform, $({}_2A_i)_{max}/{}_1A_i$, is zero in column 1, -0.15 in column 2, and -0.25 in column 3. The strengths of second waveforms of other folds formed under similar conditions can be estimated by comparison with the folds shown in Fig. 14.

The forms of folds shown in Fig. 14, locs. A3, B3, and C3, are influenced by all three component waveforms. Although the signs of ${}_1\underline{A}$ and ${}_3\underline{A}$ are positive and the sign of ${}_2\underline{A}$ is negative in all three examples, the relative magnitudes of the amplitudes differ. The amplitude ratios, or relative strengths of the component waveforms, for the top interface shown in Fig. 14, loc. A3, are:

$$ {}_2A/{}_1A = -0.17; \quad {}_3A/{}_1A = 0.02; \quad {}_3A/{}_2A = -0.12 $$

whereas at loc. B3 they are:

Figure 14. Fold forms of multilayers unconfined above but confined below. Forms derived by 3rd order analysis. Identical stiff layers. Lower medium ranges from soft ($\mu_L/\mu_1 = 0.1$) in row A to stiff ($\mu_L/\mu_1 = 1.0$) in row B to rigid ($\mu_L/\mu_1 \to \infty$) in row C. Column 1 shows interfaces composed of only first waveforms; ${}_2A_i = {}_3A_i = 0$. Columns 2 and 3 show interfaces composed of first, second, and third component waveforms at two stages of deformation of the same multilayers. For example, shortening of the multilayer shown at loc. C1 results in the fold form shown at loc. C2, and further shortening of this same multilayer results in fold form shown at loc. C3.

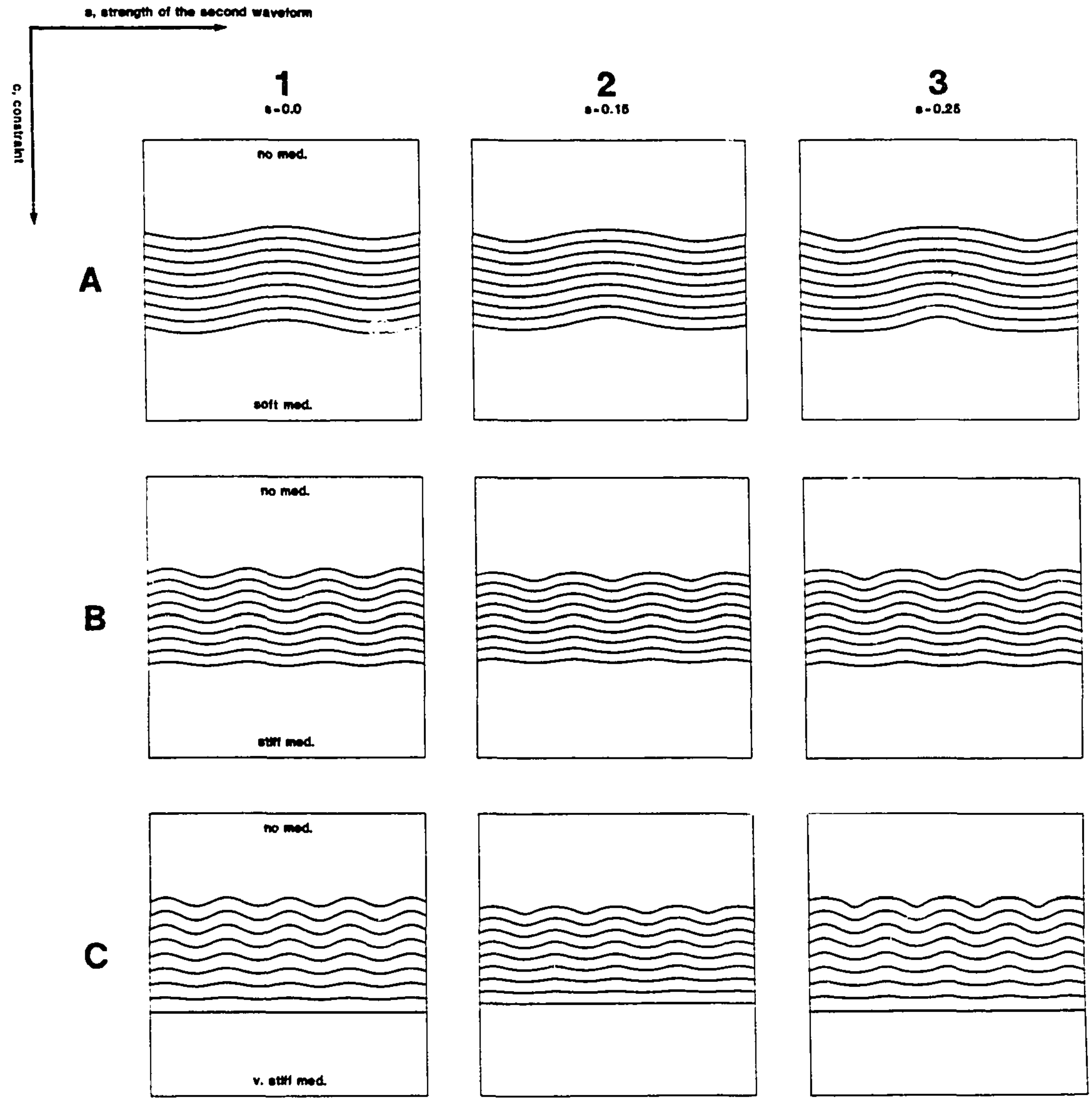

s, strength of the second waveform
c, constraint
1
s=0.0
2
s=0.15
3
s=0.25
A
B
C
no med.
soft med.
no med.
stiff med.
no med.
v. stiff med.

$$ {}_2A/{}_1A = -0.22; \quad {}_3A/{}_1A = 0.05; \quad {}_3A/{}_2A = -0.21 $$

and at loc. C3 they are

$$ {}_2A/{}_1A = -0.28; \quad {}_3A/{}_1A = 0.08; \quad {}_3A/{}_2A = -0.29 $$

These results indicate that the flattening produced in the upper interface by the second component waveform is greater at loc. C3 than at loc. A3. Yet the form of the upper interface at loc. C3 is more rounded than that at loc. A3. The reason lies in the relative strength of the third component waveform. In loc. A3, the amplitude of the third waveform is only $-0.12({}_2\underline{A})$, whereas at loc. C3 it is $-0.29({}_2\underline{A})$. The third waveform has a positive amplitude, so it sharpens crests and troughs, as shown in Fig. 8. Thus, it is the relative strength of the second waveform and the relative weakness of the third waveform that produces the flattened crests in the top interface shown in loc. A3, and it is the relative strength of both the second and third waveforms that produces the arc-and-cusp structure in the top interface shown at loc. C3. The form of the top interface shown at loc. B3 is intermediate, and the relative strength of the third waveform is intermediate between the values for the multilayers shown at locs. A3 and C3.

This completes my presentation of the essential results of the analysis of fold forms in simple, repetitive multilayers of viscous materials. In following pages I present the theory and then, in the Discussion, apply the theory to some large folds in rocks and to some small folds in experimental multilayers.

THEORY OF FOLDING OF VISCOUS MULTILAYERS

Solution for Constants

The analysis of folding of multilayers begins with an explanation of steps in the derivation of arbitrary constants that must be evaluated in order to compute the growth rates of perturbations in interfaces of layers. A representative layer is considered in some detail, but only final results are presented for confining media.

The height of each interface, between layers or between a layer and a confining medium, is described by the relation,

$$\zeta_{t,b} = \pm\, h/2 + {}_1A_{t,b}\cos(\ell x) + {}_2A_{t,b}\cos(2\ell x) + {}_3A_{t,b}\cos(3\ell x) \qquad (8)$$

plus other trigonometric terms if the analysis is carried to an order higher than 3rd. Here $\underline{t}$ refers to top and $\underline{b}$ to bottom interfaces of a layer. The first term in eq. (8) gives the mean height of the upper $(+\,\underline{h}/2)$ and lower $(-\,\underline{h}/2)$ interfaces. Trigonometric terms describe the variation of the height of the interface about its mean position.

Initially, each interface is a simple first cosine waveform and ${}_2\underline{A}_{t,b} = 0 = {}_3\underline{A}_{t,b}$. However, as the first waveform grows, the second and third waveforms develop spontaneously, so the complete analysis must consider all three waveforms.

The mechanical problem is to determine the amplitudes, ${}_i\underline{A}_{t,b}$, as functions of time. It is formulated by separating components of velocity and stress within a layer into mean and perturbed values

(Fletcher, 1974, 1977). The mean values of stress and velocity are those that solve the problem describing the uniform deformation of a layer with planar interfaces. The perturbed values of stress and velocity are those that must be added to the mean values in order to match stresses and velocities at perturbed interfaces between layers or between a layer and a confining medium.

This analysis considers multilayers subjected to uniform shortening parallel to layers and uniform thickening normal to layers; the rate of shearing deformation is zero. The mean stresses and velocities within a layer are

$$\bar{v}_x = x\bar{D}_{xx} \tag{9a}$$

$$\bar{v}_z = z\bar{D}_{zz}+(\bar{v}_z)_o = (\bar{v}_z)_o - z\bar{D}_{xx} \tag{9b}$$

$$\bar{\sigma}_{xx} = 2\mu\bar{D}_{xx} - \bar{p} \tag{9c}$$

$$\bar{\sigma}_{zz} = -2\mu\bar{D}_{xx} - \bar{p} \tag{9d}$$

$$\bar{\sigma}_{xz} = 0 \tag{9e}$$

$$\bar{p} = -(\bar{\sigma}_{xx}+\bar{\sigma}_{zz})/2 \tag{9f}$$

in which $\underline{\bar{D}}_{xx}$ is layer-parallel deformation rate. For the incompressible viscous material, $\underline{\bar{D}}_{xx} = -\underline{\bar{D}}_{zz}$. This completes the solution for the mean flow, which is exact.

The total velocities and stresses are the sums of the mean and perturbed values:

$$v_x = \bar{v}_x + \tilde{v}_x \; ; \quad v_z = \bar{v}_z + \tilde{v}_z \tag{10a}$$

$$\sigma_{xx} = \bar{\sigma}_{xx} + \tilde{\sigma}_{xx} \; ; \quad \sigma_{zz} = \bar{\sigma}_{zz} + \tilde{\sigma}_{zz} \; ; \quad \sigma_{xz} = \tilde{\sigma}_{xz} \tag{10b}$$

The perturbed values satisfy the biharmonic equation in the stream function,

$$\nabla^4\psi = 0 \tag{11a}$$

where

$$\tilde{v}_x = -(\partial\psi/\partial z) \; ; \quad \tilde{v}_z = (\partial\psi/\partial x) \tag{11b}$$

The solution is,

$$\tilde{v}_x = -\left[\{{}_ja + {}_jd + {}_jb(j\ell z)\}{}_jS + \{{}_jb + {}_jc + {}_jd(j\ell z)\}{}_jC\right]\sin(j\ell x) \tag{12a}$$

$$\tilde{v}_z = \left[\{{}_ja + {}_jb(j\ell z)\}{}_jC + \{{}_jc + {}_jd(j\ell z)\}{}_jS\right]\cos(j\ell x) \tag{12b}$$

$$\tilde{\sigma}_{xx} = -2j\mu\ell\left[\{{}_ja + 2{}_jd + {}_jb(j\ell z)\}{}_jS + \{{}_jc + 2{}_jb + {}_jd(j\ell z)\}{}_jC\right]\cos(j\ell x) - \tilde{p}_o \tag{12c}$$

$$\tilde{\sigma}_{zz} = 2j\mu\ell\left[\{{}_ja + {}_jb(j\ell z)\}{}_jS + \{{}_jc + {}_jd(j\ell z)\}{}_jC\right]\cos(j\ell x) - \tilde{p}_o \tag{12d}$$

$$\tilde{\sigma}_{xz} = -2j\mu\ell\left[\{{}_ja + {}_jd + {}_jb(j\ell z)\}{}_jC + \{{}_jc + {}_jb + {}_jd(j\ell z)\}{}_jS\right]\sin(j\ell x) \tag{12e}$$

in which

$${}_jS = \sinh(j\ell z) \; ; \quad {}_jC = \cosh(j\ell z) \tag{12f}$$

and j = 1, 2, and 3 (results summed). Here ${}_1\underline{a}$, ${}_2\underline{a}$, ${}_3\underline{a}$, ${}_1\underline{b}$ ...... ${}_2\underline{d}$, ${}_3\underline{d}$ are twelve arbitrary constants.

The arbitrary constants are eliminated by means of velocity and stress boundary conditions. In accordance with the coordinate system shown in an inset in Fig. 1, with coordinate $\underline{n}$ normal to and $\underline{s}$ parallel to an interface, the velocity and stress components normal and parallel to an interface are:

$$v_n = [v_z]_\zeta \cos(\theta) - [v_x]_\zeta \sin(\theta) \tag{13a}$$

$$v_s = [v_x]_\zeta \cos(\theta) + [v_z]_\zeta \sin(\theta) \tag{13b}$$

$$\sigma_{nn} = [\sigma_{zz}]_\zeta \cos^2(\theta) + [\sigma_{xx}]_\zeta \sin^2(\theta) - 2[\sigma_{xz}]_\zeta \cos(\theta)\sin(\theta) \tag{13c}$$

$$\sigma_{ns} = [\sigma_{zz}-\sigma_{xx}]_\zeta \cos(\theta)\sin(\theta) + [\sigma_{xz}]_\zeta [\cos^2(\theta)-\sin^2(\theta)] \tag{13d}$$

in which $[\quad]_\zeta$ indicates that the quantity is to be evaluated at the interface, $\underline{z} = \zeta$, and

$$\cos(\theta) = 1 \,/ \sqrt{1+(\partial\zeta/\partial x)^2}\;; \quad \sin(\theta) = \cos(\theta)\,(\partial\zeta/\partial x) \tag{13e}$$

where θ is the slope angle (Fig. 1).

In solving for the constants, eqs. (9) and (12) are substituted into eq. (10), $\underline{z}$ is replaced with ζ_t and ζ_b, eq. (8), at the top and bottom of a layer, respectively, and eq. (10) is substituted into eq. (13), maintaining a certain order of approximation in the results.

In the 3rd order analysis, terms containing powers of $({}_1A\ell)$ up to $({}_1A\ell)^3$ are maintained, but terms of higher order, such as $({}_1A\ell)^4$, are omitted. The quantity $({}_1A\ell)$ is the maximum slope of the first waveform, so the analysis is accurate to 3rd order in the maximum slope of the first waveform. Terms containing $({}_1A\ell)({}_2A\ell)$ are maintained, but terms of higher order, such as $({}_1A\ell)^2({}_2A\ell)$, $({}_1A\ell)({}_3A\ell)$, $(2{}_2A\ell)^2$, and $(3{}_3A\ell)^2$, are omitted, so the analysis is accurate to 1st order in maximum slopes of the second and third waveforms.

Each of the arbitrary constants, ${}_1\underline{a}$, ${}_2\underline{a}$, ... ${}_2\underline{d}$, ${}_3\underline{d}$, in eqs. (12) is actually a composite of constants, each of which is proportional to 1st or higher order in $({}_1A\ell)$, $(2{}_2A\ell)$, or $(3{}_3A\ell)$. It is helpful to rewrite the composite constants in a way that indicates explicitly their dependencies on orders of approximation. The following notation has proven to be convenient: the leading subscript indicates the waveform with which the constant is associated; the leading superscript indicates the product of maximum slopes that enters the expression for that constant. For example,

$${}_1a = {}^1_1a + {}^{12}_1a + {}^{111}_1a$$

in which ${}^1_1\underline{a}$ is for the first waveform (subscript "1") and is to 1st order in $({}_1A\ell)$ (superscript "1"); ${}^{12}_1\underline{a}$ is also for the first waveform, as is ${}^{111}_1\underline{a}$, but ${}^{12}_1\underline{a}$ is to order $({}_1A\ell)(2{}_2A\ell)$ (superscript "12") and ${}^{111}_1\underline{a}$ is to 3rd order in $({}_1A\ell)$ (superscript "111"). Similarly, ${}^2_2\underline{a}$ is for the second waveform (subscript of "2") and is to 1st order in $({}_{2}A\ell)$, whereas ${}^{11}_{2}\underline{a}$ is to 2nd order in $({}_{1}A\ell)$. This notation increases the number of constants, but it markedly simplifies the maintenance of correct orders of approximation.

The number of arbitrary constants for multilayer problems can be extremely large: even for 1st order analyses there are four constants for each layer, so for ten layers and two confining media, there are 44 arbitrary constants. For 3rd order analysis, of ten layers and two media, there are 352 constants. Therefore, I have devised a method of solution that reduces the number of independent constants for an entire multilayer by about half, from four per layer to two per interface for each waveform and each order of approximation. However, I wish to emphasize that the method involves no special assumptions and therefore in no way compromises the stated accuracy of the solution.

Two sets of constants, sigma and tau, are introduced via the expressions,

$$(\sigma_{nn})_{t,b} = \sigma_o + ({}^{1}_{1}\sigma_{t,b} + {}^{12}_{1}\sigma_{t,b} + {}^{111}_{1}\sigma_{t,b}) \cos(\ell x) + ({}^{2}_{2}\sigma_{t,b} + {}^{11}_{2}\sigma_{t,b}) \cos(2\ell x)$$

$$+ ({}^{3}_{3}\sigma_{t,b} + {}^{12}_{3}\sigma_{t,b} + {}^{111}_{3}\sigma_{t,b}) \cos(3\ell x) \tag{14a}$$

$$(\sigma_{ns})_{t,b} = ({}^{1}_{1}\tau_{t,b} + {}^{12}_{1}\tau_{t,b} + {}^{111}_{1}\tau_{t,b}) \sin(\ell x) + ({}^{2}_{2}\tau_{t,b} + {}^{11}_{2}\tau_{t,b}) \sin(2\ell x)$$

$$+ ({}^{3}_{3}\tau_{t,b} + {}^{12}_{3}\tau_{t,b} + {}^{111}_{3}\tau_{t,b}) \sin(3\ell x) \tag{14b}$$

in which the numeric subscripts and superscripts indicate waveform and order of approximation, as described above. These constants reduce the total number that needs to be determined because the constants for the top of one layer are identical to the constants for the bottom of the overlying layer.

To solve for the constants ${}_j\underline{a}$, ${}_j\underline{b}$, ${}_j\underline{c}$, ${}_j\underline{d}$, I equate (14a) to (13c) and (14b) to (13d), after eqs. (13c) and (13d) have been expanded and expressed to 3rd order accuracy. Then I use the resulting expressions to eliminate constants ${}_j\underline{a}$ ... ${}_j\underline{d}$ in eqs. (13a) and (13b). Equations (13a) and (13b), now in terms of sigma and tau, provide the boundary velocities that must be satisfied at each interface. The final results are:

$$
\begin{aligned}
(v_n)_{t,b} = {} & (\bar{v}_z)_{t,b}\cos(\theta_{t,b}) - (\bar{v}_x)_{t,b}\sin(\theta_{t,b}) \\
& + \Big\{({}^{1}_{1}\Lambda_m + {}^{12}_{1}\Lambda_m + {}^{111}_{1}\Lambda_m)({}_1C^2) + ({}^{1}_{1}\lambda_p + {}^{12}_{1}\lambda_p + {}^{111}_{1}\lambda_p)k \\
& \pm ({}^{1}_{1}\Lambda_p + {}^{12}_{1}\Lambda_p + {}^{111}_{1}\Lambda_p)({}_1S^2) \mp ({}^{1}_{1}\lambda_m + {}^{12}_{1}\lambda_m + {}^{111}_{1}\lambda_m)k \\
& + ({}_1A_{t,b}\ell/2)\big[({}^{2}_{2}\Lambda_p + {}^{11}_{2}\Lambda_p)2k - ({}^{2}_{2}\lambda_m + {}^{11}_{2}\lambda_m)({}_2C^2) \\
& \qquad \mp ({}^{2}_{2}\Lambda_m + {}^{11}_{2}\Lambda_m)2k \mp ({}^{2}_{2}\lambda_p + {}^{11}_{2}\lambda_p)({}_2S^2)\big] \\
& - ({}_2A_{t,b}\ell/2)\big[{}^{1}_{1}\Lambda_p k - {}^{1}_{1}\lambda_m({}_1C^2) \mp {}^{1}_{1}\Lambda_m k \mp {}^{1}_{1}\lambda_p({}_1S^2)\big] \\
& - ({}_1A_{t,b}\ell/2)^2\big[{}^{1}_{1}\Lambda_m({}_1C^2) + {}^{1}_{1}\lambda_p({}_1S_1C) \pm {}^{1}_{1}\Lambda_p({}_1S^2) \pm {}^{1}_{1}\lambda_m({}_1S_1C)\big]\Big\}\cos(\ell x) \\
& + \Big\{({}^{2}_{2}\Lambda_m + {}^{11}_{2}\Lambda_m)({}_2C^2) + ({}^{2}_{2}\lambda_p + {}^{11}_{2}\lambda_p)2k \pm ({}^{2}_{2}\Lambda_p + {}^{11}_{2}\Lambda_p)({}_2S^2) \mp ({}^{2}_{2}\lambda_m + {}^{11}_{2}\lambda_m)2k \\
& + ({}_1A_{t,b}\ell)\big[{}^{1}_{1}\Lambda_p k - {}^{1}_{1}\lambda_m({}_1C^2) \mp {}^{1}_{1}\Lambda_m k \mp {}^{1}_{1}\lambda_p({}_1S^2)\big]\Big\}\cos(2\ell x) \\
& + \Big\{({}^{3}_{3}\Lambda_m + {}^{12}_{3}\Lambda_m + {}^{111}_{3}\Lambda_m)({}_3C^2) + ({}^{3}_{3}\lambda_p + {}^{12}_{3}\lambda_p + {}^{111}_{3}\lambda_p)3k \\
& \pm ({}^{3}_{3}\Lambda_p + {}^{12}_{3}\Lambda_p + {}^{111}_{3}\Lambda_p)({}_3S^2) \mp ({}^{3}_{3}\lambda_m + {}^{12}_{3}\lambda_m + {}^{111}_{3}\lambda_m)3k \\
& + 3({}_1A_{t,b}\ell/2)\big[({}^{2}_{2}\Lambda_p + {}^{11}_{2}\Lambda_p)2k - ({}^{2}_{2}\lambda_m + {}^{11}_{2}\lambda_m)({}_2C^2) \\
& \qquad \mp ({}^{2}_{2}\Lambda_m + {}^{11}_{2}\Lambda_m)2k \mp ({}^{2}_{2}\lambda_p + {}^{11}_{2}\lambda_p)({}_2S^2)\big] \\
& + 3({}_2A_{t,b}\ell/2)\big[{}^{1}_{1}\Lambda_p k - {}^{1}_{1}\lambda_m({}_1C^2) \mp {}^{1}_{1}\Lambda_m k \mp {}^{1}_{1}\lambda_p({}_1S^2)\big] \\
& - ({}_1A_{t,b}\ell/2)^2\big[{}^{1}_{1}\Lambda_m({}_1C^2) + {}^{1}_{1}\lambda_p(3{}_1S_1C-2k) \\
& \qquad \pm {}^{1}_{1}\Lambda_p({}_1S^2) \pm {}^{1}_{1}\lambda_m(3{}_1S_1C+2k)\big]\Big\}\cos(3\ell x)
\end{aligned}
\tag{15a}
$$

$$
\begin{aligned}
(v_s)_{t,b} &= (\bar{v}_z)_{t,b}\sin(\theta_{t,b}) + (\bar{v}_x)_{t,b}\cos(\theta_{t,b}) \\
&+\Big\{ -({}^{1}_{1}\Lambda_p+{}^{12}_{1}\Lambda_p+{}^{111}_{1}\Lambda_p)k + ({}^{1}_{1}\lambda_m+{}^{12}_{1}\lambda_m+{}^{111}_{1}\lambda_m)({}_1C^2) \\
&\quad \pm ({}^{1}_{1}\Lambda_m+{}^{12}_{1}\Lambda_m+{}^{111}_{1}\Lambda_m)k \pm ({}^{1}_{1}\lambda_p+{}^{12}_{1}\lambda_p+{}^{111}_{1}\lambda_p)({}_1S^2) \\
&\quad + ({}_1A_{t,b}\ell/2)\big[({}^{2}_{2}\Lambda_m+{}^{11}_{2}\Lambda_m)(3\,{}_2C^2) + ({}^{2}_{2}\lambda_p+{}^{11}_{2}\lambda_p)(4\,{}_2S_2C-2k) \\
&\qquad\qquad \pm ({}^{2}_{2}\Lambda_p+{}^{11}_{2}\Lambda_p)(3\,{}_2S^2) \pm ({}^{2}_{2}\lambda_m+{}^{11}_{2}\lambda_m)(4\,{}_2S_2C+2k)\big] \\
&\quad - ({}_2A_{t,b}\ell/2)\big[{}^{1}_{1}\Lambda_m(3\,{}_1C^2) + {}^{1}_{1}\lambda_p(2\,{}_1S_1C+k) \pm {}^{1}_{1}\Lambda_p(3\,{}_1S^2) \pm {}^{1}_{1}\lambda_m(2\,{}_1S_1C-k)\big] \\
&\quad + ({}_1A_{t,b}\ell/2)^2\big[{}^{1}_{1}\Lambda_p({}_1S_1C) + {}^{1}_{1}\lambda_m({}_1C^2) \pm {}^{1}_{1}\Lambda_m({}_1S_1C) \pm {}^{1}_{1}\lambda_p({}_1S^2)\big]\Big\} \sin(\ell x) \\
&+\Big\{ -({}^{2}_{2}\Lambda_p+{}^{11}_{2}\Lambda_p)2k + ({}^{2}_{2}\lambda_m+{}^{11}_{2}\lambda_m)({}_2C^2) \pm ({}^{2}_{2}\Lambda_m+{}^{11}_{2}\Lambda_m)2k \pm ({}^{2}_{2}\lambda_p+{}^{11}_{2}\lambda_p)({}_2S^2) \\
&\quad + ({}_1A_{t,b}\ell)\big[{}^{1}_{1}\lambda_p({}_1S_1C-k) \pm {}^{1}_{1}\lambda_m({}_1S_1C+k)\big] \Big\}\sin(2\ell x) \\
&+\Big\{ -({}^{3}_{3}\Lambda_p+{}^{12}_{3}\Lambda_p+{}^{111}_{3}\Lambda_p)3k + ({}^{3}_{3}\lambda_m+{}^{12}_{3}\lambda_m+{}^{111}_{3}\lambda_m)({}_3C^2) \\
&\quad \pm ({}^{3}_{3}\Lambda_m+{}^{12}_{3}\Lambda_m+{}^{111}_{3}\Lambda_m)3k \pm ({}^{3}_{3}\lambda_p+{}^{12}_{3}\lambda_p+{}^{111}_{3}\lambda_p)({}_3S^2) \\
&\quad + ({}_1A_{t,b}\ell/2)\big[({}^{2}_{2}\Lambda_m+{}^{11}_{2}\Lambda_m)({}_2C^2) + ({}^{2}_{2}\lambda_p+{}^{11}_{2}\lambda_p)(4\,{}_2S_2C-6k) \\
&\qquad\qquad \pm ({}^{2}_{2}\Lambda_p+{}^{11}_{2}\Lambda_p)({}_2S^2) \pm ({}^{2}_{2}\lambda_m+{}^{11}_{2}\lambda_m)(4\,{}_2S_2C+6k)\big] \\
&\quad - ({}_2A_{t,b}\ell/2)\big[{}^{1}_{1}\Lambda_m({}_1C^2) - {}^{1}_{1}\lambda_p(2\,{}_1S_1C-3k) \pm {}^{1}_{1}\Lambda_p({}_1S^2) \mp {}^{1}_{1}\lambda_m(2\,{}_1S_1C+3k)\big] \\
&\quad + ({}_1A_{t,b}\ell/2)^2\big[{}^{1}_{1}\Lambda_p({}_1S_1C-2k) + {}^{1}_{1}\lambda_m(3\,{}_1C^2) \\
&\qquad\qquad \pm {}^{1}_{1}\Lambda_m({}_1S_1C+2k) \pm {}^{1}_{1}\lambda_p(3\,{}_1S^2)\big]\Big\} \sin(3\ell x) \qquad (15b)
\end{aligned}
$$

in which the upper sign in $\pm$ or $\mp$ corresponds to the top and the lower sign to the bottom of the layer. The dimensionless wavenumber, _k_, is

$$k = \pi h/L \tag{15c}$$

in which _h_ is vertical thickness and _L_ is wavelength of the first waveform, and

$${}_jS = \sinh(jk) \; ; \quad {}_jC = \cosh(jk) \tag{15d}$$

in which _j_ is waveform.

The lambda constants in eqs. (15a) and (15b) are given by:

$${}^j_j\Lambda_{p,m} = \frac{[{}^j_j\sigma_t \pm {}^j_j\sigma_b - \rho g({}_jA_t \pm {}_jA_b)]}{[4j\mu\ell({}_jS\,{}_jC \pm jk)]} \; ; \; j = 1, 2, \text{ or } 3 \text{ (no sum)} \tag{16a}$$

in which ρg is unit weight (density times acceleration of gravity).

$${}^j_j\lambda_{p,m}[4j\mu\ell({}_jS\,{}_jC \mp jk)] = [{}^j_j\tau_t \pm {}^j_j\tau_b - 4j\mu\ell\bar{D}_{xx}({}_jA_t \pm {}_jA_b)] \tag{16b}$$

$$\begin{aligned}{}^{11}_{2}\Lambda_{p,m}[2({}_2S\,{}_2C \pm 2k)] = {} & [{}^{11}_{2}\sigma_t \pm {}^{11}_{2}\sigma_b + 2\mu(\ell^2)\bar{D}_{xx}({}_1A_t^2 \pm {}_1A_b^2)]/4\mu\ell \\ & +(3\ell/4)({}_1A_t \pm {}_1A_b)({}^1_1\lambda_p)({}_1S\,{}_1C-k) \\ & + (3\ell/4)({}_1A_t \mp {}_1A_b)({}^1_1\lambda_m)({}_1S\,{}_1C+k)\end{aligned} \tag{16c}$$

$$
\begin{aligned}
{}^{11}_{2}\lambda_{p,m}\left[2({}_2S_2C \mp 2k)\right] = {} & ({}^{11}_{2}\tau_t \pm {}^{11}_{2}\tau_b)/4\mu\ell \\
& - (\ell/4)({}_1A_t \pm {}_1A_b)\left[{}^{1}_{1}\Lambda_p({}_1S_1C-3k) + {}^{1}_{1}\lambda_m(4\,{}_1C^2)\right] \\
& - (\ell/4)({}_1A_t \mp {}_1A_b)\left[{}^{1}_{1}\Lambda_m({}_1S_1C+3k) + {}^{1}_{1}\lambda_p(4\,{}_1S^2)\right]
\end{aligned}
\tag{16d}
$$

$$
\begin{aligned}
{}^{12}_{1}\Lambda_{p,m}\left[2({}_1S_1C \pm k)\right] = {} & ({}^{12}_{1}\sigma_t \pm {}^{12}_{1}\sigma_b)/2\mu\ell - 4\ell\bar{D}_{xx}\left[({}_1A_t)({}_2A_t) \pm ({}_1A_b)({}_2A_b)\right] \\
& - (3\ell/2)({}_2A_t \pm {}_2A_b)({}^{1}_{1}\lambda_p)({}_1S_1C-k) \\
& - (3\ell/2)({}_2A_t \mp {}_2A_b)({}^{1}_{1}\lambda_m)({}_1S_1C+k)
\end{aligned}
\tag{16e}
$$

$$
\begin{aligned}
{}^{12}_{1}\lambda_{p,m}\left[2({}_1S_1C \mp k)\right] = {} & ({}^{12}_{1}\tau_t \pm {}^{12}_{1}\tau_b)/2\mu\ell \\
& - 2\ell({}_1A_t \pm {}_1A_b)\left[{}^{2}_{2}\Lambda_p({}_2S_2C) + {}^{2}_{2}\lambda_m({}_2C^2)\right] \\
& - 2\ell({}_1A_t \mp {}_1A_b)\left[{}^{2}_{2}\Lambda_m({}_2S_2C) + {}^{2}_{2}\lambda_p({}_2S^2)\right] \\
& + (\ell/2)({}_2A_t \pm {}_2A_b)\left[{}^{1}_{1}\Lambda_p({}_1S_1C+3k) - {}^{1}_{1}\lambda_m(2\,{}_1C^2)\right] \\
& + (\ell/2)({}_2A_t \mp {}_2A_b)\left[{}^{1}_{1}\Lambda_m({}_1S_1C-3k) - {}^{1}_{1}\lambda_p(2\,{}_1S^2)\right]
\end{aligned}
\tag{16f}
$$

$$
\begin{aligned}
{}^{111}_{1}\Lambda_{p,m}\left[2({}_1S_1C \pm k)\right] = {} & ({}^{111}_{1}\sigma_t \pm {}^{111}_{1}\sigma_b)/2\mu\ell \\
& - (\ell^2/8)({}_1A_t^2 \pm {}_1A_b^2)\left[{}^{1}_{1}\Lambda_p({}_1S_1C-5k) + {}^{1}_{1}\lambda_m(6\,{}_1C^2)\right] \\
& - (\ell^2/8)({}_1A_t^2 \mp {}_1A_b^2)\left[{}^{1}_{1}\Lambda_m({}_1S_1C+5k) + {}^{1}_{1}\lambda_p(6\,{}_1S^2)\right]
\end{aligned}
\tag{16g}
$$

$$ {}^{111}_{\ 1}\lambda_{p,m}[2({}_1S_1C \mp k)] = [{}^{111}_{\ 1}\tau_t \pm {}^{111}_{\ 1}\tau_b + 3\mu(\ell^3)\bar{D}_{xx}({}_1A_t^3 \pm {}_1A_b^3)]/2\mu\ell $$

$$ - 2\ell({}_1A_t \pm {}_1A_b)[{}^{11}_{\ 2}\Lambda_p({}_2S_2C) + {}^{11}_{\ 2}\lambda_m({}_2C^2)] $$

$$ - 2\ell({}_1A_t \mp {}_1A_b)[{}^{11}_{\ 2}\Lambda_m({}_2S_2C) + {}^{11}_{\ 2}\lambda_p({}_2S^2)] $$

$$ - (\ell^2/8)({}_1A_t^2 \pm {}_1A_b^2)[{}^1_1\Lambda_m(6{}_1C^2) - {}^1_1\lambda_p({}_1S_1C-7k)] $$

$$ - (\ell^2/8)({}_1A_t^2 \mp {}_1A_b^2)[{}^1_1\Lambda_p(6{}_1S^2) - {}^1_1\lambda_m({}_1S_1C+7k)] \qquad (16h) $$

$$ {}^{12}_{\ 3}\Lambda_{p,m}[2({}_3S_3C \pm 3k)] = ({}^{12}_{\ 3}\sigma_t \pm {}^{12}_{\ 3}\sigma_b)/6\mu\ell $$

$$ + (4\ell/3)\bar{D}_{xx}[({}_1A_t)({}_2A_t) \pm ({}_1A_b)({}_2A_b)] $$

$$ + (4\ell/3)({}_1A_t \pm {}_1A_b)({}^2_2\lambda_p)({}_2S_2C-2k) $$

$$ + (4\ell/3)({}_1A_t \mp {}_1A_b)({}^2_2\lambda_m)({}_2S_2C+2k) $$

$$ + (5\ell/6)({}_2A_t \pm {}_2A_b)({}^1_1\lambda_p)({}_1S_1C-k) $$

$$ + (5\ell/6)({}_2A_t \mp {}_2A_b)({}^1_1\lambda_m)({}_1S_1C+k) \qquad (16i) $$

$$
\begin{aligned}
{}^{12}_{3}\lambda_{p,m}[2({}_3S_3C \mp 3k)] = &({}^{12}_{3}\tau_t \pm {}^{12}_{3}\tau_b)/6\mu\ell \\
&- (2\ell/3)({}_1A_t \pm {}_1A_b)[{}^{2}_{2}\Lambda_p({}_2S_2C-4k) + {}^{2}_{2}\lambda_m(3{}_2C^2)] \\
&- (2\ell/3)({}_1A_t \mp {}_1A_b)[{}^{2}_{2}\Lambda_m({}_2S_2C+4k) + {}^{2}_{2}\lambda_p(3{}_2S^2)] \\
&- (\ell/6)({}_2A_t \pm {}_2A_b)[{}^{1}_{1}\Lambda_p({}_1S_1C-5k) + {}^{1}_{1}\lambda_m(6{}_1C^2)] \\
&- (\ell/6)({}_2A_t \mp {}_2A_b)[{}^{1}_{1}\Lambda_m({}_1S_1C+5k) + {}^{1}_{1}\lambda_p(6{}_1S^2)] \qquad (16j)
\end{aligned}
$$

$$
\begin{aligned}
{}^{111}_{3}\Lambda_{p,m}[2({}_3S_3C \pm 3k)] = &({}^{111}_{3}\sigma_t \pm {}^{111}_{3}\sigma_b)/6\mu\ell \\
&+ (4\ell/3)({}_1A_t \pm {}_1A_b)({}^{11}_{2}\lambda_p)({}_2S_2C-2k) \\
&+ (4\ell/3)({}_1A_t \mp {}_1A_b)({}^{11}_{2}\lambda_m)({}_2S_2C+2k) \\
&+ (\ell^2/24)({}_1A_t^2 \pm {}_1A_b^2)[{}^{1}_{1}\Lambda_p(5{}_1S_1C-9k) + {}^{1}_{1}\lambda_m(14{}_1C^2)] \\
&+ (\ell^2/24)({}_1A_t^2 \mp {}_1A_b^2)[{}^{1}_{1}\Lambda_m(5{}_1S_1C+9k) + {}^{1}_{1}\lambda_p(14{}_1S^2)] \qquad (16k)
\end{aligned}
$$

$$
\begin{aligned}
{}^{111}_{3}\lambda_{p,m}[2({}_3S_3C \mp 3k)] = &[{}^{111}_{3}\tau_t \pm {}^{111}_{3}\tau_b - \mu(\ell^3)\bar{D}_{xx}({}_1A_t^3 \pm {}_1A_b^3)]/6\mu\ell \\
&- (2\ell/3)({}_1A_t \pm {}_1A_b)[{}^{11}_{2}\Lambda_p({}_2S_2C-4k) + {}^{11}_{2}\lambda_m(3{}_2C^2)] \\
&- (2\ell/3)({}_1A_t \mp {}_1A_b)[{}^{11}_{2}\Lambda_m({}_2S_2C+4k) + {}^{11}_{2}\lambda_p(3{}_2S^2)] \\
&- (\ell^2/8)({}_1A_t^2 \pm {}_1A_b^2)[{}^{1}_{1}\Lambda_m(2{}_1C^2) + {}^{1}_{1}\lambda_p(5{}_1S_1C-3k)] \\
&- (\ell^2/8)({}_1A_t^2 \mp {}_1A_b^2)[{}^{1}_{1}\Lambda_p(2{}_1S^2) + {}^{1}_{1}\lambda_m(5{}_1S_1C+3k)] \qquad (16\ell)
\end{aligned}
$$

Equations (15) are the boundary velocities at the top and bottom of each layer.

The boundary velocities for semi-infinite media are (U for upper medium, L for lower):

$$(v_n)_{U,L} = (\bar{v}_z)_{U,L}\cos(\theta_{U,L}) - (\bar{v}_x)_{U,L}\sin(\theta_{U,L})$$

$$\mp\{ {}^{1}_{1}\Lambda_{U,L} + {}^{12}_{1}\Lambda_{U,L} + {}^{111}_{1}\Lambda_{U,L} - ({}_{1}A_{U,L}\ell/2)({}^{2}_{2}\lambda_{U,L} + {}^{11}_{2}\lambda_{U,L})$$

$$+ ({}_{2}A_{U,L}\ell/2)({}^{1}_{1}\lambda_{U,L}) - ({}_{1}A_{U,L}\ell/2)^2({}^{1}_{1}\Lambda_{U,L} \mp {}^{1}_{1}\lambda_{U,L})\}\cos(\ell x)$$

$$\mp\{ {}^{2}_{2}\Lambda_{U,L} + {}^{11}_{2}\Lambda_{U,L} - ({}_{1}A_{U,L}\ell)({}^{1}_{1}\lambda_{U,L})\}\cos(2\ell x)$$

$$\mp\{ {}^{3}_{3}\Lambda_{U,L} + {}^{12}_{3}\Lambda_{U,L} + {}^{111}_{3}\Lambda_{U,L} - 3({}_{1}A_{U,L}\ell/2)({}^{2}_{2}\lambda_{U,L} + {}^{11}_{2}\lambda_{U,L})$$

$$- 3({}_{2}A_{U,L}\ell/2)({}^{1}_{1}\lambda_{U,L}) - ({}_{1}A_{U,L}\ell/2)^2[{}^{1}_{1}\Lambda_{U,L} \mp 3({}^{1}_{1}\lambda_{U,L})]\}\cos(3\ell x) \quad (17a)$$

$$(v_s)_{U,L} = (\bar{v}_z)_{U,L}\sin(\theta_{U,L}) + (\bar{v}_x)_{U,L}\cos(\theta_{U,L})$$

$$\mp\{\ {}^{1}_{1}\lambda_{U,L} + {}^{12}_{1}\lambda_{U,L} + {}^{111}_{1}\lambda_{U,L}$$

$$+ ({}_{1}A_{U,L}\ell/2)[3({}^{2}_{2}\Lambda_{U,L} + {}^{11}_{2}\Lambda_{U,L}) \mp 4({}^{2}_{2}\lambda_{U,L} + {}^{11}_{2}\lambda_{U,L})]$$

$$- ({}_{2}A_{U,L}\ell/2)[3({}^{1}_{1}\Lambda_{U,L}) \mp 2({}^{1}_{1}\lambda_{U,L})]$$

$$\mp ({}_{1}A_{U,L}\ell/2)^2({}^{1}_{1}\Lambda_{U,L} \mp {}^{1}_{1}\lambda_{U,L})\}\ \sin(\ell x)$$

$$\mp\{\ {}^{2}_{2}\lambda_{U,L} + {}^{11}_{2}\lambda_{U,L} \mp ({}_{1}A_{U,L}\ell)({}^{1}_{1}\lambda_{U,L})\}\ \sin(2\ell x)$$

$$\mp\{\ {}^{3}_{3}\lambda_{U,L} + {}^{12}_{3}\lambda_{U,L} + {}^{111}_{3}\lambda_{U,L}$$

$$+ ({}_{1}A_{U,L}\ell/2)[({}^{2}_{2}\Lambda_{U,L} + {}^{11}_{2}\Lambda_{U,L}) \mp 4({}^{2}_{2}\lambda_{U,L} + {}^{11}_{2}\lambda_{U,L})]$$

$$- ({}_{2}A_{U,L}\ell/2)[{}^{1}_{1}\Lambda_{U,L} \pm 2({}^{1}_{1}\lambda_{U,L})]$$

$$\mp ({}_{1}A_{U,L}\ell/2)^2[{}^{1}_{1}\Lambda_{U,L} \mp 3({}^{1}_{1}\lambda_{U,L})]\}\ \sin(3\ell x) \qquad (17b)$$

in which

$${}^{j}_{j}\Lambda_{U,L} = [{}^{j}_{j}\sigma_{U,L} - \rho g({}_{j}A_{U,L})]/(2j\mu\ell)\ ;\ j = 1,2,\text{or } 3\ (\text{no sum}) \qquad (18a)$$

$${}^{j}_{j}\lambda_{U,L} = [{}^{j}_{j}\tau_{U,L} - 4j\mu\ell\bar{D}_{xx}({}_{j}A_{U,L})]/(2j\mu\ell)\ ; \qquad (18b)$$

$$ {}^{11}_{2}\Lambda_{U,L} = [{}^{11}_{2}\sigma_{U,L} + 2\mu(\ell^2)\bar{D}_{xx}({}_1A_{U,L})^2]/4\mu\ell + (3\ell/4)({}_1A_{U,L})({}^1_1\lambda_{U,L}) \tag{18c} $$

$$ {}^{11}_{2}\lambda_{U,L} = ({}^{11}_{2}\tau_{U,L}/4\mu\ell) - (\ell/4)({}_1A_{U,L})[{}^1_1\Lambda_{U,L} \mp 4({}^1_1\lambda_{U,L})] \tag{18d} $$

$$ {}^{12}_{1}\Lambda_{U,L} = ({}^{12}_{1}\sigma_{U,L}/2\mu\ell) - 4\ell\bar{D}_{xx}({}_1A_{U,L})({}_2A_{U,L}) - (3\ell/2)({}_2A_{U,L})({}^1_1\lambda_{U,L}) \tag{18e} $$

$$ \begin{aligned} {}^{12}_{1}\lambda_{U,L} = {} & ({}^{12}_{1}\tau_{U,L}/2\mu\ell) - 2\ell({}_1A_{U,L})({}^2_2\Lambda_{U,L} \mp {}^2_2\lambda_{U,L}) \\ & + (\ell/2)({}_2A_{U,L})[{}^1_1\Lambda_{U,L} \pm 2({}^1_1\lambda_{U,L})] \end{aligned} \tag{18f} $$

$$ {}^{111}_{1}\Lambda_{U,L} = ({}^{111}_{1}\sigma_{U,L}/2\mu\ell) - (\ell^2/8)({}_1A_{U,L})^2[{}^1_1\Lambda_{U,L} \mp 6({}^1_1\lambda_{U,L})] \tag{18g} $$

$$ \begin{aligned} {}^{111}_{1}\lambda_{U,L} = {} & [{}^{111}_{1}\tau_{U,L} + 3\mu(\ell^3)\bar{D}_{xx}({}_1A_{U,L})^3]/2\mu\ell - 2\ell({}_1A_{U,L})({}^{11}_{2}\Lambda_{U,L} \mp {}^{11}_{2}\lambda_{U,L}) \\ & \pm (\ell^2/8)({}_1A_{U,L})^2[6({}^1_1\Lambda_{U,L}) \pm {}^1_1\lambda_{U,L}] \end{aligned} \tag{18h} $$

$$ \begin{aligned} {}^{12}_{3}\Lambda_{U,L} = {} & ({}^{12}_{3}\sigma_{U,L}/6\mu\ell) + (4\ell/3)\bar{D}_{xx}({}_1A_{U,L})({}_2A_{U,L}) + (4\ell/3)({}_1A_{U,L})({}^2_2\lambda_{U,L}) \\ & + (5\ell/6)({}_2A_{U,L})({}^1_1\lambda_{U,L}) \end{aligned} \tag{18i} $$

$$ \begin{aligned} {}^{12}_{3}\lambda_{U,L} = {} & ({}^{12}_{3}\tau_{U,L}/6\mu\ell) - (2\ell/3)({}_1A_{U,L})[{}^2_2\Lambda_{U,L} \mp 3({}^2_2\lambda_{U,L})] \\ & - (\ell/6)({}_2A_{U,L})[{}^1_1\Lambda_{U,L} \mp 6({}^1_1\lambda_{U,L})] \end{aligned} \tag{18j} $$

$$
\begin{aligned}
{}^{111}_{\;\;3}\Lambda_{U,L} = ({}^{111}_{\;\;3}\sigma_{U,L}/6\mu\ell) + (4\ell/3)({}_1A_{U,L})({}^{11}_{\;2}\lambda_{U,L}) \\
+ (\ell^2/24)({}_1A_{U,L})^2[5({}^1_1\Lambda_{U,L}) \mp 14({}^1_1\lambda_{U,L})]
\end{aligned}
\tag{18k}
$$

$$
\begin{aligned}
{}^{111}_{\;\;3}\lambda_{U,L} = [{}^{111}_{\;\;3}\tau_{U,L} - \mu(\ell^3)\bar{D}_{xx}({}_1A_{U,L})^3]/6\mu\ell \\
- (2\ell/3)({}_1A_{U,L})[{}^{11}_{\;2}\Lambda_{U,L} \mp 3({}^{11}_{\;2}\lambda_{U,L})] \\
\pm (\ell^2/8)({}_1A_{U,L})^2[2({}^1_1\Lambda_{U,L}) \mp 5({}^1_1\lambda_{U,L})]
\end{aligned}
\tag{18ℓ}
$$

The values of the constants are determined as follows. The normal velocities are equated at each interface, so for a layer $\underline{i}$ and an overlying layer $\underline{i}+1$,

$$ {}_{i+1}(v_n)_b = {}_i(v_n)_t \tag{19a} $$

The difference in tangential velocities at common interfaces depends on the type of film assumed. In general, the difference in velocity for layers $\underline{i}$ and $\underline{i}+1$ is,

$$ {}_{i+1}(v_s)_b - {}_i(v_s)_t = h_f[(1/\beta)(\sigma_{ns})|\sigma_{ns}|^{(m-1)} + (1/\mu_f)\,\sigma_{ns}] \tag{19b} $$

in which $\underline{h_f}$ is the thickness of a film separating layers, and μ_f is the coefficient of viscosity of the film. The first term in brackets in eq. (19b) is for a film of powerlaw fluid, where β and $\underline{m}$ are parameters that describe the fluid. The second term is for a film of viscous fluid. Powerlaw films are analyzed in Chapter II; in this chapter, only free slip or bonding of contacts will be considered. To use eq. (19b), substitute eq. (14b) into the right-hand-side of eq. (19b), maintaining 3rd order accuracy. For bonded contacts, μ_f and β are very large, and (19b) becomes

$$_{i+1}(v_s)_b = {}_i(v_s)_t \qquad (19b')$$

Then eqs. (19a) and (19b'), applied to each interface in the multilayer, provide sufficient equations to determine all the constants, ${}^{1}_{1}\tau_t$, ${}^{1}_{1}\sigma_t$, ${}^{11}_{2}\tau_t$ ... ${}^{111}_{3}\tau_t$, ${}^{111}_{3}\sigma_t$ ... ${}^{3}_{3}\tau_b$, ${}^{3}_{3}\sigma_b$, for the top (t) and bottom (b) of each layer.

For free slip at contacts, $\sigma_{ns} = 0$, so all the taus are zero and eq. (19b) is indeterminate. In this case, only eq. (19a) is necessary to solve for the constants ${}^{1}_{1}\sigma_t$, ${}^{1}_{1}\sigma_b$ ... ${}^{3}_{3}\sigma_t$, ${}^{3}_{3}\sigma_b$, ... ${}^{111}_{3}\sigma_t$, ${}^{111}_{3}\sigma_b$.

Growth Rates of Component Waveforms

After the constants have been determined, the growth rates of waveforms in all the interfaces are computed. To do this, one calculates the rate of change in height of an interface,

$$(\partial\zeta/\partial t) = [v_z]_\zeta - [v_x]_\zeta(\partial\zeta/\partial x) \qquad (20)$$

in which ζ is given by eq. (8).

To 3rd order in the maximum slope of the interfaces, eq. (20) provides the following expressions for the rates of growth of amplitudes:

$$
\begin{aligned}
d({}_{1}A_{t,b})/d\bar{S}_{x} = {} & - ({}_{1}A_{t,b}/\bar{S}_{x}) \\
& + (1/\bar{D}_{xx}\bar{S}_{x}) \{ ({}^{1}_{1}\Lambda_{m} + {}^{12}{}^{2}_{1}\Lambda_{m} + {}^{111}{}^{1}_{1}\Lambda_{m})({}_{1}C^{2}) + ({}^{1}_{1}\lambda_{p} + {}^{12}{}^{2}_{1}\lambda_{p} + {}^{111}{}^{1}_{1}\lambda_{p})k \\
& \pm ({}^{1}_{1}\Lambda_{p} + {}^{12}{}^{2}_{1}\Lambda_{p} + {}^{111}{}^{1}_{1}\Lambda_{p})({}_{1}S^{2}) \mp ({}^{1}_{1}\lambda_{m} + {}^{12}{}^{2}_{1}\lambda_{m} + {}^{111}{}^{1}_{1}\lambda_{m})k \\
& + ({}_{1}A_{t,b}\ell/2)[({}^{2}_{2}\Lambda_{p} + {}^{11}{}^{1}_{2}\Lambda_{p})2k - ({}^{2}_{2}\lambda_{m} + {}^{11}{}^{1}_{2}\lambda_{m})({}_{2}C^{2}) \\
& \mp ({}^{2}_{2}\Lambda_{m} + {}^{11}{}^{1}_{2}\Lambda_{m})2k \mp ({}^{2}_{2}\lambda_{p} + {}^{11}{}^{1}_{2}\lambda_{p})({}_{2}S^{2})] \\
& - ({}_{2}A_{t,b}\ell/2)[{}^{1}_{1}\Lambda_{p}k - {}^{1}_{1}\lambda_{m}({}_{1}C^{2}) \mp {}^{1}_{1}\Lambda_{m}k \mp {}^{1}_{1}\lambda_{p}({}_{1}S^{2})] \\
& - (1/2)({}_{1}A_{t,b}\ell/2)^{2}[{}^{1}_{1}\Lambda_{m}({}_{1}C^{2}) + {}^{1}_{1}\lambda_{p}(2{}_{1}S_{1}C-k) \\
& \pm {}^{1}_{1}\Lambda_{p}({}_{1}S^{2}) \pm {}^{1}_{1}\lambda_{m}(2{}_{1}S_{1}C+k)] \}
\end{aligned}
\tag{21a}
$$

$$
\begin{aligned}
d({}_{2}A_{t,b})/d\bar{S}_{x} = {} & - ({}_{2}A_{t,b}/\bar{S}_{x}) \\
& + (1/\bar{D}_{xx}\bar{S}_{x}) \{ ({}^{2}_{2}\Lambda_{m} + {}^{11}{}^{1}_{2}\Lambda_{m})({}_{2}C^{2}) + ({}^{2}_{2}\lambda_{p} + {}^{11}{}^{1}_{2}\lambda_{p})2k \\
& \pm ({}^{2}_{2}\Lambda_{p} + {}^{11}{}^{1}_{2}\Lambda_{p})({}_{2}S^{2}) \mp ({}^{2}_{2}\lambda_{m} + {}^{11}{}^{1}_{2}\lambda_{m})2k \\
& + ({}_{1}A_{t,b}\ell)[{}^{1}_{1}\Lambda_{p}k - {}^{1}_{1}\lambda_{m}({}_{1}C^{2}) \mp {}^{1}_{1}\Lambda_{m}k \mp {}^{1}_{1}\lambda_{p}({}_{1}S^{2})] \}
\end{aligned}
\tag{21b}
$$

$$
\begin{aligned}
d({}_3A_{t,b})/d\bar{S}_x = &- ({}_3A_{t,b}/\bar{S}_x) \\
&+ (1/\bar{D}_{xx}\bar{S}_x)\ \{({}^{3}_{3}\Lambda_m + {}^{12}_{\ 3}\Lambda_m + {}^{111}_{\ \ 3}\Lambda_m)({}_3C^2) + ({}^{3}_{3}\lambda_p + {}^{12}_{\ 3}\lambda_p + {}^{111}_{\ \ 3}\lambda_p)3k \\
&\qquad \pm ({}^{3}_{3}\Lambda_p + {}^{12}_{\ 3}\Lambda_p + {}^{111}_{\ \ 3}\Lambda_p)({}_3S^2) \mp ({}^{3}_{3}\lambda_m + {}^{12}_{\ 3}\lambda_m + {}^{111}_{\ \ 3}\lambda_m)3k \\
&\qquad + 3({}_1A_{t,b}\ell/2)\left[({}^{2}_{2}\Lambda_p + {}^{11}_{\ 2}\Lambda_p)2k - ({}^{2}_{2}\lambda_m + {}^{11}_{\ 2}\lambda_m)({}_2C^2)\right. \\
&\qquad\qquad \left. \mp ({}^{2}_{2}\Lambda_m + {}^{11}_{\ 2}\Lambda_m)2k \mp ({}^{2}_{2}\lambda_p + {}^{11}_{\ 2}\lambda_p)({}_2S^2)\right] \\
&\qquad + 3({}_2A_{t,b}\ell/2)\left[{}^{1}_{1}\Lambda_p k - {}^{1}_{1}\lambda_m({}_1C^2) \mp {}^{1}_{1}\Lambda_m k \mp {}^{1}_{1}\lambda_p({}_1S^2)\right] \\
&\qquad - (3/2)({}_1A_{t,b}\ell/2)^2\left[{}^{1}_{1}\Lambda_m({}_1C^2) + {}^{1}_{1}\lambda_p(2\,{}_1S\,{}_1C - k)\right. \\
&\qquad\qquad \left. \pm {}^{1}_{1}\Lambda_p({}_1S^2) \pm {}^{1}_{1}\lambda_m(2\,{}_1S\,{}_1C + k)\right]\} \qquad (21c)
\end{aligned}
$$

The identity

$$(1/\bar{S}_x)\ d\bar{S}_x = \bar{D}_{xx}dt \qquad (22)$$

has been introduced so that eq. (21) can be integrated with respect to stretch (final length over original length) rather than time.

This completes the derivation of the basic equations. For further details one may consult the appendices.

Eigenvalues, Eigenvectors, and Dominant Wavelengths

Dominant wavelengths and fold shapes for multilayers are determined using the eigenvalues and eigenvectors of the system of equations that describe the growth of amplitudes of first waveforms, eq. (21a). First, eqs. (19a) and (19b) are written for each interface as a single set of simultaneous equations:

$$s_{ij}S_j = a_{in}A_n \tag{23a}$$

in which $\underline{S}_j$ represents a column vector of sigma and tau values, $\underline{s}_{ij}$ is the matrix of coefficients, $\underline{A}_n$ is the amplitude of the first waveform in interface $\underline{n}$, and $\underline{a}_{in}$ is a matrix of coefficients. Here $\underline{j}$ ranges from one to twice the number of interfaces, and $\underline{n}$ ranges from one to the number of interfaces. Summations are implied in eq. (23a). The matrix $\underline{a}_{in}$ contains amplitudes of the first waveform, so eqs. (23a) are nonlinear.

Then eqs. (23a) are solved for the sigma and tau values

$$S_j = b_{jn}A_n \tag{23b}$$

in which

$$b_{jn} = s_{ij}^{-1}a_{in} \tag{23c}$$

By substituting the sigma and tau values, eqs. (23b), into the growth-rate equations for the first waveform, eqs. (21a), the growth-rate equations can be written in the form

$$(dA_i/d\bar{S}_x)(\bar{S}_x) = [1+q_{in}]A_n \tag{24a}$$

in which $\underline{q}_{in}$ is the amplification factor

$$q_{in} = c_{ij}b_{jn} \tag{24b}$$

and $\underline{c}_{ij}$ is the matrix of coefficients of sigma and tau in the right-hand sides of eqs. (21a).

Dominant wavelengths and fold shapes occur for the maximum growth rate of the first waveform, found by computing the maximum eigenvalue, $\underline{q}_{max} + 1$, that satisfies the equations

$$[q_{ij} + \delta_{ij}]A_j = (q_{max}+1)A_i \tag{25}$$

in which $\underline{A}_j$ and $\underline{A}_i$ are amplitudes of the first waveform. The maximum eigenvalue is one plus the maximum amplification factor for the particular wavelength of the first waveform selected. The wavelength of the first waveform that maximizes the eigenvalue is the dominant wavelength; the amplitude distribution that corresponds to the maximum eigenvalue is the eigenvector. Therefore, the eigenvalues and eigenvectors determine both the dominant wavelength and the amplitude vector corresponding to the dominant wavelength for a multilayer. In the linear analysis, both results are functions only of thickness and viscosity ratios of layers, properties of contacts between layers, and properties of the media, but in the nonlinear analysis, they are functions also of the maximum slope of the first waveform. In Chapter II, eigenvalues and eigenvectors are determined to 3rd order in maximum slopes of interfaces, but here they are determined only to 1st order.

Figure 15 shows representative multilayers with bonded (A-C) or freely slipping (D-G) contacts at interfaces. The first five multilayers (A-E) are composed of interbedded stiff and soft layers with a viscosity contrast of $\mu_1/\mu_2 = 10$, whereas the last two (F,G) are composed entirely of stiff layers. The viscosities of the media, μ_m, are indicated below the multilayers. The eigenvectors are represented in the figure by plotting the relative amplitudes of interfaces on the horizontal axis; amplitudes are normalized to a maximum of unity. The multilayers shown in Figs. 15A and 15D are identical, except contacts are bonded for the former and are free to slip for the latter. Those shown in Figs. 15B and 15E are also identical except for properties of contacts. Comparison of the amplitude distributions in these two pairs of multilayers shows that, for interbedded stiff and soft layers, the variation of amplitude with interface position is much smoother for bonded contacts than for free slip at contacts. In multilayers that slip freely, the amplitudes change markedly between tops and bottoms of soft layers but change smoothly with position in the multilayers composed of identical layers (Figs. 15F and 15G).

The amplitude vectors in Fig. 15 reflect the constraints imposed on the various multilayers. Values for the constraints were calculated with eq. (6) and are indicated below the multilayers. The lowest value of constraint is $\underline{c} \simeq 0.33$, for the multilayer of interbedded stiff and soft layers with bonded contacts and confined by soft media (Fig. 15B). The same multilayer, but with free slip at contacts (Fig. 15E), has a

Figure 15. Eigenvectors of amplitudes for a variety of multilayers, A-G. Maximum amplitudes normalized to unity. Horizontal length of interface proportional to amplitude at that interface. Properties of layers and media indicated in each diagram. Values for the constraint, c, for each multilayer were calculated with eq. (6).

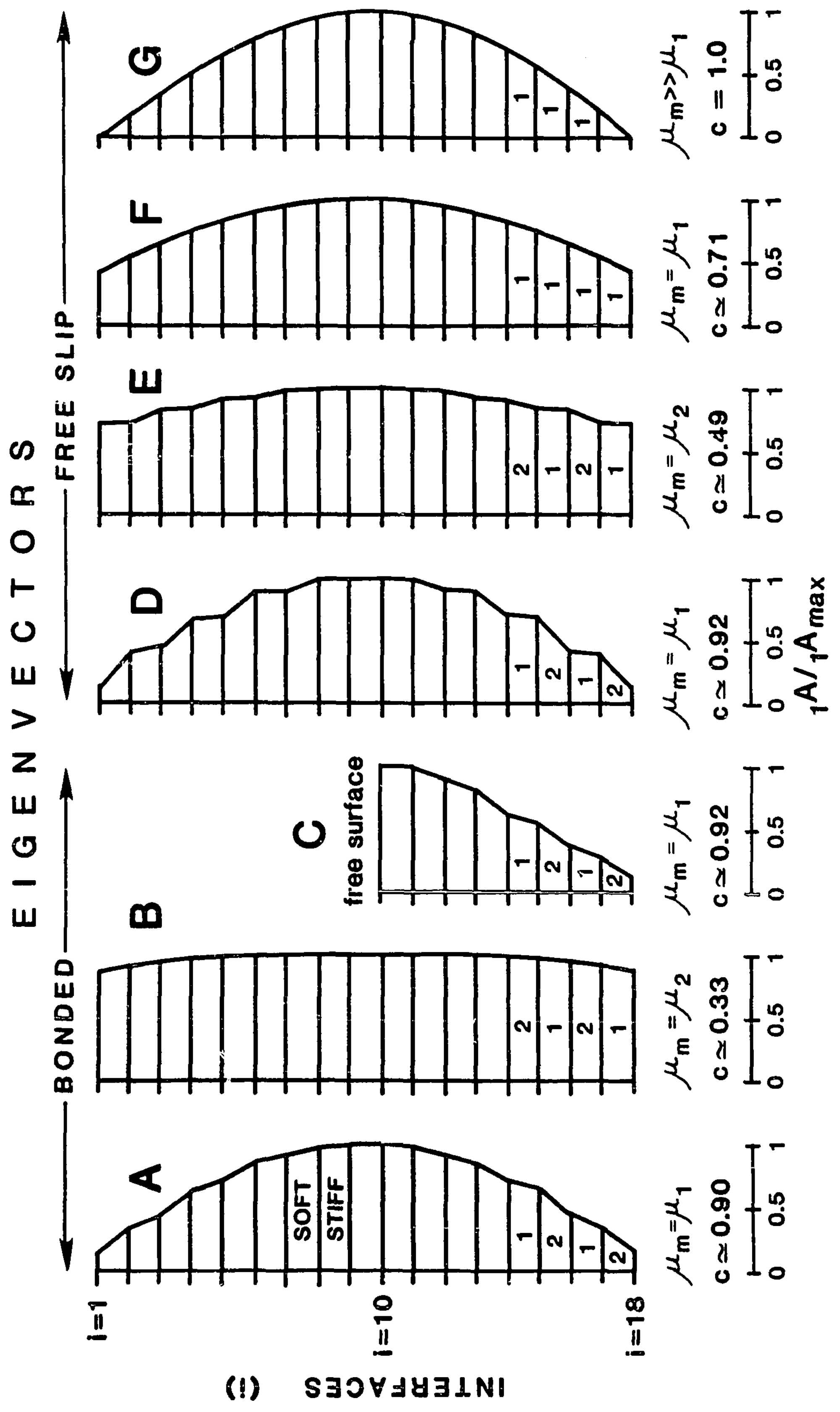

EIGENVECTORS
BONDED
FREE SLIP
A
B
C
D
E
F
G
free surface
SOFT
STIFF
i=1
i=10
i=18
INTERFACES (i)
$\mu_m=\mu_1$
$c\simeq0.90$
$\mu_m=\mu_2$
$c\simeq0.33$
$\mu_m=\mu_1$
$c\simeq0.92$
$\mu_m=\mu_1$
$c\simeq0.92$
$\mu_m=\mu_2$
$c\simeq0.49$
$\mu_m=\mu_1$
$c\simeq0.71$
$\mu_m>>\mu_1$
$c=1.0$
$_1A/_1A_{max}$
0
0.5
1

constraint of $\underline{c} \simeq 0.49$, so the constraint depends not only on the wavelength and the ratio of normal viscosity to media viscosity, μ_n/μ_m, but also on the properties of the contacts.

The rate at which a first waveform in a multilayer grows is determined by $\underline{q}_{max}$, its maximum amplification factor (eigenvalue minus one), which depends on wavelength and on the properties of the multilayer. In Fig. 16, the wavelengths are normalized with the thickness of a stiff layer. The curves labeled $\underline{A}$ through $\underline{G}$ correspond to the multilayers shown in Figs. 15A through 15G, respectively. The peak of a curve indicates, for a particular multilayer, the dominant wavelength ratio, $(L/h_1)_d$, and the maximum amplification factor, $\underline{q}_{max}$, which is the rate of growth of that dominant wavelength ratio. In general, for otherwise identical multilayers, the maximum amplification factor is larger for lower values of constraint (shown by comparison of curves $\underline{A}$ and $\underline{B}$, $\underline{D}$ and $\underline{E}$, $\underline{G}$ and $\underline{F}$) or for free slip, rather than bonding, at layer contacts (shown by comparison of curves $\underline{A}$ and $\underline{D}$, $\underline{B}$ and $\underline{E}$). The dominant wavelength ratio is larger for lower values of constraint, but slightly smaller for free slip at contacts, compared to bonded contacts.

The significance of the amplification factor is made clear by writing an approximate relation for the growth rate of the amplitude of a perturbation in an interface

$$dA/d\bar{S}_x = (A/\bar{S}_x)(1 + q) \qquad (26a)$$

If I assume that $\underline{q}$ changes insignificantly as the multilayer is shortened, then

Figure 16. Relations between amplification factor, ${}^{1}_{1}q$, of first waveform and logarithm of ratio of wavelength to thickness of stiff layer, (L/h_1), for several multilayers. Amplification factor determines rate of growth of first waveforms. Computed to 1st order accuracy in maximum slopes of first waveforms. Dominant wavelength ratio, $(L/h_1)_d$, is wavelength ratio corresponding to peak of curve. Letters near curves identify multilayers shown in Fig. 15.

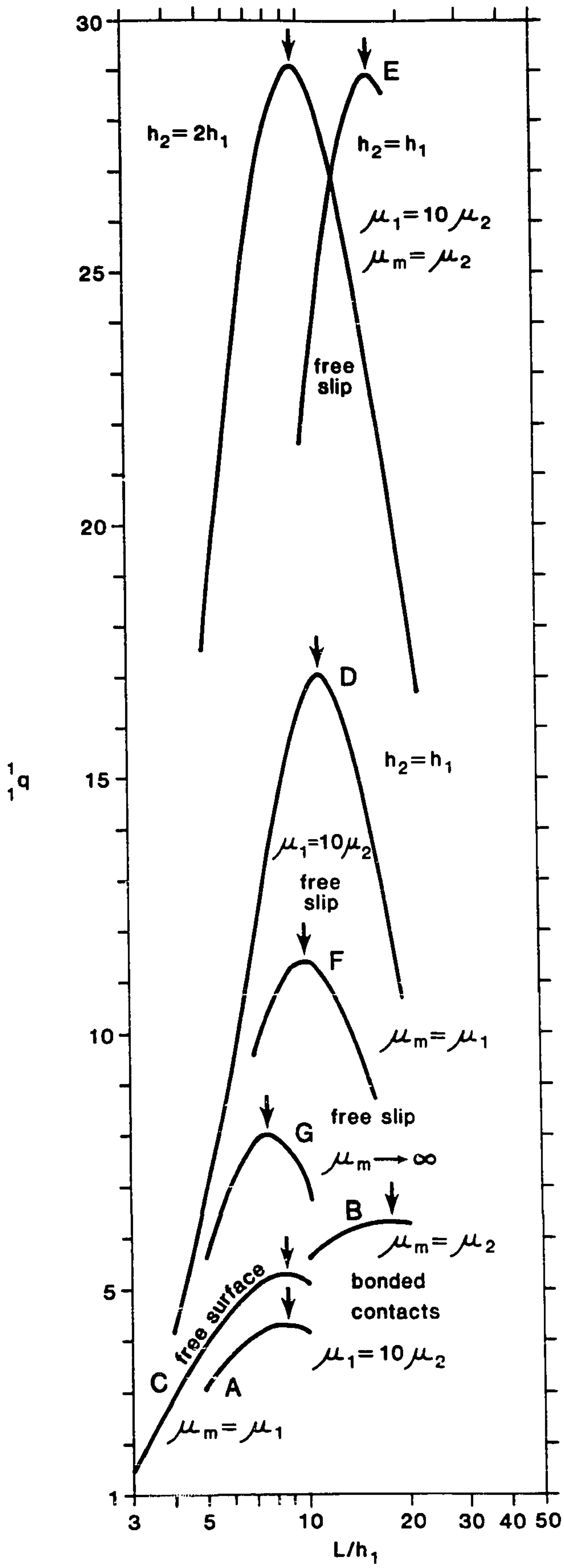

30
25
20
15
10
5
1
3
5
10
20
30
40
50
L/h1
q
E
h2= 2h1
h2= h1
μ1= 10 μ2
μm= μ2
free
slip
D
h2= h1
μ1=10μ2
free
slip
F
μm= μ1
free slip
G
μm → ∞
B
μm= μ2
free surface
bonded
contacts
μ1= 10 μ2
C
A
μm= μ1

$$A/A_o \approx (1/\bar{S}_x)^{(1+q)} = \bar{S}_z^{(1+q)} \qquad (26b)$$

in which $\bar{S}_z$ is the mean thickening of the multilayer, A_o is the initial amplitude, and A/A_o is the amplification of the perturbation. Suppose the stretch is two, so the multilayer has doubled in thickness. Then, for $q = 6.3$ (Fig. 15B), $A/A_o \cong 158$, whereas for $q = 29$ (Fig. 15E), $A/A_o \cong 10^9$.

Dominant wavelengths for multilayers can be determined to 1st order accuracy according to the theory presented here by using plots such as those in Fig. 16. Approximate values of dominant wavelengths for multilayers can be computed using the elementary folding theory (Fig. 12B, eq. 7c) presented by Johnson and Page (1976). Figure 17 compares the results of the two methods. Figure 17A compares dominant wavelength ratios for multilayers of identical layers, with free slip at contacts, confined by rigid ($\mu_m/\mu_1 \rightarrow \infty$) or by stiff ($\mu_m/\mu_1 = 1$) media. There H is the total thickness of the multilayer and N is the number of stiff layers. Dominant wavelengths computed with the two theories agree closely for N greater than six. The elementary theory underestimates dominant wavelengths for stiff media and overestimates dominant wavelengths for rigid media. Figure 17B compares dominant wavelengths computed with the 1st order analysis and the elementary analysis for multilayers with viscosity ratios of $\mu_1/\mu_2 = 10$, thickness ratios of $h_1/h_2 = 1$ and confined by rigid ($\mu_m/\mu_1 \rightarrow \infty$), stiff ($\mu_m/\mu_1 = 1$), or soft ($\mu_m/\mu_1 = 0.1$) media, for numbers of stiff layers N ranging from two to eight. For soft media, the elementary theory overestimates wavelengths,

Figure 17. Comparison of relations between dominant wavelength ratio, $(L/H)_d$, and number of stiff layers, N, according to elementary and 1st order folding theories. A. Multilayers composed of identical stiff layers. Media range from stiff, $\mu_m = \mu_1$, to rigid, $\mu_m \to \infty$. B. Multilayers composed of interbedded stiff and soft layers. Media range from soft, $\mu_m = \mu_2$, to rigid $\mu_m \to \infty$.

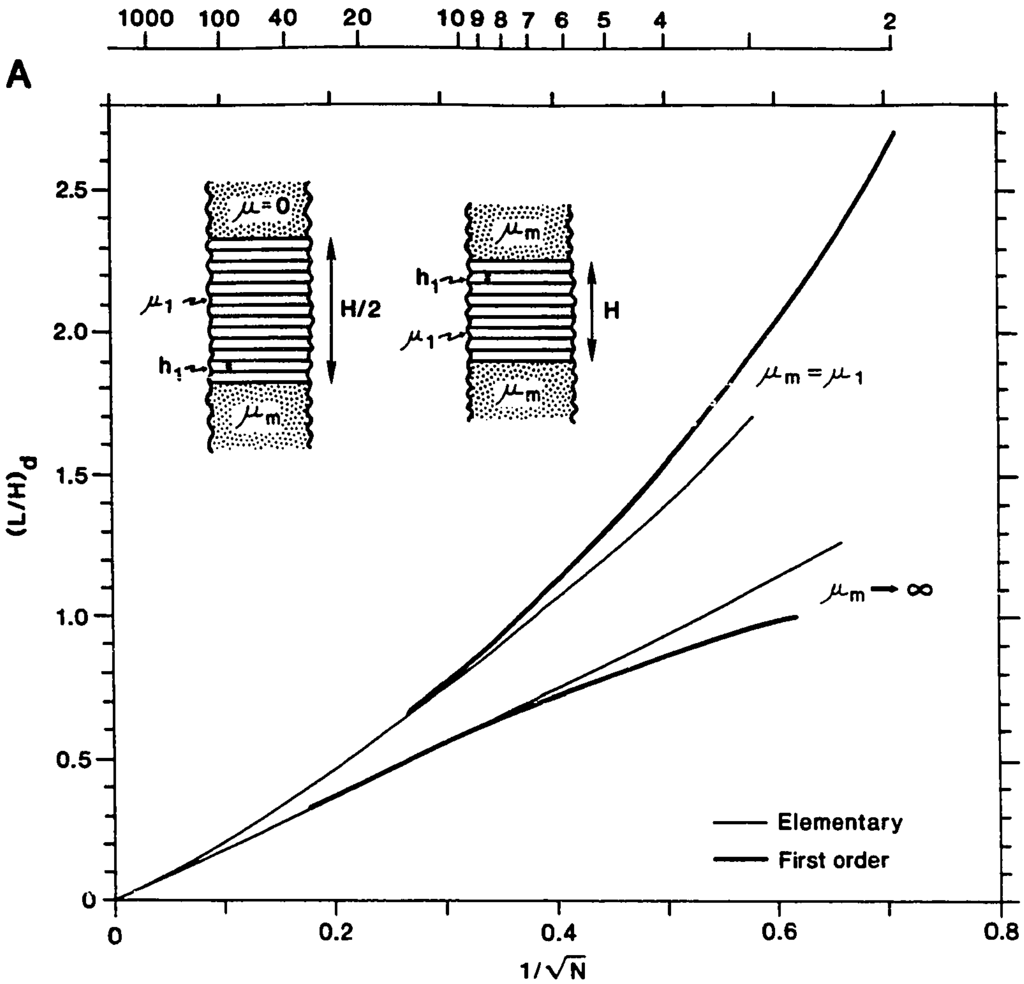
A
1000 100 40 20 10 9 8 7 6 5 4 2
μ=0
μ_1
H/2
h_1
μ_m
μ_m
h_1
μ_1
H
μ_m
$\mu_m = \mu_1$
$\mu_m \to \infty$
Elementary
First order
$(L/H)_d$
2.5
2.0
1.5
1.0
0.5
0
0
0.2
0.4
0.6
0.8
$1/\sqrt{N}$

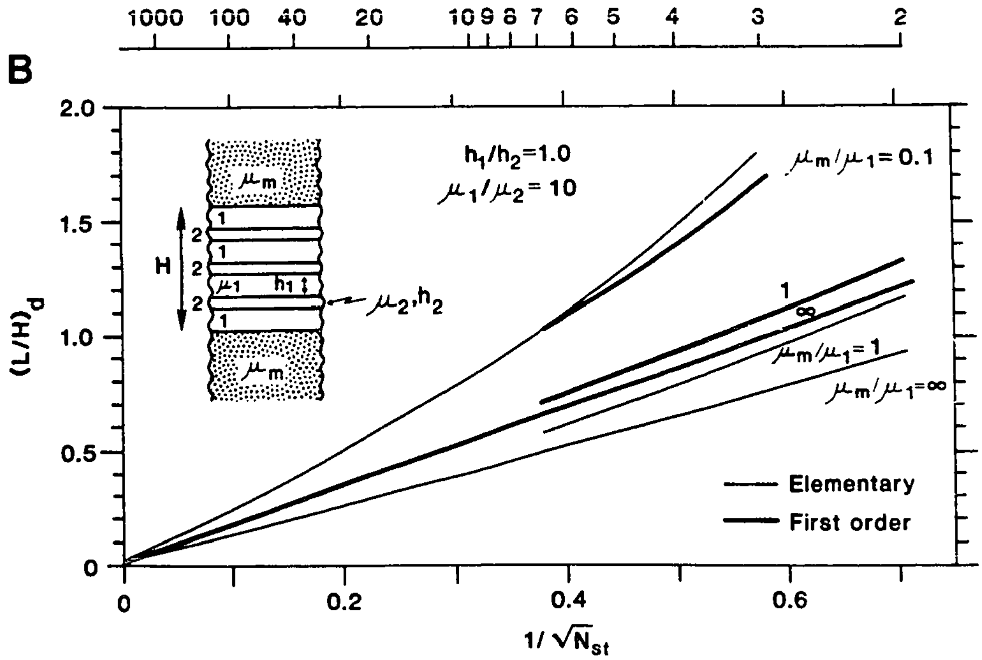
B
1000 100 40 20 10 9 8 7 6 5 4 3 2
μ_m
1
2
1
2
H
μ_1
h_1
2
1
μ_2, h_2
μ_m
h_1/h_2=1.0
μ_1/μ_2= 10
μ_m/μ_1= 0.1
1
∞
μ_m/μ_1= 1
μ_m/μ_1=∞
Elementary
First order
$(L/H)_d$
2.0
1.5
1.0
0.5
0
0
0.2
0.4
0.6
$1/\sqrt{N_{st}}$

but closely estimates them for N greater than four (total number of layers greater than nine). For stiff to rigid media, the elementary theory underestimates dominant wavelengths.

According to Fig. 17, then, elementary theory (Fig. 12) can be used to estimate dominant wavelengths for simple, repetitive multilayers. Figure 12B will provide accurate estimates for multilayers with five or more layers if the layers are identical and the media are either stiff or soft, or if the layers are interbedded stiff and soft materials and the media are soft. It will provide poorer estimates of dominant wavelengths if the layers are interbedded stiff and soft materials and the media are stiff to very stiff.

Amplification and Preferred Wavelengths

Amplification of perturbations is computed in the nonlinear, 3rd order analysis by numerically integrating eqs. (21) for all three waveforms. At each step in the integration, the constants tau and sigma must be recomputed because they depend on the amplitudes themselves. The integration is begun with a small maximum slope of the first waveform (I use one degree) and with the eigenvector of amplitudes for the initial wavelength ratio. The initial amplitudes of the second and third waveforms are zero, so these waveforms develop spontaneously as higher-order effects of the solution. The final result of the computation is an amplitude vector for each of the three waveforms. The three amplitude vectors are used in the equation for the heights of interfaces, eq. (8), and shapes of interfaces are drawn (*e.g.*, Figs. 1 through 6).

To compute the preferred wavelength, that is, the wavelength of perturbations in the first waveform that has grown the maximum amount during a given amount of shortening (Fletcher, 1974), one performs the integration indicated above for a range of initial wavelengths and determines the wavelength that corresponds to the maximum amplification. In this way, one computes the preferred vector of amplitudes of the interfaces as well as the preferred wavelength corresponding to a certain amount of stretch. For each value of stretch there is a different preferred wavelength (Fletcher, 1974). The wavelengths of folds shown in Figs. 1, 2, 3, 5, and 6 are the preferred wavelengths of the first waveforms.

The computation of preferred wavelengths can be laborious using the method outlined above. In the course of this investigation, a very simple method of estimating preferred wavelengths for single- or multi-layer folds has been developed. The method assumes only that the relation between amplification factor for the first waveform and logarithm of the wavelength-to-thickness ratio, (L/h_1), is symmetric about the logarithm of the dominant wavelength ratio $(L/h_1)_d$. For multilayer folds, the method assumes the above plus that the amplification factor changes insignificantly as the amplitude vector changes during growth of the fold. Examination of Fig. 16 indicates that the first assumption is very nearly satisfied for several multilayers. Computations of amplitude vectors suggest that the second assumption also is satisfied. As will be shown, the preferred wavelength ratio is simply related to the dominant wavelength ratio:

$$(L/h_1)_p \simeq (L/h_1)_d\ (\bar{S}_x) \tag{27a}$$

The initial wavelength ratio, which is the wavelength of the perturbation that becomes amplified the most, is

$$(L/h_1)_o \simeq (L/h_1)_d\ (\bar{S}_z)\ ;\quad \bar{S}_z = 1/\bar{S}_x \tag{27b}$$

The proof is as follows. The growth-rate equation for amplitude, $\underline{A}$, of the first waveform in any interface is determined by an equation of the form

$$[d\ell n(A/A_o)/d\ell n(\bar{S}_x)] = (1+{}_1^1q) \tag{28a}$$

in which $\underline{A_o}$ is initial amplitude of the first waveform in the interface and $(1+{}_1^1q)$ is the maximum eigenvalue. The current wavelength ratio, $(L/h_1)_c$, is related to the initial wavelength ratio, $(L/h_1)_o$, through the stretch, $\underline{\bar{S}_x}$:

$$(L/h_1)_c = (L/h_1)_o\ (\bar{S}_x)^2$$

so

$$d\ell n(\bar{S}_x) = (1/2)\ d\ell n(L/h_1)_c \tag{28b}$$

Upon substitution of eq. (28b), eq. (28a) becomes

$$[d\ell n(A/A_o)/d\ell n(L/h_1)_c] = (1+{}_1^1q)/2$$

The value of $\ell n(A/A_o)$ is the area under the curve relating $(1+{}_1^1q)/2$ and $\ell n(L/h_1)$. Examples of such curves are shown in Fig. 16. Because the curves are symmetric, the area is maximized if the wavelength ratios satisfy the following condition:

$$\ell n(L/h_1)_d - \ell n(L/h_1)_o = \ell n(L/h_1)_p - \ell n(L/h_1)_d \tag{28c}$$

or

$$(L/h_1)_p\,(L/h_1)_o = (L/h_1)_d^2 \tag{28d}$$

Equations (27) are derived using the definition

$$(L/h_1)_o = (L/h_1)_p(\bar{S}_z^2) \tag{28e}$$

in eq. (28d).

Equation (27a) is simpler than the relation derived by Sherwin and Chapple (1968) from an approximate, thin-plate analysis of single-layer folding:

$$(L/h_1)_p \simeq (L/h_1)_d \sqrt[3]{[\bar{S}_x^2(\bar{S}_x^2+1)/2]} = (L/h_1)_d\, \bar{S}_x \sqrt[3]{[(\bar{S}_x+\bar{S}_z)/2]} \tag{29}$$

which reduces to eq. (27a) for small strains; $(\bar{S}_x+\bar{S}_z)=2$. Furthermore, comparison of preferred wavelengths computed using the exact, 1st order analysis of single layers with those computed using both eq. (27a) and eq. (29) indicates that the simpler relation, eq. (27a), more closely approximates the results of the exact theory; indeed, no error was detected in eq. (27a), but results of eq. (29) differ slightly from those of the exact analysis. Equation (27a) is approximate only insofar as the relations between amplification factor and logarithm of wavelength ratio deviate from perfect symmetry about the dominant wavelength ratio and the eigenvector is different from the preferred vector of amplitudes.

Once the dominant wavelength has been computed using either the elementary theory or the 1st order theory, it is a simple matter to compute the preferred wavelength using eq. (27a) and to determine the corresponding fold form. First the dominant wavelength is calculated, starting with the estimate provided by Fig. 12B and using a computer program to solve eqs. (16). Then the value of stretch, $\underline{\bar{S}}_z$, to which the multilayer will be subjected is selected by solving the equation

$$({}_1A_{max}\ell)/({}_1A_o\ell_o) \cong \bar{S}_z^{(2+{}_1^1q)} \qquad (30)$$

in which $({}_1\underline{A}_{max}\ell)$ is the final maximum slope and $({}_1\underline{A}_o\ell_o)$ is the initial maximum slope. The quantity $1+{}_1^1q$ is the eigenvalue for the dominant wavelength. For example, for a final maximum slope angle of 20^0, an initial maximum slope angle of 1^0, and an eigenvalue of 10, a stretch of $\underline{\bar{S}}_z = 1.32$ would be computed, and a value of 1.4 esimated. Using the estimated value of stretch, the initial wavelength-to-thickness ratio, $(L/h_1)_0$, is computed with eq. (27b), and a computer program is used to solve eq. (25) for the eigenvector of initial amplitudes. Then these data are entered into a computer program that numerically integrates eqs. (21) for the growth rates of the amplitudes of component waveforms. The latter program provides results at many intermediate steps in the integration so that the evolution of the fold form can be followed. The computer programs are presented (in Microsoft BASIC) in the appendices.

Distributions of Amplitudes

In the complete 3rd order analysis the distributions of amplitudes of the first, second, and third waveforms are determined as a function of the amount of shortening or thickening of the multilayer. The normalized amplitude vectors shown in Figs. 15B and 15E reflect the distributions of amplitudes of the first waveform in these two multilayers before shortening ($\underline{S}_z = 1.0$); amplitudes of the second and third waveforms are zero. The interfaces are therefore pure cosine waves; the fold forms corresponding to these amplitude vectors are similar and resemble a very low-amplitude analogue of the fold form shown in Fig. 11, loc. A1. Normalized amplitude vectors for these same two multilayers after shortening show growth of all three waveforms (Figs. 18A and 18B, columns 1, 2 and 3, respectively). Distributions of relative strengths of second and third waveforms (columns 4 and 5, respectively) indicate the influence that these waveforms have on modifying the original, similar fold shapes. Each set of amplitude vectors corresponds to a concentric-like fold form, transformed from the initial fold form by the development of a strong second waveform. The fold form for the multilayer with bonded contacts (Fig. 18A) is shown in Fig. 6A and that for the multilayer with free slip at contacts (Fig. 18B) in Fig. 5A.

The distributions of amplitudes in Figs. 18A and 18B can be used to analyze the resultant fold forms shown in Fig. 6A and Fig. 5A, respectively, just as the diagrams in Fig. 11, columns 1 and 2, were

Figure 18. Distribution of amplitudes of first, second, and third waveforms for multilayers of interbedded stiff and soft layers confined by soft media (multilayers B and E, Fig. 15). Amplitudes in columns 1, 2, and 3 represent amplitude vectors; those in columns 4 and 5 represent distributions of relative strengths. Locs. A1 and B1: amplitudes of first waveforms normalized to maximum of one. Locs. A2 and B2: amplitudes of second waveforms normalized by maximum amplitude of first waveform. Locs. A3 and B3: amplitudes of third waveforms normalized by maximum of first. Locs. A4 and B4: amplitudes of second waveforms normalized by amplitudes of first waveforms in same interfaces. Amplitudes of second waveforms range up to -0.27 to -0.29 that of first waveforms. Locs. A5 and B5: amplitudes of third waveforms, normalized with first in same interface; negligible because they are less than 0.10($_1\underline{A}$). C. and D. Vectors of average sums, $_j\underline{A}_a$, and differences, $_j\underline{A}_s$, of amplitudes of first, second, and third waveforms, calculated according to eq. (4c). Normalized by maximum amplitude of first waveform. Dominance of $_2\underline{A}_a$ vector over $_2\underline{A}_s$ vector indicates that the layers behave as an ensemble.

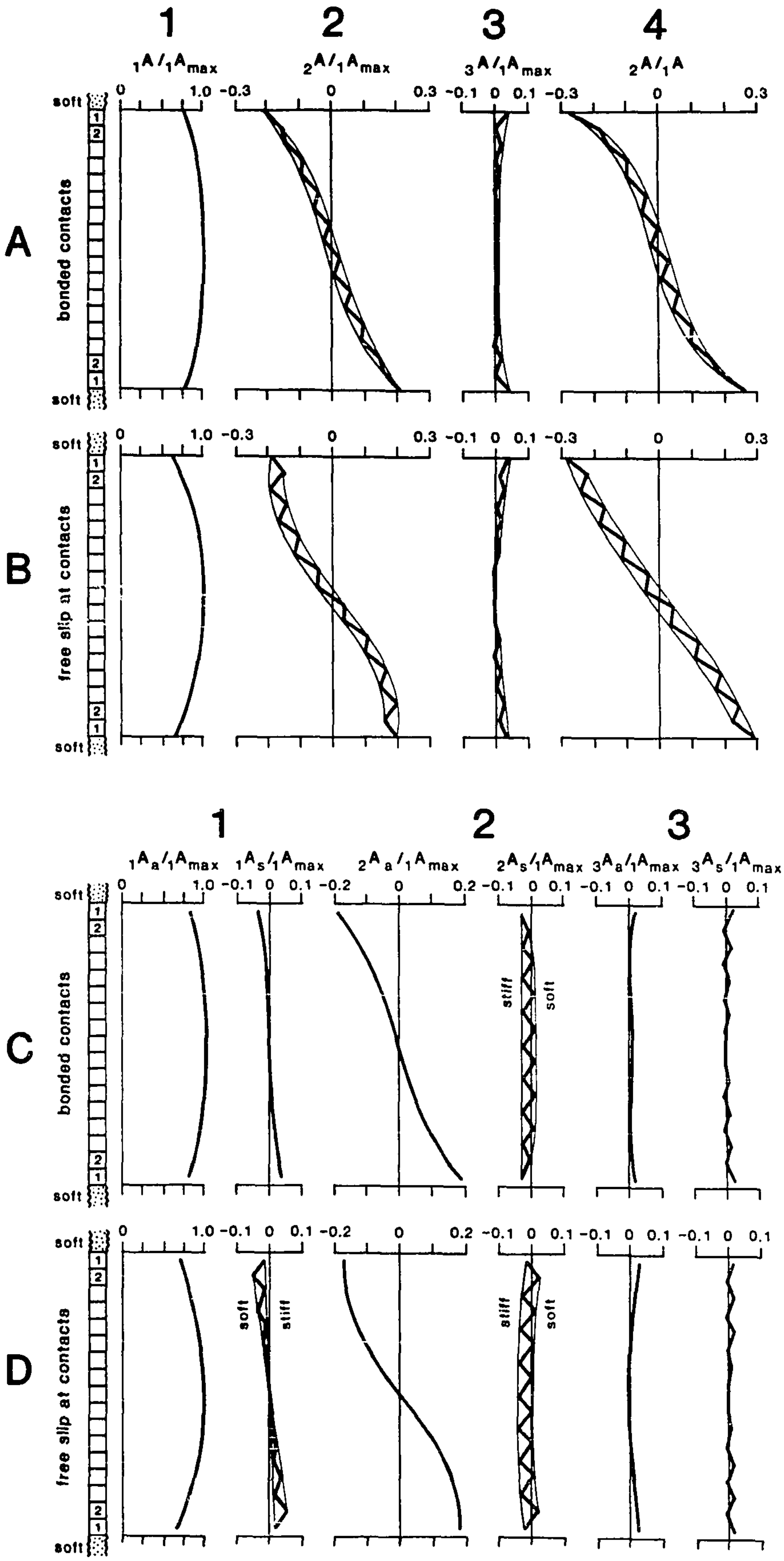

1
2
3
4
5
$_1A/_1A_{max}$
$_2A/_1A_{max}$
$_3A/_1A_{max}$
$_2A/_1A$
$_3A/_1A$
A
bonded contacts
B
free slip at contacts
C
bonded contacts
D
free slip at contacts
soft
stiff
$_1A_a/_1A_{max}$
$_1A_s/_1A_{max}$
$_2A_a/_1A_{max}$
$_2A_s/_1A_{max}$
$_3A_a/_1A_{max}$
$_3A_s/_1A_{max}$

used to geometrically analyze the resultant fold forms in Fig. 11, column 3. As discussed in conjuction with Fig. 11, the distribution of $_1\underline{A}$ amplitudes defines the multilayer folding mode of the first waveform; this distribution is represented by the amplitude vectors in Fig. 18, locs. A1 and B1. As in Fig. 11, column 1, amplitudes of the first waveform are positive throughout the multilayer. The distribution of $_2\underline{A}$ amplitudes defines the multilayer pinch-and-swell mode of the second waveform; this distribution is represented by the amplitude vectors in Fig. 18, locs. A2 and B2. As in Fig. 11, column 2, amplitudes of the second waveform are negative in the top half of the multilayer, zero at middepth, and positive in the lower half of the multilayer. Vectors of amplitudes of the third waveform are shown in Fig. 18, locs. A3 and B3. In addition, the vector of amplitudes $_1\underline{A}$ (column 1) contains information about the constraint of the multilayer, and the vector of amplitudes (column 2) plus the distribution of relative strengths (column 4) together indicate the strength of the second waveform. The <u>strength of the second waveform</u> is a single number used to characterize the multilayer, $(_2A_i)_{max}/_1A_i$; the <u>relative strength of the second waveform</u> refers to the ratio $(_2A/_1A)_i$ on any interface.

Calculation of the constraint of each multilayer using eq. (6) is straightforward because the quantity $(_1A_e/_1A_m)$ is the component plotted in Fig. 18, locs. A1 and B1, at the edges of the multilayer: the fold form is more highly constrained in the multilayer with free slip ($\underline{c}$ = 0.59) than in the multilayer with bonded contacts ($\underline{c}$ = 0.43).

However, neither vector of ${}_1\underline{A}$ amplitudes corresponds to a constrained fold form because the amplitudes do not approach zero at the upper and lower edges of the multilayers. The amplitude vectors in locs. A2 and B2 indicate the interface for which ${}_2\underline{A}$ is maximum: for both multilayers, ${}_2\underline{A}_{max}$ occurs on the outermost interfaces. The strength of the second waveform, $({}_2A_i)_{max}/{}_1A_i$, can be read directly off those same interfaces in Fig. 18, locs. A4 and B4: the strength of the second waveform is about -0.25 in both multilayers. A strength of magnitude 0.25 indicates that the effect of the second waveform is visually recognizable in the resultant fold form. Because the second waveform is strongest on the outer interfaces, flattening of crests and sharpening of troughs is greatest at the top of the multilayer, as noted in the fold forms, Fig. 6A and Fig. 5A. The strength of the third waveform, $({}_3A_i)_{max}/{}_1A_i$, is only about 0.05 (Fig. 18, locs. A3 plus A5 and B3 plus B5), so it does not have a noticeable effect on the fold form. The combination of a strong second waveform pinch-and-swell mode (Fig. 18, column 2) and the first waveform folding mode (Fig. 18, column 1) produces a concentric-like fold, as it did in Fig. 11, row A.

Figures 18A and 18B analyze the behavior of a multilayer, defined by an ensemble of interfaces. One can, instead, study the behavior of individual layers within the multilayer. For this purpose, each layer is analyzed as though it were a single-layer fold by calculating its folding and pinch-and-swell modes using eq. (4c). Plots of those calculations as vectors of the average sums and differences of interface amplitudes are shown for the multilayer with bonded contacts in Fig. 18C and for the one with free slip at contacts in Fig. 18D. The relations between position within the multilayer and amplitude of the pinch-and-swell mode for the first waveform, ${}_1\underline{A}_s/{}_1\underline{A}_{max}$, show that the soft layers accommodate much more thickening and thinning than stiff layers in the multilayer with free slip (Fig. 18, loc. D1). Both the stiff and soft layers accommodate thickening and thinning in the multilayer with bonded contacts (Fig. 18, loc. C1).

For simple, repetitive multilayers, the shapes of amplitude vectors for the first waveform reflect the constraint provided by upper and lower confining media (Fig. 15). Identical upper and lower media provide identical constraints, resulting in amplitude vectors that have symmetry about middepth in the multilayer (Fig. 19). Figure 19 shows normalized amplitude vectors and distributions of relative strengths for three multilayers of identical stiff layers with free slip at contacts and confined identically above and below by either soft ($\mu_m/\mu_1 = 0.1$) (Fig. 19A), stiff ($\mu_m/\mu_1 = 1.0$) (Fig. 19B), or rigid ($\mu_m/\mu_1 \to \infty$) (Fig. 19C) media. The corresponding fold forms are shown in Fig. 2, locs. A1, A2, and A3, respectively. The distributions of amplitudes of first waveforms (column 1) clearly reflect the differences in constraint for the three multilayers. The amplitudes of second waveforms normalized by the amplitudes of first waveforms in the same interface (column 4) show the relative strengths of the second waveforms. In all three examples, the second waveforms have little effect on the shapes of

Figure 19. Distributions of amplitudes for multilayers confined above and below by soft ($\mu_m/\mu_1 = 0.1$) (A), stiff ($\mu_m/\mu_1 = 1.0$) (B), or rigid ($\mu_m/\mu_1 \rightarrow \infty$) (C) media. Amplitude vectors of first waveforms (column 1) reflect degree of constraint.

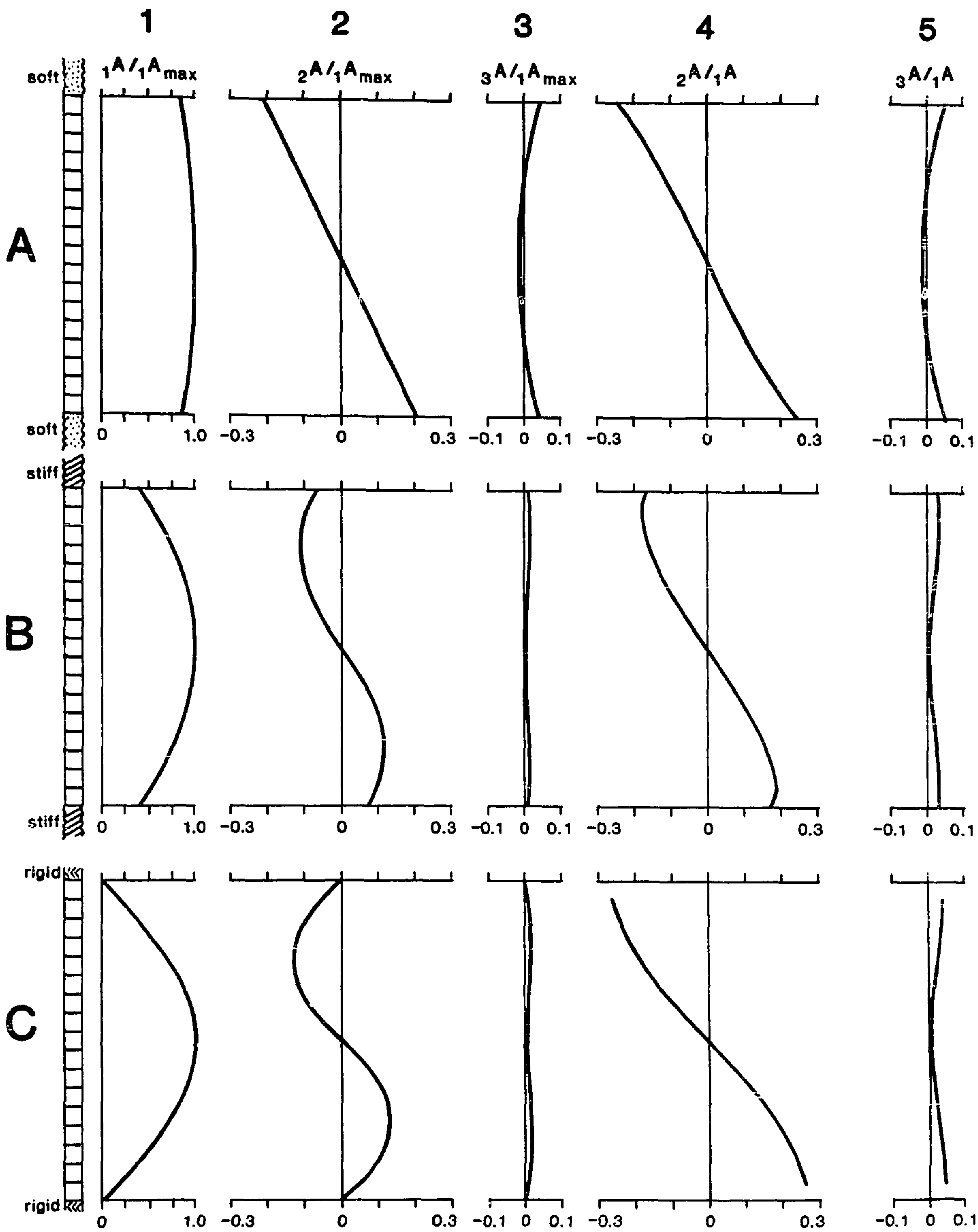
1
2
3
4
5
$_1A/_1A_{max}$
$_2A/_1A_{max}$
$_3A/_1A_{max}$
$_2A/_1A$
$_3A/_1A$
A
B
C
soft
stiff
rigid
0
1.0
-0.3
0
0.3
-0.1
0
0.1

interfaces near middepth and greater effect near the top and bottom of the multilayer.

Upper and lower confining media with different viscosities provide different constraints on simple, repetitive multilayers; symmetry of the amplitude vectors about middepth of the multilayer is lost. Figure 20 shows amplitude vectors and distributions of relative strengths for multilayers with a free upper surface and confinement below by media ranging from soft ($\mu_m/\mu_1 = 0.1$) (Fig. 20A) to rigid ($\mu_m/\mu_1 \to \infty$) (Fig. 20C). The corresponding forms of the folds are shown in Fig. 14, locs. A3, B3 and C3, respectively. The differences in constraint provided by the lower media are evident in the plots of normalized amplitudes of the first waveforms, ${}_1\underline{A}/{}_1\underline{A}_{max}$ (column 1). Amplitudes of the second and third waveforms in columns 4 and 5 are normalized by amplitudes of the first waveform in the same interface, indicating the relative strengths of the second and third waveforms in each interface. The distribution of relative strengths of the second waveform are distinctly different for the different confining media. For a soft medium, the distribution is essentially a linear function of depth (loc. A4), passing through zero slightly above middepth. For stiff lower media (loc. B4), the amplitude ratios pass through zero well above middepth, so flattened crests occur only in a few interfaces near the free upper surface of the multilayer.

Figure 20. Distributions of amplitudes for multilayers unconfined above and confined below by soft ($\mu_m/\mu_1 = 0.1$) (A), stiff ($\mu_m/\mu_1 = 1.0$) (B), or rigid ($\mu_m/\mu_1 \to \infty$) (C) medium. Multilayers composed of identical stiff layers. Relative strengths of second waveforms significant in upper and lower parts of all three multilayers. Relative strengths of third waveforms significant only in top interface in multilayers confined by stiff or rigid medium.

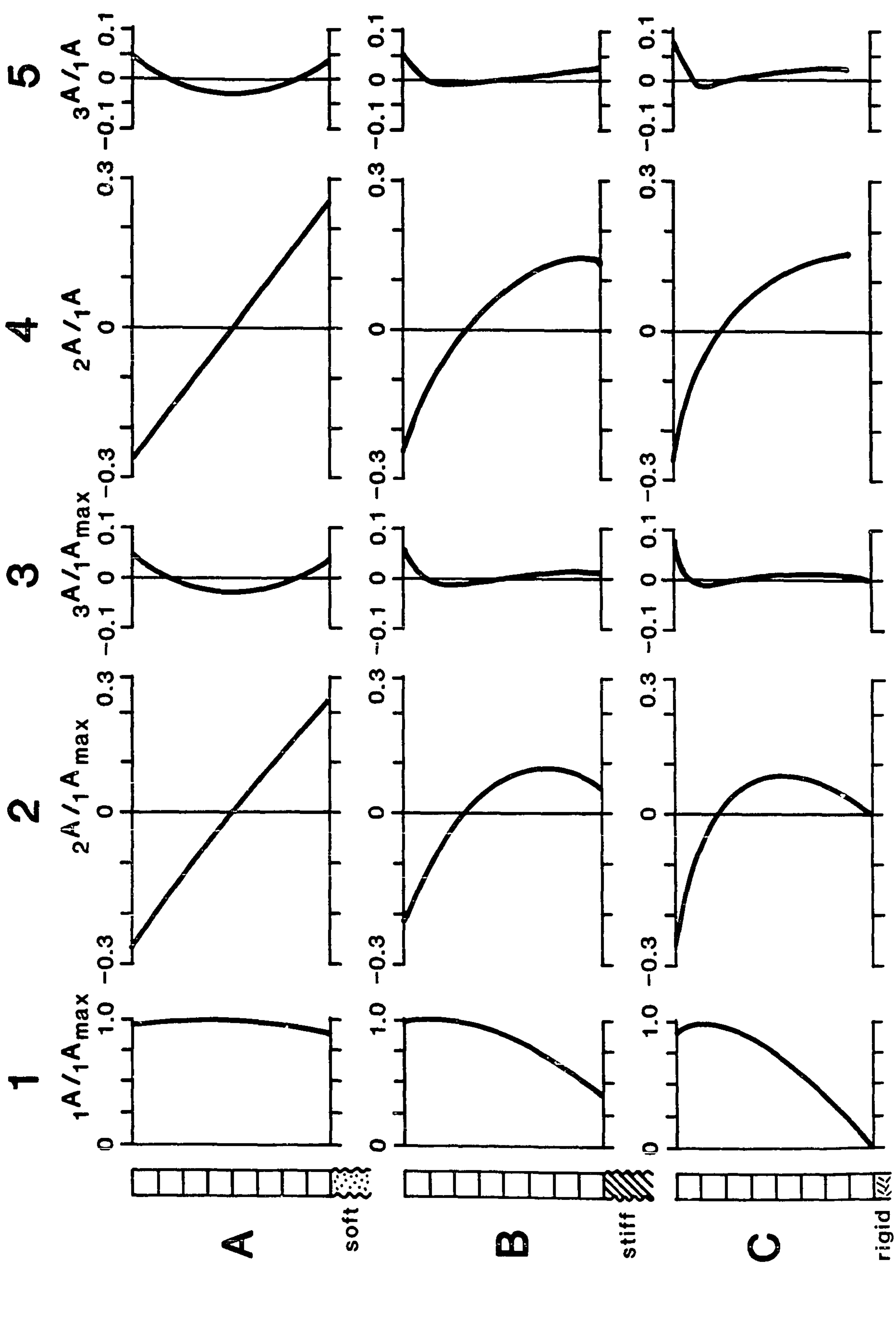

A
B
C
soft
stiff
rigid
1
2
3
4
5
$_1A/_1A_{max}$
$_2A/_1A_{max}$
$_3A/_1A_{max}$
$_2A/_1A$
$_3A/_1A$

Evolution of Fold Forms

Thus far the forms of multilayer folds have been discussed as though they were determined by a two-stage process: the initial form determined by the eigenvector of amplitudes of the first waveform, and the final form determined by the vectors of amplitudes of first, second, and, in some cases, third waveforms. The fold forms, however, evolve as the folds grow, so a fold that is virtually a similar fold at low amplitudes may become a parallel fold at moderately high amplitudes. Furthermore, the fold may remain essentially similar for much of the deformation history and then suddenly transform into a parallel form with only minor additional deformation. In this section, the growth rates of maximum amplitudes of component waveforms will be compared for shortening of multilayers B and E (Fig. 15). Then three or four stages of folding will be examined for two simple multilayers, one confined by soft media (the concentric-like fold form) and the other confined by rigid media (the internal fold form).

One measure of the growth of a fold form is the continuous increase in maximum amplitudes with increasing thickening. Although such information does not itself convey the form of the fold, it can document the evolution of a known form or allow comparison of growth rates of different fold forms. For example, Fig. 21 shows amplitude ratios for second and third waveforms and maximum slope angles of the first waveform as a function of thickening, S_z, for a multilayer with free slip at contacts and a multilayer with bonded contacts. The eigenvectors for the two multilayers are shown in Figs. 15E and 15B,

Figure 21. Relations between amplitudes of three waveforms and mean thickening for multilayers of interbedded stiff and soft layers confined by soft media. One multilayer (E, Fig. 15) has free slip at contacts, the other (B, Fig. 15) has bonded contacts. ${}_1\theta_{max}$ is maximum slope angle of first waveform. Maximum slope angle and amplitudes of second and third waveforms grow much more rapidly in multilayer with free slip than in multilayer with bonded contacts.

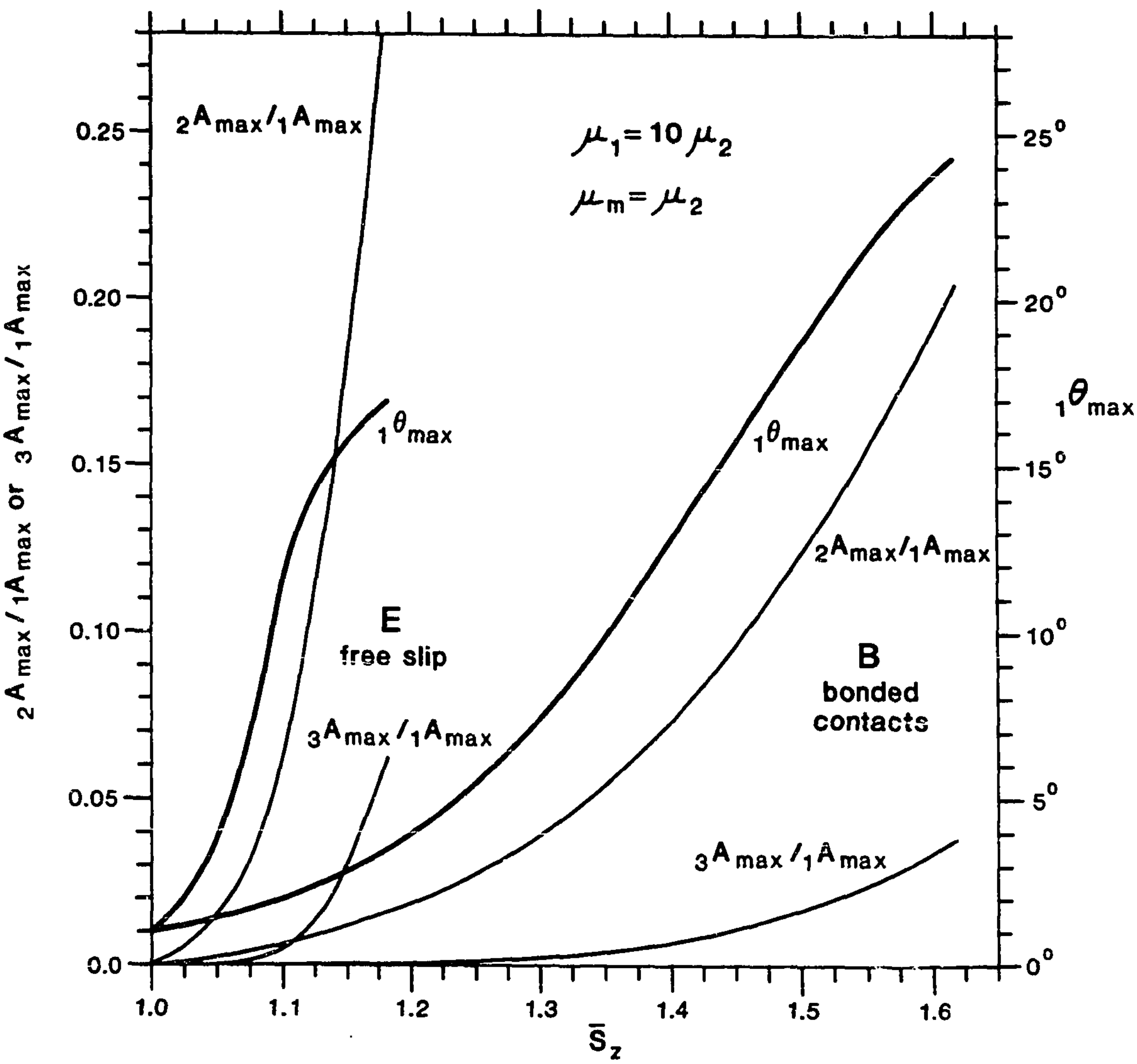

$_2A_{max}/_1A_{max}$
$\mu_1 = 10\,\mu_2$
$\mu_m = \mu_2$
$_1\theta_{max}$
$_1\theta_{max}$
$_2A_{max}/_1A_{max}$
E
free slip
B
bonded contacts
$_3A_{max}/_1A_{max}$
$_3A_{max}/_1A_{max}$
$_2A_{max}/_1A_{max}$ or $_3A_{max}/_1A_{max}$
$_1\theta_{max}$
$\bar{S}_z$
0.0
0.05
0.10
0.15
0.20
0.25
1.0
1.1
1.2
1.3
1.4
1.5
1.6
0^0
5^0
10^0
15^0
20^0
25^0

respectively. The amplitude ratios are the maximum amplitude of the second waveform, ${}_2\underline{A}_{max}$, or of the third waveform, ${}_3\underline{A}_{max}$, divided by the maximum amplitude of the first waveform, ${}_1\underline{A}_{max}$. The value of maximum slope angle of the first waveform, ${}_1\theta_{max}$, is related to the maximum amplitude of the first waveform

$$ {}_1\theta_{max} = \tan^{-1}({}_1A_{max}\ell) \tag{31} $$

All the waveforms increase in amplitude more rapidly with thickening, $\underline{\bar{S}}_z$, in the multilayer with free slip (Fig. 21, curve E) than in that with bonded contacts (Fig. 21, curve B). For example, a maximum slope angle of 16 degrees is reached at a stretch of $\underline{\bar{S}}_z = 1.16$ for the multilayer with free slip at contacts but not until a stretch of $\underline{\bar{S}}_z = 1.45$ for the multilayer with bonded contacts. In both multilayers, the initial maximum slope angle of the first waveform is one degree. For free slip at contacts, the slope angle increases slowly with stretch up to $\underline{\bar{S}}_z$ of about 1.05, then rapidly up to $\underline{\bar{S}}_z$ of 1.12, and then more slowly thereafter. The reduction in amplification of the first waveform, reflected in the tailing off of the upper part of the curve for ${}_1\theta_{max}$ in Fig. 21, is absent in the 1st order analysis and is therefore a result of the 3rd order corrections. Calculations to 3rd order accuracy indicate that, if thickening were continued, the first waveform would stop growing and then would decrease in amplitude; however, the decrease in amplitude apparently is an artifact of the 3rd order analysis and would vanish in a still higher order analysis. Presumably a higher order analysis would show that the growth rate of the first waveform decreases to nearly zero when its amplitude reaches relatively large values (corresponding to slope angles on the order of 25 to 30 degrees, depending on the multilayer). Subsequent amplification would be purely kinematic.

Ratios of ${}_2A_{max}/{}_1A_{max}$ and ${}_3A_{max}/{}_1A_{max}$ are plotted in Fig. 21 because it is the relative magnitudes of the second and third waveforms that determine non-sinusoidal fold shapes, as shown for second waveforms in Fig. 13. The amplitude maximum of the second waveform is much larger than that of the third for these multilayers. For free slip (curve E), the amplitude of the second waveform is negligible, less than $0.10({}_1A_{max})$, until the maximum slope angle in the first waveform is 10 degrees ($\bar{S}_z = 1.12$). By the time the stretch reaches 1.17, though, the amplitude of the second waveform is about $0.25({}_1A_{max})$, and the maximum slope angle is 16 degrees. At that same stretch value, the amplitude of the third waveform is only $0.05({}_1A_{max})$, so its effect on fold form is negligible.

The second waveform is somewhat weaker in the multilayer with bonded contacts (curve B, Fig. 21). It is negligible until the first waveform reaches a slope angle of about 16 degrees (as compared to 10 degrees for free slip); its amplitude reaches $0.21({}_1A_{max})$ when the maximum slope angle is about 25 degrees (as compared to 16 degrees for free slip), near the upper limit of validity of the 3rd order analysis. The amplitude of the third waveform in Fig. 21 is always negligible, less than $0.10({}_1A_{max})$, for slope angles within the limits of the theory.

The development of a particular fold form can be followed by comparing the distributions of amplitudes, rather than just maximum amplitudes, at various stages of growth. A concentric-like fold will develop in a multilayer composed of 17 identical layers confined by soft media ($\mu_m/\mu_1 = 0.1$) (Fig. 22). The initial interface form was sinusoidal; amplitudes of second and third waveforms were zero. The initial shape of the fold was defined by an eigenvector of amplitudes of first waveforms with a maximum slope angle of one degree near middepth. The amplitude component of the eigenvector for the top and bottom interfaces was 0.937 times the component at middepth, so the initial form was essentially similar.

With thickening of five percent ($\underline{\bar{S}}_z = 1.05$, Fig. 22A), the maximum slope angle increased to 5.63 degrees. The fold form remained essentially <u>similar</u>, with equally wide interface crests and troughs, because the amplitudes of the third waveform were still nearly zero and the amplitudes of the second waveform remained negligible, reaching at most 0.05 times the amplitude of the first waveform in the same interface (Fig. 22A).

As the multilayer was shortened and thickened to 6.4 percent ($\underline{\bar{S}}_z = 1.064$, Fig. 22B), though, the amplitude of the second waveform increased to about 0.09 times the amplitude of the first waveform in the top and bottom interfaces, and its effect on interface shapes became evident. The crests broadened and the troughs narrowed in interfaces in the upper half of the multilayer, so the overall form of the ensemble of

Figure 22. Three stages in growth of parallel, concentric-like fold in multilayer consisting of identical stiff layers confined by soft media. Amplitudes of first, second, and third waveforms shown beside corresponding fold. Initial form consisted of first waveforms with maximum slope angle of one degree. A. After thickening of five percent, the maximum slope angle of the first waveform was 5.63 degrees, and the waveforms remained essentially cosine waves. Maximum amplitude of second waveform about 0.05 that of first. B. After thickening of 6.4 percent, the maximum slope angle was eight degrees, and the maximum amplitude of the second waveform had reached about 0.09 that of the first. The concentric-like form has just begun to emerge. C. After thickening of eight percent, the maximum slope angle was 10.6 degrees, and the second waveform was strong (maximum amplitude 0.16 that of first). The fold form had become clearly concentric-like.

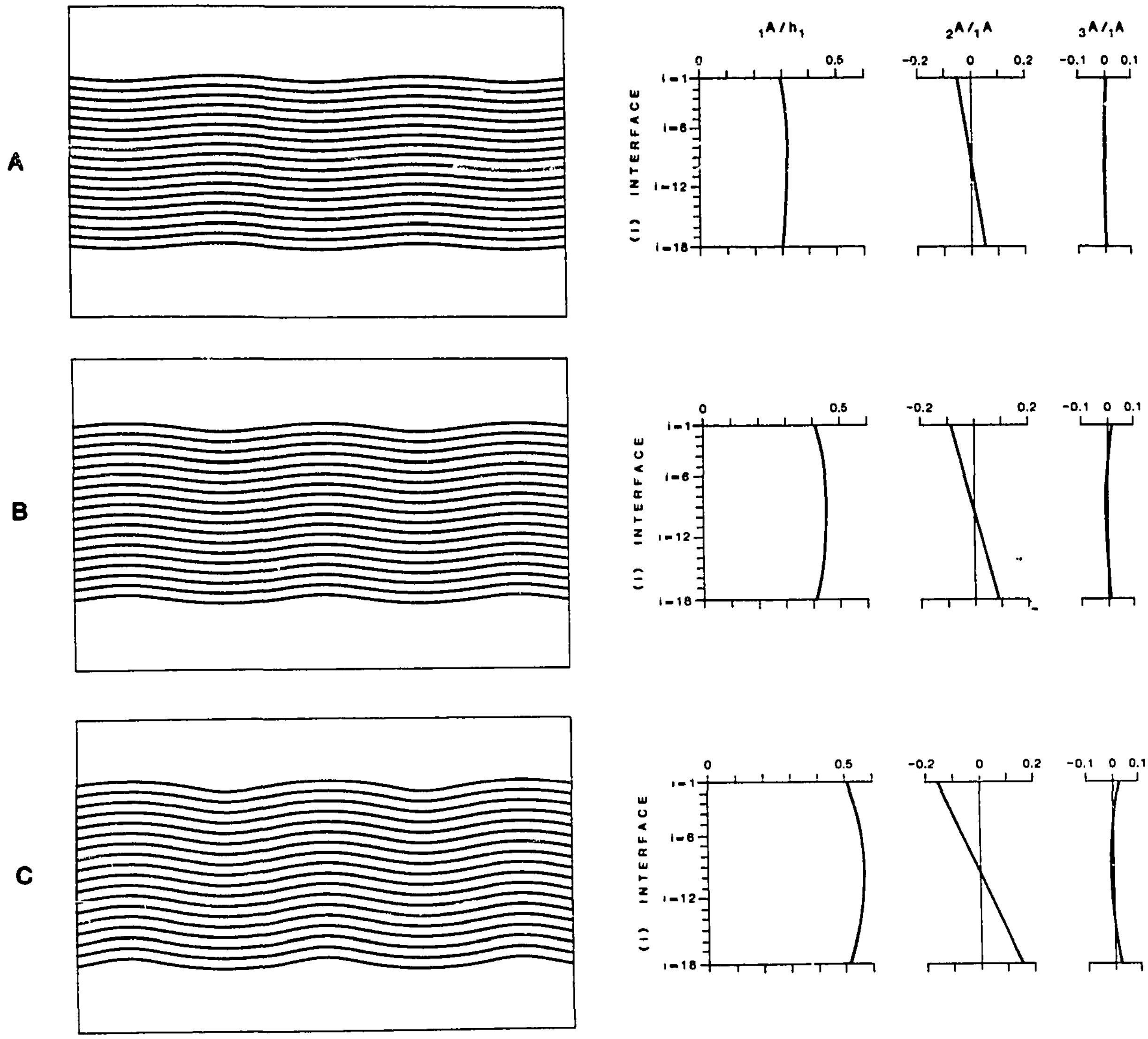
A
B
C
1A/h1
2A/1A
3A/1A
0
0.5
-0.2
0
0.2
-0.1 0 0.1
i=1
i=6
i=12
i=18
(i) INTERFACE

Figure 23. Three stages in growth of constrained, internal fold in multilayer confined by rigid media. Amplitudes of first, second, and third waveforms shown beside corresponding fold. Growth of fold much slower than that shown in Fig. 22, so thickening of multilayer during growth is marked. Initial cosinusoidal waveforms with maximum slope angle of one degree. After thickening of 33 percent, low-amplitude folds shown in A have developed. Form remains essentially sinusoidal because second waveform is still weak, as indicated to right in A. After thickening of 48 percent the fold shown in B develops. The second waveform is significant, with a maximum amplitude of about 0.16 that of the first waveform in the same interface. After thickening of 62 percent as shown in C, the characteristic pinches and flats have become well-developed in interfaces near the top and bottom of the multilayer. The second waveform is strong near 1/4 and 3/4 depths, where its amplitude is up to about 0.13 that of the first waveform in the same interface. The third waveform remains insignificant during all three stages of folding shown.

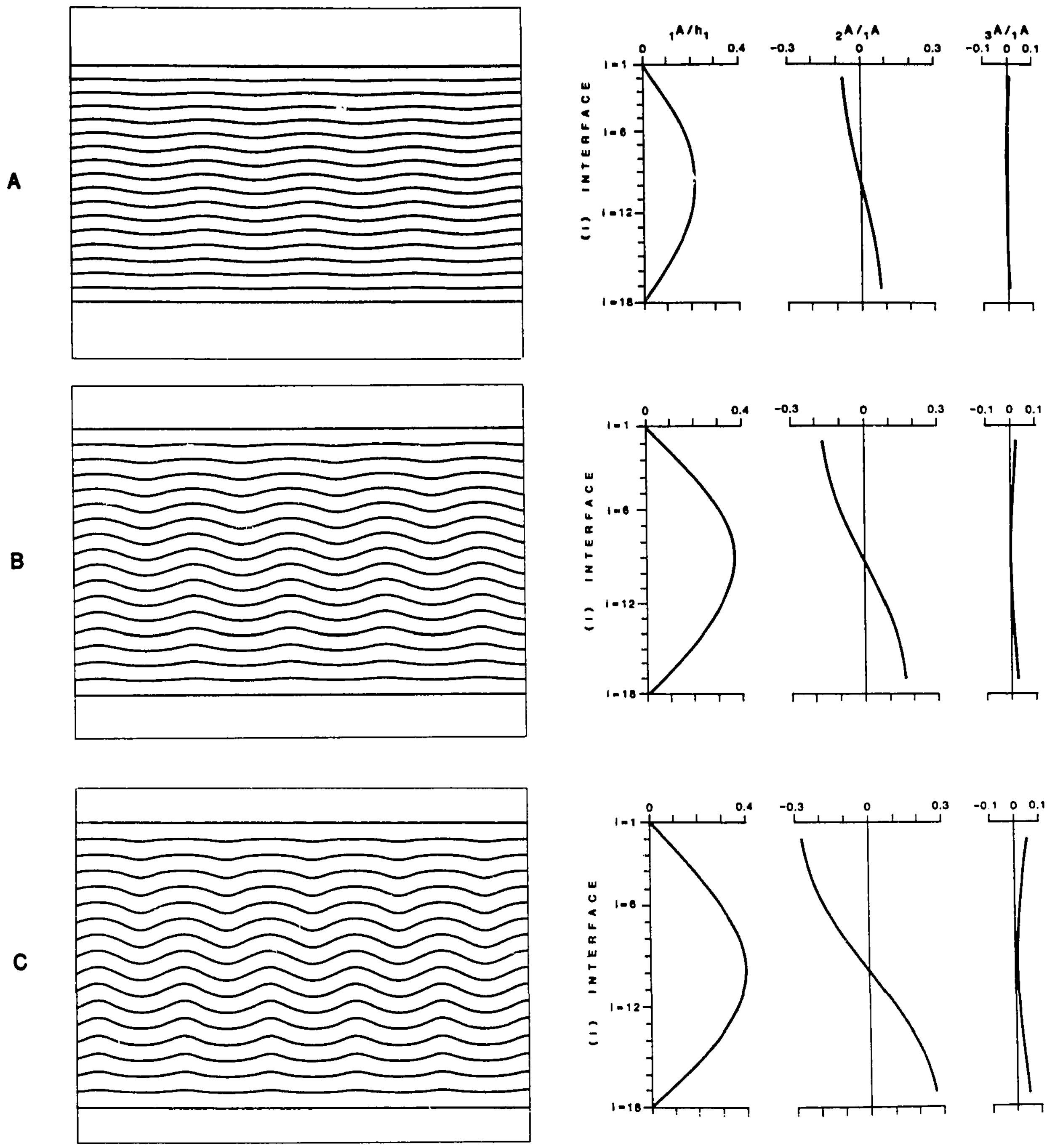
A
B
C
1A/h1
0
0.4
2A/1A
-0.3
0
0.3
3A/1A
-0.1
0
0.1
i=1
i=6
i=12
i=18
INTERFACE (i)

interfaces began to appear concentric-like. At this stage, the maximum slope angle of the first waveform was about eight degrees.

The broadening and flattening of crests in upper interfaces became even more evident as thickening increased to eight percent ($\underline{\bar{S}}_z$ = 1.08, Fig. 22C). The maximum slope angle of first waveforms was about 10.6 degrees, and the ratio ($_2\underline{A}/_1\underline{A}$) in the top and bottom interfaces increased to 0.16. As thickening increased further, to ten percent ($\underline{\bar{S}}_z$ = 1.1), the maximum amplitude of the second waveform became about 0.25 that of the first waveform (Fig. 2, loc. A1), and the fold assumed a strong concentric-like form.

Amplitude vectors for the first and second waveforms are compared in Fig. 24A for the three stages of deformation shown in Fig. 22. The three normalized amplitude vectors for the first waveform are virtually identical (Fig. 24A) although the magnitudes of the maximum amplitudes increase from 0.33 to 0.45 to 0.52 of the current thickness, $\underline{h}_1$, of a layer (Fig. 22). The shaoe of the normalized amplitude vectors for the second waveform remains essentially linear throughout folding although the magnitudes of the amplitudes increase with increasing deformation. These amplitude vector shapes together are diagnostic of the concentric-like fold form.

For the multilayer confined by soft media, the normalized amplitude vectors (Fig. 24A) closely resemble the distribution of relative strengths of amplitudes (Fig. 22). The strength of the second waveform,

Figure 24. A. Amplitude vectors for three stages of folding of a parallel, concentric-like form, shown in Fig. 22. B. Amplitude vectors for three stages of folding of a constrained, internal form, shown in Fig. 23. Amplitude vectors of first waveform are essentially identical in form although different in magnitude. Shapes of amplitude vectors for second waveform, normalized with maximum amplitude of first waveform at each stage of folding, remain fairly constant although magnitudes of elements increase with increasing deformation. The distributions of amplitudes shown in Figs. 22 and 23 indicate the strength of the second waveform compared to the first in each interface, whereas the distributions shown here indicate the change in amplitude of second waveforms from interface to interface. Amplitude vectors in A are diagnostic of the concentric-like form; those in B are diagnostic of the constrained fold form.

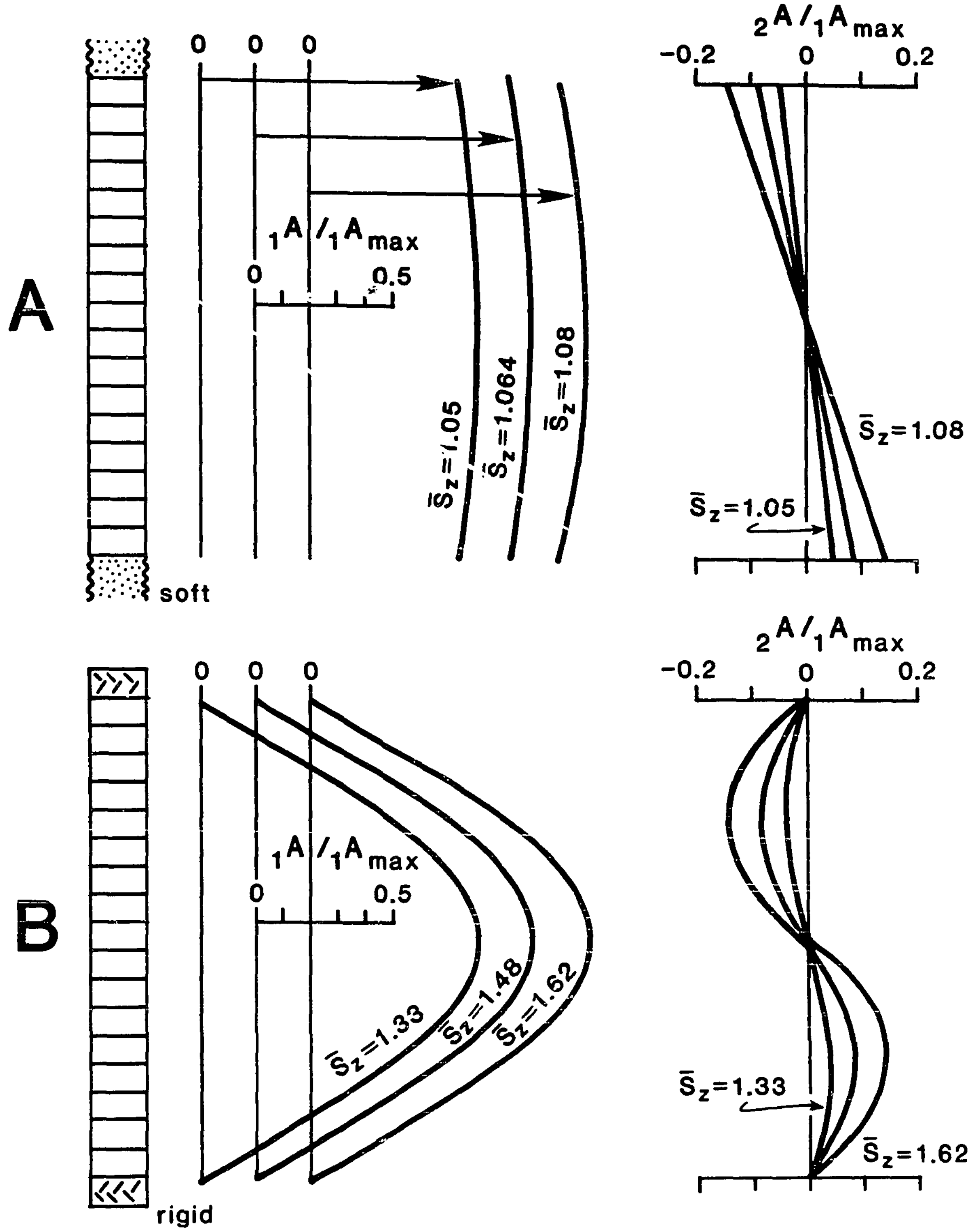

A
B
0 0 0
$_1A/_1A_{max}$
0 0.5
$\bar{S}_z=1.05$
$\bar{S}_z=1.064$
$\bar{S}_z=1.08$
$_2A/_1A_{max}$
-0.2 0 0.2
$\bar{S}_z=1.08$
$\bar{S}_z=1.05$
soft
$\bar{S}_z=1.33$
$\bar{S}_z=1.48$
$\bar{S}_z=1.62$
$\bar{S}_z=1.33$
$\bar{S}_z=1.62$
rigid

$({}_2A_i)_{max}/{}_1A_i$, equals the maximum relative strength of the second waveform, $({}_2A_i/{}_1A_i)_{max}$, and both are calculated at the outermost interfaces. This will not be the case for the second waveform in the multilayer confined by rigid media, as will be shown next.

A constrained, internal fold form will develop if the same multilayer of identical layers with free slip at contacts is confined by rigid ($\mu_m/\mu_1 \rightarrow \infty$) (Fig. 23) rather than soft media. The initial forms of interfaces were cosine waves, with maximum slope angle of one degree near middepth. As the multilayer shortened and thickened, the first waveform amplified and the second and third waveforms developed spontaneously. The amplitudes of the second waveform were essentially negligible for thickening up to 33 percent (Fig. 23A): the relative strength of the second waveform reached a maximum of only 0.075, near the boundaries; the strength of the second waveform was only 0.056, calculated at 1/4 and 3/4 depth. The fold form was controlled by the first waveforms, cosine waves with amplitudes that varied essentially cosinusoidally with vertical distance above and below middepth. The maximum slope angle of interfaces, near middepth, was about 9.4 degrees.

As thickening increased to $\underline{S}_z = 1.48$ (Fig. 23B), the maximum slope angle of the first waveform increased to about 20 degrees. The strength of the second waveform, calculated at depths of 1/4 and 3/4, increased to 0.12; the relative strength of the second waveform increased to a maximum of about 0.16 near the upper and lower, rigid boundaries. Second waveforms widened anticlines in the upper part and synclines in the lower part of the multilayer. Interfaces near the top of the multilayer had broad crests and narrow, pinched troughs; those near the bottom of the multilayer had broad troughs and narrow, pinched crests. The internal fold form had thus begun to form.

With further thickening, $\bar{\underline{S}}_z = 1.62$ (Fig. 23C), the maximum slope angle of the first waveform reached 25.4 degrees. The strength of the second waveform was 0.20 at 1/4 and 3/4 depth; the ratio $({}_2A/{}_1A)$ reached a maximum of 0.27 near the upper and lower boundaries. The third waveform never developed sufficiently to affect fold form. At 1/4 depth, the crests were broad and the troughs were narrow. Near the upper interfaces, the crests were flat and the troughs were narrow pinches, as is characteristic of the internal fold form.

Amplitude vectors for the first and second waveforms are compared in Fig. 24B for the three stages of deformation, thickening of 33 percent ($\bar{\underline{S}}_z = 1.33$), 48 percent, and 62 percent ($\bar{\underline{S}}_z = 1.62$), shown in Fig. 23 for a multilayer confined by rigid media. As in the case of the multilayer confined by soft media (Figs. 22, 24A), the three normalized amplitude vectors for the first waveform (Fig. 24B) are virtually identical, although the magnitude of the maximum amplitude increases from about 0.22 to 0.36 to 0.39 times the current thickness of a stiff layer (Fig. 23). The shape of the amplitude vectors for the second waveform remains the same throughout deformation, although the magnitudes of the normalized amplitudes increase with increased folding. These amplitude vector shapes together are diagnostic of the internal fold form.

The strength of the second waveform in a rigidly confined multilayer is calculated at 1/4 and 3/4 depth, where $_2\underline{A}$ is maximum (Fig. 24B). However, the relative strength of the second waveform, ($_2A/_1A$), is maximum near the upper and lower rigid boundaries (Fig. 23).

DISCUSSION

The theoretical analysis indicates which parameters determine fold forms and how fold forms evolve in repetitious multilayers composed of alternating stiff and soft viscous layers with bonded contacts or free slip at contacts or composed of all stiff layers with free slip at contacts. Three end-member forms can be recognized in these multilayers on the basis of theoretical analysis: parallel, constrained, and similar. Parallel, concentric-like forms develop after folds have grown to moderate amplitudes in multilayers confined by soft media. Large folds formed in layers near the ground surface will tend to be of this type because the viscosity of the overlying medium (air) is essentially zero. Constrained, internal forms develop in multilayers confined by very stiff media. Similar forms result if fold wavelengths are short relative to thicknesses of multilayers. For example, similar folds of low amplitude (sinusoidal) and high amplitude (chevron) occur in multilayers in which stiff layers are widely separated by soft interbeds. Similar, chevron folds occur at high amplitudes in thick multilayers composed only of stiff layers.

The 3rd order theoretical analysis has been motivated by structural analyses of fold forms in a variety of tectonic environments (*e.g.*, Van Hise, 1896; Kuenen and DeSitter, 1938; Hudleston, 1973; Bayly, 1974; Chapple and Spang, 1974; Ramberg and Johnson, 1976; Johnson and Page, 1976; Suppe, 1983), and by experimental or 1st order theoretical analyses of fold forms in a variety of experimental or theoretical materials (e.g., Ramberg, 1963a, 1963b; Weiss, 1968, Ghosh, 1968; Cobbold, Cosgrove, and Summers, 1971). Folds in rock and in experimental materials form in multilayers with more complex dimensional and rheological properties than those analyzed theoretically. However, by focusing on the gross forms of both the theoretical and actual folds, the origins of the gross forms can be understood. In this section, forms of some large folds in the central Appalachians will be compared with forms of folds in simple multilayers, and wavelengths and forms of smaller folds in central California will be compared with those produced theoretically in multilayers with analogous dimensional properties and rheological contrasts. Finally, selected experimental folds will be examined in light of the theory.

Berry-Buffalo Syncline and Tuscarora Mountain Anticline

In order to estimate the forms of large folds in an area northwest of Harrisburg, Pennsylvania, a composite down-plunge cross section of the Berry-Buffalo syncline and the adjacent Tuscarora Mountain anticline has been constructed (Aytuna, 1984) using parts of three 15-minute quadrangles mapped by the Pennsylvania Geological Survey and measurements of bedding attitudes at strategic locations (Fig. 25A). The cross section shows only parts of the folds, but an estimate of the gross forms of the folds is shown in Fig. 25B.

Figure 25. Some large folds in the central Appalachians, Pennsylvania. A. Composite, down-plunge cross section of Berry-Buffalo syncline and Tuscarora Mountain anticline (from Aytuna, 1984, Ch. I, fig. 10A). B. Gross form of the folds in A.

A

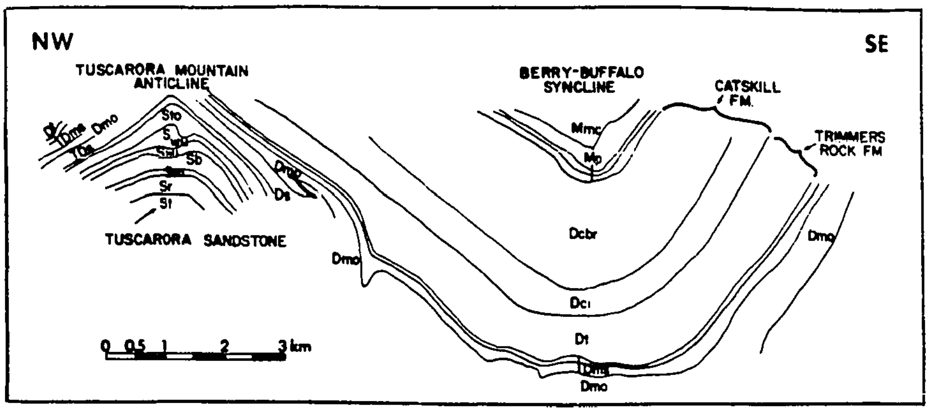
NW
SE
TUSCARORA MOUNTAIN ANTICLINE
BERRY-BUFFALO SYNCLINE
CATSKILL FM.
TRIMMERS ROCK FM
TUSCARORA SANDSTONE
Dmo
Sb
Sr
St
Mmc
Mp
Dcbr
Dci
Dt
0 0.5 1 2 3 km

B

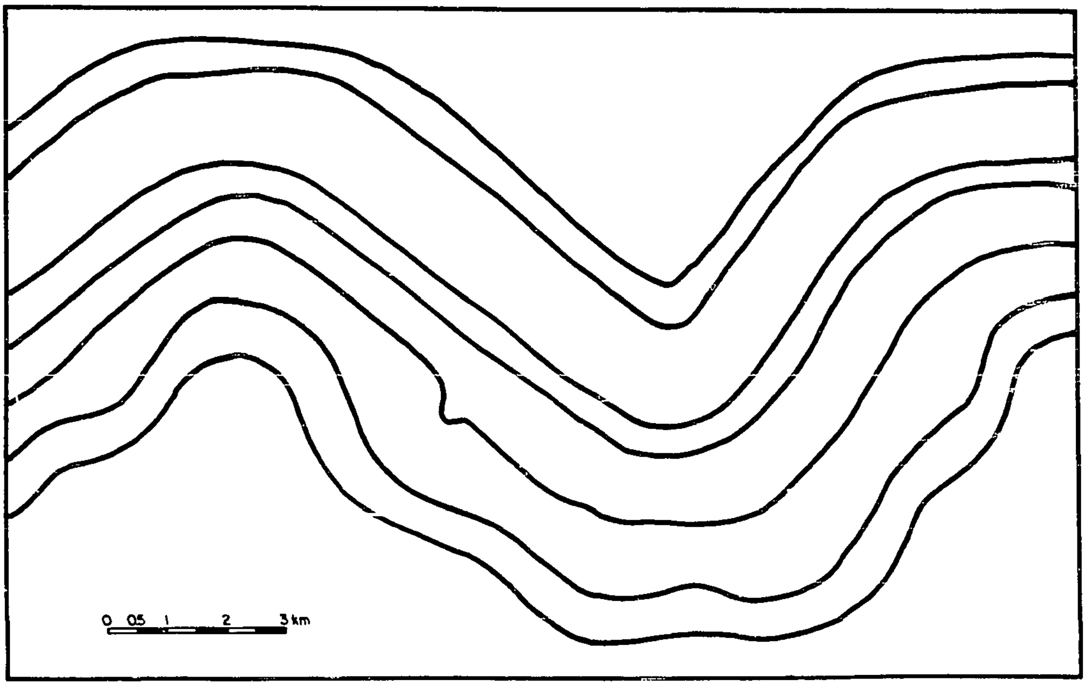
0 0.5 1 2 3 km

The largest folds in the central Appalachians, including the Berry-Buffalo syncline, have wavelengths of 11 to 18 km and involve rocks from the Cambrian to the Pennsylvanian. Intermediate-sized folds have wavelengths of about 3 km and are best developed at the levels of the Tuscarora, Juniata, and Bald Eagle Formations of Late Ordovician and Early Silurian ages, shown as the lowest layer of the cross section in Fig. 25B. The wavelengths of the large folds shown in Fig. 25 appear to be controlled by the Devonian, Catskill and Trimmers Rock formations, whereas the wavelengths of folds in the Tuscarora Sandstone and Juniata Formation appear to be controlled by the thicknesses of those units as well as by the occurrence of relatively soft units above and below (Nickelsen, 1963; Aytuna, 1984).

Although folds of at least two very different wavelengths are present in the central Appalachians (Fig. 25A), the 3rd order analysis presented here deals only with simple multilayers in which all folds have the same wavelength, so my results relate only to the gross forms of the large folds (Fig. 25B). The large folds formed just below the ground surface and are underlain by the Reedsville or Martinsburg Formation, which probably behaved much as a soft to moderately stiff medium. Therefore, among the 3rd order theoretical models, the one that relates most closely to the conditions inferred for these folds is that shown in Fig. 14, loc. A3: a multilayer with no medium above and a soft medium below. The gross fold forms also correspond: the flattening which is apparent in the Berry-Buffalo syncline (Fig. 25A) is present also in Fig. 14, loc. A3, which shows flattening of crests and sharpening of troughs in the upper part of the multilayer and flattening of troughs and sharpening of crests in the lower part of the multilayer.

Thus, the gross form of the large Appalachian folds is reproduced by folding of a theoretical multilayer subjected to the same idealized conditions of confinement as inferred for the actual folds. The correspondence between the theoretical fold forms and the gross form of the actual folds would presumably improve if the theoretical multilayer represented more closely the actual structural-lithic units. Other physical parameters of the fold forms, such as wavelength-to-thickness ratio, could then be compared. However, a complex multilayer, designed by examination of the stratigraphic section, is required to model the central Appalachian folds (Aytuna, 1984). Another discrepancy between the actual and theoretical fold forms is that the slopes of limbs in the Appalachian folds are much larger than those in the theoretical multilayer, which are at the limit ($\sim 20^{\circ}$) allowed in the 3rd order analysis. A theoretical solution carried to a higher order of accuracy in the maximum slope of the layering would permit limb dips in the resulting theoretical fold forms to approach those in the actual folds.

The preceding discussion illustrates that one way to analyze an actual fold form is to idealize its conditions of folding and determine the corresponding theoretical fold form, for which the distributions of amplitudes are known. This method is relatively simple but limits the accuracy of the analysis to that of the existing theoretical models. An alternative procedure would be to analyze the shapes of actual interface waveforms. This method would identify the number of component waveforms and perhaps suggests the order of accuracy required adequately to describe the fold.

In the theoretical analysis I derive amplitudes of component waveforms in interfaces between layers and compute the theoretical fold forms by synthesizing the waveforms. One can reverse the process for fold forms in the field or laboratory by performing least-squares analyses of each interface using Fourier series. If the origin of coordinate $\underline{x}$ is selected at the axis of the Tuscarora Mountain anticline (Fig. 25A), the height of each interface can be described by a cosinusoidal Fourier series

$$\zeta = \zeta_0 + {}_1A\cos(\ell x) + {}_2A\cos(2\ell x) + {}_3A\cos(3\ell x) + \ldots\ {}_nA\cos(n\ell x) \qquad (32)$$

in which ζ_0 is the mean height for that interface, ${}_i\underline{A}$ are amplitudes of component waveforms, and $\ell = 2\pi/L$, in which $\underline{L}$ is the wavelength of the first waveform. Stabler (1968) and Hudleston (1973) explain the application of Fourier analysis to determination of interface shape.

Using least-squares analysis, I determined amplitudes of the first five component waveforms in eq. (32) that best describe the forms of individual interfaces shown in Fig. 25B; I sequentially recombined those component waveforms to discover the contribution of each one to interface form (Fig. 26). In the fold form determined by the first waveform alone (Fig. 26A), each interface shape is purely cosinusoidal,

Figure 26. Results of Fourier analysis of gross fold form shown in Fig. 25B. A. Form according to first waveform. B. Form synthesized from first and second waveforms. C. First, second, and third waveforms. D. First through fourth waveforms. E. First through fifth waveforms. The gross form of the large folds in Fig. 25B is reproduced with the first through third waveforms, C; the fold with shorter wavelengths in Silurian and Ordovician rocks do not appear until the fourth and fifth waveforms are added, in D and E.

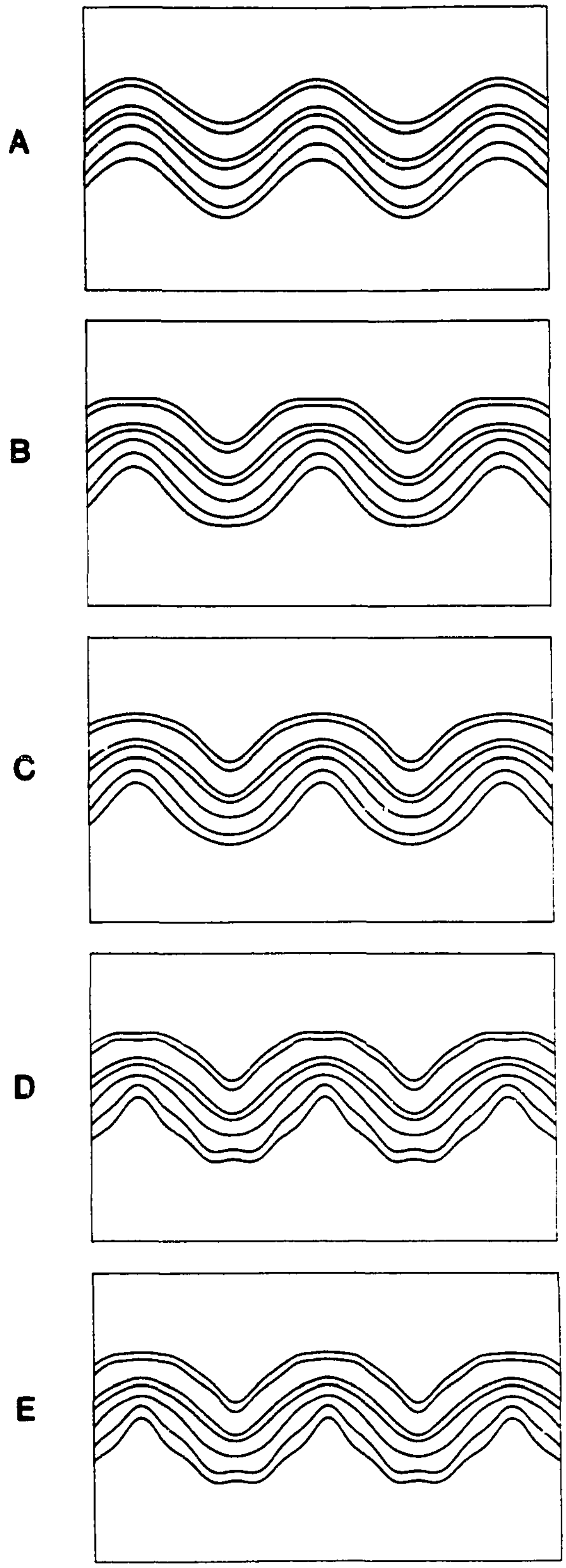
A
B
C
D
E

and the fold form poorly matches the gross form constructed on the basis of field information (Fig. 25B). Summing the first and second waveforms in each interface produces a fold form in which the crests are flattened and the troughs are sharpened in upper interfaces (Fig. 26B). Summing the first through third waveforms (Fig. 26C) further sharpens the synclines but rounds the anticlines. The fourth waveform re-flattens the crests and produces waviness in the lower two interfaces (Fig. 26D), and the fifth waveform has insignificant effect on fold form (Fig. 26E). On the bases of this analysis of component waveforms and the high slopes of the actual interfaces, I would suggest that a theoretical analysis carried to at least 4th order in maximum slopes of the first waveforms would be required to simulate closely the forms of folds shown in Fig. 25B. This example from the Appalachians serves to illustrate, however, that the gross forms of the folds can be understood using the 3rd order analysis and some deductions about the conditions of folding.

Folds in Riverbank Exposure, Huasna Syncline

Figure 27A is a composite, down-plunge cross section of the southern end of the Huasna syncline, centered about 15 km north of Santa Maria and 20 km southeast of San Luis Obispo, California (Johnson and Page, 1976). The Huasna syncline is about 30 km long and 12 km wide and plunges 20 to 30 degrees at its southern end. At midlength, the syncline is exposed within Pliocene sandstones, where it is broad and open, with gently dipping limbs. In the southern part (Fig. 27A), it is exposed within Oligocene to Pliocene rocks and ranges from an open form

Figure 27. Forms of folds in southern end of Huasna syncline, California, as determined by constructing a down-plunge cross section (from Johnson and Page, 1976, fig. 6). A. Down-plunge section, showing folds with several distinct wavelengths. B. Ideal form of folds in Riverbank Exposure, showing how the folds probably would appear had they not formed near the crest of a larger anticline. Solid lines are relatively well-controlled contacts; dashed lines are estimated.

A

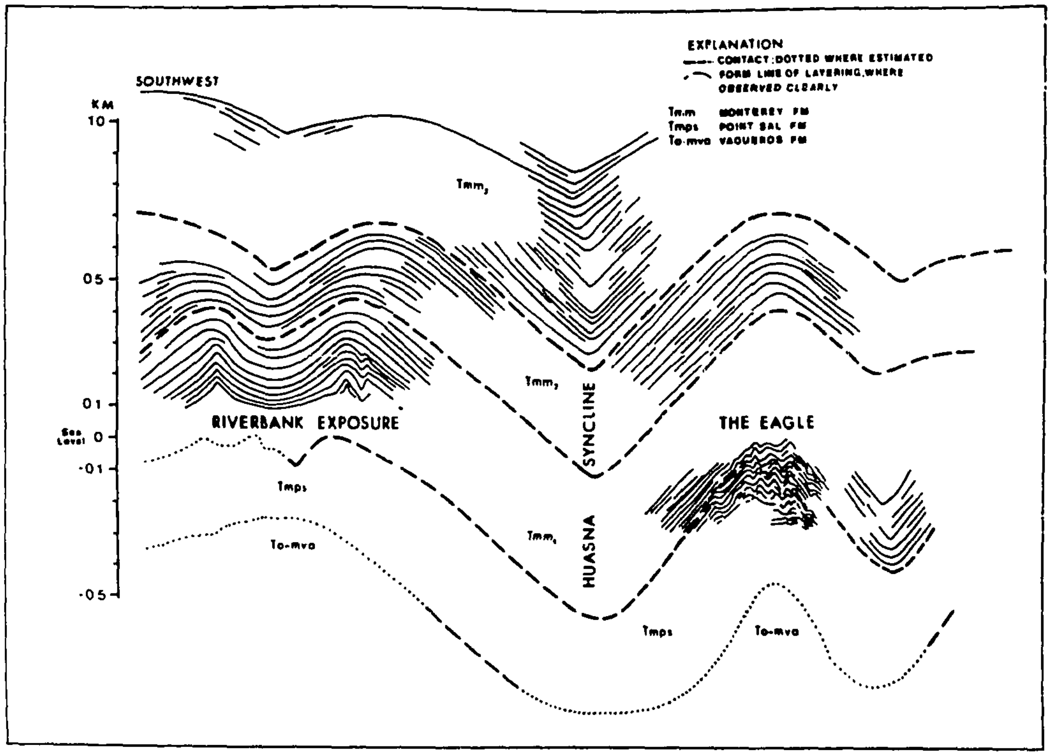
EXPLANATION
CONTACT: DOTTED WHERE ESTIMATED
FORM LINE OF LAYERING, WHERE OBSERVED CLEARLY
Tm.m MONTEREY FM
Tmps POINT SAL FM
To-mvo VAQUEROS FM
SOUTHWEST
KM
10
05
01
Sea Level 0
-01
-05
RIVERBANK EXPOSURE
HUASNA SYNCLINE
THE EAGLE
Tmps
To-mvo

B

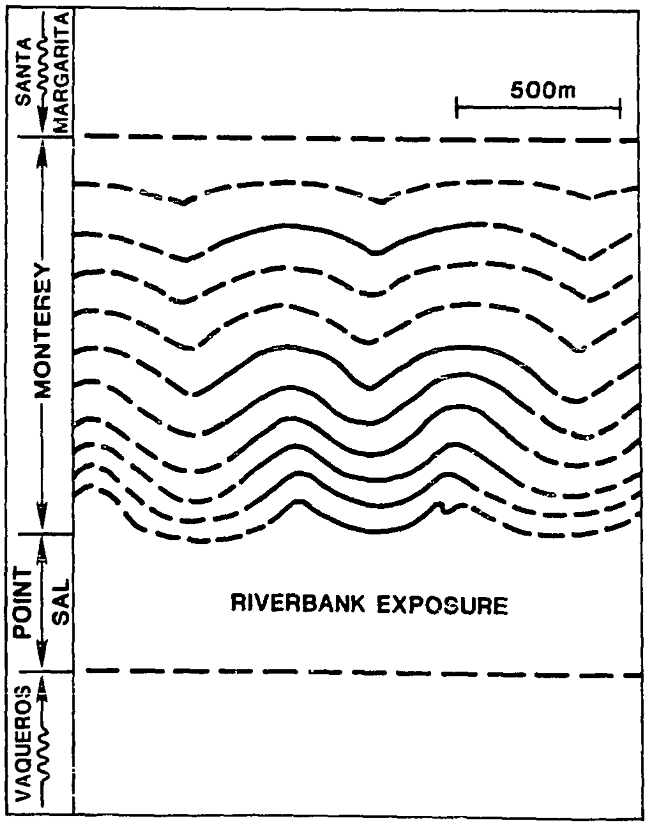
SANTA MARGARITA
MONTEREY
POINT SAL
VAQUEROS
500m
RIVERBANK EXPOSURE

with gentle limbs in Pliocene rocks to a tight chevron-like form in underlying Middle Miocene rocks.

At either side of the axis of the Huasna syncline, within the Monterey Formation, are smaller folds with wavelengths on the order of one-half to one km. I will analyze the folds labeled "Riverbank Exposure" in the left half of the structural section (Fig. 27A) because their good exposure along the bank of the Cuyama River and in road cuts permits observation of fold form and measurement of folding parameters. The idealized shapes of these folds are nearly classic concentric-like forms, with open outer arcs and sharply bent layers in cores (Fig. 27B). The forms grade upward, toward the contact with the Pliocene Santa Margarita Formation, into smooth, broad warps with narrow pinches; they grade downward, in the lower part of the Monterey Formation and the upper part of the Point Sal Formation, into intense and chaotic folding similar in scale to that at The Eagle (Fig. 27A).

Field study of the rocks involved in the Riverbank Exposure folding (Johnson and Page, 1976) indicates that folding in the Monterey was controlled by structural-lithic units which are 30 to 40 m thick, bounded by gouge zones 1 to 3 cm thick, and composed of lithologic layers which are only 0.5 to 8 cm thick. In addition, there are small faults oriented at an acute angle to bedding which accommodated 4 to 10 cm of reverse slip and which are spaced 30 to 35 m apart. The spacing between crests of the anticlines is about 500 m, and about 1.2 km of section is involved in the folding, so the ratio of wavelength to total thickness, (L/H), for the Riverbank folds is about 0.42. The structural units involved in the folding shown in Fig. 27B: are relatively massive sandstone below (Vaqueros Fm.); overlain by interbedded soft shale and siliceous shale and dolomite (Point Sal Fm.), containing numerous surfaces and zones of slip; which, in turn, are overlain by predominant siliceous shale and porcelanite (Monterey Fm.) with surfaces of bedding-plane slip spaced 30 to 40 m apart; all of which is overlain by relatively massive sandstone (Huasna member, Santa Margarita Fm.) (Johnson and Page, 1976).

These field observations, which suggest that the multilayered rock behaved much as a series of stiff layers between which slip was accommodated in thin shear zones, can be represented theoretically as a simple, repetitive multilayer. There is no reason to suspect significant differences in viscosities of layers, so I assume that $\mu_1 = \mu_2$. I assume that layer contacts were frictionless, for example as a result of high pore-water pressure. I also assume that the rocks above and below behaved as homogeneous, viscous media, with thicknesses somewhat greater than the wavelength of the folds, so I treat the media as infinite half spaces.

According to eq. (7d), for these conditions, the dominant wavelength for rigid media would be

$$(L_d/H)_R \cong 1.9 \sqrt[2]{1/N}$$

where $\underline{N}$ is the number of layers. The field observations indicate that $\underline{h}_1$ = 30 to 40 m, so I assume $\underline{h}_1$ = 35 m. The total section involved in folding is about $\underline{H}$ = 1200 m, so $\underline{N} \cong 34$, and $(L_d/H)_R \cong 0.33$. Using this value, and assuming that the media have the same stiffness as the layers, $\mu_m/\mu_n = 1$, one computes the dominant wavelength for stiff media, according to Fig. 12B, as $(L_d/H)_S \cong 0.38$.

On the other hand, if the medium below is one hundredth as stiff as the layers,

$$\mu_m = (\mu_U + \mu_L)/2 = (\mu_1 + 0.01\mu_1)/2 \simeq 0.51\mu_1$$

and $\mu_m/\mu_n = 0.51$. According to Fig. 12B, $(L_d/H)_S \simeq 0.43$. Thus $(L_d/H)_S$ is estimated as 0.38 to 0.43. This range includes the measured value of 0.42.

If the low-angle faults are included as boundaries between structural-lithic units, then the average thickness of units would be estimated to be on the order of 15 m, and the number of layers would be about 80. In this case, the dominant wavelength ratio would be 0.27 if the upper and lower media were both stiff. This is much smaller than both the ratio of 0.38 computed for 34 layers and the observed ratio of about 0.42.

The wavelength of the folds in the Riverbank Exposure may be closer to the preferred wavelength than the dominant wavelength, because the wavelength of the perturbation that amplifies the most for a given amount of stretch is the preferred wavelength. However one needs to know or to be able to estimate the shortening in order to compute the preferred wavelength. I do not know the amount of shortening responsible for the folds in the Riverbank Exposure, but the amount should not be less than the difference between the wavelength, $\underline{L}$, and the arclength, $\underline{s}$. According to estimates from Fig. 27B, $(s-L)/s = 1/7$ to $1/11$, so the amount of shortening was 9 to 14 percent. Let us assume 15 percent. Then the stretch $\underline{\bar{S}}_x = (1.0 - 0.15) = 0.85$ and, according to eq. (27a), the preferred wavelength ratio is

$$(L_p/H)_S = \bar{S}_x(L_d/H)_S = 0.85(L_d/H)_S \simeq 0.32 \text{ to } 0.37$$

This is somewhat lower than the ratio of 0.42 observed in the structural cross section. It would seem, then, that the average number of structural units involved in the folding was even less than the 34 units estimated by examination of part of the section involved in the folding.

The folds in the Riverbank Exposure (Fig. 27B) appear to be hybrids, reflecting an overlying confining medium with properties similar to those of the stiff layers and an underlying medium that is soft. These conditions most closely match those for the theoretical multilayer shown in Fig. 14, loc. B3, turned upside down because the multilayer shown at loc. B3 is confined by a stiff medium below and no medium above. The fold forms in Fig. 27B also resemble closely those in loc. B3.

The component waveforms needed to describe the form of the reconstructed Riverbank Exposure folds (Fig. 27B) can be identified using eq. (32) and the method described in the preceding example. Data only from the observed contacts, represented by solid lines in Fig. 27B, were used in the Fourier analysis. Fourth and fifth waveforms contribute insignificantly to the correspondence between the reconstructed form (Fig. 27B) and the synthesized form (Fig. 28).

Experimental Folds in Elastic Multilayers

Folds with a wide range of forms have been produced in multilayers composed of materials with a variety of properties, including rubber, gelatin, paper cards, potter's clay, modeling clay, silly putty, foliated rocks and single crystals (e.g., Kuenen and DeSitter, 1938; Currie, Patnode and Trump, 1962; Ramberg, 1963b; Ghosh, 1968; Donath, 1968; Weiss, 1968; Hudleston, 1973; Johnson, 1977; Latham, 1979). Here consideration will be restricted to multilayers of elastic materials, for two reasons: First, the conditions of the experiments are known. Second, using the same materials to produce fold forms of various types provides experimental control; the possibility that the fold forms are solely a result of peculiar properties of the layers themselves, such as plastic or brittle yielding, can be eliminated. The experiments show that fold forms can be changed merely by changing certain experimental conditions.

Fold forms developed in experimental multilayers consisting of stiff rubber strips and soft gelatin are shown in Fig. 29. Column 1 shows fold forms produced in multilayers with free slip at interfaces or in multilayers of interbedded stiff and soft materials with bonded contacts. Column 2 shows fold forms produced in multilayers of

Figure 28. Fourier analysis of first three waveforms for folds in Riverbank Exposure, Fig. 27B. Only solid lines in Fig. 27B used for analysis. A. First waveforms only. B. First plus second waveforms. C. First through third waveforms. The second waveform flattens crests or troughs of several bedding surfaces, and the third waveform primarily rounds troughs and sharpens crests in the bottom bedding surface.

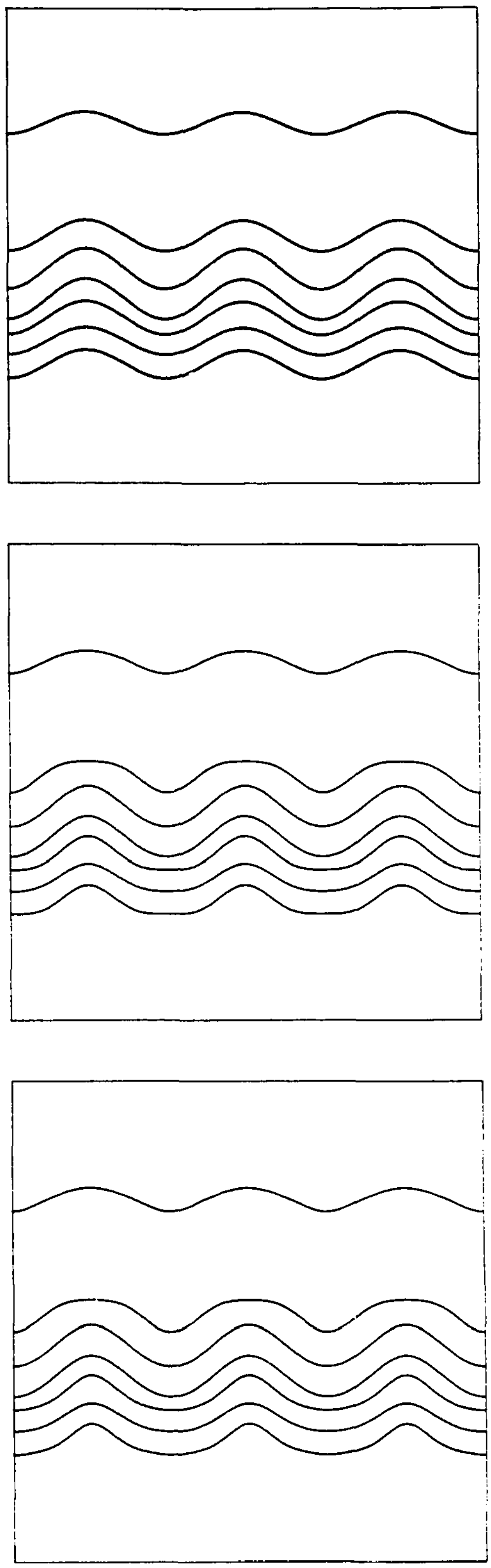

A

B

C

Figure 29. Fold forms developed in experimental multilayers consisting of stiff rubber strips and soft gelatin. Drawn from photographs. Two stages (I, II) in the development of the folds are shown for each multilayer. All subjected to layer-parallel shortening and layer-normal thickening. Column 1: Multilayers with lubricated contacts or interbedded stiff and soft layers. Loc. A1, stiff layers with lubricated contacts confined by rigid media. Loc. B1, interbedded stiff and soft layers confined by rigid media. Loc. C1, interbedded stiff and soft layers. Thickness ratio $h_2/h_1 = 3$. Confined by medium-soft media. Loc. D1, interbedded stiff and soft layers confined by soft media. Thickness ratio $h_2/h_1 = 1$. Column 2: Multilayers of stiff layers in frictional contact with one another. At loc. A2 the media are rigid, and at loc. D2 the media are soft. At loc. D2, the upper half of the multilayer is composed of thin layers and the lower half is composed of thick layers.

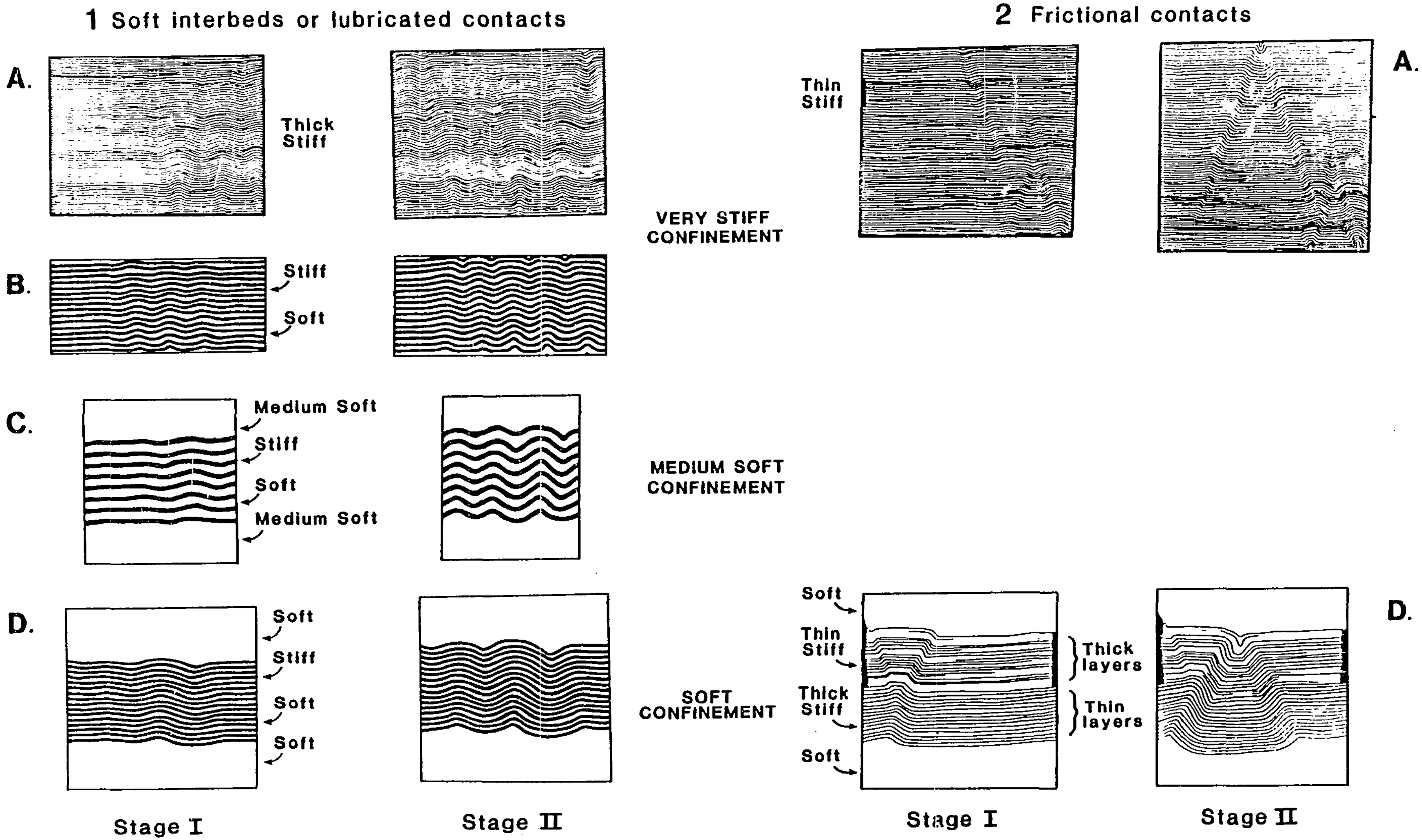

1 Soft interbeds or lubricated contacts
2 Frictional contacts
A.
Thick Stiff
Thin Stiff
A.
VERY STIFF CONFINEMENT
B.
Stiff
Soft
C.
Medium Soft
Stiff
Soft
Medium Soft
MEDIUM SOFT CONFINEMENT
D.
Soft
Stiff
Soft
Soft
SOFT CONFINEMENT
Soft
Thin Stiff
Thick Stiff
Soft
Thick layers
Thin layers
D.
Stage I
Stage II
Stage I
Stage II

identical layers with significant contact strength (friction), making slippage difficult. The latter folds are kink-like, a form that I investigate in Chapter II by treating contact strength via a film of powerlaw material at layer contacts.

All the theoretical forms described in this chapter have been derived by assuming zero slip at contacts (bonded) or free slip at contacts (zero friction), and none of the forms resembles the kink-like folds shown in Fig. 29, column 2.

The two figures at loc. A1 show two stages in the development of folds in a multilayer consisting of 68 rubber strips confined by stiff media. The contacts between strips were lubricated with silicone grease. As the multilayer was shortened parallel to layers, folds initiated and grew near the right-hand end of the multilayer (stage I), but with further shortening folds developed throughout the width of the multilayer (stage II). The form of the folds is nearly identical to the ideal <u>constrained</u>, <u>internal folds</u> (Fig. 2, loc. A3), particularly in the example with 40 identical stiff viscous layers (Fig. 3).

In elastic materials, the wavelength of the fold is essentially the dominant wavelength; the concept of a preferred wavelength is irrelevant. Therefore, wavelengths of these experimental folds will be compared to dominant wavelengths predicted by theory. According to the elementary theory, eq. (7d), the dominant wavelength ratio should be,

$$(L_d/H)_R \cong 1.9 \sqrt[2]{1/N} \cong 0.23; \quad (N = 68)$$

if contacts between layers were frictionless. The wavelength-to-thickness ratio for folds shown at middepth in Fig. 29, loc. A1, stage I, is about 0.26. The average wavelength ratio for the four complete anticlines at middepth in Fig. 29, loc. A1, stage II, is about 0.24; the ratio for only the two larger anticlines on the right is about 0.26. Thus the observed wavelengths closely correspond to, but are slightly larger than, the dominant wavelengths predicted by the elementary theory. The 1st order part of the exact theory developed here would predict the same dominant wavelength as the elementary theory (Fig. 17A).

Figure 29, loc. B1, shows two stages in the development of folds in a multilayer of interbedded stiff and soft layers confined above and below by essentially rigid media. The folds in stage II are internal folds (*e.g.*, Fig. 2A), with the characteristic flats and pinches near the upper and lower boundaries of the multilayer. The contacts are bonded; the modulus ratio of the stiff and soft layers is $G_1/G_2 = 45$; and the thickness ratio is $h_1/h_1 = 1$. Assuming a viscosity ratio of $\mu_1/\mu_2 = 45$, the normal viscosity of the multilayer (eq. 1b) is

$$\mu_n/\mu_1 = [1/(h_1+h_2)][h_1+(\mu_2/\mu_1)h_2] = 0.51$$

and the dominant wavelength ratio is, according to the elementary theory (eq. 7c),

$$(L_d/H)_R = 1.9 \sqrt[2]{1/N_p} \sqrt[4]{(\mu_1/\mu_n)/(1+h_2/h_1)^3} = 0.34$$

in which $\underline{N}_p$ is the number of pairs of stiff and soft layers ($\underline{N}_p = 16$). Compared to the exact, 1st order theory presented here, the elementary theory slightly underestimates the dominant wavelength ratio for a viscosity ratio of stiff to soft layers of ten (Fig. 17B), so it presumably underestimates the wavelength ratio for a viscosity ratio of 45. The average wavelength ratio for the three anticlines at middepth in Fig. 29, loc. B1, stage I, is 0.36, and that for five anticlines at middepth in stage II is 0.35, so the elementary theory, again, slightly underestimates the wavelengths in the elastic materials.

Figure 29, loc. C1, shows folds in a multilayer of interbedded stiff and soft layers confined by moderately soft media: $G_1/G_2 = 67$ and $G_1/G_m = 28$. The thickness of soft layers is three times the thickness of stiff layers: $h_1/h_2 = 1/3$. The 3rd order theoretical fold form that is most closely analogous to the fold form shown in Fig. 29, loc. C1, is shown in Fig. 5B. In the theoretical fold, however, the ratios are $\mu_1/\mu_2 = 10$ and $\mu_1/\mu_m = 10$, so the contrast in material properties is much stronger in the experimental example than in the theoretical example. Nevertheless, the tendency for the fold form to be <u>similar</u> if the degree of independence of stiff layers, $\underline{d}$, is large (Fig. 5), is apparent in the experimental folds, Fig. 29, loc. C1, even though $\underline{d}$ is only about 0.20.

The dominant wavelength is calculated by assuming that $h_2/h_1 = 3$; $\mu_1/\mu_m = 28$; $\mu_1/\mu_2 = 67$; and that $\underline{N} = 8$. In order to use Fig. 12B to compute the dominant wavelength for soft media, eq. (7c) must first be used to compute the dominant wavelength for the same multilayer confined by rigid media. According to eq. (1b), $\mu_n/\mu_1 = 0.26$, and according to eq. (7c), $(L_d/H)_R = 0.33$. The ratio of normal viscosity of the multilayer to viscosity of the media is $\mu_n/\mu_m = 7.3$, so according to Fig. 12B, $(L_d/H)_S \simeq 0.62\ (0.906) \simeq 0.56$. The factor 0.906, which corrects for the thickness of the multilayer, is required because elementary theory assumes soft interbeds on either side of stiff layers, whereas in the experiment outer stiff layers contact the confining media. The wavelength ratio of low-amplitude folds shown in Fig. 29, loc. C1, stage I, is about 0.53, so the elementary theory narrowly overestimates the wavelength for these folds.

Finally, the form of experimental folds in a multilayer composed of 16 stiff and 15 soft layers confined by soft media ($G_1/G_2 = 22 = G_1/G_m$; $h_1/h_2 = 1$) is a nearly perfect concentric-like form (Fig. 29, loc. D1). Contacts between layers are bonded, so the experimental conditions are most like the theoretical conditions assumed in the derivation, to 3rd order accuracy, of Fig. 1. The concentric-like form was shown to be characteristic of multilayers with low $\underline{d}$, confined by soft media, and folded to moderate amplitudes. At loc. D1, $\underline{d} \simeq 0.05$, as compared to $\underline{d} \simeq 0.20$ for the folds shown at loc. C1.

The wavelength of the experimental folds is analyzed by assuming that $\mu_1/\mu_2 = 22 = \mu_1/\mu_m$. Thus, $\mu_n/\mu_1 = 0.52$ and, according to eq. (7c), $(L_d/H)_R = 0.33$. Further, $\mu_n/\mu_m = 11.4$, so according to Fig. 12B, $(L_d/H)_S = 0.70$ to 0.74. Measurements of folds shown in Fig. 29, loc. D1, result in a calculated wavelength ratio of 0.73 to 0.74, essentially the same as the dominant wavelength ratio computed with the elementary theory.

The results presented here indicate that fold forms in viscous materials are nearly identical to those produced experimentally in elastic materials, including experimental folds shown by Currie, Patnode, and Trump (1962), Ramberg (1963b), and Johnson and Honea (1975). The close correspondence of fold forms indicates that the forms are controlled largely by nonlinearities in equations that describe boundary conditions at contacts between layers, which are the same for elastic and viscous materials, rather than by nonlinearities in the material behaviors, which exist for elastic materials (Johnson, 1977, Ch. 10) but not for viscous materials. One significant difference between folding of elastic and viscous multilayers is that the chevron form typically is weakly developed at the preferred wavelength in viscous materials (Figs. 1, 2, and 5), whereas it can be strongly developed in elastic materials (Fig. 29, loc. D1; also, Johnson and Ellen, 1974, fig. 20). Although the chevron form can be produced in viscous multilayers if wavelengths of folds are relatively short (Fig. 4B), a strong chevron form probably generally reflects some kind of yielding within layers at hinges, a phenomenon that is lacking in the viscous material but is possible in elastic, elastic-plastic, and nonlinear fluid materials (Johnson, 1977).

REFERENCES

Aytuna, S., 1984. Forms of Large Folds in the Central Appalachians, Pennsylvania. Ph.D. Dissertation, Department of Geology, University of Cincinnati, Cincinnati, Ohio, 228 pp.

Bayly, M. B., 1974. An energy calculation concerning the roundness of folds. Tectonophysics, 24: 291-316.

Biot, M. A., 1957. Folding instability of a layered viscoelastic medium under compression. Proceedings of the Royal Society of London, Ser. A, 242: 444-454.

Biot, M. A., 1959. On the instability and folding deformation of a layered viscoelastic medium in compression. Journal of Applied Mechanics, 26: 393-400.

Biot, M. A., 1961. Theory of folding of stratified viscoelastic media and its implications in tectonics and orogenesis. Geological Society of America Bulletin, 72: 1595-1620.

Biot, M. A., 1963. Internal buckling under initial stress in finite elasticity. Proceedings of the Royal Society of London, Ser. A, 273: 306-328.

Biot, M. A., 1964. Theory of internal buckling of a confined multilayered structure. Geological Society of America Bulletin, 75: 563-568.

Biot, M. A., 1965a. Further development of the theory of internal buckling of multilayers. Geological Society of America Bulletin, 76: 833-840.

Biot, M. A., 1965b. Theory of similar folding of the first and second kind. Geological Society of America Bulletin, 76: 251-258.

Chapple, W. M. and Spang, J. H., 1974. Significance of layer-parallel slip during folding of layered sedimentary rocks. Geological Society of America Bulletin, 85: 1523-1534.

Cobbold, P. R., Cosgrove, J. W. and Summers, J.M., 1971. Development of internal structures in deformed anisotropic rocks. Tectonophysics, 12: 23-53.

Currie, J. B., Patnode, H. W. and Trump, R. P., 1962. Development of folds in sedimentary strata. Geological Society of America Bulletin, 73: 655-674.

Donath, F. A., 1968. Experimental study of kink-band development in strongly anisotropic rock. In: A. J. Baer and D. K. Norris (Editors), Proceedings, Conference on Reseach in Tectonics. Geological Society of Canada Paper 68-52: 255-293.

Fletcher, R. C., 1974. Wavelength selection in the folding of a single layer with power-law rheology. American Journal of Science, 274: 1029-1043.

Fletcher, R. C., 1977. Folding of a single viscous layer: Exact infinitesimal-amplitude solution. Tectonophysics, 39: 593-606.

Fletcher, R. C., 1979. The shape of single-layer folds at small but finite amplitude. Tectonophysics, 60: 77-87.

Fletcher, R. C., 1982. Analysis of the flow in layered fluids at small, but finite, amplitude with application to mullion structures. Tectonophysics, 81: 51-66.

Ghosh, S. K., 1968. Experiments of buckling of multilayers which permit inter-layer gliding. Tectonophysics, 6: 207-249.

Honea, E. and Johnson, A. M., 1976. Part IV, Development of sinusoidal and kink folds in multilayers confined by rigid boundaries. Tectonophysics, 30: 197-239.

Hudleston, P. J., 1973. Fold morphology and some geometrical implications of theories of fold development. Tectonophysics, 16: 1-46.

Johnson, A. M., 1969. Development of folds within Carmel Formation, Arches National Monument, Utah. Tectonophysics, 8: 31-77.

Johnson, A. M., 1970. Physical Processes in Geology. Freeman, Cooper and Company, San Francisco, 577 pp.

Johnson, A. M., 1977. Styles of Folding. Elsevier, New York, 406 p.

Johnson, A. M., 1982. Fold forms in multilayers--A study for students. Unpublished manuscript. Presented in lecture to Geological Society London, 28 April. Geology Library, University of Cincinnati, Cincinnati, Ohio, 93 pp.

Johnson, A. M. and Ellen, S. D., 1974. A theory of concentric, kink, and sinusoidal folding and of monoclinal flexuring of compressible, elastic multilayers. Part I, Introduction. Tectonophysics, 21: 301-339.

Johnson, A. M. and Honea, E., 1975. Part III, Transition from sinusoidal to concentric-like to chevron folds. Tectonophysics, 27: 1-38.

Johnson, A. M. and Page, B. M., 1976. Part VII, Development of folds within Huasna syncline, San Luis Obispo County, California. Tectonophysics, 33: 97-143.

Kuenen, Ph. H. and De Sitter, L. U., 1938. Experimental investigation into the mechanism of folding. Leidsche Geologische Mededeelingen, 9: 217-239.

Latham, J-P., 1979. Experimentally developed folds in a material with a planar mineral fabric. Tectonophysics, 57: T1-T8.

Latham, J-P., 1985a. The influence of nonlinear material properties and resistance to bending on the development of internal structures. Journal of Structural Geology, 7: 225-236.

Latham, J-P., 1985b. A numerical investigation and geological discussion of the relationship between folding, kinking, and faulting. Journal of Structural Geology, 7: 237-249.

Nickelsen, R. P., 1963. Fold patterns and continuous deformation mechanisms of the central Pennsylvania folded Appalachians. In: Pittsburgh Geological Society, Guidebook, Tectonics and Cambrian-Ordovician Stratigraphy, Central Appalachians of Pennsylvania, 13-29.

Ramberg, H., 1959. Evolution of ptygmatic folding. Norsk Geologisk Tidsskrift, 39: 99-152.

Ramberg, H., 1962. Contact strain and folding instability of a multilayered body under compression. Geologische Rundschau, 51: 405-439.

Ramberg, H., 1963a. Fluid dynamics of viscous buckling applicable to folding of layered rocks. American Association of Petroleum Geologists, 47: 484-505.

Ramberg, H., 1963b. Strain distribution and geometry of folds. Bulletin of the Geological Institutions of the University of Uppsala, 42: 1-20.

Ramberg, H., 1964. Selective buckling of composite layers with contrasted rheological properties, A theory for simultaneous formation of several orders of folds. Tectonophysics, 1: 307-341.

Ramberg, H., 1970. Folding of laterally compressed multilayers in the field of gravity I; II. Physics of the Earth and Planetary Interiors, 2: 203-232 (Part I); 4: 83-120 (Part II).

Ramberg, I. B. and Johnson, A. M., 1976. Part V, Asymmetric folding in interbedded chert and shale of the Franciscan Complex, San Francisco Bay area, California. Tectonophysics, 32: 295-320.

Sherwin, J. and Chapple, W. M., 1968. Wavelengths of single layer folds: A comparison between theory and observation. American Journal of Science, 266: 167-179.

Smith, R. B., 1975. Unified theory of the onset of folding, boudinage, and mullion structure. Geological Society of America Bulletin, 86: 1601-1609.

Smith, R. B., 1977. Formation of folds, boudinage, and mullions in non-Newtonian materials. Geological Society of America Bulletin, 88: 312-320.

Smith, R. B., 1979. The folding of a strongly non-Newtonian layer. American Journal of Science, 279: 272-287.

Stabler, C. L., 1968. Simplified Fourier analysis of fold shapes. Tectonophysics, 6: 343-350.

Suppe, J., 1983. Geometry and kinematics of fault-bend folding. American Journal of Science, 283: 684-721.

Van Hise, C. R., 1896. Principles of North American pre-Cambrian Geology. U. S. Geological Survey, 16th Annual Report, 571-874.

Weiss, L. E., 1968. Flexural-slip folding of foliated model materials. In: A. J. Baer and D. K. Norris (Editors), Proceedings, Conference on Research in Tectonics. Geological Survey of Canada Paper 68-52: 294-333.

CHAPTER II

FORMATION OF KINK AND BOX FOLDS IN VISCOUS MULTILAYERS

ABSTRACT

Different forms of folds can be produced by shortening of identical viscous multilayers merely by changing the wavelengths of folds and the behavior of layer contacts.

Theoretical analysis presented here shows that the folds are kink or box forms if slip is localized along short segments of layer contacts; slip is localized if interfaces have finite adhesional strength or some other type of nonlinear resistance to slip. The folds are concentric-like or chevron forms if slip is distributed all along layer contacts; slip is distributed if interfaces have low adhesional strength or constant resistance to slip.

The theory also shows that different forms of folds can be produced in identical viscous multilayers by changing the wavelength of folds relative to the thickness of the multilayer being folded. Parallel folds, including kink and concentric-like forms, develop if the thickness of the multilayer is on the order of the folding wavelength. Similar folds, such as box and chevron forms, develop if the thickness of the multilayer is large compared to the folding wavelength.

INTRODUCTION

Several quite different methods of research have focused on causes of kink folds, which are bands or, more typically, sets of bands of finite width within which foliated elements are rotated relative to those outside the bands (Fig. 1). One method is experimentation and is represented by a relatively rich literature (Paterson and Weiss, 1966; Ghosh, 1968; Donath, 1968; Weiss, 1968; Johnson, 1970; Ellen, 1971; Cobbold and others, 1971; Scofield, 1975; Ramberg and Johnson, 1976; Reches and Johnson, 1976). The experiments, which have involved such diverse materials as phyllite, decks of paper cards, plasticene, rubber, potter's clay, and cardboard, demonstrate that kink folding can occur as a result of layer-parallel compression of strongly foliated materials with a variety of properties and subject to boundary conditions ranging from rigidly confined to softly confined. In addition to indicating the general conditions necessary for kink folding to occur, the experiments provide opportunities to observe the inception, growth, and propagation of kink bands.

Another method of research is field observation, which has largely verified that the kinds of structures observed in experiments closely resemble those observed in foliated

Figure 1. Kink fold near Northumberland, Pennsylvania at the confluence of the east and west branches of the Susquehanna River in the central Appalachians. The short limb of the fold defines the kink band, which dips steeply to the right. Beds within the kink band are rotated relative to those outside the kink band.

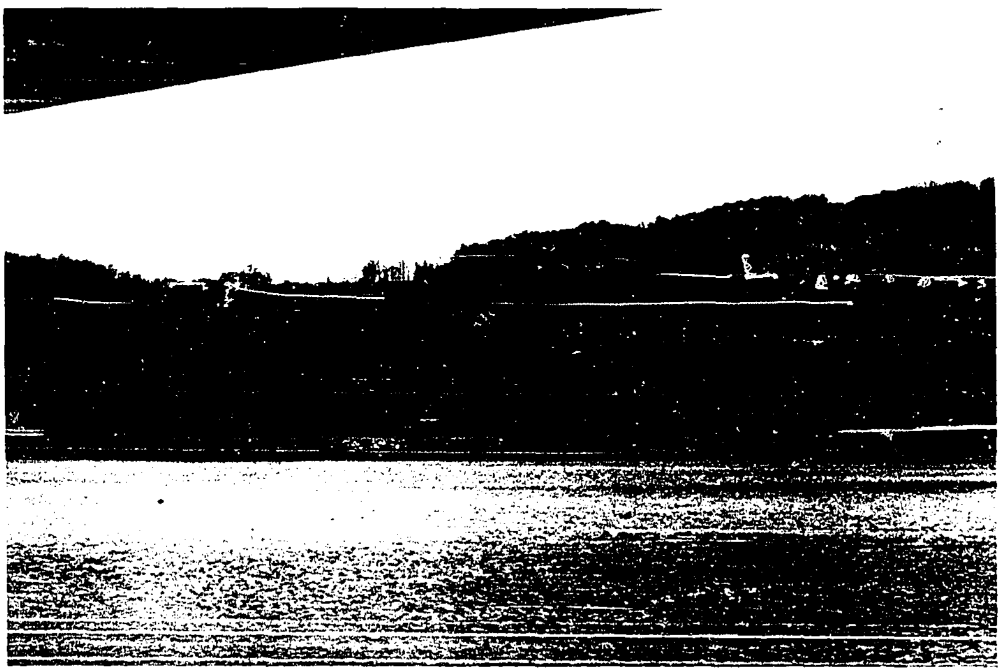

materials in the field (e.g., Dewey, 1965; Clifford, 1968; Anderson, 1968; Ellen, 1971; Ramberg and Johnson, 1976).

A third method is theoretical analysis. To date, theoretical analyses of kink folding have followed two directions. One, introduced by Biot (1965a), treats multilayers as continua and investigates conditions under which the differential equations governing such continua have different types of solutions. For example, Biot (1965b) suggested that folds of "the first kind" (sinusoidal, internal instability) form in materials in which the normal modulus (of elasticity) is greater than the shear modulus and that folds of "the second kind" (kink) form in materials in which the shear modulus is greater than the normal modulus. The latter conditions are associated with the existence of two or four real characteristics, which allow certain discontinuities to exist. Thus, the Biot approach recognizes that kink folds form in highly foliated materials and represents the foliated materials by anisotropic elastic materials.

Biot's approach to kink folding was followed subsequently by Johnson (1970), Cobbold and others (1971), Ellen (1971), and Latham (1985a, 1985b). Ellen (1971) recognized that real characteristics could not exist for the simple elastic materials discussed by Biot, so he analyzed elastic-plastic materials. Latham (1985a, 1985b) reworked the Biot method and concluded that four real characteristics can exist in layers of powerlaw rheology. Latham (1985a) added couple stresses to the behavior of the fundamental element of the foliated material in order to account for bending resistance. Biot's approach was the basis for a discussion of relations between lines of discontinuity and various kinds of faults, folds, and flexures (Johnson and Ellen, 1974) and for studies of conditions that favor folding on the one hand and faulting on the other (Johnson, 1980; Latham, 1985b).

The second theoretical approach to kink folding treats multilayers as stacks of discrete layers with contact strength. This approach originated during a study of axial fracturing and subsequent faulting by buckling of bands containing small columns of rock in granite (Peng and Johnson, 1972) and was subsequently applied to research on fold forms (Honea and Johnson, 1976; Reches and Johnson, 1976; Collier, 1978). Layers were assumed to behave as elastic materials. Contact properties were represented by simple adhesion or by Coulomb strength, involving both adhesion and friction. Honea and Johnson (1976) showed that finite adhesional contact strength can result in the development of kink forms in elastic multilayers by allowing slip to occur only locally along layer contacts.

My research follows this second theoretical approach. I consider multilayers composed of discrete layers so that I can investigate details of fold form. This has an advantage over the Biot approach, which focuses on the characteristics that the theory generates rather than on fold form. The Biot approach, however, has the advantage of being able to investigate discontinuous structures. I treat linear viscous layers because the folding of viscous material is easier to analyze than the buckling of elastic material and because viscous material probably more closely resembles the behavior of rocks than does elastic material. I model nonlinear resistance to slip at layer contacts either by representing the rate of slip at contacts as a nonlinear function of the contact shear stress or by including thin interbeds of nonlinear material between thick viscous layers. My models of nonlinear resistance to slip at contacts closely relate to adhesional contact strength, which is a highly nonlinear resistance to slip.

My theoretical analysis differs from that of Honea and Johnson (1976) in that it can model nonlinear resistance to slip at contacts using folding theory derived to 3rd order accuracy in slopes of interfaces. As a result, I can describe both the development of localized slip at layer contacts and the consequent evolution of a conjugate, kink-like fold from an initial, sinusoidal perturbation.

Methods of analyzing the folding of viscous layers to 1st order accuracy were developed by Biot (e.g., 1959, 1961, 1965a), Ramberg (e.g., 1962, 1970), Fletcher (1974, 1977), and Smith (1975, 1977). First order analyses provide dominant wavelengths and amplitude distributions for the initial perturbation. However, they are restricted to infinitesimal amplitudes and thus can only describe the initial, sinusoidal shape of the perturbation.

Study of non-sinusoidal fold forms requires higher order analyses. Fletcher (1979, 1982) extended the 1st order analysis to 2nd order accuracy in maximum slopes of interfaces of a layer. As a result, he was able to describe the evolution of a concentric-like fold from a sinusoidally perturbed single layer. My analysis of folding of viscous multilayers in Chapter I extends this method to 3rd order accuracy. The 3rd order analysis can treat relatively high-amplitude folding (maximum slopes of 25-30° in some problems).

Previous theoretical analyses of single- or multi-layer folding of viscous materials were unable to address localized slip because they were restricted either to bonded contacts, for which slip is zero, or to free slip, for which layers slip everywhere. By characterizing the behavior of layer contacts as a resistance to slip, I am able to model localized slip at layer contacts in addition to zero slip and free slip at contacts. In this chapter I incorporate the general model of contact properties into the equations which I have derived to 3rd order accuracy to describe the development of fold forms in viscous multilayers.

One purpose of this chapter is to investigate not only the conditions under which kink-like folds will form, but also the conditions under which they will not form. Honea and Johnson (1976) attempted to determine conditions under which idealized "kink folds" would develop on the one hand and "sinusoidal folds" would develop on the other. More recently, Latham (1985b) has used Biot's model (1965a), with powerlaw rheology of layers, to suggest conditions under which folds of various forms should develop. Latham (1985b) suggests that two parameters control fold form: "intrinsic anisotropy" and "induced anisotropy." Intrinsic anisotropy is defined as the ratio of the averaged normal modulus to the averaged shear modulus of the multilayer, and induced anisotropy is related to the power of the exponent of the powerlaw materials composing the multilayer. Latham suggests that, for low intrinsic anisotropy and low power, the folding is passive (kinematic). If intrinsic anisotropy is high and power is low, the folding is "similar" (actually, a combination of chevron folds and the pattern Biot terms "internal instability"). If intrinsic anisotropy is low and power is high, the multilayer faults or shears within narrow zones. Finally, if both anisotropy and power are high, kink folds form. These qualitative results are consistent with those suggested by Honea and Johnson (1976) and Johnson (1980).

As in the work by Honea and Johnson (1976), I focus on the properties of contacts between layers as the most likely seat of different forms of folds. I describe the behavior of contacts with a powerlaw model. My results will show that it is the nonlinear behavior (powerlaw exponent > 1.0) of the layer contacts that is responsible for the kink-like and box forms. Increasing the powerlaw exponent enhances the kink-like appearance of the theoretical fold forms. Linear behavior (powerlaw exponent = 1.0) of contacts results in sinusoidal, concentric-like, and chevron fold forms. Thus the power of the powerlaw exponent plays a critical role in the development of fold form, as noted by Latham (1985b).

The chapter is organized as follows. First, I describe the properties of contacts between layers and present the results of my theoretical analysis of fold forms in viscous multilayers by describing and geometrically analyzing the fold forms that develop for different types of layer contacts. Then I present the theoretical model. The influence of contact properties on fold form is investigated by solving equations for multilayers of infinite thickness. Analysis of multilayers with finite thickness shows the effect of confinement on the forms and growth of folds. The focus will be on multilayers with localized slip at layer contacts, but results for multilayers with bonded or frictionless contacts are presented for comparison.

THE REPRESENTATIVE MULTILAYER

The simple, repetitive multilayers I analyze in this chapter consist of identical layers of constant coefficient of internal viscosity (Fig. 2). Each multilayer is confined above and below by infinitely thick, viscous media and subjected to uniform rates of horizontal shortening and vertical thickening. The contacts between the top layer and the overburden and between the bottom layer and the substratum are frictionless, allowing free slip there.

Initial perturbations of interfaces between layers are positive cosinusoidal waveforms. The amplitudes and wavelengths are selected on the basis of an analysis of eigenvalues and eigenvectors, as will be explained in following pages. The maximum slope angle of the perturbation is initially one degree.

The model I have selected for contact properties relates rate of slip, $\delta \underline{v}_s$, between layers to magnitude of shear stress, σ_{ns}, applied at contacts (Fig. 3). Each layer contact is represented by some specified resistance to slip described for the general case by a powerlaw relationship between the rate of slip and the contact shear stress.

If the powerlaw exponent is one, the resistance to slip is constant all along the layer contacts, and the rate of slip is a linear function of the contact shear stress

Figure 2. Representative multilayer. Simple finite multilayer containing an initial, low amplitude perturbation and subject to uniform rates of horizontal shortening, $-\bar{D}_{xx}$, and vertical thickening, $\bar{D}_{zz}$. Multilayer, of total thickness H, consists of identical layers, of individual thickness h and coefficient of internal viscosity μ_ℓ, and is confined above and below by infinitely thick media with coefficient of internal viscosity μ_m.

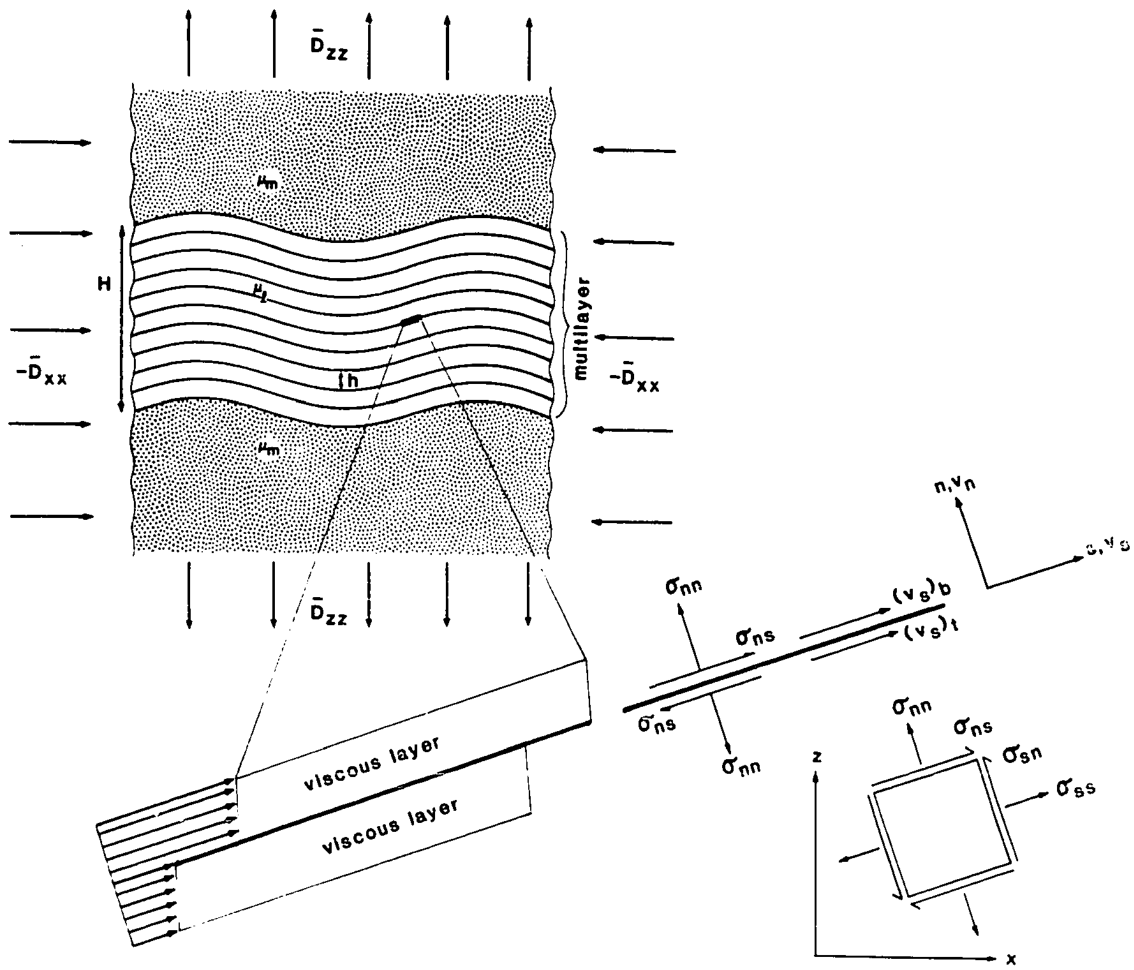

$\bar{D}_{zz}$
μ_m
H
μ_l
h
multilayer
$-\bar{D}_{xx}$
$-\bar{D}_{xx}$
μ_m
$\bar{D}_{zz}$
viscous layer
viscous layer
n, v_n
s, v_s
σ_{nn}
$(v_s)_b$
σ_{ns}
$(v_s)_t$
σ_{ns}
σ_{nn}
σ_{nn}
σ_{ns}
σ_{sn}
σ_{ss}
z
x

Figure 3. Powerlaw relationship between rate of slip, $\delta \underline{v}_s$, and shear stress, σ_{ns}, at layer contacts for several values of the powerlaw exponent, $\underline{m}$.

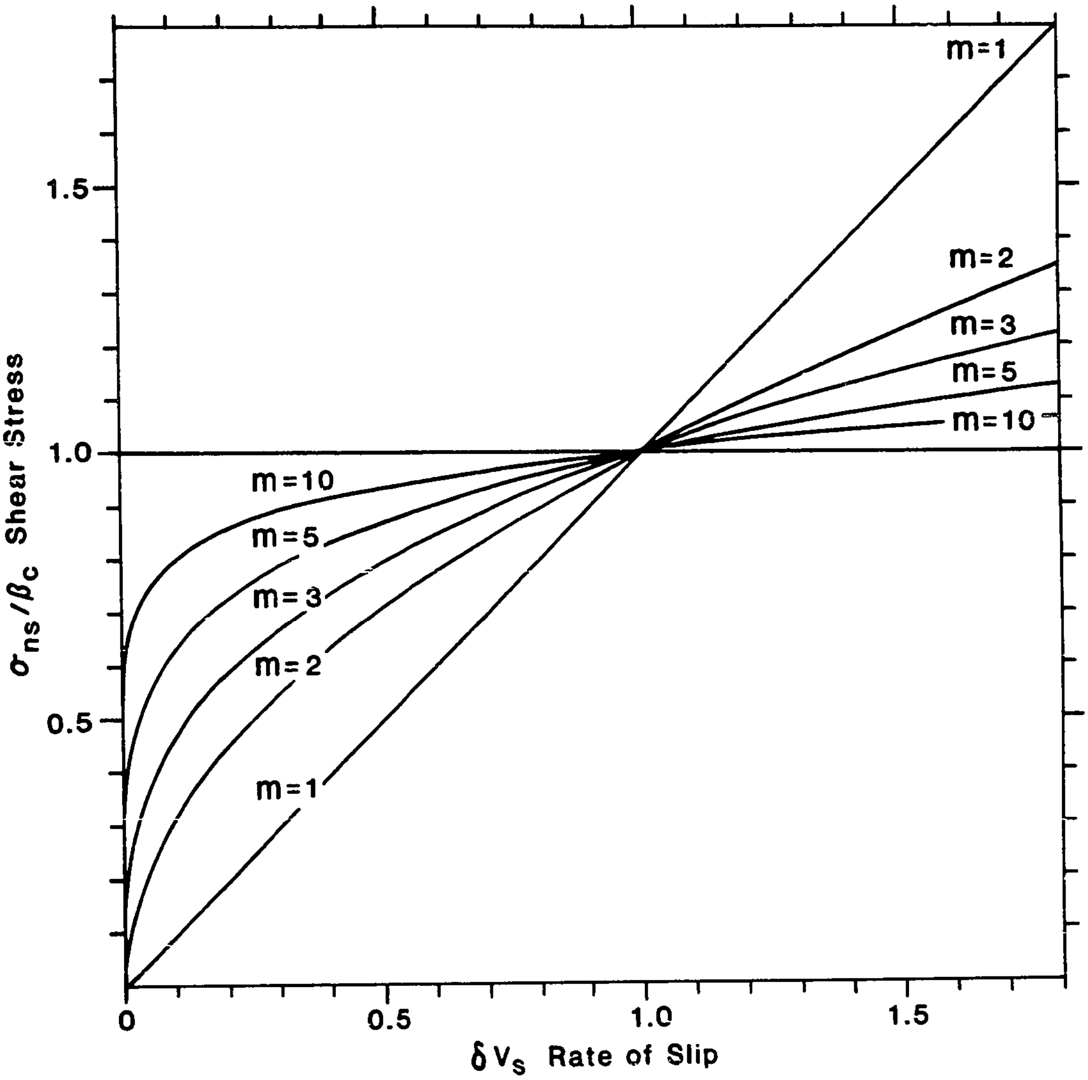

m=1
m=2
m=3
m=5
m=10
m=10
m=5
m=3
m=2
m=1
1.5
1.0
0.5
σ_{ns}/β_c Shear Stress
0
0.5
1.0
1.5
δV_s Rate of Slip

(m = 1, Fig. 3). Resistance to slip ranges from infinite, in which case contacts are bonded, to zero, in which case contacts slip freely. Constant, finite resistance to slip produces slip which is distributed along layer contacts.

If the powerlaw exponent is greater than one, the resistance to slip varies with position along the contact, and the rate of slip is a nonlinear function of the contact shear stress (m > 1, Fig. 3). Nonlinear resistance to slip is closely related to adhesional contact strength and produces slip which is localized along layer contacts.

EXAMPLES OF FOLD FORMS

Different fold forms can be produced in identical viscous multilayers merely by changing the behavior of contacts between layers. Fold forms generated theoretically in multilayers with free slip at contacts and with localized slip at contacts (m = 2.0) are compared in Fig. 4. The form of the multilayer with free slip at contacts (Fig. 4A) is concentric-like; the form of the multilayer with localized slip at contacts (Fig. 4B) is kink-like. Thus a slight change in contact properties (from m = 1.0 to m = 2.0) markedly changes fold form.

In the concentric-like fold (Fig. 4A), the upper interfaces define broad, rounded anticlines which are separated by narrow, sharpened synclines; these forms change gradually down through the multilayer until, at the lower

Figure 4. Effect of rheology of layer contacts on fold forms in simple finite multilayers confined by soft media (μ_m/μ_l = 0.01). Each multilayer has folded at its preferred wavelength ratio, $(\underline{L}/\underline{H})_p$, where $\underline{H}$ is the total thickness of the multilayer: $(\underline{L}/\underline{H})_p$ is 1.2 for the multilayer with free slip at contacts (Fig. 4A) and is 5.5 for the multilayer with localized slip at contacts (Fig. 4B).
A. Concentric-like fold form in multilayer with free slip at contacts. B. Kink-like fold form in multilayer with localized slip at contacts.

A

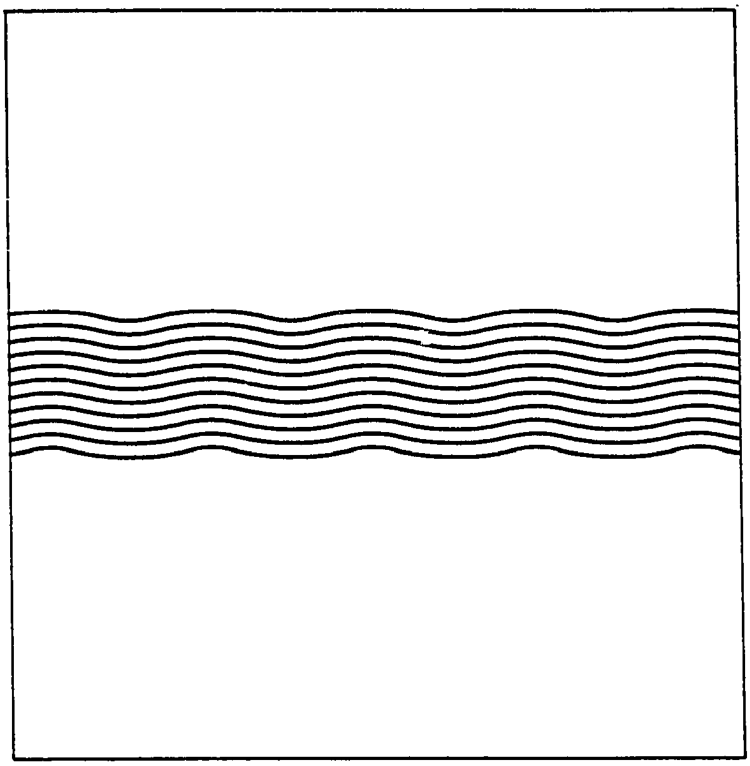

B

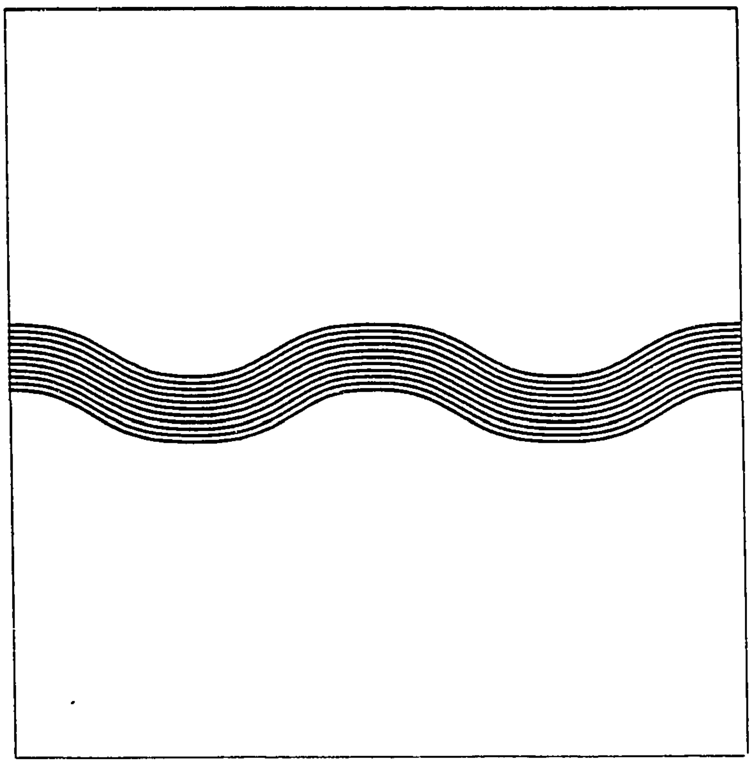

interfaces, broad, rounded synclines are separated by narrow, sharpened anticlines. The interfaces at middepth are of approximately sinusoidal shape. The axial planes of these folds are vertical; the inflection surfaces dip toward axial planes in anticlines and away from axial planes in synclines.

In the kink-like fold (Fig. 4B), the inflection surfaces are inclined to the vertical, as in the concentric-like fold, but both the inner and outer arcs of anticlines and synclines are flattened and the limbs are straightened and steepened. The form of each limb resembles a monoclinal flexure and is strikingly similar to the "kinkform" derived by Honea and Johnson (1976) for elastic multilayers with adhesional contact strength.

Different fold forms also can be produced theoretically by changing the wavelength of folds relative to the total thickness of the multilayer being folded, as illustrated in Fig. 5 for two multilayers with free slip at contacts (Fig. 5A) and for two multilayers with localized slip at contacts (Fig. 5B). Folds in multilayers with very low ratios of wavelength to total thickness ($\underline{L}/\underline{H} << 1$) are shown in column 1; folds in multilayers with wavelengths on the order of the multilayer thickness ($\underline{L}/\underline{H} \cong 1$) are shown in column 2. The fold wavelength is 12 to 13 times the thickness of a single layer, ($\underline{L}/\underline{h}$) = 12 to 13, in all four examples.

Figure 5. Effect on fold form of wavelength *L* relative to total thickness *H* of multilayer.
Wavelength-to-total-thickness ratio, (*L*/*H*), is very low in multilayers shown in column 1 and approximately equal to 1 in multilayers shown in column 2.
Wavelength-to-single-layer-thickness ratio, (*L*/*h*), is 12 in all four multilayers. A. Free slip at contacts. Chevron folds form in multilayers of infinite thickness (loc. A1); concentric-like folds form in multilayers of finite thickness (loc. A2). B. Localized slip at contacts. Box folds form in multilayers of infinite thickness (loc. B1); kink-like folds form in multilayers of finite thickness (loc. B2).

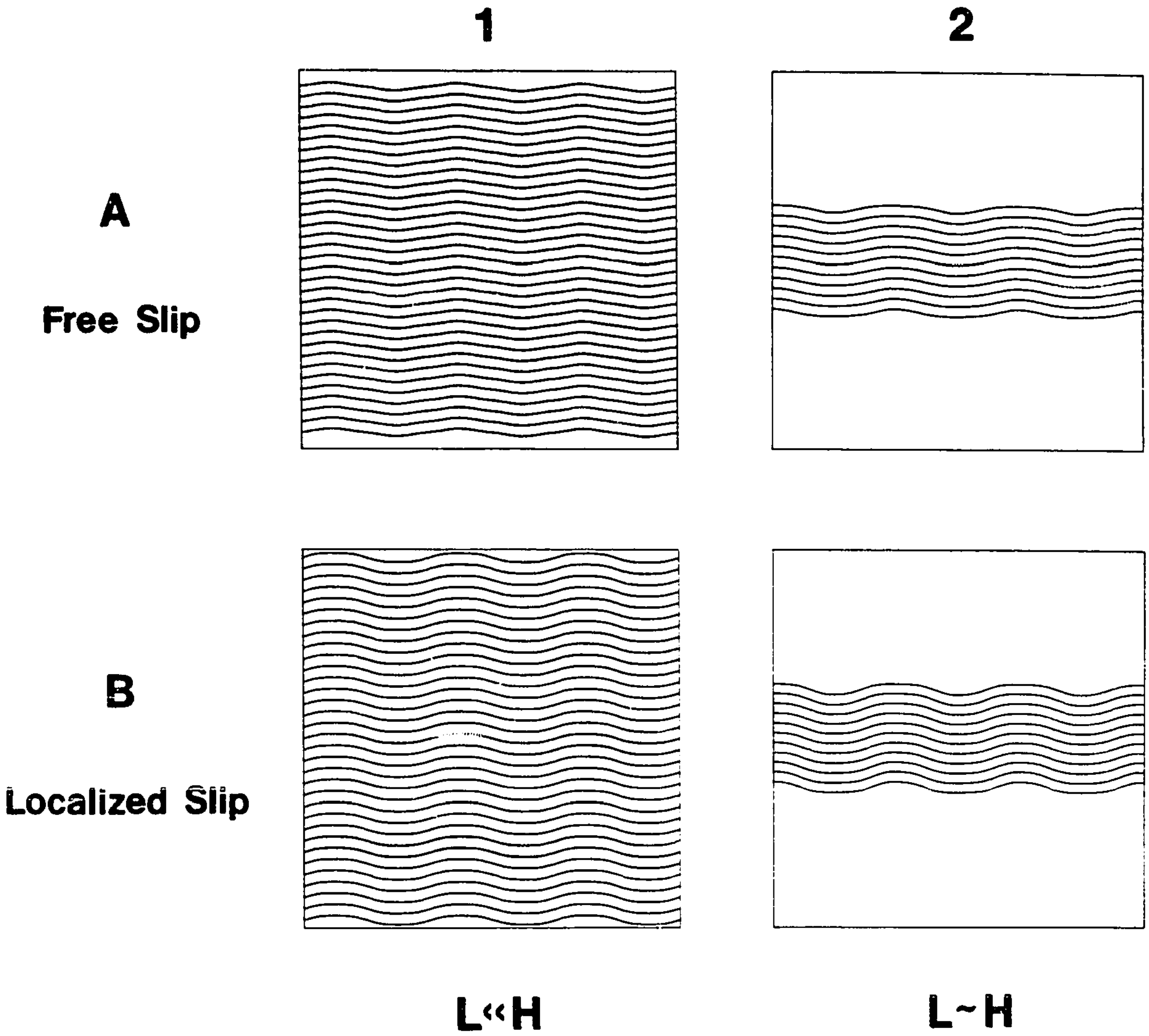
1
2
A
Free Slip
B
Localized Slip
L«H
L~H

The folds in very thick multilayers (column 1) are similar in form because the shape of each layer must be identical to that of its neighbors. The folds in thin multilayers (column 2) tend to be parallel in form and reflect the tendency for individual layers to maintain uniform orthogonal thicknesses.

The parallel, concentric-like fold, which develops in thin multilayers with free slip at contacts (Fig. 5, loc. A2), is absent in the corresponding very thick multilayer (Fig. 5, loc. A1). Instead, the folds are similar, chevron folds.

A parallel, kink-like fold develops in thin multilayers with localized slip at contacts (loc. B2), whereas a similar, box fold, a kink-like fold with vertical inflection surfaces, develops in the corresponding very thick multilayer (loc. B1).

Hybrid forms of folds with short wavelengths develop in thick multilayers: layers at middepth fold as though the multilayer were infinitely thick; layers near top and bottom are affected by the relative viscosity of the confining media. Thus in a finite multilayer composed of 59 layers with free slip at contacts, chevron folds develop at middepth (Fig. 6A). In the same multilayer with localized slip at contacts (m = 2) (Fig. 6B), box folds develop at middepth. Because these multilayers are confined by rigid media, fold amplitudes must die out at upper and lower

Figure 6. Hybrid fold forms in thick (59 layers) viscous multilayers confined by very stiff media (μ_m/μ_ℓ = 1000).
A. Free slip at contacts. Wavelength-to-total-thickness ratio, (L/H), is 0.06. Chevron folds form at middepth; constrained folds form in upper and lower quarters.
B. Localized slip at contacts. (L/H) = 0.14. Box folds form at middepth; kink-like folds form in upper and lower quarters.

A

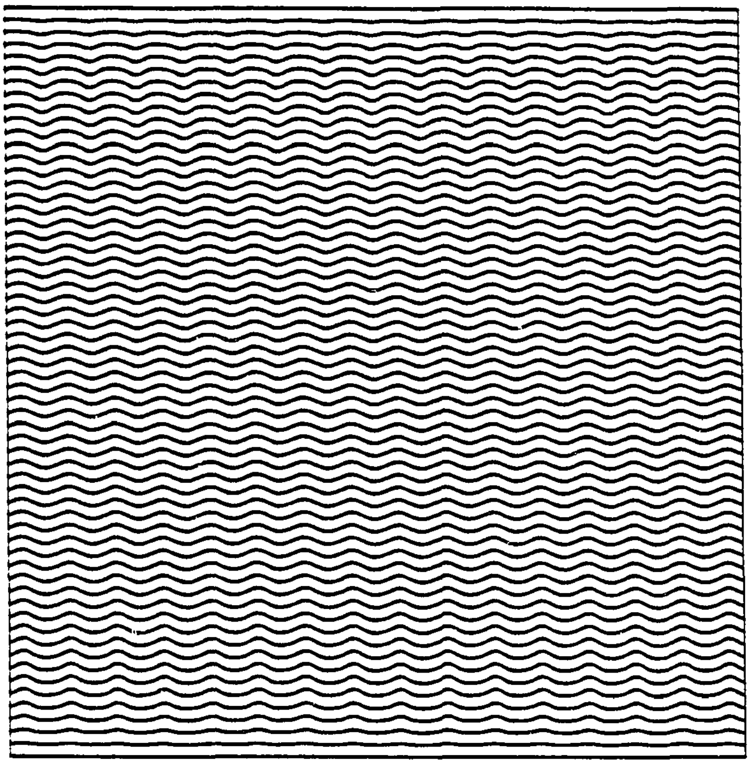

B

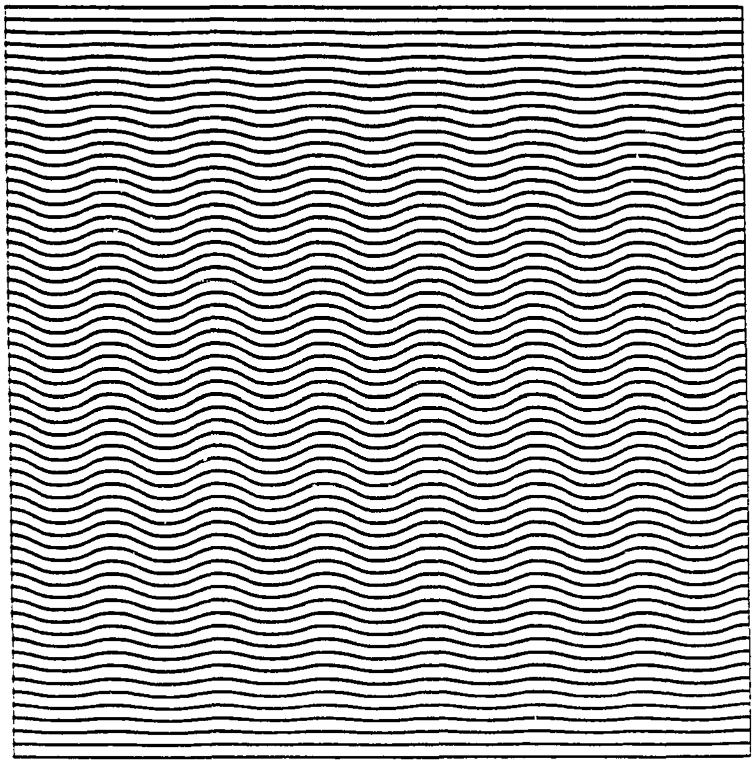

interfaces. Accordingly, the chevron folds blend into constrained folds in the upper and lower quarters of the multilayer (Fig. 6A), and the box folds become kink-like in the upper and lower quarters of the multilayer (Fig. 6B).

GEOMETRIC ANALYSIS OF THE FOLD FORMS

The fold forms which develop in simple multilayers with free slip at contacts and with localized slip at contacts (Figs. 4 through 6) can be described in terms of differences in amplitudes and wavelengths of component waveforms at layer interfaces. A <u>fold form</u> is a pattern defined by the shapes of all the layer interfaces in a single- or multi-layer. The shape of a single interface in a multilayer is a <u>resultant waveform</u> which can be described by the superposition of <u>component waveforms</u>. The component waveform is a single sinusoidal or cosinusoidal waveform and is the fundamental element of shape.

As the typical multilayer containing solely a first cosinusoidal waveform is shortened, cosinusoidal <u>second</u>, <u>third</u>, and <u>fourth waveforms</u> spontaneously develop. The wavelength of the second waveform is $\underline{L}/2$, one half that of the first waveform; the wavelength of the third is $\underline{L}/3$; and the fourth is $\underline{L}/4$.

The <u>mode</u> of the <u>first waveform</u>, the component waveform of wavelength $\underline{L}$, is the pattern defined by the first waveforms in the entire collection of interfaces, and for conditions studied here it is always a folding mode: the sign of the amplitude of the first waveform is the same throughout the multilayer (Fig. 7A). The mode of the second waveform is a pinch-and-swell mode: the sign of the amplitude of the second waveform in the upper part of the multilayer is opposite that in the lower part (Fig. 7B). The mode of the third waveform is a folding mode; the sign of the amplitude of the third waveform can be positive or negative (Fig. 7C), depending on the conditions of folding. The fourth waveform forms a pinch-and-swell mode (Fig. 7D).

The fold form in a finite multilayer with free slip at contacts (Fig. 5, loc. A2) essentially reflects the contributions of only first and second waveforms. Figure 8A shows part of the fold train from Fig. 5, loc. A2, and Fig. 8B shows the first and second component waveforms individually for each interface. The concentric-like fold form shown in Fig. 8A is the result of the summation of the waveforms shown in Fig. 8B. On the uppermost interface, for example, the second waveform reduces the upward deflection in the anticline and increases the downward deflection in the syncline. At the inflection point of the first waveform, the second waveform deflects the interface upward. The second waveform, therefore, flattens the peak and sharpens the trough produced by the first waveform and moves the inflection point closer to the sharpened trough. At the

Figure 7. Modes of component waveforms. A. Folding mode formed by first component waveforms (wavelength L) with positive amplitudes. B. Pinch-and-swell mode of second component waveforms (wavelength L/2) with negative amplitudes in upper half of multilayer and positive amplitudes in lower half of multilayer. C. Folding mode of third component waveforms (wavelength L/3) with negative amplitudes. D. Pinch-and-swell mode of fourth component waveform (wavelength L/4).

A

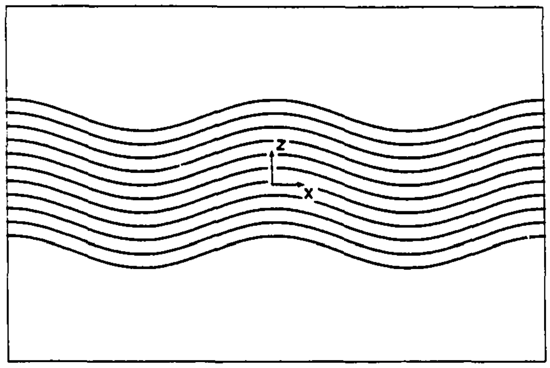

B

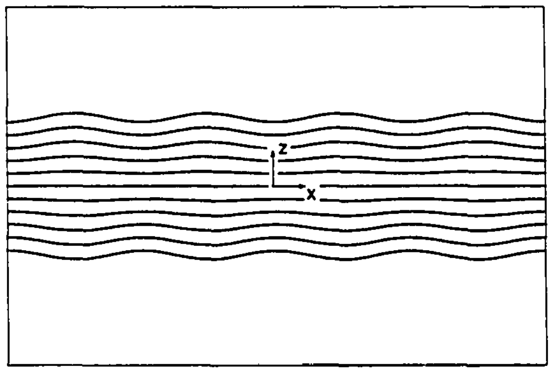

C

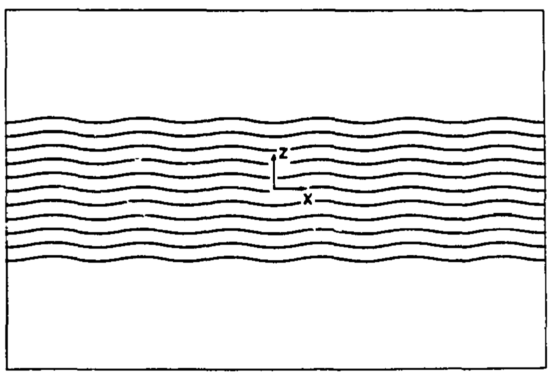

D

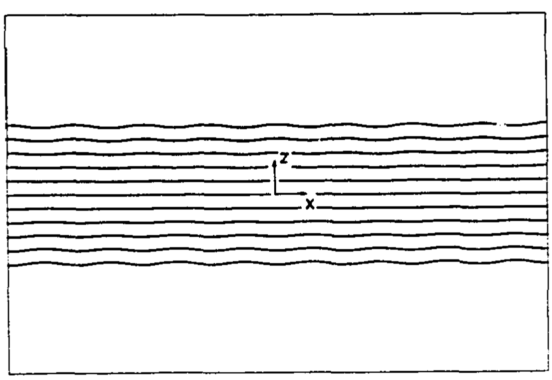

Figure 8. Effect of second component waveform on form of fold. A. Concentric-like fold form in finite multilayer with free slip at contacts. Shape of each interface is resultant waveform produced by addition of first and second component waveforms. B. Individual first and second component waveforms at each interface.

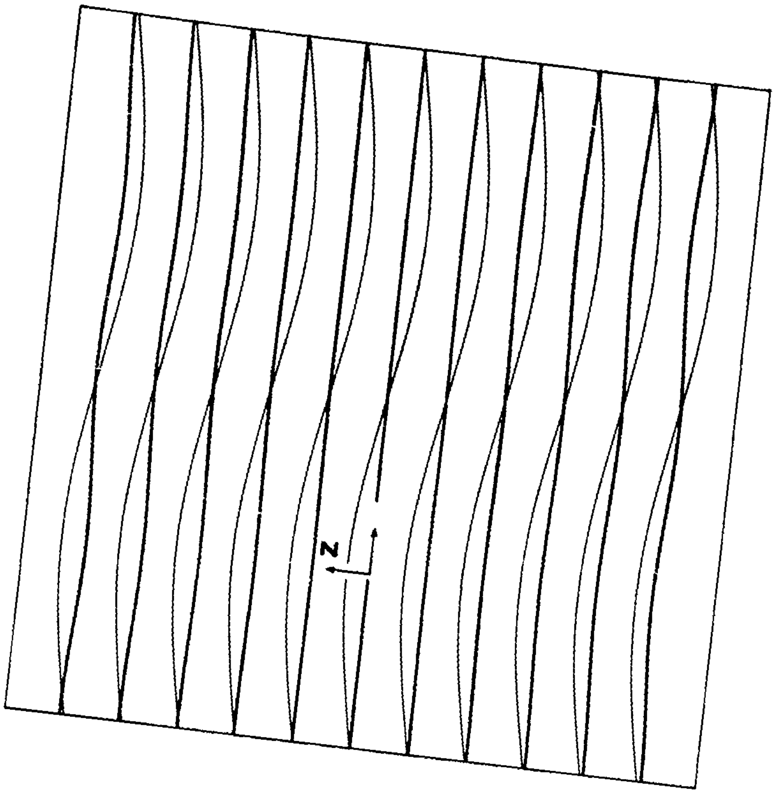

B

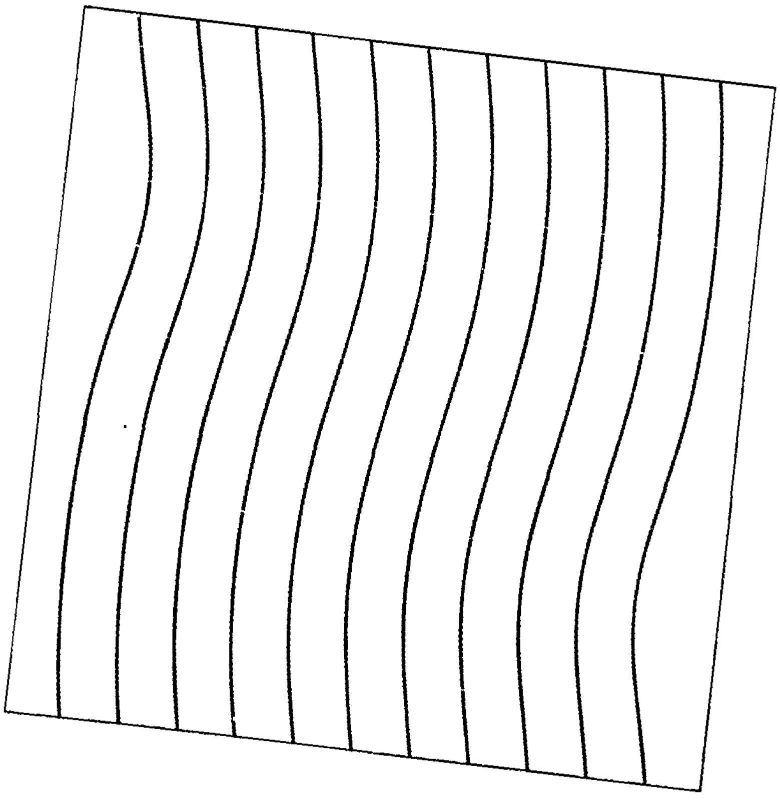

A

lowermost interface the effect of the second waveform is reversed because its sign is opposite. There the peak is enhanced and narrowed and the trough is reduced and broadened. Thus the concentric-like fold shown in Fig. 8A reflects the superposition of a positive, cosinusoidal, folding mode and a negative, cosinusoidal, pinch-and-swell mode.

Analyses of very thick multilayers are ideal for illustrating effects of third waveforms on the shapes of folds because second and fourth waveforms cannot develop in such multilayers. Because the amplitude of each waveform is constant throughout an infinitely thick multilayer, the third waveform has the same effect on the shape of each interface. Parts of the fold trains in infinitely thick multilayers with free slip at contacts and with localized slip at contacts (Fig. 5, locs. A1 and B1) are shown in Fig. 9, locs. A1 and B1, respectively. The first and third waveforms, shown individually for each interface in Fig. 9, locs. A2 and B2, are both cosinusoidal.

The amplitude of the first waveform has a positive sign in both infinitely thick multilayers; the amplitude of the third waveform has a positive sign in the multilayer with free slip (Fig. 9, loc. A2) and a negative sign in the multilayer with localized slip (Fig. 9, loc. B2).

The fold in the infinitely thick multilayer with free slip is a chevron fold. The third waveform sharpens the

Figure 9. Effect of third component waveform on form of fold. Shape of each interface shown in column 1 is resultant waveform produced by addition of individual first and third component waveforms at that interface, shown in column 2. A. Chevron fold form in infinitely thick multilayer with free slip at contacts results from addition of first and third component waveforms which both have positive amplitudes. B. Box fold form in infinitely thick multilayer with localized slip at contacts results from addition of first component waveform with positive amplitude and third component waveform with negative amplitude.

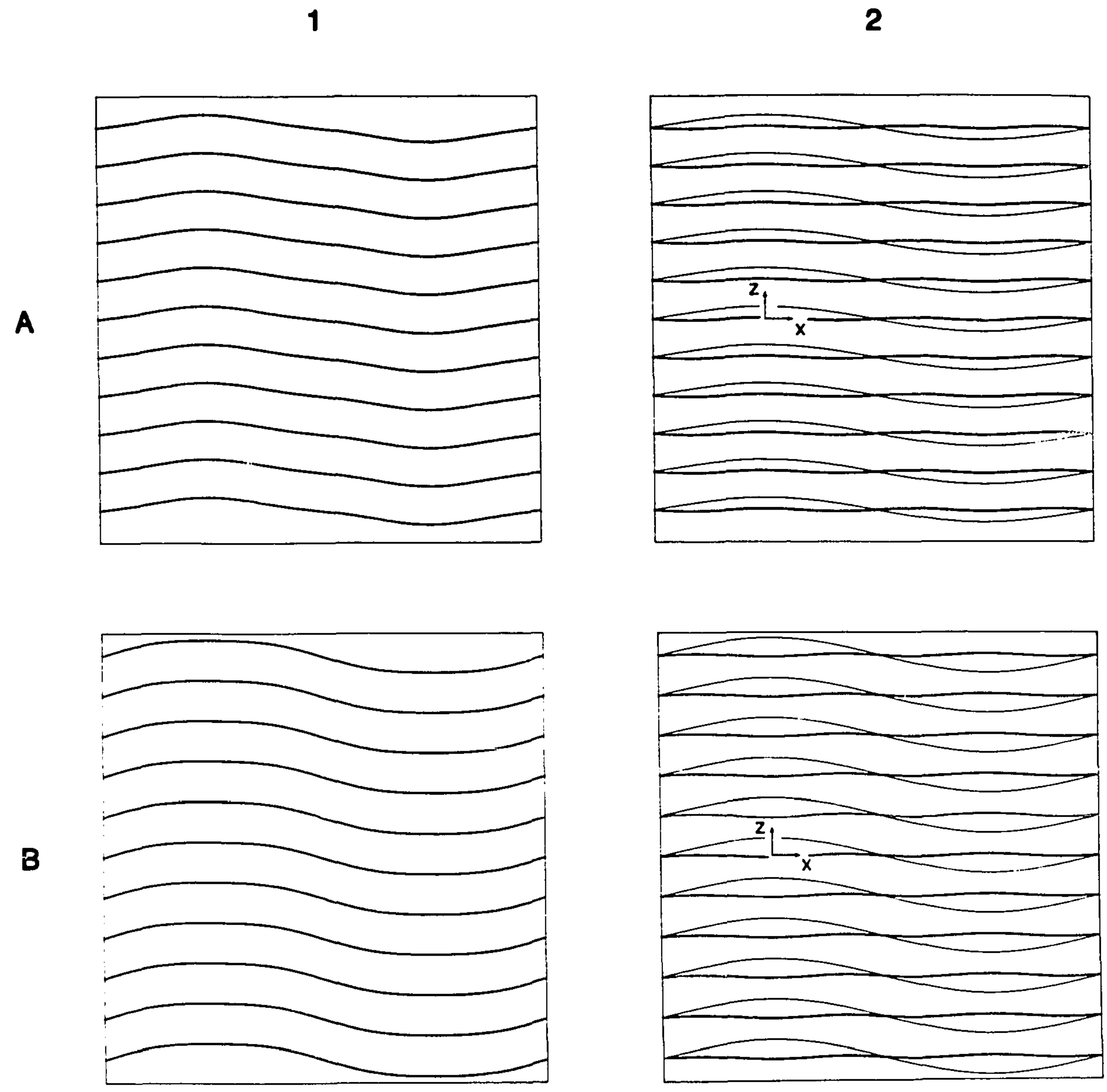

1
2
A
B
z
x
z
x

fold at crests and troughs of the first waveform, decreases the upward deflection on either side of a crest, and decreases the downward deflection on either side of a trough. Thus the hinges sharpen and narrow and the limbs straighten and lengthen to produce the chevron shape as a result of the superposition of the first and third component waveforms.

The fold in the multilayer with localized slip at contacts (Fig. 9, loc. B1) is a box fold. The amplitude of the third waveform has the opposite sign, so it flattens crests and troughs produced by the first waveform, increases the upward deflection on either side of the crests, and increases the downward deflection on either side of the troughs. The net effect of the combination of first and third component waveforms is the box fold, characterized by flattened and broadened hinges, shortened, straightened, and steepened limbs, and vertical inflection surfaces.

The degree to which a second or third waveform will modify the shape of the interface is determined by the relative amplitudes of the combining waveforms. Parts of a concentric-like fold (Fig. 5, loc. A2) and a kink-like fold (Fig. 5, loc. B2) are reproduced in Fig. 10, locs. A1 and B1, respectively, and analyzed in terms of amplitude-to-thickness ratios of first, second, third, and fourth component waveforms (${}_1\underline{A}/\underline{h}$, ${}_2\underline{A}/\underline{h}$, ${}_3\underline{A}/\underline{h}$, and ${}_4\underline{A}/\underline{h}$) (column 2) and amplitude ratios (${}_2\underline{A}/{}_1\underline{A}$), (${}_3\underline{A}/{}_1\underline{A}$), and

Figure 10. Relative amplitudes of component waveforms in finite multilayers. Ratio of wavelength to thickness of single layer, ($\underline{L}/\underline{h}$), is 12 for fold forms shown in column 1. Amplitude-to-thickness ratios for component waveforms on each interface are shown in column 2; individual amplitude ratios for each interface are shown in column 3.
A. Concentric-like fold form in finite multilayer with free slip at layer contacts. The maximum amplitude of the second waveform, ${}_2\underline{A}_{max}$, which occurs on the outer interfaces, is six times larger than ${}_3\underline{A}_{max}$ (loc. A2) and ∓ 0.20 times as large as ${}_1\underline{A}_{max}$ (loc. A3). B. Kink-like fold form in finite multilayer with localized slip at layer contacts. The maximum amplitude of the third waveform, which occurs at middepth, is $-0.06({}_1\underline{A}_{max})$; ${}_2\underline{A}_{max}$ is $\pm 0.15({}_3\underline{A}_{max})$ (loc. B3).

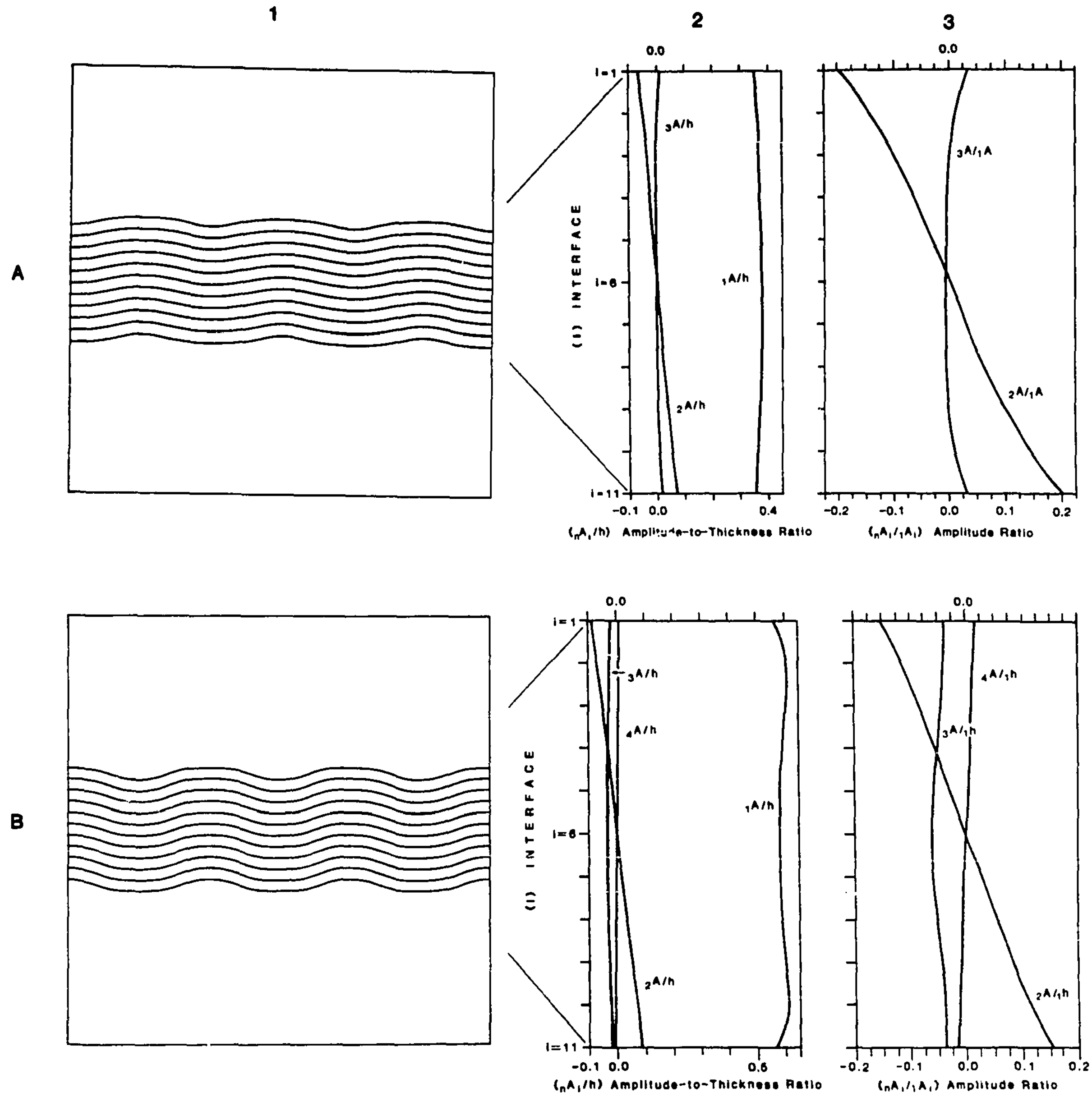
1
2
3
A
B
0.0
I=1
I=6
I=11
(I) INTERFACE
$_3A/h$
$_1A/h$
$_2A/h$
$_4A/h$
$_3A/_1A$
$_2A/_1A$
$_4A/_1h$
$_3A/_1h$
$_2A/_1h$
-0.1 0.0 0.4
-0.1 0.0 0.6
-0.2 -0.1 0.0 0.1 0.2
($_nA_i/h$) Amplitude-to-Thickness Ratio
($_nA_i/_1A_i$) Amplitude Ratio

$({}_{4}\underline{A}/{}_{1}\underline{A})$ (column 3).

That the concentric-like fold form is a consequence of the development of a strong second waveform is demonstrated by the geometric analysis in Fig. 8 and by the analysis of relative amplitudes in Fig. 10, locs. A2 and A3. For the fold form shown in Fig. 10, loc. A1, the absolute magnitudes of the amplitudes of the second waveforms are much larger than those of the third (loc. A2), and the largest ${}_{2}\underline{A}$ is about $\mp 0.2({}_{1}\underline{A})$ on the outermost interfaces (loc. A3). The third waveform slightly sharpens crests and troughs of the first waveforms in the upper and lower interfaces of the multilayer.

That the kink-like fold form with flattened hinges and straightened limbs is a consequence of the development of a strong second waveform and a strong third waveform with a negative amplitude is demonstrated by the geometric analysis in Fig. 9B and by the analysis of relative amplitudes in Figs. 10B and 10C. The largest ${}_{2}\underline{A}$ is about $\mp 0.15({}_{1}\underline{A})$ on the outermost interfaces; the largest ${}_{3}\underline{A}$ is about $-0.06({}_{1}\underline{A})$ at middepth. The third component waveform with negative amplitude produces the flattened hinges and straightened limbs, and the second waveform produces the inclination of the axial planes to the vertical. The inclination of the axial planes differentiates the box from the kink-like fold.

ANALYSIS OF FOLDING

I showed the different forms of folds which develop in multilayers with free slip and with localized slip at layer contacts and analyzed the forms in terms of their component waveforms in preceding pages. Here I will derive the theoretical model of slip at contacts and explain, by means of analytical expressions which describe the folding, how the signs and amplitudes of component waveforms depend on variables such as the rate of slip at layer contacts, the wavelength-to-thickness ratio, and the number of layers.

Properties of Layer Contacts

The behavior of layer contacts is modeled by a powerlaw relationship between rate of slip, $\delta \underline{v}_s$, and magnitude of shear stress, σ_{ns}, applied at contacts between layers:

$$\delta v_s = (\sigma_{ns}/\beta_c)\,|\sigma_{ns}/\beta_c|^{(m-1)} \qquad (1)$$

where β_c is a material constant and $\underline{m}$ is the powerlaw exponent, also assumed to be a material constant. The relationship between rate of slip and contact shear stress is illustrated for several values of $\underline{m}$ in Fig. 3.

The coefficient of contact viscosity, Ξ, is the local slope of the curve describing slip at that contact and is itself an inverse powerlaw function of the contact shear stress:

$$\Xi = (\beta_c/m)|\beta_c/\sigma_{ns}|^{(m-1)} \quad (2)$$

Contact viscosity increases as the shear stress decreases.

Combining eqs. (1) and (2) gives

$$\sigma_{ns} = m\Xi(\delta v_s) \quad (3)$$

The coefficient of contact viscosity, times the power m, is thus the resistance to slip at layer contacts.

The coefficient of contact viscosity, Ξ, essentially controls the contact properties of the multilayers I analyze. According to eq. (2), Ξ depends on both β_c and m. Suppose that σ_{ns}/β_c is unity, which occurs at the crossover point shown in Fig. 3. Then the slope of the curve, the contact viscosity, simplifies at that point to β_c/m (eq. 2). At the crossover point, Ξ is inversely proportional to m and proportional to β_c. The effect of the power m for other conditions depends upon whether the state of stress corresponds to a point above or below the crossover point. If above, the effect of increasing m is to decrease the contact viscosity, and if below, the effect is to increase the contact viscosity. The contact viscosity always increases with increasing β_c, as eq. (2) indicates.

A special case occurs for m = 1. Then the contact viscosity is equal to β_c, resistance to slip is constant everywhere along a contact, and rate of slip is a linear function of the shear stress (Fig. 3). As β_c becomes very large, the contacts become effectively bonded, and as β_c approaches zero, contacts slip freely.

Another special case occurs for $\underline{m} \to \infty$. In general, because the powerlaw exponent $\underline{m}$ is greater than one, the rate of slip at layer contacts increases nonlinearly with the contact shear stress, eq. (1). As $\underline{m}$ becomes very large, eq. (1) describes a contact with finite strength (Fig. 3), as shown by Smith (1979).

Thus, by specifying the coefficient of contact viscosity, Ξ, relative to the thickness, $\underline{h}$, and the <u>coefficient of internal viscosity</u>, μ_ℓ, of the layers, one can model free slip ($h\Xi \ll \mu_\ell$), linear or nonlinear viscous slip ($h\Xi < \mu_\ell$), or bonding ($h\Xi \geq \mu_\ell$) at layer contacts.

The nonlinear relation between shear stress and rate of slip, eq. (1), can have a profound effect on fold form by localizing interface slip. The dependence of the powerlaw ($\underline{m} > 1.0$) contact viscosity on the local magnitude of the contact shear stress, eq. (2), causes resistance to slip to vary along contacts. At places along layer contacts where stress is higher, the resistance to slip is lower, which produces a local increase in the rate of slip. As a result, slip on the contact becomes <u>localized</u> where the shear stress is maximal.

<u>Extension of Coulomb's Law</u>. My study of fold forms in multilayers with nonlinear resistance to slip at contacts was motivated by studies of folding of multilayers with

Coulomb adhesional contact strength (Honea and Johnson, 1976; Reches and Johnson, 1976). For example, Honea and Johnson (1976) showed that kink forms develop in response to layer-parallel compression in multilayers with finite contact strength which allows slip to occur locally along layer contacts.

Finite contact strength on a plane of potential failure commonly is modeled theoretically by Coulomb's Law:

$$\sigma_{ns} \leq \pm\ (C - \sigma'_{nn} \tan\phi) \qquad (4)$$

where σ_{ns} is the shear stress at the contact, $\underline{C}$ is the cohesive strength, σ'_{nn} is the effective normal stress across the contact, and $\tan\phi$ is the coefficient of contact friction. The expression $(C - \sigma'_{nn} \tan\phi)$ is the finite contact strength which must be overcome by the shear stress for slip to occur between layers.

The shear stress along a cosinusoidally perturbed contact varies with horizontal position. According to eq. (4), then, local slip could occur along parts of the perturbed contact while the rest of the contact remained bonded. The disadvantage of the application of Coulomb's Law to perturbed contacts is that, once the criterion for slip is met locally, the behavior of the contact becomes a discontinuous function of the stress.

I chose a powerlaw function of the shear stress to describe slip at contacts because it can model nonlinear resistance to slip but has the mathematical advantage that its behavior is a continuous function of stress. In analogy with the coefficient of contact friction, $\tan\phi$, which describes resistance to slip if interfaces have a finite strength, a coefficient of contact viscosity, Ξ, describes resistance to slip if interfaces have powerlaw or linear viscous rheologies.

Various constant and nonuniform resistances to slip can be incorporated into the familiar Coulomb's Law, eq. (4), by adding a time-dependent term:

$$\sigma_{ns} = \pm\ (C - \sigma'_{nn}\ \tan\phi) + m\Xi(\delta v_s) \tag{5}$$

where Ξ is the coefficient of contact viscosity, $\underline{m}$ is the powerlaw exponent, and $\delta\underline{v}_s$ is the rate of slip at the contact,

$$\delta v_s = (v_s)_b - (v_s)_t \tag{6}$$

Here, $(\underline{v}_s)_b$ and $(\underline{v}_s)_t$ are the velocities parallel to the interface on either side of the contact (Fig. 2). The rate of slip, $\delta\underline{v}_s$, can be expressed by rearranging eq. (5):

$$\delta v_s = [\sigma_{ns} \mp (C - \sigma'_{nn}\ \tan\phi)]/(m\Xi)\ ;$$

$$|\sigma_{ns}| \geq C - \sigma'_{nn}\ \tan\phi \tag{7}$$

<u>Local slip</u> occurs when the equality in eq. (7) is met only locally while other portions of the contact remain

bonded. Local slip on a perturbed interface is possible if the contacts are completely described by adhesional strength ($\delta \underline{v}_s$ becomes indeterminate).

Localized slip is the approximation that the powerlaw function makes to local slip. Localized slip occurs when the inequality in eq. (7) is true everywhere along the contact and the local rate of slip is controlled by the local resistance to slip, or local contact viscosity, Ξ. In this chapter, the rate of slip depends solely on the contact viscosity; the contact strength is equal to zero. Equation (7) then reduces to eq. (3).

Model of Contacts. The rheological model of contact behavior is derived by describing the behavior of a thin, interlayer film in the limit as the thickness of the film goes to zero. The powerlaw formulation of the Reiner-Rivlin simple fluid is assumed to describe the interlayer films. For plane strain, the shear stress parallel to interface films of powerlaw rheology is:

$$\sigma_{ns} = \beta'[(D_{ss}^2 + D_{ns}^2)^{(1-m)/m}]^{1/2}(D_{ns}) \tag{8a}$$

in which $\underline{D}$ is the deformation rate,

$$D_{ij} = (1/2)(\partial v_i/\partial x_j + \partial v_j/\partial x_i) \tag{8b}$$

β' is a material constant, and $\underline{m}$ is the powerlaw exponent, also assumed to be a material constant. The powerlaw fluid is treated as a thin film so that it cannot thicken or thin significantly, in which case $\underline{D}_{nn} = 0 = \underline{D}_{ss}$, and eq. (8a) can be written in the form

$$(\sigma_{ns}/\beta) = [2/|\sigma_{ns}/\beta|^{(m-1)}]\ D_{ns} \tag{9}$$

where β is a material constant. The rate of shearing deformation is given by the rate of slip, $\delta\underline{v}_s$, between adjacent layers across the film and by the thickness, $\delta\underline{n}$, of the film:

$$D_{ns} = (1/2)(\delta v_s/\delta n) \tag{10}$$

For a powerlaw film, therefore, the rate of slip is

$$\delta v_s = [(\sigma_{ns}/\beta)|\sigma_{ns}/\beta|^{(m-1)}](\delta n) \tag{11}$$

By analogy, eq. (1) describes the rate of slip at a contact between two layers:

$$\delta v_s = (\sigma_{ns}/\beta_c)|\sigma_{ns}/\beta_c|^{(m-1)} \tag{1}$$

where β_c is a property of the contact.

The patterns of slip along layer contacts are quite different for contacts with different resistances to slip, as shown schematically in Fig. 11. The shear stress along the upper contact of a cosinusoidally folded layer (Fig. 11A) within a multilayer varies sinusoidally, to 1st order, along an interface with a non-zero resistance to slip (Fig. 11B):

<u>Figure</u> <u>11</u>. Variation of shear stress, σ_{ns}, and rate of slip, $\delta \underline{v}_s$, along interface between layers. A. Interface between cosinusoidally folded layers. B. Sinusoidal variation of σ_{nn} along upper contact of layer. C., D., E. Variation of $\delta \underline{v}_s$ along contacts with constant resistance to slip ($\underline{m}$ = 1), variable resistance to slip ($\underline{m}$ > 1), and strength k, respectively. The variation of $\delta \underline{v}_s$ along the contact with variable resistance (D) resembles that on the contact with strength (E).

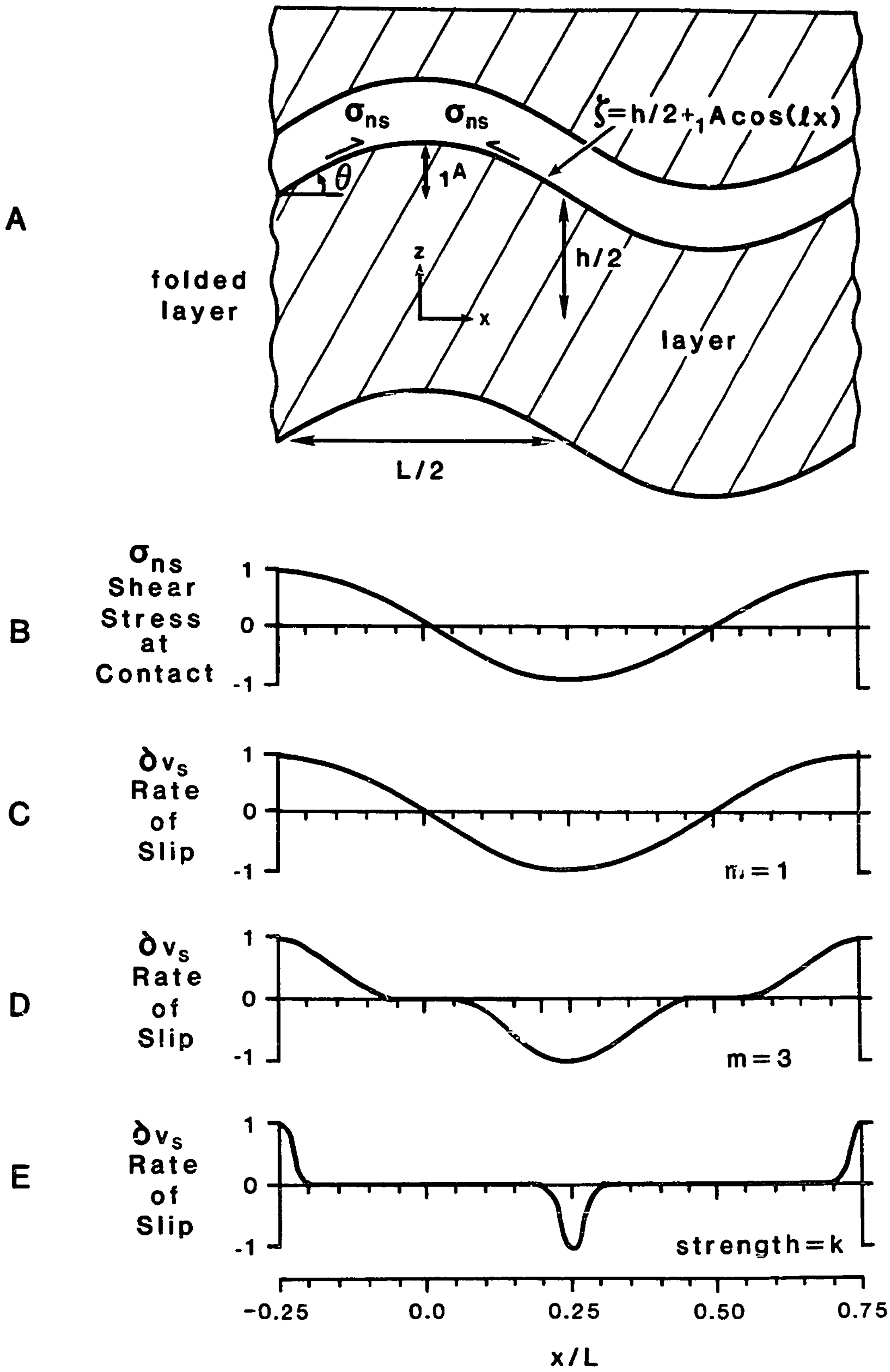
A
folded layer
layer
σns
σns
ζ=h/2+₁Acos(ℓx)
θ
₁A
h/2
z
x
L/2
B
σns Shear Stress at Contact
C
δvs Rate of Slip
m=1
D
δvs Rate of Slip
m=3
E
δvs Rate of Slip
strength=k
1
0
-1
-0.25
0.0
0.25
0.50
0.75
x/L

$$\sigma_{ns} = 4\mu_\ell \bar{D}_{xx}({}_1A\ell)\ \sin(\ell x) \tag{12}$$

The rate of slip at a contact is, according to eqs. (3) and (12),

$$\delta v_s = (1/m\Xi)[4\mu_\ell \bar{D}_{xx}({}_1A\ell)]\ \sin(\ell x) \tag{13}$$

For a constant resistance to slip ($m = 1$), the rate of slip varies sinusoidally with position, as shown in Fig. 11C and eq. (13). The magnitude of the slip depends on the contrast between the contact viscosity, Ξ, and the internal viscosity of the layers, μ_ℓ.

For a nonuniform resistance to slip ($m > 1$), the variation of the rate of slip at the interface is more complicated (Fig. 11D) and resembles that in a plastic material with strength (Fig. 11E): a plastic material of shear strength k will slip locally where the shear stress at the contact is equal to the strength; this occurs first, and perhaps exclusively, at the inflection points of the fold. In the nonlinear, powerlaw model, slip is localized in the vicinity of the inflection points (Fig. 11D).

Selection of m. In all of the analyses presented in this chapter, the powerlaw exponent m is restricted to values of one, two, or three in conjunction with the decision to derive an analytical solution for the folding accurate to 3rd order in the maximum slope of the first waveform. Relative to the center of a layer, the height, ζ, of a point along an interface at the top of a layer is initially

$$\zeta = h/2 + {}_1A \cos(\ell x) \tag{14}$$

where $\ell = 2\pi/\underline{L}$ and $\underline{L}$ is the wavelength of the fold (Fig. 11A); the left subscript refers to the waveform with which the amplitude is associated. The maximum slope of the interface is

$$\tan(\theta)_{max} = {}_1A\ell \tag{15}$$

where θ is the slope angle. The boundary stresses, σ_{nn} and σ_{ns}, and velocities, $\underline{v}_n$ and $\underline{v}_s$, at a point with coordinates ($\underline{x}$,$\underline{z}$) on an interface are derived in terms of powers of the maximum slope, (${}_1A\ell$). The order of approximation of a solution is defined in terms of the largest power to which the maximum slope is raised (Fletcher, 1977, 1979, 1982). For a 3rd order solution, then, terms proportional to (${}_1A\ell$), $({}_1A\ell)^2$, and $({}_1A\ell)^3$ are retained.

The 3rd order analysis of an initial, cosinusoidal waveform with wavelength $\underline{L}$ reveals that second, third, and fourth component waveforms may develop spontaneously. In the solutions presented here, only terms proportional to (${}_2A\ell$), (${}_3A\ell$), (${}_4A\ell$), or (${}_1A\ell$)(${}_2A\ell$) are retained.

Increasing the power $\underline{m}$ beyond three not only increases the nonlinearity of the contact behavior but also increases the amount of algebra required to solve problems because the analytical solution would need to be derived to a correspondingly higher order of accuracy. Selection of $\underline{m}$ = 2 or 3 permits an investigation of the fundamental effects of nonlinearity without posing an intractable algebraic problem.

Anisotropy. The anisotropy of a multilayer is defined as the ratio of the effective normal and shear viscosities. For a representative element of a multilayer with nonlinear resistance to slip at contacts, the effective shear, μ_s, and normal, μ_n, viscosities are:

$$1/\mu_s = 1/\mu_\ell + 1/(h\Xi) \qquad (16a)$$

$$\mu_n = \mu_\ell \qquad (16b)$$

According to eqs. (2), (12), and (16), the anisotropy is

$$\mu_n/\mu_s = 1 + \{\underline{m}[\underline{4}({}_1\underline{A}\underset{\sim}{\ell})]^{(m-1)}/\hat{\beta}\} \ \underline{\sin}^{(m-1)}(\underset{\sim}{\ell}\underline{x}) \qquad (17a)$$

where

$$\hat{\beta} = (\beta_c)^m h/[\mu_\ell(\mu_\ell \bar{D}_{xx})^{(m-1)}] \qquad (17b)$$

For constant resistance to slip at contacts ($\underline{m}$ = 1), the coefficient of contact viscosity, Ξ, is constant. Therefore, the shear viscosity, eq. (16a), and the anisotropy, eq. (17a), are constant. Anisotropy varies from one for bonded contacts to infinity for free slip at contacts. The corresponding $\hat{\beta}$ ranges from infinity for bonded contacts to zero for free slip at contacts.

For variable resistance to slip at contacts, however, the contact viscosity and the anisotropy vary with position along the interface. The anisotropy of a multilayer with nonlinear contact viscosity decreases from a maximum at the inflection points, where $\ell\underline{x} = \pm\pi/2$, to a minimum at the hinges of the fold, where $\ell\underline{x} = \pm\pi$. The maximum anisotropy, α,

$$\alpha = (\mu_n/\mu_s)_{max} = 1 + m[4({}_1A\ell)]^{(m-1)}/\beta \qquad (18)$$

According to eq. (18), the maximum anisotropy of a simple multilayer with nonlinear contact viscosity is a function of the maximum slope at inflection points along an interface, the powerlaw exponent $\underline{m}$, and the constant β. If an initial maximum anisotropy and an initial maximum slope are selected for the multilayer, eq. (18) can be used to compute the constant β.

Because the maximum slope (${}_1A\ell$) increases during folding, the anisotropy increases during folding. Early in folding, when slopes are low, the anisotropy is close to one, and the multilayer folds slowly as a single, thick layer. Later in folding, when slopes are higher, the anisotropy is higher, the layers slip relative to one another, and the multilayer folds much more rapidly.

Mean and Perturbed Flows

The height of each interface in the multilayer is described by the relation

$$\zeta_{t,b} = \pm(h/2) + {}_1A_{t,b}\cos(\ell x) + {}_2A_{t,b}\cos(2\ell x) + {}_3A_{t,b}\cos(3\ell x) \qquad (19)$$

Here, t refers to top and b refers to bottom interfaces of a layer, and h is the thickness of a single layer. Initially, each interface is a simple first cosine waveform. However, as the first waveform grows, the second, third, and fourth waveforms develop spontaneously.

The mechanical problem is to determine the amplitudes, ${}_jA_{t,b}$, as functions of time. It is formulated by separating components of velocity and stress within a layer into mean and perturbed values (Fletcher, 1974, 1977). The mean values of stress and velocity are those that solve the problem describing the uniform deformation of a layer with planar interfaces. The perturbed values of stress and velocity are those that must be added to the mean values in order to match stresses and velocities at perturbed interfaces between layers or between a layer and a confining medium.

This analysis considers multilayers subjected to uniform shortening parallel to layers and uniform thickening normal to layers; the rate of shearing deformation is zero.

The mean stresses and velocities (indicated with a bar) within a layer are

$$\bar{v}_x = x \, \bar{D}_{xx} \tag{20a}$$

$$\bar{v}_z = z \, \bar{D}_{zz} + (\bar{v}_z)_o = (\bar{v}_z)_o - z \, \bar{D}_{xx} \tag{20b}$$

$$\bar{\sigma}_{xx} = 2\mu_\ell \bar{D}_{xx} - \bar{p} \tag{20c}$$

$$\bar{\sigma}_{zz} = - 2\mu_\ell \bar{D}_{xx} - \bar{p} \tag{20d}$$

$$\bar{\sigma}_{xz} = 0 \tag{20e}$$

$$\bar{p} = - (\bar{\sigma}_{xx} + \bar{\sigma}_{zz})/2 \tag{20f}$$

in which $\underline{\bar{D}}_{xx}$ is layer-parallel deformation rate. For the incompressible viscous material, $\underline{\bar{D}}_{xx} = -\underline{\bar{D}}_{zz}$. This completes the solution for the mean flow, which is exact.

The total velocities and stresses are the sums of the mean and perturbed (indicated by a tilde) values:

$$v_x = \bar{v}_x + \tilde{v}_x \tag{21a}$$

$$v_z = \bar{v}_z + \tilde{v}_z \tag{21b}$$

$$\sigma_{xx} = \bar{\sigma}_{xx} + \tilde{\sigma}_{xx} \tag{21c}$$

$$\sigma_{zz} = \bar{\sigma}_{zz} + \tilde{\sigma}_{zz} \tag{21d}$$

$$\sigma_{xz} = \tilde{\sigma}_{xz} \tag{21e}$$

The perturbed values satisfy the biharmonic equation in the stream function,

$$\nabla^4\psi = 0 \tag{22}$$

where

$$\tilde{v}_x = -(\partial\psi/\partial z) \tag{23a}$$

$$\tilde{v}_z = (\partial\psi/\partial x) \tag{23b}$$

The solution is

$$\tilde{v}_x = -[\{{}_ja + {}_jd + {}_jb(j\ell z)\}{}_jS + \{{}_jb + {}_jc + {}_jd(j\ell z)\}{}_jC] \sin(j\ell x) \tag{24a}$$

$$\tilde{v}_z = [\{{}_ja + {}_jb(j\ell z)\}{}_jC + \{{}_jc + {}_jd(j\ell z)\}{}_jS] \cos(j\ell x) \tag{24b}$$

$$\tilde{\sigma}_{xx} = -2j\mu\ell[\{{}_ja + 2{}_jd + {}_jb(j\ell z)\}{}_jS + \{{}_jc + 2{}_jb + {}_jd(j\ell z)\}{}_jC] \cos(j\ell x) - \tilde{p}_o \tag{24c}$$

$$\tilde{\sigma}_{zz} = 2j\mu\ell[\{{}_ja + {}_jb(j\ell z)\}{}_jS + \{{}_jc + {}_jd(j\ell z)\}{}_jC] \cos(j\ell x) - \tilde{p}_o \tag{24d}$$

$$\tilde{\sigma}_{xz} = -2j\mu\ell[\{{}_ja + {}_jd + {}_jb(j\ell z)\}{}_jC + \{{}_jc + {}_jb + {}_jd(j\ell z)\}{}_jS] \sin(j\ell x) \tag{24e}$$

in which

$${}_jS = \sinh(j\ell z) \ ; \ {}_jC = \cosh(j\ell z) \tag{24f}$$

and j = 1, 2, 3, and 4 (results summed). Here, ${}_j\underline{a}$, ${}_j\underline{b}$, ${}_j\underline{c}$, and ${}_j\underline{d}$ are arbitrary constants.

The arbitrary constants are eliminated by means of velocity and stress boundary conditions. Equation (1), in conjunction with eq. (6), provides one of the boundary conditions at interfaces between layers. Additional boundary conditions are provided by equating normal velocities, $\underline{v}_n$, normal stresses, σ_{nn}, and shear stresses, σ_{ns}, at interfaces.

The growth rates of waveforms in all the interfaces are determined by computing the rate of change in height of an interface

$$(\partial\xi/\partial t) = [v_z]_\xi - [v_x]_\xi(\partial\xi/\partial x) \qquad (25)$$

in which ξ is given by eq. (19). The equations for the growth of the component waveforms take the general form:

$$d({}_nA)/d\bar{S}_x = +[({}_nA)/\bar{S}_x](1 + q); \quad n=1,2,3,4 \qquad (26)$$

where $\underline{\bar{S}}_x$ is horizontal shortening (stretch), $\underline{h}_o/\underline{h}$, which ranges from one to zero; ${}_n\underline{A}$ is current amplitude; ${}_n\underline{A}_o$ is initial amplitude; and $\underline{n}$ denotes the component waveform. The term (1 + $\underline{q}$) is the amplification factor for the waveforms. In the case of kinematic amplification, $\underline{q}$ is zero; the kinematic amplification factor is always equal to one. Dynamic amplification of the perturbed interface is represented by g. In this chapter, the term "amplification factor" will refer to the dynamic amplification factor, g.

The basic equations are derived in further detail in the appendices.

Growth and Shapes of Similar Folds in Very Thick Multilayers

I showed in previous pages that the geometrical differences between forms of chevron and box folds, which develop near middepth in thick multilayers or everywhere within infinitely thick multilayers, are results of the opposite signs of their third component waveforms. Here I show that the characteristic shapes of chevron and box folds develop spontaneously, even if the initial perturbation in a multilayer is simply a sinusoidal shape, and that the opposite signs of the third waveforms are results of rheological properties of layer contacts.

First I compare amplification factors for the first, cosinusoidal waveform in various types of multilayers. I briefly discuss dominant and preferred wavelengths, which have been investigated at length for various systems in Chapter I and elsewhere (Fletcher, 1974, 1977). Then I present amplification factors that control the growth of the third waveforms. I analyze three multilayers:

1. Multilayers with constant resistance to slip at layer contacts. Of these, I consider two special cases:

A. Bonded contacts. The contact viscosity is so high that layers cannot slip and interfaces between layers are merely passive markers.

B. Free slip at contacts. The contact viscosity is so low that layers slip freely.

2. Multilayers with variable resistance to slip at layer contacts. In this case, slip is localized.

<u>Amplification Factors</u>. The amplitudes of the first and third waveforms grow according to the following expressions:

$$d({}_{1}A)/d\bar{S}_x = ({}_{1}A/\bar{S}_x)[1 + {}^{1}_{1}\underline{q} + {}^{11}{}^{1}_{1}\underline{q}] \qquad (27a)$$

$$d({}_{3}A)/d\bar{S}_x = ({}_{3}A/\bar{S}_x)[1 + {}^{3}_{3}\underline{q}] + ({}_{1}A/\bar{S}_x)[{}^{11}{}^{1}_{3}\underline{q}] \qquad (27b)$$

The heights of interfaces, relative to centers of layers, are

$$\zeta = h/2 + {}_{1}A\cos(\ell x) + {}_{3}A\cos(3\ell x) \qquad (28)$$

The subscripts and superscripts used in eqs. (27) are interpreted as follows. The left subscript identifies the waveform with which the variable is associated. The left superscript indicates the product of maximum slopes that enters the expression for that variable. For example, ${}^{11}{}^{1}_{3}\underline{q}$ is an amplification factor for the third waveform, and it is accurate to 3rd order in $({}_{1}A\ell)$, the slope of the first waveform. The factors ${}^{1}_{1}\underline{q}$ and ${}^{3}_{3}\underline{q}$ are accurate to 1st order in the amplitudes of the first and third waveforms, respectively.

The full expressions for the amplification factors for multilayers with frictionless contacts, localized slip at contacts ($\underline{m}$ = 3), and bonded contacts are compared in Table I. All the dynamic amplification factors for bonded contacts are zero, so perturbations in the multilayer will be amplified solely kinematically. The 1st order amplification factors for the first and third waveforms, ${}^{1}_{1}\underline{g}$ and ${}^{3}_{3}\underline{g}$, respectively, are both zero for the multilayer with localized slip at contacts. Therefore, to 1st and 2nd orders, the multilayer behaves as though it has bonded contacts. Of the three considered, only the multilayer with free slip at contacts has nonzero 1st order amplification factors, ${}^{1}_{1}\underline{g}$ and ${}^{3}_{3}\underline{g}$.

Both the multilayer with free slip at contacts and the multilayer with localized slip at contacts have significant 3rd order amplification factors, ${}^{111}_{1}\underline{g}$ and ${}^{111}_{3}\underline{g}$, which drive the growth of the first and third waveforms, respectively. Because ${}^{111}_{1}\underline{g}$ and ${}^{111}_{3}\underline{g}$ have opposite signs for free slip and localized slip at contacts (Table I), they have quite different effects on the folds in those multilayers.

For the multilayer with localized slip, the amplification factor for the first waveform, ${}^{111}_{1}\underline{g}$, is always positive (Table I) but approaches a limiting value at long wavelengths (Fig. 12). There is no finite dominant wavelength for which amplification is maximized.

TABLE I

AMPLIFICATION FACTORS FOR INFINITELY THICK MULTILAYERS

	Free Slip at Contacts	Localized Slip at Contacts ($\underline{m}$ = 3)	Bonded Contacts
${}^{1}_{1}q$ =	$+ [2k/({}_1S_1C-k)]$	0	0
${}^{111}_{1}q$ =	$- [({}_1A\ell)^2/2({}_1S_1C-k)^2][+ 4({}_1S_1C)^2$ $- 2({}_1S)^2({}_2C/{}_2S)({}_1S_1C-k)$ $+ ({}_1S_1C)k + k^2]$	$+ 48[({}_1A\ell)^2/\hat{\beta}](k/{}_1S)^2$	0
${}^{3}_{3}q$ =	$+ [6k/({}_3S_3C-3k)]$	0	0
${}^{111}_{3}q$ =	$+ [({}_1A\ell)^2/4({}_1S_1C-k)({}_3S_3C-3k)][- 6({}_1S_3C)({}_1C_3S+{}_1S_3C)$ $+ 4({}_1S)^2({}_2C/{}_2S)(3{}_3S_3C-k)$ $+ 5({}_1S_1C)k + 3({}_3S_3C)k - 2k^2]$	$- 48[({}_1A\ell)^2/\hat{\beta}](k/{}_3S)^2$	0

TABLE I continued

where

L is the wavelength of the first waveform

h is the thickness of one layer; h_o is the initial thickness of one layer

k is the dimensionless wavenumber of the first waveform: $k = (2\pi/L)(h/2)$

$\bar{S}_x$ is the horizontal stretch: $\bar{S}_x = h_o/h$

${}_nS = \sinh(nk)$; ${}_nC = \cosh(nk)$

${}_nA_o$ is the initial amplitude of waveform n

$1/\hat{\beta} = [1/(\beta_c)^3 h][\mu_\ell(\mu_\ell \bar{D}_{xx})^2]$

Figure 12. Relationship between amplification factor $_1q$ and wavelength-to-thickness ratio (L/h) for first waveform in infinitely thick multilayers. A finite dominant wavelength exists in an infinitely thick multilayer with free slip at contacts but not in one with localized slip at contacts. The dashed lines indicate combinations of $(_1A\ell)^2/\beta$ and (L/h) for which eqs. (27a) are not strictly valid. The magnitude of the 1st order term in σ_{ns} was assumed to be much greater than the magnitudes of the higher order terms. In cubing σ_{ns}, therefore, higher order terms were considered negligible. However, magnitudes of the higher order terms in σ_{ns} increase with increasing ($_1A\ell$) and may become significant at certain combinations of slope and low wavelength-to-thickness ratio.

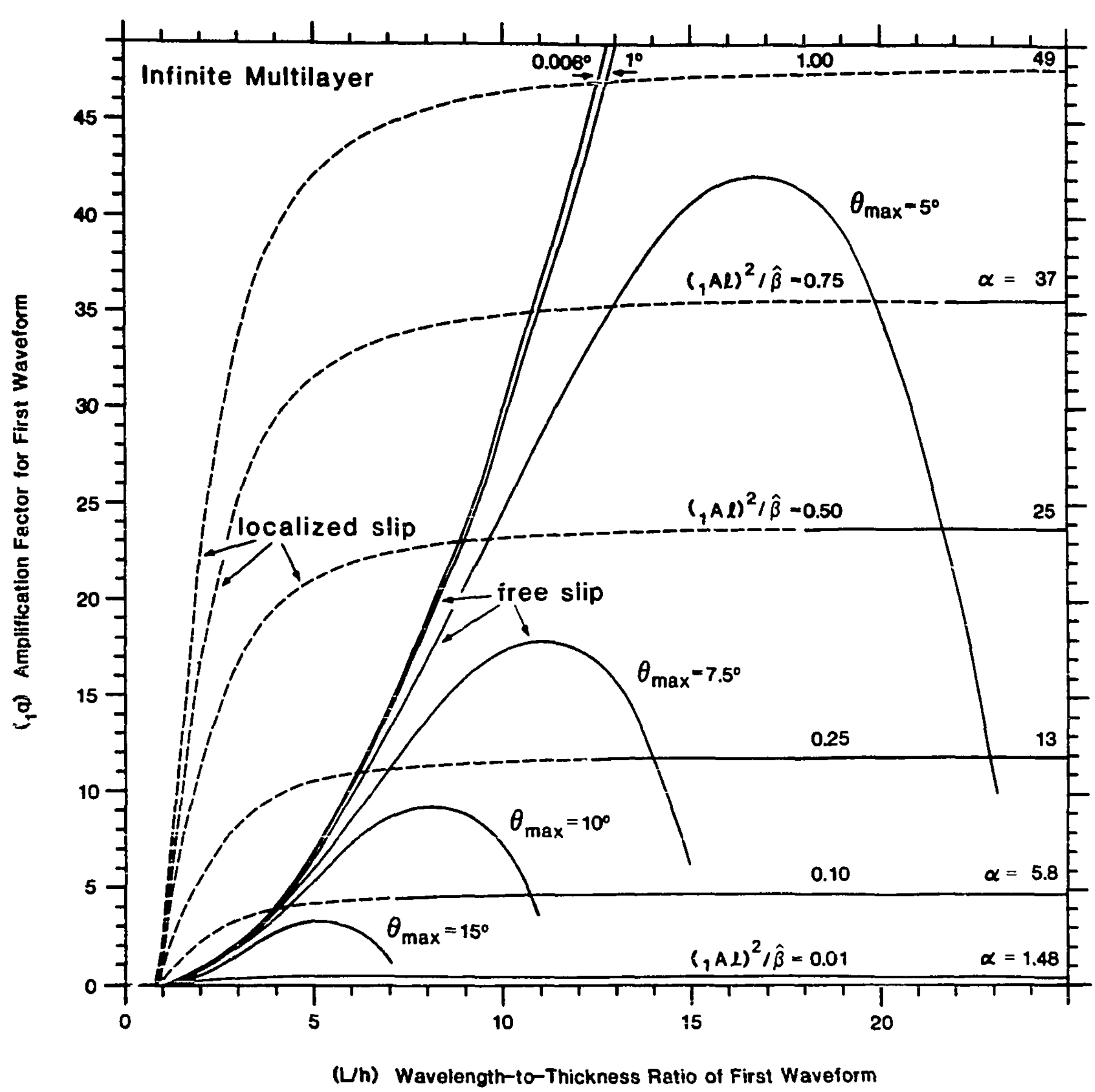

Infinite Multilayer
0.006°
1°
1.00
49
θ_{max}=5°
$({}_1A\ell)^2/\hat{\beta}$=0.75
α = 37
$({}_1A\ell)^2/\hat{\beta}$=0.50
25
localized slip
free slip
θ_{max}=7.5°
0.25
13
θ_{max}=10°
0.10
α = 5.8
θ_{max}=15°
$({}_1A\ell)^2/\hat{\beta}$ = 0.01
α = 1.48
$({}_1a)$ Amplification Factor for First Waveform
(L/h) Wavelength-to-Thickness Ratio of First Waveform

Although finite dominant wavelengths are absent in infinitely thick multilayers according to 1st order analyses of viscous and elastic multilayers (Ramberg, 1962, 1963, 1964; Honea and Johnson, 1976), they exist to 3rd order accuracy in the simple viscous multilayer with free slip at contacts. To 3rd order, the amplitude of the first waveform is driven by both 1st and 3rd order contributions. The 1st order amplification factor for the first waveform, ${}^{1}_{1}\underline{g}$, is positive and increases indefinitely with increasing wavelength; the 3rd order amplification factor for the first waveform, ${}^{111}_{1}\underline{g}$, is negative, and its magnitude increases with increasing wavelength (Table I). Together, ${}^{1}_{1}\underline{g}$ and ${}^{111}_{1}\underline{g}$ produce a finite dominant wavelength, Fig. 12. Several dominant wavelengths for the multilayer with free slip at contacts are listed in Table II.

The preferred wavelength-to-thickness ratio is the wavelength ratio of the perturbation that has achieved the highest amplification, $({}_1A/{}_1A_0)$, for a given amount of horizontal shortening, $\underline{S}_x$. Preferred wavelength ratios for infinitely thick multilayers with free slip at contacts are indicated by the peaks of the curves in Fig. 13.

Whereas the magnitudes of the amplification factors for the first waveform are important because they determine the amplitudes of the folds, the magnitudes and signs of the amplification factors for the third waveform are important because they determine the forms of the folds. The

Figure 13. Relationship between amplification (${}_1\underline{A}/{}_1\underline{A}_o$) of first waveform and wavelength-to-thickness ratio ($\underline{L}/\underline{h}$) for selected values of horizontal shortening $\bar{\underline{S}}_x$ in an infinitely thick multilayer with free slip at contacts. The ($\underline{L}/\underline{h}$) that has become most amplified after a given amount of shortening is $(\underline{L}/\underline{h})_p$, the preferred wavelength ratio.

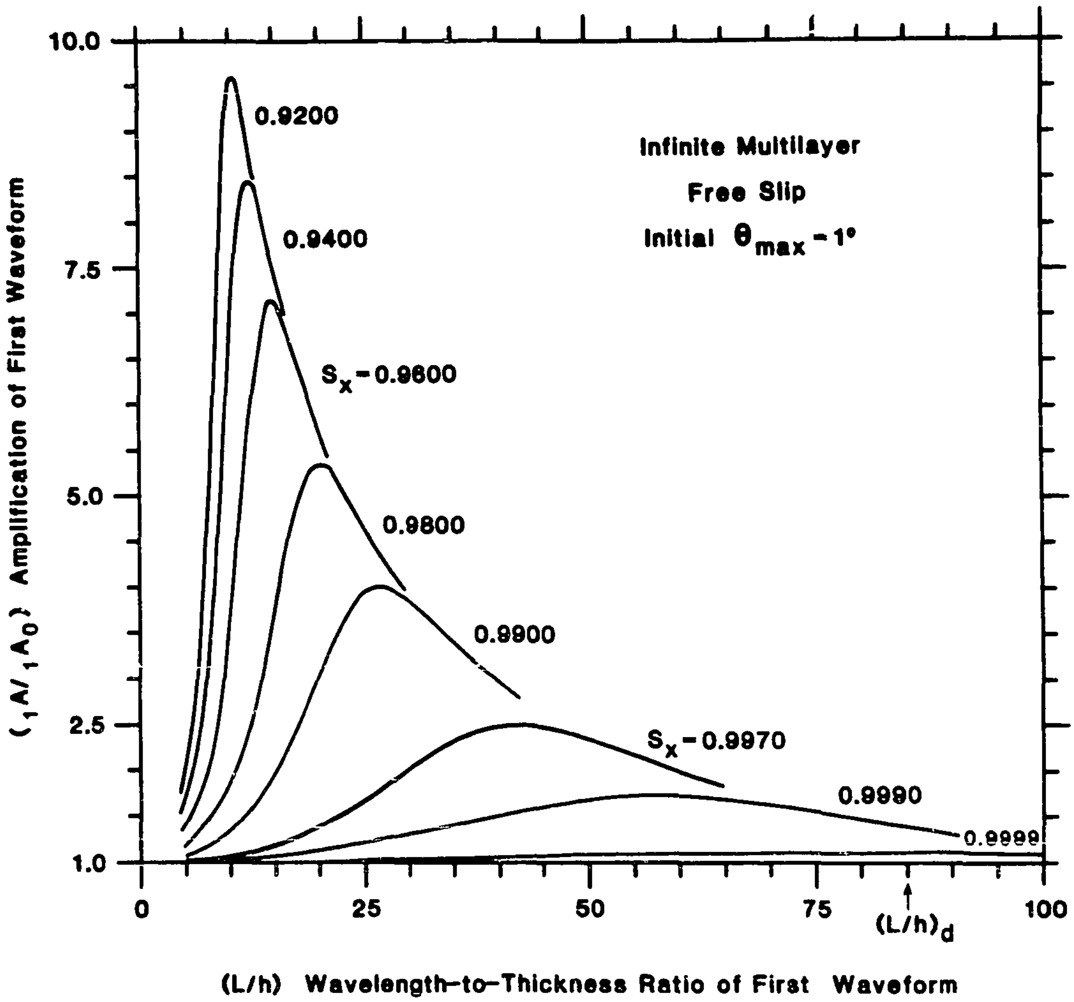
Infinite Multilayer
Free Slip
Initial θmax = 1°
0.9200
0.9400
Sx = 0.9600
0.9800
0.9900
Sx = 0.9970
0.9990
0.9999
10.0
7.5
5.0
2.5
1.0
0
25
50
75
100
(L/h)d
(1A/ 1A0) Amplification of First Waveform
(L/h) Wavelength-to-Thickness Ratio of First Waveform

amplification factors for the third waveform are positive for free slip at contacts and negative for localized slip at contacts, for all wavelengths (Table I, Fig. 14). According to eq. (27b), the positive values of ${}^{3}_{3}\underline{g} + {}^{11}{}^{1}_{3}\underline{g}$ for free slip produce a positive third waveform. The result is the chevron fold (Fig. 5, loc. A1). On the other hand, the negative value of ${}^{11}{}^{1}_{3}\underline{g}$ for localized slip at contacts results in a negative third waveform. The result is the box fold (Fig. 5, loc. B1).

Changes in Amplification Factors during Folding. One of the interesting results of analyses of folding to 3rd order accuracy is that amplification factors can change markedly during folding. For example, the amplification factor for the dominant wavelength in the case of free slip reduces considerably as the maximum slope angle of the multilayer increases from 1° to 15° during folding (Table II). Values of the amplification factors during folding are determined by using values for the current amplitudes and wavelength ratios in the expressions in Table I. Values for the amplitudes during folding are found, in turn, by integrating eqs. (27) with respect to horizontal stretch, $\underline{S}_x$, which is the variable I use to keep track of the shortening.

Each instant during the growth of a particular fold can be identified by a single point in Fig. 12, and a line connecting successive points describes the path of

Figure 14. Relationship between amplification factors ${}^{3}_{3}g$ and ${}^{11}_{\ 3}g$ for the third waveform and wavelength-to-thickness ratio (L/h) for the first waveform in infinitely thick multilayers.

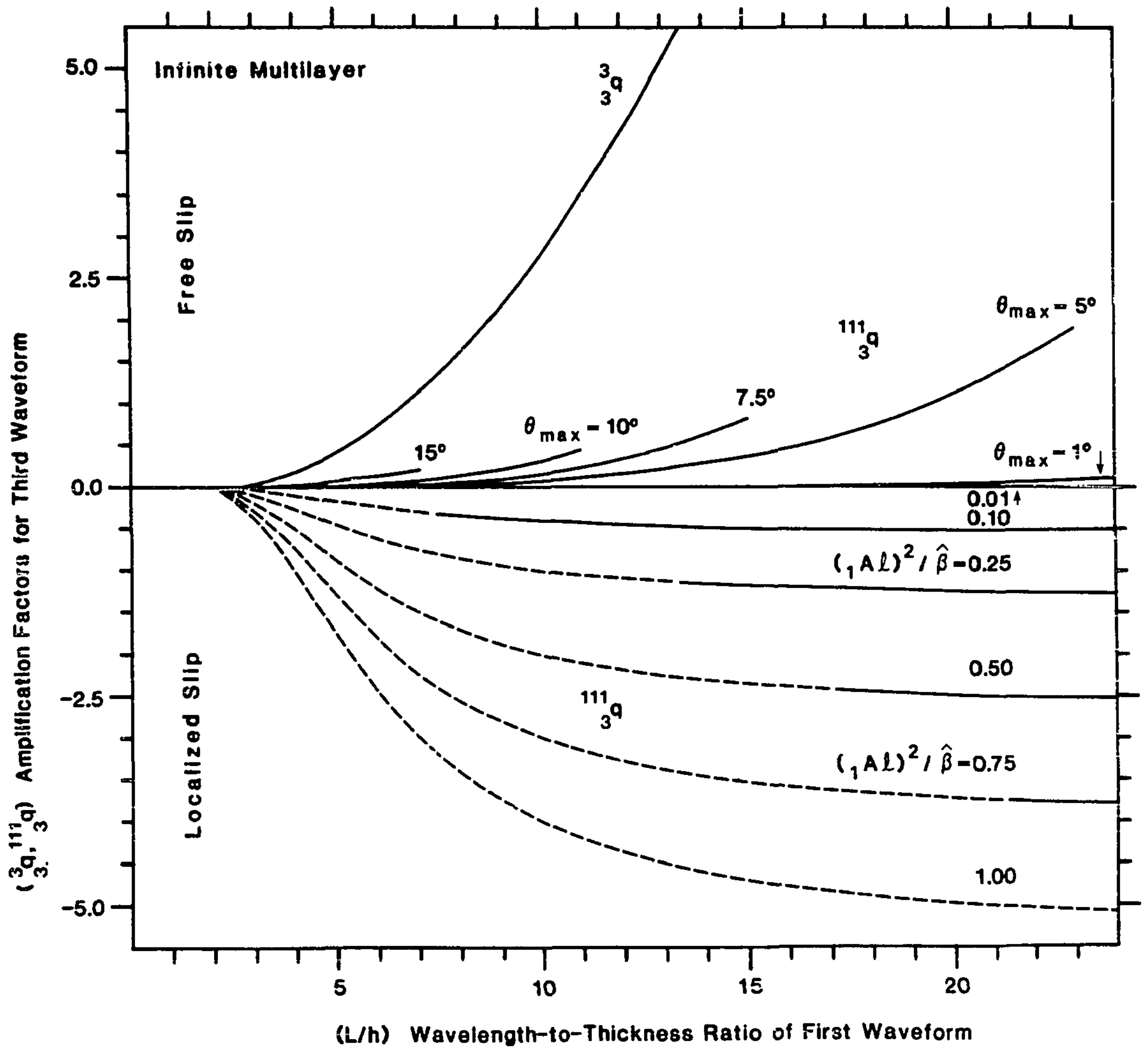

Infinite Multilayer
Free Slip
Localized Slip
$_3^3q$
$_3^{111}q$
$\theta_{max} = 5°$
7.5°
$\theta_{max} = 10°$
15°
$\theta_{max} = 1°$
0.01
0.10
$({}_1A\ell)^2/\hat{\beta} = 0.25$
0.50
$({}_1A\ell)^2/\hat{\beta} = 0.75$
1.00
5.0
2.5
0.0
-2.5
-5.0
5
10
15
20
$({}_3^3q, {}_3^{111}q)$ Amplification Factors for Third Waveform
(L/h) Wavelength-to-Thickness Ratio of First Waveform

TABLE II

DOMINANT WAVELENGTH-TO-THICKNESS RATIOS IN AN INFINITELY THICK MULTILAYER WITH FREE SLIP AT CONTACTS

Maximum Slope Angle	Dominant Fold Wavelength	Dominant Fold Amplification Factor
$\tan^{-1}({}_1A\ell)$	$(L/h)_d$	$({}_1q)_{max}$
1°	85	1100
5°	17	42
7.5°	11	18
10°	8	9
15°	5	3

amplification factors during folding. Several paths of amplification factors for first waveforms are shown in Figs. 15A and 15B.

The amplification factor $_{1}\underline{g}$ (= $^{\mathrm{I}}_{1}\underline{g}$ + $^{\mathrm{II}}_{1}\underline{g}$) decreases sharply as the slope of the perturbation increases in a multilayer with free slip at contacts (Fig. 15A). The reason is given in Table I: the positive contribution, $^{\mathrm{I}}_{1}\underline{g}$, is independent of slope, but the absolute magnitude of the negative contribution, $^{\mathrm{II}}_{1}\underline{g}$, increases as the square of the slope.

In striking contrast, the amplification factor $_{1}\underline{g}$ characteristically remains nearly constant and then suddenly increases with increase in slope of a perturbation in multilayers with localized slip at contacts (Fig. 15B). Again, the reason is given in Table I: the amplification factor for the first waveform, $^{\mathrm{II}}_{1}\underline{g}$, is positive and proportional to the square of the maximum slope of the perturbation.

Paths of amplification factors in multilayers with localized slip (Fig. 15B) reflect unstable yielding of contacts. As the slope increases, the anisotropy increases and the contact viscosity decreases, which further drives the folding. Comparison of paths $\underline{B}$-$\underline{B}$' and $\underline{A}$-$\underline{A}$' (Fig. 15B) suggests that a critical slope must be reached for unstable yielding to begin. Perturbation $\underline{A}$ has an initial slope greater than the critical value and immediately yields

Figure 15. Selected paths of progressive change in amplification factor $_1g$ during folding. A. In an infinitely thick multilayer with free slip at contacts, $_1g$ decreases as the slope of the perturbation increases. B. In an infinitely thick multilayer with localized slip at contacts, $_1g$ increases as the slope of the perturbation increases.

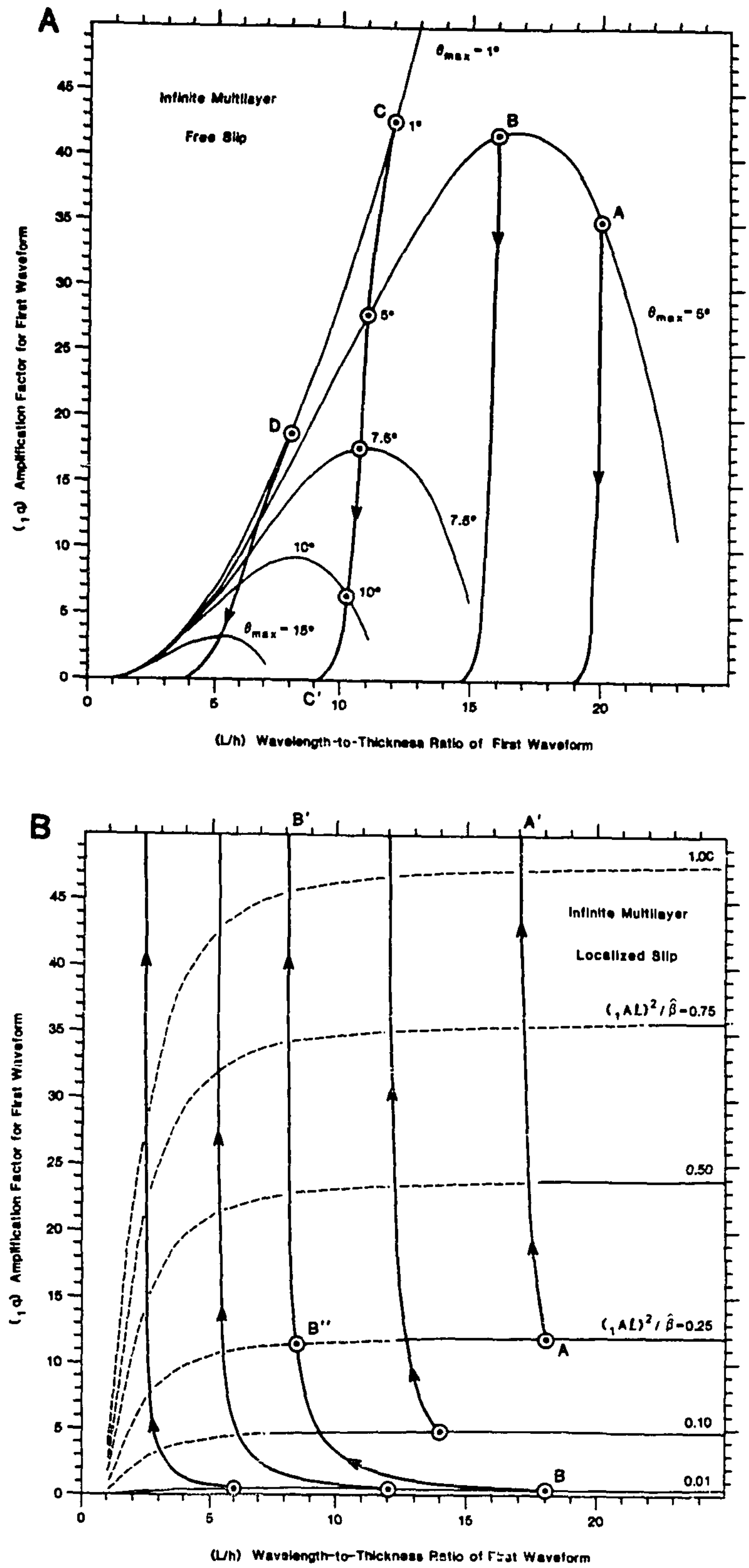
A
Infinite Multilayer
Free Slip
θ_{max} = 1°
C
1°
B
A
5°
θ_{max} = 5°
D
7.5°
7.5°
10°
10°
θ_{max} = 15°
C'
($_1a$) Amplification Factor for First Waveform
(L/h) Wavelength-to-Thickness Ratio of First Waveform
B
B'
A'
1.00
Infinite Multilayer
Localized Slip
$(_1AL)^2/\beta$=0.75
0.50
B''
$(_1AL)^2/\beta$=0.25
A
0.10
B
0.01
($_1a$) Amplification Factor for First Waveform
(L/h) Wavelength-to-Thickness Ratio of First Waveform

unstably as folding begins. Perturbation $\underline{B}$, however, has an initial slope below the critical value; shortening (decrease of $\underline{L}/\underline{h}$) increases the maximum slope, but yielding is stable until the critical slope is achieved, in the vicinity of point $\underline{B}''$.

Evolution of a Box Fold. Examination of several steps in the formation of a box fold from a simple, cosinusoidal perturbation allows one to correlate the change in form of the fold to the change in amplification factors. Analysis of the differential equations describing the rates of growth of the component waveforms, eqs. (27), reveals how the fold form grows (Fig. 16). Analysis of the integrated form of these equations reveals how the fold form appears (Fig. 17). Each of these approaches will be used to study the evolution of the box fold shown in Fig. 5, loc. B1.

The paths of the amplification factors for the first and third waveforms, ${}^{11}{}_{1}^{1}\underline{q}$ and ${}^{11}{}_{3}^{1}\underline{q}$, are superimposed on graphs showing the relationship between amplification factor and current wavelength ratio, $(\underline{L}/\underline{h})_c$, contoured for constant values of $({}_1\underline{A}\ell)^2/\beta$, in Fig. 16. The material property β is constant, so the lines are contours of equal current slope and equal current anisotropy.

The paths in Fig. 16 document the continuous evolution of the box fold shown in Fig. 5, loc. B1. The five points indicated by Roman numerals in Fig. 16 are analyzed in Table III. Initial conditions are represented at point I

<u>Figure</u> <u>16</u>. Paths of progressive change in amplification factors ${}^{111}_{\;\;\;1}\underline{g}$ and ${}^{111}_{\;\;\;3}\underline{g}$ during growth of box fold shown in Fig. 5, loc. B1. While the slope and anisotropy remain low, the amplification factors increase slowly; at a slope and anisotropy between points III and IV, the amplification factors begin to increase rapidly, reflecting unstable yielding of contacts. As explained in the caption to Fig. 12, the dashed lines indicate combinations of $({}_1A\ell)^2/\hat{\beta}$ and ($\underline{L}/\underline{h}$) for which the limits of the 3rd order solution have been exceeded. Where the paths of the amplification factors encounter a dashed line, the equations describing the growth of the fold are out-of-bounds because higher-order terms discounted by the 3rd order analysis are no longer negligible. The essence of the stage V fold form is present at stage IV; continuing the folding into the dashed region exaggerates the elements sufficiently to make the fold form visible for illustration but does not change the nature of the effect of the third waveform.

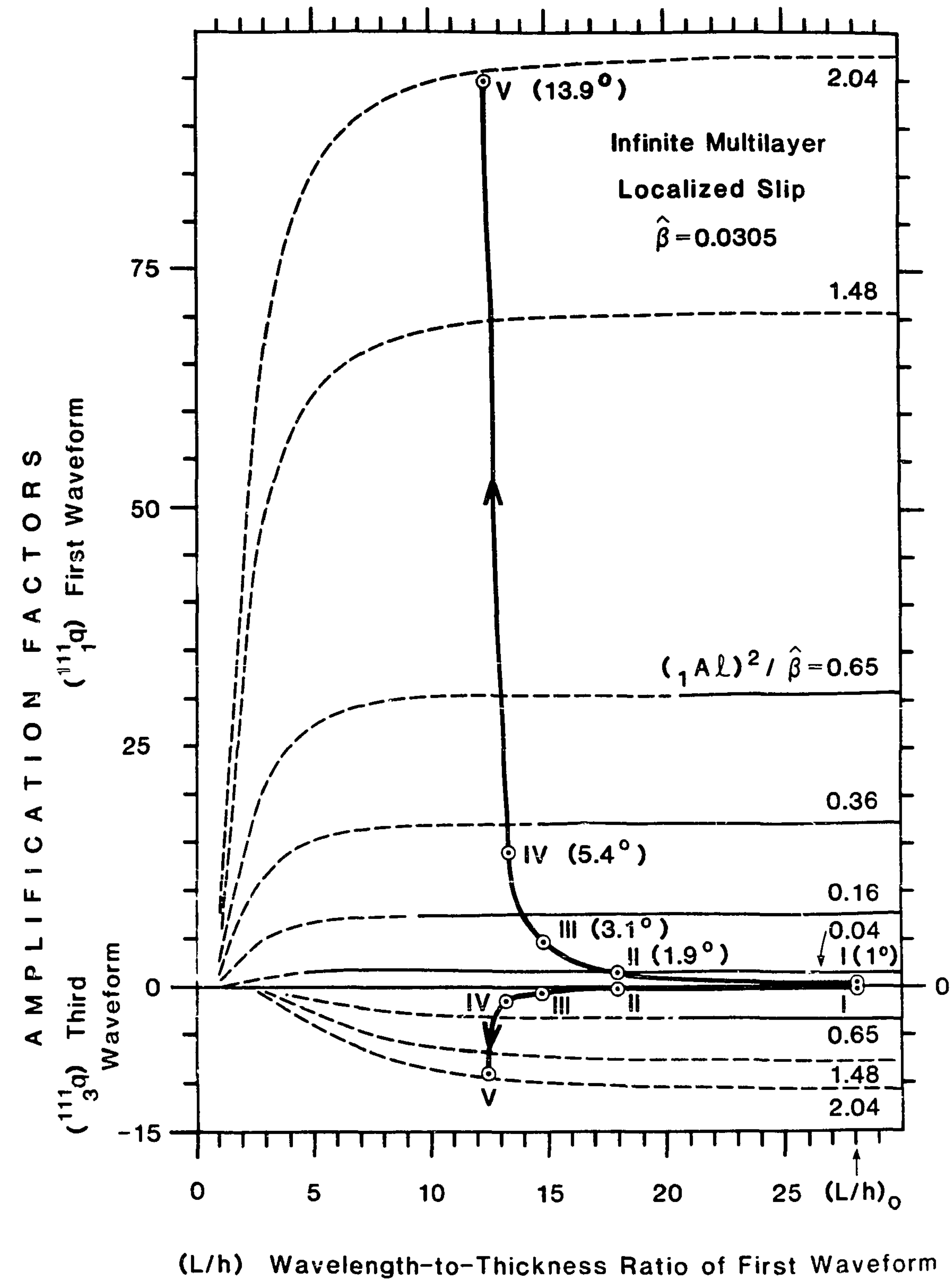

V (13.9°)
2.04
Infinite Multilayer
Localized Slip
$\hat{\beta}$=0.0305
75
1.48
50
AMPLIFICATION FACTORS
($^{111}_{1}q$) First Waveform
($_{1}A\ell)^2 / \hat{\beta}$=0.65
25
0.36
IV (5.4°)
0.16
III (3.1°)
0.04
II (1.9°)
I (1°)
0
IV
III
II
I
0.65
($^{111}_{3}q$) Third Waveform
1.48
V
2.04
-15
0
5
10
15
20
25
(L/h)$_0$
(L/h) Wavelength-to-Thickness Ratio of First Waveform

TABLE III

ANISOTROPY AND AMPLIFICATION FACTORS AT
FIVE STAGES IN EVOLUTION OF BOX FOLD SHOWN IN FIG. 5, LOC. B1

Stage	$\bar{S}_x$	(L/h)	$\tan^{-1}({}_1A\ell)$	Anisotropy (μ_n/μ_s)	Amplification Factors	
					$(1 + {}^{111}_{1}q)$	${}^{111}_{3}q$
I	1.0	28.0	1°	1.48	1.48	-0.05
II	0.80	17.9	2°	2.80	2.78	-0.18
III	0.72	14.6	3°	5.77	5.70	-0.46
IV	0.69	13.1	5°	15.29	15.02	-1.34
V	0.67	12.4	14°	97.92	95.87	-8.91

(Fig. 16, Table III): wavelength-to-thickness ratio $(L/H)_o = 28$; maximum slope of the first waveform $({}_1A\ell)_o = \tan(1°) = 0.017$; $({}_1A\ell)_o^2/\beta = 0.01$; anisotropy $\alpha_o = 1.48$.

Starting from the initial conditions (point I), the amplification factors increase slowly early in the shortening. When the multilayer has shortened by 20 percent ($\bar{\underline{S}}_x = 0.80$; point II, Fig. 16), the wavelength-to-thickness ratio has reduced from 28 to 17.9, about one-third its original value (Table III). The amplification factors have tripled, but folding remains largely kinematic.

As the maximum slope angle of the first waveform reaches four or five degrees (between points III and IV, Fig. 16), the magnitudes of the amplification factors begin to increase rapidly with further shortening. Points III and IV correspond to shortening of 28 to 31 percent ($\bar{\underline{S}}_x$ of 0.72 to 0.69).

Between points IV and V (Fig. 16), the shortening increases slightly, from 31 to 33 percent ($\bar{\underline{S}}_x$ from 0.69 to 0.67), but the amplification factors for the first and third waveforms, ${}^{11}_{1}\underline{g}$ and ${}^{11}_{3}\underline{g}$, both increase by an order of magnitude (Table III). Folding has become dynamic. The rapid increase in amplification factors reflects the phenomenon of unstable yielding of contacts, which is the driving mechanism of folding in multilayers with nonlinear resistance to slip at contacts.

The left-hand column in Fig. 17 shows the fold forms corresponding to points II to V in Fig. 16. The middle column shows the individual amplitude-to-thickness ratios, ${}_1\underline{A}/\underline{h}$ and ${}_3\underline{A}/\underline{h}$. The right-hand column shows the ratio ${}_3\underline{A}/{}_1\underline{A}$ and demonstrates that the amplitude of the third waveform is increasing relative to that of the first during shortening. The ratio ${}_3\underline{A}/{}_1\underline{A}$ indicates the relative strength that the third waveform has in modifying the shape of the fold.

Initially, stages I through III, the shape of the interfaces is essentially cosinusoidal because the magnitude of the ratio ${}_3\underline{A}/{}_1\underline{A}$ is less than 0.04. By stage III, the slope has increased from 1° to only 3°, so even the first waveform is subtle.

A discernible box fold begins to emerge as unstable yielding at contacts begins (between points III and IV). At stage IV, the maximum slope angle of the first waveform is 5°, ${}_3\underline{A}/{}_1\underline{A} = -0.06$, and the third waveform is starting to flatten crests and troughs and to localize steepening in limbs. By stage V, the slope angle of the first waveform has increased to 14° and the amplitude of the first waveform is 2.5 times that in stage IV, so the fold is quite perceptible (Fig. 17). In addition, the strength of the third waveform has increased to eight percent, ${}_3\underline{A}/{}_1\underline{A} = -0.08$. The resultant fold form is a box fold with a maximum slope angle of 17°:

Figure 17. Four stages in evolution of the box fold shown in Fig. 5, loc. B1. A. Fold forms. B. Amplitudes of first and third waveforms for each interface. C. Relative amplitudes for each interface. At point IV, the slope is 5°, ${}_3\underline{A}$ is $-0.06({}_1\underline{A})$, and flattening of hinges is just discernible. By point V, the slope is 14°, ${}_3\underline{A}$ is $-0.08({}_1\underline{A})$, and flattening of the hinges is distinct.

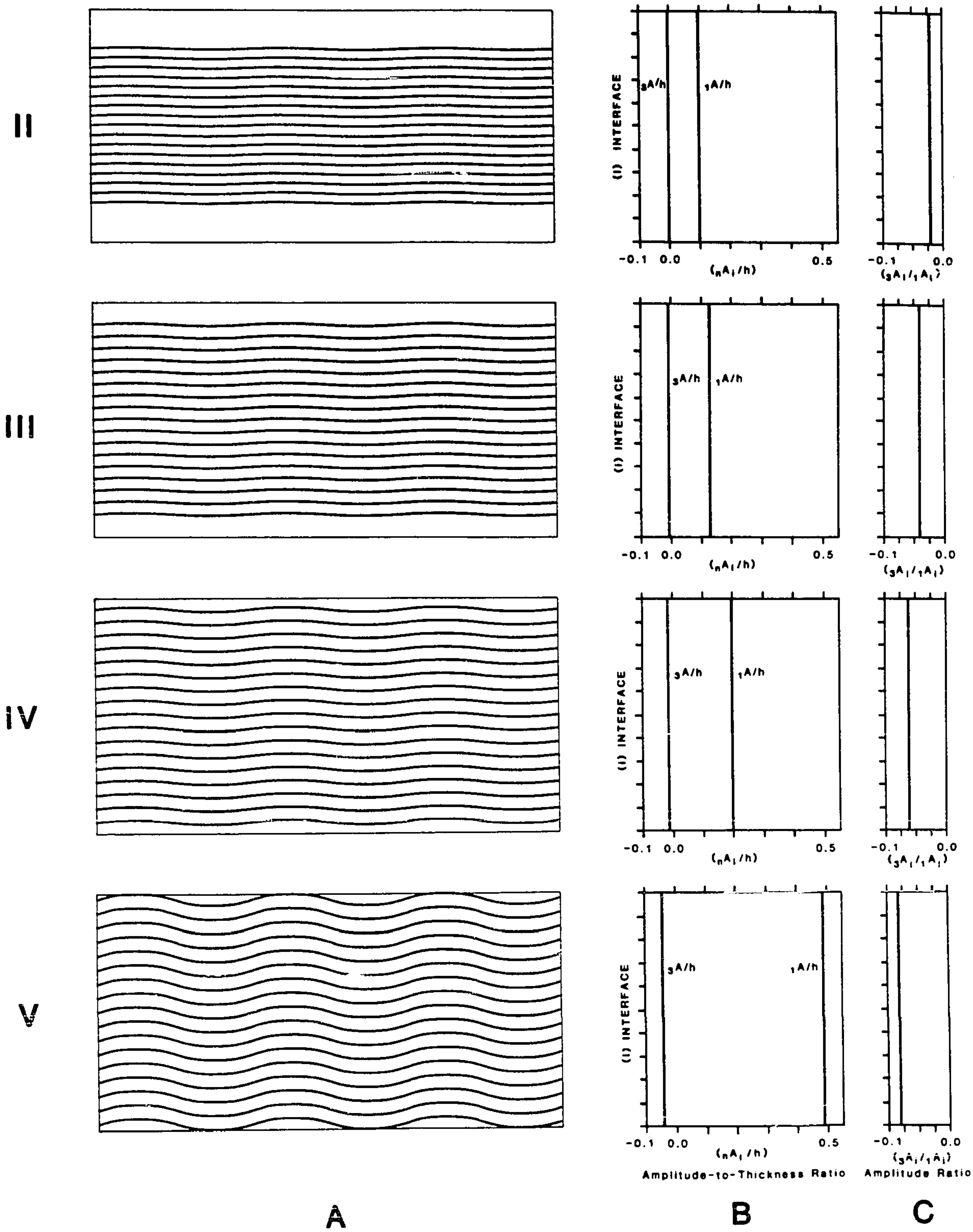
II
III
IV
V
(I) INTERFACE
3A/h
1A/h
-0.1 0.0 0.5
(nAi/h)
-0.1 0.0
(3Ai/1Ai)
Amplitude-to-Thickness Ratio
Amplitude Ratio
A
B
C

$$(\partial\zeta/\partial x)_{x=-L/4} = ({}_1A\ell)[1 - 3({}_3A/{}_1A)] \qquad (29)$$

because $\tan^{-1}({}_1A\ell) = 14°$ and ${}_3\underline{A}/{}_1\underline{A} = -0.08$.

In these ways Figs. 16 and 17 show how a simple, cosinusoidal initial perturbation, with maximum slope angle of 1°, evolves into a box fold.

Folding of Finite Multilayers

Analysis of folding of infinitely thick multilayers allows one to investigate basic causes of similar fold forms and to write closed form expressions for amplification factors. Investigation of parallel fold types, including concentric-like and kink-like folds, requires multilayers to be of finite thickness.

Three significant changes occur in the folding of the three standard multilayers -- with bonded contacts, free slip at contacts, and localized slip at contacts -- if the multilayer thickness is made finite:

1. Both even and odd waveforms grow, to 3rd order, in finite multilayers. First, second, and third waveforms grow in multilayers with free slip or bonded contacts. First through fourth waveforms grow in multilayers with localized slip if the power, $\underline{m}$, is 2. (If $\underline{m} = 3$, only the first through third waveforms grow).
2. A multilayer with localized slip at contacts has finite dominant and preferred wavelengths.
3. A bonded multilayer behaves as a single layer with free

slip at contacts.

<u>Eigenvectors and Eigenvalues for the First Waveform</u>. Each interface in a finite multilayer can have different amplitudes of component waveforms, and growth of each waveform can, in principle, be affected by all the other amplitudes in all the other interfaces. The differential equations that describe the growth of the waveforms are nonlinear, but the description of amplitude distributions is considerably simplified by extraction of eigenvectors and eigenvalues from the differential equations for the first waveform. Use of eigenvectors and eigenvalues to analyze linear differential equations is discussed in Chapter I and by Ramberg (1970) and Smith (1975, 1977).

The equations that describe the growth of the first waveform in each interface, to 3rd order accuracy, are a system of <u>n</u> coupled, nonlinear differential equations:

$$d({}_{1}A_{i})/d(\ell n\bar{S}_{x}) = {}_{1}A_{i} + ({}_{1}A_{j})[{}^{1}_{1}q_{ij} + {}^{11}_{1}q_{ij} + {}^{111}_{1}q_{ij}]$$

$$i=1,2...n;\; j=1,2...n \qquad (30a)$$

where <u>n</u> is the number of interfaces in the multilayer (summation on repeated indices). Expressions for the <u>q</u>'s are provided in the appendices.

My approach to the analysis of eqs. (30a) is to determine iteratively the eigenvalues and eigenvectors of the system of equations. The eigenvalue of greatest absolute value equals one plus the maximum amplification factor, $_1g_{max}$, for the first waveform for the system of layers. The ratio of wavelength to thickness ($\underline{L}/\underline{h}$) that maximizes the eigenvalue is the initial dominant wavelength $(\underline{L}/\underline{h})_d$. The eigenvector corresponding to the eigenvalue represents the relative amplitudes of the first waveforms in the interfaces of the multilayer. Thus the amplitude in one interface is specified and the eigenvector determines the others.

Eigenvectors for finite multilayers confined by soft media ($\underline{R} = \mu_{media}/\mu_{layers} = 0.01$) are shown in Fig. 18 for a range of initial wavelength ratios. The maximum slope was 1°, but each eigenvector has been normalized to 1.0. These eigenvectors were used to design the forms of the initial perturbations in the finite multilayers shown in Figs. 4 and 5.

If the contacts slip freely (Fig. 18A), the initial perturbation has nearly the same amplitude at every interface for all wavelength ratios. If slip at contacts is localized (Fig. 18B) or if contacts are bonded (Fig. 18C), the eigenvectors vary with wavelength ratio: at low ($\underline{L}/\underline{h}$), the amplitude of the initial perturbation is much lower on the outer interfaces than on the middle interfaces; at larger ($\underline{L}/\underline{h}$), the amplitudes become more nearly uniform.

Relationships between amplification factor and wavelength ratio are compared for infinitely thick and

Figure 18. Eigenvectors at selected wavelength-to-thickness ratios ($\underline{L}/\underline{h}$) for finite multilayers confined by soft media (μ_m/μ_ℓ = 0.01). A. Free slip at contacts. B. Localized slip at contacts. C. Bonded contacts.

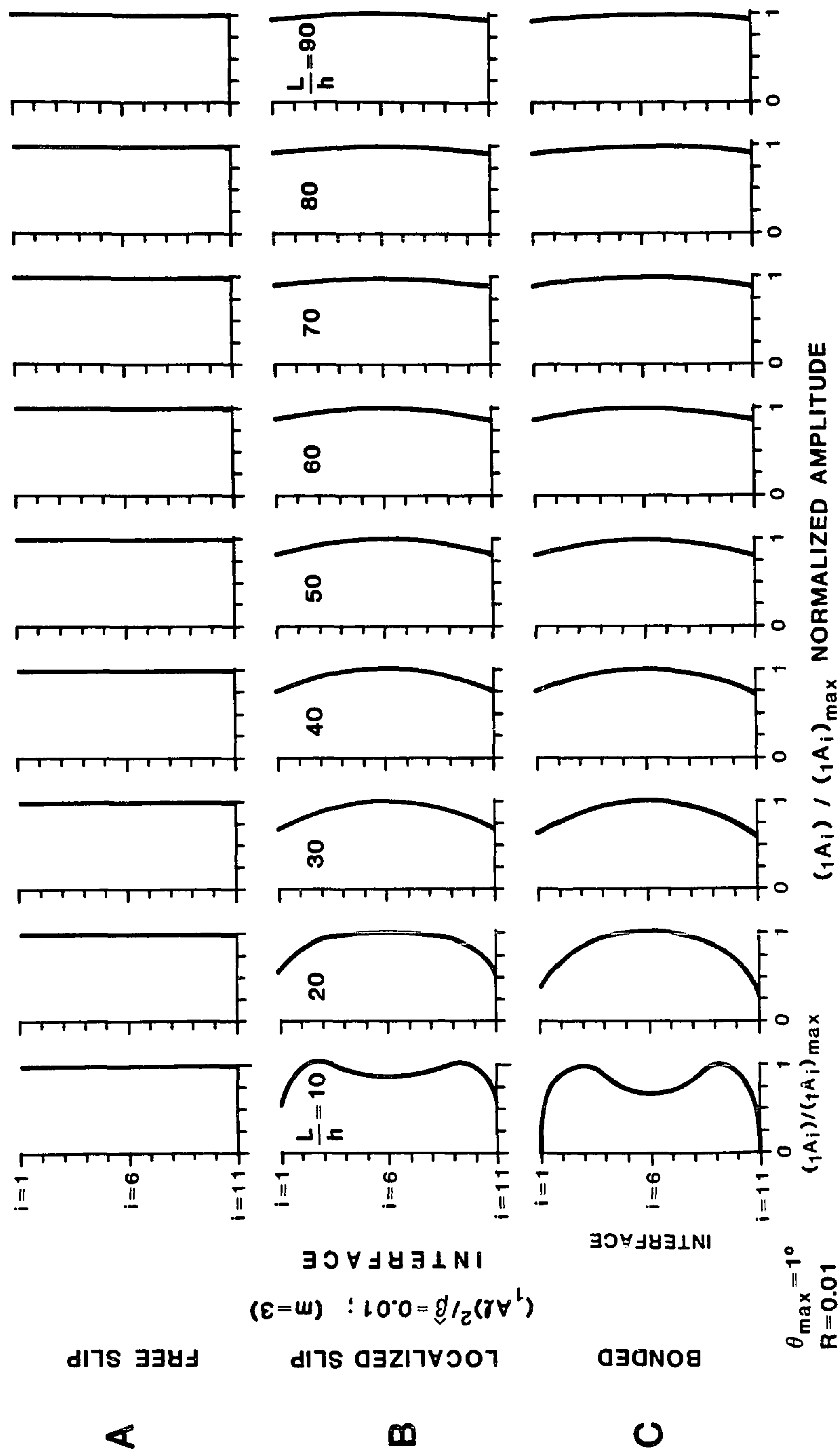
A
B
C
FREE SLIP
LOCALIZED SLIP
BONDED
$({}_1A\ell)^2/\mathcal{g} = 0.01$; (m=3)
INTERFACE
INTERFACE
$\theta_{max} = 1°$
R=0.01
$\frac{L}{h} = 10$
20
30
40
50
60
70
80
$\frac{L}{h} = 90$
i=1
i=6
i=11
$({}_1A_i)/({}_1A_i)_{max}$
$({}_1A_i)$ / $({}_1A_i)_{max}$ NORMALIZED AMPLITUDE

unconfined finite multilayers in Fig. 19. For all the multilayers considered, amplification factors are higher for unconfined finite multilayers than for the corresponding infinitely thick multilayers (Table IVa,b). For free slip at contacts, dominant wavelength ratios are slightly larger in the unconfined finite multilayer than in the infinitely thick multilayer (Table IVc,d).

Unconfined finite multilayers with bonded contacts and with localized slip at contacts ($\underline{m}$ = 3) have similar dominant wavelength ratios and amplification factors. The dominant wavelength ratios are an order of magnitude greater than those in the multilayer with free slip at contacts; however, the amplification factors are nearly identical (Fig. 19, Table IV).

For multilayers with free slip at contacts and with bonded contacts, the difference in dominant wavelength ratio is a function only of the number of layers in the multilayer. Because all the multilayers in this chapter have frictionless contacts with the confining media, the 10-layer multilayer with bonded contacts is equivalent to a multilayer consisting of one thick layer with free slip at contacts.

Increasing confinement produces lower dominant wavelength ratios and lower amplification factors (Fig. 20, Table IV). Comparing various multilayers with localized slip at contacts to one with bonded contacts, the dominant

Figure _19_. Relationship between amplification factor $_1\underline{q}$ and wavelength-to-thickness ratio ($\underline{L}/\underline{h}$) for the first waveform in infinitely thick and unconfined finite multilayers. The dominant wavelength ratio in unconfined finite multilayers with bonded contacts or with localized slip at contacts is an order of magnitude greater than the dominant wavelength ratio in the corresponding multilayer with free slip at contacts.

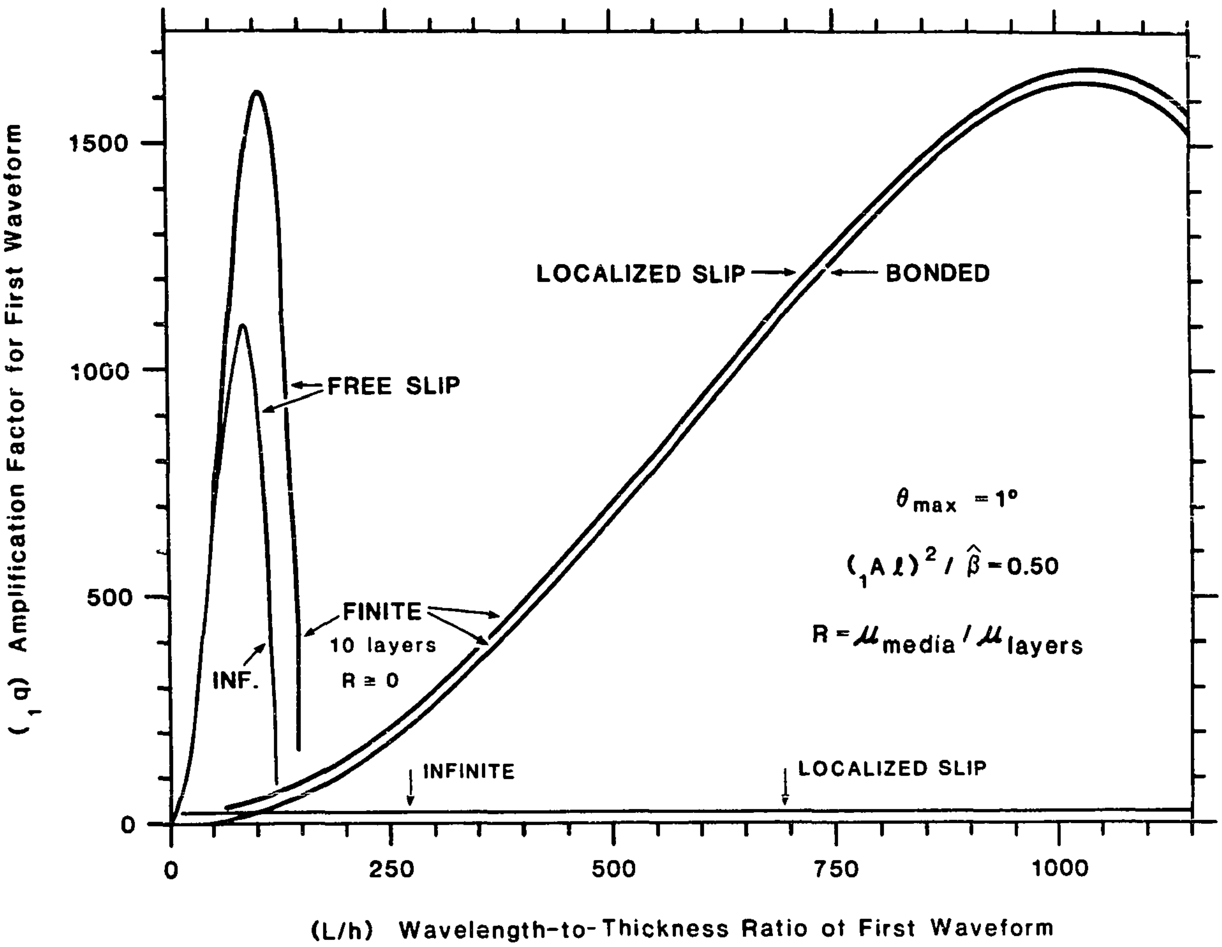

1500
1000
500
0
250
750
FREE SLIP
LOCALIZED SLIP
BONDED
FINITE
10 layers
R ≥ 0
INF.
INFINITE
LOCALIZED SLIP
$\theta_{max} = 1°$
$({}_1A\ell)^2 / \hat{\beta} = 0.50$
$R = \mu_{media} / \mu_{layers}$
$({}_1q)$ Amplification Factor for First Waveform
(L/h) Wavelength-to-Thickness Ratio of First Waveform

TABLE IV

MAXIMUM AMPLIFICATION FACTORS AND DOMINANT WAVELENGTH-TO-THICKNESS RATIOS IN MULTILAYERS OF FINITE AND INFINITE THICKNESS

a. Maximum Amplification Factors $({}_1q)_{max}$ in Multilayers of Finite Thickness

α \ R	0	0.01	0.1
∞ (free slip)	1641	118	26
13	1654	29	12
5.8	1647	27	7
1 (bonded)	1642	25	5

b. Maximum Amplification Factors $({}_1q)_{max}$ in Multilayers of Infinite Thickness

α	
∞ (free slip)	1100
13	12
5.8	5
1 (bonded)	0

c. Dominant Wavelength-to-Thickness Ratios $(L/h)_d$ in Multilayers of Finite Thickness

α \ R	0	0.01	0.1
∞ (free slip)	104	35	16
13	1036	138	18
5.8	1038	154	55
1 (bonded)	1040	165	82

d. Dominant Wavelength-to-Thickness Ratios $(L/h)_d$ in Multilayers of Infinite Thickness

α	
∞ (free slip)	85
13	∞
5.8	∞
1 (bonded)	0

$R = \mu_{media}/\mu_{layers}$ α = anisotropy

10 layers $m = 3$

Figure 20. Relationship between amplification factor ${}_1g$ and wavelength-to-thickness ratio (L/h) for finite multilayers confined by soft media ($\mu_m/\mu_\ell = 0.01$). As the anisotropy of the multilayer increases, the dominant wavelength ratio decreases and its associated ${}_1g$ increases.

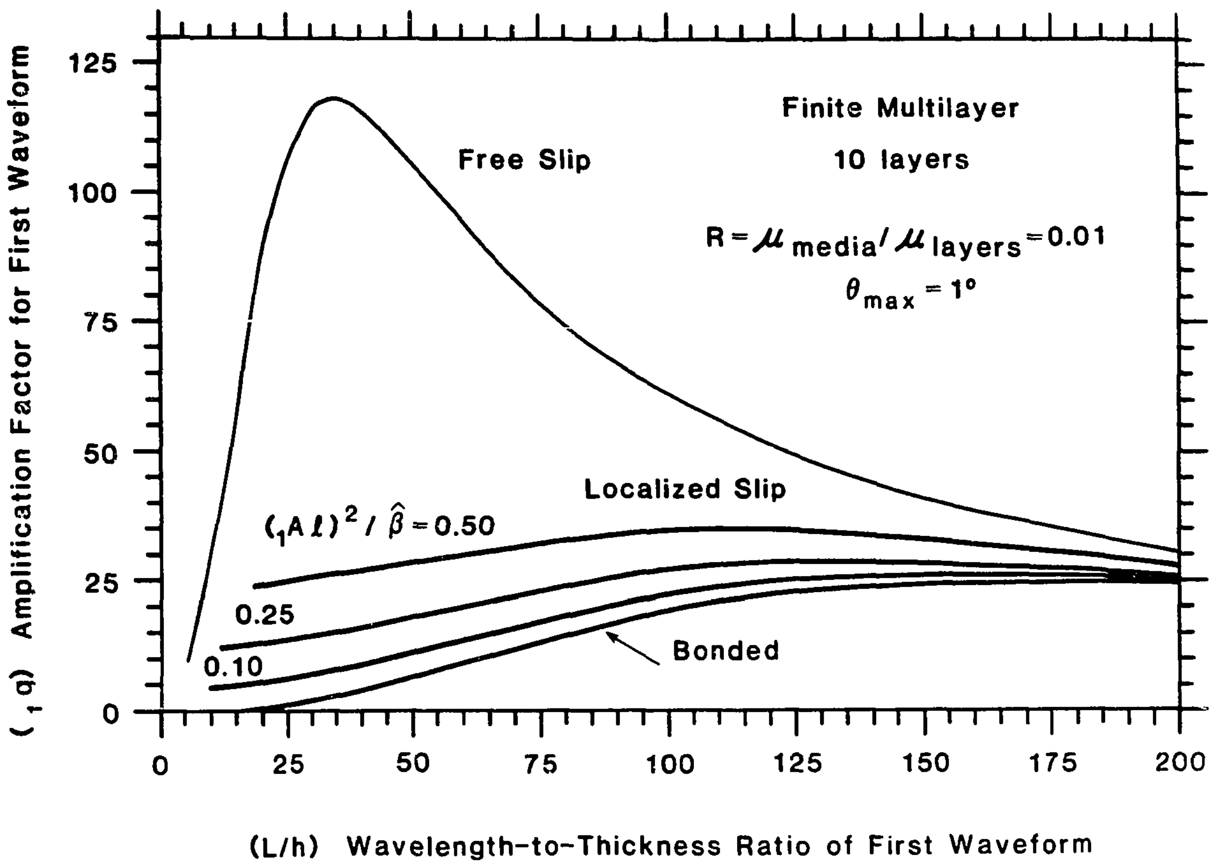

Finite Multilayer
10 layers
R = μ media / μ layers = 0.01
θ max = 1°
Free Slip
Localized Slip
(₁A ℓ)² / β̂ = 0.50
0.25
0.10
Bonded
125
100
75
50
25
0
0
25
50
75
100
125
150
175
200
(₁q) Amplification Factor for First Waveform
(L/h) Wavelength-to-Thickness Ratio of First Waveform

wavelength ratio is always found to be larger -- and the amplification factor always lower -- for the multilayer with bonded contacts (anisotropy = 1.0). As the anisotropy of the multilayer increases (as the $({}_{1}A\ell)^{2}/\beta$ ratio increases), $(\underline{L}/\underline{h})_{d}$ is reduced and ${}_{1}\underline{q}_{max}$ is increased (Table IV).

<u>Amplification Factors for Second, Third, and Fourth Waveforms</u>. Equations describing the growth of the second, third, and fourth waveforms in a finite multilayer are, to 3rd order accuracy:

$$d({}_{2}A_{i})/d(\ell n\bar{S}_{x}) = {}_{2}A_{i} + ({}_{2}A_{j})[{}^{2}_{2}q_{ij}] + ({}_{1}A_{j})[{}^{11}_{2}q_{ij} + {}^{111}_{2}q_{ij}] \tag{30b}$$

$$d({}_{3}A_{i})/d(\ell n\bar{S}_{x}) = {}_{3}A_{i} + ({}_{3}A_{j})[{}^{3}_{3}q_{ij}] + ({}_{1}A_{j})[{}^{11}_{3}q_{ij} + {}^{111}_{3}q_{ij}] \tag{30c}$$

$$d({}_{4}A_{i})/d(\ell n\bar{S}_{x}) = {}_{4}A_{i} + ({}_{4}A_{j})[{}^{4}_{4}q_{ij}] + ({}_{1}A_{j})[{}^{111}_{4}q_{ij}] \tag{30d}$$

Expressions for the $\underline{q}$'s are provided in the appendices. Initial growth rates for the second, third, and fourth component waveforms are determined by the quantities $({}^{11}_{2}\underline{q} + {}^{111}_{2}\underline{q})$, $({}^{11}_{3}\underline{q} + {}^{111}_{3}\underline{q})$, and $({}^{111}_{4}\underline{q})$, respectively, because ${}_{2}\underline{A}_{j}$, ${}_{3}\underline{A}_{j}$, and ${}_{4}\underline{A}_{j}$ are zero initially. Initial values of these amplification factors can be calculated for each interface using the eigenvector of values ${}_{1}\underline{A}_{j}$, found by solving eq. (30a), and are designated ${}_2\underline{q}$, ${}_3\underline{q}$, and ${}_4\underline{q}$, respectively.

A critical amplification factor for the development of strong concentric-like and kink-like forms in multilayers is ${}_2\underline{q}$, the amplification factor for the second waveform. Relations among ${}_2\underline{q}$, wavelength ratio, properties of confining media, and properties of interfaces between layers are shown in Fig. 21.

Figure 21A shows that the amplification factor of the second waveform can be relatively large for multilayers with free slip at contacts, depending on the wavelength ratio and the relative stiffness, $\underline{R}$, of the confining media. As relative stiffness increases from very soft to soft, $\underline{R}$ = 0.01 to 0.1, the maximum amplification factor decreases, and the corresponding wavelength-to-thickness ratio decreases from about 23 to 18.

The amplification factor of the second waveform for the multilayers with localized slip depends on the order of approximation and the exponential power. For 3rd order analysis and power $\underline{m}$ = 2, the strength of the amplification factor is determined largely by the anisotropy of the multilayer, that is, the $({}_1A\ell)^{(m-1)}/\beta$ ratio. As anisotropy increases, the amplification factor increases (Fig. 21B). For 3rd order analysis and $\underline{m}$ = 3, the amplification factor is very small (Fig. 21A); one would have to perform a 4th order analysis to see a strong second waveform for a power

Figure 21. Relationship between amplification factor ${}_2\underline{q}$ for the second waveform and wavelength-to-thickness ratio ($\underline{L}/\underline{h}$) for the first waveform for unconfined and confined finite multilayers. A. Confinement by soft media (μ_m/μ_ℓ = 0.01) maximizes ${}_2\underline{q}$ for a particular initial ($\underline{L}/\underline{h}$). To 3rd order, maximum values of ${}_2\underline{q}$ are significantly higher in the multilayer with free slip at contacts than in the multilayer with localized slip at contacts ($\underline{m}$ = 3). B. Increase in anisotropy of multilayer with localized slip at contacts ($\underline{m}$ = 2) increases the maximum value of ${}_2\underline{q}$.

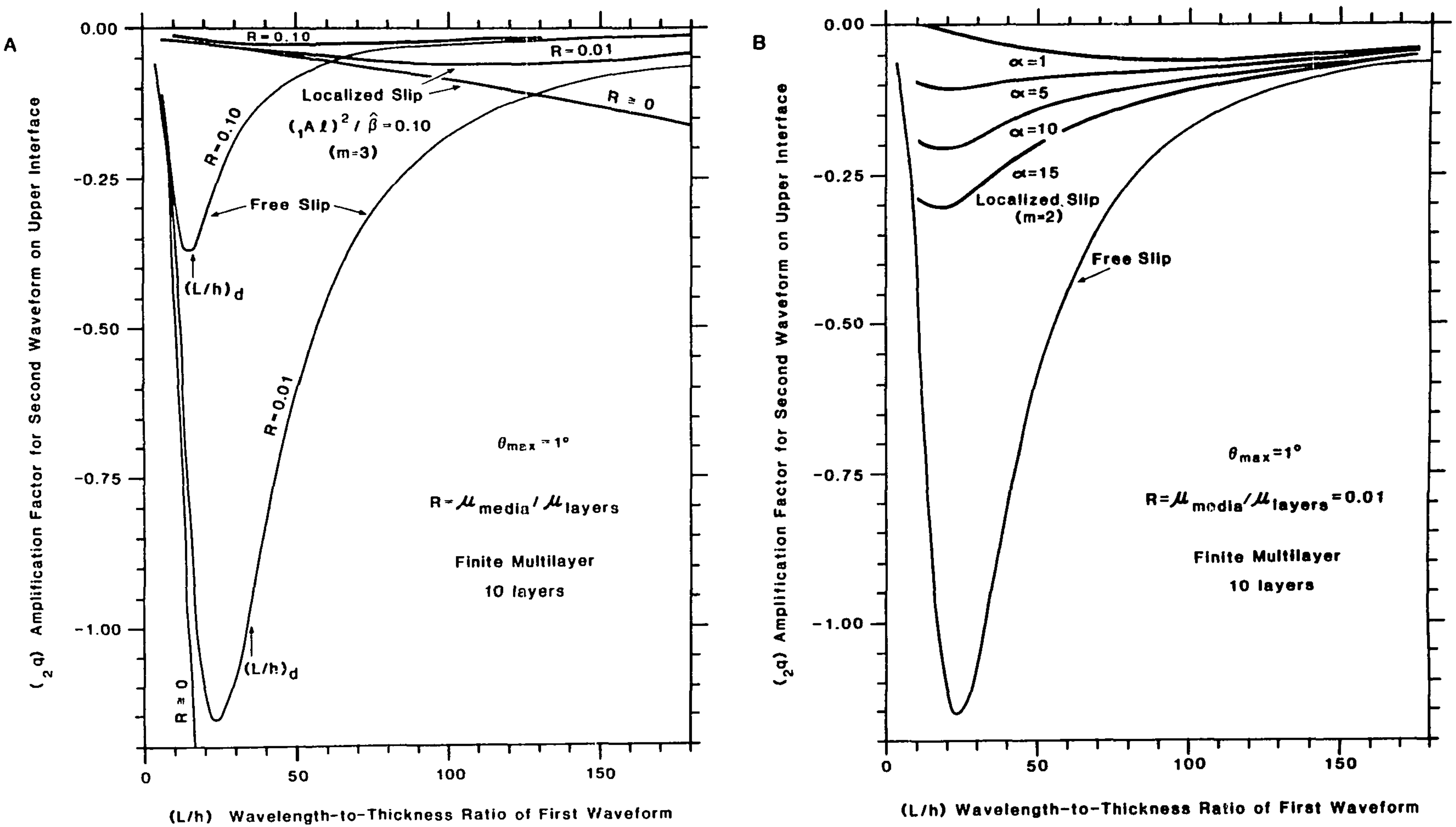
A
0.00
-0.25
-0.50
-0.75
-1.00
0
50
100
150
R=0.10
R=0.01
R ≥ 0
Localized Slip
$({}_1A\ell)^2 / \hat{\beta} = 0.10$
(m=3)
R=0.10
Free Slip
(L/h)d
R=0.01
(L/h)d
R ≥ 0
$\theta_{max} = 1°$
$R = \mu_{media} / \mu_{layers}$
Finite Multilayer
10 layers
(2q) Amplification Factor for Second Waveform on Upper Interface
(L/h) Wavelength-to-Thickness Ratio of First Waveform
B
0.00
-0.25
-0.50
-0.75
-1.00
0
50
100
150
α=1
α=5
α=10
α=15
Localized Slip
(m=2)
Free Slip
$\theta_{max} = 1°$
$R = \mu_{media} / \mu_{layers} = 0.01$
Finite Multilayer
10 layers
(2q) Amplification Factor for Second Waveform on Upper Interface
(L/h) Wavelength-to-Thickness Ratio of First Waveform

$\underline{m} = 3$.

The relative magnitudes of ${}_2\underline{q}$, shown in Fig. 21 for finite multilayers with different contact properties, are reflected in the corresponding fold forms. The second waveform is well developed in multilayers with free slip at contacts (Fig. 4A, Fig. 5, loc. A2) and in multilayers with localized slip at contacts, provided $\underline{m} = 2$ (Fig. 4B, Fig. 5, loc. B2). However, the second waveform is poorly developed in multilayers with localized slip for the case $\underline{m} = 3$ if the analysis is carried only to 3rd order accuracy.

The third waveform also is critical to the determination of fold form. If the third waveform is strong, its sign determines whether the folds will be chevron-like or kink-like. Relations between the initial amplification factor of the third waveform, ${}_3\underline{q}$, and the initial wavelength ratio of the first waveform are shown in Fig. 22. The sign of ${}_3\underline{q}$ is negative for multilayers with localized slip at contacts (Fig. 22). The negative sign corresponds to a negative third waveform, which is responsible for the box form and the steep limbs of the kink-like form (Figs. 5B, 6B).

The amplification factor for the third waveform is generally small for the finite multilayer with free slip at contacts and consequently has minor effect on the form of such multilayers (Fig. 10A). However, for thick multilayers and short wavelengths, the amplification factor for the

Figure 22. Relationship between amplification factor $_3\underline{q}$ for the third waveform and wavelength-to-thickness ratio ($\underline{L}/\underline{h}$) for the first waveform for unconfined and confined finite multilayers. Confinement by soft media (μ_m/μ_ℓ = 0.01) maximizes $_3\underline{q}$ for a particular initial ($\underline{L}/\underline{h}$). Maximum values of $_3\underline{q}$ are significantly higher in multilayers with localized slip at contacts ($\underline{m}$ > 1.0) than in multilayers with free slip at contacts.

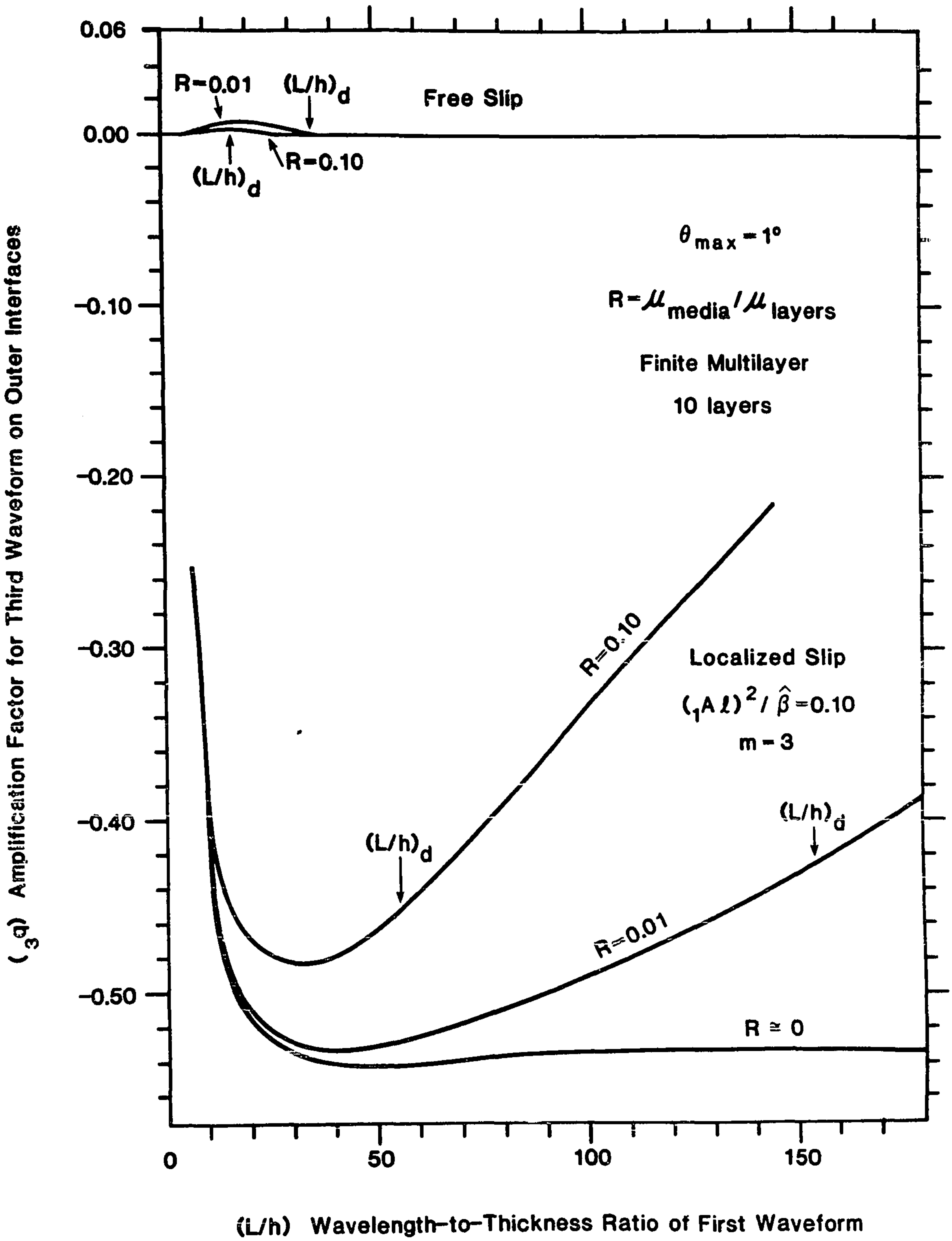
0.06
0.00
-0.10
-0.20
-0.30
-0.40
-0.50
R=0.01
(L/h)d
Free Slip
R=0.10
(L/h)d
θmax = 1°
R=μmedia/μlayers
Finite Multilayer
10 layers
Localized Slip
(1Aℓ)²/β̂=0.10
m=3
R=0.10
(L/h)d
(L/h)d
R=0.01
R ≃ 0
0
50
100
150
(3q) Amplification Factor for Third Waveform on Outer Interfaces
(L/h) Wavelength-to-Thickness Ratio of First Waveform

third waveform becomes large and the chevron form becomes distinct (Fig. 5, loc. A1, Fig. 6A).

DISCUSSION

The analysis of folding of multilayers consisting of identical viscous layers shows that different fold forms can be produced by changing the properties of the layer contacts or the wavelengths of the first waveforms. In the Discussion I will focus on two aspects of the theoretical analysis:

1. The theoretical kink-like folds invariably are pervasive, whereas kink bands commonly are isolated.
2. The form of folds generated by a particular theoretical analysis depends on the combination of the order of approximation and the power of the powerlaw contact property selected in performing that analysis.

All the folds shown in this chapter are pervasive: regardless of contact properties, the waveforms repeat indefinitely along each interface. Pervasive folding in viscous multilayers with free or localized slip at contacts is a result of assumptions that all the interfaces are initially perturbed into cosinusoidal waveforms of low amplitude and that the powerlaw exponent _m_ is one, two, or three. But only the latter assumption is fundamental. One could relax the first assumption and introduce a local perturbation into the multilayer. However, unless the properties of the multilayer allow the perturbation to grow only locally, waveforms would spontaneously grow in the multilayer on either side of the local perturbation, producing pervasive folds. This was shown by Reches and Johnson (1977) experimentally and theoretically for elastic materials.

Apparently, the second assumption, that *m* is one, two, or three, must be changed to produce the local deformation that characterizes isolated kink bands. Honea and Johnson (1976) have shown that a particular form of isolated flexure, a "kinkform," can exist in a multilayer with finite, plastic, adhesional contact strength. Smith (1979) has demonstrated that a powerlaw material behaves as a plastic material with strength as *m* approaches infinity, so slip will become local in a multilayer with powerlaw rheology at contacts as the power *m* increases indefinitely. Also, Latham (1985b) concludes that, for multilayers composed of powerlaw material, a large powerlaw exponent results in local deformation. For these reasons, the differences between forms of isolated kink-like folds and the pervasive kink-like folds I have investigated can be removed by indefinitely increasing the power exponent, *m*, in the equations that describe contact properties between layers. We have seen in this chapter that removal of these differences is inessential to understanding the general conditions responsible for kink folding.

The second aspect of the theoretical analysis that I feel should be discussed is the necessity of selecting an appropriate combination of order of approximation, O, and powerlaw exponent, m, to investigate fold form. The fold form predicted by the theoretical approximation depends on the relationship between the exponent, m, and the order of the solution, O, as follows. (In all examples, the multilayers are composed of identical layers and confined by soft media.)

1. O < m. Folding described by analyses in which the order of the solution is less than the exponent power is purely kinematic; it reflects merely passive deformation of interfaces.

For example, 0th order analysis of a multilayer with constant resistance to slip at contacts (m = 1) is kinematic. A kinematic analysis does not reveal much about fold form. It is less obvious, but true, that a 1st order analysis cannot be used to investigate fold form of multilayers with variable resistance to slip at contacts (m > 1). Any 1st order analysis of a multilayer with localized slip at contacts (m > 1) is equivalent to a kinematic analysis, as is a 2nd order analysis of folding of a multilayer with contact behavior described by m = 3.

2. O = m. If the order of the solution O and the power m are equal, analyses of multilayer folding describe the growth of essentially *similar* folds.

If slip at contacts is distributed, a 1st order solution for folding of a multilayer with $\underline{m} = 1$ produces nearly <u>similar</u> cosinusoidal fold forms because no waveforms other than the first develop. If slip at contacts is localized, a 3rd order analysis with $\underline{m} = 3$ describes the growth of nearly <u>similar</u>, box folds.

3. $\underline{O} > \underline{m}$. Analyses of folding in which $\underline{O}$ is greater than $\underline{m}$ can produce distinctly non-<u>similar</u> fold forms, and results of these analyses are the ones that provide the most information about fold form.

In a 2nd order analysis of folding of a finite multilayer for which $\underline{m} = 1$, a strong second waveform develops which modifies the cosinusoidal shape, resulting in a concentric-like fold. A 3rd order analysis of this multilayer may produce no new information about fold form, because the third waveform is very weak, as shown in Chapter I. Under some conditions, though, the analysis determines a strong third waveform which further refines the fold form to produce a combination of concentric-like and chevron forms.

Similarly, a 3rd order analysis of folding for which $\underline{m} = 2$ describes the development of strong second and third waveforms which produce a kink-like fold form in finite multilayers.

On the basis of this understanding of my theoretical results, I would anticipate that a 4th or higher order analysis of multilayers with nonlinear resistance to slip described by m = 3 would also produce kink-like folds in finite multilayers.

REFERENCES CITED

Anderson, T.B., 1968. The geometry of a natural orthorhombic system of kink bands. In: A.J. Baer and D.K. Norris (Editors), Proceedings, Conference on Research in Tectonics. Geological Survey of Canada Paper 68-52: 200-220.

Biot, M.A., 1959. On the instability and folding deformation of a layered viscoelastic medium in compression. Journal of Applied Mechanics, 26: 393-400.

Biot, M.A., 1961. Theory of folding of stratified viscoelastic media and its implications in tectonics and orogenesis. Geological Society of America Bulletin, 72: 1595-1620.

Biot, M.A., 1965a. Mechanics of Incremental Deformations. John Wiley & Sons, Inc., New York, 504 pp.

Biot, M.A., 1965b. Theory of similar folding of the first and second kind. Geological Society of America Bulletin, 76: 251-258.

Clifford, P.M., 1968. Kink band development in the Lake St. Joseph area, northwestern Ontario. In: A.J. Baer and D.K. Norris (Editors), Proceedings, Conference on Research in Tectonics. Geological Survey of Canada Paper 68-52: 229-241

Cobbold, P.R., Cosgrove, J.W. and Summers, J.M., 1971. Development of internal structures in deformed anisotropic rocks. Tectonophysics, 12: 23-53.

Collier, M., 1978. Ultimate locking angles for conjugate and monoclinal kink bands. Tectonophysics, 48: T1-T6.

Dewey, J.F., 1965. Nature and origin of kink-bands. Tectonophysics, 1: 459-494.

Donath, F.A., 1968. Experimental study of kink-band development in strongly anisotropic rock. In: A.J. Baer and D.K. Norris (Editors), Proceedings, Conference on Research in Tectonics. Geological Survey of Canada Paper 68-52: 255-293.

Ellen, S.D., 1971. The development of folds in layered chert of the Franciscan Assemblage near San Francisco, California. Ph.D. dissertation, Department of Geology, Stanford University, Stanford, California, 330 pp.

Fletcher, R.C., 1974. Wavelength selection in the folding of a single layer with power-law rheology. American Journal of Science, 274: 1029-1043.

Fletcher, R.C., 1977. Folding of a single viscous layer: Exact infinitesimal-amplitude solution. Tectonophysics, 39: 593-606.

Fletcher, R.C., 1979. The shape of single-layer folds at small but finite amplitude. Tectonophysics, 60: 77-87.

Fletcher, R.C., 1982. Analysis of the flow in layered fluids at small, but finite, amplitude with application to mullion structures. Tectonophysics, 81: 51-66.

Ghosh, S.K., 1966. Experimental tests of buckling folds in relation to strain ellipsoid in simple shear deformations. Tectonophysics, 3: 169-185.

Honea, E., 1975. The effect of contact strength on the shape of buckle folds. Ph.D. dissertation, Department of Geology, Stanford University, Stanford, California, 89 pp.

Honea, E. and Johnson, A.M., 1976. Part IV, Development of sinusoidal and kink folds in multilayers confined by rigid boundaries. Tectonophysics, 30: 197-239.

Johnson, A.M., 1970. Physical Processes in Geology. Freeman, Cooper & Co., San Francisco, 577 pp.

Johnson, A.M., 1980. Folding and faulting of strain-hardening sedimentary rocks. Tectonophysics, 62: 251-278.

Johnson, A.M. and Ellen, S.D., 1974. A theory of concentric, kink, and sinusoidal folding and of monoclinal flexuring of compressible, elastic multilayers. Part I, Introduction. Tectonophysics, 21: 301-339.

Latham, J-P., 1985a. The influence of nonlinear material properties and resistance to bending on the development of internal structures. Journal of Structural Geology, 7: 225-236.

Latham, J-P., 1985b. A numerical investigation and geological discussion of the relationship between folding, kinking, and faulting. Journal of Structural Geology, 7: 237-249.

Paterson, M.S. and Weiss, L.E., 1966. Experimental deformation and folding in phyllite. Geological Society of America Bulletin, 77: 343-374.

Peng, S. and Johnson, A.M., 1972. Crack growth and faulting in cylindrical specimens of Chelmsford granite. International Journal of Rock Mechanics and Mining Sciences, 9: 37-86.

Ramberg, H., 1962. Contact strain and folding instability of a multilayered body under compression. Geologische Rundschau, 51: 405-439.

Ramberg, H., 1963. Fluid dynamics of viscous buckling applicable to folding of layered rocks. American Association of Petroleum Geologists, 47: 484-505.

Ramberg, H., 1964. Selective buckling of composite layers with contrasted rheological properties, A theory for simultaneous formation of several orders of folds. Tectonophysics, 1: 307-341.

Ramberg, H., 1970. Folding of laterally compressed multilayers in the field of gravity I; II. Physics of the Earth and Planetary Interiors, 2: 203-232 (Part I); 4: 83-120 (Part II).

Ramberg, I.B. and Johnson, A.M., 1976. Part V, Asymmetric folding in interbedded chert and shale of the Franciscan Complex, San Francisco Bay area, California. Tectonophysics, 32: 295-320.

Reches, Z. and Johnson, A.M., 1976. Part VI, Asymmetric folding and monoclinal kinking. Tectonophysics, 35: 295-334.

Reches, Z. and Johnson, A.M., 1977. Development of monoclines, Part II: Theoretical analysis of monoclines. Geological Society of America Memoir 151: 273-311.

Scofield, D.H., 1975. Fold forms in the Monterey and Santa Margarita Formations along Lopez Canyon, Tar Spring Ridge (7 1/2 ') Quadrangle, San Luis Obispo County, California. M.S. thesis, Department of Geology, Stanford University, Stanford, California, 61 pp.

Smith, R.B., 1975. Unified theory of the onset of folding, boudinage, and mullion structure. Geological Society of America Bulletin, 86: 1601-1609.

Smith, R.B., 1977. Formation of folds, boudinage, and mullions in non-Newtonian materials. Geological Society of America Bulletin, 88: 312-320.

Smith, R.B., 1979. The folding of a strongly non-Newtonian layer. American Journal of Science, 279: 272-287.

Weiss, L.E., 1968. Flexural-slip folding of foliated model materials. In: A.J. Baer and D.K. Norris (Editors), Proceedings, Conference on Research in Tectonics. Geological Survey of Canada Paper 68-52: 294-333.

CHAPTER III

OPPOSITE SENSES OF FOLD ASYMMETRY

ABSTRACT

If the orientation of the principal compressive stress is oblique to layering, viscous multilayers fold in response to the layer-parallel shortening and develop asymmetric interfaces in response to the layer-parallel shearing deformation. For a given sense of layer-parallel shear stress, the sense of asymmetry of folds can be reversed by changing only the behavior of the layer contacts: If the resistance to slip at layer contacts is a constant, the resistance is the same everywhere along interfaces, and folds develop the sense of asymmetry of drag folds. If the resistance to slip at layer contacts is a function of shear stress, however, the resistance is lower on slopes facing one way and higher on slopes facing the other way, and folds develop the sense of asymmetry of monoclinal kink folds.

The orientations of axial planes of drag folds and monoclinal kink folds differ fundamentally with respect to the orientation of layer-parallel shearing. The axial planes of drag folds on the limb of a large fold are approximately parallel to the axial plane of the large fold, but the axial planes of monoclinal kink folds dip toward the axial plane of the large fold.

INTRODUCTION

Folds may have opposite senses of asymmetry for a given sense of layer-parallel shear (Fig. 1). The short limb of a drag fold (Figs. 1, 2A) faces right in response to right-lateral simple shear strain parallel to layering and faces left for left-lateral simple shear strain parallel to layering. The short limb of a monoclinal kink fold (Figs. 1, 2B), however, faces left for right-lateral shear and faces right for left-lateral shear. The central purpose of this chapter is to explain the conditions responsible for the opposite senses of asymmetry of drag folds and monoclinal kink folds.

This research on fold asymmetry is partly motivated by my field study (Chapter IV) of minor folds on the southeast limb of the New Bloomfield anticline, near the confluence of the Juniata and Susquehanna rivers, central Pennsylvania. Minor folds with opposite senses of asymmetry (Fig. 3) are exposed in adjacent roadcuts on the same limb of the major fold. All but one of the minor folds in the northern roadcut (on left in Fig. 3) have the sense of asymmetry of drag folds because their short limbs all dip toward the axial plane of the major anticline. The minor fold in the southern roadcut (on right in Fig. 3) has the sense of asymmetry of a monoclinal kink fold because its short, steep

<u>Figure 1</u>. Opposite senses of asymmetry of idealized drag and monoclinal kink folds. The sense of shear responsible for asymmetry of folds is indicated by arrows and implied by position in larger fold. The short limb of a <u>drag fold</u> (<u>d</u>) faces right in response to right-lateral simple shear strain parallel to layering and faces left for left-lateral simple shear strain parallel to layering. The short limb of a <u>monoclinal kink fold</u> (<u>k</u>) faces left for right-lateral shear and faces right for left-lateral shear. Traces of axial planes (<u>a</u>) shown for both minor and major folds.

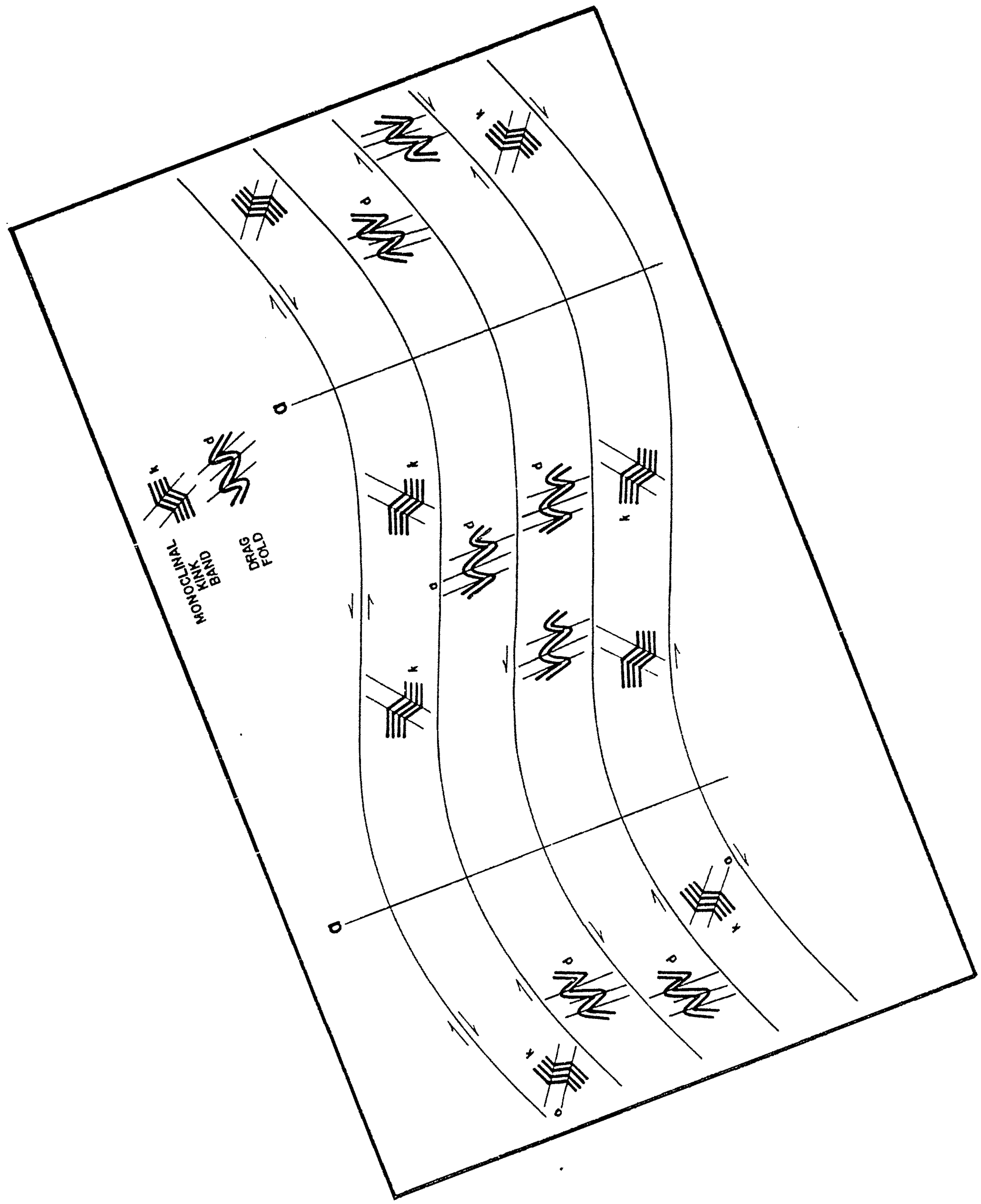
MONOCLINAL KINK BAND
DRAG FOLD
k
d
a
a

Figure 2. A. Folds with the sense of asymmetry of drag folds near the core of an anticline within the Huasna Syncline, California (from Johnson and Page, 1976, fig. 8). The sense of shear is right-lateral on the left side of the drawing and left-lateral on the right. B. Folds with the sense of asymmetry of monoclinal kink folds on the east limb of the Wills Mountain Anticline, near Pinto, West Virginia. The sense of shear is left-lateral on this limb of the anticline.

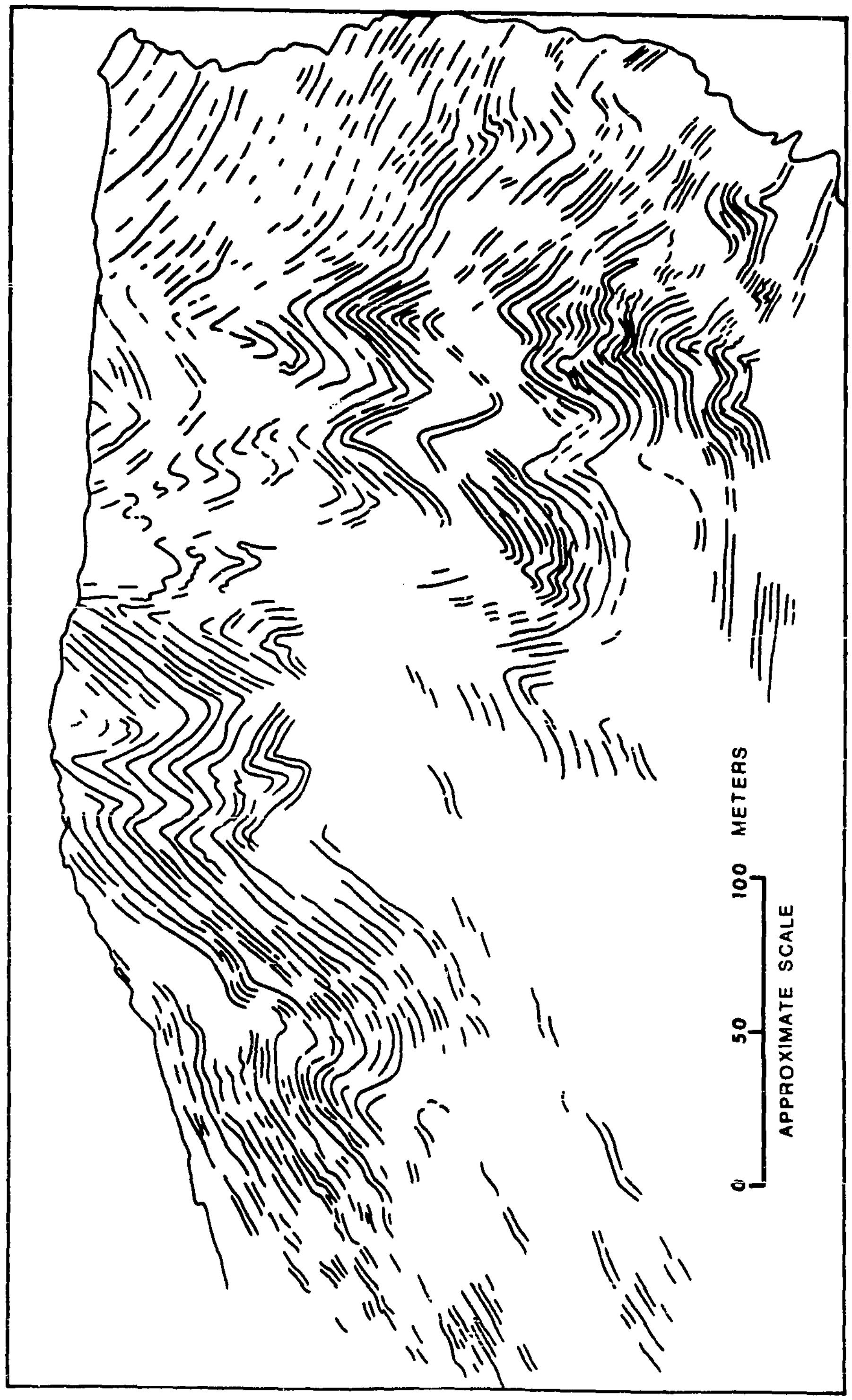
0 50 100 METERS
APPROXIMATE SCALE

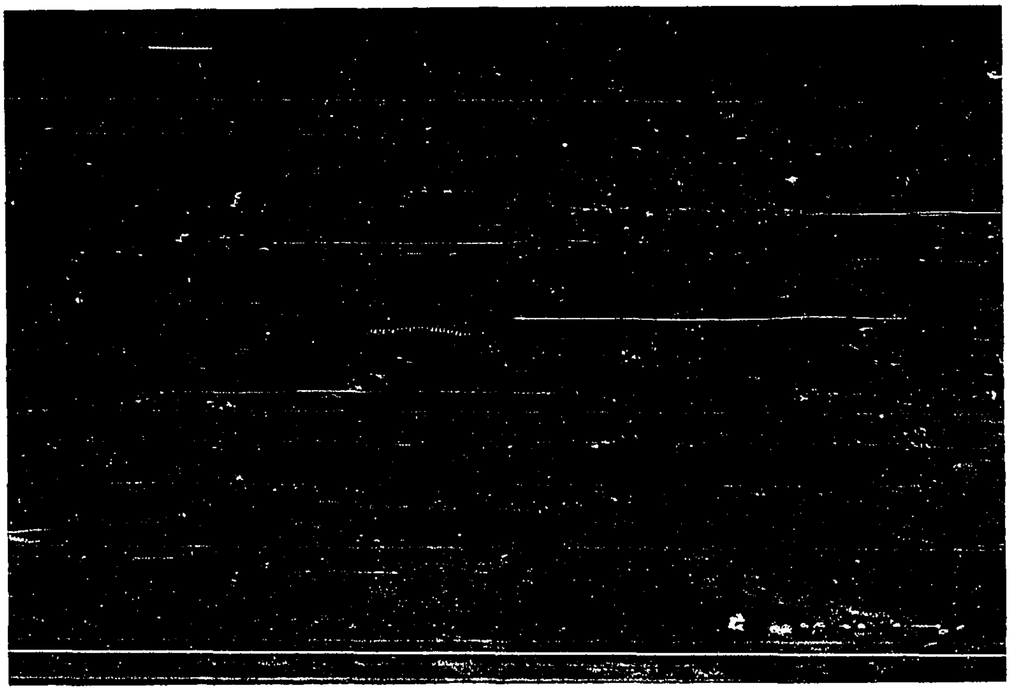

Figure 3. Minor folds with opposite senses of asymmetry on the southeast limb of the New Bloomfield anticline, central Pennsylvania. The sense of shear is left-lateral on this limb of the major anticline. Chevron and concentric-like folds with drag fold asymmetry in northern roadcut on the left; kink-like fold with monoclinal kink fold asymmetry in southern roadcut on the right.

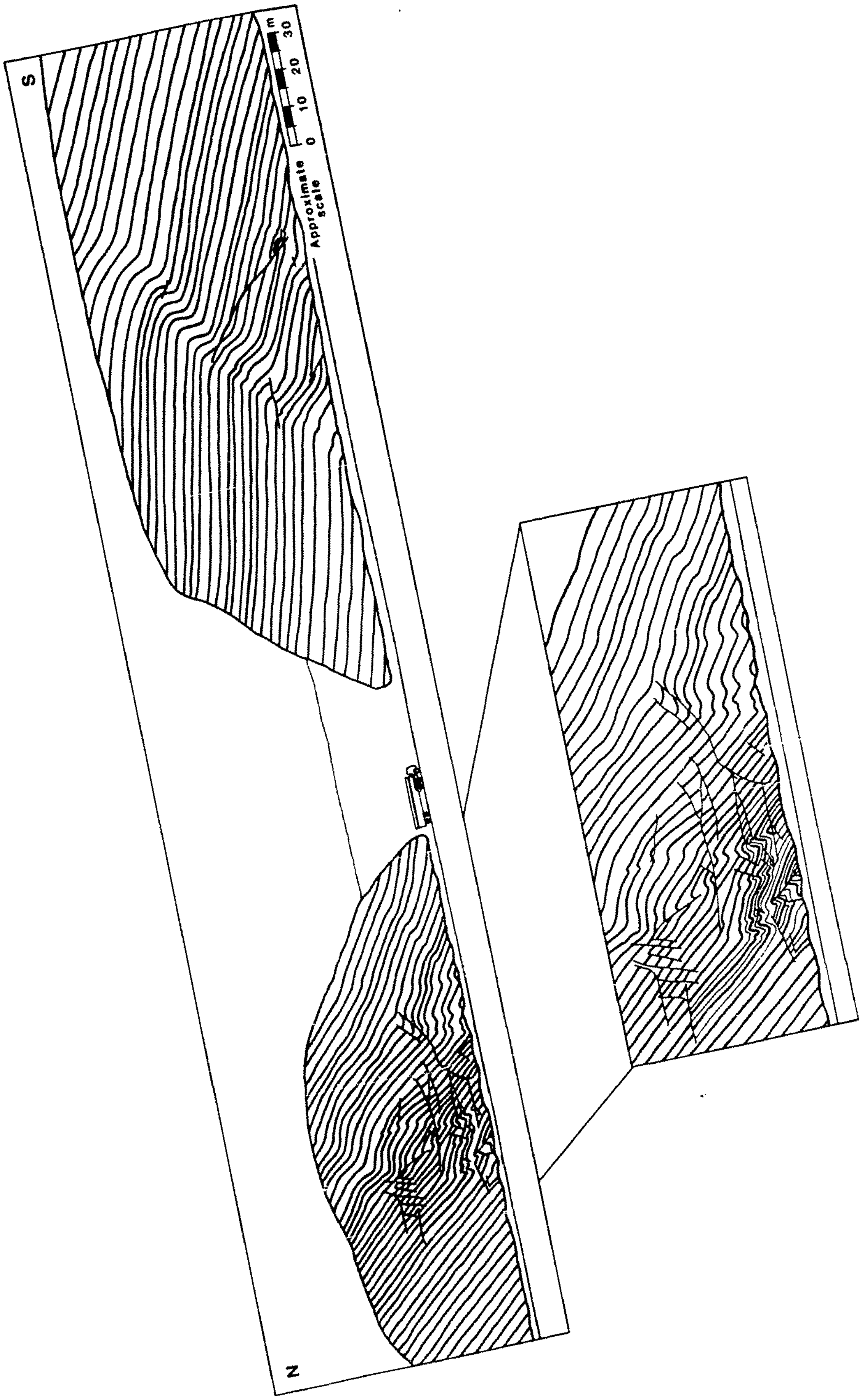
S
Approximate scale
0 10 20 30 m
N

limb dips away from the axial plane of the major anticline.

In this chapter, I focus on the sense of asymmetry of folds rather than on the forms of asymmetric folds. For example, the drag folds in the roadcut shown on the left in Fig. 3 are tight chevron folds near the left end of the roadcut and relatively open, almost concentric-like folds slightly right of center in the roadcut. Yet despite their different forms, these folds have the same sense of asymmetry. The forms of the relatively open, concentric-like drag folds resemble parts of the fold with monoclinal kink fold asymmetry (in roadcut shown on right in Fig. 3), but these have opposite senses of asymmetry. In Chapters I and II, I discuss parameters which control forms of folds. In the following pages, I address the causes of opposite senses of fold asymmetry.

PREVIOUS WORK AND STATEMENT OF PROBLEM

Drag Folds

Hans Ramberg (1963) explained that drag folds develop in response to a combination of layer-parallel shortening and shear (Fig 4). The shortening is responsible for the folding; the shear is responsible for the asymmetry. Ramberg (1963) reasoned that the formation of drag folds on the limbs of large folds requires either that the large and small folds grow simultaneously or that the small folds form

Figure 4. Minor folds with drag fold sense of asymmetry developed in response to layer-parallel shear strain on limbs of major fold, according to Ramberg (1963) (from Ramberg, 1963, fig. 6).

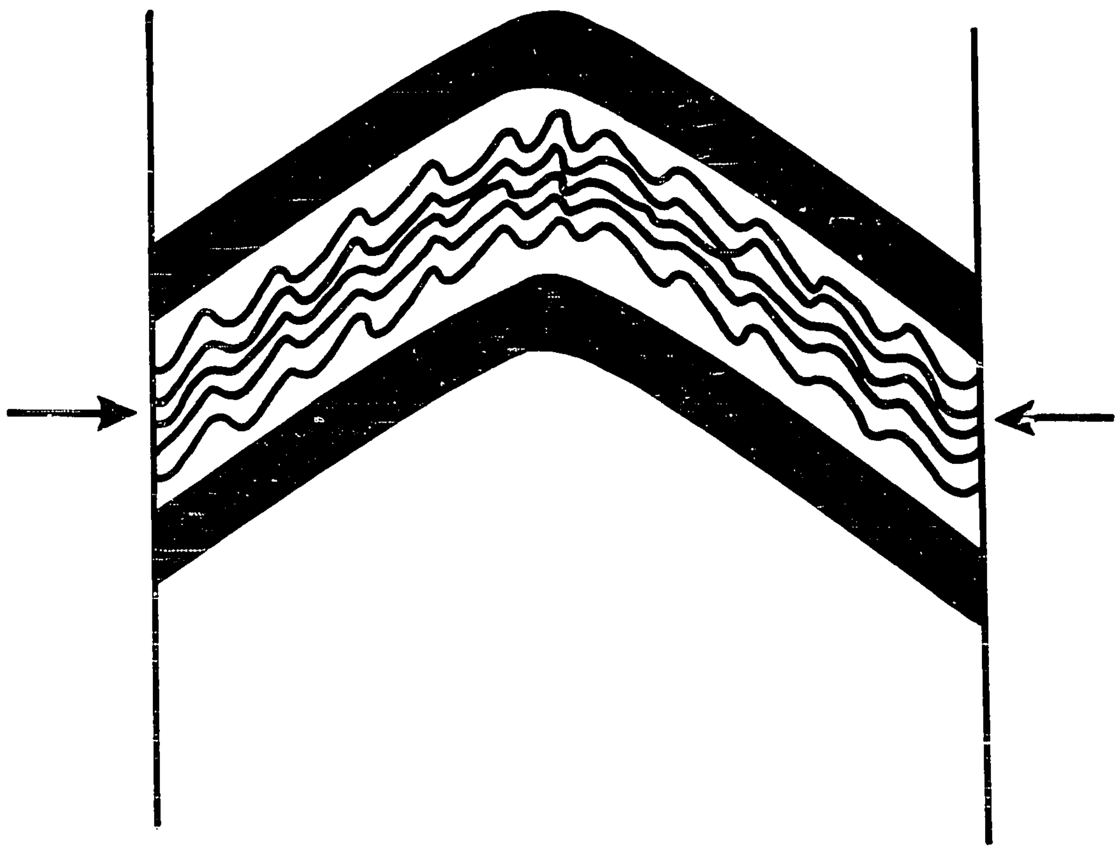

first, so that shear on the limbs of the large folds can cause the small folds to become asymmetric. According to Ramberg (1963), the deformation responsible for the asymmetry of drag folds is passive, or kinematic.

Ivar Ramberg and Johnson (1976) applied H. Ramberg's concept of drag folding to a field study of asymmetric folds in interbedded cherts and shales of the Franciscan Complex and to a collateral experimental study of asymmetric folding in elastic multilayers composed of rubber strips or interbedded rubber and gelatin strips. In the experiments, drag folds formed as a result of layer-parallel shortening and simultaneous or subsequent simple shear in elastic multilayers composed of stiff layers with lubricated contacts or of interbedded stiff and soft layers. I. Ramberg and Johnson showed that during simple shear, the asymmetry of drag folds is produced by passive reorientation of layers in limbs much as predicted by H. Ramberg's kinematic model.

Other studies of drag folds have been restricted primarily to single layers. Ghosh (1966) produced drag folds in single layers of modeling clay embedded in putty, materials with relatively low contrasts in properties. Treagus (1973) theoretically analyzed the effects of shear on folding of single viscous layers in soft media and concluded that dominant wavelength is independent of shear. Manz and Wickham (1978) had difficulty in producing experimentally asymmetric folds in ethyl cellulose layers and media having viscosity contrasts ranging from 20 to 100. Similarly, Anthony and Wickham (1978) were unable to produce strong asymmetric folds using finite-element solutions for single layers in media with viscosity contrasts ranging from 17 to 42.

This was essentially the level of understanding of drag folding at the time my research began.

Monoclinal Kink Folds

Dewey (1965) recognized on the basis of field study of faults and associated asymmetric folds that the sense of asymmetry of monoclinal kink folds is opposite to that of drag folds (Fig. 1). Subsequent experiments by Weiss (1968), Donath (1968), Johnson (1970), Ellen (1971), Cobbold and others (1971), Gay and Weiss (1974), and I. Ramberg and Johnson (1976), and subsequent field, experimental, and theoretical studies by Reches and Johnson (1976), confirmed the relation between sense of layer-parallel shear stress and sense of monoclinal kink fold asymmetry shown in Fig. 1.

The sense of asymmetry of monoclinal kink folds has been explained qualitatively by Reches and Johnson (1976) and by Reches (1979) in the context of the theory of kink folding developed by Honea and Johnson (1976). They considered a multilayer containing various irregularities in slope (Fig. 5), with the contacts between layers having

Figure 5. The sense and magnitude of the local contact shear stress in multilayers with finite strength at layer contacts (from Reches and Johnson, 1976, fig. 11). A. The sense and magnitude of the local shear stress depends only on the sign and magnitude of the local slope if multilayer is subjected only to mean horizontal compression. B. Sense and magnitude of local shear stress depends also on sense and magnitude of mean horizontal shear stress if principal compressive stress is not horizontal.

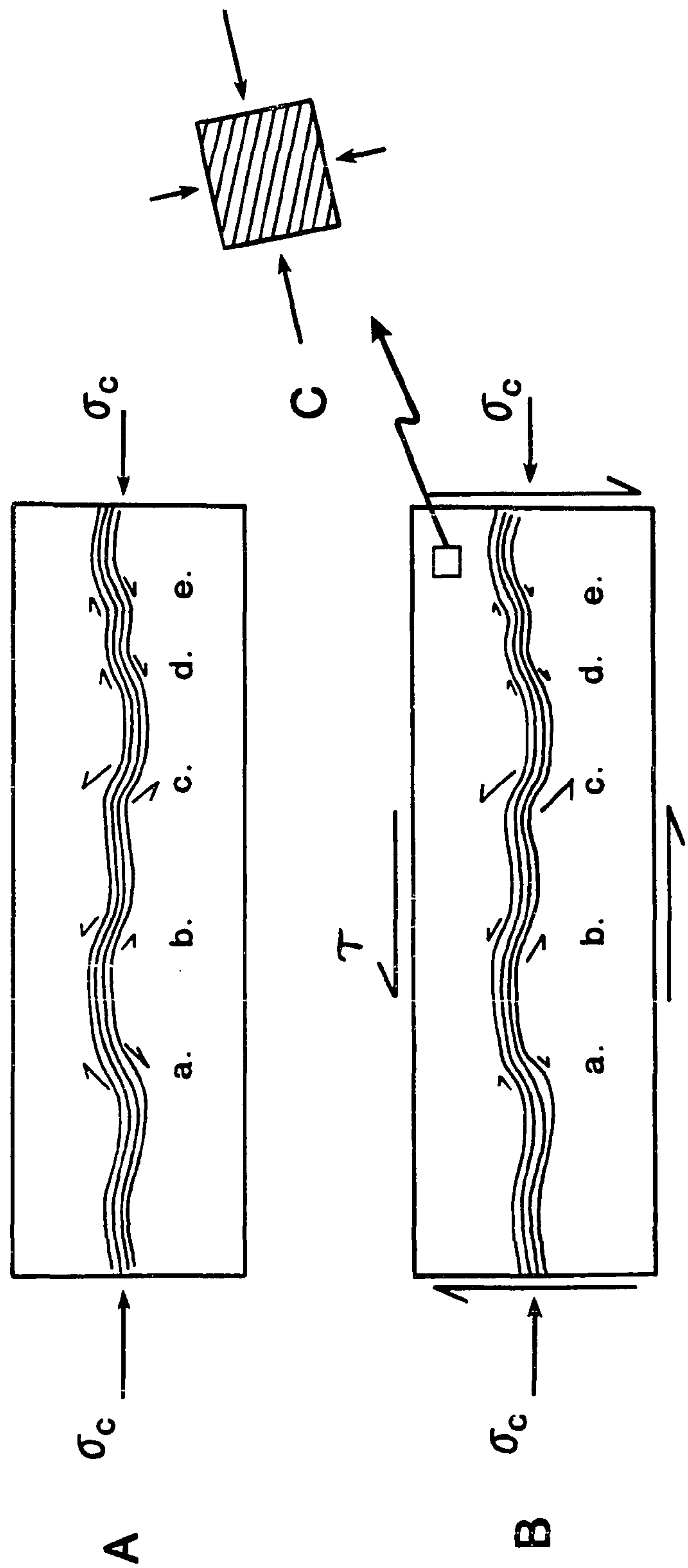

A
B
C
σ_c
σ_c
σ_c
σ_c
a.
b.
c.
d.
e.
a.
b.
c.
d.
e.
τ

finite strength, as described by Coulomb's Law.

If the multilayer is subjected solely to mean horizontal compression, σ_c, the initial irregularities produce shear locally at contacts between layers; the shear stress is zero where slopes are zero and maximal where slopes are maximal. Thus, the shear stresses are largest at points a and c (Fig. 5A), but at these points the sense of shear is opposite. Contacts yield simultaneously at points a and c, and the resulting kink bands are conjugate (Honea and Johnson, 1976).

Consider the same multilayer as being subjected not only to a mean horizontal compression, σ_c, but also to a mean horizontal, left-lateral shear stress, τ (Fig. 5B). The magnitude of the mean shear is less than the contact shear strength, so contacts between flat layers remain bonded. As a result of superposition of the mean shear stress on the local shear stresses produced by the interaction of the irregularities (at a, b, c, d, and e) and the layer-parallel compression, however, the layer-parallel shear stresses are locally <u>increased</u> to exceed the shear strength at points b and c, but locally <u>decreased</u> at points a, d, and e (Fig. 5B). Accordingly, yielding will occur first at point c, then at point b. Yielding will not occur at points a, d, or e for this state of stress. For this reason, left-lateral shear stress favors initiation of right-lateral kink folding (Reches and Johnson, 1976).

This was essentially the state of understanding of monoclinal kink folds at the time my research was initiated.

Focus of Paper

Together, the studies by Hans Ramberg (1963) on the causes of drag folds and the studies by Reches and Johnson (1976) on the causes of monoclinal kink folds account for the opposite senses of asymmetry of the two kinds of folds. Neither of these studies, however, proceeded significantly beyond qualitative analysis of conditions causing the different kinds of folds or the different senses of asymmetry. There was no bridge between the ideas developed in the studies of drag folding and those treating monoclinal kink folding; there were no equations to describe the growth of either type of asymmetric fold from an initial, symmetric perturbation.

In this chapter I present a comprehensive, theoretical model of asymmetric folding of viscous multilayers. The model is designed to include not only the two end members considered by Ramberg (1963) and by Reches and Johnson (1976), but also to cover the continuum of intermediate behaviors.

To determine the conditions under which folds with drag fold asymmetry form in preference to folds with monoclinal kink fold asymmetry, I consider the folding of simple, repetitive, viscous multilayers. As in the work by Honea and Johnson (1976) on conjugate kink folding and by Reches and Johnson (1976) on monoclinal kink folding, my research focuses on the properties of contacts between layers as the most likely source for different senses of fold asymmetry. As I will show, this requires a 2nd order theoretical analysis.

MEAN FLOW AND CONTACT PROPERTIES

Mean Stresses, Deformation Rates, and Velocities

Components of velocity and stress within the layer are separated into mean and perturbed values (e.g., Fletcher, 1974, 1977); the mean values of stress and velocity are those that solve the problem describing the uniform deformation of a layer with planar interfaces, and the perturbed values of stress and velocity are those that must be added to the mean values to match stresses and velocities at perturbed interfaces.

The mean stresses and velocities within a layer are:

$$\bar{v}_x = x\bar{D}_{xx} + 2z\bar{D}_{xz} + (\bar{v}_x)_o \tag{1a}$$

$$\bar{v}_z = z\bar{D}_{zz} + (\bar{v}_z)_o = -z\bar{D}_{xx} + (\bar{v}_z)_o \tag{1b}$$

$$\bar{\sigma}_{xx} = 2\mu_\ell\bar{D}_{xx} - \bar{p} \tag{1c}$$

$$\bar{\sigma}_{zz} = -2\mu_\ell\bar{D}_{xx} - \bar{p} \tag{1d}$$

$$\bar{\sigma}_{xz} = 2\mu_\ell\bar{D}_{xz} \tag{1e}$$

$$\bar{p} = -(\bar{\sigma}_{xx} + \bar{\sigma}_{zz})/2 \tag{1f}$$

in which $\underline{\bar{D}}_{ij}$ is the mean deformation rate,

$$\bar{D}_{ij} = (1/2)(\partial\bar{v}_i/\partial x_j + \partial\bar{v}_j/\partial x_i) \tag{1g}$$

and μ_ℓ is the coefficient of viscosity for a layer. For incompressible viscous materials, $\underline{\bar{D}}_{xx} = -\underline{\bar{D}}_{zz}$; for the simple shearing assumed here, $(\partial\bar{v}_z/\partial x) = 0$.

The orientation of maximum compression, $\bar{\sigma}_c$, within a stiff, viscous layer is defined by the angle $\bar{\theta}$, measured clockwise from the $\underline{x}$-direction (Fig. 6), which lies in the plane of the unperturbed layering. The ratio of the mean shear stress, $\underline{\sigma}_{xz}$, to the difference of the mean normal stresses, $\underline{\sigma}_{xx}$ and $\underline{\sigma}_{zz}$, is

$$\bar{\sigma}_{xz}/(\bar{\sigma}_{xx} - \bar{\sigma}_{zz}) = -(1/2)\tan(2\bar{\theta}) \tag{2a}$$

Within viscous layers, therefore,

$$\bar{\sigma}_{xz} = -2\mu_\ell\bar{D}_{xx}\tan(2\bar{\theta}) \tag{2b}$$

or

$$\bar{D}_{xz}/\bar{D}_{xx} = -\tan(2\bar{\theta}) \tag{2c}$$

For the boundary conditions, I have elected to specify a combination of uniform, layer-parallel normal deformation rate, $\underline{\bar{D}}_{xx}$, and uniform, layer-parallel shear stress, $\bar{\sigma}_{xz}$. The multilayer and confining medium are allowed to shear in

Figure 6. Representative multilayer of total thickness H composed of identical layers of thickness h and coefficient of viscosity μ_l and confined by media of infinite thickness and coefficient of viscosity μ_m. Interfaces between layers initially perturbed into symmetric, cosinusoidal waveforms. Multilayer and media subjected to uniform rates of layer-parallel shortening, $\bar{D}_{xx}$, and layer-parallel simple shearing, $\bar{\sigma}_{xz}$. Orientation of maximum compression, $\bar{\sigma}_c$, defined by angle $\bar{\theta}$, measured clockwise from the x-direction.

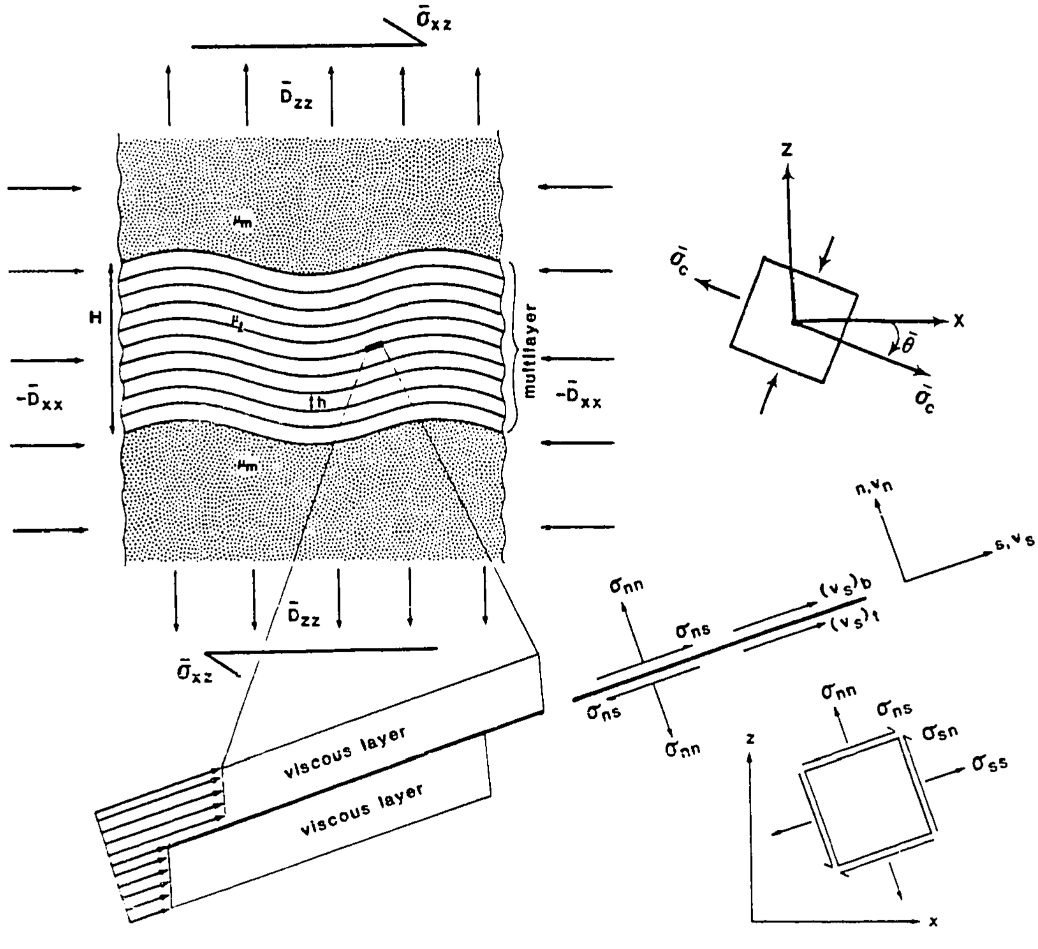

$\bar{\sigma}_{xz}$
$\bar{D}_{zz}$
μ_m
H
μ_l
multilayer
h
$-\bar{D}_{xx}$
$-\bar{D}_{xx}$
μ_m
$\bar{D}_{zz}$
$\bar{\sigma}_{xz}$
viscous layer
viscous layer
z
x
σ_c'
θ'
σ_c'
n, v_n
s, v_s
σ_{nn}
$(v_s)_b$
σ_{ns}
$(v_s)_t$
σ_{ns}
σ_{nn}
σ_{nn}
σ_{ns}
σ_{sn}
σ_{ss}
z
x

a combination of mean pure shearing, as specified by $\underline{\bar{D}}_{xx} - \underline{\bar{D}}_{zz}$, and mean layer-parallel simple shearing, $2\underline{\bar{D}}_{xz}$. The mean velocities specified for a layer, eqs. (1a) and (1b), reflect this choice.

Because $\bar{\sigma}_{xz}$ is constant throughout the multilayer, the mean shearing deformation, $\underline{\bar{D}}_{xz}$, varies locally according to the viscosity of the layer. However, an averaged mean shearing deformation for the entire multilayer, $(\underline{\bar{D}}_{xz})_{ave}$, can be related to the mean shear stress through the mean shear viscosity, $\bar{\mu}_s$, of the multilayer:

$$\bar{\sigma}_{xz} = 2\bar{\mu}_s(\bar{D}_{xz})_{ave} \tag{3}$$

Then, for a principal compressive deformation rate $\underline{\bar{D}}_c$ acting at an angle $\bar{\theta}'$ clockwise to the layering,

$$(\bar{D}_{xz})_{ave}/(\bar{D}_{xx} - \bar{D}_{zz}) = -(1/2)\ \tan(2\bar{\theta}') \tag{4a}$$

which is analogous to eq. (2a) for the mean stresses. For incompressible materials,

$$(\bar{D}_{xz})_{ave}/\bar{D}_{xx} = -\ \tan(2\bar{\theta}') \tag{4b}$$

Combining eqs. (2b), (3), and (4b), a relationship can be derived among the orientation of the principal stresses, the orientation of the principal deformation rates, and the mean anisotropy, $\bar{\alpha}$, of the multilayer:

$$\bar{\alpha} = \tan(2\bar{\theta}')/\tan(2\bar{\theta}) \tag{5a}$$

According to eqs. (2c) and (4b),

$$\bar{\alpha} = (\bar{D}_{xz})_{ave}/(\bar{D}_{xz})_{stiff\ layers} \tag{5b}$$

The mean anisotropy, $\bar{\alpha}$, is the ratio of the normal to mean shear viscosity of the multilayer.

Properties of Contacts between Layers

Model of contacts. The model I have selected to describe contact properties relates rate of slip, $\delta \underline{v}_s$, between layers to magnitude of shear stress, σ_{ns}, applied at contacts (Fig. 7). If contacts between layers are bonded, $\delta \underline{v}_s$ is zero, and if contacts between layers slip freely, σ_{ns} is zero. These two end member conditions, bonded contacts and free slip at contacts, can be considered extremes of either contact strength or contact viscosity.

If, as Honea and Johnson (1976) assumed, contacts have a finite strength described by Coulomb's Law of contact friction, then

$$|\sigma_{ns}| \leq C - \sigma_{nn} \tan(\Phi) \tag{6}$$

in which σ_{ns} is the shear stress parallel to the interface, σ_{nn} is the stress normal to the interface, $\underline{C}$ is adhesion, and Φ is angle of internal friction. (Normal stresses are negative if compressive.) If the inequality in eq. (6) is satisfied, the contacts are bonded, and if adhesion and friction are zero, contacts slip freely.

Figure 7. Powerlaw relationship between rate of slip, $\delta \underline{v}_s$, and shear stress, σ_{ns}, at layer contacts for several values of the powerlaw exponent, $\underline{m}$.

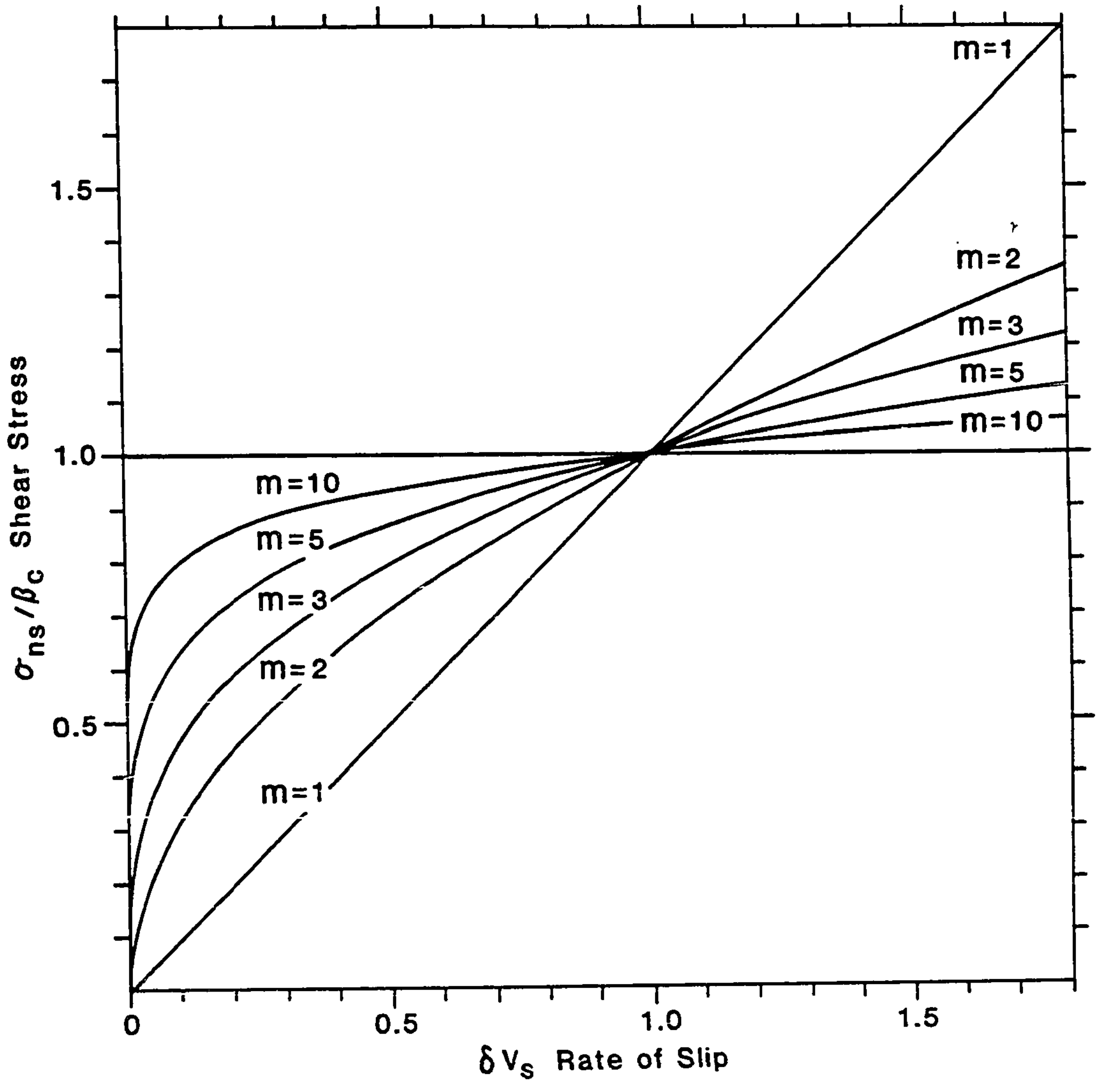

m=1
m=2
m=3
m=5
m=10
m=10
m=5
m=3
m=2
m=1
1.5
1.0
0.5
σ_{ns}/β_c Shear Stress
0
0.5
1.0
1.5
δV_s Rate of Slip

If, as I assumed in Chapter II, contacts have a contact viscosity of powerlaw form, then

$$\delta v_s = \sigma_{ns}/(\Xi m) \qquad (7a)$$

in which $\underline{m}$ is the powerlaw exponent and Ξ is the coefficient of contact viscosity. In this model, the rate of slip is a powerlaw function of the shear stress:

$$\delta v_s = (\sigma_{ns}/\beta_c)\ |\sigma_{ns}/\beta_c|^{(m-1)} \qquad (7b)$$

where β_c is a constant. The slope of the relation between contact shear stress and rate of slip is the coefficient of contact viscosity

$$d(\sigma_{ns})/d(\delta v_s) = \Xi = (\beta_c/m)\ |\sigma_{ns}/\beta_c|^{(1-m)} \qquad (7c)$$

The contact viscosity describes the resistance to slip at the interface. If Ξ is very large, contacts are bonded, and if Ξ is very small, contacts slip freely.

The powerlaw formulation of contact viscosity, eq. (7c), can model resistance to slip ranging from constant ($\underline{m}$ = 1) to highly nonlinear ($\underline{m} \to \infty$). A plot of the relation between (σ_{ns}/β_c) and $\delta \underline{v}_s$, Fig. 7, shows that the powerlaw model of contact viscosity, eq. (7), closely resembles the model of contact strength, eq. (6), particularly as the exponent $\underline{m}$ becomes large.

At the crossing point, where the curves for different powers cross in Fig. 7, the coefficient of contact viscosity is

$$\Xi = (\beta_c/m); \ (\sigma_{ns}/\beta_c) = 1 \tag{7d}$$

Thus Ξ at that point is controlled by the parameter β_c as well as by the power m. The parameter β_c plays two roles. The lower the magnitude of β_c, the lower the shear stress σ_{ns} at which the ratio (σ_{ns}/β_c) is unity; and the lower the magnitude of β_c, the lower the contact viscosity at the crossing point. The power m also plays two roles. The higher the value of m, the more strength-like the relation between rate of slip and shear stress; the higher the value of m, the lower the contact viscosity at the crossing point.

Rate of Slip. The rate of slip at layer contacts is

$$\delta v_s = (v_s)_b - (v_s)_t \tag{8}$$

where $(v_s)_b$ and $(v_s)_t$ are the velocities parallel to the interface on either side of the contact (Fig. 6); b refers to the bottom of overlying layer and t to the top of underlying layer.

The shear stress at layer contacts, σ_{ns}, depends both on the mean shear stress, $\bar{\sigma}_{xz}$, which is a function of the inclination of the principal compressive stress to planar interfaces, and on the perturbed shear stress, $\hat{\tau}$, which is a function of the local slope of the perturbed interfaces. The shear stress at the contact is

$$\sigma_{ns} = \bar{\sigma}_{xz} + \tilde{\tau} \tag{9a}$$

As shown in Chapters I and II, $\tilde{\tau}$ is

$$\tilde{\tau} = {}_0\tau + {}_1\tau \sin(\ell x) + {}_2\tau \sin(2\ell x) + {}_3\tau \cos(2\ell x) \tag{9b}$$

where the constants ${}_1\tau$, ${}_2\tau$, and ${}_3\tau$ are amplitudes of the perturbed shear stress distribution.

The rate of slip at an interface described by a powerlaw resistance to slip is expressed as a series expansion to 2nd order of eqs. (7) and (9a) in the perturbed shear stress at the interface:

$$\delta v_s = (1/\beta_c)\ \bar{\sigma}_{xz}\ \{|\bar{\sigma}_{xz}/\beta_c|^{(m-1)} +$$

$$m|\bar{\sigma}_{xz}/\beta_c|^{(m-2)}(\tilde{\tau}/\beta_c) +$$

$$[m(m-1)/2]|\bar{\sigma}_{xz}/\beta_c|^{(m-3)}(\tilde{\tau}/\beta_c)^2\} \tag{10a}$$

If the powerlaw exponent $\underline{m}$ is greater than one, the rate of slip is a nonlinear function of the contact shear stress. If $\underline{m}$ equals one, eq. (10a) simplifies to a linear function of the shear stress

$$\delta v_s = (1/\beta_c)[\bar{\sigma}_{xz} + \tilde{\tau}] \tag{10b}$$

in which the coefficient of contact viscosity is β_c, a constant.

Velocity jump at layer contacts. The total mean velocity parallel to flat layering, $\bar{v}_x$, is a consequence of both the layer-parallel normal and shearing deformation rates, respectively $\bar{D}_{xx}$ and $\bar{D}_{xz}$ (eq. 1a). Using eq. (1e), we can write an expression for $\bar{v}_x$ at the top of a single representative layer as

$$\bar{v}_x = \bar{D}_{xx}x + (\bar{\sigma}_{xz}/\mu_\ell)\zeta_t + (\bar{v}_x)_o \tag{11}$$

where ζ_t is the height of the top interface with reference to the middle of the layer,

$$\zeta_t = h/2 + A\cos(\ell x) + B\cos(2\ell x) + C\sin(2\ell x) \tag{12}$$

and h is the thickness of a layer.

If the mean shear stress, $\bar{\sigma}_{xz}$, is zero, the mean layer-parallel velocity reflects only the shortening, through $\bar{D}_{xx}x$. If the mean simple shearing stress is not zero, however, a velocity gradient across the layer is produced which is inversely proportional to the viscosity of the layer. Thus the mean velocity parallel to layering increases from the middle to the top of the layer.

At the contacts between layers, there is a velocity jump in the x-direction that depends on the rate of slip parallel to the contact, eq. (10). The mean part of the velocity jump in the x-direction is the difference in mean velocities at the top (t) of one layer and at the bottom (b) of the overlying layer:

$$(\bar{v}_x)_b - (\bar{v}_x)_t = (\bar{\sigma}_{xz})\zeta[1/(\mu_\ell)_b - 1/(\mu_\ell)_t] + (\bar{\sigma}_{xz}/\beta_c)^m + \Delta(\bar{v}_x)_o \tag{13}$$

where the last term, $\Delta(\underline{\bar{v}}_x)_o$, acts as a correction to the mean velocity jump at the layer contacts.

Anisotropy. I define the anisotropy of a multilayer as the ratio of the normal to the effective shear viscosities. For a representative element of a multilayer consisting of identical viscous layers with powerlaw resistance to slip at layer contacts, the effective coefficient of shear viscosity, μ_s, and the normal viscosity, μ_n, are:

$$1/\mu_s = 1/\mu_\ell + 1/(\Xi h) \tag{14a}$$

$$\mu_n = \mu_\ell \tag{14b}$$

in which $\underline{h}$ is the thickness of a layer and Ξ is the coefficient of contact viscosity, eq. (7c).

Combined with eqs. (7c) and (9a), eqs. (14) provide an expression for the anisotropy, α:

$$\alpha = \mu_n/\mu_s = 1 + (\mu_\ell/h)(m/\beta_c) \; |(\bar{\sigma}_{xz} + \tilde{\tau})/\beta_c|^{(m-1)} \tag{15}$$

According to eq. (15), the value of the anisotropy depends on both the mean shear stress and on the perturbed shear stress. The mean shear stress, $\bar{\sigma}_{xz}$, in turn, is a function of the mean orientation, $\bar{\theta}$, of the layering. The perturbed shear stress, $\tilde{\tau}$, is a function of the local orientation, $\tilde{\theta}$, of the layering.

I define the mean anisotropy, $\bar{\alpha}$, of a multilayer as the value of the anisotropy calculated with the mean shear viscosity:

$$\bar{\alpha} = \mu_n/\bar{\mu}_s = 1 + (\mu_l/h)(m/\beta_c)\ |\bar{\sigma}_{xz}/\beta_c|^{(m-1)} \tag{16a}$$

or

$$\bar{\alpha} = 1 + (m/\beta)\ |2\ \tan(2\bar{\theta})|^{(m-1)} \tag{16b}$$

where

$$\beta = (\beta_c)h/[\mu_l|\mu_l\bar{D}_{xx}/\beta_c|^{(m-1)}] \tag{16c}$$

and eq. (2b) has been used to express the mean shear stress in terms of the angle $\bar{\theta}$.

According to eq. (16b), the mean value of the anisotropy for a multilayer is a function of the powerlaw exponent $\underline{m}$, the inclination of the layering to the principal stresses, $\bar{\theta}$, and a parameter, β, which is a function of the mean deformation rate, $\underline{\bar{D}}_{xx}$, causing folding. Anisotropy ranges from one for contacts with infinite resistance to slip (bonded) to infinity for contacts with zero resistance to slip (free slip). The corresponding value for β ranges from infinity for infinite resistance to slip to zero for zero resistance to slip.

The mean anisotropy is related to the proportion of the mean layer-parallel velocity that is accommodated by a velocity jump at an interface compared to the proportion that is accommodated by deformation within a layer. For the mean value of the anisotropy, eq. (16a) can be rewritten as

$$\bar{\alpha} = 1 + (\mu_{\ell}/h)(1/\bar{S}) \tag{17}$$

where $\bar{S}$ is the mean value of the contact viscosity, eq. (7c), computed assuming zero perturbation. Using eqs. (1e) and (7a), eq. (17) becomes

$$\bar{\alpha} = 1 + m(\delta\bar{v}_x/\Delta\bar{v}_x) \tag{18}$$

where $\delta\bar{v}_x$ is the mean velocity jump at the interface and $\Delta\bar{v}_x$ is the increase in mean layer-parallel velocity across the thickness, h, of a layer. If there is no slip at contacts, the anisotropy equals one, and all shearing deformation is accommodated within the layer. If there is zero resistance to slip at contacts (free slip), the anisotropy is very large and much of the shearing deformation is accommodated as slip at the interfaces.

Thus we have seen two ways of understanding the mean anisotropy of a multilayer composed entirely of stiff, viscous layers. Equation (18) shows that the anisotropy is related to the partitioning of shearing between the layers and the interfaces. Equation (5b) shows that the anisotropy is also related to the difference in orientations of principal far-field deformation rates and principal far-field mean stresses.

GEOMETRIC PROPERTIES OF ASYMMETRY

Although fold form is a property of the entire package of interfaces in a multilayer, asymmetry is a property of a single interface. Each interface in a multilayer can have a different strength of asymmetry and, in some multilayers, a different sense of asymmetry.

The waveform one observes in an interface is a resultant waveform, defined here in terms of cosinusoidal and sinusoidal component waveforms. Differences in the sense and strength of asymmetry which develops at interfaces in simple multilayers with constant or variable resistance to slip at contacts can be understood in terms of differences in the amplitudes, signs, and wavelengths of the component waveforms.

I define the asymmetry, $\mathring{A}$, operationally to be the difference in the lengths of the left- and right- dipping limbs of an interface waveform divided by the sum of the lengths of the left- and right- dipping limbs, with both sets measured parallel to the wavetrain (the x-axis in my analyses) (Fig. 8):

$$\mathring{A} = (\lambda_{LD} - \lambda_{RD})/(\lambda_{LD} + \lambda_{RD}) \qquad (19)$$

The lengths of the limbs are measured from crests to troughs, which are defined as positions of zero slope on the interface waveform.

If the shape of an interface (Fig. 8) is described by an equation of the form,

$$\zeta = h/2 + A\cos(\ell x) + B\cos(2\ell x) + C\sin(2\ell x) \qquad (20a)$$

the positions of crests and troughs can be derived from

$$\begin{aligned}(\partial\zeta/\partial x) &= 0\\ &= -(A\ell)\sin(\ell x) - (2B\ell)\sin(2\ell x)\\ &\quad + (2C\ell)\cos(2\ell x) \qquad (20b)\end{aligned}$$

Let two troughs and a crest be defined by the positions

$$\ell x_1 = \varepsilon_1; \quad \ell x_2 = \pi + \varepsilon_2; \quad \ell x_3 = -\pi + \varepsilon_3 \qquad (21)$$

in which ε_1, ε_2, and ε_3 are:

$$\varepsilon_1 = \sin^{-1}\{2[(C/A)\cos(2\varepsilon_1) - (B/A)\sin(2\varepsilon_1)]\} \qquad (22a)$$

$$\varepsilon_2 = \varepsilon_3 = \sin^{-1}\{-2[(C/A)\cos(2\varepsilon_3) - (B/A)\sin(2\varepsilon_3)]\} \qquad (22b)$$

Using eqs. (21) to describe the lengths of the left- and right- dipping limbs on the interface, the asymmetry, $\underline{\mathring{A}}$ (eq. 19), becomes

$$\mathring{A} = (\varepsilon_1 - \varepsilon_2)/\pi \qquad (23a)$$

Asymmetry, $\underline{\mathring{A}}$, is determined by substituting into eq. (23a) the values for ε_1, ε_2, and ε_3, obtained by solving

Figure 8. Asymmetric interface waveform. Lengths of left- and right- dipping limbs designated as λ_{LD} and λ_{RD}, respectively.

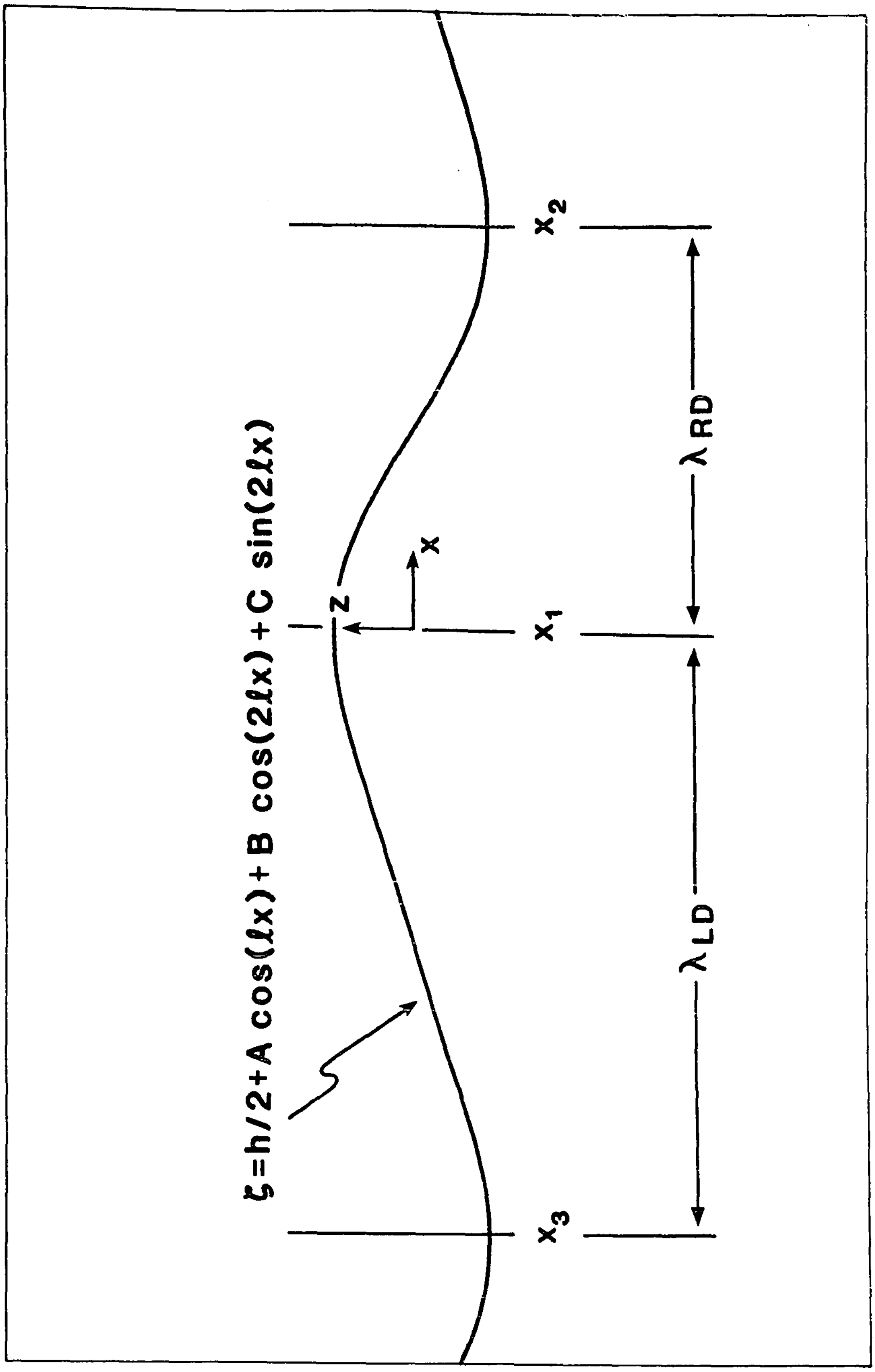

ζ=h/2+A cos(ℓx)+B cos(2ℓx)+C sin(2ℓx)
x
z
x₂
x₁
x₃
λRD
λLD

eqs. (22). Table I lists the asymmetry, $\mathring{A}$, computed using eqs. (22), for various values of C/A and B/A.

A 1st order approximation to $\mathring{A}$ can be derived as follows. The 1st order approximations to eqs. (22) are

$$\varepsilon_1 \cong 2(C/A)/[1 + 4(B/A)] \tag{24a}$$

$$\varepsilon_2 = \varepsilon_3 \cong -2(C/A)/[1 - 4(B/A)] \tag{24a}$$

Substituting eqs. (24) into eq. (23a), we find

$$\mathring{A} \cong (4/\pi)(C/A)/\{1 - [4(B/A)]^2\}; \quad |B/A|<<(1/4) \tag{23b}$$

The 1st order expression in eq. (23b) indicates the nature of the dependence of $\mathring{A}$ on C/A and B/A.

The magnitude, or <u>strength</u>, of asymmetry $\mathring{A}$ increases as the disparity in the lengths of the fold limbs increases (eq. 19). The strength of the asymmetry also increases as the ratios of amplitudes of the component waveforms, C/A and B/A, increase (Table I, eq. 23b). If C is zero, the asymmetry $\mathring{A}$ is zero and the waveform is symmetric. If C is nonzero, the magnitude of asymmetry increases with the amplitudes B and C.

I have arbitrarily defined the <u>sign</u> of the asymmetry $\mathring{A}$ to be positive if the left-dipping limb is longer than the right (Fig. 8). A positive sense of asymmetry corresponds also to a positive C/A ratio but is independent of the sign of the B/A ratio (eqs. 22, 23b).

TABLE I

ASYMMETRY Å CORRESPONDING TO VARIOUS RATIOS OF AMPLITUDES OF COMPONENT WAVEFORMS

± B/A	C/A	Å
0	0.05	0.063
	0.10	0.119
	0.15	0.167
	0.20	0.207
	0.25	0.239
	0.30	0.265
0.10	0.05	0.073
	0.10	0.133
	0.15	0.180
	0.20	0.217
	0.25	0.247
	0.30	0.271
0.20	0.05	0.123
	0.10	0.179
	0.15	0.216
	0.20	0.245
	0.25	0.268
	0.30	0.289

Interfaces in a multilayer <u>drift</u>, or undergo a phase shift, in response to layer-parallel shear. The drift is measured by a <u>phase angle</u>, ϕ, which necessarily enters the trigonometric terms used to describe each interface shape (eq. 20a) in the multilayer. If the phase angle is the same on all interfaces, the resultant waveforms are in phase throughout the multilayer. If the phase angle varies from interface to interface, the resultant waveforms are out of phase.

The height of a single interface subjected to a phase shift is

$$\zeta = h/2 + A\cos(\ell x+\phi) + B\cos(2\ell x+2\phi) + C\sin(2\ell x+2\phi) \qquad (25a)$$

As in the previous example, eq. (20b), the positions of peaks and troughs can be determined by the relation

$$(\partial\zeta/\partial x) = 0 = -(A\ell)\sin(\ell x+\phi) - (2B\ell)\sin(2\ell x+2\phi) + (2C\ell)\cos(2\ell x+2\phi) \qquad (25b)$$

The amount of phase shift has no affect on asymmetry.

Although the asymmetry of a composite waveform in an interface can be described quantitatively by the operational asymmetry, $\dot{\underline{A}}$, effects of various component waveforms on interface asymmetry and shape can be best appreciated visually. Illustrations of the addition of component waveforms to produce a resultant waveform are shown in Fig. 9. Column 1 contains four identical first component waveforms of positive amplitude A. Each of these first waveforms is added to a second component waveform of cosine or sine form and amplitude B or C, respectively, shown in column 2. Column 3 shows the resultant waveforms.

The effects of the second waveform depend on the sign of its amplitude and whether it is a sine or cosine wave. Addition of a cosinusoidal second waveform (rows A and B) to a cosinusoidal first waveform produces a symmetric resultant waveform. For example, the second component waveform shown in loc. A2 has a positive amplitude and sharpens the crests and flattens the troughs defined by the first waveform, as shown in loc. A3. Addition of the cosinusoidal second component waveform moves the inflection points of the first component waveforms closer to the sharpened crests but does not affect the positions of the crests.

Addition of a sinusoidal second component waveform (rows C and D) to a first component waveform produces an asymmetric resultant waveform. For example, a sinusoidal second component waveform of positive amplitude C (loc. C2) steepens the dip and decreases the length of right-dipping limbs, and shallows the dip and increases the length of left-dipping limbs (loc. C3). A sinusoidal second component

<u>Figure 9</u>. Asymmetry and shapes of interfaces determined by addition of two component waveforms. Cosinusoidal first component waveforms of positive amplitudes in column 1; cosinusoidal and sinusoidal second component waveforms, of positive or negative amplitudes, in column 2. Each row, A-D, illustrates the addition of a waveform in column 1 to a waveform in column 2 to produce a resultant waveform in column 3. Addition of a cosinusoidal second waveform (rows A and B) to a cosinusoical first waveform produces a <u>symmetric</u> resultant waveform. Addition of a sinusoidal second waveform (rows C and D) to a cosinusoidal first waveform produces an <u>asymmetric</u> resultant waveform.

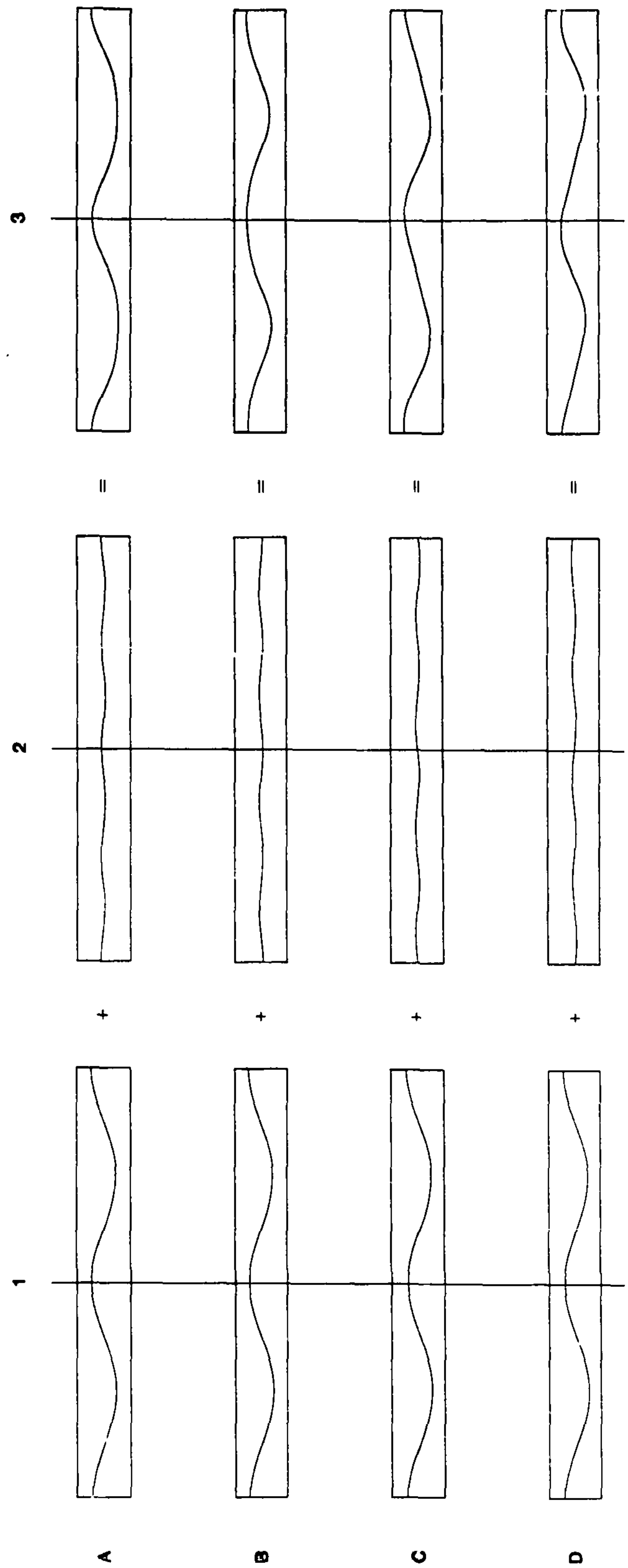

1
2
3
A
B
C
D

waveform with a negative amplitude C (loc. D2) produces a resultant waveform with the opposite asymmetry: steeper, shorter left-dipping limbs and shallower, longer right-dipping limbs (loc. D3). Addition of the sinusoidal second component waveform moves the positions of the crests closer to the inflection points on the steepened limbs but does not affect the positions of the inflection points.

The effectiveness of a second component waveform in modifying the interface shape produced by the first component waveform alone depends on the relative strength of the second waveform. The relative strength of the second waveform at an interface is measured by the ratio of its amplitude to that of the first waveform on that interface. The relative strength of the second cosinusoidal waveform in Fig. 9, loc. A3, is B/A = 0.20; in loc. D3, the relative strength of the second sinusoidal waveform is C/A = -0.20.

As the strength of the second sinusoidal waveform increases, the shape of the interface becomes more asymmetric. Asymmetry is difficult to recognize visually when the C/A ratio falls below about 0.08, that is, when Å is less than about 0.1.

Nine resultant waveforms produced by adding a positive sinusoidal second waveform to a positive cosinusoidal first waveform are shown in Fig. 10. The strength of the second waveform, C/A, and the operational asymmetry, Å, for each interface are indicated to the right of that interface. At

Figure 10. Values of asymmetry, Å, for various interface waveforms. Asymmetry Å increases with increasing strength of the sinusoidal second component waveform, measured by ratio C/A, where C is the amplitude of the sinusoidal second waveform and A is the amplitude of the first waveform. Asymmetry is difficult to recognize visually if Å is less than about 0.1.

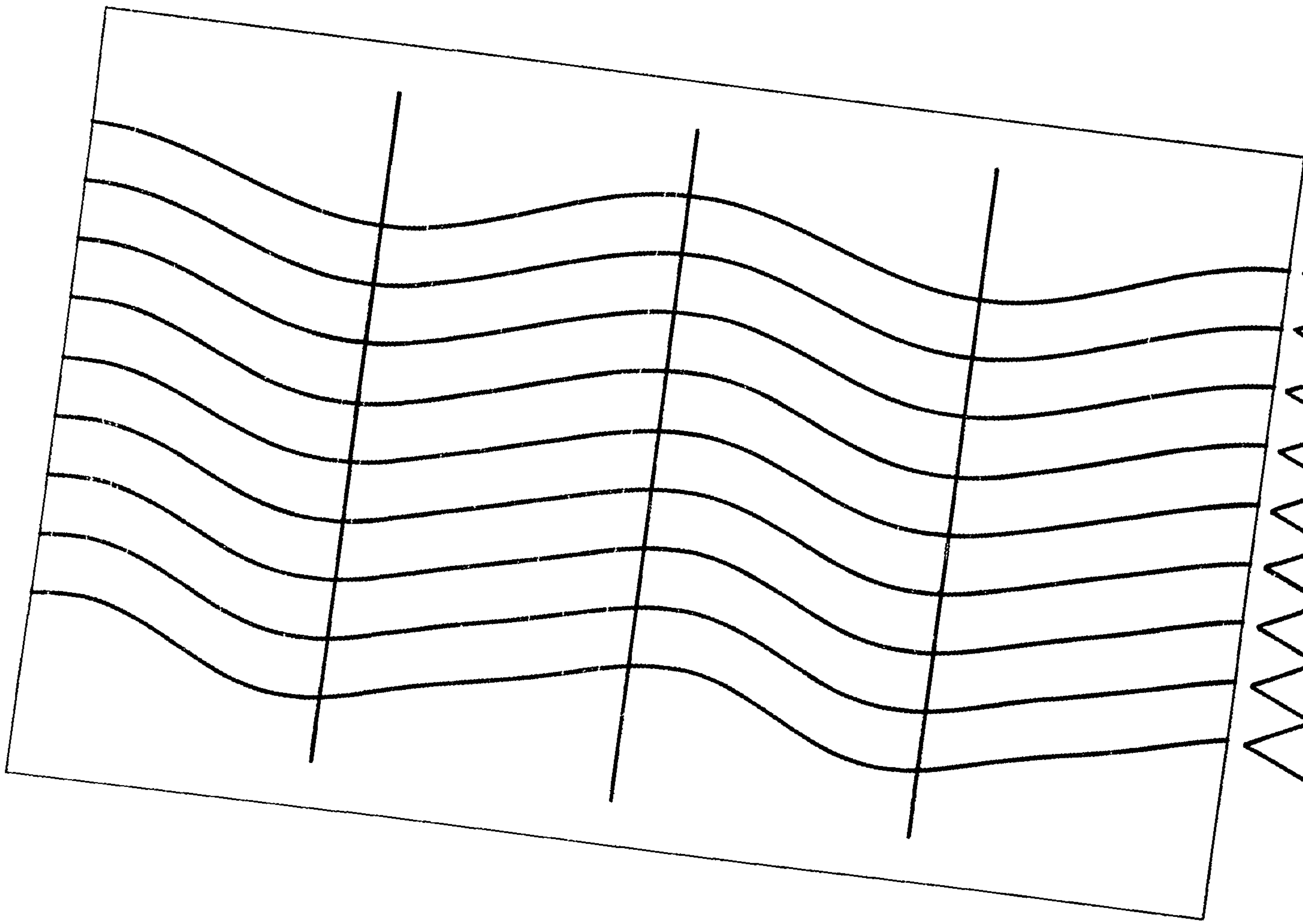

C/A	Å
0.0	0.0
0.050	0.062
0.075	0.092
0.100	0.119
0.125	0.144
0.150	0.167
0.175	0.188
0.200	0.207
0.225	0.223

a $\underline{C}/\underline{A}$ ratio of zero, the interface shape is symmetric.

ANALYSIS OF ASYMMETRY IN INFINITELY THICK MULTILAYERS

I will show that jumps in the mean layer-parallel velocities across interfaces are responsible for the spontaneous development of the first and second waveforms that produce both the drift and the opposite senses of asymmetry described in preceding pages.

I will first analyze infinitely thick multilayers. Equations that describe folding of multilayers are greatly simplified when adapted to infinitely thick multilayers because no terms are needed to account for media or for differences among layers. Fold forms are similar, and each interface in an infinitely thick multilayer can be described by a combination of two folding-mode waveforms, $\underline{A}\cos(\ell \underline{x})$ and $\underline{C}\sin(2\ell \underline{x})$. $\underline{B}$, the amplitude of the cosinusoidal second component waveform, is zero. Asymmetry is the result of growth of $\underline{C}$, the amplitude of the sinusoidal second waveform.

The mean velocity parallel to layering offsets each interface an identical amount from its neighboring interfaces, introducing a phase shift, ϕ, between pairs of neighboring interfaces. Every interface, therefore, continues to bear an identical relationship to the center of its underlying layer, and the height of each interface can be written as

$$\zeta = h/2 + A\cos(\ell x+\phi) + C\sin(2\ell x+2\phi) \qquad (26)$$

The equations for growth of the two component waveforms and the phase angle are

$$dA/d\bar{S}_x = -(A/\bar{S}_x)\ (1 + {}^{1}_{1}q) \qquad (27a)$$

$$dC/d\bar{S}_x = -(C/\bar{S}_x)\ (1 + {}^{2}_{2}q) + (A/\bar{S}_x)\ {}^{1}_{2}q \qquad (27b)$$

$$d\phi/d\bar{S}_x = -(1/\bar{S}_x)\ r \qquad (27c)$$

$$\bar{S}_x = h_o/h = L/L_o \qquad (27d)$$

where $\bar{S}_x$ is the horizontal stretch (shortening); A and C are current amplitudes; r is a drift factor; and q is an amplification factor. Expressions for the amplification factors are presented below; I will discuss each set, eqs. (28), eqs. (29), and eqs. (30), in following pages.

I consider three infinitely thick multilayers which differ only in the nature of the rate of slip at layer contacts:

1. The Ramberg model of drag folds. (Bonded contacts). The rate of slip at layer contacts is zero, and the interfaces serve only as passive markers.
2. General drag fold model. The rate of slip at layer contacts is a linear function of the contact shear stress.
3. Monoclinal kink fold model. The rate of slip at layer

<u>Bonded Contacts</u> ($\underline{m} = 1.0$; $\bar{\alpha} = 1.0$)

$$ {}_1^1q = 0 \qquad (28a)$$

$$ {}_2^2q = 0 \qquad (28b)$$

$$ {}_2^{11}q = -(A\ell)\ \tan(2\bar{\theta}) \qquad (28c)$$

$$ r = -2k\ \tan(2\bar{\theta}) \qquad (28d)$$

<u>Constant Resistance to Slip at Contacts</u> ($\underline{m} = 1.0$; $\bar{\alpha} \geq 1.0$)

$$ {}_1^1q = [2k/({}_1S_1C-k)](1 - {}_1F) \qquad (29a)$$

$$ {}_2^2q = [4k/({}_2S_2C-2k)](1 - {}_2F) \qquad (29b)$$

$$ {}_2^{11}q = -(A\ell)\ \tan(2\bar{\theta}) \left[1 + ({}_2^2q/16)\ \{4 + u[2({}_2S/{}_1S)^2-1] + 4(k/{}_1S)^2(\bar{\alpha}-1)u[2({}_2S_2C/k)-({}_1S_1C/k)-1]\} \right] \qquad (29c)$$

$$ r = -2k\ \tan(2\bar{\theta})\ [1 + (\bar{\alpha}-1)u] \qquad (29d)$$

$$ u = \frac{(1/A\ell)^2 - 1}{(1/A\ell)^2 + 3/4 + (\bar{\alpha}-1)k({}_1S_1C+k)/({}_1S^2)} \qquad (29e)$$

<u>Variable Resistance to Slip at Contacts</u> ($\underline{m} > 1.0$; $\bar{\alpha} \geq 1.0$)

$$ {}^{1}_{1}q = [2k/({}_{1}S_{1}C-k)](1 - {}_{1}F) \tag{30a} $$

$$ {}^{2}_{2}q = [4k/({}_{2}S_{2}C-2k)](1 - {}_{2}F) \tag{30b} $$

$$ {}^{11}_{2}q = -(A\ell)\ \tan(2\bar{\theta}) \Big[1 + [{}^{2}_{2}q/(16m)]\ \{4m + u[2({}_{2}S/{}_{1}S)^{2}-1] + 4(k/{}_{1}S)^{2}(\bar{\alpha}-1)u[2({}_{2}S_{2}C/k)-({}_{1}S_{1}C/k)-1] - 4m(m-1)[{}_{1}F/\tan(2\bar{\theta})]^{2}\} \Big] \tag{30c} $$

$$ r = -2k\ \tan(2\bar{\theta})\ [1 + (\bar{\alpha}-1)u/m] \tag{30d} $$

$$ u = \frac{(1/A\ell)^{2} - m\{1 - (m-1)[{}_{1}F/\tan(2\bar{\theta})]^{2}\}}{(1/A\ell)^{2} + 3/4 + (\bar{\alpha}-1)k({}_{1}S_{1}C+k)/({}_{1}S^{2})} \tag{30e} $$

where

$$ {}_{n}F = \frac{{}_{n}S^{2}}{{}_{n}S^{2} + (\bar{\alpha}-1)2nk({}_{n}S_{n}C-nk)} $$

$$ \tan(2\bar{\theta}) = -(1/2)\ \bar{\sigma}_{xz}/(\bar{D}_{xx}\mu_{\ell}) $$

$$ {}_{n}C = \cosh(nk);\quad {}_{n}S = \sinh(nk) $$

$$ k = \pi h/L $$

contacts is a nonlinear function of the contact shear stress.

<u>Ramberg Model</u>

I first investigate asymmetry in the case of an infinitely thick multilayer composed of identical layers with bonded contacts. The multilayer behaves as a homogeneous, viscous material, and interfaces are merely passive markers. Horizontal compression, parallel to interfaces, amplifies perturbations in interfaces kinematically, as shown in Chapter I. With the addition of mean simple shear parallel to flat interfaces, both asymmetry and drift develop kinematically, as indicated by the non-zero amplification factor, ${}^{1}_{2}\underline{g}$, and drift factor, $\underline{r}$, eqs. (28).

I identify the model of passive interfaces subjected both to layer-parallel shortening and shear with Ramberg's model because both ascribe the development of asymmetry to a kinematic superposition of shear strain onto folds (Ramberg, 1963).

The equations for kinematic folding are relatively simple and can be written completely here. From eqs. (27) and (28), we find

$$dA/d\bar{s}_x = -(A/\bar{s}_x) \qquad (31a)$$

$$dC/d\bar{s}_x = -(C/\bar{s}_x) - (1/\bar{s}_x)\ A\ (A\ell)\ \tan(2\bar{\theta}) \qquad (31b)$$

$$d\phi/d\bar{S}_x = (1/\bar{S}_x)\ 2k\ \tan(2\bar{\theta}) \tag{31c}$$

in which

$$k = \pi h/L \tag{31d}$$

Integrating eqs. (31), we obtain:

$$A = A_o/\bar{S}_x \tag{32a}$$

$$C = (A_o/2)(A_o\ell_o)\ \tan(2\bar{\theta})\ (1 - \bar{S}_x^2)/\bar{S}_x^3 \tag{32b}$$

$$\phi = -k\ \tan(2\bar{\theta})\ (1 - \bar{S}_x^2) \tag{32c}$$

The first waveform amplifies only in response to layer-parallel shortening (eq. 32a). Both the amplitude $\underline{C}$ of the second waveform and the drift are zero without layer-parallel shear ($\bar{\theta} = 0$) (eqs. 32b,c). The amplitude of the second waveform depends on the square of the amplitude of the first waveform -- the square of the perturbed thickness of the layer -- whereas the magnitude of the phase angle depends on the mean thickness, $\underline{h}$, of the layer. Therefore, layer-parallel displacement of a point by the second waveform depends on the position of that point on the perturbed interface, but the lateral displacement caused by the drift is the same for every point along an interface. The second waveform changes the shape of the interface, but the drift does not.

The strength of the second waveform, $\underline{C}/\underline{A}$, indicates the magnitude of the asymmetry. According to eqs. (32a) and (32b),

$$(C/A) = (1/2)(A_o \ell_o)\ \tan(2\bar{\theta})\ (1 - \bar{S}_x^2)/\bar{S}_x^2 \qquad (33a)$$

A 1st order approximation to the operational asymmetry, $\underline{\mathring{A}}$, can be derived from eqs. (33a) and (23b)

$$\mathring{A} \cong (2/\pi)(A_o \ell_o)\ \tan(2\bar{\theta})\ (1 - \bar{S}_x^2)/\bar{S}_x^2 \qquad (33b)$$

The sense of asymmetry of folds is determined by the sign of $\underline{C}/\underline{A}$, relative to the sense of layer-parallel shear stress. For passive interfaces, the sign of $\underline{C}/\underline{A}$, eq. (33a), and of $\underline{\mathring{A}}$, eq. (33b), is positive if the layer-parallel shear is positive (right-lateral) and negative if the layer-parallel shear is negative (left-lateral). Thus, the sense of asymmetry recorded by a passive interface must be that of a drag fold; this is consistent with the result Ramberg (1963) obtained.

The phase angle, ϕ, enters the argument of the sine and cosine functions to describe the drift of waveforms. The phase shift can also be expressed as an angular drift, φ, which is the inclination after deformation of a line that was originally vertical. The relationship between φ and ϕ is:

$$\tan(\varphi) = -\ (\phi/\ell)\ (2/h) = -\ \phi/k \qquad (33c)$$

The angular drift, eq. (33c), can be expressed in terms of

$\bar{\theta}$ for passive interfaces by using eq. (32c)

$$\tan(\phi) = \tan(2\bar{\theta})\,(1 - \bar{S}_x^2) \tag{33d}$$

According to eq. (33d), the angular drift of passive interfaces is positive (right-lateral) if the layer-parallel shear is positive, and it is negative (left-lateral) if the layer-parallel shear is negative.

Kinematic growth of both component waveforms during layer-parallel shortening and shearing of an infinitely thick multilayer with bonded contacts is analyzed in Fig. 11. The multilayer contains an initial, symmetric, cosinusoidal perturbation (Fig. 11A) with a maximum slope of 20°. The orientation of the principal compression is $\bar{\theta}$ = 40° clockwise with respect to bedding.

Kinematic amplification of the first component waveform results solely from the layer-parallel compression (eq. 32a, Fig. 11B). Deformation resulting from the mean, layer-parallel shear stress produces drift and asymmetry of interface waveforms (eqs. 32b,c). The effect of superimposing the drift on the first waveforms (Fig. 11B) is shown in Fig. 11C: each interface waveform is symmetric but offset from its neighbors. The asymmetry is added in Fig. 11D: each resultant interface waveform is asymmetric, with the short, steep limb dipping to the right. During deformation of a multilayer subjected to layer-parallel shortening and shearing, $\underline{A}$, $\underline{C}$, and ϕ grow simultaneously,

Figure 11. Analysis of kinematic growth of component waveforms and phase angle during layer-parallel shortening and shearing of infinitely thick multilayer with bonded contacts. A. Initial, symmetric perturbation consists of first component waveforms. B. Kinematic amplification of first waveforms in response to layer-parallel shortening maintains symmetry of interfaces. C. Drift of waveforms shown in B results in offset of neighboring, symmetric interfaces. D. In addition to producing the drift shown in C, layer-parallel shearing deformation causes waveforms at bonded contacts to develop the sense of asymmetry of drag folds.

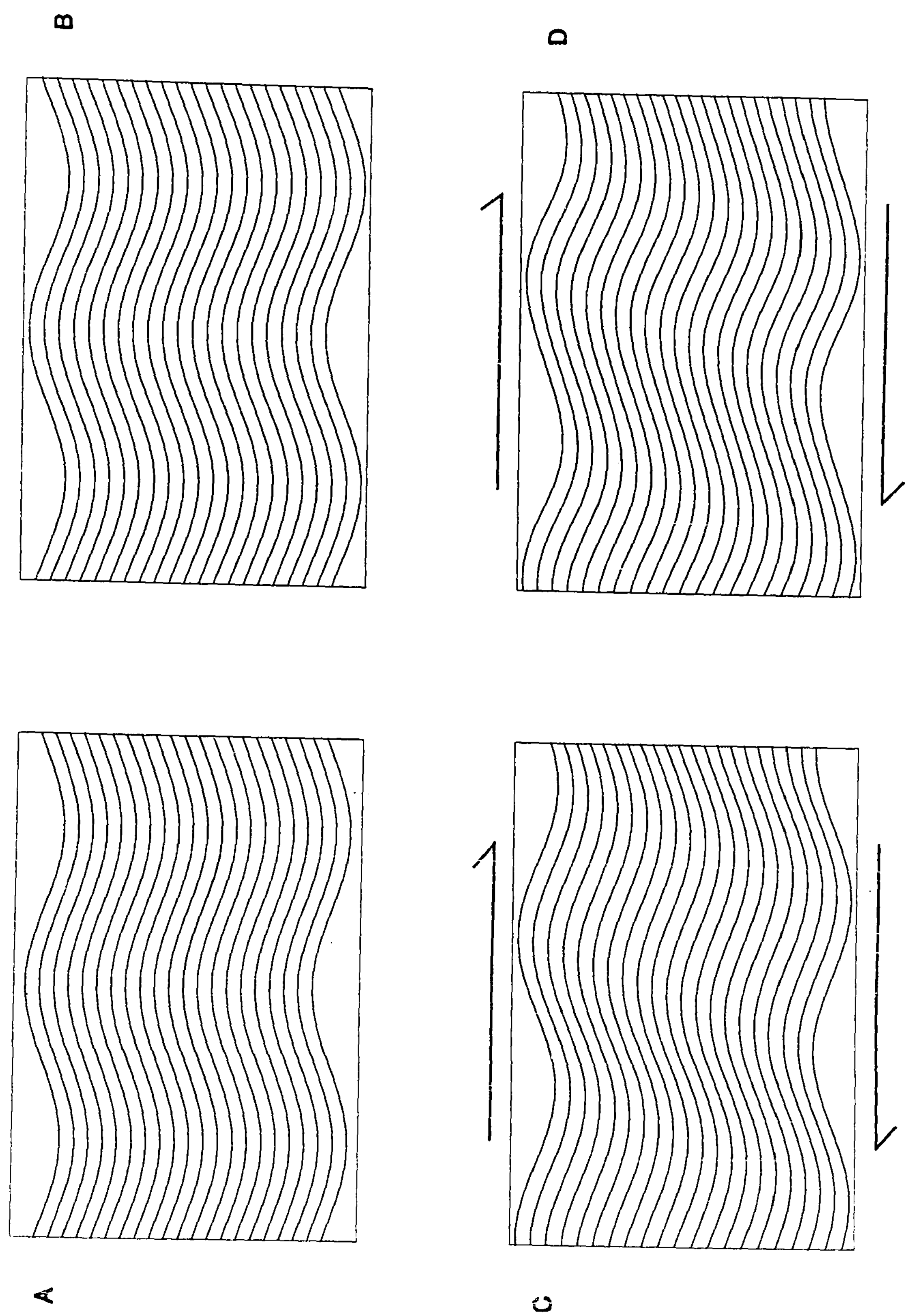
A
B
C
D

transforming the fold form shown in Fig. 11A directly into that shown in Fig. 11D.

Kinematic growth of $\underline{A}$, $\underline{C}$, and ϕ according to the H. Ramberg model is closely related to, but not equivalent to, simple shear strain of passive folds, which is the model of drag folds analyzed by I. Ramberg and Johnson (1976). Here I briefly examine kinematic amplification resulting solely from simple shear.

In simple shear, the deformed position ($\underline{x}$,$\underline{z}$) of a material point with initial position ($\underline{X}$,$\underline{Z}$), is

$$x = X + Z \tan(\psi) \tag{34a}$$

$$z = Z = h/2 + A \cos(\ell X) \tag{34b}$$

where ψ is the angle of simple shear strain, $\underline{h}/2$ is the mean vertical distance from the origin of coordinates, and $\underline{A} \cos(\ell \underline{X})$ is the initial shape of a symmetric, passive perturbation. The angle of simple shear strain, ψ, is the angle of inclination resulting from simple shear of an initially vertical line in homogeneous material. Thus, although ψ is closely related to the drift angle, ϕ, eqs. (33c,d), ϕ is not equal to ψ because ϕ arises from compression as well as from shear; ϕ would equal ψ if $\underline{\bar{D}}_{xx}$ were zero ($\underline{\bar{S}}_x = 1$).

The simple shear strain of pre-existing, passive, symmetric waveforms produces asymmetric interface waveforms

(Fig. 12A) which are virtually identical to waveforms produced by kinematic amplification of perturbations subjected simultaneously to layer-parallel normal and shearing deformations (Fig. 12B). Figure 12A shows a multilayer subjected to simple shear strain, with ψ = 20°. Figure 12B shows the same multilayer kinematically deformed by layer-parallel compression and simple shear; $\underline{\bar{S}}_x$ is 0.97 (three percent shortening), $\bar{\theta}$ is 40°, and ϕ is 20°. Both sets of interface waveforms are asymmetric, and both have the sense of asymmetry of a drag fold.

General Drag Fold Model

Drag folds occur in identical multilayers in which the resistance to slip at contacts is constant. The coefficient of contact viscosity, Ξ, which reduces to a constant for $\underline{m}$ = 1 (eq. 7c), can range from infinity (bonded contacts) to zero (free slip). The corresponding mean anisotropy of the multilayer, $\bar{\alpha}$, can range from one for bonded contacts to very large for free slip (eq. 17). Viscous slip, which is characterized by a constant, finite resistance to slip at contacts, is a behavior intermediate between these two extremes.

A sinusoidal second component waveform and fold asymmetry are consequences of layer-parallel shear stress. The second waveform starts to grow as a 2nd order interaction between the mean layer-parallel velocity and the

Figure 12. Simple shear strain of symmetric waveforms (A) and layer-parallel shortening and shearing deformation of symmetric perturbation (B) produce virtually identical resultant waveforms with drag fold asymmetry. Multilayer shown in B is analyzed in Fig. 11.

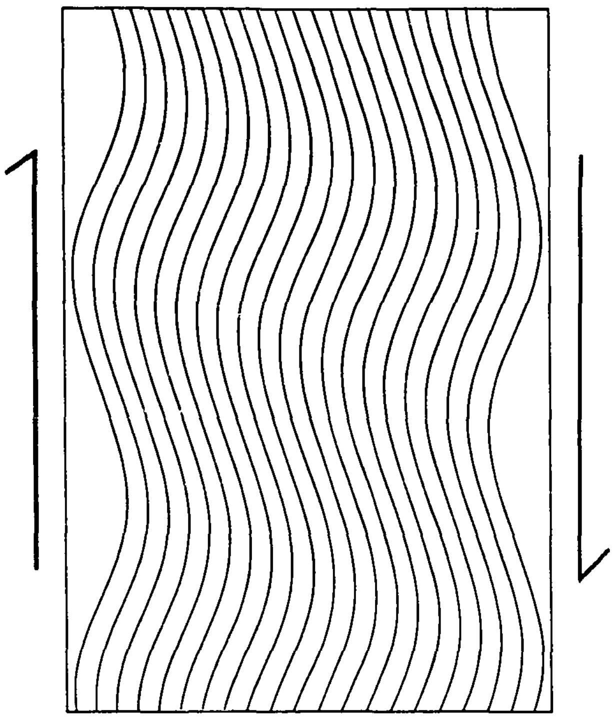

B

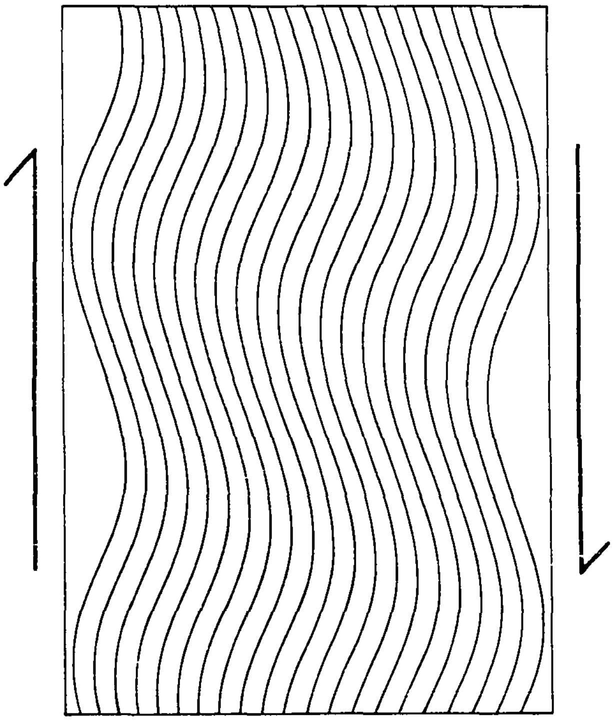

A

perturbed interface (eq. 29b). Once growth of a second waveform has been initiated, both the layer-parallel compression, through the amplification factor ${}^{0}_{2}\underline{q}$, and the mean shear, through the amplification factor ${}^{1}_{2}\underline{q}$, promote its continued development.

Growth of the second waveform in an infinitely thick multilayer is driven by a discontinuity in the mean layer-parallel velocity, $\bar{\underline{v}}_x$, at each interface. The mean layer-parallel velocity jump, in turn, is driven by the mean shear stress (eq. 13). If contacts are bonded, the $\bar{\underline{v}}_x$ discontinuity can arise only if the layers have perturbed interfaces and different viscosities. If the layers have a finite resistance to slip at contacts, however, a discontinuity in $\bar{\underline{v}}_x$ can also be generated by slip at interfaces.

The sense of asymmetry of the resultant waveform at an interface with constant resistance to slip is always the asymmetry of a drag fold. The amplitude of the second waveform, $\underline{C}$, takes its sign from that of the mean shear stress because in the expressions for ${}^{1}_{2}\underline{q}$, the coefficient of the mean shear stress is positive for all wavelengths and anisotropies (eq. 29c).

The Ramberg model of bonded contacts correctly determines the sense of asymmetry of drag folds at interfaces with viscous slip, but considerably underestimates the magnitude of the asymmetry. The strength of the second waveform, $\underline{C}/\underline{A}$, and the magnitude of the asymmetry, $\underline{\hat{A}}$ (eqs. 22, 24a), increase with anisotropy (curve $\underline{m}$ = 1, Fig. 13A). For anisotropy of $\bar{\alpha} = 2.0$, $\underline{C}/\underline{A} = 0.113$, and the asymmetry is $\underline{\hat{A}} = 0.133$; for anisotropy of $\bar{\alpha} = 8.3$, $\underline{C}/\underline{A} = 0.3$, and $\underline{\hat{A}} = 0.265$. The strength of the second waveform, $\underline{C}/\underline{A}$, is about 0.063 and the corresponding asymmetry is $\underline{\hat{A}} = 0.078$ for the Ramberg model of drag folding ($\bar{\alpha} = 1.0$, Fig. 13A).

The increase of the phase angle, ϕ, in multilayers with finite, constant resistance to slip at contacts is controlled by a drift factor, $\underline{r}$, eq. (29d). The value of the drift factor for interfaces which accommodate deformation by slip is greater than the kinematic value produced by deformation that is confined to layers (eq. 28d). The drift factor increases in magnitude with anisotropy and is inversely proportional to the wavelength of the first waveform, eq. (29d). The factor $\underline{u}$, eq. (29e), limits the growth of the phase angle at large slopes and anisotropies: $\underline{u}$ is always positive, ranging from one to zero for slopes ranging from 0° to 45° and approaching zero as anisotropy becomes large.

Neither asymmetry nor drift develops, to 2nd order, in multilayers with free slip at contacts. In the limit of very large anisotropy (free slip), the contacts offer no resistance to slip, so the contact viscosity is zero and the contact shear stress is zero.

Figure 13. Relations between sense and strength of asymmetry $\mathring{A}$, strength of second waveform, C/A, nonlinearity of contact behavior, m, mean anisotropy, $\bar{\alpha}$, and orientation of maximum compression, $\bar{\theta}$. A. Strength of asymmetry $\mathring{A}$ increases with $\bar{\alpha}$ for constant resistance to slip at contacts (m = 1) and is maximized at intermediate value of $\bar{\alpha}$ for variable resistance to slip at contacts (m > 1). Monoclinal kink fold asymmetry can develop if contacts have variable resistance to slip. B. Tendency toward drag fold asymmetry increases with $\bar{\theta}$. Strength of asymmetry increases with $\bar{\theta}$ for constant resistance to slip at contacts and decreases with $\bar{\theta}$ for variable resistance to slip at contacts.

A.

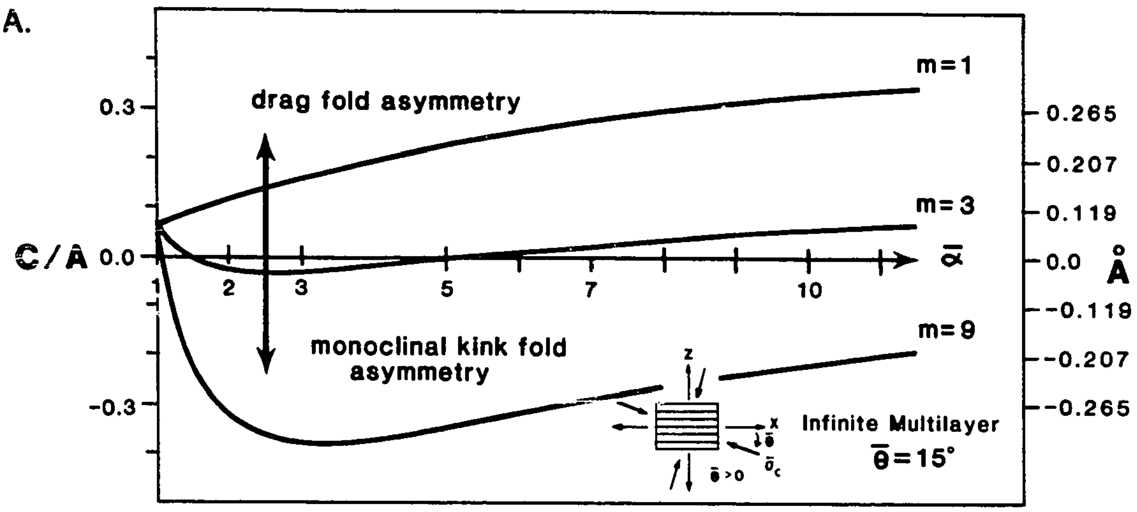

drag fold asymmetry
monoclinal kink fold asymmetry
m=1
m=3
m=9
C/A
0.3
0.0
-0.3
1
2
3
5
7
10
0.265
0.207
0.119
0.0
-0.119
-0.207
-0.265
Å
Infinite Multilayer
$\bar{\theta}=15°$

B.

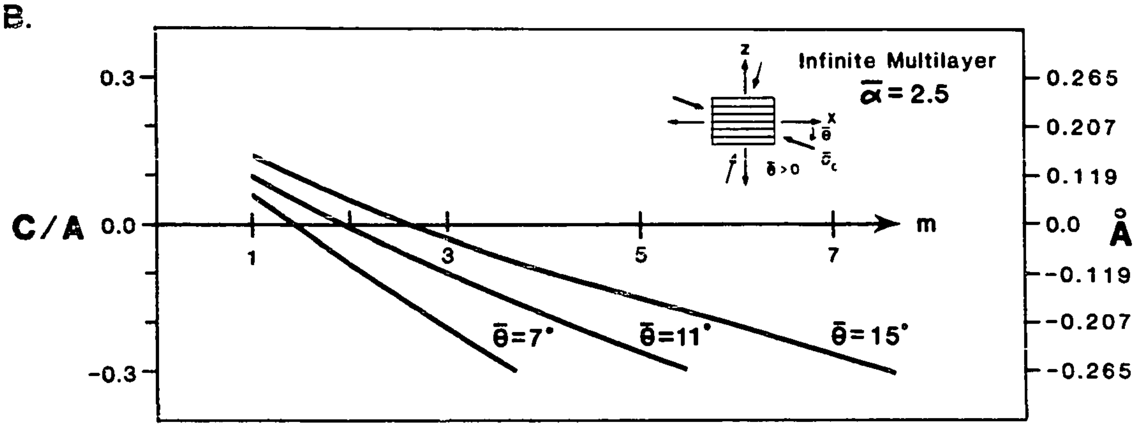

Infinite Multilayer
$\bar{\alpha}=2.5$
C/A
0.3
0.0
-0.3
1
3
5
7
m
$\bar{\theta}=7°$
$\bar{\theta}=11°$
$\bar{\theta}=15°$
0.265
0.207
0.119
0.0
-0.119
-0.207
-0.265
Å

Growth of the first cosinusoidal component waveform is a function of the layer-parallel compression and the anisotropy of the multilayer. Therefore, the amplification factor for the first waveform, ${}_1^1\underline{q}$, reduces not only to that for bonded contacts if the anisotropy is one but also to that for free slip at contacts if the anisotropy is very large:

$$\text{bonded contacts:} \quad {}_1^1q = 0 \tag{35a}$$

$$\text{viscous slip:} \quad {}_1^1q = \left[\frac{2k}{({}_1S_1C-k)}\right]\left[1 - \frac{({}_1S^2)}{\{({}_1S^2)+(\bar{\alpha}-1)2k({}_1S_1C-k)\}}\right] \tag{35b}$$

$$\text{free slip:} \quad {}_1^1q = \left[\frac{2k}{({}_1S_1C-k)}\right] \tag{35c}$$

For viscous slip at contacts, the amplification factor for the first component waveform, eq. (35b), is intermediate between the amplification factors that would occur for the two end members, eqs. (35a, 35c). As the anisotropy of the multilayer increases, ${}_1^1\underline{q}$ increases.

<u>Monoclinal Kink Fold Model</u>

Folds with monoclinal kink fold asymmetry occur in multilayers with variable resistance to slip at layer contacts. Variable resistance to slip is modeled by a powerlaw rheology for which the powerlaw exponent, $\underline{m}$, is greater than 1.0. According to this model, eq. (7c), the contact slipperiness (the inverse of viscosity) is

$$1/\Xi = (m/\beta_c)\ |\sigma_{ns}/\beta_c|^{(m-1)} \tag{36a}$$

Using the expression for the contact shear stress, eq. (9), the expression for the contact slipperiness can be expanded to

$$1/\Xi = 1/\bar{\Xi} + (1/\bar{\Xi})(m-1)(\tilde{\tau}/\bar{\sigma}_{xz}) + \ldots \tag{36b}$$

in which the mean contact slipperiness, generated solely by the mean shear stress, is

$$1/\bar{\Xi} = (m/\beta_c)\ |\bar{\sigma}_{xz}/\beta_c|^{(m-1)} \tag{36c}$$

The perturbed shear stress in eq. (36b) can be replaced by a sinusoidal function of $\underline{x}$, $¦\tau \sin(\ell \underline{x})$, and the expression for contact slipperiness becomes:

$$1/\Xi = 1/\bar{\Xi} + (1/\bar{\Xi})(m-1)(¦\tau/\bar{\sigma}_{xz})\ \sin(\ell x) \tag{36d}$$

Equation (36d) holds one of the keys to understanding different senses of asymmetric folding, as I will explain in following pages. The equation shows that the slipperiness consists of two terms: The first term is a mean value, $1/\bar{\Xi}$, and is constant along interfaces between layers. The second term, a perturbed value, is nonzero only if $\underline{m}$ is greater than 1.0. The effect of this term is to reduce the slipperiness on limbs facing one way and to increase the slipperiness on limbs facing the other way.

The contact slipperiness is used in the expression for anisotropy, eq. (15). The mean value in eq. (36d) determines the mean anisotropy, eq. (16a). The form of the perturbed value in eq. (36d) indicates that anisotropy to first and to higher orders of approximation will be a function of the local slope of interfaces between layers and therefore will be a function of position along layer contacts.

The rate of slip at layer contacts is expressed in terms of contact shear stress in eq. (10a), which can be rewritten as

$$\delta v_s = (\bar{\sigma}_{xz}/\bar{\Xi} m) + (1/\bar{\Xi})\{\tilde{\tau} + [(m-1)/2](\tilde{\tau}/\bar{\sigma}_{xz})\tilde{\tau}\} \tag{37a}$$

A more general expression incorporating the form of eq. (37a) is

$$\delta v_s = (\delta v_s)_0 + (\delta v_s)_1 + (\delta v_s)_2 \tag{37b}$$

The 0th order contribution to the rate of slip, (eq. 37a), is proportional to the mean contact slipperiness and to the mean shear stress and can be expressed in terms of mean anisotropy, eq. (17):

$$(\delta v_s)_0 = (\bar{\sigma}_{xz}/\bar{\Xi} m) = (\bar{\sigma}_{xz})(h/\mu_\ell)(\bar{\alpha}-1)/m \tag{38a}$$

In a 0th order analysis, therefore, the rate of slip is proportional to the slope of a straight line on a plot in stress and slip space (Fig. 7) that connects the point at the origin of coordinates to the point that represents the contact shear stress and rate of slip. The slope of that line is $\Xi\underline{m}$.

The 0th order rate of slip contributes to the growth of the phase shift, eq. (30d). Because the drift factor $\underline{r}$ is inversely proportional to $\underline{m}$, drift of contacts with variable resistance to slip is less than that of contacts with constant resistance to slip, eq. (29d), for low slopes of the first waveform; the rate of growth of ϕ is essentially kinematic if $\underline{m}$ is large.

The 1st order, perturbed contribution to the rate of slip is proportional to the magnitude of the perturbed shear stress:

$$(\delta v_s)_1 = (\bar{\alpha}-1)(h/\mu_\ell)(\tfrac{1}{2}\tau)\ \sin(\ell x) \qquad (38b)$$

The constant of proportionality is the mean contact viscosity, Ξ, which is the local slope of the curve that relates $\delta\underline{v}_s$ and σ_{ns}, Fig. 7. In a 1st order analysis, then, the slipperiness is constant everywhere along perturbed interfaces and is determined by the mean inclination, $\bar{\theta}$, of the far-field stresses in stiff layers.

To 1st order, the rate of slip is proportional to the mean anisotropy. In this respect, multilayers both with linear and nonlinear contact properties behave alike. Folding occurs to 1st order in an infinitely thick multilayer because the mean shear stress lowers the resistance to slip at layer contacts. Without layer-parallel mean shear stress, the resistance to slip would be infinite to 1st order, as noted in Chapter II for multilayers subjected solely to layer-parallel shortening.

The 2nd order contribution to the rate of slip in eq. (37a) is:

$$(\delta v_s)_2 = (1/2)[(1/\bar{S})(m-1)({}^{1}_{1}\tau/\bar{\sigma}_{xz})\ \sin(\ell x)]\ ({}^{1}_{1}\tau)\ \sin(\ell x) \tag{38c}$$

According to eq. (38c), 2nd order folding of multilayers with variable resistance to slip at contacts is controlled by a 1st order perturbed slipperiness, eq. (36d), which varies with the local slope of the perturbed interface.

The rate of slip at interfaces will be different on limbs facing in opposite directions, according to the 2nd order analysis. The local resistance to slip depends on the relative signs of the mean shear stress and the perturbed shear stress. The sign of the perturbed shear stress, ${}^{1}_{1}\tau\ \sin(\ell \underline{x})$, is a function of the sign of the slope of the first cosinusoidal waveform. The resistance to slip is lower on positive slopes of the first waveform if mean shear stress is positive because the positive mean shear stress and the positive perturbed shear stress together produce a higher contact shear stress. The resistance to slip is higher on negative slopes of the perturbation because the mean and perturbed shear stresses have opposite signs.

Using a trigonometric identity, the 2nd order contribution to the rate of slip (eq. 38c) can be rewritten:

$$(\delta v_s)_2 = (1/4)[(1/\Xi)(m-1)({}^1_1\tau/\bar{\sigma}_{xz})]\ ({}^1_1\tau)\ [1 - \cos(2\ell x)] \tag{38d}$$

By increasing the magnitude of the factor $\underline{u}$, eq. (30e), the $\underline{x}$-independent term in eq. (38d) strengthens the terms in eq. (30c) which promote drag fold asymmetry.

The sinusoidal second component waveform that produces monoclinal kink fold asymmetry is driven by the $\underline{x}$-dependent term in the 2nd order contribution to the rate of slip, eq. (38d). The last term in ${}^1_2\underline{q}$, eq. (30c), can be expressed as

$${}^1_2q = \ldots$$
$$-[1/(A\bar{D}_{xx})]\{{}^2_2q/[64(\bar{\alpha}-1)k]\}\ (1/\Xi)(\bar{m}-1)({}^1_1\tau/\bar{\sigma}_{xz})\ ({}^1_1\tau) \tag{39}$$

which makes clear its dependence on the 2nd order rate of slip, eq. (38d). Because the sign of the last term in ${}^1_2\underline{q}$ is opposite to those of the rest of the terms in ${}^1_2\underline{q}$, eq. (30c), the last term can reverse the sign of the amplitude $\underline{C}$ of the second waveform and thereby produce the monoclinal kink fold sense of asymmetry.

Thus, for a positive sense of mean shear stress, monoclinal kink fold asymmetry can form because the resistance to slip is lower on positive slopes and higher on negative slopes.

The asymmetry, $\underline{A}$, of folds in infinitely thick multilayers with variable resistance to slip at contacts is a function of the strength of the second waveform, $\underline{C}/\underline{A}$, which in turn depends on the mean anisotropy, $\bar{\alpha}$, the degree of nonlinearity of the resistance, $\underline{m}$, and the orientation, $\bar{\theta}$, of principal stresses in stiff layers (Fig. 13). The strength of the asymmetry, $\underline{A}$, is indicated by the strength of the second waveform, $\underline{C}/\underline{A}$, and the sense of asymmetry is indicated by the sign of $\underline{C}/\underline{A}$ relative to the sign of the mean shear stress. Figure 13 was constructed for a positive mean shear stress, so a positive $\underline{C}/\underline{A}$ in that figure indicates the sense of asymmetry of a drag fold and a negative $\underline{C}/\underline{A}$ indicates the sense of asymmetry of a monoclinal kink fold. For all the relations shown in Fig. 13, the multilayers are infinitely thick and consist of identical layers. The initial wavelength-to-thickness ratio is 35, the initial slope of the first waveform is 1°, and the final slope is 15°.

The strength of the second component waveform, $\underline{C}/\underline{A}$, is plotted in Fig. 13B as a function of the powerlaw exponent $\underline{m}$ for different magnitudes of the mean shear stress, as measured by the inclination $\bar{\theta}$ of the maximum compressive stress, $\bar{\sigma}_c$. For a given mean layer-parallel compression and shear stress, corresponding to an inclination of $\bar{\theta} = 11°$, for example, fold asymmetry progresses from drag asymmetry ($\underline{C}/\underline{A} > 0$) to zero asymmetry ($\underline{C}/\underline{A} = 0$) to monoclinal kink asymmetry ($\underline{C}/\underline{A} < 0$) as the power $\underline{m}$ is increased (Fig. 13B). For $\bar{\theta} = 7°$, the sense of asymmetry reverses ($\underline{C}/\underline{A} = 0$) at $\underline{m} = 1.4$; for $\bar{\theta} = 11°$, $\underline{C}/\underline{A} = 0$ at $\underline{m} = 1.95$; and for $\bar{\theta} = 15°$, $\underline{C}/\underline{A} = 0$ at $\underline{m} = 2.6$.

As the relative magnitude of the mean shear stress is increased, that is, as $\bar{\theta}$ is increased, fold asymmetry tends toward drag fold asymmetry for any value of $\underline{m}$ (Fig. 13B). For constant resistance to slip at contacts ($\underline{m} = 1$), the sense of asymmetry is that of a drag fold and the strength of asymmetry increases with increasing magnitude of the mean shear stress. For variable resistance to slip at contacts ($\underline{m} > 1$), the sense of asymmetry is that of a monoclinal kink fold, and the strength of asymmetry decreases with increasing magnitude of the mean shear stress.

Relations between the strength and sense of the asymmetry and the anisotropy, $\bar{\alpha}$, are shown for different values of $\underline{m}$ in Fig. 13A. As the anisotropy increases, the strength of the asymmetry increases for constant resistance to slip at contacts ($\underline{m} = 1$). For variable resistance to slip at contacts ($\underline{m} > 1$), in contrast, the strength of the monoclinal kink fold asymmetry is maximum at an intermediate value of anisotropy. For the conditions assumed for construction of Fig. 13A, asymmetry is maximum at $\bar{\alpha} \cong 3$. As the multilayer anisotropy is increased beyond three, the strength of the asymmetry decreases.

For variable resistance to slip at layer contacts (for example, $\underline{m}$ = 3) and low anisotropy ($\bar{\alpha} \cong 1$, Fig. 13A), the mean resistance to slip is high, so the contact behaves as though it were bonded all along its length. Consequently, the component waveform of amplitude $\underline{C}$ is initiated kinematically. The sign of d$\underline{C}$/d$\underline{t}$ is positive, and the resultant waveforms have the asymmetry of drag folds.

As anisotropy increases slightly ($1 < \bar{\alpha} < 1.3$), the mean resistance to slip decreases, but the total resistance is distinctly lower on slopes facing one way and higher on slopes facing the other way. The component waveform with amplitude $\underline{C}$ grows more slowly than it did kinematically. The resultant waveform still has the sense of asymmetry of drag folds, but the strength is weaker.

As the anisotropy increases beyond about 1.3, the amplitude, $\underline{C}$, of the second waveform becomes negative because the sign of d$\underline{C}$/d$\underline{t}$ becomes negative; the sense of asymmetry of monoclinal kink folds develops.

At an even higher anisotropy ($\bar{\alpha} \cong 5.5$), the mean resistance to slip may be sufficiently low so that the difference in resistance to slip on the two sets of slopes is negligible. Then the sign of d$\underline{C}$/d$\underline{t}$ will become positive, and the sense of asymmetry of interface waveforms will become that of a drag fold.

Figure 14 shows boundaries between domains of drag fold and monoclinal kink fold asymmetries, as the sense of

Figure 14. Domains of combinations of thickness-to-wavelength ratio, $\underline{h}/\underline{L}$, and orientation of maximum compression, $\bar{\theta}$, which favor development of monoclinal kink fold or drag fold asymmetry in infinitely thick multilayers. Domain boundaries are defined by the $d\underline{C}/d\underline{t} = 0$ contour.

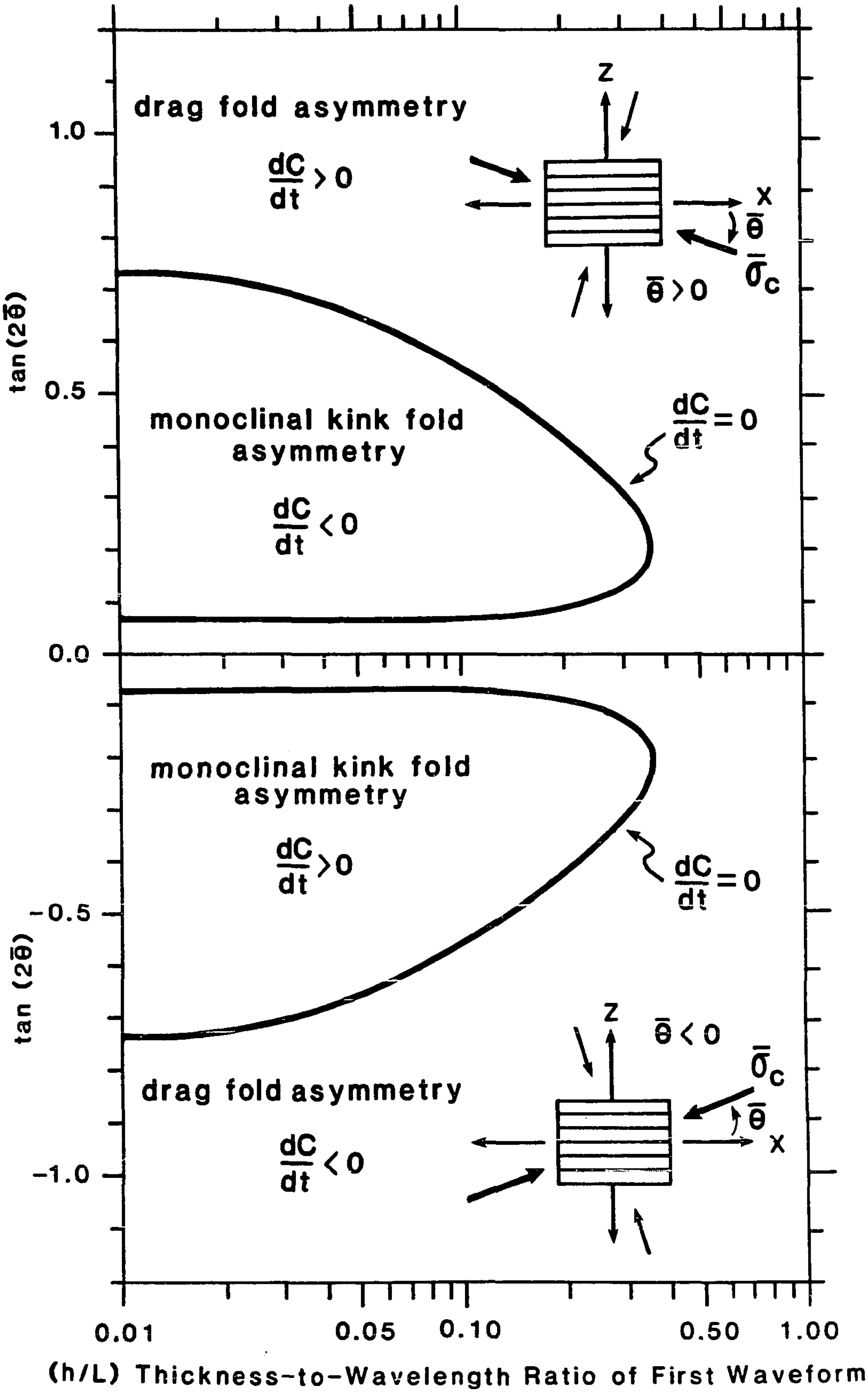

drag fold asymmetry
$\frac{dC}{dt} > 0$
z
x
$\bar{\theta}$
$\bar{\sigma}_c$
$\bar{\theta} > 0$
monoclinal kink fold asymmetry
$\frac{dC}{dt} < 0$
$\frac{dC}{dt} = 0$
monoclinal kink fold asymmetry
$\frac{dC}{dt} > 0$
$\frac{dC}{dt} = 0$
z
$\bar{\theta} < 0$
$\bar{\sigma}_c$
$\bar{\theta}$
x
drag fold asymmetry
$\frac{dC}{dt} < 0$
1.0
0.5
0.0
-0.5
-1.0
tan (2$\bar{\theta}$)
tan (2$\bar{\theta}$)
0.01
0.05
0.10
0.50
1.00
(h/L) Thickness-to-Wavelength Ratio of First Waveform

asymmetry varies with thickness-to-wavelength ratio, $\underline{h}/\underline{L}$, and orientation of maximum compression, $\bar{\theta}$. The domain boundaries are defined as conditions at which $d\underline{C}/d\underline{t} = 0$. The sign of $d\underline{C}/d\underline{t}$ depends on the sign of the mean shear stress. For positive $\bar{\theta}$, corresponding to a positive mean shear stress (Fig. 14A), the $d\underline{C}/d\underline{t} = 0$ contour encloses a region of negative values of $d\underline{C}/d\underline{t}$. For negative mean shear stress (Fig. 14B), this region contains positive values of $d\underline{C}/d\underline{t}$.

Only the positive state of mean shear stress will be shown in following figures. The discussions will apply equally to the negative state of mean shear stress if appropriate sign changes are made.

In Fig. 15, the nonlinear contacts are described by $\underline{m} = 5$. To focus on the dependence of mean anisotropy, $\bar{\alpha}$, on $\bar{\theta}$, I rewrite eq. (16b) as

$$\bar{\alpha} - 1 = R\ |\tan(2\bar{\theta})|^{(m-1)} \tag{40a}$$

where

$$R = (m/\bar{\beta})(2)^{(m-1)} \tag{40b}$$

and $\bar{\beta}$ is defined in eq. (16c). For the construction of Fig. 15, $\underline{R}$ was selected to be 50 and $\underline{m} = 5$.

The parameters that control the sign of $d\underline{C}/d\underline{t}$ can be investigated in more detail by making assumptions which further simplify eq. (30b). At long wavelength, $\underline{L}$, the

<u>Figure 15</u>. Domains of monoclinal kink fold and drag fold asymmetries for positive orientation of maximum compression, $\bar{\theta}$, in infinitely thick multilayer with variable resistance to slip at contacts ($\underline{m}$ = 5).

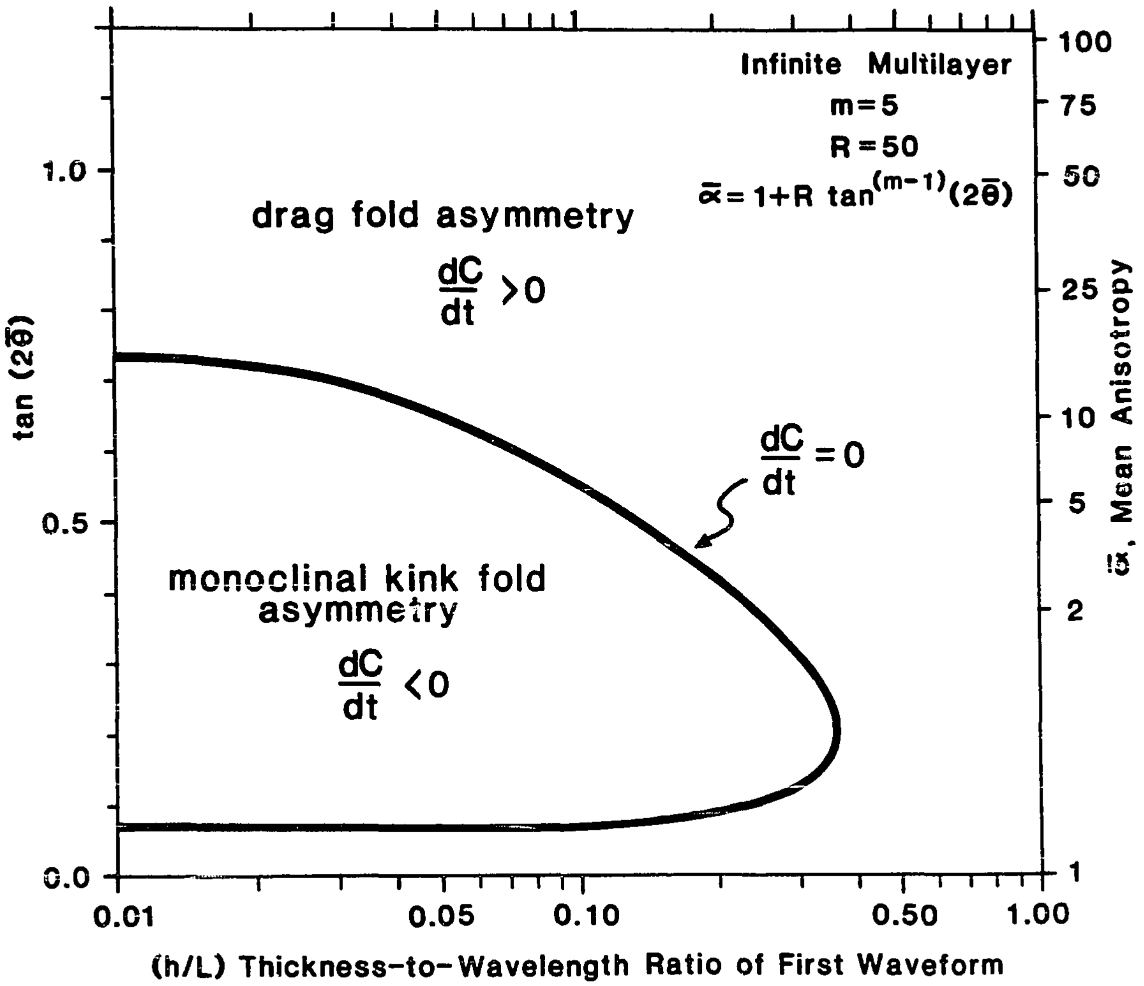

Infinite Multilayer
m=5
R=50
$\bar{\alpha} = 1+R\ \tan^{(m-1)}(2\bar{\theta})$
drag fold asymmetry
$\frac{dC}{dt} > 0$
$\frac{dC}{dt} = 0$
monoclinal kink fold asymmetry
$\frac{dC}{dt} < 0$
tan $(2\bar{\theta})$
1.0
0.5
0.0
100
75
50
25
10
5
2
1
$\bar{\alpha}$, Mean Anisotropy
0.01
0.05
0.10
0.50
1.00
(h/L) Thickness-to-Wavelength Ratio of First Waveform

parameter <u>k</u> becomes small, and for small <u>k</u>, sinh(<u>nk</u>) approaches <u>nk</u> and cosh(<u>nk</u>) approaches unity. Thus, for long wavelengths, ${}^1_{\frac{1}{2}}q$ becomes

Ramberg model (bonded) (eq. 28c):

$$ {}^1_{\frac{1}{2}}q = -(A\ell)\ \tan(2\bar{\theta}) \tag{41a}$$

Constant resistance to slip (eq. 29c):

$$ {}^1_{\frac{1}{2}}q = -(A\ell)\ \tan(2\bar{\theta})\ [1 + R(11/4 + 2R)] \tag{41b}$$

Variable resistance to slip (eq. 30c):

$$ {}^1_{\frac{1}{2}}q = -(A\ell)\ \tan(2\bar{\theta})\ \Big\{ 1 + R|\tan(2\bar{\theta})|^{(m-1)}[1 + 7/(4m) + (2R/m)|\tan(2\bar{\theta})|^{(m-1)} - (m-1)/\tan^2(2\bar{\theta})] \Big\} \tag{41c}$$

for the three models of contact slip I have considered. These are the terms that are responsible for the initiation of a second sinusoidal waveform, which, in turn, determines the asymmetry at interfaces.

Let us examine the term in braces in eq. (41c) for the model of variable resistance to slip. The first term, "1", is the kinematic amplification factor resulting from shearing deformation within a layer. It is the only term considered in the Ramberg model, eq. (41a). The other terms in eq. (41c) represent dynamic amplification factors resulting from slip at layer contacts.

The first three terms within brackets in eq. (41c),

$$1 + 7/(4m) + (2R/m)|\tan(2\bar{\theta})|^{(m-1)}$$

are a result of the constant, mean resistance to slip. The sign of these three terms is always positive, so they always enhance the kinematic term, that is, these three terms always contribute to growth of the waveform that causes the fold to have drag asymmetry. If $\underline{m} = 1$, these terms simplify to a constant, $(11/4 + 2\underline{R})$, as indicated in eq. (41b). Furthermore, if $\underline{m}$ becomes very large, these terms approach unity.

The last term in brackets in eq. (41c),

$$-(m-1)/\tan^2(2\bar{\theta})$$

results from the perturbed resistance to slip at contacts and produces unequal rates of slip on interface limbs with different slopes. This term, which is negative for all values of $\underline{m}$ and $\bar{\theta}$, can reduce and even reverse the sign of the amplification factor, making $d\underline{C}/d\underline{t}$ negative and producing interface waveforms with the sense of asymmetry of monoclinal kink folds. The magnitude of the term is relatively large for low inclinations of the principal compressive stress and decreases, slowly at first and then more rapidly, for increasing $\bar{\theta}$.

The domain of monoclinal kink folding described by the $d\underline{C}/d\underline{t} = 0$ contour for long wavelengths (left side of Fig. 15) can be explained using eq. (41c) for fixed $\underline{m}$ and $\underline{R}$.

If the maximum compressive stress is parallel to the layering, $\bar{\theta}$ is zero and the mean anistropy is $\bar{\alpha} = 1$, so $d\underline{C}/d\underline{t}$ is kinematic and positive.

If the maximum compression is inclined to layering, $\bar{\theta}$ is nonzero. For non-zero values of $\bar{\theta}$, the sign of eq. (41c) depends on the interplay between eqs. (40a) and (40b). Initiation and growth of the second waveform will be zero when the term in brackets in eq. (41c) is zero, which occurs for conditions satisfying

$$1 + R[1 + 7/(4m)]\ |\tan(2\bar{\theta})|^{(m-1)} + (2R^2/m)|\tan(2\bar{\theta})|^{[2(m-1)]}$$

$$- R(m-1)\ |\tan(2\bar{\theta})|^{(m-3)} = 0 \qquad (42a)$$

For relatively small values of $\bar{\theta}$, the negative term in eq. (42a), proportional to $|\tan(2\bar{\theta})|^{(m-3)}$, dominates; this term produces monoclinal kink asymmetry. At relatively high values of $\bar{\theta}$, the other, positive terms in eq. (42a) dominate; these terms produce drag fold asymmetry. Thus, the lower part of the loop, near $\underline{h}/\underline{L} = 0.01$ (Fig. 15), is the transition between bonded contacts, with $\bar{\theta} = 0$, and monoclinal kink fold asymmetry, with $\bar{\theta}$ small. The upper part of the loop is the transition from monoclinal asymmetry to very easy slip at contacts.

Monoclinal kink fold asymmetry develops in multilayers with initial conditions plotting within the domain where $d\underline{C}/d\underline{t} < 0$. Contours of $\underline{C}/\underline{A}$ corresponding to final slope values of $(A\ell) = \tan(15°)$ have been plotted in Fig. 16 relative to the initial $d\underline{C}/d\underline{t} = 0$ curve (Fig. 15). The degree of asymmetry which develops at the interface is larger for longer wavelengths and for values of $\bar{\theta}$ plotting closer to the middle of the domain. However, the shortening required to produce the slope of $(A\ell) = \tan(15°)$ for points near the bottom of the domain is much larger than that near the top of the domain.

The effect of $\underline{m}$ on the position of the $d\underline{C}/d\underline{t} = 0$ curve is illustrated in Fig. 17. For a powerlaw exponent $\underline{m} = 3$, the sign of eq. (41c) is negative for very small $\bar{\theta}$. As $\underline{m}$ is made larger, a larger value of $\bar{\theta}$ is required to reverse the sign of eq. (41c), and the interval of $\bar{\theta}$ values for which $d\underline{C}/d\underline{t}$ is negative is reduced (Fig. 17). Thus, for larger values of $\underline{m}$, the domain of monoclinal kink fold asymmetry shifts to higher $\bar{\theta}$ values and operates over a narrower range of $\bar{\theta}$ values.

In the limit of very large $\underline{m}$, which describes contact strength, the range of monoclinal kink asymmetry becomes a single value of $\bar{\theta}$ below which the contacts remain bonded and at which monoclinal kink asymmetry develops. This is the critical angle for unstable yielding of contacts, discussed by Reches and Johnson (1976).

Equation (42a) can be simplified and rearranged for large $\underline{m}$ to give an upper limit to the $\bar{\theta}$ at which drag fold asymmetry will occur:

Figure 16. Contours of C/A, the strength of the second sinusoidal waveform, for final slope values of $(A\ell) = \tan(15°)$ at interfaces with monoclinal kink fold asymmetry in multilayers with variable resistance to slip at contacts (m = 5).

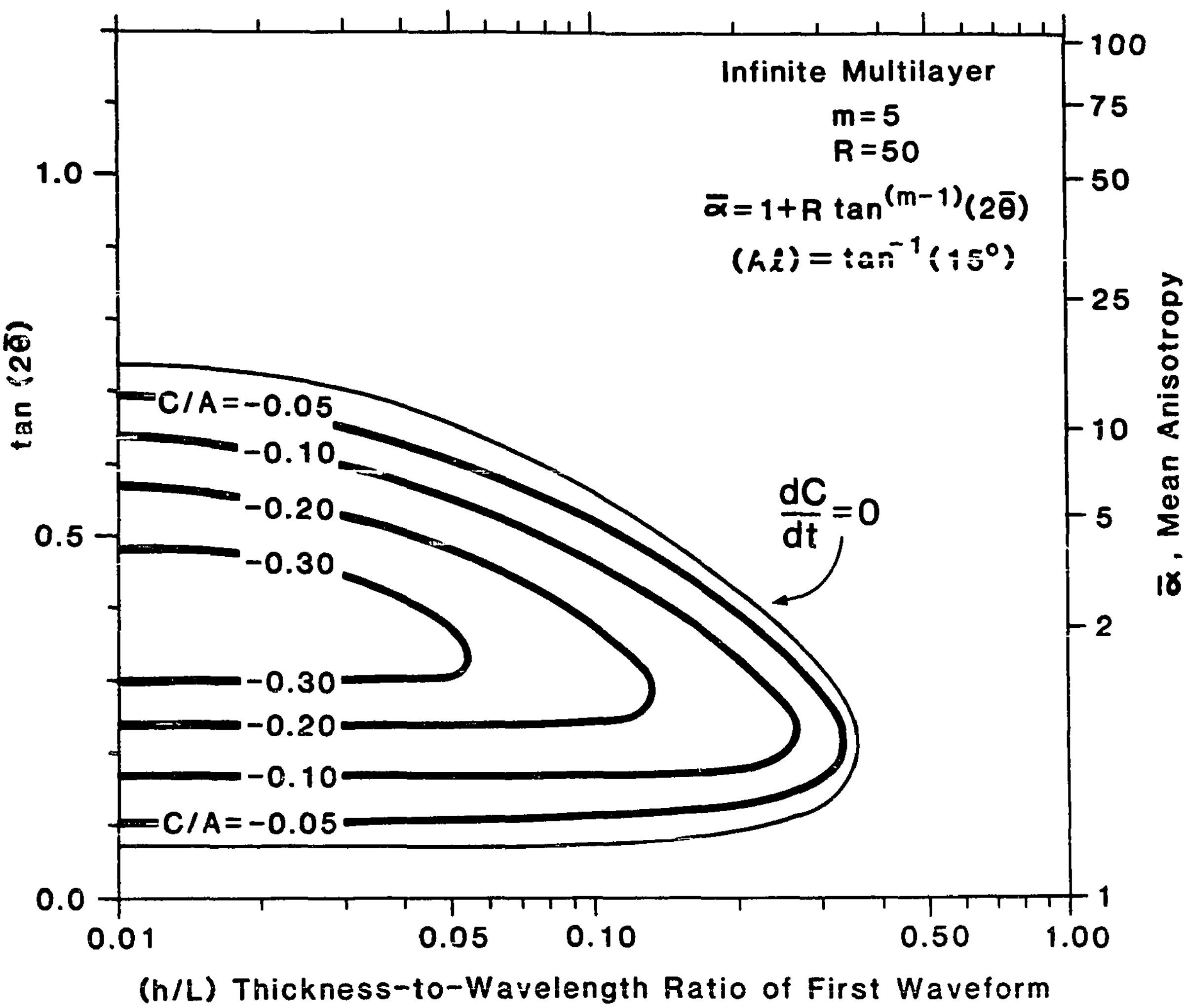

Infinite Multilayer
m=5
R=50
$\bar{\alpha}=1+R\tan^{(m-1)}(2\bar{\theta})$
$(A\ell)=\tan^{-1}(15°)$
C/A=-0.05
-0.10
-0.20
-0.30
-0.30
-0.20
-0.10
C/A=-0.05
$\frac{dC}{dt}=0$
1.0
0.5
0.0
tan (2θ̄)
100
75
50
25
10
5
2
1
$\bar{\alpha}$, Mean Anisotropy
0.01
0.05
0.10
0.50
1.00
(h/L) Thickness-to-Wavelength Ratio of First Waveform

Figure 17. Effect of exponent $\underline{m}$ on position of $d\underline{C}/d\underline{t} = 0$ curve defining domain boundaries.

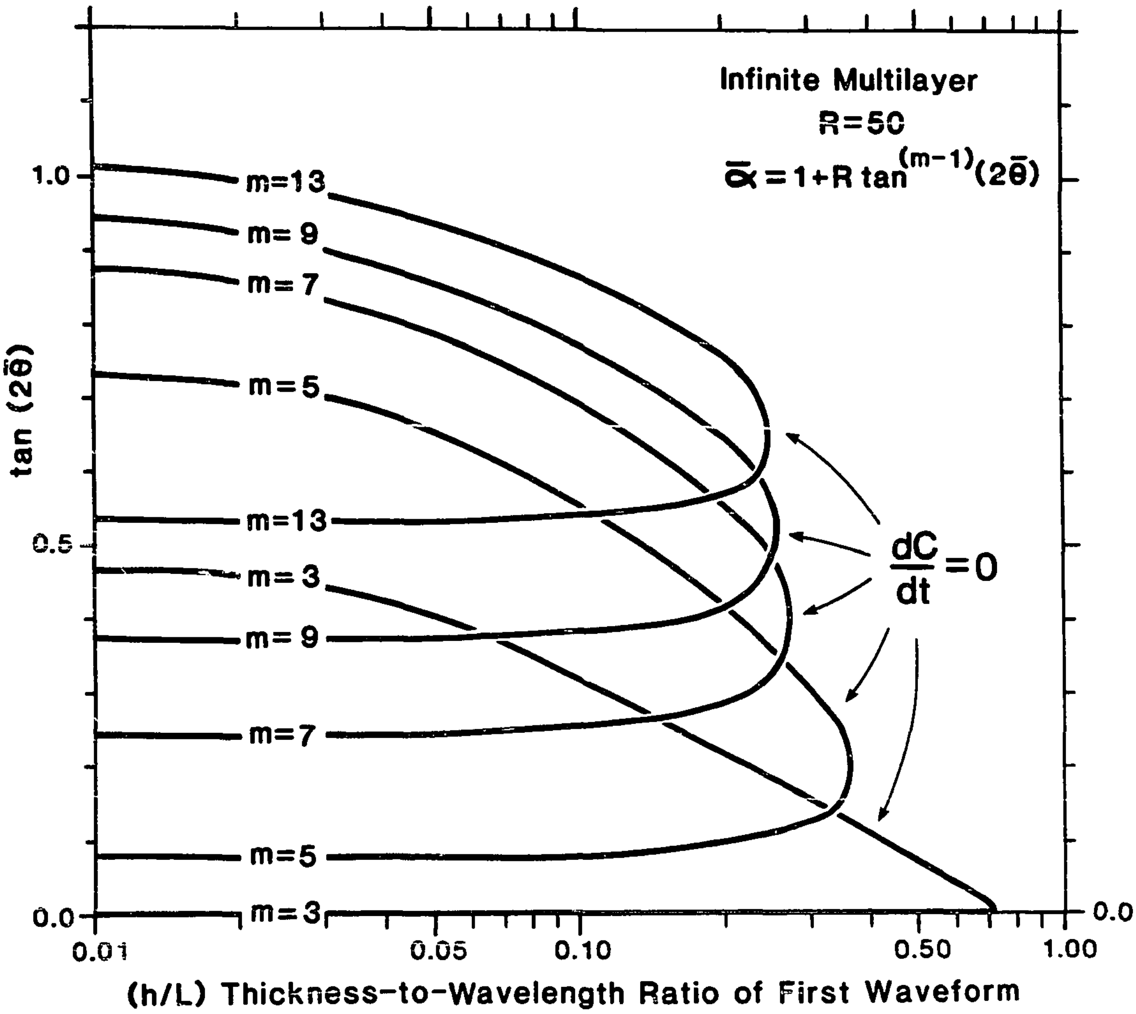

Infinite Multilayer
R=50
$\bar{\alpha} = 1 + R\tan^{(m-1)}(2\bar{\theta})$
m=13
m= 9
m= 7
m=5
m=13
m= 3
m= 9
m=7
m=5
m=3
$\frac{dC}{dt} = 0$
tan (2θ̄)
1.0
0.5
0.0
0.0
0.01
0.05
0.10
0.50
1.00
(h/L) Thickness-to-Wavelength Ratio of First Waveform

$$1/R = |\tan(2\bar{\theta})|^{(m-3)}\,[m - \tan^2(2\bar{\theta})] \qquad (42b)$$

Equation (42b) is possible only if

$$\tan(2\bar{\theta}) \leq \sqrt{m} \qquad (42c)$$

Thus

$$\bar{\theta} \leq 45^\circ$$

which gives the maximum $\bar{\theta}$ for drag fold asymmetry.

ASYMMETRY IN FINITE MULTILAYERS

Analysis of folding of multilayers with a finite number of layers enclosed by media of infinite thickness is more complicated than analysis of infinitely thick multilayers. For example, each interface in a multilayer of finite thickness can have a unique phase angle and set of amplitudes of component waveforms which determine its asymmetry. In principle, some interfaces in a finite multilayer can have one sense of asymmetry and others can have the opposite sense of asymmetry. However, the explanations of asymmetry of interfaces in infinitely thick multilayers apply equally to asymmetry of interfaces in finite multilayers.

The simple, finite, repetitive multilayer I analyze has a total thickness _H_ consisting of 11 identical layers of thickness h and coefficient of viscosity μ_l and is confined above and below by thick media with coefficient of viscosity μ_m (Fig. 6). The multilayer is subjected to a combination of layer-parallel compression and simple shear. The interfaces between layers are initially perturbed into cosinusoidal waveforms, the amplitudes of which are determined by an analysis of eigenvalues and eigenvectors, as explained in Chapter I. The eigenvalues determine the dominant wavelength for the multilayer. Each interface, originally described by a cosine wave of amplitude A, evolves, according to my 2nd order analysis, into a waveform containing two cosine waveforms and one sine waveform:

$$\zeta_{t,b} = \pm h/2 + A_{t,b}\cos(\ell x+\phi_{t,b}) + B_{t,b}\cos(2\ell x+2\phi_{t,b}) + C_{t,b}\sin(2\ell x+2\phi_{t,b}) \tag{43}$$

in which t is top and b is bottom of a layer.

In following paragraphs I will determine the conditions under which folds with drag asymmetry and monoclinal kink fold asymmetry develop in finite multilayers; I will examine the effect that layer-parallel shear can have on dominant wavelengths of multilayer folds; and I will analyze some examples of theoretical asymmetric folds in finite multilayers.

Domains of Asymmetry

Through study of Figs. 15, 16, and 17, I showed conditions under which folds with monoclinal kink asymmetry will develop in finite multilayers, primarily emphasizing effects of inclination, θ, of the far-field compression, that is, the relative magnitude of the layer-parallel shear stress, and the ratio of layer thickness to wavelength, h/L. I showed that the boundary between the two types of asymmetry is unbounded for long wavelengths.

A similar diagram for a finite multilayer with 11 layers is shown in Fig. 18. The same material constants were assumed as in Fig. 15, the boundary from which has been superimposed in Fig. 18. The two contours of $dC/dt = 0$ closely correspond for short wavelengths (right-hand end) and diverge markedly for h/L ratios smaller than 0.05, that is, for wavelengths L greater than $20h$. Thus, except for long wavelengths, the discussion of conditions of sense of asymmetry of waveforms in interfaces of infinitely thick multilayers applies to multilayers of both finite and infinite thicknesses.

Dominant Wavelength

A spectacular effect of layer-parallel shear on folding of finite multilayers with variable resistance to slip at contacts is the reduction of wavelengths of folds that develop in such multilayers. If layer-parallel shear stress

Figure 18. Comparison of positions of $d\underline{C}/d\underline{t} = 0$ curves for finite multilayer confined by soft media ($\mu_m/\mu_\ell = 0.1$) and for corresponding infinitely thick multilayer (Fig. 15). Domain of monoclinal kink asymmetry for finite multilayer is limited to wavelengths shorter than the dominant wavelength for bonded contacts (anisotropy $\tilde{\alpha} = 1$).

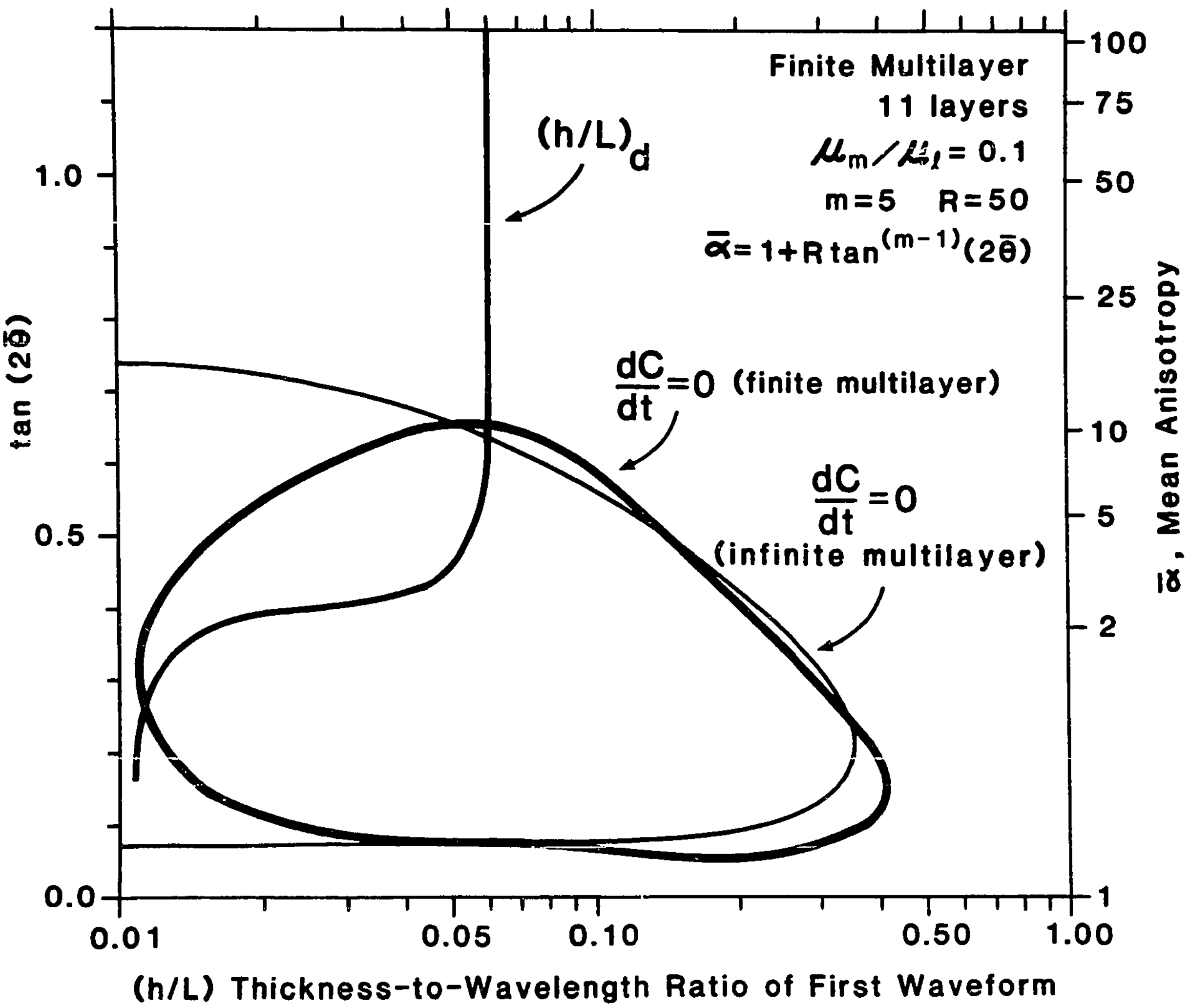

Finite Multilayer
11 layers
$\mu_m/\mu_l = 0.1$
m=5 R=50
$\bar{\alpha} = 1 + R\tan^{(m-1)}(2\bar{\theta})$
$(h/L)_d$
$\frac{dC}{dt}=0$ (finite multilayer)
$\frac{dC}{dt}=0$ (infinite multilayer)
tan $(2\bar{\theta})$
$\bar{\alpha}$, Mean Anisotropy
1.0
0.5
0.0
100
75
50
25
10
5
2
1
0.01
0.05
0.10
0.50
1.00
(h/L) Thickness-to-Wavelength Ratio of First Waveform

is zero, the contacts between layers are bonded, and the multilayer folds as a thick unit, as discussed in Chapter I. If, on the other hand, layer-parallel shear stress is relatively high, the contacts are virtually free to slip, and the multilayer folds as though contacts were frictionless.

I measure the resistance to slip in simple multilayers by the anisotropy for linear contact behavior and by the mean anisotropy for nonlinear contact behavior:

$$\alpha = 1 + (\mu_l / h\beta_c); \qquad \text{linear } (m = 1; \text{ eq. 16a})$$

$$\bar{\alpha} = 1 + R\,|\tan(2\bar{\theta})|^{(m-1)}; \qquad \text{nonlinear } (m > 1; \text{ eq. 40a})$$

where R is defined in eqs. (16c) and (40b). As the anisotropy approaches one, the contacts are bonded, and as the anisotropy approaches infinity, the contacts slip freely.

The marked effect of anisotropy on amplification factor, ${}^{1}_{1}g$, for the first waveform, as a function of thickness-to-wavelength ratio, h/L, is shown in Fig. 19. For $\bar{\alpha} \cong 1$, ${}^{1}_{1}g \cong 4$, and for $\bar{\alpha} \cong 100$, ${}^{1}_{1}g \cong 27$. The viscosity ratio of media and layers for Fig. 19 is $\mu_m/\mu_l = 0.1$. The relations between ${}^{1}_{1}g$ and h/L (Fig. 19) depend only on anisotropy and are thus valid whether the contacts between layers have constant or variable resistances to slip.

Figure 19. Increase in amplification factor for the first waveform, ${}^{1}_{1}\underline{q}$, and decrease in dominant wavelength with increasing mean anisotropy, $\bar{\alpha}$, of multilayer.

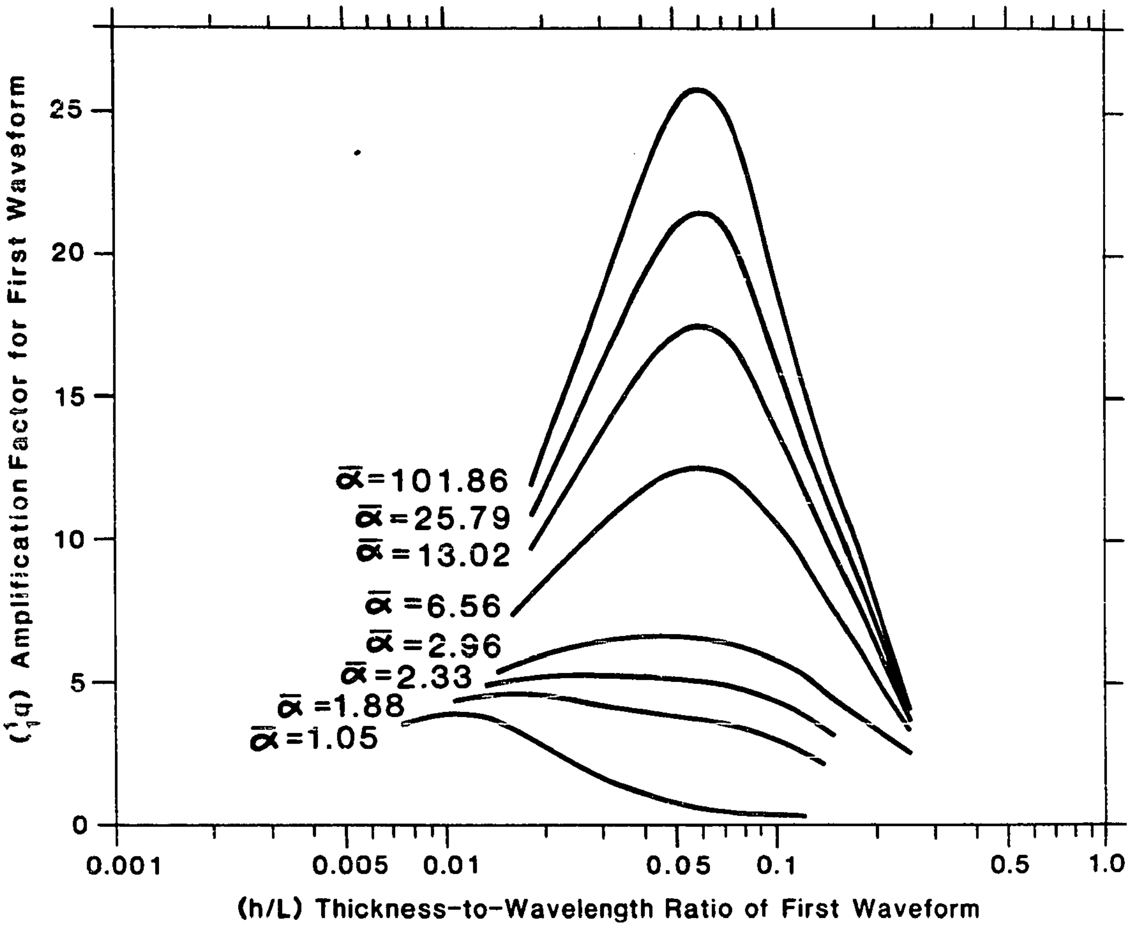

25
20
15
10
5
0
0.001
0.005
0.01
0.05
0.1
0.5
1.0
$\bar{\alpha}$=101.86
$\bar{\alpha}$=25.79
$\bar{\alpha}$=13.02
$\bar{\alpha}$=6.56
$\bar{\alpha}$=2.96
$\bar{\alpha}$=2.33
$\bar{\alpha}$=1.88
$\bar{\alpha}$=1.05
(^1_1q) Amplification Factor for First Waveform
(h/L) Thickness-to-Wavelength Ratio of First Waveform

The peaks of the curves correspond to the dominant wavelengths. The dominant wavelength for the multilayer with the highest resistance to slip at layer contacts (mean anisotropy closest to 1.0), according to Fig. 19, is about 95$\underline{h}$. The dominant wavelength decreases as the anisotropy increases. The dominant wavelength for the multilayer with the highest anisotropy, $\bar{\alpha}$ = 102, is about 18$\underline{h}$ (Fig. 19). Thus there is a five-fold decrease in wavelength as the anisotropy increases from about 1 to 100.

According to Fig. 19, however, multilayers fold at the dominant wavelength corresponding to free slip at contacts for mean anisotropies greater than about 5. As the anisotropy changes from 5 to 1, the dominant wavelength goes through a transition from that of nearly free slip at contacts to that of bonded contacts.

The relations between dominant wavelength and anisotropy for multilayers confined by media ranging from very soft to very stiff are shown in Fig. 20. For stiff media, the dominant wavelengths are smaller for low anisotropy than for high anisotropy, although the variation is small. For very soft media, μ_m/μ_ℓ = 0.01, anisotropy ranging from 1 to at least 14 affects the dominant wavelength, although the effect is greatest for anisotropies between 8 and 12. For soft media, μ_m/μ_ℓ = 0.10, the change in dominant wavelength is drastic for anisotropies between 1 and 4, as noted earlier.

Figure 20. Comparison of change in dominant wavelength with increasing anisotropy for finite multilayers confined by media ranging from very soft ($\mu_m/\mu_\ell = 0.01$) to very stiff ($\mu_m/\mu_\ell = 10$).

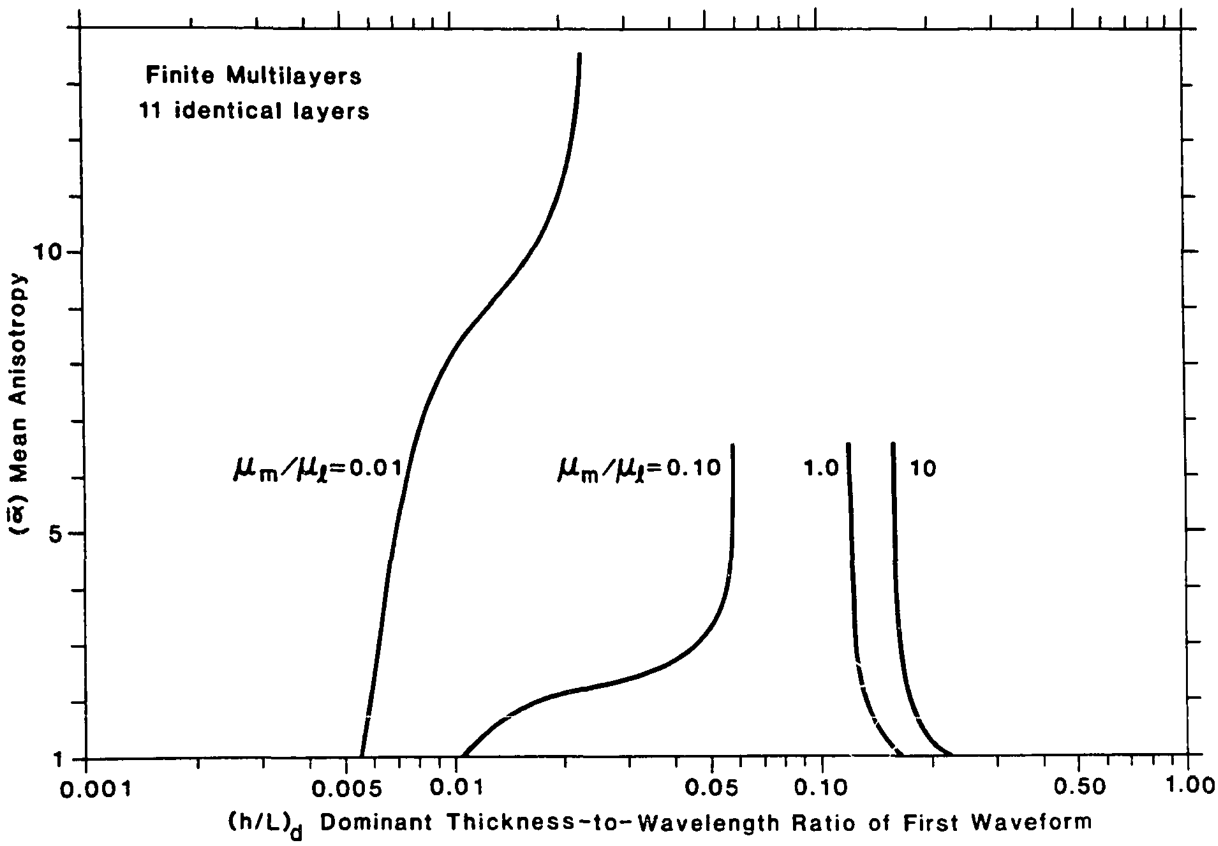
Finite Multilayers
11 identical layers
μ_m/μ_l=0.01
μ_m/μ_l=0.10
1.0
10
($\bar{\alpha}$) Mean Anisotropy
10
5
1
0.001
0.005
0.01
0.05
0.10
0.50
1.00
$(h/L)_d$ Dominant Thickness-to-Wavelength Ratio of First Waveform

The relation between the dominant wavelength of the first waveform and the sense of asymmetry of folding on the middle interface of 11-layer multilayers is shown in Fig. 18. The dominant wavelengths are shown as functions of tan($2\bar{\delta}$), rather than of anisotropy, and $\underline{R}$ was assumed to be 50 for the analyses.

Figure 18 shows that the domain of monoclinal kink fold asymmetry is limited to wavelengths shorter than the dominant wavelengths for bonded contacts. As the anisotropy of the multilayer increases, the dominant wavelength becomes shorter; at an anisotropy of 1.2, the curve for dominant wavelength crosses into the domain of monoclinal kink fold asymmetry. The decrease in dominant wavelength with increasing anisotropy is most dramatic in the vicinity of the wavelength which is halfway between those for bonded contacts and free slip at contacts. The dominant wavelength decreases from 55$\underline{h}$ at an anisotropy of 2.0 to 25$\underline{h}$ for an anisotropy of 2.6. Dominant wavelengths in multilayers with anisotropies greater than about 10 fall outside the domain of monoclinal kink asymmetry. Interface waveforms in these multilayers have the asymmetry of drag folds.

Once the dominant wavelength has been determined for a multilayer, the preferred wavelength can be calculated according to the method described in Chapter I. The wavelengths of folds I will show in following pages are at or near the preferred wavelengths corresponding to the anisotropy of the multilayer.

Examples of Asymmetric Folds

I have shown that interfaces with different senses of asymmetry can be produced in simple multilayers of infinite or finite thickness by changing the behavior of layer contacts. Two finite multilayers are shown in Fig. 21 which differ only in the behavior of the contacts. The multilayers in row A, Fig. 21, have constant resistance to slip ($\underline{m}$ = 1) at layer contacts. The multilayers shown in row B, Fig. 21, have variable resistance to slip ($\underline{m}$ = 5). Both multilayers in column 1, Fig. 21, were subjected to right-lateral sense of layer-parallel shear, and both multilayers in column 2, Fig. 21, were subjected to left-lateral sense of layer-parallel shear.

If resistance to slip at layer contacts is constant ($\underline{m}$ = 1; Fig. 21A), interfaces exhibit both a relative offset and an asymmetric shape. For the right-lateral sense of shear shown in loc. A1, the sense of asymmetry is that of a drag fold because the short limb on the interface waveform dips to the right; the sense of relative offset of interfaces is right-lateral because each layer has shifted to the right compared to the layer below. For the left-lateral sense of shear shown in loc. A2, the sense of asymmetry is that of a drag fold because the short limb on the interface waveform dips to the left; the sense of

Figure 21. Sense of asymmetry in finite multilayers with constant resistance to slip ($\underline{m}$ = 1) (row A) and variable resistance to slip ($\underline{m}$ = 5) (row B) at contacts. Multilayers with constant resistance to slip at contacts have drag fold sense of asymmetry because the short limbs on interface waveforms dip to the right for right-lateral sense of shear (loc. A1) and to the left for left-lateral sense of shear (loc. A2). Multilayers with variable resistance to slip at contacts have monoclinal kink fold asymmetry because short limbs dip to the left for right-lateral sense of shear and to the right for left-lateral sense of shear.

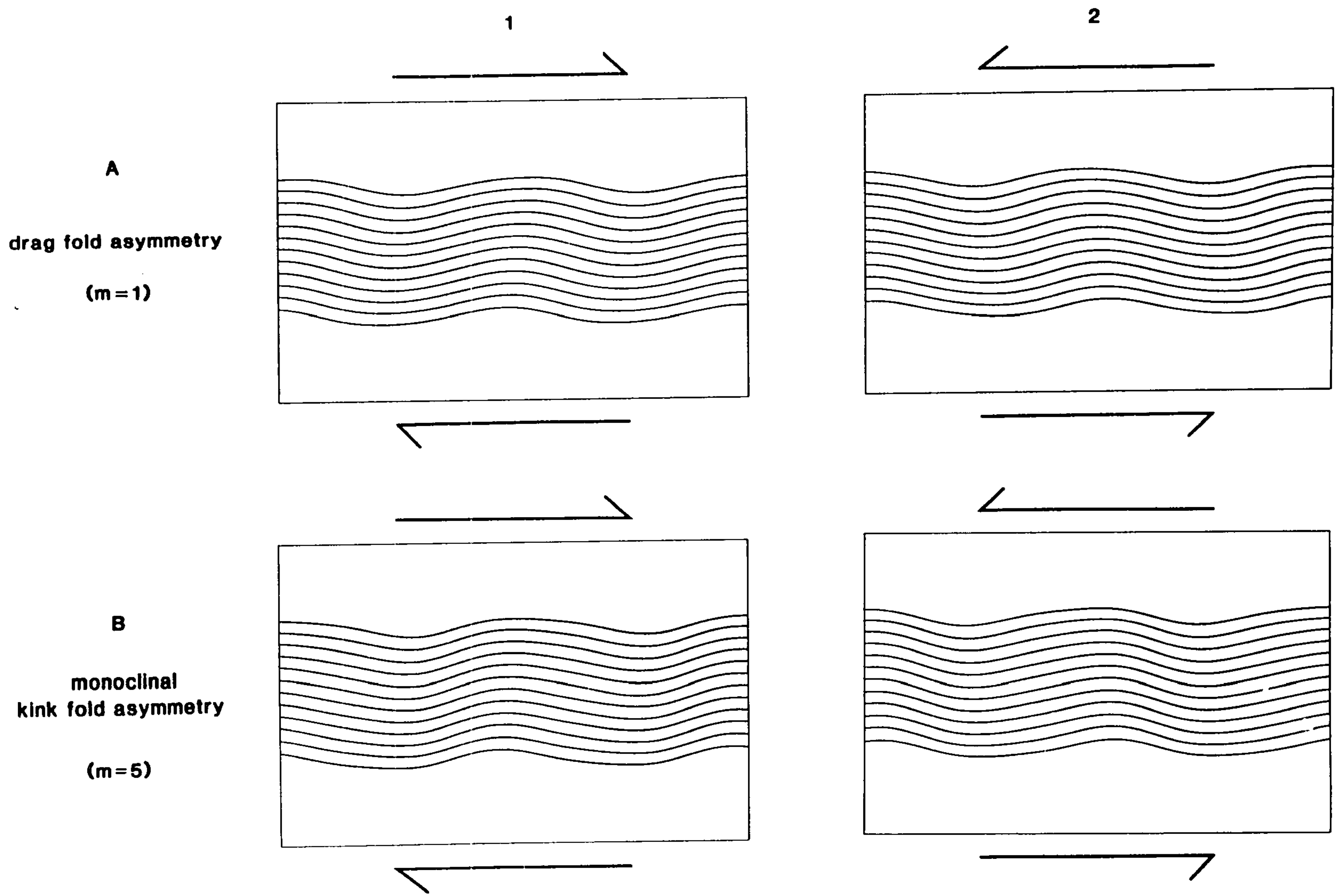
1
2
A
drag fold asymmetry
(m=1)
B
monoclinal
kink fold asymmetry
(m=5)

relative offset of interfaces is left-lateral.

If resistance to slip at layer contacts is variable ($\underline{m}$ > 1; Fig. 21B), the sense of asymmetry is reversed. The interfaces shown in loc. B1 have the sense of asymmetry of a monoclinal kink fold because, for the right-lateral sense of shear stress applied to the multilayer, the short limbs on the interface waveforms dip to the left. The individual interfaces appear to be approximately in phase. For the left-lateral sense of shear shown in loc. B2, the fold has the sense of asymmetry of a monoclinal kink fold because the short limb on the interface waveform dips to the right.

The strength of the asymmetry of folds with monoclinal kink fold asymmetry increases with $\underline{m}$, the powerlaw exponent describing nonlinear contact behavior. The sense of asymmetry in the three multilayers shown in Fig. 22 is that of a monoclinal kink fold, but the strength of asymmetry of the fold in Fig. 22C ($\underline{m}$ = 7) is stronger than that in Fig. 22A ($\underline{m}$ = 3). The asymmetry is weak ($\underline{\AA}$ = -0.05) for the fold shown in Fig. 22A, strong ($\underline{\AA}$ = -0.14) for the fold shown in Fig. 22B, and very strong ($\underline{\AA}$ = -0.20) for the fold shown in Fig. 22C.

The apparent offset of layer interfaces, on the other hand, decreases as the power $\underline{m}$ increases (Fig. 22). Relative drift of layer interfaces is reduced for larger $\underline{m}$ (eq. 30d). In addition, the cosinusoidal second waveform of amplitude $\underline{B}$ is stronger for the multilayer shown in Fig. 22C

Figure 22. Increase in strength of asymmetry $\mathring{\underline{A}}$ of folds with monoclinal kink fold asymmetry with increase in powerlaw exponent $\underline{m}$ describing nonlinear contact behavior.

C. m=7

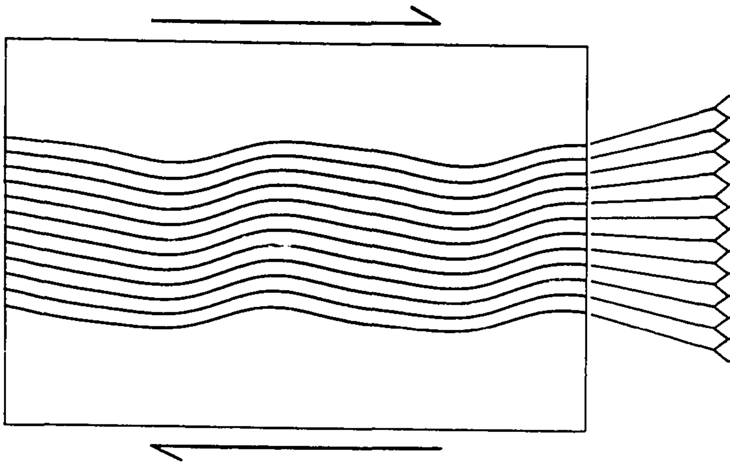

B/A	C/A	Å
-0.14	-0.18	-0.21
-0.11	-0.19	-0.21
-0.08	"	-0.20
-0.05	"	"
-0.03	"	"
-0.01	"	"
0.01	"	"
0.03	"	"
0.05	"	"
0.08	"	-0.20
0.11	-0.19	-0.21
0.14	-0.18	-0.21

B. m=5

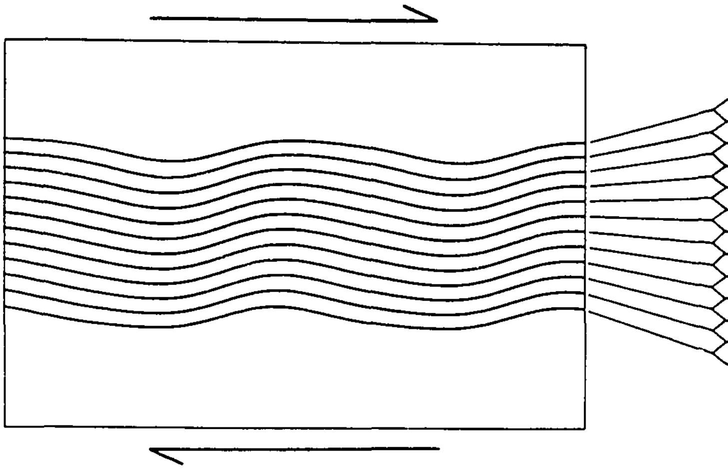

B/A	C/A	Å
-0.12	-0.10	-0.14
-0.10	-0.11	"
-0.07	"	"
-0.05	-0.11	"
-0.03	-0.12	"
-0.01	"	"
0.01	"	"
0.03	-0.12	"
0.05	-0.11	"
0.07	"	"
0.10	-0.11	"
0.12	-0.10	-0.14

A. m=3

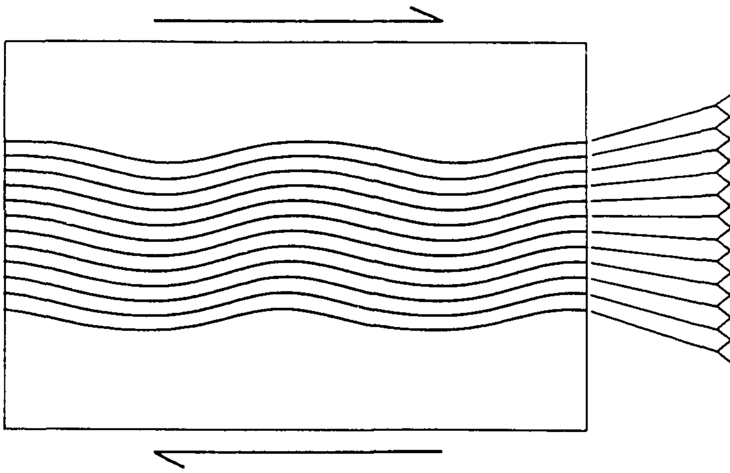

B/A	C/A	Å
-0.10	-0.02	-0.04
-0.09	-0.03	-0.04
-0.06	-0.03	-0.05
-0.04	-0.04	"
-0.03	"	"
-0.01	"	"
0.01	"	"
0.03	"	"
0.04	-0.04	"
0.06	-0.03	-0.05
0.09	-0.03	-0.04
0.10	-0.02	-0.04

than for the one shown in Fig. 22A. This component waveform, which tends to maintain the uniform orthogonal thickness of a finite multilayer (discussed in Chapter II), reduces the relative drift between layer interfaces.

DISCUSSION

The 2nd order analysis of viscous multilayers subjected to principal compression oblique to layering demonstrates that layer-parallel compression causes folding of the multilayer and that layer-parallel shearing causes individual interfaces to drift and to develop asymmetry. Although properties of the layers and the layer contacts control the wavelength and rate of growth of the folds, properties of the layer contacts control the sense and strength of drift and asymmetry.

Each increase in the order of accuracy of the solution adds to our understanding of the effects of layer-parallel compression and shear on multilayer folds:

1. 0th order solution. An analysis carried to 0th order accuracy reveals that the mean shearing deformation causes interface waveforms to drift. The sense of drift is always the same as that of the mean layer-parallel shear stress. The amount that the drift exceeds the kinematic value, the value in a homogeneous material, is a function of the anisotropy and the nonlinearity of the multilayer. The drift increases with anisotropy and decreases with

nonlinearity (with m). For large m, the amount of drift reduces to the kinematic value.

Layer-parallel compression produces kinematic shortening of layers.

2. 1st order solution. The 1st order analysis shows that folding of multilayers is a result of layer-parallel compression. For multilayers with the same anisotropy, the wavelength and rate of growth of the folds are the same whether contact behavior is linear or nonlinear. For nonlinear contact behavior, however, the mean shear stress reduces the resistance to slip at layer contacts. This, in turn, increases the anisotropy and rate of growth and shortens the dominant wavelength of the fold.

3. 2nd order solution. To 2nd order, two additional component waveforms develop spontaneously. The layer-parallel compression initiates a second cosinusoidal component waveform which tends to maintain uniform orthogonal thickness of layers (Fletcher, 1974). The layer-parallel shear stress initiates a second sinusoidal component waveform which causes the resultant waveforms at interfaces to become asymmetric. Contacts with constant resistance to slip ($m = 1$) develop the sense of asymmetry of drag folds; contacts with variable resistance to slip ($m > 1$) develop the sense of asymmetry of monoclinal kink folds.

4. 3rd order solution. Here I anticipate effects of mean

shear which would be revealed by an analysis carried to 3rd order accuracy. In a 3rd order analysis, the shape of an interface will be determined by component waveforms of three different wavelengths

$$\zeta = A\cos(\ell x+\phi) + B\cos(2\ell x+2\phi) + C\sin(2\ell x+2\phi) + D\cos(3\ell x+3\phi) + E\sin(3\ell x+3\phi) \quad (44)$$

The cosinusoidal third component waveform of amplitude $\underline{D}$ arises as a result of layer-parallel shortening; the sinusoidal third component waveform of amplitude $\underline{E}$ is a result of layer-parallel shearing deformation.

To 3rd order, the behavior of layer contacts affects fold form as well as fold asymmetry. The effect of contact properties on fold forms resulting solely from layer-parallel compression is investigated to 3rd order accuracy in Chapters I and II. A suite of fold forms, including sinusoidal, concentric-like, and chevron folds (Fig. 23A), can be produced in viscous multilayers with constant resistance to slip between layers. The multilayers may be confined by stiff or soft media and may consist of all stiff layers or of interbedded stiff and soft layers, provided the layer contacts or the soft interbeds behave linearly. A different suite of fold forms, including box folds with vertical axial planes and kink-like folds with inclined axial planes (Fig. 23B), can be produced in

Figure 23. Effect of contact properties on theoretical fold forms produced solely by layer-parallel compression ($\bar{\theta} = 0$) and determined to 3rd order accuracy. A. Constant resistance to slip at contacts. Chevron folds form in multilayers of infinite thickness (loc. A1); concentric-like folds form in multilayers of finite thickness (loc. A2). B. Variable resistance to slip at contacts. Box folds form in multilayers of infinite thickness (loc. B1); kink-like folds form in multilayers of finite thickness (loc. B2).

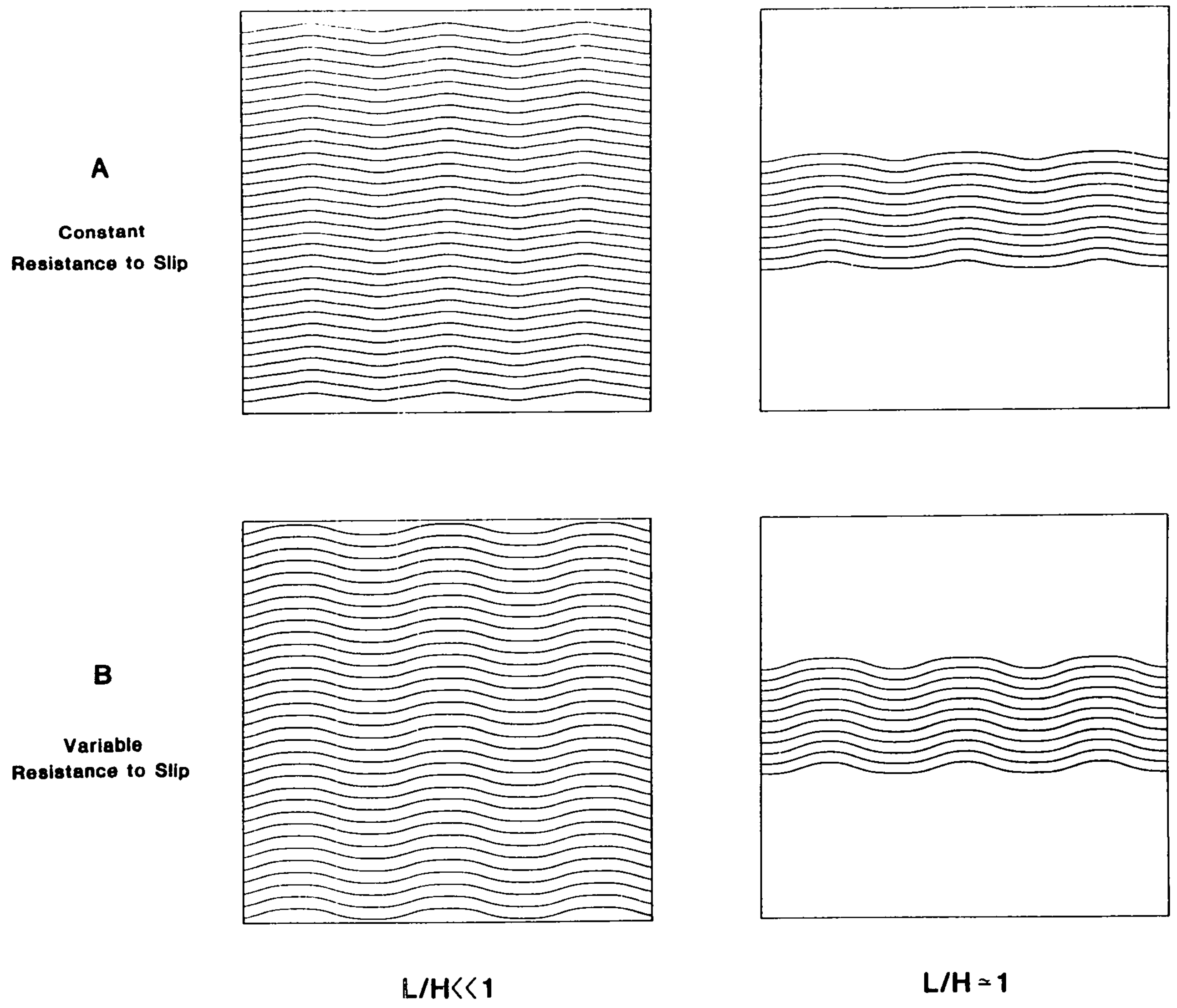
A
Constant
Resistance to Slip
B
Variable
Resistance to Slip
L/H<<1
L/H ≃ 1

otherwise identical multilayers by imposing variable resistance to slip between layers. Resistance to slip between stiff layers may be provided by thin interbeds with nonlinear properties or by nonlinear contact viscosities. Moreover, isolated kink folds presumably can occur if the resistance to slip is highly nonlinear, as in the contact strength assumed by Honea and Johnson (1976).

Multilayers with constant resistance to slip at contacts develop concentric-like and chevron folds, to 3rd order, as a result of layer-parallel compression, and develop drag fold asymmetry, to 2nd order, as a result of layer-parallel shear. I anticipate that an asymmetric chevron fold form, much like that shown in Fig. 24A, would develop in thick, viscous multilayers with constant resistance to slip at contacts subjected to principal compression oblique to layering. I simulated this fold by adding the 3rd order solution for a chevron fold form (Fig. 23, loc. A1), produced by a positive amplitude $\underline{D}$ of the third cosinusoidal component waveform, eq. (44), to the 2nd order solution for drag fold asymmetry (Fig. 21, loc. A1).

Multilayers with variable resistance to slip at contacts develop kink-like and box folds, to 3rd order, as a result of layer-parallel compression, and develop monoclinal kink fold asymmetry, to 2nd order, as a result of layer-parallel shear. I anticipate that an asymmetric

Figure 24. Anticipated effects of layer-parallel shear stress on 3rd order theoretical fold forms. A. Asymmetric chevron fold form in thick viscous multilayer with constant resistance to slip at contacts. B. Asymmetric kink-like fold form in finite viscous multilayer with variable resistance to slip at contacts. Fold forms in A and B simulated by adding 3rd order solution determined for layer-parallel compression alone (Fig. 23, locs. A1 and B2, respectively) to 2nd order solution determined for combination of layer-parallel compression and shear (Fig. 21, locs. A1 and B1, respectively).

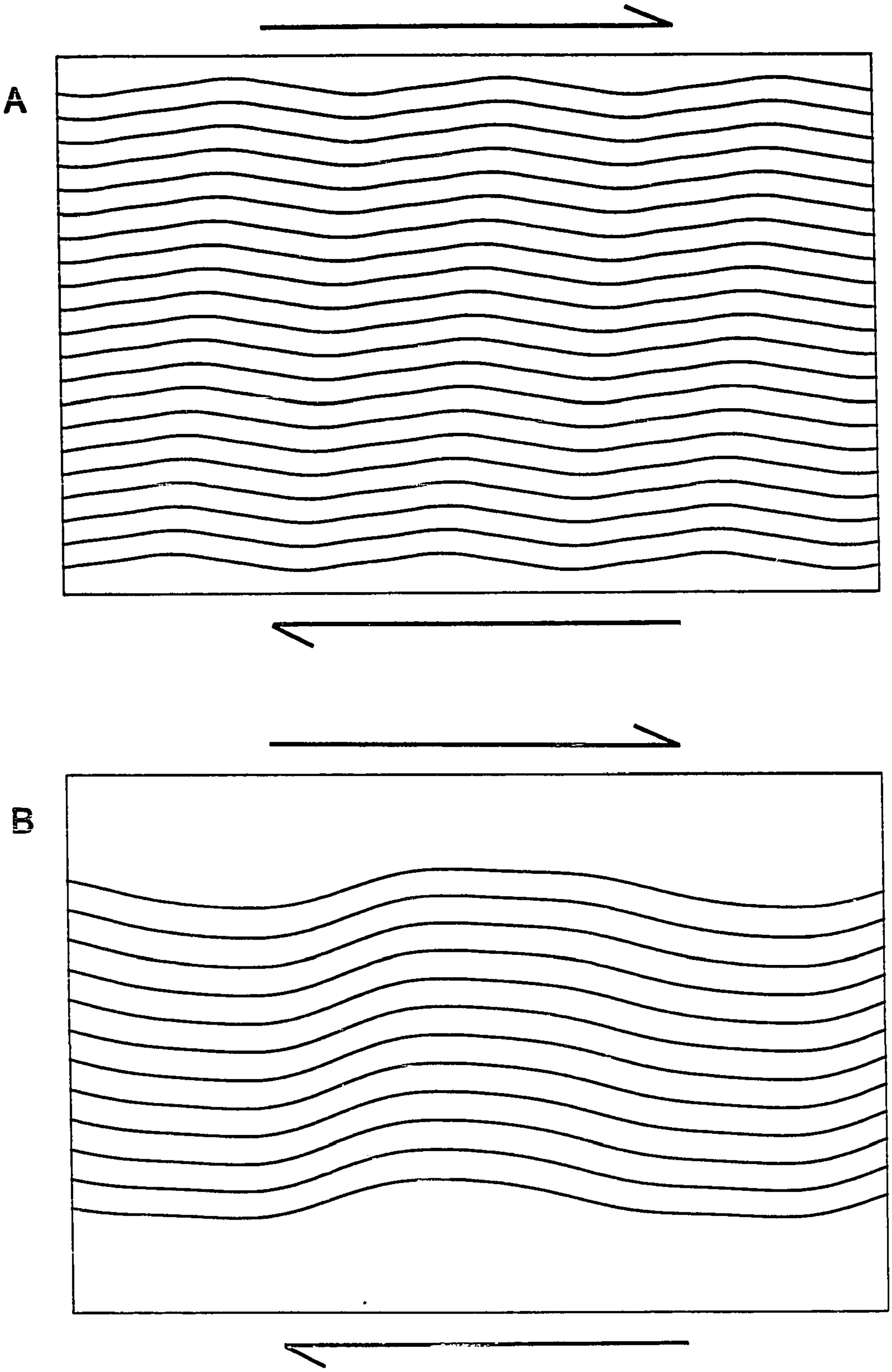
A
B

kink-like fold form, much like that shown in Fig. 24B, would develop in a finite multilayer with variable resistance to slip at contacts. I simulated this fold form by adding the 3rd order solution for a kink-like fold (Fig. 23, loc. B2), produced by a negative amplitude D of the third cosinusoidal waveform, eq. (44), to the 2nd order solution for monoclinal kink fold asymmetry (Fig. 21, loc. B1).

A consistent difference I have observed between folds with drag and those with monoclinal kink asymmetry is the orientation of the axial plane of the fold relative to the orientation of the simple shearing deformation. The trace of the axial plane of a drag fold is reoriented, with respect to a line perpendicular to the direction of layer-parallel shearing, in the same sense as the simple shearing deformation. As a result, a drag fold on the limb of a large fold (Figs. 1, 2A, 3A) has an axial plane which is approximately parallel to the axial plane of the large fold. The trace of the axial plane of the monoclinal kink fold, on the other hand, is oriented in the opposite sense. Consequently, the axial plane of a monoclinal kink fold on the limb of a large fold (Figs. 1, 2B, 3B) dips toward the axial plane of the large fold.

The different inclinations of the axial planes of drag folds and monoclinal kink folds is a fundamental distinction which appears even in a 0th order analysis of the effects of layer-parallel shear. To 0th order, interfaces at contacts with constant resistance to slip develop a sense of relative offset, due to drift, which is the same as the sense of applied mean shearing stress. The amount of relative offset is less at contacts with variable resistance to slip in an otherwise equivalent multilayer, and approaches kinematic values for large m. The trace of the axial plane, which is defined by a line connecting corresponding hingepoints on successive interfaces, is initially normal to layering. As a result of the shearing deformation, the trace of the axial plane is inclined from the vertical a maximal amount for linear contact behavior and a minimal amount for highly nonlinear contact behavior.

The sinusoidal third component waveform of amplitude E, eq. (44), probably contributes to differences of dips of axial planes of asymmetric folds. The trace of the axial plane in the kink-like fold shown in Fig. 25 is inclined in a direction opposite to that in Fig. 24B. I reversed the plunge direction of this line by adding a third sinusoidal component waveform of positive amplitude E to the fold form simulated in Fig. 24B. For the fold shown in Fig. 25, I removed the drift to emphasize the inclination of the axial plane. Thus I anticipate that a 3rd order analysis of layer-parallel shear stress will produce the diagnostic, opposite inclinations of axial planes in drag folds and monoclinal kink folds that are observed in nature.

Figure 25. Asymmetric kink-like fold form with trace of axial plane oriented, with respect to a line perpendicular to the direction of layer-parallel shearing, in the opposite sense as the simple shearing deformation. Fold form simulated by adding anticipated 3rd order effect of layer-parallel shearing deformation to fold form shown in Fig. 24B.

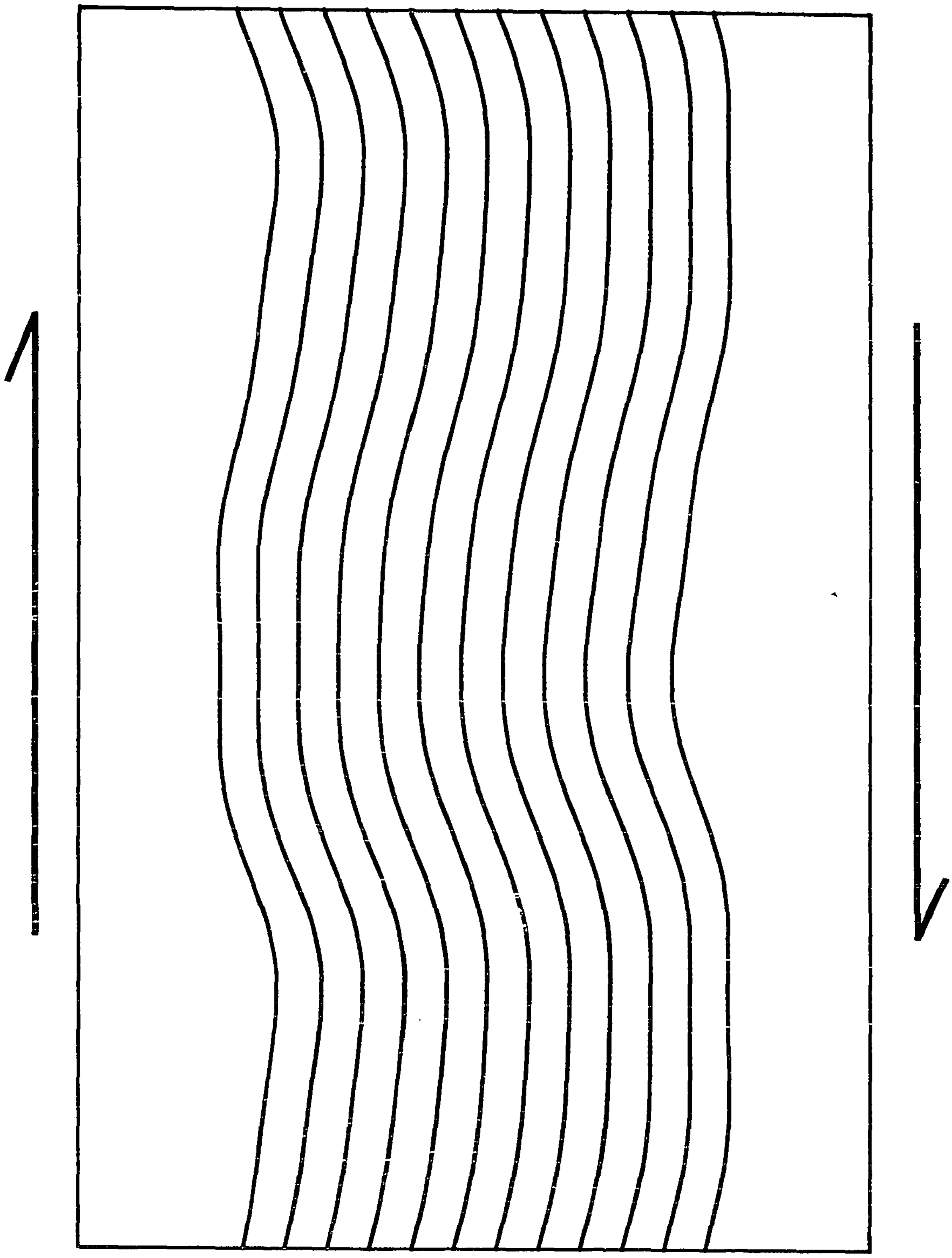

REFERENCES CITED

Anthony, M. and Wickham, J., 1978. Finite-element simulation of asymmetric folding. Tectonophysics, 47: 1-14.

Cobbold, P.R., Cosgrove, J.W. and Summers, J.M., 1971. Development of internal structures in deformed anisotropic rocks. Tectonophysics, 12: 23-53.

Dewey, J.F., 1965. Nature and origin of kink-bands. Tectonophysics, 1: 459-494.

Donath, F.A., 1968. Experimental study of kink-band development in strongly anisotropic rock. In: A.J. Baer and D.K. Norris (Editors), Proceedings, Conference on Research in Tectonics. Geological Society of Canada Paper 68-52: 255-293.

Ellen, S.D., 1971. The development of folds in layered chert of the Franciscan Assemblage near San Francisco, California. Ph.D. dissertation, Department of Geology, Stanford University, Stanford, California, 330 pages.

Fletcher, R.C., 1974. Wavelength selection in the folding of a single layer with power-law rheology. American Journal of Science, 274: 1029-1043.

Fletcher, R.C., 1977. Folding of a single viscous layer: Exact infinitesimal-amplitude solution. Tectonophysics, 39: 593-606.

Gay, N.C. and Weiss, L.E., 1974. The relationship between principal stress directions and the geometry of kinks in foliated rocks. Tectonophysics, 21: 287-300.

Ghosh, S.K., 1966. Experimental tests of buckling folds in relation to strain ellipsoid in simple shear deformations. Tectonophysics, 3: 169-185.

Honea, E. and Johnson, A.M., 1976. Part IV, Development of sinusoidal and kink folds in multilayers confined by rigid boundaries. Tectonophysics, 30: 197-239.

Johnson, A.M., 1970. Physical Processes in Geology. Freeman, Cooper & Co., San Francisco, 577 pp.

Johnson, A.M. and Page, B.M., 1976. Part VII, Development of folds within Huasna syncline, San Luis Obispo County, California. Tectonophysics, 33: 97-143.

Manz, R. and Wickham., J., 1978. Experimental Analysis of Folding in Simple Shear. Tectonophysics, 44: 79-90.

Ramberg, H., 1963. Evolution of drag folds. Geological Magazine, v. 100, no. 2: 7-105.

Ramberg, I.B. and Johnson, A.M., 1976. Part V, Asymmetric folding in interbedded chert and shale of the Franciscan Complex, San Francisco Bay area, California. Tectonophysics, 32: 295-320.

Reches, Z., 1979. Deformation of a foliated medium. Tectonophysics, 57: 119-129.

Reches, Z. and Johnson, A.M., 1976. Part VI, Asymmetric folding and monoclinal kinking. Tectonophysics, 35: 295-334.

Treagus, S.H., 1973. Buckling stability of a viscous single-layer system, oblique to the principal compression. Tectonophysics, 19: 2271-289.

Weiss, L.E., 1968. Flexural-slip folding of foliated model materials. In: A.J. Baer and D.K. Norris (Editors), Proceedings, Conference on Research in Tectonics. Geological Survey of Canada Paper 68-52: 294-333.

CHAPTER IV

ASYMMETRY OF SMALL FOLDS IN THE CENTRAL APPALACHIANS

ABSTRACT

Among the variety of fold forms which occur on the southeast limb of the New Bloomfield anticline, two are particularly intriguing because they have opposite senses of asymmetry. One fold form has the sense of asymmetry associated with drag folds -- its short, steep limb dips toward the axial plane of the major anticline. The other fold form has the sense of asymmetry associated with a monoclinal kink fold -- its short, steep limb dips away from the axial plane of the major anticline.

The folds occur in the Upper Devonian Trimmers Rock and Brallier formations and are exposed in roadcuts on Highway 22/322, six km north of the confluence of the Juniata and Susquehanna Rivers in central Pennsylvania. The monoclinal kink fold occurs within units of massive siltstone, each about 20 m thick, alternating with units of massive mudstone or interbedded mudstone and siltstone. The drag folds occur lower in the section in an interbedded siltstone and mudstone sequence.

The exposures of complete, small-scale folds occurring in adjacent roadcuts within the same stratigraphic unit present an excellent opportunity to investigate deformation mechanisms responsible for different senses of fold asymmetry. Both fold forms consist predominantly of

straight segments separated by relatively narrow hinge zones. Layer-parallel slip is a common deformation mechanism in both types of asymmetric folds. The slip surfaces within the chevron folds, with drag-fold asymmetry, occur in both limbs and in hinges; the slip surfaces within the monoclinal kink fold are more prevalent in the hinges and on the short, steep limb.

Enigmatic folds occur in rocks between the chevron folds and the large monoclinal kink fold. On the one hand, these folds have the asymmetry of drag folds and their axial planes are subparallel to the axial plane of the major fold. On the other hand, the concentration of slip surfaces in short limbs of these folds is the same as that in the monoclinal kink fold. I tentatively interpret them to be kink folds, part of a conjugate set, that formed at a different time than the chevron and monoclinal kink folds.

INTRODUCTION

It is generally assumed in structural geology that parasitic folds that form on the limb of a developing larger fold tend to be asymmetric because they are subjected to simple shearing by the larger fold. This assumption is substantially correct because it does not specify the sense of asymmetry. On the other hand, Pumpelly's Rule (Wilson, 1960) of structural geology states that parasitic folds have the sense of asymmetry of drag folds and therefore can be used to infer the location of structural features of the large folds. Pumpelly's Rule can be quite misleading because monoclinal kink folds develop a sense of asymmetry opposite to that of drag folds in response to the same sense of shear.

According to theory presented in Chapter III, folds in multilayers with constant resistance to slip at contacts develop the sense of asymmetry of a drag fold, but folds in multilayers with variable resistance to slip at contacts develop the sense of asymmetry of a monoclinal kink fold. Thus, the theory indicates that a difference in properties of thin interbeds or of contacts between layers can cause fold asymmetry to be opposite in different parts of a rock section being folded. Pumpelly's Rule is therefore valid only for multilayers with certain physical properties.

In this chapter I describe small folds in the Trimmers Rock and Brallier formations within the southeastern limb of the New Bloomfield anticline (Fig. 1), in central Pennsylvania. Study of the small folds was part of the motivation for the theoretical analysis of fold asymmetry presented in Chapter III; examination of the small folds provides an opportunity to apply some of the results of the theoretical analyses presented in Chapters I, II and III. After describing the small folds I will use the observations and the results of the theoretical analyses to estimate the conditions responsible for the folding.

STRATIGRAPHIC AND STRUCTURAL SETTING

Small, asymmetric folds, with wavelengths of 10 to 60 m and with opposite senses of asymmetry, are exposed in a series of roadcuts along Highway 22/322 on the east side of the Juniata River, a few km northwest of its confluence with the Susquehanna River in central Pennsylvania. The outcrops expose part of the southeast limb of the New Bloomfield anticline (Fig. 1), a large, first order fold* with a wavelength of 15 km. At the Juniata River, the anticline is

---

*Orders of folds should not be confused with order of approximation used in the theoretical analysis. The concept of orders of folds is an old one (*e.g.*, Rogers, 1858, p. 887; Van Hise, 1896); the notion is that folds of distinctly different sizes form roughly at the same time in a complex multilayered rock sequence. Nickelsen (1963) has

Figure 1. Study site on the southeast limb of the New Bloomfield anticline near the confluence of the Juniata and Susquehanna rivers, central Pennsylvania. The map shows traces of contacts between some of the rock units included on part of the Pennsylvania State Geologic Map (Gray and others, 1960).

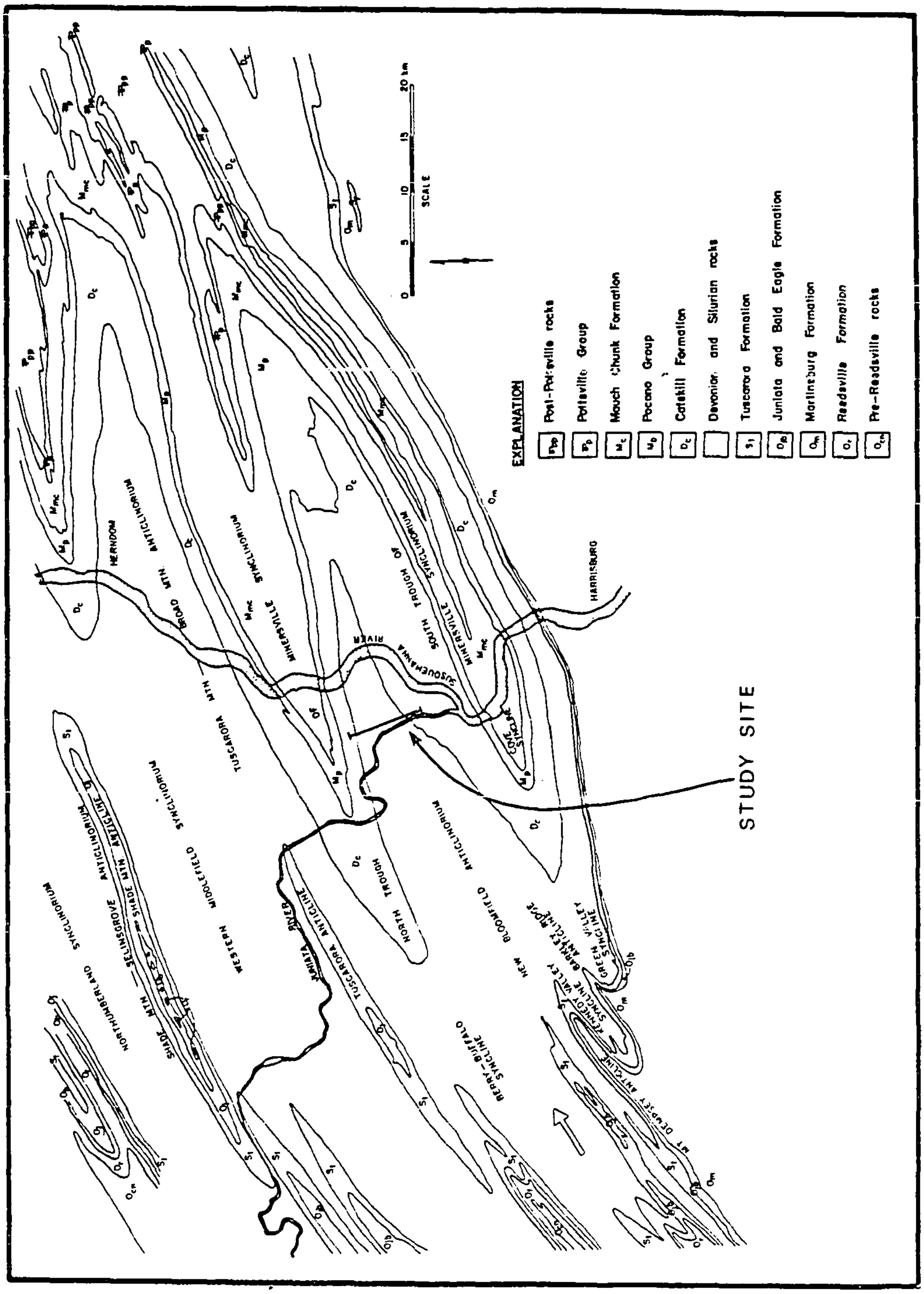
EXPLANATION
Post-Pottsville rocks
Pottsville Group
Mauch Chunk Formation
Pocono Group
Catskill Formation
Devonian and Silurian rocks
Tuscarora Formation
Juniata and Bald Eagle Formation
Martinsburg Formation
Reedsville Formation
Pre-Reedsville rocks
0 5 10 15 20 km
SCALE
STUDY SITE
HARRISBURG
SUSQUEHANNA RIVER
JUNIATA RIVER
TUSCARORA ANTICLINE
NORTH TROUGH
SOUTH TROUGH OF MINERSVILLE SYNCLINORIUM
MINERSVILLE SYNCLINORIUM
BROAD MTN. ANTICLINORIUM
HERNDON
TUSCARORA MTN.
WESTERN MIDDLEFIELD SYNCLINORIUM
SHADE MTN.
SELINSGROVE ANTICLINORIUM
NORTHUMBERLAND SYNCLINORIUM
NEW BLOOMFIELD ANTICLINORIUM
PERRY-BUFFALO SYNCLINE
COVE SYNCLINE
MT. DEMPSEY ANTICLINE

asymmetric, with a steeper northwest limb (Fig. 2). Its axis plunges to the northeast at angles of 5 to 20 degrees (Dyson, 1963).

The small, asymmetric folds indicated in Fig. 2 occur in the central part of the Trimmers Rock-Brallier formations (610 m undivided, upper Devonian) (Dtrb, Fig. 2). The upper part is predominantly siltstones of the Trimmers Rock Formation. This lithology grades downward into increasingly finer siltstones, mudstones, and shales. The lowest part of the section (75 m) is predominantly shaly Brallier Formation (Dyson, 1963, p. 22). The constituents of the siltstones and mudstones in both the Trimmers Rock and Brallier formations include a large fraction of quartz grains (Frakes, 1967; Samuels, 1979). The siltstones are generally cemented by silica and locally by carbonates (Faill and Wells, 1974).

---

provided a useful classification of sizes or orders of folds in the Appalachians: First-order folds are anticlinoria and synclinoria with wavelengths of 11 to 18 km and involve rocks from the Cambrian to the Pennsylvanian. Second-order folds have wavelengths of 2.5 to 3 km and are best developed at the levels of the Tuscarora and Bald Eagle formations. Third-order folds have wavelengths of several meters to one kilometer. They are best developed in the middle Silurian and middle Devonian rocks above the Rose Hill Shale and below and Hamilton Group. Fourth-order folds have wavelengths ranging from a few tens of centimeters to a few meters. Fifth-order folds are smaller than these.

Figure 2. Cross section through the New Bloomfield anticline. The location of the line of section is indicated on Fig. 1. The location of contacts and faults is taken from the geologic map of the northern half of the New Bloomfield quadrangle, Pennsylvania (Dyson, 1963).

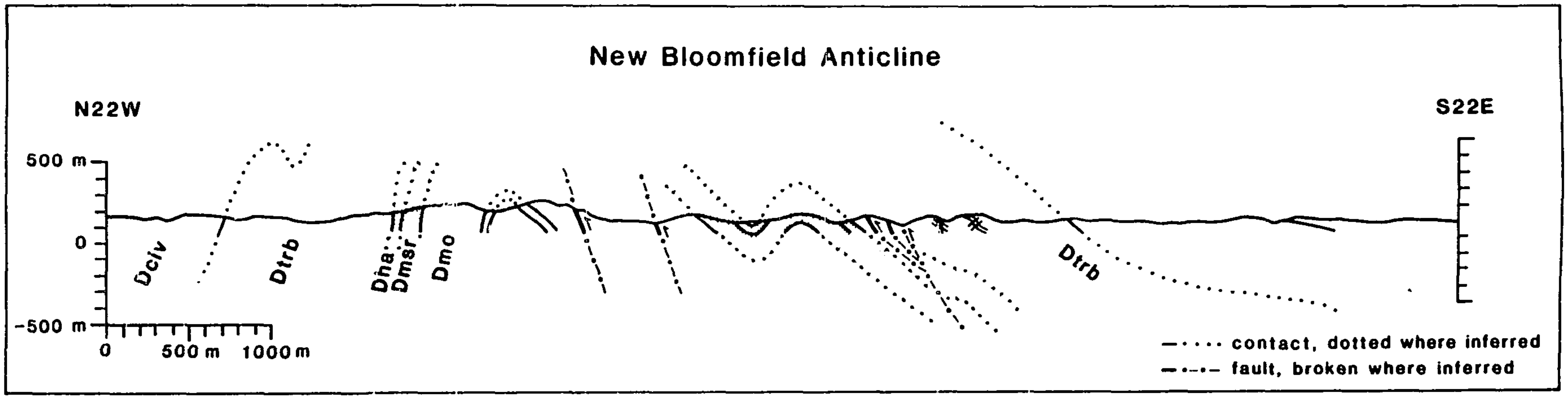
New Bloomfield Anticline
N22W
S22E
500 m
0
-500 m
0
500 m
1000 m
Dclv
Dtrb
Dha
Dmsr
Dmo
Dtrb
contact, dotted where inferred
fault, broken where inferred

Layer contacts of the siltstone and mudstone beds within the Trimmers Rock-Brallier unit may be planar and persistent, irregular, or gradational (Frakes, 1967). The Trimmers Rock Formation is characterized by very hard graywacke siltstone beds up to two meters thick which appear massive or structureless but have planar upper and lower contacts. The planar contacts persist over long distances within an outcrop but may wedge out within an exposure. Interbeds of shale and mudstone may be totally absent or may constitute the bulk of the local section. The siltstones commonly form resistant ledges and weather as yellowish blocks equal in thickness to the bed thickness. Siltstones of the Brallier Formation are also graywackes and have planar basal contacts, but upper contacts are gradational with overlying shales.

THE SMALL, ASYMMETRIC FOLDS

All the small folds (Figs. 3 and 4) in the roadcuts are characterized by relatively straight limbs and narrow hinges; some of the folds are chevron-shaped and others are kink-shaped. Relative to the position of the folds on the limb of the New Bloomfield anticline, the small folds can be differentiated by sense of asymmetry and by orientation of axial planes. All but one of the minor, asymmetric folds in the northern roadcut (on left in Figs. 3 and 4) have the

<u>Figure 3</u>. Small asymmetric folds on the southeast limb of the New Bloomfield anticline are exposed in roadcuts along highway 22/322 on the east side of the Juniata River about 33 km northwest of Harrisburg, Pennsylvania.

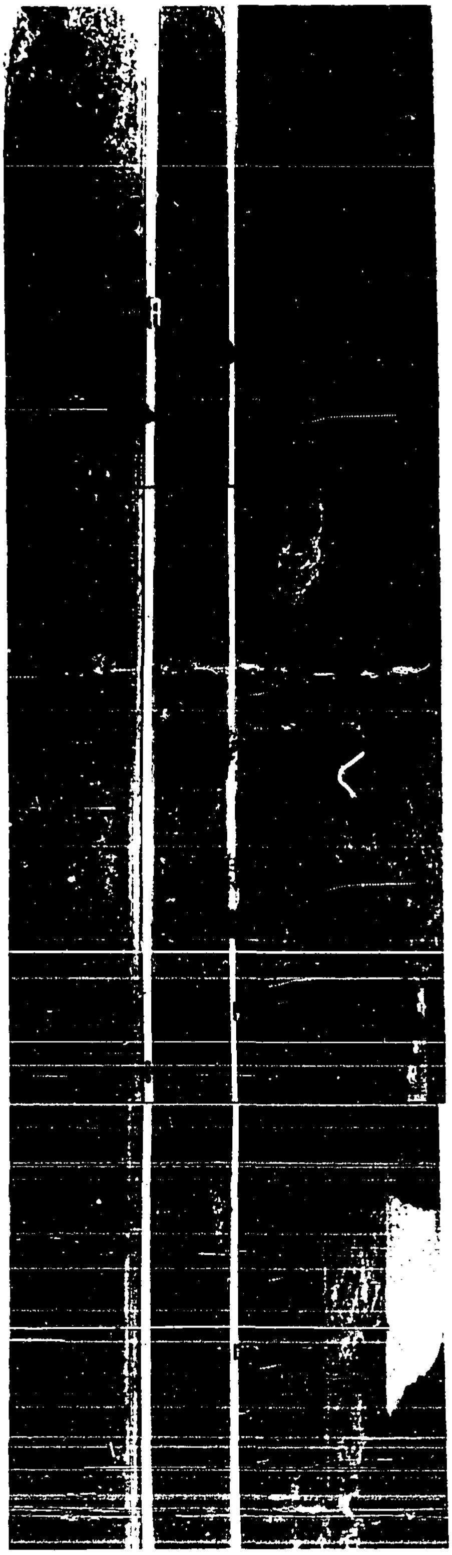

Figure 4. Controlled sketch of minor folds exposed in the roadcuts shown in photographs in Fig. 3. Chevron folds with drag fold asymmetry in northern part of the northern roadcut (on left); large monoclinal kink fold in southern roadcut (on right).

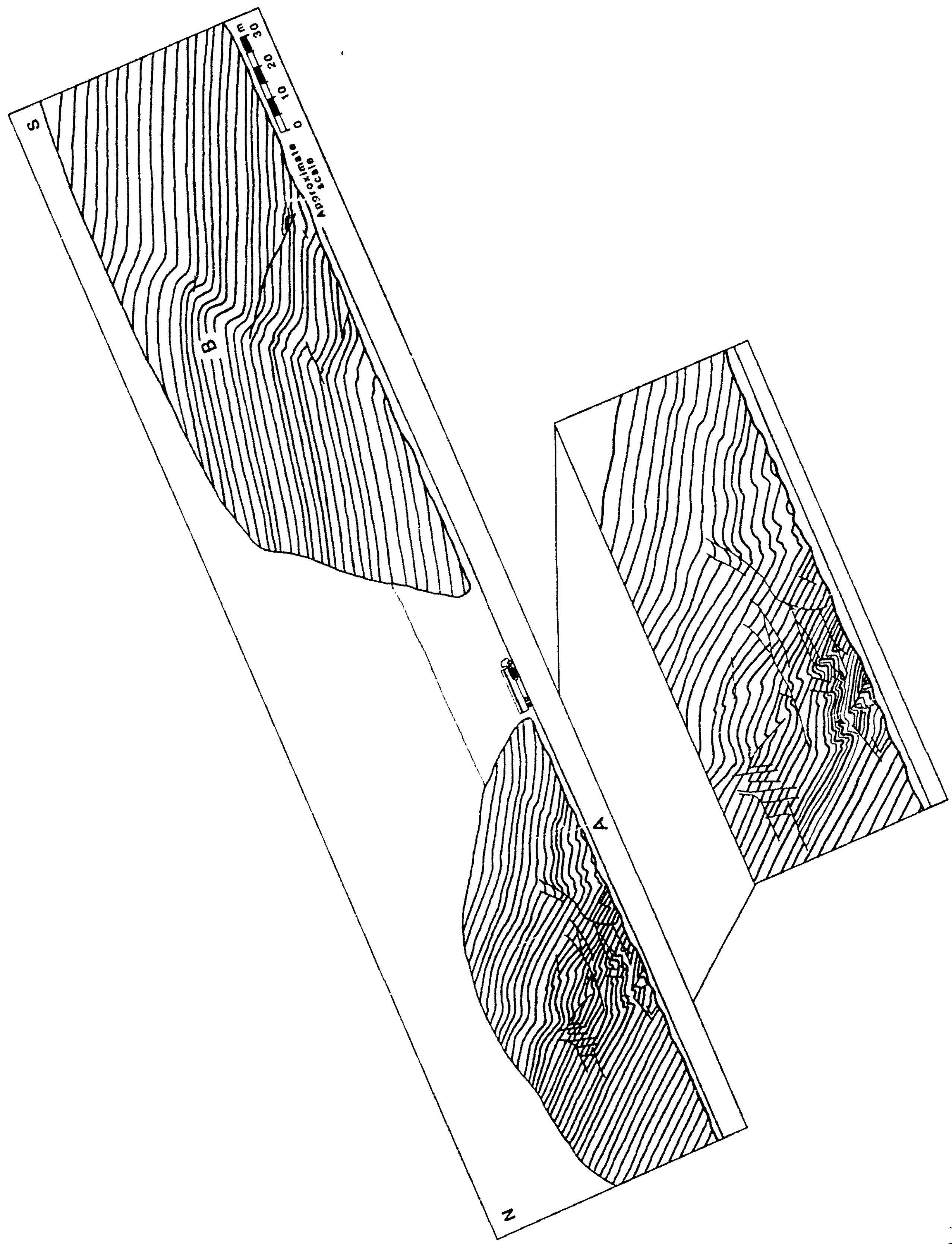
S
Approximate scale
0
10
20
30
m
B
A
N

sense of asymmetry of a drag fold because their short, steep limbs dip toward the axial plane of the major anticline. The minor fold in the southern roadcut (on right in Figs. 3 and 4) and one of the minor folds in the northern roadcut have the sense of asymmetry of a monoclinal kink fold because their short, steep limbs dip away from the axial plane of the major anticline.

Plots of structural elements on stereographic projections (Fig. 5) indicate that layers in the two roadcuts were folded about axes with approximately the same attitude and that bedding-plane slip was essentially normal to fold axes. Poles to bedding around a synclinal hinge (location A, Fig. 4) indicate a fold axis that plunges 10°, N73E (solid triangle in Fig. 5A); a similar plot of poles to bedding around a kink hinge (northern hinge, location B, Fig. 4) indicates a fold axis that plunges 15°, N76E (solid triangle in Fig. 5B).

Fold axes were also derived from the attitudes of slickenlines on bedding planes by assuming that the direction of the slickenlines is perpendicular to the fold axis. Axes were derived for one fold with drag-fold asymmetry (open circles, Fig. 5A) and one fold with monoclinal kink-fold asymmetry (open circles, Fig. 5B). The fold axes derived from orientations of slickenlines cluster about the fold axes (indicated by solid triangles) determined from the attitudes of bedding planes. Therefore,

Figure 5. Stereoplots of poles to bedding and fold axes. Lower hemisphere projection, Wulff net. A. Structural data for asymmetric fold at location A, Fig. 4. B. Structural data for monoclinal kink fold at location B, Fig. 4.

A

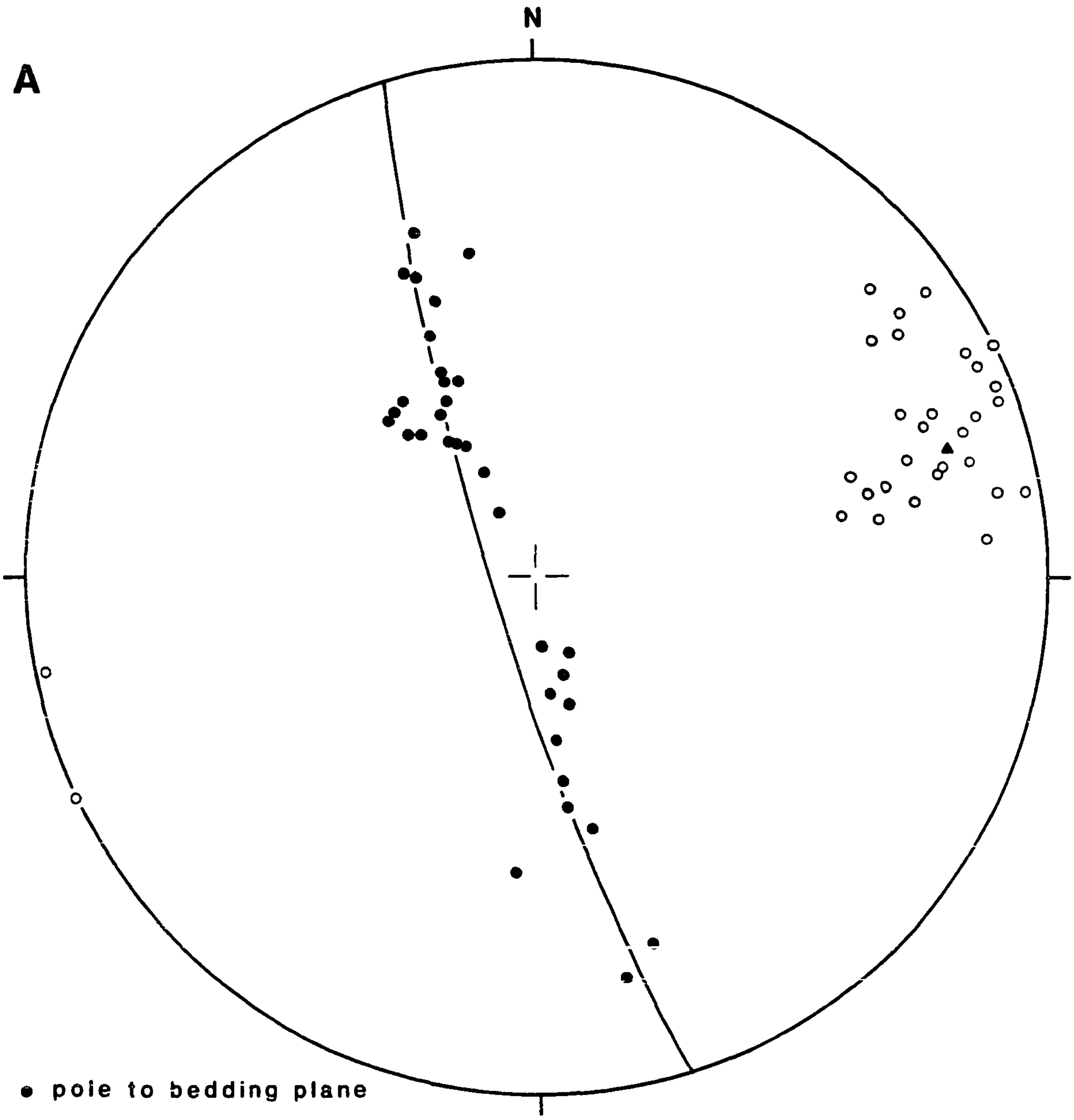

● pole to bedding plane

○ fold axis calculated from slickenline

▲ fold axis calculated from bedding planes

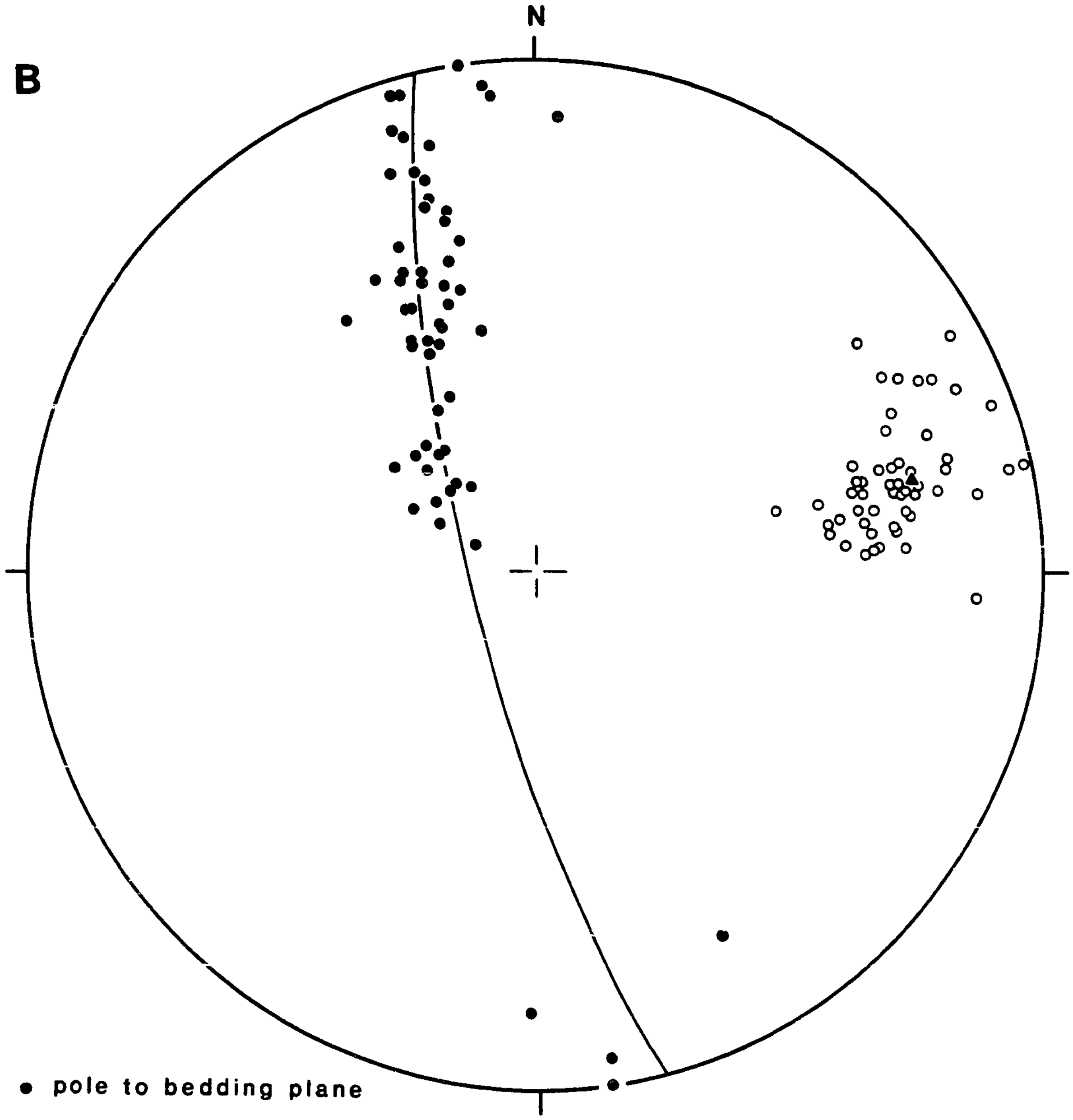

• pole to bedding plane

○ fold axis calculated from slickenline

▲ fold axis calculated from bedding planes bedding-plane slip was essentially normal to fold axes for these small, asymmetric folds, as it was for many other folds in the central Appalachians analyzed by Nickelsen (1963) and by Faill (1973).

The axial planes of most of the folds in the northern roadcut (on left in Fig. 4) tend to be vertical or to dip steeply to the southeast. The axial planes of the large fold in the southern roadcut and the fold in the southern part of the northern roadcut dip approximately 40 degrees to the northwest. The dip of the axial planes of the larger fold is interrupted in the vicinity of a conspicuous reverse fault (Fig. 4). Below the fault, the axial planes dip approximately 45° NW, but above the fault, they dip 30° NW.

The fold in the southern roadcut (on right in Fig. 4) occurs in rocks characterized by marked changes. At the upper end of the fold the short limb is in mudstones containing a few siltstones. Below that, the short limb cuts through a package of four rock units, each about 20 m thick. The units alternate from predominantly mudstone to predominantly siltstone.

This fold is an isolated structure, and I consider it to be a monoclinal kink fold. The bedding in the long limbs on either side of the kink limb dips 20 to 25° SE. In the kink limb, the bedding dips southeast much more steeply, in places slightly through vertical.

The asymmetric folds in the northern part of the northern roadcut are in interbedded mudstones and siltstones (Fig. 6A). Thicknesses both of siltstones and of mudstones are generally a few cm to a few dm. The short limb of these folds dips to the northwest. Tight hinges grade upsection or downsection into more rounded forms. The folds have a chevron form, and I consider them to be <u>chevron drag folds</u>. The folds are repetitive structures but die out along the bedding.

The asymmetric folds in the central part of the northern roadcut are in a section of predominantly siltstone, containing many beds up to three dm thick (location A, Fig. 4; Fig. 6B). Mudstone interbeds are one to five cm thick. Some of the layers in the folds have a relatively open, almost concentric-like form, but many are sharp and chevron-like (Fig. 6B). My first interpretation of these folds was that they are drag folds of concentric-like form or of combinations of concentric-like and chevron forms. However, I now interpret them to be kink folds, partly on the basis of my study of deformation mechanisms which I will discuss next.

MECHANISMS OF DEFORMATION

The nearly complete exposure of folds with opposite senses of asymmetry occurring in adjacent roadcuts along the Juniata River within the same stratigraphic unit appeared to present an excellent opportunity to investigate deformation

Figure 6. Photographs of some asymmetric folds in the northern roadcut shown (on left) in Fig. 4. A. Chevron folds with drag fold asymmetry. B. Asymmetric folds left of location A, Fig. 4.

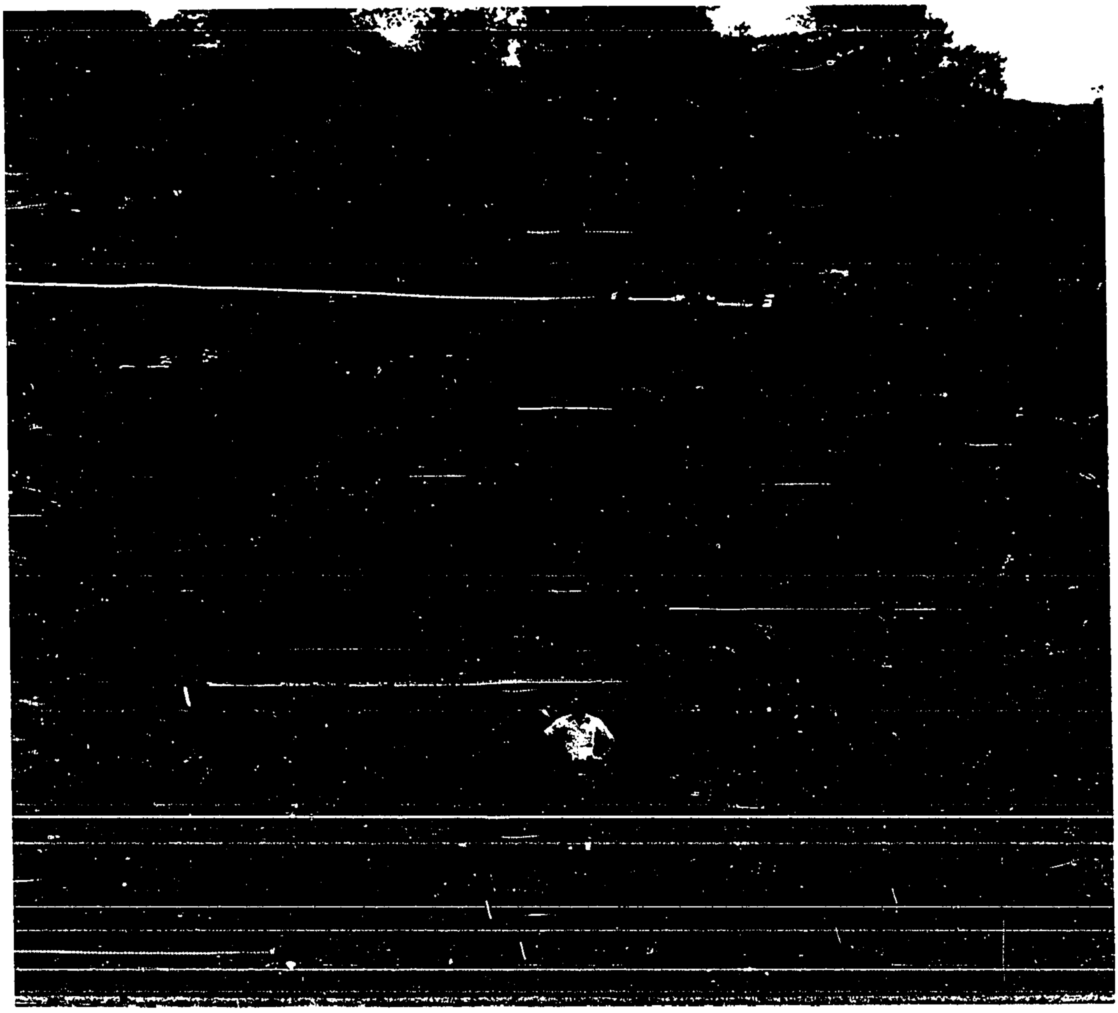

mechanisms responsible for different asymmetric folds. With this in mind, I examined in detail parts of the small folds in the roadcuts and mapped my observations of slip surfaces and faults on enlarged photographs of the outcrops. I recognized bedding-plane faults in the field by the presence of slickensides, and the lines shown in Figs. 7B and 8B represent only those surfaces on which I observed slickenlines.

Slip between mechanical units, as manifested in layer-parallel, bedding-plane faults, was a common mechanism of deformation in all the folds. Bedding-plane faults are prevalent in the hinges and on both limbs of the asymmetric chevron folds shown at the left in Fig. 4.

The number of bedding-plane faults is relatively few on the long limbs outside the large monoclinal kink band but increases in the hinge and on the short, steep limb, as shown in Fig. 7B; bedding-plane slip was almost non-existent in layers on either side of the kink band, but was intense within both hinges and the short, steep limb.

A similar phenomenon can be observed in the asymmetric folds in the central and southern parts of the northern roadcut (location A, Fig. 4; Fig. 6B). Bedding-plane faults are much more common in the hinges and on the short, steep limb (Fig. 8). The spacing of bedding-plane faults defines the thicknesses and numbers of mechanical units, which are thus more numerous in the hinges and on the short, steep

Figure 7. Location and distribution of slip surfaces on part of monoclinal kink fold. A. Area of map shown in Fig. 7B is along bench above upper highway at location B, Fig. 4. B. Map of slickenlined faults in monoclinal kink fold. Faults along axial plane dip to the north (left). Layer-parallel (bedding-plane) faults are more numerous in the hinges and on the short, steep limb, and are much less abundant outside the kink band.

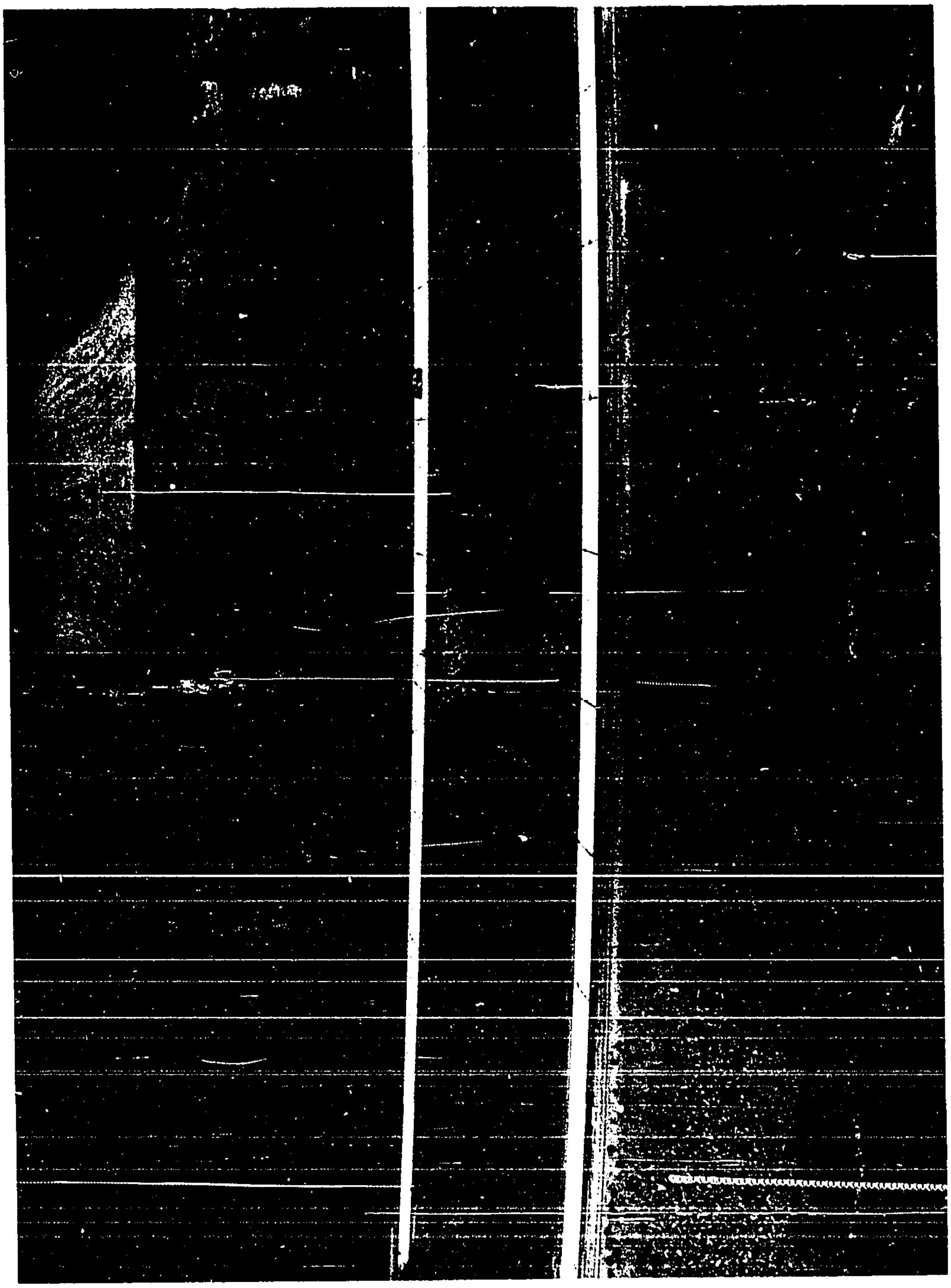


0 0.5 1.0 m

Figure 8. Location and distribution of slip surfaces on asymmetric fold at location A, Fig. 4. A. Photograph of fold mapped in detail in Fig. 8B. B. Map of slickenlined layer-parallel faults. Bedding-plane faults are more numerous in hinges and on short, steep limb. Veins in synclinal hinge are indicated by dotted lines. Stippled areas are covered.

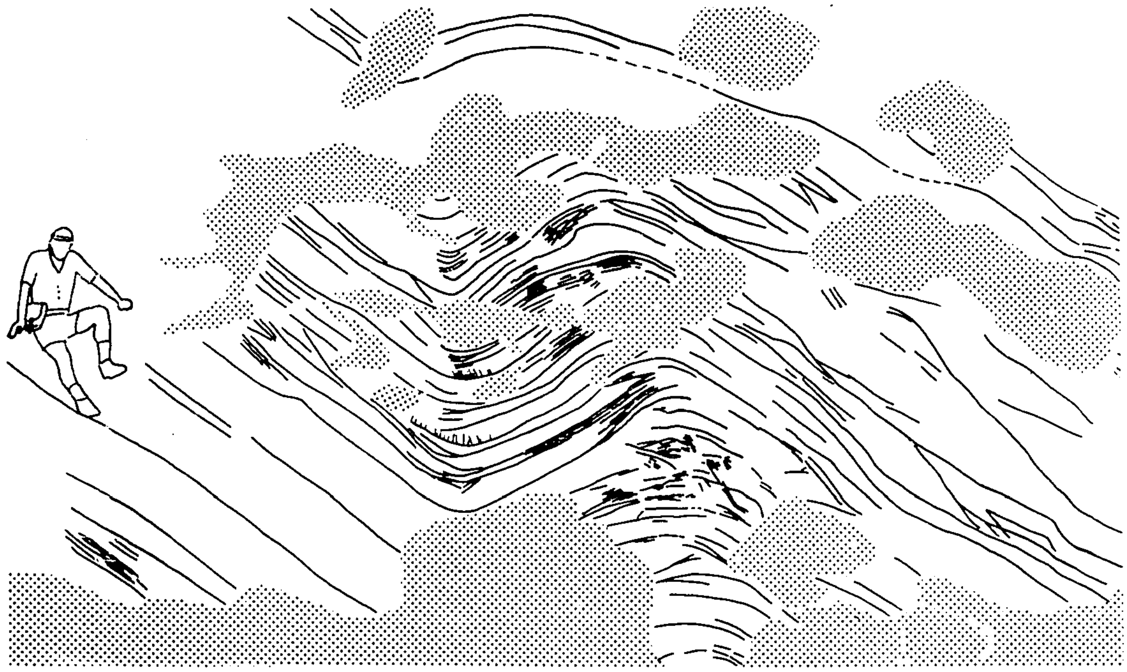

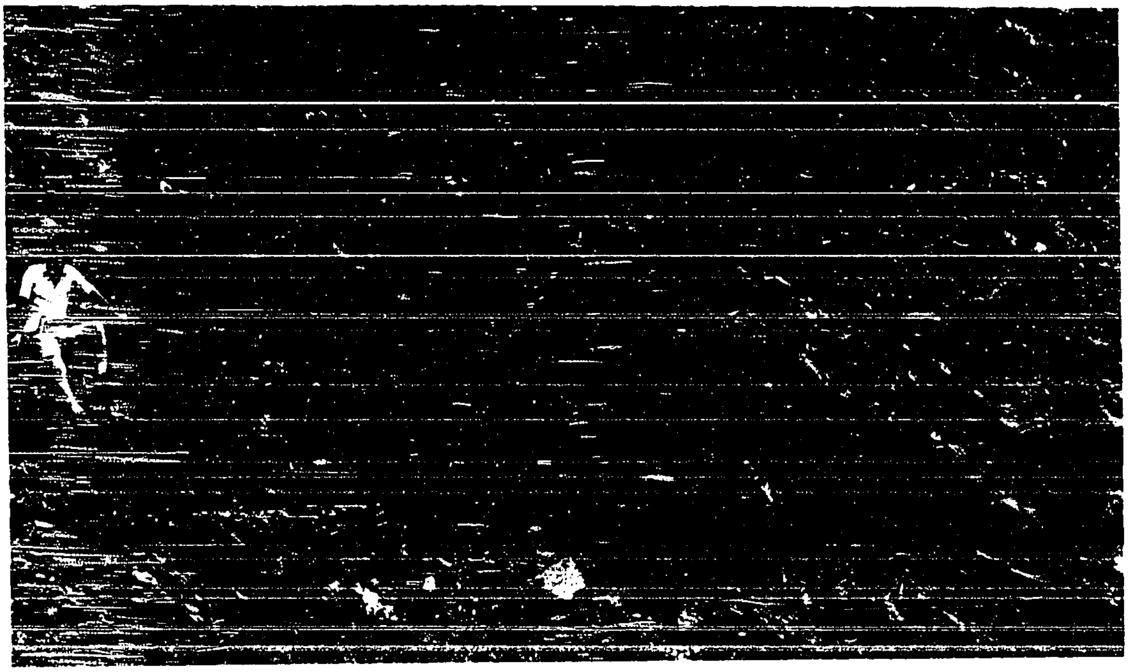

limbs. The slip surfaces tend to follow bedding planes, but may cut across bedding, especially in the hinge areas.

The larger number of bedding-plane faults on the short, steep limb is evident on a finer scale, too. Figure 9 shows a detailed map of traces of fractures in a layer in the synclinal hinge shown in the center of Fig. 8B. The layer is bounded above and below by through-going, bedding-plane faults. Several bedding-plane faults enter the hinge area from the short, steep limb on the right and terminate in the vicinity of the hinge, so they do not extend into the long limb on the left. The bedding-plane faults are strongly slickenlined.

Each fault terminates by branching into several small offshoots, almost all of which trend upward, reflecting right-lateral shear on the faults (e.g., Segall and Pollard, 1983). Bedding-plane faults in hinges may bifurcate to form wedge-shaped units, and the wedges may slip over each other as observed by Cloos (1964). Faill (1973) reported that the slickenline directions on wedge faults are congruent with those on bedding planes, and inferred on this basis that slip on wedge faults was simultaneous with slip on bedding planes, which occurred during folding.

Right-lateral shear is also reflected in filled fault steps (Segall and Pollard, 1983), shown in black in Fig. 9. The filled steps are rhombohedral-shaped in cross section. Each fault surface consists of a series of stepped fault

<u>Figure 9</u>. Detailed map of traces of fractures in a layer in the synclinal hinge of the asymmetric fold shown in Fig. 8. Right-lateral shear is indicated by the offset of mechanical hinges from the fold trough, by the shape of the filled rhombohedrons, by the orientation of small cracks at the ends of bedding-plane faults, and by the larger number of bedding-plane faults on the short limb.

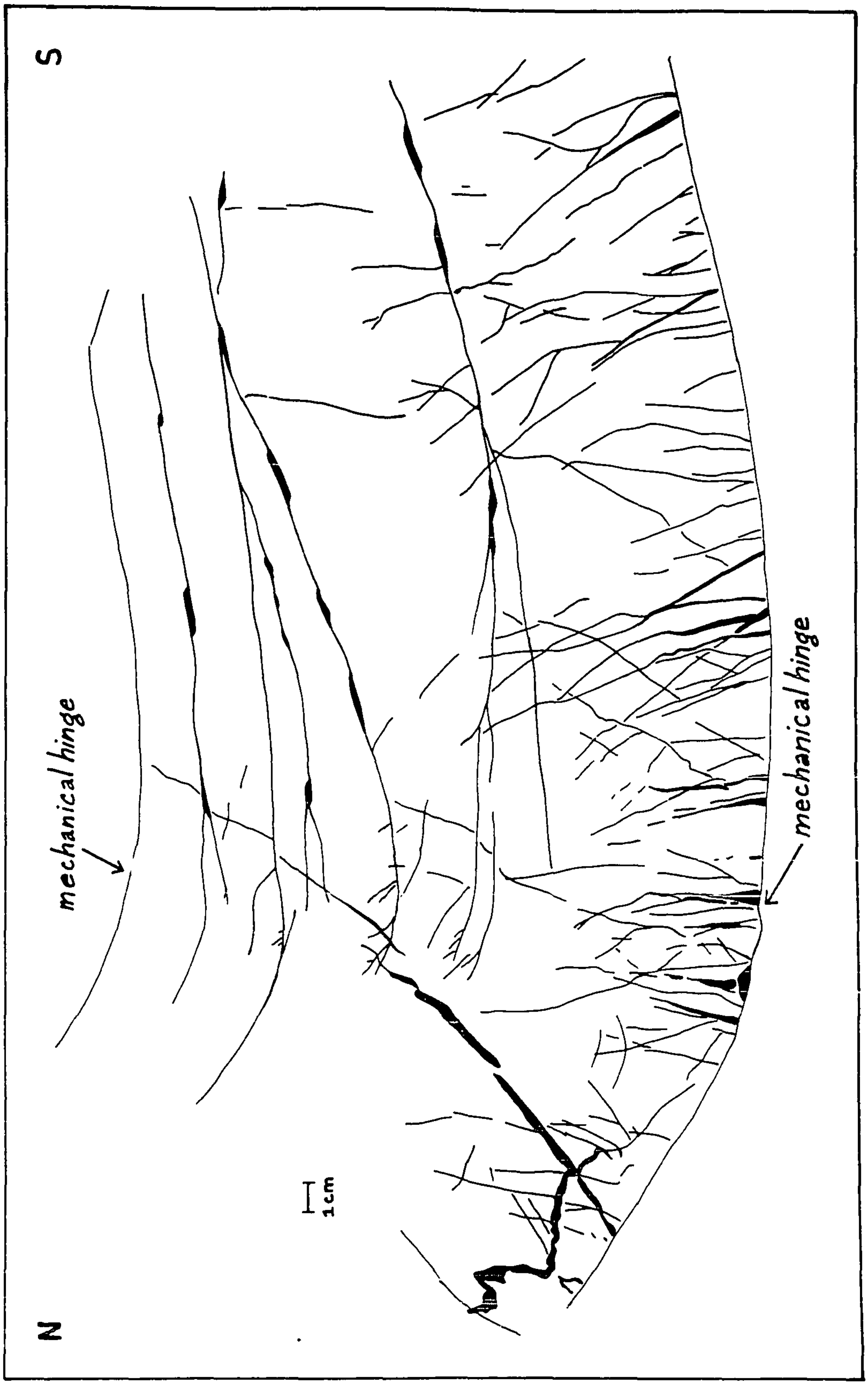
S
N
mechanical hinge
mechanical hinge
1 cm

segments, and the slickenside steps, which show up clearly in this cross section (Fig. 9), occur where fault steps overlap.

Veins perpendicular to bedding are related to stepped slickensides in the synclinal hinge of the drag fold (Fig. 10). Each slickenlined slip zone around the curved hinge consists of a series of overlapping surfaces connected by a short segment at an angle to the bedding plane reminiscent of a ramp between two levels of a thrust surface. Individual slickenlined surfaces seem to be rooted at one end to a bedding-perpendicular vein.

The mechanical hinge of each layer interface in a fold can be defined by determining where the slip direction reverses. The bed shown in Fig. 9 is bounded by bedding-plane faults, and the sense of movement indicated by the slickenside steps reverses direction along the faults. Interestingly, the mechanical hinges for the bed are not located at the troughs of the interfaces of the fold, but are offset slightly to the left (north). Offset of the mechanical hinge from the trough probably is a result of superimposition of layer-parallel compression and shear, and the sense of offset in this example indicates right-lateral shear relative to the local orientation of the bedding-plane faults.

The right-lateral shear, which is reflected in the offset of mechanical hinges (Fig. 10), the shape of the

Figure 10. Observed relationship between veins and overlapping slickenlined surfaces on lower bedding plane in hinge mapped in Fig. 9. A. Photograph focusing on the lower bedding surface. B. Illustration of observed rooting of individual slickenlined surfaces at one end to bedding-perpendicular veins.

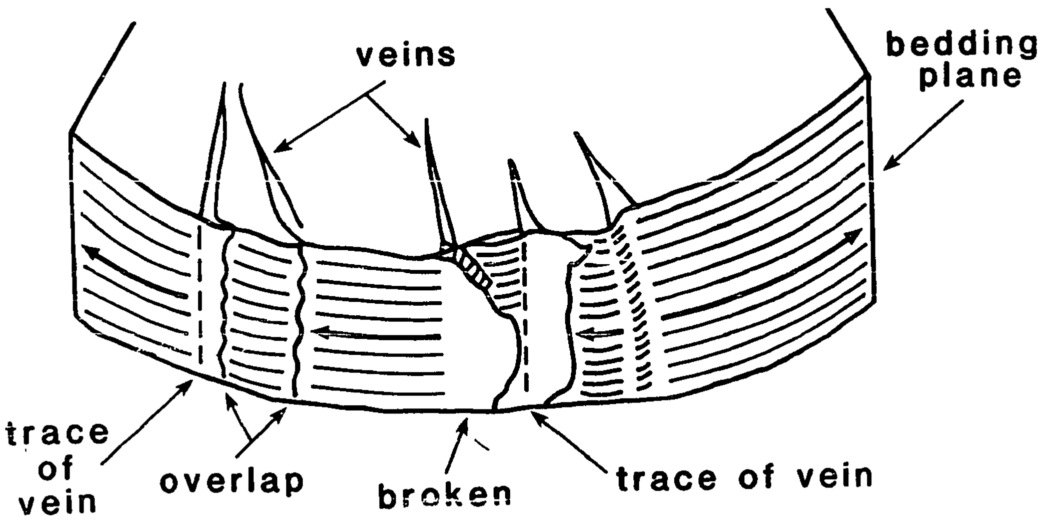
veins
bedding plane
trace of vein
overlap
broken
trace of vein

filled rhombohedrons (Fig. 9), the larger number of bedding-plane faults on the left limb (Fig. 8), and the orientation of small cracks at the ends of bedding-plane faults (Fig. 9), is inconsistent with the setting of the small folds on the limb of the New Bloomfield anticline. There, the shear should have been left lateral, as viewed in the figures described herein.

In summary, detailed mapping of the folds shown in previous pages provides some information about deformation mechanisms during folding, but provides no information about differences in rheological properties of layers or of contacts in the folds with different asymmetries. In all the folds, flexural slip was accommodated by slip along bedding-plane faults. In the chevron folds in the northern roadcut (Fig. 6A), shear appears to have been distributed as well within shaly interbeds between siltstone layers. Examination of numerous fold hinges in concentric-like, kink-like and chevron folds in the Trimmers Rock-Brallier unit indicates that bending in all types of folds typically was eased by the existence or development of bedding-plane faults and that bending was accomplished by internal deformation of layers, not by visible faulting or fracturing. Thus the deformation mechanisms were the same qualitatively, but presumably not quantitatively, in all the folds.

DISCUSSION

The field work was aimed originally at documenting an example of folds which I assumed had formed simultaneously with opposite senses of asymmetry. Instead, the field observations have provided an interesting challenge to the assumption that the asymmetric folds formed simultaneously. The descriptions of the asymmetric folds in the Trimmers Rock-Brallier unit on the southeastern limb of the New Bloomfield anticline raise several problems regarding interpretation of the conditions during folding.

Folds with opposite senses of asymmetry occur in the same or adjacent roadcuts. Folding theory indicates that such folds could have formed simultaneously, or at least under the same stress state, provided the properties of interbeds or contacts between layers were different where the fold asymmetries are different. Theory developed in Chapter III indicates that folds with drag-fold asymmetry will form if the interbeds or contacts have constant resistance to slip, whereas folds with monoclinal-kink asymmetry will form if the interbeds or contacts have variable resistance to slip (for example, contact strength or nonlinear contacts). The theory, however, provides no information about how one is to determine rock properties.

The field descriptions indicate that the chevron folds in the northern end of the northern roadcut (Fig. 6A) occur within a sequence of interbedded siltstones and mudstones. The asymmetric folds in the central part of that roadcut occur within a sequence of predominant siltstone. The large monoclinal kink fold in the southern outcrop occurs within a package of predominant siltstone units alternating with predominant mudstone units, each about 20 dm thick. Thus the rock units involved in folding are not obviously different rheologically.

The difficulty of recognizing differences in properties of rocks responsible for different fold forms is perhaps typical. Asymmetric folds of chevron shape are common near San Francisco in parts of the Franciscan Assemblege, consisting of interbedded cherts and shales (Ramberg and Johnson, 1976). A few monoclinal and conjugate kink folds occur in the same sequence, but apparently where shale interbeds are thinner. Multilayered rock consisting of interbedded limestone and shale, near Cody, Wyoming, contains well developed monoclinal-kink folds (Aydin, M.S. thesis, 1973; Reches and Johnson, 1976).

The essential differences in properties of the rocks near San Francisco and near Cody may well be a result of pore-water pressures at the times of folding. Where pore-water pressures are high, the shales will have low strength and behave essentially as linear viscous materials, for which theory predicts drag-fold asymmetry. Where pore-water pressures are low, the shales will have high strength and behave as highly nonlinear materials, for which theory predicts monoclinal-kink asymmetry (Chapter III).

The same may well be true for the folds in the Trimmers Rock-Brallier unit in central Pennsylvania. The pore-water pressures might have been higher when and where the chevron folds formed. However, I have no relevant observations with which to evaluate this speculation.

An observation that supports the interpretation that most of the folds in the northern outcrop have drag-fold asymmetry and that one fold in the northern outcrop and the large fold in the southern roadcut have monoclinal kink asymmetry is the marked difference in orientation of axial planes. As shown in Fig. 4, the traces of axial planes of all but one of the folds in the northern roadcut are essentially vertical whereas the traces of axial planes of the large fold in the southern roadcut and of one of the small folds near the southern edge of the northern roadcut are inclined 30 to 45 degrees from the horizon. These orientations are consistent with the orientations of axial planes of minor, asymmetric folds that form at the same time as the major fold, as shown in Fig. 1, Chapter III.

On the basis of these observations, I would (indeed, I did) tentatively conclude that the folds with opposite asymmetry formed under the same general state of layer-parallel shortening and (left-lateral) layer-parallel shear. The field observations suggest that the rocks that folded with the opposite asymmetry are nearly identical, so I presume that the properties of the rocks were the same at the times the folds formed but that the strengths of contacts or interbeds were different. For example, strength may have been reduced by higher pore-water pressures in the part of the section where the chevron folds formed.

The tentative conclusion is questioned, however, by several additional observations. The folds in the central part of the northern roadcut (Figs. 4, 6B, and 8A) resemble kink folds. These folds are closely associated with a kink fold with opposite asymmetry at the southern end of the northern roadcut. The concentration of slip surfaces in the short limb of these folds (Fig. 8B) is closely related to that in the limb of the monoclinal kink fold (Fig. 7B), in the southern roadcut. In contrast, the chevron folds in the northern part of the northern roadcut have slip surfaces on both limbs and even in hinges.

The marked development of slip surfaces on the limb of the large kink fold in the southern roadcut, Fig. 7B, is as expected. Reches and Johnson (1976) showed that the sense of asymmetry of local, monoclinal-kink folds can be explained in terms of early yielding of layer contacts along interfaces facing right for left-lateral shear and facing left for right-lateral shear. I showed in Chapter III that the same type of explanation can be derived for multilayers with nonlinear contact properties.

A possible explanation for the high concentration of slip surfaces on the short limb of the asymmetric fold mapped in detail (Fig. 8B) is that the slip surfaces were generated late in the folding, after the folds had become markedly asymmetric. In this way, the shear stress could be larger on the short limb than the long limb (as one can demonstrate with a Mohr diagram, for example). Yielding could thus have occurred on the short limb of the fold shown in Fig. 8B.

However, study of Fig. 9 indicates that, in the limb of a layer within that fold, the slip accommodated along surfaces within the layer was sufficiently large to produce the slope of the limb by simple shear. This contradicts the assumption that the slip surfaces formed late, after the limb had been strongly tilted. Alternatively, the fold considered, until now, as a drag fold might in fact be a kink fold, part of a conjugate set in the southern end of the northern roadcut. This interpretation contradicts the assumption that all the folds formed when the rocks were subjected to the same stress state. However, the initial assumption of simultaneity was made only for simplicity.

I would mention one final difficulty facing interpretation of the small folds. All the folds are either local or localized. How can the theory of asymmetric folding, which is based on the assumption that folding is repetitive, be relevant to local or localized folding? I believe that the theory qualitatively is relevant to localized folding in spite of the fact that it assumes an infinite train of waveforms. There is no reason to suspect that the prediction of sense of asymmetry would be changed by a theory that addresses local or localized folding. The 3rd-order theory developed in this dissertation is unable to solve problems involving local folding, but it could be extended, in principle, to very high powers in the powerlaw equations, which would allow local folding, as discussed in Chapter II.

However, I feel that the localization of folding is important because it probably reflects changes of rock properties or stress states along layering. For example, folding in the Trimmers Rock-Brallier unit may have been localized by faulting deeper in the section. Perhaps the overall shearing accommodated by the drag folding in the northern roadcut (left end of Fig. 4) reflects localized shearing near the termination of a low-angle reverse or thrust fault, such as those suggested in the regional cross section of the New Bloomfield anticline (Fig. 2). According to the theoretical analysis (Chapter III), the localized shearing would not only produce asymmetry of folds but would allow contacts to slip locally and thereby cause the folds to be localized. Thus I suggest that the localized folding is a result of layer-parallel shortening and shear localized near a terminating thrust fault.

On the basis of my study of the minor folds exposed in the roadcuts (Fig. 4), I would suggest the following sequence of events during their formation: Early in the growth of the New Bloomfield anticline and of a thrust fault in its southeastern limb, minor folds were initiated near the termination of the thrust fault. The rocks were subjected to layer-parallel compression, and the first folds formed were symmetric chevron folds in the thinly interbedded siltstones and shales and conjugate kink folds in the relatively massive siltstones immediately overlying them. As the New Bloomfield anticline grew, shearing increased on its limbs, and the chevron folds became drag folds and the large monoclinal kink fold in the southern roadcut initiated and developed. The conjugate kink folds changed insignificantly, although the dip of the right-facing limb reduced and the dip of the left-facing limb increased slightly as a result of the layer-parallel shear strain. Most of the shear strain was accommodated in the shaly unit containing the chevron folds by shearing and faulting of the folds (Fig. 4).

REFERENCES

Aydin, A., 1973. Field Study and Theoretical Analysis of Some Small Faults in Montana, Wyoming, and Utah. M.S. thesis, Department of Geology, Stanford University, Stanford, California, 51 pages.

Cloos, E., 1964. Wedging, bedding plane slips, and gravity tectonics in the Appalachians. In: W.D. Lowry, ed., Tectonics of the Southern Appalachians. VPI Department of Geological Sciences Memoir I: 63-70.

Dyson, J.L., 1963. Geology and Mineral Resources of the Northern Half of the New Bloomfield Quadrangle. Atlas A 137ab. Pennsylvania Geological Survey, Harrisburg, Pennsylvania, 63 pages.

Faill, R.T., 1973. Kink-band folding, Valley and Ridge Province, Pennsylvania. Geological Society of America, 84: 1289-1314

Faill, R.T. and Wells, R.B., 1974. Geology and Mineral Resources of the Millerstown Quadrangle, Perry, Juniata, and Snyder Counties, Pennsylvania. Atlas 136. Pennsylvania Geological Survey, Harrisburg, Pennsylvania, 276.

Frakes, L.A., 1967. Stratigraphy of the Devonian Trimmers Rock in Eastern Pennsylvania. Bulletin G 51, Pennsylvania Geological Survey, Harrisburg, Pennsylvania,

Gray, C., Conlin, R.R., Hoskins, D.M., and Shepps, V.C., 1960. Geologic map of Pennsylvania, 1/250,000. Pennsylvania Topographic and Geologic Survey, 4th series.

Nickelsen, R.P., 1963. Fold patterns and continuous deformation mechanisms of the Central Pennsylvania folded Appalachians. In: Tectonics and Cambrian-Ordovician Stratigraphy in the Central Appalachians of Pennsylvania. Field Conference sponsored by the Pittsburgh Geological Society and the Appalachian Geological Society: 15-28.

Ramberg, I.B. and Johnson, A.M., 1976. Part V, Asymmetric folding in interbedded chert and shale of the Franciscan Complex, San Francisco Bay area, California.

Tectonophysics, 32: 295-320.

Reches, Z. and Johnson, A.M., 1976. Part VI, Asymmetric folding and monoclinal kinking. Tectonophysics, 35: 295-334.

Rogers, H.D., 1858. The Geology of Pennsylvania, A Government Survey. 2 vols. and atlas. J.B. Lippincott and Co., Philadelphia.

Samuels, N.D., 1979. The Sedimentology and Petrology of the Brallier Formation - Upper Devonian Turbidite Slope Facies of the Central Appalachians. M.S. Thesis, Department of Geology, University of Cincinnati, Cincinnati, Ohio, 153 pages.

Segall, P. and Pollard, D.D., 1983. Nucleation and growth of strike slip faults in granite. Journal of Geophysical Research, v. 88, p. 555-568.

Van Hise, C.R., 1896. Principles of North American Pre-Cambrian Geology.

Wilson, G., 1960. The tectonic significance of small scale structures, and their importance to the geologist in the field. Annales de la Societe Geologique de Belgique, T. LXXXIV: 424-548.

APPENDIX

APPENDIX

INTRODUCTION

The Appendix consists of three parts: In Appendix A, I present the method of analysis of uniform shortening of viscous multilayers and extend the analysis to 3rd order accuracy. In Appendix B, I expand the analysis to include layer-parallel shearing deformation in addition to layer-parallel shortening. In both analyses, I derive equations for the mean and perturbed stresses and velocities, the stress and velocity boundary conditions, and the rates of growth of amplitudes.

The differential equations for rates of growth of amplitudes of waveforms are integrated numerically on a computer. In Appendix C, I list computer programs for calculating amplitudes of waveforms to 3rd order accuracy in multilayers subjected to maximum compression parallel to layering ("Folding3rdOrder.bas") and to 2nd order accuracy in multilayers subjected to maximum compression oblique to layering ("Shear.bas"). I also list computer programs for analyzing the corresponding infinitely thick multilayers ("Infmult.bas" and "Infshear.bas", respectively). Finally, I present a computer program for calculating eigenvalues and eigenvectors for the 3rd order analysis ("Eigen.bas").

APPENDIX A

Folding theory analyzes the deformation of a single- or multi-layer in response to applied stresses and velocities. The method that I follow in analyzing the deformation of viscous multilayers was developed by Fletcher (1977) for a single viscous layer embedded in viscous media.

The multilayers I analyze consist of linear viscous layers and are confined above and below by infinitely thick, viscous media. The application of stresses and velocities to the multilayer and media produces internal stresses and velocities which result in the flow of the viscous material. The flow of the viscous materials is governed by the equilibrium equations (the equations of motion), the rheological equations, and the boundary conditions.

The multilayer and media are shortened at a uniform rate by applied layer-parallel compression. The resulting flow of the material at any point within the system is a combination of a mean and a perturbed flow.

The mean flow is uniform throughout the layer and throughout the duration of the deformation because it results from the uniform rate of deformation of a layer with planar interfaces at their mean positions. If interfaces are perturbed about their mean position, a perturbed flow arises which varies both with position in the layer and with time.

Folding occurs if the perturbed flow is unstable, that is, if the perturbed flow increases the departure of the interface from its mean position, which in turn increases the magnitude of the perturbed flow.

We keep track of the response of the layers to the deformation by calculating the change in position of material points on the interfaces of the layers. The position of points on the interface is described by ζ, the height of the interface above the origin of coordinates. In my analyses, the origin of coordinates for each layer is at middepth in that layer, which has a vertical thickness h. The heights of the top (t) and bottom (b) interfaces of a single layer are initially:

$$\zeta_t = h/2 + {}_1A_t \cos(\ell x) \tag{1a}$$

$$\zeta_b = -h/2 + {}_1A_b \cos(\ell x) \tag{1b}$$

The mean positions of the top and bottom interfaces are $h/2$ and $-h/2$, respectively; the variation of points about the mean position is described initially by a cosinusoidal function of amplitude ${}_1A$.

Changes in the heights of points on the interface show the evolution of the interface during deformation. The change in mean height records the amount that the layer has shortened and thickened. The change in perturbed height describes the change in shape of the interface.

The height of the interface changes at any point because of the local flow of the viscous material in response to stresses and velocities at that point. The flow of the material must satisfy the boundary conditions, which specify the relationships of internal stresses and velocities across the interfaces of layers.

An exact description of the interface position is necessary to satisfy the boundary conditions exactly. We can describe the mean height of the interface exactly, so we satisfy the boundary conditions exactly if the layers have planar interfaces. We only describe the perturbed position of the interface approximately, so the solution to the boundary conditions is accordingly approximate when the layer interfaces have a non-planar shape. The approximation enters the analysis only where the position of the interface must be specified in the boundary equations, so the degree of approximation of the analyses is very closely controlled.

The perturbed height of the interface, the shape of the interface, changes initially because the mean internal stresses interact with the perturbed interface. The interaction sets up a perturbed flow and causes the perturbation of the interface to grow and to change shape. Growth of the perturbation further feeds the perturbing flow, which further changes the shape of the interface.

Additional waveforms are necessary to describe the change in shape of an initial, cosinusoidal waveform. The interactions feed the growth of existing waveforms and generate new ones. Each new waveform generates a new perturbed flow. The accuracy with which we describe the deformed shape of the interface determines the number of waveforms we use.

The order of approximation refers to the maximum power to which the slope of the original perturbation is raised. The order of approximation in turn limits the slope which the perturbation may attain and still remain within the limits of the theory. For a 3rd order solution, then, terms proportional to $({}_1\underline{A}\ell)$, $({}_1\underline{A}\ell)^2$, and $({}_1\underline{A}\ell)^3$ are retained, whereas terms proportional to $({}_1\underline{A}\ell)^4$ or to other powers larger than three are considered negligible. The 3rd order analysis of an initial, cosinusoidal waveform with wavelength $\underline{L}$ reveals that second, third, and fourth waveforms, with wavelengths $\underline{L}/2$, $\underline{L}/3$, and $\underline{L}/4$, respectively, develop spontaneously. In the solutions presented here, only terms proportional to $({}_2\underline{A}\ell)$, $({}_3\underline{A}\ell)$, $({}_4\underline{A}\ell)$, or $({}_1\underline{A}\ell)({}_2\underline{A}\ell)$ are retained.

The description of the shape of the interface to 3rd order accuracy involves the use of as many as four component waveforms. Other waveforms may be generated during the deformation, but we consider them to be negligible, to 3rd order accuracy.

To 3rd order, we write the height of the interface in terms of its mean position and a variation about that mean that is described in terms of four component waveforms:

$$\zeta_t = h/2 + {}_1A_t \cos(\ell x) + {}_2A_t \cos(2\ell x)$$

$$+ {}_3A_t \cos(3\ell x) + {}_4A_t \cos(4\ell x) \qquad (2a)$$

$$\zeta_b = -h/2 + {}_1A_b \cos(\ell x) + {}_2A_b \cos(2\ell x)$$

$$+ {}_3A_b \cos(3\ell x) + {}_4A_b \cos(4\ell x) \qquad (2b)$$

The total velocities and stresses within a layer are the sums of the mean and perturbed values,

$$v_x = \bar{v}_x + \tilde{v}_x \qquad (3a)$$

$$v_z = \bar{v}_z + \tilde{v}_z \qquad (3b)$$

$$\sigma_{xx} = \bar{\sigma}_{xx} + \tilde{\sigma}_{xx} \qquad (3c)$$

$$\sigma_{zz} = \bar{\sigma}_{zz} + \tilde{\sigma}_{zz} \qquad (3d)$$

$$\sigma_{xz} = \bar{\sigma}_{xz} + \tilde{\sigma}_{xz} \qquad (3e)$$

For convenience, we analyze the mean and perturbed values separately and then add the two solutions.

The mean stresses and velocities within the layer are

$$\bar{v}_x = x\bar{D}_{xx} \qquad (4a)$$

$$\bar{v}_z = z\bar{D}_{zz} + (\bar{v}_z)_o = (\bar{v}_z)_o - z\bar{D}_{xx} \qquad (4b)$$

$$\bar{\sigma}_{xx} = 2\mu\bar{D}_{xx} - \bar{p} \qquad (4c)$$

$$\bar{\sigma}_{zz} = -2\mu\bar{D}_{xx} - \bar{p} \tag{4d}$$

$$\bar{\sigma}_{xz} = 0 \tag{4e}$$

$$\bar{p} = -(\bar{\sigma}_{xx} + \bar{\sigma}_{zz})/2 \tag{4f}$$

The layer-parallel deformation rate, or shortening rate, is $\underline{\bar{D}}$:

$$\bar{D}_{ij} = (1/2)(\partial\bar{v}_i/\partial x_j + \partial\bar{v}_j/\partial x_i) \tag{4g}$$

For incompressible materials, the rate of layer-parallel shortening is equal to the rate of layer-normal thickening

$$\bar{D}_{xx} = -\bar{D}_{zz} \tag{4h}$$

The perturbed values satisfy the biharmonic equation in the stream function, ψ:

$$\nabla^4\psi = 0 \tag{5a}$$

The stream function ψ for this problem is

$$\psi = (1/j\ell)\ {}_jg(z)\ \sin(j\ell x);\ j = 1,2,3,4 \text{ (results summed)} \tag{5b}$$

in which ℓ is the wavenumber, $\ell = 2\pi/\underline{L}$, $\underline{L}$ is the wavelength of the perturbation, and ${}_j\underline{g}$ are functions of $\underline{z}$.

The perturbed velocities are derivatives of the stream function:

$$\tilde{v}_z = \partial\psi/\partial x;\ \tilde{v}_x = -\partial\psi/\partial z \tag{5c}$$

Performing the derivatives indicated in eq. (5c) provides solutions for the perturbed velocities. The solutions for the perturbed stresses are derived by substituting the perturbed velocities into the rheological equations. The results are:

$$\tilde{v}_z = [\{{}_j a + {}_j b(j\ell z)\} \cosh(j\ell z)$$

$$+ \{{}_j c + {}_j d(j\ell z)\} \sinh(j\ell z)] \cos(j\ell x) \tag{6a}$$

$$\tilde{v}_x = -[\{{}_j a + {}_j d + {}_j b(j\ell z)\} \sinh(j\ell z)$$

$$+ \{{}_j b + {}_j c + {}_j d(j\ell z)\} \cosh(j\ell z)] \sin(j\ell x) \tag{6b}$$

$$\tilde{\sigma}_{zz} = 2j\mu\ell[\{{}_j a + {}_j b(j\ell z)\} \sinh(j\ell z)$$

$$+ \{{}_j c + {}_j d(j\ell z)\} \cosh(j\ell z)] \cos(j\ell x) - \tilde{p}_o \tag{6c}$$

$$\tilde{\sigma}_{xx} = -2j\mu\ell[\{{}_j a + 2{}_j d + {}_j b(j\ell z)\} \sinh(j\ell z)$$

$$+ \{{}_j c + 2{}_j b + {}_j d(j\ell z)\} \cosh(j\ell z)] \cos(j\ell x) - \tilde{p}_o \tag{6d}$$

$$\tilde{\sigma}_{xz} = -2j\mu\ell[\{{}_j a + {}_j d + {}_j b(j\ell z)\} \cosh(j\ell z)$$

$$+ \{{}_j c + {}_j b + {}_j d(j\ell z)\} \sinh(j\ell z)] \sin(j\ell x) \tag{6e}$$

in which $\underline{j}$ = 1,2,3,4 (results summed).

Each of the four waveforms used to describe the shape of the interface gives rise to a set of perturbed stresses and velocities, generated from eq. (6) by letting $\underline{j}$ take on values of one, two, three, and four. The quantities ${}_1\underline{a}$, ${}_2\underline{a}$,

${}_3\underline{a}$, ${}_4\underline{a}$, ${}_1\underline{b}$, ..., ${}_4\underline{d}$ in eq. (6) are arbitrary constants which will be eliminated by means of the velocity and stress boundary conditions.

So far, the equations for the perturbed stresses and velocities are exact and apply at any point within the layer. However, we need to describe the stresses and velocities at the interfaces. Insofar as the description of the position of the interface is approximate, the expressions for the stresses and velocities at the interface become approximate. Because I describe the shape of the interface to 3rd order accuracy, I derive the expressions for the perturbed stresses and velocities to 3rd order accuracy.

The 3rd order expressions for the perturbed stresses and velocities are derived by substituting the 3rd order expression for the height of the interface, ζ (eq. 2), for $\underline{z}$ in eq. (6), maintaining 3rd order accuracy. The same order of approximation is used in the series expansion for the cosh and sinh functions, which also contain the approximation for the height of the interface.

Expressions for the perturbed stresses and velocities, to 3rd order accuracy, are:

$$[\tilde{v}_z] = [\{{}_ja \pm {}_jbjk\}({}_jC) + \{\pm{}_jc + {}_jdjk\}({}_jS)]\ \cos(j\ell x)$$

$$+\ j[\{{}_jb + {}_jc \pm {}_jdjk\}({}_jC)$$

$$+\ \{\pm{}_ja \pm {}_jd + {}_jbjk\}({}_jS)]\ ({}_1A\ell)\cos(\ell x)\ \cos(j\ell x)$$

$$+\ j[\{{}_jb + {}_jc \pm {}_jdjk\}({}_jC)$$

$$+\ \{\pm{}_ja \pm {}_jd + {}_jbjk\}({}_jS)]\ ({}_2A\ell)\cos(2\ell x)\ \cos(j\ell x)$$

$$+\ (j^2/2)[\{{}_ja + 2{}_jd \pm {}_jbjk\}({}_jC)$$

$$+\ \{\pm{}_jc \pm 2{}_jb + {}_jdjk\}({}_jS)]\ [({}_1A\ell)\cos(\ell x)]^2\ \cos(j\ell x) \tag{7a}$$

$$[\tilde{v}_x] = -\ [\{{}_jb + {}_jc \pm {}_jdjk\}({}_jC) + \{\pm{}_ja \pm {}_jd + {}_jbjk\}({}_jS)]\ \sin(j\ell x)$$

$$-\ j[\{{}_ja + 2{}_jd \pm {}_jbjk\}({}_jC)$$

$$+\ \{\pm{}_jc \pm 2{}_jb + {}_jdjk\}({}_jS)]\ ({}_1A\ell)\cos(\ell x)\ \sin(j\ell x)$$

$$-\ j[\{{}_ja + 2{}_jd \pm {}_jbjk\}({}_jC)$$

$$+\ \{\pm{}_jc \pm 2{}_jb + {}_jdjk\}({}_jS)]\ ({}_2A\ell)\cos(2\ell x)\ \sin(j\ell x)$$

$$-\ (j^2/2)[\{{}_jc + 3{}_jb \pm {}_jdjk\}({}_jC)$$

$$+\ \{\pm{}_ja \pm 3{}_jd + {}_jbjk\}({}_jS)]\ [({}_1A\ell)\cos(\ell x)]^2\ \sin(j\ell x) \tag{7b}$$

$$[\tilde{\sigma}_{zz}] = 2j\mu\ell[\{{}_jc\pm{}_jdjk\}({}_jC) + \{\pm{}_ja+{}_jbjk\}({}_jS)]\cos(\ell x)$$

$$+ 2(j^2)\mu\ell[\{{}_ja+{}_jd\pm{}_jbjk\}({}_jC)$$

$$+ \{\pm{}_jc\pm{}_jb+{}_jdjk\}({}_jS)]\ ({}_1A\ell)\cos(\ell x)\ \cos(j\ell x)$$

$$+ 2(j^2)\mu\ell[\{{}_ja+{}_jd\pm{}_jbjk\}({}_jC)$$

$$+ \{\pm{}_jc\pm{}_jb+{}_jdjk\}({}_jS)]\ ({}_2A\ell)\cos(2\ell x)\ \cos(j\ell x)$$

$$+ 2(j^3/2)\mu\ell[\{{}_jc+2{}_jb\pm{}_jdjk\}({}_jC)$$

$$+ \{\pm{}_ja\pm2{}_jd+{}_jbjk\}({}_jS)]\ [({}_1A\ell)\cos(\ell x)]^2\ \cos(j\ell x)$$

$$- \bar{p}_o + \rho gz \tag{7c}$$

$$[\tilde{\sigma}_{xx}] = -\ 2j\mu\ell[\{{}_jc+2{}_jb\pm{}_jdjk\}({}_jC)$$

$$+ \{\pm{}_ja\pm2{}_jd+{}_jbjk\}({}_jS)]\ \cos(j\ell x)$$

$$- 2(j^2)\mu\ell[\{{}_ja+3{}_jd\pm{}_jbjk\}({}_jC)$$

$$+ \{\pm{}_jc\pm3{}_jb+{}_jdjk\}({}_jS)]\ ({}_1A\ell)\cos(\ell x)\ \cos(j\ell x)$$

$$- 2(j^2)\mu\ell[\{{}_ja+3{}_jd\pm{}_jbjk\}({}_jC)$$

$$+ \{\pm{}_jc\pm3{}_jb+{}_jdjk\}({}_jS)]\ ({}_2A\ell)\cos(2\ell x)\ \cos(j\ell x)$$

$$- 2(j^3/2)\mu\ell[\{{}_jc+4{}_jb\pm{}_jdjk\}({}_jC)$$

$$+ \{\pm{}_ja\pm4{}_jd+bjk\}({}_jS)]\ [({}_1A\ell)\cos(\ell x)]^2\ \cos(j\ell x)$$

$$- \bar{p}_o + \rho gz \tag{7d}$$

$$[\tilde{\sigma}_{xz}] = -2j\mu\ell[\{_ja+_jd\pm_jbjk\}(_jC) + \{\pm_jc\pm_jb+_jdjk\}(_jS)]\ \sin(j\ell x)$$

$$- 2(j^2)\mu\ell[\{_jc+2_jb\pm_jdjk\}(_jC)$$

$$+ \{\pm_ja\pm 2_jd+_jbjk\}(_jS)]\ (_1A\ell)\cos(\ell x)\ \sin(j\ell x)$$

$$- 2(j^2)\mu\ell[\{_jc+2_jb\pm_jdjk\}(_jC)$$

$$+ \{\pm_ja\pm 2_jd+_jbjk\}(_jS)]\ (_2A\ell)\cos(2\ell x)\ \sin(j\ell x)$$

$$- 2(j^3/2)\mu\ell[\{_ja+3_jd\pm_jbjk\}(_jC)$$

$$+ \{\pm_jc\pm 3_jb+_jdjk\}(_jS)]\ [(_1A\ell)\cos(\ell x)]^2\ \sin(j\ell x) \qquad (7e)$$

in which

$_j\underline{C} = \cosh(\underline{jk})$ and $_j\underline{S} = \sinh(\underline{jk})$

$\underline{j}$ is the waveform number ($\underline{j}$ = 1,2,3, or 4)

$\underline{k} = \ell(\underline{h}/2)$

ℓ is the wavenumber, $\ell = 2\pi/L$

$\underline{L}$ is the wavelength of the first component waveform

$\underline{h}$ is the vertical thickness of a layer.

The "±" sign refers to the top (+) and bottom (-) of a layer.

Each of the arbitrary constants in eq. (7) is actually a composite of constants, each of which is proportional to 1st or higher order in $({}_1\underline{A}\ell)$, $(2_2\underline{A}\ell)$, $(3_3\underline{A}\ell)$, or $(4_4\underline{A}\ell)$. It is helpful to rewrite the composite constants in a way that indicates explicitly their dependencies on orders of approximation. The following notation has proven to be convenient: the leading subscript indicates the waveform with which the constant is associated; the leading superscript indicates the product of maximum slopes that enters the expression for that constant. For example,

$$ {}_1a = {}^1_1a + {}^{11}_{1}a + {}^{12}_{1}a + {}^{111}_{1}a \tag{8a} $$

in which ${}^1_1\underline{a}$ is for the first waveform (subscript "1") and is to 1st order in $({}_1\underline{A}\ell)$ (superscript "1"); ${}^{11}_{1}\underline{a}$ is also for the first waveform, as are ${}^{12}_{1}\underline{a}$ and ${}^{111}_{1}\underline{a}$, but ${}^{11}_{1}\underline{a}$ is to 2nd order in the slope of the first waveform $({}_1\underline{A}\ell)$ (superscript "11"), ${}^{12}_{1}\underline{a}$ is to order $({}_1\underline{A}\ell)(2_2\underline{A}\ell)$ (superscript "12"), and ${}^{111}_{1}\underline{a}$ is to 3rd order in $({}_1\underline{A}\ell)$ (superscript "111"). Similarly, the constant ${}_2\underline{a}$ stands for a composite of constants

$$ {}_2a = {}^2_2a + {}^{11}_{2}a + {}^{12}_{2}a + {}^{111}_{2}a \tag{8b} $$

in which ${}^2_2\underline{a}$ is for the second waveform (subscript "2") and is to 1st order in $(2_2\underline{A}\ell)$ (superscript "2"), whereas ${}^{11}_{2}\underline{a}$ and ${}^{111}_{2}\underline{a}$ are to 2nd and 3rd orders, respectively, in $({}_1\underline{A}\ell)$.

The expanded expressions for the constants for the third and fourth waveforms are:

$$ {}_{3}a = {}^{3}_{3}a + {}^{11}_{3}a + {}^{12}_{3}a + {}^{111}_{3}a \tag{8c} $$

$$ {}_{4}a = {}^{4}_{4}a + {}^{12}_{4}a + {}^{111}_{4}a \tag{8d} $$

Finally, we rewrite the expressions for the perturbed stresses and velocities, eq. (7), using the components of the arbitrary constants, eq. (8), and trigonometric identities to regroup terms according to waveform. The expressions for the perturbed stresses and velocities become:

$$
\begin{aligned}
[\check{v}_z] = \Big\{ & [\{{}^{1}_{1}a \pm {}^{1}_{1}bk\}({}_{1}C) + \{\pm {}^{1}_{1}c + {}^{1}_{1}dk\}({}_{1}S)] \\
&+ [\{{}^{11}_{1}a \pm {}^{11}_{1}bk\}({}_{1}C) + \{\pm {}^{11}_{1}c + {}^{11}_{1}dk\}({}_{1}S)] \\
&+ (1/2)[\{{}^{1}_{1}b + {}^{1}_{1}c \pm {}^{1}_{1}dk\}({}_{1}C) + \{\pm {}^{1}_{1}a \pm {}^{1}_{1}d + {}^{1}_{1}bk\}({}_{1}S)]({}_{2}A\ell) \\
&+ [\{{}^{2}_{2}b + {}^{2}_{2}c \pm 2{}^{2}_{2}dk\}({}_{2}C) + \{\pm {}^{2}_{2}a \pm {}^{2}_{2}d + 2{}^{2}_{2}bk\}({}_{2}S)]({}_{1}A\ell) \\
&+ [\{{}^{12}_{1}a \pm {}^{12}_{1}bk\}({}_{1}C) + \{\pm {}^{12}_{1}c + {}^{12}_{1}dk\}({}_{1}S)] \\
&+ (3/8)[\{{}^{1}_{1}a + 2{}^{1}_{1}d \pm {}^{1}_{1}bk\}({}_{1}C) + \{\pm {}^{1}_{1}c \pm 2{}^{1}_{1}b + {}^{1}_{1}dk\}({}_{1}S)]({}_{1}A\ell)^2 \\
&+ [\{{}^{11}_{2}c + {}^{11}_{2}b \pm 2{}^{11}_{2}dk\}({}_{2}C) + \{\pm {}^{11}_{2}a \pm {}^{11}_{2}d + 2{}^{11}_{2}bk\}({}_{2}S)]({}_{1}A\ell) \\
&+ [\{{}^{111}_{1}a \pm {}^{111}_{1}bk\}({}_{1}C) + \{\pm {}^{111}_{1}c + {}^{111}_{1}dk\}({}_{1}S)] \Big\} \qquad \cos(\ell x) \\
+ \\
\Big\{ & [\{{}^{2}_{2}a \pm 2{}^{2}_{2}bk\}({}_{2}C) + \{\pm {}^{2}_{2}c + 2{}^{2}_{2}dk\}({}_{2}S)] \\
&+ (1/2)[\{{}^{1}_{1}b + {}^{1}_{1}c \pm {}^{1}_{1}dk\}({}_{1}C) + \{\pm {}^{1}_{1}a \pm {}^{1}_{1}d + {}^{1}_{1}bk\}({}_{1}S)]({}_{1}A\ell) \\
&+ [\{{}^{11}_{2}a \pm 2{}^{11}_{2}bk\}({}_{2}C) + \{\pm {}^{11}_{2}c + 2{}^{11}_{2}dk\}({}_{2}S)] \\
&+ [\{{}^{12}_{2}a \pm 2{}^{12}_{2}bk\}({}_{2}C) + \{\pm {}^{12}_{2}c + 2{}^{12}_{2}dk\}({}_{2}S)]
\end{aligned}
$$

$$+\ (1/2)[\{{}^{1}{}^{1}_{1}c+{}^{1}{}^{1}_{1}b\pm{}^{1}{}^{1}_{1}dk\}({}_{1}C)$$
$$+\ \{\pm{}^{1}{}^{1}_{1}a\pm{}^{1}{}^{1}_{1}d+{}^{1}{}^{1}_{1}bk\}({}_{1}S)]({}_{1}A\ell)$$

$$+\ (3/2)[\{{}^{1}{}^{1}_{3}c+{}^{1}{}^{1}_{3}b\pm 3{}^{1}{}^{1}_{3}dk\}({}_{3}C)$$
$$+\ \{\pm{}^{1}{}^{1}_{3}a\pm{}^{1}{}^{1}_{3}d+3{}^{1}{}^{1}_{3}bk\}({}_{3}S)]({}_{1}A\ell)$$

$$+\ [\{{}^{11}{}^{1}_{2}a\pm 2{}^{11}{}^{1}_{2}bk\}({}_{2}C)+\{\pm{}^{11}{}^{1}_{2}c+2{}^{11}{}^{1}_{2}dk\}({}_{2}S)]\ \Big\}\qquad \cos(2\ell x)$$

$+$

$$\Big\{\ [\{{}^{3}_{3}a\pm 3{}^{3}_{3}bk\}({}_{3}C)+\{\pm{}^{3}_{3}c+3{}^{3}_{3}dk\}({}_{3}S)]$$

$$+\ [\{{}^{1}{}^{1}_{3}a\pm 3{}^{1}{}^{1}_{3}bk\}({}_{3}C)+\{\pm{}^{1}{}^{1}_{3}c+3{}^{1}{}^{1}_{3}dk\}({}_{3}S)]$$

$$+\ (1/2)[\{{}^{1}_{1}b+{}^{1}_{1}c\pm{}^{1}_{1}dk\}({}_{1}C)+\{\pm{}^{1}_{1}a\pm{}^{1}_{1}d+{}^{1}_{1}bk\}({}_{1}S)]({}_{2}A\ell)$$

$$+\ [\{{}^{2}_{2}b+{}^{2}_{2}c\pm 2{}^{2}_{2}dk\}({}_{2}C)+\{\pm{}^{2}_{2}a\pm{}^{2}_{2}d+2{}^{2}_{2}bk\}({}_{2}S)]({}_{1}A\ell)$$

$$+\ [\{{}^{1}{}^{2}_{3}a\pm 3{}^{1}{}^{2}_{3}bk\}({}_{3}C)+\{\pm{}^{1}{}^{2}_{3}c+3{}^{1}{}^{2}_{3}dk\}({}_{3}S)]$$

$$+\ (1/8)[\{{}^{1}_{1}a+2{}^{1}_{1}d\pm{}^{1}_{1}bk\}({}_{1}C)+\{\pm{}^{1}_{1}c\pm 2{}^{1}_{1}b+{}^{1}_{1}dk\}({}_{1}S)]({}_{1}A\ell)^{2}$$

$$+\ [\{{}^{1}{}^{1}_{2}c+{}^{1}{}^{1}_{2}b\pm 2{}^{1}{}^{1}_{2}dk\}({}_{2}C)+\{\pm{}^{1}{}^{1}_{2}a\pm{}^{1}{}^{1}_{2}d+2{}^{1}{}^{1}_{2}bk\}({}_{2}S)]({}_{1}A\ell)$$

$$+\ [\{{}^{11}{}^{1}_{3}a\pm 3{}^{11}{}^{1}_{3}bk\}({}_{3}C)+\{\pm{}^{11}{}^{1}_{3}c+3{}^{11}{}^{1}_{3}dk\}({}_{3}S)]\ \Big\}\qquad \cos(3\ell x)$$

$+$

$$\Big\{\ [\{{}^{4}_{4}a\pm 4{}^{4}_{4}bk\}({}_{4}C)+\{\pm{}^{4}_{4}c+4{}^{4}_{4}dk\}({}_{4}S)]$$

$$+\ [\{{}^{1}{}^{2}_{4}a\pm 4{}^{1}{}^{2}_{4}bk\}({}_{4}C)+\{\pm{}^{1}{}^{2}_{4}c+4{}^{1}{}^{2}_{4}dk\}({}_{4}S)]$$

$$+\ (1/2)[\{{}^{1}{}^{1}_{1}c+{}^{1}{}^{1}_{1}b\pm{}^{1}{}^{1}_{1}dk\}({}_{1}C)$$
$$+\ \{\pm{}^{1}{}^{1}_{1}a\pm{}^{1}{}^{1}_{1}d+{}^{1}{}^{1}_{1}bk\}({}_{1}S)]({}_{1}A\ell)$$

$$+\ (3/2)[\{{}^{1}{}^{1}_{3}c+{}^{1}{}^{1}_{3}b\pm 3{}^{1}{}^{1}_{3}dk\}({}_{3}C)$$
$$+\ \{\pm{}^{1}{}^{1}_{3}a\pm{}^{1}{}^{1}_{3}d+3{}^{1}{}^{1}_{3}bk\}({}_{3}S)]({}_{1}A\ell)$$

$$+\ [\{{}^{11}{}^{1}_{4}a\pm 4{}^{11}{}^{1}_{4}bk\}({}_{4}C)+\{\pm{}^{11}{}^{1}_{4}c+4{}^{11}{}^{1}_{4}dk\}({}_{4}S)]\ \Big\}\qquad \cos(4\ell x)$$

$+$

$$+\ (1/2)[\{{}^{1}_{1}b+{}^{1}_{1}c\pm{}^{1}_{1}dk\}({}_{1}C)+\{\pm{}^{1}_{1}a\pm{}^{1}_{1}d+{}^{1}_{1}bk\}({}_{1}S)]({}_{1}A\ell)\qquad (9a)$$

$$
\begin{aligned}
[\tilde{v}_x] = \Big\{ & - [\{{}^{1}_{1}b+{}^{1}_{1}c\pm{}^{1}_{1}dk\}({}_{1}C) + \{\pm{}^{1}_{1}a\pm{}^{1}_{1}d+{}^{1}_{1}bk\}({}_{1}S)] \\
& - [\{{}^{11}_{1}b+{}^{11}_{1}c\pm{}^{11}_{1}dk\}({}_{1}C) + \{\pm{}^{11}_{1}a\pm{}^{11}_{1}d+{}^{11}_{1}bk\}({}_{1}S)] \\
& + (1/2)[\{{}^{1}_{1}a+2{}^{1}_{1}d\pm{}^{1}_{1}bk\}({}_{1}C) + \{\pm{}^{1}_{1}c\pm 2{}^{1}_{1}b+{}^{1}_{1}dk\}({}_{1}S)]({}_{2}A\ell) \\
& - [\{{}^{2}_{2}a+2{}^{2}_{2}d\pm 2{}^{2}_{2}bk\}({}_{2}C) + \{\pm{}^{2}_{2}c\pm 2{}^{2}_{2}b+2{}^{2}_{2}dk\}({}_{2}S)]({}_{1}A\ell) \\
& - [\{{}^{12}_{1}b+{}^{12}_{1}c\pm{}^{12}_{1}dk\}({}_{1}C) + \{\pm{}^{12}_{1}a\pm{}^{12}_{1}d+{}^{12}_{1}bk\}({}_{1}S)] \\
& - (1/8)[\{{}^{1}_{1}c+3{}^{1}_{1}b\pm{}^{1}_{1}dk\}({}_{1}C) + \{\pm{}^{1}_{1}a\pm 3{}^{1}_{1}d+{}^{1}_{1}bk\}({}_{1}S)]({}_{1}A\ell)^2 \\
& - [\{{}^{11}_{2}a+2{}^{11}_{2}d\pm 2{}^{11}_{2}bk\}({}_{2}C) \\
& \qquad\qquad + \{\pm{}^{11}_{2}c\pm 2{}^{11}_{2}b+2{}^{11}_{2}dk\}({}_{2}S)]({}_{1}A\ell) \\
& - [\{{}^{111}_{1}b+{}^{111}_{1}c\pm{}^{111}_{1}dk\}({}_{1}C) \\
& \qquad\qquad + \{\pm{}^{111}_{1}a\pm{}^{111}_{1}d+{}^{111}_{1}bk\}({}_{1}S)] \Big\} \qquad \sin(\ell x) \\
+ & \\
\Big\{ & - [\{{}^{2}_{2}b+{}^{2}_{2}c\pm 2{}^{2}_{2}dk\}({}_{2}C) + \{\pm{}^{2}_{2}a\pm{}^{2}_{2}d+2{}^{2}_{2}bk\}({}_{2}S)] \\
& - (1/2)[\{{}^{1}_{1}a+2{}^{1}_{1}d\pm{}^{1}_{1}bk\}({}_{1}C) + \{\pm{}^{1}_{1}c\pm 2{}^{1}_{1}b+{}^{1}_{1}dk\}({}_{1}S)]({}_{1}A\ell) \\
& - [\{{}^{11}_{2}b+{}^{11}_{2}c\pm 2{}^{11}_{2}dk\}({}_{2}C) + \{\pm{}^{11}_{2}a\pm{}^{11}_{2}d+2{}^{11}_{2}bk\}({}_{2}S)] \\
& - [\{{}^{12}_{2}b+{}^{12}_{2}c\pm 2{}^{12}_{2}dk\}({}_{2}C) + \{\pm{}^{12}_{2}a\pm{}^{12}_{2}d+2{}^{12}_{2}bk\}({}_{2}S)] \\
& - (1/2)[\{{}^{11}_{1}a+2{}^{11}_{1}d\pm{}^{11}_{1}bk\}({}_{1}C) \\
& \qquad\qquad + \{\pm{}^{11}_{1}c\pm 2{}^{11}_{1}b+{}^{11}_{1}dk\}({}_{1}S)]({}_{1}A\ell) \\
& - (3/2)[\{{}^{11}_{3}a+2{}^{11}_{3}d\pm 3{}^{11}_{3}bk\}({}_{3}C) \\
& \qquad\qquad + \{\pm{}^{11}_{3}c\pm 2{}^{11}_{3}b+3{}^{11}_{3}dk\}({}_{3}S)]({}_{1}A\ell) \\
& - [\{{}^{111}_{2}b+{}^{111}_{2}c\pm 2{}^{111}_{2}dk\}({}_{2}C) \\
& \qquad\qquad + \{\pm{}^{111}_{2}a\pm{}^{111}_{2}d+2{}^{111}_{2}bk\}({}_{2}S)] \Big\} \qquad \sin(2\ell x) \\
+ & \\
\Big\{ & - [\{{}^{3}_{3}b+{}^{3}_{3}c\pm 3{}^{3}_{3}dk\}({}_{3}C) + \{\pm{}^{3}_{3}a\pm{}^{3}_{3}d+3{}^{3}_{3}bk\}({}_{3}S)] \\
& - [\{{}^{11}_{3}b+{}^{11}_{3}c\pm 3{}^{11}_{3}dk\}({}_{3}C) + \{\pm{}^{11}_{3}a\pm{}^{11}_{3}d+3{}^{11}_{3}bk\}({}_{3}S)] \\
& - (1/2)[\{{}^{1}_{1}a+2{}^{1}_{1}d\pm{}^{1}_{1}bk\}({}_{1}C) + \{\pm{}^{1}_{1}c\pm 2{}^{1}_{1}b+{}^{1}_{1}dk\}({}_{1}S)]({}_{2}A\ell) \\
& - [\{{}^{2}_{2}a+2{}^{2}_{2}d\pm 2{}^{2}_{2}bk\}({}_{2}C) + \{\pm{}^{2}_{2}c\pm 2{}^{2}_{2}b+2{}^{2}_{2}dk\}({}_{2}S)]({}_{1}A\ell)
\end{aligned}
$$

$$- [\{{}^{1}{}^{2}_{3}b+{}^{1}{}^{2}_{3}c\pm 3\,{}^{1}{}^{2}_{3}dk\}({}_{3}C) + \{\pm{}^{1}{}^{2}_{3}a\pm{}^{1}{}^{2}_{3}d+3\,{}^{1}{}^{2}_{3}bk\}({}_{3}S)]$$

$$- (1/8)[\{{}^{1}_{1}c+3\,{}^{1}_{1}b\pm{}^{1}_{1}dk\}({}_{1}C) + \{\pm{}^{1}_{1}a\pm 3\,{}^{1}_{1}d+{}^{1}_{1}bk\}({}_{1}S)]({}_{1}A\ell)^{2}$$

$$- [\{{}^{1}{}^{1}_{2}a+2\,{}^{1}{}^{1}_{2}d\pm 2\,{}^{1}{}^{1}_{2}bk\}({}_{2}C) + \{\pm{}^{1}{}^{1}_{2}c\pm 2\,{}^{1}{}^{1}_{2}b+2\,{}^{1}{}^{1}_{2}dk\}({}_{2}S)]({}_{1}A\ell)$$

$$- [\{{}^{11}{}^{1}_{3}b+{}^{11}{}^{1}_{3}c\pm 3\,{}^{11}{}^{1}_{3}dk\}({}_{3}C) + \{\pm{}^{11}{}^{1}_{3}a\pm{}^{11}{}^{1}_{3}d+3\,{}^{11}{}^{1}_{3}bk\}({}_{3}S)] \Big\} \quad \sin(3\ell x)$$

$$+$$

$$\Big\{ - [\{{}^{4}_{4}b+{}^{4}_{4}c\pm 4\,{}^{4}_{4}dk\}({}_{4}C) + \{\pm{}^{4}_{4}a\pm{}^{4}_{4}d+4\,{}^{4}_{4}bk\}({}_{4}S)]$$

$$- [\{{}^{1}{}^{2}_{4}b+{}^{1}{}^{2}_{4}c\pm 4\,{}^{1}{}^{2}_{4}dk\}({}_{4}C) + \{\pm{}^{1}{}^{2}_{4}a\pm{}^{1}{}^{2}_{4}d+4\,{}^{1}{}^{2}_{4}bk\}({}_{4}S)]$$

$$- (3/2)[\{{}^{1}{}^{1}_{3}a+2\,{}^{1}{}^{1}_{3}d\pm 3\,{}^{1}{}^{1}_{3}bk\}({}_{3}C) + \{\pm{}^{1}{}^{1}_{3}c\pm 2\,{}^{1}{}^{1}_{3}b+3\,{}^{1}{}^{1}_{3}dk\}({}_{3}S)]({}_{1}A\ell)$$

$$- [\{{}^{11}{}^{1}_{4}b+{}^{11}{}^{1}_{4}c\pm 4\,{}^{11}{}^{1}_{4}dk\}({}_{4}C) + \{\pm{}^{11}{}^{1}_{4}a\pm{}^{11}{}^{1}_{4}d+4\,{}^{11}{}^{1}_{4}bk\}({}_{4}S)] \Big\} \quad \sin(4\ell x)$$

(9b)

$$[\tilde{\sigma}_{zz}] = \Big\{2\mu\ell[\{{}^{1}_{1}c\pm{}^{1}_{1}dk\}({}_{1}C) + \{\pm{}^{1}_{1}a+{}^{1}_{1}bk\}({}_{1}S)]$$

$$+ 2\mu\ell[\{{}^{1}{}^{1}_{1}c\pm{}^{1}{}^{1}_{1}dk\}({}_{1}C) + \{\pm{}^{1}{}^{1}_{1}a+{}^{1}{}^{1}_{1}bk\}({}_{1}S)]$$

$$+ \mu\ell[\{{}^{1}_{1}a+{}^{1}_{1}d\pm{}^{1}_{1}bk\}({}_{1}C) + \{\pm{}^{1}_{1}c\pm{}^{1}_{1}b+{}^{1}_{1}dk\}({}_{1}S)]({}_{2}A\ell)$$

$$+ 4\mu\ell[\{{}^{2}_{2}a+{}^{2}_{2}d\pm 2\,{}^{2}_{2}bk\}({}_{2}C) + \{\pm{}^{2}_{2}c\pm{}^{2}_{2}b+2\,{}^{2}_{2}dk\}({}_{2}S)]({}_{1}A\ell)$$

$$+ 2\mu\ell[\{{}^{1}{}^{2}_{1}c\pm{}^{1}{}^{2}_{1}dk\}({}_{1}C) + (\pm{}^{1}{}^{2}_{1}a+{}^{1}{}^{2}_{1}bk\}({}_{1}S)]$$

$$+ (3\mu\ell/4)[\{{}^{1}_{1}c+2\,{}^{1}_{1}b\pm{}^{1}_{1}dk\}({}_{1}C) + \{\pm{}^{1}_{1}a\pm 2\,{}^{1}_{1}d+{}^{1}_{1}bk\}({}_{1}S)]({}_{1}A\ell)^{2}$$

$$+ 4\mu\ell[\{{}^{1}{}^{1}_{2}a+{}^{1}{}^{1}_{2}d\pm 2\,{}^{1}{}^{1}_{2}bk\}({}_{2}C) + \{\pm{}^{1}{}^{1}_{2}c\pm{}^{1}{}^{1}_{2}b+2\,{}^{1}{}^{1}_{2}dk\}({}_{2}S)]({}_{1}A\ell)$$

$$+ 2\mu\ell[\{{}^{11}{}^{1}_{1}c\pm{}^{11}{}^{1}_{1}dk\}({}_{1}C) + \{\pm{}^{11}{}^{1}_{1}a+{}^{11}{}^{1}_{1}bk\}({}_{1}S)] \Big\} \quad \cos(\ell x)$$

$$+$$

$$\Big\{ + 4\mu\ell[\{{}^{2}_{2}c\pm 2\,{}^{2}_{2}dk\}({}_{2}C) + \{\pm{}^{2}_{2}a+2\,{}^{2}_{2}bk\}({}_{2}S)]$$

$$+ \mu\ell[\{{}^{1}_{1}a+{}^{1}_{1}d\pm{}^{1}_{1}bk\}({}_{1}C) + \{\pm{}^{1}_{1}c\pm{}^{1}_{1}b+{}^{1}_{1}dk\}({}_{1}S)]({}_{1}A\ell)$$

$$+\ 4\mu\ell[\{{}^{1}{}^{1}_{2}c \pm 2\,{}^{1}{}^{1}_{2}dk\}({}_{2}C) + \{\pm\,{}^{1}{}^{1}_{2}a + 2\,{}^{1}{}^{1}_{2}bk\}({}_{2}S)]$$

$$+\ 4\mu\ell[\{{}^{1}{}^{2}_{2}c \pm 2\,{}^{1}{}^{2}_{2}dk\}({}_{2}C) + \{\pm\,{}^{1}{}^{2}_{2}a + 2\,{}^{1}{}^{2}_{2}bk\}({}_{2}S)]$$

$$+\ \mu\ell[\{{}^{1}{}^{1}_{1}a + {}^{1}{}^{1}_{1}d \pm {}^{1}{}^{1}_{1}bk\}({}_{1}C) + \{\pm\,{}^{1}{}^{1}_{1}c \pm {}^{1}{}^{1}_{1}b + {}^{1}{}^{1}_{1}dk\}({}_{1}S)]({}_{1}A\ell)$$

$$\begin{aligned}+\ 9\mu\ell[\{{}^{1}{}^{1}_{3}a + {}^{1}{}^{1}_{3}d \pm 3\,{}^{1}{}^{1}_{3}bk\}({}_{3}C) \\ + \{\pm\,{}^{1}{}^{1}_{3}c \pm {}^{1}{}^{1}_{3}b + 3\,{}^{1}{}^{1}_{3}dk\}({}_{3}S)]({}_{1}A\ell)\end{aligned}$$

$$+\ 4\mu\ell[\{{}^{11}{}^{1}_{2}c \pm 2\,{}^{11}{}^{1}_{2}dk\}({}_{2}C) + \{\pm\,{}^{11}{}^{1}_{2}a + 2\,{}^{11}{}^{1}_{2}bk\}({}_{2}S)]\ \Big\} \qquad \cos(2\ell x)$$

$+$

$$\Big\{\ +\ 6\mu\ell[\{{}^{3}_{3}c \pm 3\,{}^{3}_{3}dk\}({}_{3}C) + \{\pm\,{}^{3}_{3}a + 3\,{}^{3}_{3}bk\}({}_{3}S)]$$

$$+\ 6\mu\ell[\{{}^{1}{}^{1}_{3}c \pm 3\,{}^{1}{}^{1}_{3}dk\}({}_{3}C) + \{\pm\,{}^{1}{}^{1}_{3}a + 3\,{}^{1}{}^{1}_{3}bk\}({}_{3}S)]$$

$$+\ \mu\ell[\{{}^{1}_{1}a + {}^{1}_{1}d \pm {}^{1}_{1}bk\}({}_{1}C) + \{\pm\,{}^{1}_{1}c \pm {}^{1}_{1}b + {}^{1}_{1}dk\}({}_{1}S)]({}_{2}A\ell)$$

$$+\ 4\mu\ell[\{{}^{2}_{2}a + {}^{2}_{2}d \pm 2\,{}^{2}_{2}bk\}({}_{2}C) + \{\pm\,{}^{2}_{2}c \pm {}^{2}_{2}b + 2\,{}^{2}_{2}dk\}({}_{2}S)]({}_{1}A\ell)$$

$$+\ 6\mu\ell[\{{}^{1}{}^{2}_{3}c \pm 3\,{}^{1}{}^{2}_{3}dk\}({}_{3}C) + \{\pm\,{}^{1}{}^{2}_{3}a + 3\,{}^{1}{}^{2}_{3}bk\}({}_{3}S)]$$

$$\begin{aligned}+\ (\mu\ell/4)[\{{}^{1}_{1}c + 2\,{}^{1}_{1}b \pm {}^{1}_{1}dk\}({}_{1}C) \\ + \{\pm\,{}^{1}_{1}a \pm 2\,{}^{1}_{1}d + {}^{1}_{1}bk\}({}_{1}S)]({}_{1}A\ell)^{2}\end{aligned}$$

$$\begin{aligned}+\ 4\mu\ell[\{{}^{1}{}^{1}_{2}a + {}^{1}{}^{1}_{2}d \pm 2\,{}^{1}{}^{1}_{2}bk\}({}_{2}C) \\ + \{\pm\,{}^{1}{}^{1}_{2}c \pm {}^{1}{}^{1}_{2}b + 2\,{}^{1}{}^{1}_{2}dk\}({}_{2}S)]({}_{1}A\ell)\end{aligned}$$

$$\begin{aligned}+\ 6\mu\ell[\{{}^{11}{}^{1}_{3}c \pm 3\,{}^{11}{}^{1}_{3}dk\}({}_{3}C) \\ + \{\pm\,{}^{11}{}^{1}_{3}a + 3\,{}^{11}{}^{1}_{3}bk\}({}_{3}S)]\ \Big\}\end{aligned} \qquad \cos(3\ell x)$$

$+$

$$\Big\{\ +\ 8\mu\ell[\{{}^{4}_{4}c \pm 4\,{}^{4}_{4}dk\}({}_{4}C) + \{\pm\,{}^{4}_{4}a + 4\,{}^{4}_{4}bk\}({}_{4}S)]$$

$$+\ 8\mu\ell[\{{}^{1}{}^{2}_{4}c \pm 4\,{}^{1}{}^{2}_{4}dk\}({}_{4}C) + \{\pm\,{}^{1}{}^{2}_{4}a + 4\,{}^{1}{}^{2}_{4}bk\}({}_{4}S)]$$

$$\begin{aligned}+\ 9\mu\ell[\{{}^{1}{}^{1}_{3}a + {}^{1}{}^{1}_{3}d \pm 3\,{}^{1}{}^{1}_{3}bk\}({}_{3}C) \\ + \{\pm\,{}^{1}{}^{1}_{3}c \pm {}^{1}{}^{1}_{3}b + 3\,{}^{1}{}^{1}_{3}dk\}({}_{3}S)]({}_{1}A\ell)\end{aligned}$$

$$\begin{aligned}+\ 8\mu\ell[\{{}^{11}{}^{1}_{4}c \pm 4\,{}^{11}{}^{1}_{4}dk\}({}_{4}C) \\ + \{\pm\,{}^{11}{}^{1}_{4}a + 4\,{}^{11}{}^{1}_{4}bk\}({}_{4}S)]\ \Big\}\end{aligned} \qquad \cos(4\ell x)$$

$+$

$$+\ \mu\ell[\{{}^{1}_{1}a+{}^{1}_{1}d\pm{}^{1}_{1}bk\}({}_{1}C)\ +\ \{\pm{}^{1}_{1}c\pm{}^{1}_{1}b+{}^{1}_{1}dk\}({}_{1}S)]({}_{1}A\ell)$$

$$+\ \mu\ell[\{{}^{1}{}^{1}_{1}a+{}^{1}{}^{1}_{1}d\pm{}^{1}{}^{1}_{1}bk\}({}_{1}C)\ +\ \{\pm{}^{1}{}^{1}_{1}c\pm{}^{1}{}^{1}_{1}b+{}^{1}{}^{1}_{1}dk\}({}_{1}S)]({}_{1}A\ell)$$

$$-\ \not{p}_{o}\ -\ \rho g z \tag{9c}$$

$$[\sigma_{xx}]\ =\ \Big\{\ -\ 2\mu\ell[\{{}^{1}_{1}c+2{}^{1}_{1}b\pm{}^{1}_{1}dk\}({}_{1}C)\ +\ \{\pm{}^{1}_{1}a\pm2{}^{1}_{1}d+{}^{1}_{1}bk\}({}_{1}S)]$$

$$-\ 2\mu\ell[\{{}^{1}{}^{1}_{1}c+2{}^{1}{}^{1}_{1}b\pm{}^{1}{}^{1}_{1}dk\}({}_{1}C)\ +\ \{\pm{}^{1}{}^{1}_{1}a\pm2{}^{1}{}^{1}_{1}d+{}^{1}{}^{1}_{1}bk\}({}_{1}S)]$$

$$-\ \mu\ell[\{{}^{1}_{1}a+3{}^{1}_{1}d\pm{}^{1}_{1}bk\}({}_{1}C)\ +\ \{\pm{}^{1}_{1}c\pm3{}^{1}_{1}b+{}^{1}_{1}dk\}({}_{1}S)]({}_{2}A\ell)$$

$$-\ 4\mu\ell[\{{}^{2}_{2}a+3{}^{2}_{2}d\pm2{}^{2}_{2}bk\}({}_{2}C)$$
$$+\ \{\pm{}^{2}_{2}c\pm3{}^{2}_{2}b+2{}^{2}_{2}dk\}({}_{2}S)]({}_{1}A\ell)$$

$$-\ 2\mu\ell[\{{}^{1}{}^{2}_{1}c+2{}^{1}{}^{2}_{1}b\pm{}^{1}{}^{2}_{1}dk\}({}_{1}C)\ +\ \{\pm{}^{1}{}^{2}_{1}a\pm2{}^{1}{}^{2}_{1}d+{}^{1}{}^{2}_{1}bk\}({}_{1}S)]$$

$$-\ (3\mu\ell/4)[\{{}^{1}_{1}c+4{}^{1}_{1}b\pm{}^{1}_{1}dk\}({}_{1}C)$$
$$+\ \{\pm{}^{1}_{1}a\pm4{}^{1}_{1}d+{}^{1}_{1}bk\}({}_{1}S)]({}_{1}A\ell)^{2}$$

$$-\ 4\mu\ell[\{{}^{1}{}^{1}_{2}a+3{}^{1}{}^{1}_{2}d\pm2{}^{1}{}^{1}_{2}bk\}({}_{2}C)$$
$$+\ \{\pm{}^{1}{}^{1}_{2}c\pm3{}^{1}{}^{1}_{2}b+2{}^{1}{}^{1}_{2}dk\}({}_{2}S)]({}_{1}A\ell)$$

$$-\ 2\mu\ell[\{{}^{11}{}^{1}_{1}c+2{}^{11}{}^{1}_{1}b\pm{}^{11}{}^{1}_{1}dk\}({}_{1}C)$$
$$+\ \{\pm{}^{11}{}^{1}_{1}a\pm2{}^{11}{}^{1}_{1}d+{}^{11}{}^{1}_{1}bk\}({}_{1}S)]\ \Big\}\qquad\cos(\ell x)$$

$$+$$

$$\Big\{\ -\ 4\mu\ell[\{{}^{2}_{2}c+2{}^{2}_{2}b\pm2{}^{2}_{2}dk\}({}_{2}C)\ +\ \{\pm{}^{2}_{2}a\pm2{}^{2}_{2}d+2{}^{2}_{2}bk\}({}_{2}S)]$$

$$-\ \mu\ell[\{{}^{1}_{1}a+3{}^{1}_{1}d\pm{}^{1}_{1}bk\}({}_{1}C)\ +\ \{\pm{}^{1}_{1}c\pm3{}^{1}_{1}b+{}^{1}_{1}dk\}({}_{1}S)]({}_{1}A\ell)$$

$$-\ 4\mu\ell[\{{}^{1}{}^{1}_{2}c+2{}^{1}{}^{1}_{2}b\pm2{}^{1}{}^{1}_{2}dk\}({}_{2}C)$$
$$+\ \{\pm{}^{1}{}^{1}_{2}a\pm2{}^{1}{}^{1}_{2}d+2{}^{1}{}^{1}_{2}bk\}({}_{2}S)]$$

$$-\ 4\mu\ell[\{{}^{1}{}^{2}_{2}c+2{}^{1}{}^{2}_{2}b\pm2{}^{1}{}^{2}_{2}dk\}({}_{2}C)\ +\ \{\pm{}^{1}{}^{2}_{2}a\pm2{}^{1}{}^{2}_{2}d+2{}^{1}{}^{2}_{2}bk\}({}_{2}S)]$$

$$-\ \mu\ell[\{{}^{1}{}^{1}_{1}a+3{}^{1}{}^{1}_{1}d\pm{}^{1}{}^{1}_{1}bk\}({}_{1}C)$$
$$+\ \{\pm{}^{1}{}^{1}_{1}c\pm3{}^{1}{}^{1}_{1}b+{}^{1}{}^{1}_{1}dk\}({}_{1}S)]({}_{1}A\ell)$$

$$-\ 9\mu\ell[\{{}^{1}{}^{1}_{3}a+3{}^{1}{}^{1}_{3}d\pm3{}^{1}{}^{1}_{3}bk\}({}_{3}C)$$
$$+\ \{\pm{}^{1}{}^{1}_{3}c\pm3{}^{1}{}^{1}_{3}b+3{}^{1}{}^{1}_{3}dk\}({}_{3}S)]({}_{1}A\ell)$$

$$-\ 4\mu\ell[\{{}^{11}{}^{1}_{2}c+2{}^{11}{}^{1}_{2}b\pm2{}^{11}{}^{1}_{2}dk\}({}_{2}C)$$
$$+\ \{\pm{}^{11}{}^{1}_{2}a\pm2{}^{11}{}^{1}_{2}d+2{}^{11}{}^{1}_{2}bk\}({}_{2}S)]\ \Big\}\qquad\cos(2\ell x)$$

$$+$$

$$\{ - 6\mu\ell[\{{}^{3}_{3}c+2{}^{3}_{3}b\pm 3{}^{3}_{3}dk\}({}_{3}C) + \{\pm{}^{3}_{3}a\pm 2{}^{3}_{3}d+3{}^{3}_{3}bk\}({}_{3}S)]$$

$$- 6\mu\ell[\{{}^{1}{}^{1}_{3}c+2{}^{1}{}^{1}_{3}b\pm 3{}^{1}{}^{1}_{3}dk\}({}_{3}C) + \{\pm{}^{1}{}^{1}_{3}a\pm 2{}^{1}{}^{1}_{3}d+3{}^{1}{}^{1}_{3}bk\}({}_{3}S)]$$

$$- \mu\ell[\{{}^{1}_{1}a+3{}^{1}_{1}d\pm{}^{1}_{1}bk\}({}_{1}C) + \{\pm{}^{1}_{1}c\pm 3{}^{1}_{1}b+{}^{1}_{1}dk\}({}_{1}S)]({}_{2}A\ell)$$

$$- 4\mu\ell[\{{}^{2}_{2}a+3{}^{2}_{2}d\pm 2{}^{2}_{2}bk\}({}_{2}C) + \{\pm{}^{2}_{2}c\pm 3{}^{2}_{2}b+2{}^{2}_{2}dk\}({}_{2}S)]({}_{1}A\ell)$$

$$- 6\mu\ell[\{{}^{1}{}^{2}_{3}c+2{}^{1}{}^{2}_{3}b\pm 3{}^{1}{}^{2}_{3}dk\}({}_{3}C) + \{\pm{}^{1}{}^{2}_{3}a\pm 2{}^{1}{}^{2}_{3}d+3{}^{1}{}^{2}_{3}bk\}({}_{3}S)]$$

$$- (\mu\ell/4)[\{{}^{1}_{1}c+4{}^{1}_{1}b\pm{}^{1}_{1}dk\}({}_{1}C) + \{\pm{}^{1}_{1}a\pm 4{}^{1}_{1}d+{}^{1}_{1}bk)({}_{1}S)]({}_{1}A\ell)^{2}$$

$$- 4\mu\ell[\{{}^{1}{}^{1}_{2}a+3{}^{1}{}^{1}_{2}d\pm 2{}^{1}{}^{1}_{2}bk\}({}_{2}C) + \{\pm{}^{1}{}^{1}_{2}c\pm 3{}^{1}{}^{1}_{2}b+2{}^{1}{}^{1}_{2}dk\}({}_{2}S)]({}_{1}A\ell)$$

$$- 6\mu\ell[\{{}^{11}{}^{1}_{3}c+2{}^{11}{}^{1}_{3}b\pm 3{}^{11}{}^{1}_{3}dk\}({}_{3}C) + \{\pm{}^{11}{}^{1}_{3}a\pm 2{}^{11}{}^{1}_{3}d+3{}^{11}{}^{1}_{3}bk\}({}_{3}S)] \} \qquad \cos(3\ell x)$$

$$+$$

$$\{ - 8\mu\ell[\{{}^{4}_{4}c+2{}^{4}_{4}b\pm 4{}^{4}_{4}dk\}({}_{4}C) + \{\pm{}^{4}_{4}a\pm 2{}^{4}_{4}d+4{}^{4}_{4}bk\}({}_{4}S)]$$

$$- 8\mu\ell[\{{}^{1}{}^{2}_{4}c+2{}^{1}{}^{2}_{4}b\pm 4{}^{1}{}^{2}_{4}dk\}({}_{4}C) + \{\pm{}^{1}{}^{2}_{4}a\pm 2{}^{1}{}^{2}_{4}d+4{}^{1}{}^{2}_{4}bk\}({}_{4}S)]$$

$$- 9\mu\ell[\{{}^{1}{}^{1}_{3}a+3{}^{1}{}^{1}_{3}d\pm 3{}^{1}{}^{1}_{3}bk\}({}_{3}C) + \{\pm{}^{1}{}^{1}_{3}c\pm 3{}^{1}{}^{1}_{3}b+{}^{1}{}^{1}_{3}dk\}({}_{3}S)]({}_{1}A\ell)$$

$$- 8\mu\ell[\{{}^{11}{}^{1}_{4}c+2{}^{11}{}^{1}_{4}b\pm 4{}^{11}{}^{1}_{4}dk\}({}_{4}C) + \{\pm{}^{11}{}^{1}_{4}a\pm 2{}^{11}{}^{1}_{4}d+4{}^{11}{}^{1}_{4}bk\}({}_{4}S)] \} \qquad \cos(4\ell x)$$

$$+$$

$$- \mu\ell[\{{}^{1}_{1}a+3{}^{1}_{1}d\pm{}^{1}_{1}bk\}({}_{1}C) + \{\pm{}^{1}_{1}c\pm 3{}^{1}_{1}b+{}^{1}_{1}dk\}({}_{1}S)]({}_{1}A\ell)$$

$$- \mu\ell[\{{}^{1}{}^{1}_{1}a+3{}^{1}{}^{1}_{1}d\pm{}^{1}{}^{1}_{1}bk\}({}_{1}C) + \{\pm{}^{1}{}^{1}_{1}c\pm 3{}^{1}{}^{1}_{1}b+{}^{1}{}^{1}_{1}dk\}({}_{1}S)]({}_{1}A\ell)$$

$$- \tilde{p}_{o} - \rho g z \tag{9d}$$

$$\begin{aligned}
[\tilde{\sigma}_{xz}] = \Big\{ & -2\mu\ell[\{{}^{1}_{1}a+{}^{1}_{1}d\pm{}^{1}_{1}bk\}({}_{1}C) + \{\pm{}^{1}_{1}c\pm{}^{1}_{1}b+{}^{1}_{1}dk\}({}_{1}S)] \\
& - 2\mu\ell[\{{}^{1}{}^{1}_{1}a+{}^{1}{}^{1}_{1}d\pm{}^{1}{}^{1}_{1}bk\}({}_{1}C) + \{\pm{}^{1}{}^{1}_{1}c\pm{}^{1}{}^{1}_{1}b+{}^{1}{}^{1}_{1}dk\}({}_{1}S)] \\
& + \mu\ell[\{{}^{1}_{1}c+2{}^{1}_{1}b\pm{}^{1}_{1}dk\}({}_{1}C) + \{\pm{}^{1}_{1}a\pm 2{}^{1}_{1}d+{}^{1}_{1}bk\}({}_{1}S)]({}_{2}A\ell) \\
& - 4\mu\ell[\{{}^{2}_{2}c+2{}^{2}_{2}b\pm 2{}^{2}_{2}dk\}({}_{2}C) + \{\pm{}^{2}_{2}a\pm 2{}^{2}_{2}d+2{}^{2}_{2}bk\}({}_{2}S)]({}_{1}A\ell) \\
& - 2\mu\ell[\{{}^{1}{}^{2}_{1}a+{}^{1}{}^{2}_{1}d\pm{}^{1}{}^{2}_{1}bk\}({}_{1}C) + \{\pm{}^{1}{}^{2}_{1}c\pm{}^{1}{}^{2}_{1}b+{}^{1}{}^{2}_{1}dk\}({}_{1}S)] \\
& - (\mu\ell/4)[\{{}^{1}_{1}a+3{}^{1}_{1}d\pm{}^{1}_{1}bk\}({}_{1}C) \\
& \qquad + \{\pm{}^{1}_{1}c\pm 3{}^{1}_{1}b+{}^{1}_{1}dk\}({}_{1}S)]({}_{1}A\ell)^{2} \\
& - 4\mu\ell[\{{}^{1}{}^{1}_{2}c+2{}^{1}{}^{1}_{2}b\pm 2{}^{1}{}^{1}_{2}dk\}({}_{2}C) \\
& \qquad + \{\pm{}^{1}{}^{1}_{2}a\pm 2{}^{1}{}^{1}_{2}d+2{}^{1}{}^{1}_{2}bk\}({}_{2}S)]({}_{1}A\ell) \\
& - 2\mu\ell[\{{}^{11}{}^{1}_{1}a+{}^{11}{}^{1}_{1}d\pm{}^{11}{}^{1}_{1}bk\}({}_{1}C) \\
& \qquad + \{\pm{}^{11}{}^{1}_{1}c\pm{}^{11}{}^{1}_{1}b+{}^{11}{}^{1}_{1}dk\}({}_{1}S)] \Big\} \qquad \sin(\ell x)
\end{aligned}$$

$+$

$$\begin{aligned}
\Big\{ & - 4\mu\ell[\{{}^{2}_{2}a+{}^{2}_{2}d\pm 2{}^{2}_{2}bk\}({}_{2}C) + \{\pm{}^{2}_{2}c\pm{}^{2}_{2}b+2{}^{2}_{2}dk\}({}_{2}S)] \\
& - \mu\ell[\{{}^{1}_{1}c+2{}^{1}_{1}b\pm{}^{1}_{1}dk\}({}_{1}C) + \{\pm{}^{1}_{1}a\pm 2{}^{1}_{1}d+{}^{1}_{1}bk\}({}_{1}S)]({}_{1}A\ell) \\
& - 4\mu\ell[\{{}^{1}{}^{1}_{2}a+{}^{1}{}^{1}_{2}d\pm 2{}^{1}{}^{1}_{2}bk\}({}_{2}C) + \{\pm{}^{1}{}^{1}_{2}c\pm{}^{1}{}^{1}_{2}b+2{}^{1}{}^{1}_{2}dk\}({}_{2}S)] \\
& - 4\mu\ell[\{{}^{1}{}^{2}_{2}a+{}^{1}{}^{2}_{2}d\pm 2{}^{1}{}^{2}_{2}bk\}({}_{2}C) + \{\pm{}^{1}{}^{2}_{2}c\pm{}^{1}{}^{2}_{2}b+2{}^{1}{}^{2}_{2}dk\}({}_{2}S)] \\
& - \mu\ell[\{{}^{1}{}^{1}_{1}c+2{}^{1}{}^{1}_{1}b\pm{}^{1}{}^{1}_{1}dk\}({}_{1}C) \\
& \qquad + \{\pm{}^{1}{}^{1}_{1}a\pm 2{}^{1}{}^{1}_{1}d+{}^{1}{}^{1}_{1}bk\}({}_{1}S)]({}_{1}A\ell) \\
& - 9\mu\ell[\{{}^{1}{}^{1}_{3}c+2{}^{1}{}^{1}_{3}b\pm 3{}^{1}{}^{1}_{3}dk\}({}_{3}C) \\
& \qquad + \{\pm{}^{1}{}^{1}_{3}a\pm 2{}^{1}{}^{1}_{3}d+3{}^{1}{}^{1}_{3}bk\}({}_{3}S)]({}_{1}A\ell) \\
& - 4\mu\ell[\{{}^{11}{}^{1}_{2}a+{}^{11}{}^{1}_{2}d\pm 2{}^{11}{}^{1}_{2}bk\}({}_{2}C) \\
& \qquad + \{\pm{}^{11}{}^{1}_{2}c\pm{}^{11}{}^{1}_{2}b+2{}^{11}{}^{1}_{2}dk\}({}_{2}S)] \Big\} \qquad \sin(2\ell x)
\end{aligned}$$

$+$

$$\begin{aligned}
\Big\{ & - 6\mu\ell[\{{}^{3}_{3}a+{}^{3}_{3}d\pm 3{}^{3}_{3}bk\}({}_{3}C) + \{\pm{}^{3}_{3}c\pm{}^{3}_{3}b+3{}^{3}_{3}dk\}({}_{3}S)] \\
& - 6\mu\ell[\{{}^{1}{}^{1}_{3}a+{}^{1}{}^{1}_{3}d\pm 3{}^{1}{}^{1}_{3}bk\}({}_{3}C) + \{\pm{}^{1}{}^{1}_{3}c\pm{}^{1}{}^{1}_{3}b+3{}^{1}{}^{1}_{3}dk\}({}_{3}S)] \\
& - \mu\ell[\{{}^{1}_{1}c+2{}^{1}_{1}b\pm{}^{1}_{1}dk\}({}_{1}C) + \{\pm{}^{1}_{1}a\pm 2{}^{1}_{1}d+{}^{1}_{1}bk\}({}_{1}S)]({}_{2}A\ell) \\
& - 4\mu\ell[\{{}^{2}_{2}c+2{}^{2}_{2}b\pm 2{}^{2}_{2}dk\}({}_{2}C) + \{\pm{}^{2}_{2}a\pm 2{}^{2}_{2}d+2{}^{2}_{2}bk\}({}_{2}S)]({}_{1}A\ell) \\
& - 6\mu\ell[\{{}^{1}{}^{2}_{3}a+{}^{1}{}^{2}_{3}d\pm 3{}^{1}{}^{2}_{3}bk\}({}_{3}C) + \{\pm{}^{1}{}^{2}_{3}c\pm{}^{1}{}^{2}_{3}b+3{}^{1}{}^{2}_{3}dk\}({}_{3}S)]
\end{aligned}$$

$$- (\mu\ell/4)[\{{}^{1}_{1}a+3{}^{1}_{1}d\pm{}^{1}_{1}bk\}({}_{1}C)$$
$$+ \{\pm{}^{1}_{1}c\pm3{}^{1}_{1}b+{}^{1}_{1}dk\}({}_{1}S)]({}_{1}A\ell)^{2}$$

$$- 4\mu\ell[\{{}^{1}{}^{1}_{2}c+2{}^{1}{}^{1}_{2}b\pm2{}^{1}{}^{1}_{2}dk\}({}_{2}C)$$
$$+ \{\pm{}^{1}{}^{1}_{2}a\pm2{}^{1}{}^{1}_{2}d+2{}^{1}{}^{1}_{2}bk\}({}_{2}S)]({}_{1}A\ell)$$

$$- 6\mu\ell[\{{}^{11}{}^{1}_{3}a+{}^{11}{}^{1}_{3}d\pm3{}^{11}{}^{1}_{3}bk\}({}_{3}C)$$
$$+ \{\pm{}^{11}{}^{1}_{3}c\pm{}^{11}{}^{1}_{3}b+3{}^{11}{}^{1}_{3}dk\}({}_{3}S)] \Big\} \qquad \sin(3\ell x)$$

$+$

$$\Big\{ - 8\mu\ell[\{{}^{4}_{4}a+{}^{4}_{4}d\pm4{}^{4}_{4}bk\}({}_{4}C) + \{\pm{}^{4}_{4}c\pm{}^{4}_{4}b+4{}^{4}_{4}dk\}({}_{4}S)]$$

$$- 8\mu\ell[\{{}^{1}{}^{2}_{4}a+{}^{1}{}^{2}_{4}d\pm4{}^{1}{}^{2}_{4}bk\}({}_{4}C) + \{\pm{}^{1}{}^{2}_{4}c\pm{}^{1}{}^{2}_{4}b+4{}^{1}{}^{2}_{4}dk\}({}_{4}S)]$$

$$- 9\mu\ell[\{{}^{1}{}^{1}_{3}c+2{}^{1}{}^{1}_{3}b\pm3{}^{1}{}^{1}_{3}dk\}({}_{3}C)$$
$$+ \{\pm{}^{1}{}^{1}_{3}a\pm2{}^{1}{}^{1}_{3}d+3{}^{1}{}^{1}_{3}bk\}({}_{3}S)]({}_{1}A\ell)$$

$$- 8\mu\ell[\{{}^{11}{}^{1}_{4}a+{}^{11}{}^{1}_{4}d\pm4{}^{11}{}^{1}_{4}bk\}({}_{4}C)$$
$$+ \{\pm{}^{11}{}^{1}_{4}c\pm{}^{11}{}^{1}_{4}b+4{}^{11}{}^{1}_{4}dk\}({}_{4}S)] \Big\} \qquad \sin(4\ell x) \qquad (9e)$$

The complete expressions for the velocities and stresses, eqs. (3), are found by summing the individual expressions for the mean and perturbed values, eqs. (4) and (9), respectively.

The constants are eliminated by application of the stress and velocity boundary conditions. The boundary conditions pertain to the stresses and velocities normal and parallel to the interface. Using the coordinate system shown in Fig. 1, Chapter I, with coordinate $\underline{n}$ normal to and $\underline{s}$ parallel to an interface, the velocity and stress components normal and parallel to an interface are:

$$v_n = [v_z]_\zeta \cos(\theta) - [v_x]_\zeta \sin(\theta) \tag{10a}$$

$$v_s = [v_x]_\zeta \cos(\theta) + [v_z]_\zeta \sin(\theta) \tag{10b}$$

$$\sigma_{nn} = [\sigma_{zz}]_\zeta \cos^2(\theta) + [\sigma_{xx}]_\zeta \sin^2(\theta) - 2[\sigma_{xz}]_\zeta \cos(\theta)\sin(\theta) \tag{10c}$$

$$\sigma_{ns} = [\sigma_{zz} - \sigma_{xx}]_\zeta \cos(\theta)\sin(\theta) + [\sigma_{xz}]_\zeta [\cos^2(\theta)-\sin^2(\theta)] \tag{10d}$$

in which $[\ \ ]_\zeta$ indicates that the quantity is to be evaluated at the interface, $\underline{z} = \zeta$ (eq. 2), and

$$\cos(\theta) = 1/\surd[1+(\partial\zeta/\partial x)^2; \quad \sin(\theta) = \cos(\theta)\ (\partial\zeta/\partial x) \tag{10e}$$

where θ is the slope angle (Fig. 1, Ch. I).

The number of arbitrary constants for multilayer problems can be extremely large. For each waveform and each order of approximation, four stress and velocity conditions can be written for each layer and two for each confining medium. For each waveform and each order of approximation, there are 44 boundary conditions which must be solved simultaneously for the 44 unknown constants in a confined, 10-layer multilayer. For 3rd order analysis of ten layers and two media, there are potentially 660 constants.

In the course of the derivations presented here, I have devised a method that reduces the number of constants by about half, from four per layer to two per interface for each waveform and each order of approximation. The new method applies the same stress and velocity boundary conditions as the previous method, but applies them sequentially rather than simultaneously.

In the new method, the stress boundary conditions are applied first to eliminate half the constants. The stress boundary conditions state that the normal and shear stresses in two adjacent layers, or in a layer and adjacent medium, must be equal at the interface between the two layers, or layer and medium. The stress boundary conditions are written:

$$(\sigma_{nn})_b = (\sigma_{nn})_t \tag{11a}$$

$$(\sigma_{ns})_b = (\sigma_{ns})_t \tag{11b}$$

The sequence of operations in the new method of solution is:

1) Expand the interface stresses, eq. (10c,d), to 3rd order and substitute the 3rd order expressions for the stresses, eqs. (3c,d,e), found by summing eqs. (4c,d,e) and (9c,d,e). The results are:

$$(\sigma_{nn})_{t,b} = -2\mu\bar{D}_{xx} + 2\mu\bar{D}_{xx}({}_1A_{t,b}\ell)^2 - \bar{p}_o - \bar{\bar{p}}_o \pm \rho g(h/2)$$

$$- \mu\ell[\{{}^{1}_{1}a+{}^{1}_{1}d\pm{}^{1}_{1}bk\}({}_1C) + \{\pm{}^{1}_{1}c\pm{}^{1}_{1}b+{}^{1}_{1}dk\}({}_1S)]({}_1A_{t,b}\ell)$$

$$- \mu\ell[\{{}^{11}_{1}a+{}^{11}_{1}d\pm{}^{11}_{1}bk\}({}_1C)$$
$$+ \{\pm{}^{11}_{1}c\pm{}^{11}_{1}b+{}^{11}_{1}dk\}({}_1S)]({}_1A_{t,b}\ell)$$

$+$

$$\{ 4\mu\bar{D}_{xx}({}_1A_{t,b}\ell)({}_2A_{t,b}2\ell) + \rho g({}_1A_{t,b})$$

$$+ 2\mu\ell[\{{}^{1}_{1}c\pm{}^{1}_{1}dk\}({}_1C) + \{\pm{}^{1}_{1}a+{}^{1}_{1}bk\}({}_1S)]$$

$$+ 2\mu\ell[\{{}^{11}_{1}c\pm{}^{11}_{1}dk\}({}_1C) + \{\pm{}^{11}_{1}a+{}^{11}_{1}bk\}({}_1S)]$$

$$- 3\mu\ell[\{{}^{1}_{1}a+{}^{1}_{1}d\pm{}^{1}_{1}bk\}({}_1C) + \{\pm{}^{1}_{1}c\pm{}^{1}_{1}b+{}^{1}_{1}dk\}({}_1S)]({}_2A_{t,b}\ell)$$

$$+ 2\mu\ell[\{{}^{12}_{1}c\pm{}^{12}_{1}dk\}({}_1C) + \{\pm{}^{12}_{1}a+{}^{12}_{1}bk\}({}_1S)]$$

$$- (\mu\ell/4)[\{5{}^{1}_{1}c+6{}^{1}_{1}b\pm 5{}^{1}_{1}dk\}({}_1C)$$
$$+ (\pm 5{}^{1}_{1}a\pm 6{}^{1}_{1}d+5{}^{1}_{1}bk\}]({}_1A_{t,b}\ell)^2$$

$$+ 2\mu\ell[\{{}^{111}_{1}c\pm{}^{111}_{1}dk\}({}_1C)$$
$$+ \{\pm{}^{111}_{1}a+{}^{111}_{1}bk\}({}_1S)] \} \qquad \cos(\ell x)$$

$+$

$$\{ -2\mu\bar{D}_{xx}({}_1A_{t,b}\ell)^2 + \rho g({}_2A_{t,b})$$

$$+ 4\mu\ell[\{{}^{2}_{2}c\pm 2{}^{2}_{2}dk\}({}_2C) + \{\pm{}^{2}_{2}a+2{}^{2}_{2}bk\}({}_2S)]$$

$$+\ 3\mu\ell[\{{}^{1}_{1}a+{}^{1}_{1}d\pm{}^{1}_{1}bk\}({}_{1}C)\ +\ (\pm{}^{1}_{1}c\pm{}^{1}_{1}b+{}^{1}_{1}dk\}({}_{1}S)]({}_{1}A_{t,b}\ell)$$

$$+\ 4\mu\ell[\{{}^{1}{}^{1}_{2}c\pm 2\,{}^{1}{}^{1}_{2}dk\}({}_{2}C)\ +\ \{\pm{}^{1}{}^{1}_{2}a+2\,{}^{1}{}^{1}_{2}bk\}({}_{2}S)]$$

$$+\ 4\mu\ell[\{{}^{1}{}^{2}_{2}c\pm 2\,{}^{1}{}^{2}_{2}dk\}({}_{2}C)\ +\ \{\pm{}^{1}{}^{2}_{2}a+2\,{}^{1}{}^{2}_{2}bk\}({}_{2}S)]$$

$$+\ 3\mu\ell[\{{}^{1}{}^{1}_{1}a+{}^{1}{}^{1}_{1}d\pm{}^{1}{}^{1}_{1}bk\}({}_{1}C)$$
$$+\ \{\pm{}^{1}{}^{1}_{1}c\pm{}^{1}{}^{1}_{1}b+{}^{1}{}^{1}_{1}dk\}({}_{1}S)]({}_{1}A_{t,b}\ell)$$

$$+\ 3\mu\ell[\{{}^{1}{}^{1}_{3}a+{}^{1}{}^{1}_{3}d\pm 3\,{}^{1}{}^{1}_{3}bk\}({}_{3}C)$$
$$+\ \{\pm{}^{1}{}^{1}_{3}c\pm{}^{1}{}^{1}_{3}b+3\,{}^{1}{}^{1}_{3}dk\}({}_{3}S)]({}_{1}A_{t,b}\ell)$$

$$+\ 4\mu\ell[\{{}^{11}{}^{1}_{2}c\pm 2\,{}^{11}{}^{1}_{2}dk\}({}_{2}C)$$
$$+\ \{\pm{}^{11}{}^{1}_{2}a+2\,{}^{11}{}^{1}_{2}bk\}({}_{2}S)]\ \Big\}\qquad \cos(2\ell x)$$

$$+$$

$$\Big\{\ -4\mu\bar{D}_{xx}({}_{1}A_{t,b}\ell)({}_{2}A_{t,b}2\ell)\ +\ \rho g({}_{3}A_{t,b})$$

$$+\ 6\mu\ell[\{{}^{3}_{3}c\pm 3\,{}^{3}_{3}dk\}({}_{3}C)\ +\ \{\pm{}^{3}_{3}a+3\,{}^{3}_{3}bk\}({}_{3}S)]$$

$$+\ 6\mu\ell[\{{}^{1}{}^{1}_{3}c\pm 3\,{}^{1}{}^{1}_{3}dk\}({}_{3}C)\ +\ \{\pm{}^{1}{}^{1}_{3}a+3\,{}^{1}{}^{1}_{3}bk\}({}_{3}S)]$$

$$+\ 5\mu\ell[\{{}^{1}_{1}a+{}^{1}_{1}d\pm{}^{1}_{1}bk\}({}_{1}C)\ +\ \{\pm{}^{1}_{1}c\pm{}^{1}_{1}b+{}^{1}_{1}dk\}({}_{1}S)]({}_{2}A_{t,b}\ell)$$

$$+\ 8\mu\ell[\{{}^{2}_{2}a+{}^{2}_{2}d\pm 2\,{}^{2}_{2}bk\}({}_{2}C)\ +\ \{\pm{}^{2}_{2}c\pm{}^{2}_{2}b+2\,{}^{2}_{2}dk\}({}_{2}S)]({}_{1}A_{t,b}\ell)$$

$$+\ 6\mu\ell[\{{}^{1}{}^{2}_{3}c\pm 3\,{}^{1}{}^{2}_{3}dk\}({}_{3}C)\ +\ \{\pm{}^{1}{}^{2}_{3}a+3\,{}^{1}{}^{2}_{3}bk\}({}_{3}S)]$$

$$+\ (\mu\ell/4)[\{9\,{}^{1}_{1}c+14\,{}^{1}_{1}b\pm 9\,{}^{1}_{1}dk\}({}_{1}C)$$
$$+\ (\pm 9\,{}^{1}_{1}a\pm 14\,{}^{1}_{1}d+9\,{}^{1}_{1}bk\}({}_{1}S)]({}_{1}A_{t,b}\ell)^{2}$$

$$+\ 8\mu\ell[\{{}^{1}{}^{1}_{2}a+{}^{1}{}^{1}_{2}d\pm 2\,{}^{1}{}^{1}_{2}bk\}({}_{2}C)$$
$$+\ \{\pm{}^{1}{}^{1}_{2}c\pm{}^{1}{}^{1}_{2}b+2\,{}^{1}{}^{1}_{2}dk\}({}_{2}S)]({}_{1}A_{t,b}\ell)$$

$$+\ 6\mu\ell[\{{}^{11}{}^{1}_{3}c\pm 3\,{}^{11}{}^{1}_{3}dk\}({}_{3}C)$$
$$+\ \{\pm{}^{11}{}^{1}_{3}a+3\,{}^{11}{}^{1}_{3}bk\}({}_{3}S)]\ \Big\}\qquad \cos(3\ell x)$$

$$+$$

$$\Big\{\ +\ \rho g({}_{4}A_{t,b})$$

$$+\ 8\mu\ell[\{{}^{4}_{4}c\pm 4\,{}^{4}_{4}dk\}({}_{4}C)\ +\ \{\pm{}^{4}_{4}a+4\,{}^{4}_{4}bk\}({}_{4}S)]$$

$$+\ 8\mu\ell[\{{}^{1}{}^{2}_{4}c\pm 4\,{}^{1}{}^{2}_{4}dk\}({}_{4}C)\ +\ \{\pm{}^{1}{}^{2}_{4}a+4\,{}^{1}{}^{2}_{4}bk\}({}_{4}S)]$$

$$+\ 15\mu\ell[\{{}^{1}{}^{1}_{3}a+{}^{1}{}^{1}_{3}d\pm 3\,{}^{1}{}^{1}_{3}bk\}({}_{3}C)$$
$$+\ \{\pm{}^{1}{}^{1}_{3}c\pm{}^{1}{}^{1}_{3}b+3\,{}^{1}{}^{1}_{3}dk\}({}_{3}S)]({}_{1}A_{t,b}\ell)$$

$$+\ 8\mu\ell[\{{}^{111}_{4}c \pm 4\,{}^{111}_{4}dk\}({}_{4}C)$$
$$+\ \{\pm\,{}^{111}_{4}a + 4\,{}^{111}_{4}bk\}({}_{4}S)]\ \Big\} \qquad \cos(4\ell x)$$

(12a)

$$(\sigma_{ns})_{t,b} = \Big\{\ 4\mu\bar{D}_{xx}({}_{1}A_{t,b}\ell) - 3\mu\bar{D}_{xx}({}_{1}A_{t,b}\ell)^{3}$$

$$-\ 2\mu\ell[\{{}^{1}_{1}a + {}^{1}_{1}d \pm {}^{1}_{1}bk\}({}_{1}C) + \{\pm\,{}^{1}_{1}c \pm {}^{1}_{1}b + {}^{1}_{1}dk\}({}_{1}S)]$$

$$-\ 2\mu\ell[\{{}^{11}_{1}a + {}^{11}_{1}d \pm {}^{11}_{1}bk\}({}_{1}C) + \{\pm\,{}^{11}_{1}c \pm {}^{11}_{1}b + {}^{11}_{1}dk\}({}_{1}S)]$$

$$-\ \mu\ell[\{3\,{}^{1}_{1}c + 2\,{}^{1}_{1}b \pm 3\,{}^{1}_{1}dk\}({}_{1}C)$$
$$+\ \{\pm 3\,{}^{1}_{1}a \pm 2\,{}^{1}_{1}d + 3\,{}^{1}_{1}bk\}({}_{1}S)]({}_{2}A_{t,b}\ell)$$

$$-\ 4\mu\ell[\{{}^{2}_{2}b\}({}_{2}C) + \{\pm\,{}^{2}_{2}d\}({}_{2}S)]({}_{1}A_{t,b}\ell)$$

$$-\ 2\mu\ell[\{{}^{12}_{1}a + {}^{12}_{1}d \pm {}^{12}_{1}bk\}({}_{1}C) + \{\pm\,{}^{12}_{1}c \pm {}^{12}_{1}b + {}^{12}_{1}dk\}({}_{1}S)]$$

$$+\ (\mu\ell/4)[\{7\,{}^{1}_{1}a + {}^{1}_{1}d \pm 7\,{}^{1}_{1}bk\}({}_{1}C)$$
$$+\ \{\pm 7\,{}^{1}_{1}c \pm {}^{1}_{1}b + 7\,{}^{1}_{1}dk\}({}_{1}S)]({}_{1}A_{t,b}\ell)^{2}$$

$$-\ 4\mu\ell[\{{}^{11}_{2}b\}({}_{2}C) + \{\pm\,{}^{11}_{2}d\}({}_{2}S)]({}_{1}A_{t,b}\ell)$$

$$-\ 2\mu\ell[\{{}^{111}_{1}a + {}^{111}_{1}d \pm {}^{111}_{1}bk\}({}_{1}C)$$
$$+\ \{\pm\,{}^{111}_{1}c \pm {}^{111}_{1}b + {}^{111}_{1}dk\}({}_{1}S)]\ \Big\} \qquad \sin(\ell x)$$

$+$

$$\Big\{\ 4\mu\bar{D}_{xx}({}_{2}A_{t,b}2\ell)$$

$$-\ 4\mu\ell[\{{}^{2}_{2}a + {}^{2}_{2}d \pm 2\,{}^{2}_{2}bk\}({}_{2}C) + \{\pm\,{}^{2}_{2}c \pm {}^{2}_{2}b + 2\,{}^{2}_{2}dk\}({}_{2}S)]$$

$$-\ \mu\ell[\{3\,{}^{1}_{1}c + 4\,{}^{1}_{1}b \pm 3\,{}^{1}_{1}dk\}({}_{1}C)$$
$$+\ \{\pm 3\,{}^{1}_{1}a \pm 4\,{}^{1}_{1}d + 3\,{}^{1}_{1}bk\}({}_{1}S)]({}_{1}A_{t,b}\ell)$$

$$-\ 4\mu\ell[\{{}^{11}_{2}a + {}^{11}_{2}d \pm 2\,{}^{11}_{2}bk\}({}_{2}C) + \{\pm\,{}^{11}_{2}c \pm {}^{11}_{2}b + 2\,{}^{11}_{2}dk\}({}_{2}S)]$$

$$-\ 4\mu\ell[\{{}^{12}_{2}a + {}^{12}_{2}d \pm 2\,{}^{12}_{2}bk\}({}_{2}C) + \{\pm\,{}^{12}_{2}c \pm {}^{12}_{2}b + 2\,{}^{12}_{2}dk\}({}_{2}S)]$$

$$-\ \mu\ell[\{3\,{}^{11}_{1}c + 4\,{}^{11}_{1}b \pm 3\,{}^{11}_{1}dk\}({}_{1}C)$$
$$+\ \{\pm 3\,{}^{11}_{1}a \pm 4\,{}^{11}_{1}d + 3\,{}^{11}_{1}bk\}({}_{1}S)]({}_{1}A_{t,b}\ell)$$

$$-\ 3\mu\ell[\{{}^{11}_{3}c + 4\,{}^{11}_{3}b \pm 3\,{}^{11}_{3}dk\}({}_{3}C)$$
$$+\ \{\pm\,{}^{11}_{3}a \pm 4\,{}^{11}_{3}d + 3\,{}^{11}_{3}bk\}({}_{3}S)]({}_{1}A_{t,b}\ell)$$

$$-\ 4\mu\ell[\{{}^{111}_{2}a + {}^{111}_{2}d \pm 2\,{}^{111}_{2}bk\}({}_{2}C)$$
$$+\ \{\pm\,{}^{111}_{2}c \pm {}^{111}_{2}b + 2\,{}^{111}_{2}dk\}({}_{2}S)]\ \Big\} \qquad \sin(2\ell x)$$

$$
\begin{aligned}
+ \\
& \Big\{ \; 4\mu\bar{D}_{xx}({}_{3}A_{t,b}3\ell) + \mu\bar{D}_{xx}({}_{1}A_{t,b}\ell)^{3} \\
& - 6\mu\ell[\{{}^{3}_{3}a+{}^{3}_{3}d \pm 3{}^{3}_{3}bk\}({}_{3}C) + \{\pm{}^{3}_{3}c\pm{}^{3}_{3}b+3{}^{3}_{3}dk\}({}_{3}S)] \\
& - 6\mu\ell[\{{}^{1}{}^{1}_{3}a+{}^{1}{}^{1}_{3}d \pm 3{}^{1}{}^{1}_{3}bk\}({}_{3}C) + \{\pm{}^{1}{}^{1}_{3}c\pm{}^{1}{}^{1}_{3}b+3{}^{1}{}^{1}_{3}dk\}({}_{3}S)] \\
& - \mu\ell[\{5{}^{1}_{1}c+6{}^{1}_{1}b\pm 5{}^{1}_{1}dk\}({}_{1}C) \\
& \qquad\qquad + \{\pm 5{}^{1}_{1}a\pm 6{}^{1}_{1}d+5{}^{1}_{1}bk\}({}_{1}S)]({}_{2}A_{t,b}\ell) \\
& - 4\mu\ell[\{2{}^{2}_{2}c+3{}^{2}_{2}b\pm 4{}^{2}_{2}dk\}({}_{2}C) \\
& \qquad\qquad + \{\pm 2{}^{2}_{2}a\pm 3{}^{2}_{2}d+4{}^{2}_{2}bk\}({}_{2}S)]({}_{1}A_{t,b}\ell) \\
& - 6\mu\ell[\{{}^{1}{}^{2}_{3}a+{}^{1}{}^{2}_{3}d\pm 3{}^{1}{}^{2}_{3}bk\}({}_{3}C) \\
& \qquad\qquad\qquad + \{\pm{}^{1}{}^{2}_{3}c\pm{}^{1}{}^{2}_{3}b+3{}^{1}{}^{2}_{3}dk\}({}_{3}S)] \\
& - (\mu\ell/4)[\{9{}^{1}_{1}a+15{}^{1}_{1}d\pm 9{}^{1}_{1}bk\}({}_{1}C) \\
& \qquad\qquad + \{\pm 9{}^{1}_{1}c\pm 15{}^{1}_{1}b+9{}^{1}_{1}dk\}({}_{1}S)]({}_{1}A_{t,b}\ell)^{2} \\
& - 4\mu\ell[\{2{}^{1}{}^{1}_{2}c+3{}^{1}{}^{1}_{2}b\pm 4{}^{1}{}^{1}_{2}dk\}({}_{2}C) \\
& \qquad\qquad + \{\pm 2{}^{1}{}^{1}_{2}a\pm 3{}^{1}{}^{1}_{2}d+4{}^{1}{}^{1}_{2}bk\}({}_{2}S)]({}_{1}A_{t,b}\ell) \\
& - 6\mu\ell[\{{}^{11}{}^{1}_{3}a+{}^{11}{}^{1}_{3}d\pm 3{}^{11}{}^{1}_{3}bk\}({}_{3}C) \\
& \qquad\qquad + \{\pm{}^{11}{}^{1}_{3}c\pm{}^{11}{}^{1}_{3}b+3{}^{11}{}^{1}_{3}dk\}({}_{3}S)] \;\Big\} \qquad \sin(3\ell x) \\
+ \\
& \Big\{ \; 4\mu\bar{D}_{xx}({}_{4}A_{t,b}4\ell) \\
& - 8\mu\ell[\{{}^{4}_{4}a+{}^{4}_{4}d\pm 4{}^{4}_{4}bk\}({}_{4}C) + \{\pm{}^{4}_{4}c\pm{}^{4}_{4}b+4{}^{4}_{4}dk\}({}_{4}S)] \\
& - 8\mu\ell[\{{}^{1}{}^{2}_{4}a+{}^{1}{}^{2}_{4}d\pm 4{}^{1}{}^{2}_{4}bk\}({}_{4}C) + \{\pm{}^{1}{}^{2}_{4}c\pm{}^{1}{}^{2}_{4}b+4{}^{1}{}^{2}_{4}dk\}({}_{4}S)] \\
& - 3\mu\ell[\{5{}^{1}{}^{1}_{3}c+8{}^{1}{}^{1}_{3}b\pm 15{}^{1}{}^{1}_{3}dk\}({}_{3}C) \\
& \qquad\qquad + \{\pm 5{}^{1}{}^{1}_{3}a\pm 8{}^{1}{}^{1}_{3}d+15{}^{1}{}^{1}_{3}bk\}({}_{3}S)]({}_{1}A_{t,b}\ell) \\
& - 8\mu\ell[\{{}^{11}{}^{1}_{4}a+{}^{11}{}^{1}_{4}d\pm 4{}^{11}{}^{1}_{4}bk\}({}_{4}C) \\
& \qquad\qquad + \{\pm{}^{11}{}^{1}_{4}c\pm{}^{11}{}^{1}_{4}b+4{}^{11}{}^{1}_{4}dk\}({}_{4}S)] \;\Big\} \qquad \sin(4\ell x)
\end{aligned}
\tag{12b}
$$

2) Introduce 3rd order expressions for the normal and shear stresses at the interface, σ_{nn} and σ_{ns}, which are written in terms of two new constants, σ and τ. These expressions are:

$$
\begin{aligned}
(\sigma_{nn})_{t,b} = \sigma_o &+ ({}^{1}_{1}\sigma_{t,b} + {}^{11}_{1}\sigma_{t,b} + {}^{12}_{1}\sigma_{t,b} + {}^{111}_{1}\sigma_{t,b}) \cos(\ell x) \\
&+ ({}^{2}_{2}\sigma_{t,b} + {}^{11}_{2}\sigma_{t,b} + {}^{12}_{2}\sigma_{t,b} + {}^{111}_{2}\sigma_{t,b}) \cos(2\ell x) \\
&+ ({}^{3}_{3}\sigma_{t,b} + {}^{11}_{3}\sigma_{t,b} + {}^{12}_{3}\sigma_{t,b} + {}^{111}_{3}\sigma_{t,b}) \cos(3\ell x) \\
&+ ({}^{4}_{4}\sigma_{t,b} + {}^{12}_{4}\sigma_{t,b} + {}^{111}_{4}\sigma_{t,b}) \cos(4\ell x)
\end{aligned}
\tag{13a}
$$

$$
\begin{aligned}
(\sigma_{ns})_{t,b} = \tau_o &+ ({}^{1}_{1}\tau_{t,b} + {}^{11}_{1}\tau_{t,b} + {}^{12}_{1}\tau_{t,b} + {}^{111}_{1}\tau_{t,b}) \sin(\ell x) \\
&+ ({}^{2}_{2}\tau_{t,b} + {}^{11}_{2}\tau_{t,b} + {}^{12}_{2}\tau_{t,b} + {}^{111}_{2}\tau_{t,b}) \sin(2\ell x) \\
&+ ({}^{3}_{3}\tau_{t,b} + {}^{11}_{3}\tau_{t,b} + {}^{12}_{3}\tau_{t,b} + {}^{111}_{3}\tau_{t,b}) \sin(3\ell x) \\
&+ ({}^{4}_{4}\tau_{t,b} + {}^{12}_{4}\tau_{t,b} + {}^{111}_{4}\tau_{t,b}) \sin(4\ell x)
\end{aligned}
\tag{13b}
$$

3) Equate the expressions for the interface stresses written in terms of arbitrary constants for the layer, eq. (12), to the expressions written in terms of arbitrary constants for the interface, eq. (13); equate (12a) to (13a) and (12b) to (13b). The interface constants, σ and τ, are thereby expressed in terms of the layer constants, $\underline{a}$, $\underline{b}$, $\underline{c}$, and $\underline{d}$. A pair of equations, one for σ and one for τ, can be written for each combination of order and waveform contained in eq. (8). An example is shown in eqs. (14) for the 1st order

constants for the first waveform:

$$ {}^1_1\sigma_{t,b} = \rho g({}_1A_{t,b}) + 2\mu\ell[\{{}^1_1c \pm {}^1_1dk\}({}_1C) $$

$$ + \{\pm\ {}^1_1a + {}^1_1bk\}({}_1S)] \tag{14a} $$

$$ {}^1_1\tau_{t,b} = 4\mu\bar{D}_{xx}({}_1A_{t,b}\ell) - 2\mu\ell[\{{}^1_1a + {}^1_1d \pm {}^1_1bk\}({}_1C) $$

$$ + \{\pm\ {}^1_1c \pm {}^1_1b + {}^1_1dk\}({}_1S)] \tag{14b} $$

4. However, we need expressions for the layer constants, a, b, c, and d, in terms of the interface constants, σ and τ. We derive these expressions by solving each pair of equations, such as (14a) and (14b), simultaneously. The expressions for the layer constants in terms of the interface constants are:

$$ {}_ja = [{}_j\Lambda_m\{jk({}_jS) + {}_jC\} + {}_j\lambda_p\{jk({}_jC)\}] \tag{15a} $$

$$ {}_jb = -[{}_j\Lambda_p({}_jS) + {}_j\lambda_m({}_jC)] \tag{15b} $$

$$ {}_jc = [{}_j\Lambda_p\{jk({}_jC) + {}_jS\} + {}_j\lambda_m\{jk({}_jS)\}] \tag{15c} $$

$$ {}_jd = -[{}_j\Lambda_m({}_jC) + {}_j\lambda_p({}_jS)] \tag{15d} $$

In deriving eqs. (15), we have introduced new constants, lambda. The constants lambda for each combination of order and waveform contain the corresponding interface constants and the interaction terms responsible for generating that waveform-order combination. The values of lambda are:

$$ {}^{j}_{j}\Lambda_{p,m} = \frac{[{}^{j}_{j}\sigma_t \pm {}^{j}_{j}\sigma_b - \rho g({}_{j}A_t \pm {}_{j}A_b)]}{[4j\mu\ell({}_{j}S_{j}C \pm jk)]} \text{ ; } j = 1,\ 2,\ \text{or } 3 \text{ (no sum)} \qquad (16a) $$

in which $\rho \underline{g}$ is unit weight (density times acceleration of gravity).

$$ {}^{j}_{j}\lambda_{p,m}[4j\mu\ell({}_{j}S_{j}C \mp jk)] = [{}^{j}_{j}\tau_t \pm {}^{j}_{j}\tau_b - 4j\mu\ell\bar{D}_{xx}({}_{j}A_t \pm {}_{j}A_b)] \qquad (16b) $$

$$ \begin{aligned} {}^{11}_{2}\Lambda_{p,m}[2({}_{2}S_{2}C \pm 2k)] = {} & [{}^{11}_{2}\sigma_t \pm {}^{11}_{2}\sigma_b + 2\mu(\ell^2)\bar{D}_{xx}({}_{1}A_t^2 \pm {}_{1}A_b^2)]/4\mu\ell \\ & +(3\ell/4)({}_{1}A_t \pm {}_{1}A_b)({}^{1}_{1}\lambda_p)({}_{1}S_{1}C-k) \\ & + (3\ell/4)({}_{1}A_t \mp {}_{1}A_b)({}^{1}_{1}\lambda_m)({}_{1}S_{1}C+k) \qquad (16c) \end{aligned} $$

$$ \begin{aligned} {}^{11}_{2}\lambda_{p,m}[2({}_{2}S_{2}C \mp 2k)] = {} & ({}^{11}_{2}\tau_t \pm {}^{11}_{2}\tau_b)/4\mu\ell \\ & - (\ell/4)({}_{1}A_t \pm {}_{1}A_b)[{}^{1}_{1}\Lambda_p({}_{1}S_{1}C-3k) + {}^{1}_{1}\lambda_m(4{}_{1}C^2)] \\ & - (\ell/4)({}_{1}A_t \mp {}_{1}A_b)[{}^{1}_{1}\Lambda_m({}_{1}S_{1}C+3k) + {}^{1}_{1}\lambda_p(4{}_{1}S^2)] \qquad (16d) \end{aligned} $$

$$ \begin{aligned} {}^{12}_{1}\Lambda_{p,m}[2({}_{1}S_{1}C \pm k)] = {} & ({}^{12}_{1}\sigma_t \pm {}^{12}_{1}\sigma_b)/2\mu\ell - 4\ell\bar{D}_{xx}[({}_{1}A_t)({}_{2}A_t) \pm ({}_{1}A_b)({}_{2}A_b)] \\ & - (3\ell/2)({}_{2}A_t \pm {}_{2}A_b)({}^{1}_{1}\lambda_p)({}_{1}S_{1}C-k) \\ & - (3\ell/2)({}_{2}A_t \mp {}_{2}A_b)({}^{1}_{1}\lambda_m)({}_{1}S_{1}C+k) \qquad (16e) \end{aligned} $$

$$
\begin{aligned}
{}^{12}_{1}\lambda_{p,m}[2({}_1S_1C \mp k)] = {} & ({}^{12}_{1}\tau_t \pm {}^{12}_{1}\tau_b)/2\mu\ell \\
& - 2\ell({}_1A_t \pm {}_1A_b)[{}^{2}_{2}\Lambda_p({}_2S_2C) + {}^{2}_{2}\lambda_m({}_2C^2)] \\
& - 2\ell({}_1A_t \mp {}_1A_b)[{}^{2}_{2}\Lambda_m({}_2S_2C) + {}^{2}_{2}\lambda_p({}_2S^2)] \\
& + (\ell/2)({}_2A_t \pm {}_2A_b)[{}^{1}_{1}\Lambda_p({}_1S_1C+3k) - {}^{1}_{1}\lambda_m(2{}_1C^2)] \\
& + (\ell/2)({}_2A_t \mp {}_2A_b)[{}^{1}_{1}\Lambda_m({}_1S_1C-3k) - {}^{1}_{1}\lambda_p(2{}_1S^2)]
\end{aligned}
\tag{16f}
$$

$$
\begin{aligned}
{}^{111}_{1}\Lambda_{p,m}[2({}_1S_1C \pm k)] = {} & ({}^{111}_{1}\sigma_t \pm {}^{111}_{1}\sigma_b)/2\mu\ell \\
& - (\ell^2/8)({}_1A_t^2 \pm {}_1A_b^2)[{}^{1}_{1}\Lambda_p({}_1S_1C-5k) + {}^{1}_{1}\lambda_m(6{}_1C^2)] \\
& - (\ell^2/8)({}_1A_t^2 \mp {}_1A_b^2)[{}^{1}_{1}\Lambda_m({}_1S_1C+5k) + {}^{1}_{1}\lambda_p(6{}_1S^2)]
\end{aligned}
\tag{16g}
$$

$$
\begin{aligned}
{}^{111}_{1}\lambda_{p,m}[2({}_1S_1C \mp k)] = {} & [{}^{111}_{1}\tau_t \pm {}^{111}_{1}\tau_b + 3\mu(\ell^3)\bar{D}_{xx}({}_1A_t^3 \pm {}_1A_b^3)]/2\mu\ell \\
& - 2\ell({}_1A_t \pm {}_1A_b)[{}^{11}_{2}\Lambda_p({}_2S_2C) + {}^{11}_{2}\lambda_m({}_2C^2)] \\
& - 2\ell({}_1A_t \mp {}_1A_b)[{}^{11}_{2}\Lambda_m({}_2S_2C) + {}^{11}_{2}\lambda_p({}_2S^2)] \\
& - (\ell^2/8)({}_1A_t^2 \pm {}_1A_b^2)[{}^{1}_{1}\Lambda_m(6{}_1C^2) - {}^{1}_{1}\lambda_p({}_1S_1C-7k)] \\
& - (\ell^2/8)({}_1A_t^2 \mp {}_1A_b^2)[{}^{1}_{1}\Lambda_p(6{}_1S^2) - {}^{1}_{1}\lambda_m({}_1S_1C+7k)]
\end{aligned}
\tag{16h}
$$

$$ {}^{12}_{3}\Lambda_{p,m}[2({}_{3}S_{3}C \pm 3k)] = ({}^{12}_{3}\sigma_t \pm {}^{12}_{3}\sigma_b)/6\mu\ell $$

$$ + (4\ell/3)\bar{D}_{xx}[({}_{1}A_t)({}_{2}A_t) \pm ({}_{1}A_b)({}_{2}A_b)] $$

$$ + (4\ell/3)({}_{1}A_t \pm {}_{1}A_b)({}^{2}_{2}\lambda_p)({}_{2}S_{2}C-2k) $$

$$ + (4\ell/3)({}_{1}A_t \mp {}_{1}A_b)({}^{2}_{2}\lambda_m)({}_{2}S_{2}C+2k) $$

$$ + (5\ell/6)({}_{2}A_t \pm {}_{2}A_b)({}^{1}_{1}\lambda_p)({}_{1}S_{1}C-k) $$

$$ + (5\ell/6)({}_{2}A_t \mp {}_{2}A_b)({}^{1}_{1}\lambda_m)({}_{1}S_{1}C+k) \tag{16i} $$

$$ {}^{12}_{3}\lambda_{p,m}[2({}_{3}S_{3}C \mp 3k)] = ({}^{12}_{3}\tau_t \pm {}^{12}_{3}\tau_b)/6\mu\ell $$

$$ - (2\ell/3)({}_{1}A_t \pm {}_{1}A_b)[{}^{2}_{2}\Lambda_p({}_{2}S_{2}C-4k) + {}^{2}_{2}\lambda_m(3{}_{2}C^2)] $$

$$ - (2\ell/3)({}_{1}A_t \mp {}_{1}A_b)[{}^{2}_{2}\Lambda_m({}_{2}S_{2}C+4k) + {}^{2}_{2}\lambda_p(3{}_{2}S^2)] $$

$$ - (\ell/6)({}_{2}A_t \pm {}_{2}A_b)[{}^{1}_{1}\Lambda_p({}_{1}S_{1}C-5k) + {}^{1}_{1}\lambda_m(6{}_{1}C^2)] $$

$$ - (\ell/6)({}_{2}A_t \mp {}_{2}A_b)[{}^{1}_{1}\Lambda_m({}_{1}S_{1}C+5k) + {}^{1}_{1}\lambda_p(6{}_{1}S^2)] \tag{16j} $$

$$ {}^{111}_{\ \ 3}\Lambda_{p,m}[2({}_{3}S_{3}C \pm 3k)] = ({}^{111}_{\ \ 3}\sigma_t \pm {}^{111}_{\ \ 3}\sigma_b)/6\mu\ell $$

$$ + (4\ell/3)({}_{1}A_t \pm {}_{1}A_b)({}^{11}_{\ 2}\lambda_p)({}_{2}S_{2}C-2k) $$

$$ + (4\ell/3)({}_{1}A_t \mp {}_{1}A_b)({}^{11}_{\ 2}\lambda_m)({}_{2}S_{2}C+2k) $$

$$ + (\ell^2/24)({}_{1}A_t^2 \pm {}_{1}A_b^2)[{}^{1}_{1}\Lambda_p(5{}_{1}S_{1}C-9k) + {}^{1}_{1}\lambda_m(14{}_{1}C^2)] $$

$$ + (\ell^2/24)({}_{1}A_t^2 \mp {}_{1}A_b^2)[{}^{1}_{1}\Lambda_m(5{}_{1}S_{1}C+9k) + {}^{1}_{1}\lambda_p(14{}_{1}S^2)] \tag{16k} $$

$$
\begin{aligned}
{}^{111}_{3}\lambda_{p,m}\left[2({}_{3}S_{3}C \mp 3k)\right] = {} & \left[{}^{111}_{3}\tau_{t} \pm {}^{111}_{3}\tau_{b} - \mu(\ell^{3})\bar{D}_{xx}({}_{1}A_{t}^{3} \pm {}_{1}A_{b}^{3})\right]/6\mu\ell \\
& - (2\ell/3)({}_{1}A_{t} \pm {}_{1}A_{b})\left[{}^{11}_{2}\Lambda_{p}({}_{2}S_{2}C-4k) + {}^{11}_{2}\lambda_{m}(3_{2}C^{2})\right] \\
& - (2\ell/3)({}_{1}A_{t} \mp {}_{1}A_{b})\left[{}^{11}_{2}\Lambda_{m}({}_{2}S_{2}C+4k) + {}^{11}_{2}\lambda_{p}(3_{2}S^{2})\right] \\
& - (\ell^{2}/8)({}_{1}A_{t}^{2} \pm {}_{1}A_{b}^{2})\left[{}^{1}_{1}\Lambda_{m}(2_{1}C^{2}) + {}^{1}_{1}\lambda_{p}(5_{1}S_{1}C-3k)\right] \\
& - (\ell^{2}/8)({}_{1}A_{t}^{2} \mp {}_{1}A_{b}^{2})\left[{}^{1}_{1}\Lambda_{p}(2_{1}S^{2}) + {}^{1}_{1}\lambda_{m}(5_{1}S_{1}C+3k)\right] \qquad (16\ell)
\end{aligned}
$$

$$ {}^{11}_{1}\Lambda_{p,m}[2({}_1S_1C\pm k)] = ({}^{11}_{1}\sigma_t \pm {}^{11}_{1}\sigma_b)/2\mu\ell \qquad (16m) $$

$$ {}^{11}_{1}\lambda_{p,m}[2({}_1S_1C\mp k)] = ({}^{11}_{1}\tau_t \pm {}^{11}_{1}\tau_b)/2\mu\ell \qquad (16n) $$

$$ {}^{12}_{2}\Lambda_{p,m}[2({}_2S_2C\pm 2k)] = ({}^{12}_{2}\sigma_t \pm {}^{12}_{2}\sigma_b)/4\mu\ell \qquad (16o) $$

$$ {}^{12}_{2}\lambda_{p,m}[2({}_2S_2C\mp 2k)] = ({}^{12}_{2}\tau_t \pm {}^{12}_{2}\tau_b)/4\mu\ell \qquad (16p) $$

$$ \begin{aligned} {}^{111}_{2}\Lambda_{p,m}[2({}_2S_2C\pm 2k)] &= ({}^{111}_{2}\sigma_t \pm {}^{111}_{2}\sigma_b)/4\mu\ell \\ &+ (3\ell/4)({}_1A_t\pm{}_1A_b)[{}^{11}_{1}\lambda_p({}_1S_1C-k)+{}^{11}_{3}\lambda_p({}_3S_3C-3k)] \\ &+ (3\ell/4)({}_1A_t\mp{}_1A_b)[{}^{11}_{1}\lambda_m({}_1S_1C+k)+{}^{11}_{3}\lambda_m({}_3S_3C+3k)] \end{aligned} \qquad (16q) $$

$$ \begin{aligned} {}^{111}_{2}\lambda_{p,m}[2({}_2S_2C\mp 2k)] &= ({}^{111}_{2}\tau_t\pm{}^{111}_{2}\tau_b)/4\mu\ell \\ &- (\ell/4)({}_1A_t\pm{}_1A_b)[{}^{11}_{1}\Lambda_p({}_1S_1C-3k)+4\,{}^{11}_{1}\lambda_m({}_1C^2)] \\ &- (\ell/4)({}_1A_t\mp{}_1A_b)[{}^{11}_{1}\Lambda_m({}_1S_1C+3k)+4\,{}^{11}_{1}\lambda_p({}_1S^2)] \\ &- (3\ell/4)({}_1A_t\pm{}_1A_b)[{}^{11}_{3}\Lambda_p 3({}_3S_3C-k)+4\,{}^{11}_{3}\lambda_m({}_3C^2)] \\ &- (3\ell/4)({}_1A_t\mp{}_1A_b)[{}^{11}_{3}\Lambda_m 3({}_3S_3C+k)+4\,{}^{11}_{3}\lambda_p({}_3S^2)] \end{aligned} \qquad (16r) $$

$$ {}^{11}_{3}\Lambda_{p,m}[2({}_3S_3C\pm 3k)] = ({}^{11}_{3}\sigma_t \pm {}^{11}_{3}\sigma_b)/6\mu\ell \qquad (16s) $$

$$ {}^{11}_{3}\lambda_{p,m}[2({}_3S_3C\mp 3k)] = ({}^{11}_{3}\tau_t \pm {}^{11}_{3}\tau_b)/6\mu\ell \qquad (16t) $$

$$ {}^{12}_{4}\Lambda_{p,m}[2({}_4S_4C\pm 4k)] = ({}^{12}_{4}\sigma_t \pm {}^{12}_{4}\sigma_b)/8\mu\ell \qquad (16u) $$

$$ {}^{12}_{4}\lambda_{p,m}[2({}_4S_4C\mp 4k)] = ({}^{12}_{4}\tau_t \pm {}^{12}_{4}\tau_b)/8\mu\ell \qquad (16v) $$

$$ \begin{aligned} {}^{111}_{4}\Lambda_{p,m}[2({}_4S_4C\pm 4k)] &= ({}^{111}_{4}\sigma_t \pm {}^{111}_{4}\sigma_b)/8\mu\ell \\ &+ (15\ell/8)({}_1A_t\pm{}_1A_b)[{}^{11}_{3}\lambda_p({}_3S_3C-3k)] \\ &+ (15\ell/8)({}_1A_t\mp{}_1A_b)[{}^{11}_{3}\lambda_m({}_3S_3C+3k)] \end{aligned} \qquad (16w) $$

$$ \begin{aligned} {}^{111}_{4}\lambda_{p,m}[2({}_4S_4C\mp 4k)] &= ({}^{111}_{4}\tau_t\pm{}^{111}_{4}\tau_b)/8\mu\ell \\ &- (3\ell/8)({}_1A_t\pm{}_1A_b)[{}^{11}_{3}\Lambda_p 3({}_3S_3C-5k)+8\,{}^{11}_{3}\lambda_m({}_3C^2)] \\ &- (3\ell/8)({}_1A_t\mp{}_1A_b)[{}^{11}_{3}\Lambda_m 3({}_3S_3C+5k)+8\,{}^{11}_{3}\lambda_p({}_3S^2)] \end{aligned} \qquad (16x) $$

The interface velocities can now be written in terms of the interface stress constants. First, we expand the expressions for the interface velocities, eqs. (10a,b), to 3rd order. Then we substitute the 3rd order expressions for the mean and perturbed velocities, eq. (3a,b), using eqs. (4a,b) and (9a,b), into the expanded expressions for the interface velocities. Now the interface velocities are expressed, to 3rd order, in terms of the layer constants. We rewrite the interface velocities in terms of the interface stress constants using eqs. (15).

The resulting expressions for the velocities normal and tangential to the interface are:

$$
\begin{aligned}
(v_n)_{t,b} = {} & (\bar{v}_z)_{t,b}\cos(\theta_{t,b}) - (\bar{v}_x)_{t,b}\sin(\theta_{t,b}) \\
& + \Big\{ ({}^{1}_{1}\Lambda_m + {}^{11}_{\;1}\Lambda_m + {}^{12}_{\;1}\Lambda_m + {}^{111}_{\;\;1}\Lambda_m)({}_{1}C^2) \\
& + ({}^{1}_{1}\lambda_p + {}^{11}_{\;1}\lambda_p + {}^{12}_{\;1}\lambda_p + {}^{111}_{\;\;1}\lambda_p)k \\
& \pm ({}^{1}_{1}\Lambda_p + {}^{11}_{\;1}\Lambda_p + {}^{12}_{\;1}\Lambda_p + {}^{111}_{\;\;1}\Lambda_p)({}_{1}S^2) \\
& \mp ({}^{1}_{1}\lambda_m + {}^{11}_{\;1}\lambda_m + {}^{12}_{\;1}\lambda_m + {}^{111}_{\;\;1}\lambda_m)k \\
& + ({}_{1}A_{t,b}\ell/2)[({}^{2}_{2}\Lambda_p + {}^{11}_{\;2}\Lambda_p)2k - ({}^{2}_{2}\lambda_m + {}^{11}_{\;2}\lambda_m)({}_{2}C^2) \\
& \qquad \mp ({}^{2}_{2}\Lambda_m + {}^{11}_{\;2}\Lambda_m)2k \mp ({}^{2}_{2}\lambda_p + {}^{11}_{\;2}\lambda_p)({}_{2}S^2)] \\
& - ({}_{2}A_{t,b}\ell/2)[{}^{1}_{1}\Lambda_p k - {}^{1}_{1}\lambda_m({}_{1}C^2) \mp {}^{1}_{1}\Lambda_m k \mp {}^{1}_{1}\lambda_p({}_{1}S^2)] \\
& - ({}_{1}A_{t,b}\ell/2)^2[{}^{1}_{1}\Lambda_m({}_{1}C^2) + {}^{1}_{1}\lambda_p({}_{1}S_{1}C) \\
& \qquad \pm {}^{1}_{1}\Lambda_p({}_{1}S^2) \pm {}^{1}_{1}\lambda_m({}_{1}S_{1}C)] \Big\} \qquad \cos(\ell x)
\end{aligned}
$$

$+$

$$
\begin{aligned}
& + \Big\{ ({}^{2}_{2}\Lambda_m + {}^{11}_{\;2}\Lambda_m + {}^{12}_{\;2}\Lambda_m + {}^{111}_{\;\;2}\Lambda_m)({}_{2}C^2) \\
& + ({}^{2}_{2}\lambda_p + {}^{11}_{\;2}\lambda_p + {}^{12}_{\;2}\lambda_p + {}^{111}_{\;\;2}\lambda_p)2k
\end{aligned}
$$

$$\pm \left({}^{2}_{2}\Lambda_p+{}^{11}_{2}\Lambda_p+{}^{12}_{2}\Lambda_p+{}^{111}_{2}\Lambda_p\right)\left({}_{2}S^2\right)$$

$$\mp \left({}^{2}_{2}\lambda_m+{}^{11}_{2}\lambda_m+{}^{12}_{2}\lambda_m+{}^{111}_{2}\lambda_m\right)2k$$

$$+ \left({}_{1}A_{t,b}\ell\right)\left[{}^{1}_{1}\Lambda_p k-{}^{1}_{1}\lambda_m\left({}_{1}C^2\right)\mp{}^{1}_{1}\Lambda_m k\mp{}^{1}_{1}\lambda_p\left({}_{1}S^2\right)\right]$$

$$+ \left({}_{1}A_{t,b}\ell\right)\left[{}^{11}_{1}\Lambda_p k-{}^{11}_{1}\lambda_m\left({}_{1}C^2\right)\mp{}^{11}_{1}\Lambda_m k\mp{}^{11}_{1}\lambda_p\left({}_{1}S^2\right)\right]$$

$$+ \left({}_{1}A_{t,b}\ell\right)\left[{}^{11}_{3}\Lambda_p 3k-{}^{11}_{3}\lambda_m\left({}_{3}C^2\right)\right.$$

$$\left.\mp{}^{11}_{3}\Lambda_m 3k\mp{}^{11}_{3}\lambda_p\left({}_{3}S^2\right)\right] \Big\} \qquad \cos(2\ell x)$$

$$+$$

$$+ \Big\{ \left({}^{3}_{3}\Lambda_m+{}^{11}_{3}\Lambda_m+{}^{12}_{3}\Lambda_m+{}^{111}_{3}\Lambda_m\right)\left({}_{3}C^2\right)$$

$$+ \left({}^{3}_{3}\lambda_p+{}^{11}_{3}\lambda_p+{}^{12}_{3}\lambda_p+{}^{111}_{3}\lambda_p\right)3k$$

$$\pm \left({}^{3}_{3}\Lambda_p+{}^{11}_{3}\Lambda_p+{}^{12}_{3}\Lambda_p+{}^{111}_{3}\Lambda_p\right)\left({}_{3}S^2\right)$$

$$\mp \left({}^{3}_{3}\lambda_m+{}^{11}_{3}\lambda_m+{}^{12}_{3}\lambda_m+{}^{111}_{3}\lambda_m\right)3k$$

$$+ 3\left({}_{1}A_{t,b}\ell/2\right)\left[\left({}^{2}_{2}\Lambda_p+{}^{11}_{2}\Lambda_p\right)2k - \left({}^{2}_{2}\lambda_m+{}^{11}_{2}\lambda_m\right)\left({}_{2}C^2\right)\right.$$

$$\left.\mp\left({}^{2}_{2}\Lambda_m+{}^{11}_{2}\Lambda_m\right)2k \mp \left({}^{2}_{2}\lambda_p+{}^{11}{}_{2}\lambda_p\right)\left({}_{2}S^2\right)\right]$$

$$+ 3\left({}_{2}A_{t,b}\ell/2\right)\left[{}^{1}_{1}\Lambda_p k-{}^{1}_{1}\lambda_m\left({}_{1}C^2\right)\mp{}^{1}_{1}\Lambda_m k\mp{}^{1}_{1}\lambda_p\left({}_{1}S^2\right)\right]$$

$$- \left({}_{1}A_{t,b}\ell/2\right)^2\left[{}^{1}_{1}\Lambda_m\left({}_{1}C^2\right)+{}^{1}_{1}\lambda_p\left(3\,{}_{1}S_{1}C-2k\right)\right.$$

$$\left.\pm{}^{1}_{1}\Lambda_p\left({}_{1}S^2\right)\pm{}^{1}_{1}\lambda_m\left(3\,{}_{1}S_{1}C+2k\right)\right] \Big\} \qquad \cos(3\ell x)$$

$$+$$

$$+ \Big\{ \left({}^{4}_{4}\Lambda_m+{}^{12}_{4}\Lambda_m+{}^{111}_{4}\Lambda_m\right)\left({}_{4}C^2\right)$$

$$+ \left({}^{4}_{4}\lambda_p+{}^{12}_{4}\lambda_p+{}^{111}_{4}\lambda_p\right)4k$$

$$\pm \left({}^{4}_{4}\Lambda_p+{}^{12}_{4}\Lambda_p+{}^{111}_{4}\Lambda_p\right)\left({}_{4}S^2\right)$$

$$\mp \left({}^{4}_{4}\lambda_m+{}^{12}_{4}\lambda_m+{}^{111}_{4}\lambda_m\right)4k$$

$$+ 2\left({}_{1}A_{t,b}\ell\right)\left[{}^{11}_{3}\Lambda_p 3k-{}^{11}_{3}\lambda_m\left({}_{3}C^2\right)\right.$$

$$\left.\mp{}^{11}_{3}\Lambda_m 3k\mp{}^{11}_{3}\lambda_p\left({}_{3}S^2\right)\right] \Big\} \qquad \cos(4\ell x)$$

(17a)

$$
\begin{aligned}
(v_s)_{t,b} = {} & (\bar{v}_z)_{t,b}\sin(\theta_{t,b}) + (\bar{v}_x)_{t,b}\cos(\theta_{t,b}) \\
& + \Big\{ - ({}^{1}_{1}\Lambda_p + {}^{1}{}^{1}_{1}\Lambda_p + {}^{1}{}^{2}_{1}\Lambda_p + {}^{11}{}^{1}_{1}\Lambda_p)k \\
& + ({}^{1}_{1}\lambda_{m+}{}^{1}{}^{1}_{1}\lambda_m + {}^{1}{}^{2}_{1}\lambda_m + {}^{11}{}^{1}_{1}\lambda_m)({}_{1}C^2) \\
& \pm ({}^{1}_{1}\Lambda_m + {}^{1}{}^{1}_{1}\Lambda_m + {}^{1}{}^{2}_{1}\Lambda_m + {}^{11}{}^{1}_{1}\Lambda_m)k \\
& \pm ({}^{1}_{1}\lambda_p + {}^{1}{}^{1}_{1}\lambda_p + {}^{1}{}^{2}_{1}\lambda_p + {}^{11}{}^{1}_{1}\lambda_p)({}_{1}S^2) \\
& + ({}_{1}A_{t,b}\ell/2)[({}^{2}_{2}\Lambda_m + {}^{1}{}^{1}_{2}\Lambda_m)(3_2C^2) + ({}^{2}_{2}\lambda_p + {}^{1}{}^{1}_{2}\lambda_p)(4_2S_2C-2k) \\
& \qquad \pm ({}^{2}_{2}\Lambda_p + {}^{1}{}^{1}_{2}\Lambda_p)(3_2S^2) \pm ({}^{2}_{2}\lambda_m + {}^{1}{}^{1}_{2}\lambda_m)(4_2S_2C+2k)] \\
& - ({}_{2}A_{t,b}\ell/2)[{}^{1}_{1}\Lambda_m(3_1C^2) + {}^{1}_{1}\lambda_p(2_1S_1C+k) \\
& \qquad \pm {}^{1}_{1}\Lambda_p(3_1S^2) \pm {}^{1}_{1}\lambda_m(2_1S_1C-k)] \\
& + ({}_{1}A_{t,b}\ell/2)^2[{}^{1}_{1}\Lambda_p({}_{1}S_1C) + {}^{1}_{1}\lambda_m({}_{1}C^2) \\
& \qquad \pm {}^{1}_{1}\Lambda_m({}_{1}S_1C) \pm {}^{1}_{1}\lambda_p({}_{1}S^2)] \Big\} \qquad \sin(\ell x) \\
+ & \\
& + \Big\{ - ({}^{2}_{2}\Lambda_p + {}^{1}{}^{1}_{2}\Lambda_p + {}^{1}{}^{2}_{2}\Lambda_p + {}^{11}{}^{1}_{2}\Lambda_p)2k \\
& + ({}^{2}_{2}\lambda_{m+}{}^{1}{}^{1}_{2}\lambda_m + {}^{1}{}^{2}_{2}\lambda_m + {}^{11}{}^{1}_{2}\lambda_m)({}_{2}C^2) \\
& \pm ({}^{2}_{2}\Lambda_m + {}^{1}{}^{1}_{2}\Lambda_m + {}^{1}{}^{2}_{2}\Lambda_m + {}^{11}{}^{1}_{2}\Lambda_m)2k \\
& \pm ({}^{2}_{2}\lambda_p + {}^{1}{}^{1}_{2}\lambda_p + {}^{1}{}^{2}_{2}\lambda_p + {}^{11}{}^{1}_{2}\lambda_p)({}_{2}S^2) \\
& + ({}_{1}A_{t,b}\ell)[({}^{1}_{1}\lambda_p + {}^{1}{}^{1}_{1}\lambda_p)({}_{1}S_1C-k) \pm ({}^{1}_{1}\lambda_m + {}^{1}{}^{1}_{1}\lambda_m)({}_{1}S_1C+k)] \\
& + ({}_{1}A_{t,b}\ell)[2{}^{1}{}^{1}_{3}\Lambda_m({}_{3}C^2) + 3{}^{1}{}^{1}_{3}\lambda_p({}_{3}S_3C-k) \\
& \qquad \pm 2{}^{1}{}^{1}_{3}\Lambda_p({}_{3}S^2) \pm 3{}^{1}{}^{1}_{3}\lambda_m({}_{3}S_3C+k)] \Big\} \qquad \sin(2\ell x) \\
+ & \\
& + \Big\{ - ({}^{3}_{3}\Lambda_p + {}^{1}{}^{1}_{3}\Lambda_p + {}^{1}{}^{2}_{3}\Lambda_p + {}^{11}{}^{1}_{3}\Lambda_p)3k \\
& + ({}^{3}_{3}\lambda_{m+}{}^{1}{}^{1}_{3}\lambda_m + {}^{1}{}^{2}_{3}\lambda_m + {}^{11}{}^{1}_{3}\lambda_m)({}_{3}C^2) \\
& \pm ({}^{3}_{3}\Lambda_m + {}^{1}{}^{1}_{3}\Lambda_m + {}^{1}{}^{2}_{3}\Lambda_m + {}^{11}{}^{1}_{3}\Lambda_m)3k \\
& \pm ({}^{3}_{3}\lambda_p + {}^{1}{}^{1}_{3}\lambda_p + {}^{1}{}^{2}_{3}\lambda_p + {}^{11}{}^{1}_{3}\lambda_p)({}_{3}S^2) \\
& + ({}_{1}A_{t,b}\ell/2)[({}^{2}_{2}\Lambda_m + {}^{1}{}^{1}_{2}\Lambda_m)({}_{2}C^2) + ({}^{2}_{2}\lambda_p + {}^{1}{}^{1}_{2}\lambda_p)(4_2S_2C-6k)
\end{aligned}
$$

$$\pm({}^{2}_{2}\Lambda_p+{}^{1}{}^{1}_{2}\Lambda_p)({}_{2}S^2) \quad \pm \quad ({}^{2}_{2}\lambda_m+{}^{1}{}^{1}_{2}\lambda_m)(4\,{}_{2}S_2C+6k)]$$

$$-\quad ({}_{2}A_{t,b}\ell/2)[{}^{1}_{1}\Lambda_m({}_{1}C^2)-{}^{1}_{1}\lambda_p(2\,{}_{1}S_1C-3k)$$

$$\pm{}^{1}_{1}\Lambda_p({}_{1}S^2)\mp{}^{1}_{1}\lambda_m(2\,{}_{1}S_1C+3k)]$$

$$+\quad ({}_{1}A_{t,b}\ell/2)^2[{}^{1}_{1}\Lambda_p({}_{1}S_1C-2k)+{}^{1}_{1}\lambda_m(3\,{}_{1}C^2)$$

$$\pm{}^{1}_{1}\Lambda_m({}_{1}S_1C+2k)\pm{}^{1}_{1}\lambda_p(3\,{}_{1}S^2)] \quad \Big\} \qquad \sin(3\ell x)$$

$$+$$

$$+\quad \Big\{ \quad -\quad ({}^{4}_{4}\Lambda_p+{}^{1}{}^{2}_{4}\Lambda_p+{}^{11}{}^{1}_{4}\Lambda_p)4k$$

$$+\quad ({}^{4}_{4}\lambda_m+{}^{1}{}^{2}_{4}\lambda_m+{}^{11}{}^{1}_{4}\lambda_m)({}_{4}C^2)$$

$$\pm\quad ({}^{4}_{4}\Lambda_m+{}^{1}{}^{2}_{4}\Lambda_m+{}^{11}{}^{1}_{4}\Lambda_m)4k$$

$$\pm\quad ({}^{4}_{4}\lambda_p+{}^{1}{}^{2}_{4}\lambda_p+{}^{11}{}^{1}_{4}\lambda_p)({}_{4}S^2)$$

$$+\quad ({}_{1}A_{t,b}\ell)[{}^{1}{}^{1}_{3}\Lambda_m({}_{3}C^2)+3\,{}^{1}{}^{1}_{3}\lambda_p({}_{3}S_3C-2k)$$

$$\pm{}^{1}{}^{1}_{3}\Lambda_p({}_{3}S^2)\pm 3\,{}^{1}{}^{1}_{3}\lambda_m({}_{3}S_3C+2k)] \quad \Big\} \qquad \sin(4\ell x)$$

(17b)

The derivation of the velocities for the upper and lower confining media uses the same equations as used for the layers and follows the same progression of steps. The derivation for the media is different, however, in that:

1. The perturbed velocities and stresses in the media must vanish with increasing distance above or below the multilayer-medium interface. As a result, the four arbitrary constants, a, b, c, d, used to describe stresses and velocities in a layer are reduced to two in each medium. For the upper medium, a and b are zero; for the lower medium, c and d are zero.

2. The origins of coordinates for the media are at the multilayer-medium interfaces. The term for the mean position of the interfaces, which was $\pm(h/2)$ for a layer, is zero for the media, and the heights, ζ, of the upper (U) and lower (L) multilayer-medium interfaces becomes:

$$\zeta_{U,L} = {}_1A_{U,L}\cos(\ell x) + {}_2A_{U,L}\cos(2\ell x) + {}_3A_{U,L}\cos(3\ell x) + {}_4A_{U,L}\cos(4\ell x) \quad (18)$$

As a result, the variable k used in the derivation for a layer, is zero for the media because k is a function of the mean height of the interface.

The expressions for the lambda constants for the upper (U) and lower (L) media are:

$$ {}^{j}_{j}\Lambda_{U,L} = [{}^{j}_{j}\sigma_{U,L} - \rho g({}_{j}A_{U,L})]/(2j\mu\ell) \text{ ; } j = 1,2,\text{or } 3 \text{ (no sum)} \tag{19a} $$

$$ {}^{j}_{j}\lambda_{U,L} = [{}^{j}_{j}\tau_{U,L} - 4j\mu\ell\bar{D}_{xx}({}_{j}A_{U,L})]/(2j\mu\ell) \text{ ;} \tag{19b} $$

$$ {}^{11}_{2}\Lambda_{U,L} = [{}^{11}_{2}\sigma_{U,L} + 2\mu(\ell^2)\bar{D}_{xx}({}_{1}A_{U,L})^2]/4\mu\ell + (3\ell/4)({}_{1}A_{U,L})({}^{1}_{1}\lambda_{U,L}) \tag{19c} $$

$$ {}^{11}_{2}\lambda_{U,L} = ({}^{11}_{2}\tau_{U,L}/4\mu\ell) - (\ell/4)({}_{1}A_{U,L})[{}^{1}_{1}\Lambda_{U,L} \mp 4({}^{1}_{1}\lambda_{U,L})] \tag{19d} $$

$$ {}^{12}_{1}\Lambda_{U,L} = ({}^{12}_{1}\sigma_{U,L}/2\mu\ell) - 4\ell\bar{D}_{xx}({}_{1}A_{U,L})({}_{2}A_{U,L}) - (3\ell/2)({}_{2}A_{U,L})({}^{1}_{1}\lambda_{U,L}) \tag{19e} $$

$$ \begin{aligned} {}^{12}_{1}\lambda_{U,L} = {} & ({}^{12}_{1}\tau_{U,L}/2\mu\ell) - 2\ell({}_{1}A_{U,L})({}^{2}_{2}\Lambda_{U,L} \mp {}^{2}_{2}\lambda_{U,L}) \\ & + (\ell/2)({}_{2}A_{U,L})[{}^{1}_{1}\Lambda_{U,L} \pm 2({}^{1}_{1}\lambda_{U,L})] \end{aligned} \tag{19f} $$

$$ {}^{111}_{1}\Lambda_{U,L} = ({}^{111}_{1}\sigma_{U,L}/2\mu\ell) - (\ell^2/8)({}_{1}A_{U,L})^2[{}^{1}_{1}\Lambda_{U,L} \mp 6({}^{1}_{1}\lambda_{U,L})] \tag{19g} $$

$$ \begin{aligned} {}^{111}_{1}\lambda_{U,L} = {} & [{}^{111}_{1}\tau_{U,L} + 3\mu(\ell^3)\bar{D}_{xx}({}_{1}A_{U,L})^3]/2\mu\ell - 2\ell({}_{1}A_{U,L})({}^{11}_{2}\Lambda_{U,L} \mp {}^{11}_{2}\lambda_{U,L}) \\ & \pm (\ell^2/8)({}_{1}A_{U,L})^2[6({}^{1}_{1}\Lambda_{U,L}) \pm {}^{1}_{1}\lambda_{U,L}] \end{aligned} \tag{19h} $$

$$ \begin{aligned} {}^{12}_{3}\Lambda_{U,L} = {} & ({}^{12}_{3}\sigma_{U,L}/6\mu\ell) + (4\ell/3)\bar{D}_{xx}({}_{1}A_{U,L})({}_{2}A_{U,L}) + (4\ell/3)({}_{1}A_{U,L})({}^{2}_{2}\lambda_{U,L}) \\ & + (5\ell/6)({}_{2}A_{U,L})({}^{1}_{1}\lambda_{U,L}) \end{aligned} \tag{19i} $$

$$ {}^{12}_{\ 3}\lambda_{U,L} = ({}^{12}_{\ 3}\tau_{U,L}/6\mu\ell) - (2\ell/3)({}_1A_{U,L})[{}^{2}_{2}\Lambda_{U,L} \mp 3({}^{2}_{2}\lambda_{U,L})] $$

$$ - (\ell/6)({}_2A_{U,L})[{}^{1}_{1}\Lambda_{U,L} \mp 6({}^{1}_{1}\lambda_{U,L})] \qquad (19j) $$

$$ {}^{111}_{\ \ 3}\Lambda_{U,L} = ({}^{111}_{\ \ 3}\sigma_{U,L}/6\mu\ell) + (4\ell/3)({}_1A_{U,L})({}^{11}_{\ 2}\lambda_{U,L}) $$

$$ + (\ell^2/24)({}_1A_{U,L})^2[5({}^{1}_{1}\Lambda_{U,L}) \mp 14({}^{1}_{1}\lambda_{U,L})] \qquad (19k) $$

$$ {}^{111}_{\ \ 3}\lambda_{U,L} = [{}^{111}_{\ \ 3}\tau_{U,L} - \mu(\ell^3)\bar{D}_{xx}({}_1A_{U,L})^3]/6\mu\ell $$

$$ - (2\ell/3)({}_1A_{U,L})[{}^{11}_{\ 2}\Lambda_{U,L} \mp 3({}^{11}_{\ 2}\lambda_{U,L})] $$

$$ \pm (\ell^2/8)({}_1A_{U,L})^2[2({}^{1}_{1}\Lambda_{U,L}) \mp 5({}^{1}_{1}\lambda_{U,L})] \qquad (19\ell) $$

$$ {}^{1}{}^{1}_{1}\Lambda_{U,L} = {}^{1}{}^{1}_{1}\sigma_{U,L}/2\mu\ell \tag{19m} $$

$$ {}^{1}{}^{1}_{1}\lambda_{U,L} = {}^{1}{}^{1}_{1}\tau_{U,L}/2\mu\ell \tag{19n} $$

$$ {}^{1}{}^{2}_{2}\Lambda_{U,L} = {}^{1}{}^{2}_{2}\sigma_{U,L}/4\mu\ell \tag{19o} $$

$$ {}^{1}{}^{2}_{2}\lambda_{U,L} = {}^{1}{}^{2}_{2}\tau_{U,L}/4\mu\ell \tag{19p} $$

$$ \begin{aligned} {}^{11}{}^{1}_{2}\Lambda_{U,L} &= {}^{11}{}^{1}_{2}\sigma_{U,L}/4\mu\ell \\ &\quad + (3/4)({}_{1}A_{U,L}\ell)({}^{1}{}^{1}_{1}\lambda_{U,L} + {}^{1}{}^{1}_{3}\lambda_{U,L}) \end{aligned} \tag{19q} $$

$$ \begin{aligned} {}^{11}{}^{1}_{2}\lambda_{U,L} &= {}^{11}{}^{1}_{2}\tau_{U,L}/4\mu\ell \\ &\quad - ({}_{1}A_{U,L}\ell/4)({}^{1}{}^{1}_{1}\Lambda_{U,L} \mp 4\,{}^{1}{}^{1}_{1}\lambda_{U,L}) \\ &\quad - 3({}_{1}A_{U,L}\ell/4)(3\,{}^{1}{}^{1}_{3}\Lambda_{U,L} \mp 4\,{}^{1}{}^{1}_{3}\lambda_{U,L}) \end{aligned} \tag{19r} $$

$$ {}^{1}{}^{1}_{3}\Lambda_{U,L} = {}^{1}{}^{1}_{3}\sigma_{U,L}/6\mu\ell \tag{19s} $$

$$ {}^{1}{}^{1}_{3}\lambda_{U,L} = {}^{1}{}^{1}_{3}\tau_{U,L}/6\mu\ell \tag{19t} $$

$$ {}^{1}{}^{2}_{4}\Lambda_{U,L} = {}^{1}{}^{2}_{4}\sigma_{U,L}/8\mu\ell \tag{19u} $$

$$ {}^{1}{}^{2}_{4}\lambda_{U,L} = {}^{1}{}^{2}_{4}\tau_{U,L}/8\mu\ell \tag{19v} $$

$$ \begin{aligned} {}^{11}{}^{1}_{4}\Lambda_{U,L} &= {}^{11}{}^{1}_{4}\sigma_{U,L}/8\mu\ell \\ &\quad + (15/8)({}_{1}A_{U,L}\ell)({}^{1}{}^{1}_{3}\lambda_{U,L}) \end{aligned} \tag{19w} $$

$$ \begin{aligned} {}^{11}{}^{1}_{4}\lambda_{U,L} &= {}^{11}{}^{1}_{4}\tau_{U,L}/8\mu\ell \\ &\quad - (3/8)({}_{1}A_{U,L}\ell)(3\,{}^{1}{}^{1}_{3}\Lambda_{U,L} \mp 8\,{}^{1}{}^{1}_{3}\lambda_{U,L}) \end{aligned} \tag{19x} $$

The expressions for the velocities normal and tangential to the interface for the media are:

$$
\begin{aligned}
(v_n)_{U,L} = {} & (\bar{v}_z)_{U,L} \cos(\theta_{U,L}) - (\bar{v}_x)_{U,L} \sin(\theta_{U,L}) \\
& \mp \Big\{ {}^{1}_{1}\Lambda_{U,L} + {}^{11}_{1}\Lambda_{U,L} + {}^{12}_{1}\Lambda_{U,L} + {}^{111}_{1}\Lambda_{U,L} \\
& \quad - ({}_{1}A_{U,L}\ell/2)({}^{2}_{2}\lambda_{U,L} + {}^{11}_{2}\lambda_{U,L}) + ({}_{2}A_{U,L}\ell/2)({}^{1}_{1}\lambda_{U,L}) \\
& \quad - ({}_{1}A_{U,L}\ell/2)^2({}^{1}_{1}\Lambda_{U,L} \mp {}^{1}_{1}\lambda_{U,L}) \Big\} \cos(\ell x) \\
+ & \\
& \mp \Big\{ {}^{2}_{2}\Lambda_{U,L} + {}^{11}_{2}\Lambda_{U,L} + {}^{12}_{2}\Lambda_{U,L} + {}^{111}_{2}\Lambda_{U,L} \\
& \quad - ({}_{1}A_{U,L}\ell)({}^{1}_{1}\lambda_{U,L} + {}^{11}_{1}\lambda_{U,L} + {}^{11}_{3}\lambda_{U,L}) \Big\} \cos(2\ell x) \\
+ & \\
& \mp \Big\{ {}^{3}_{3}\Lambda_{U,L} + {}^{11}_{3}\Lambda_{U,L} + {}^{12}_{3}\Lambda_{U,L} + {}^{111}_{3}\Lambda_{U,L} \\
& \quad - 3({}_{1}A_{U,L}\ell/2)({}^{2}_{2}\lambda_{U,L} + {}^{11}_{2}\lambda_{U,L}) - 3({}_{2}A_{U,L}\ell/2)({}^{1}_{1}\lambda_{U,L}) \\
& \quad - ({}_{1}A_{U,L}\ell/2)^2({}^{1}_{1}\Lambda_{U,L} \mp 3{}^{1}_{1}\lambda_{U,L}) \Big\} \cos(3\ell x) \\
+ & \\
& \mp \Big\{ {}^{4}_{4}\Lambda_{U,L} + {}^{12}_{4}\Lambda_{U,L} + {}^{111}_{4}\Lambda_{U,L} \\
& \quad - 2({}_{1}A_{U,L}\ell)({}^{11}_{3}\lambda_{U,L}) \Big\} \cos(4\ell x)
\end{aligned}
\qquad (20a)
$$

$$
\begin{aligned}
(v_s)_{U,L} = {} & (\bar{v}_z)_{U,L} \sin(\theta_{U,L}) + (\bar{v}_x)_{U,L} \cos(\theta_{U,L}) \\
& \mp \Big\{ {}^{1}_{1}\lambda_{U,L} + {}^{11}_{1}\lambda_{U,L} + {}^{12}_{1}\lambda_{U,L} + {}^{111}_{1}\lambda_{U,L} \\
& \quad + ({}_{1}A_{U,L}\ell/2)[3({}^{2}_{2}\Lambda_{U,L}+{}^{11}_{2}\Lambda_{U,L}) \mp 4({}^{2}_{2}\lambda_{U,L} + {}^{11}_{2}\lambda_{U,L})] \\
& \quad - ({}_{2}A_{U,L}\ell/2)[3({}^{1}_{1}\Lambda_{U,L}) \mp 2({}^{1}_{1}\lambda_{U,L})] \\
& \quad \mp ({}_{1}A_{U,L}\ell/2)^2[{}^{1}_{1}\Lambda_{U,L} \mp ({}^{1}_{1}\lambda_{U,L})] \Big\} \sin(\ell x) \\
+ &
\end{aligned}
$$

$$\mp \Big\{ {}^{2}_{2}\lambda_{U,L} + {}^{1}{}^{1}_{2}\lambda_{U,L} + {}^{1}{}^{2}_{2}\lambda_{U,L} + {}^{11}{}^{1}_{2}\lambda_{U,L}$$

$$\mp ({}_{1}A_{U,L}\ell)({}^{1}_{1}\lambda_{U,L} + {}^{1}{}^{1}_{1}\lambda_{U,L})$$

$$+ ({}_{1}A_{U,L}\ell)(2\,{}^{1}{}^{1}_{3}\Lambda_{U,L} \mp 3\,{}^{1}{}^{1}_{3}\lambda_{U,L}) \Big\} \sin(2\ell x)$$

$$+$$

$$\mp \Big\{ {}^{3}_{3}\lambda_{U,L} + {}^{1}{}^{1}_{3}\lambda_{U,L} + {}^{1}{}^{2}_{3}\lambda_{U,L} + {}^{11}{}^{1}_{3}\lambda_{U,L}$$

$$+ ({}_{1}A_{U,L}\ell/2)[({}^{2}_{2}\Lambda_{U,L} + {}^{1}{}^{1}_{2}\Lambda_{U,L}) \mp 4({}^{2}_{2}\lambda_{U,L}+{}^{1}{}^{1}_{2}\lambda_{U,L})]$$

$$- ({}_{2}A_{U,L}\ell/2)[{}^{1}_{1}\Lambda_{U,L} \pm 2({}^{1}_{1}\lambda_{U,L})]$$

$$\mp ({}_{1}A_{U,L}\ell/2)^{2}({}^{1}_{1}\Lambda_{U,L} \mp 3\,{}^{1}_{1}\lambda_{U,L}) \Big\} \sin(3\ell x)$$

$$+$$

$$\mp \Big\{ {}^{4}_{4}\Lambda_{U,L} + {}^{1}{}^{2}_{4}\Lambda_{U,L} + {}^{11}{}^{1}_{4}\Lambda_{U,L}$$

$$+ ({}_{1}A_{U,L}\ell)[{}^{1}{}^{1}_{3}\Lambda_{U,L} \mp 3({}^{1}{}^{1}_{3}\lambda_{U,L})] \Big\} \sin(4\ell x) \qquad (20b)$$

The velocity boundary conditions are applied to determine values for the interface constants.

For all the multilayers I analyze, the normal velocity components must match at each interface:

$$(v_n)_b = (v_n)_t \tag{21a}$$

The tangential velocity boundary condition controls the nature of the slip at layer contacts. The theoretical model of slip at layer contacts is derived in Chapter II. In general, the difference in velocities of two layers, or of a layer and a medium, across their mutual interface is a function of the interface shear stress, σ_{ns}, and of parameters which describe the ability of the contact to resist slip. The boundary condition is:

$$(v_s)_b - (v_s)_t = (h_f)(\sigma_{ns}/\beta)\,|\sigma_{ns}/\beta|^{(m-1)} \tag{21b}$$

in which $\underline{h}_f$ is the thickness of the film separating the layers, and β and $\underline{m}$ are parameters describing a powerlaw fluid.

By specifying the nature of the resistance to slip at the contact, one can use the tangential boundary condition to describe a wide variety of slip conditions: no slip at contacts (bonded contacts), viscous slip at contacts, free slip at contacts, or localized slip at contacts.

The power $\underline{m}$ of the powerlaw expression determines whether the film behaves as a linear viscous fluid (powerlaw exponent $\underline{m}$ equals one) or a nonlinear fluid (powerlaw exponent $\underline{m}$ greater than one).

If the powerlaw exponent $\underline{m}$ is one, the material constant β reduces to the coefficient of viscosity, μ_f, of the film. The resistance to slip at contacts is constant, and slip is distributed along layer contacts.

For bonded contacts, the coefficient of viscosity of the film, μ_f, is very large. The resistance to slip is then infinite, and the rate of slip at contacts is zero:

$$(v_s)_b - (v_s)_t = 0 \tag{22a}$$

For viscous slip at contacts, the coefficient of viscosity is finite. The resistance to slip is then finite and constant all along the interface, and the rate of slip is a linear function of the contact shear stress

$$(v_s)_b - (v_s)_t = (h_f)(\sigma_{ns}/\mu_f) \tag{22b}$$

The tangential velocity boundary condition is indeterminate if there is free slip at contacts. In that case, the interface shear stress, σ_{ns}, is zero, and all the τ constants are zero. For free slip at contacts, the normal velocity boundary condition is sufficient to determine all the σ interface constants.

If the powerlaw exponent $\underline{m}$ is greater than one, the film is a nonlinear material. The resistance to slip then varies with position on the interface, which produces localized slip at layer contacts. The rate of slip at contacts then becomes a nonlinear function of the contact shear stress, eq. (21b).

To use the tangential velocity boundary condition, one substitutes the 3rd order expression for the contact shear stress, σ_{ns}, written in terms of the τ interface constants, into the velocity boundary condition, eq. (21b):

$$(v_s)_b - (v_s)_t =$$

$$(h_f/\beta^m) \Big\{ [\tau_0 + {}_1\tau \sin(\ell x) + {}_2\tau \sin(2\ell x) + {}_3\tau \sin(3\ell x)]$$

$$|\tau_0 + {}_1\tau \sin(\ell x) + {}_2\tau \sin(2\ell x) + {}_3\tau \sin(3\ell x)|^{(m-1)} \Big\} \qquad (23)$$

Here, each τ is a composite variable: ${}_1\tau = {}^1_1\tau + {}^{1}{}^2_1\tau + {}^{11}{}^1_1\tau$; ${}_2\tau = {}^2_2\tau + {}^{1}{}^1_2\tau$; and ${}_3\tau = {}^3_3\tau + {}^{1}{}^2_3\tau + {}^{11}{}^1_3\tau$.

The absolute value of the shear stress in the boundary condition, eq. (21b), is taken by using binomial series to express the square root of the square of the shear stress.

For a 3rd order analysis, the powerlaw exponent $\underline{m}$ is limited to values of one, two, or three. If the exponent were greater than three, then additional waveforms, ones not contained in the 3rd order description of the height of the interface, ζ (eq. 2), would be produced upon substituting the 3rd order expression for the contact shear stress into the 3rd order velocity boundary condition, eq. (21b).

The 3rd order expression for the tangential velocity boundary condition, valid for powerlaw exponents of one, two, or three, is:

$$
\begin{aligned}
(v_s)_b - (v_s)_t = (h_f/\beta^m)[\,|{}^{1}_{1}\tau|/\sqrt{2}\,]^{(m-1)} \\
\Big\{\; {}^{1}_{1}\tau[1 + (m-1)/4]\,\sin(\ell x) \\
+ ({}^{1}{}^{2}_{1}\tau + {}^{11}{}^{1}_{1}\tau)\,\sin(\ell x) \\
+ m({}^{2}_{2}\tau + {}^{1}{}^{1}_{2}\tau)\,\sin(2\ell x) \\
+ ({}^{3}_{3}\tau + {}^{1}{}^{2}_{3}\tau + {}^{11}{}^{1}_{3}\tau)\,\sin(3\ell x) \\
- [(m-1)/4]({}^{1}_{1}\tau)\sin(3\ell x) \\
- [3(m-1)/4]({}^{2}_{2}\tau + {}^{1}{}^{1}_{2}\tau)\,\sin(4\ell x)\;\Big\}
\end{aligned}
\qquad (24a)
$$

Different waveforms and τ constants will remain in the 3rd order expression for different values of the powerlaw exponent $\underline{m}$,

For a powerlaw exponent of one, the rate of slip, eq. (24a), reduces to a linear function of the first three waveforms:

$$
\begin{aligned}
(v_s)_b - (v_s)_t = (h_f/\mu_f)\,\Big\{({}^{1}_{1}\tau + {}^{1}{}^{2}_{1}\tau + {}^{11}{}^{1}_{1}\tau)\,\sin(\ell x) \\
+ ({}^{2}_{2}\tau + {}^{1}{}^{1}_{2}\tau)\,\sin(2\ell x) \\
+ ({}^{3}_{3}\tau + {}^{1}{}^{2}_{3}\tau + {}^{11}{}^{1}_{3}\tau)\,\sin(3\ell x)\;\Big\}
\end{aligned}
\qquad (24b)
$$

For a powerlaw exponent of two, the rate of slip, eq. (21b), becomes a nonlinear function of all four waveforms:

$$(v_s)_b - (v_s)_t = (h_f/\beta^2)[|{}^1_1\tau|/\sqrt{2}]$$

$$\{ (5/4)({}^1_1\tau) \sin(\ell x)$$

$$- (1/4)({}^1_1\tau) \sin(3\ell x)$$

$$+ 2({}^2_2\tau + {}^{1}{}^1_2\tau) \sin(2\ell x)$$

$$- (3/4)({}^2_2\tau + {}^{1}{}^1_2\tau) \sin(4\ell x) \} \qquad (24c)$$

For a powerlaw exponent m of three, the rate of slip, eq. (21b), is also a nonlinear function, but only of two waveforms:

$$(v_s)_b - (v_s)_t = (h_f/\beta^3)({}^1_1\tau)^3 [(3/4) \sin(\ell x)$$

$$- (1/4) \sin(3\ell x)] \qquad (24d)$$

To 3rd order and for an exponent of three, all the τ constants except ${}^1_1\tau$ are zero.

To solve for the interface stresses, the equation matching the normal velocity boundary condition, eq. (21a), and one of the tangential velocity boundary conditions, eq. (24 a, b, or c), are applied to each interface in a multilayer, and the set of interfaces stresses is determined simultaneously. A different set of velocity boundary conditions is solved for each set of constants corresponding to a different combination of waveform and order of approximation. Thus, the 15 sets of constants listed in eq. (8) are determined by 15 sets of velocity boundary conditions.

As an example, I will use the velocity boundary conditions to determine the interface stress constants for the first waveform to 1st order.

I write the velocity boundary conditions for the multilayer in matrix form. To illustrate the method, I will consider an arbitrary multilayer composed of three layers of different thicknesses and viscosities confined above and below by infinitely thick, viscous media. Individual layers and media are identified by the variable *L*; individual interfaces between layers are identified by the variable *I*:

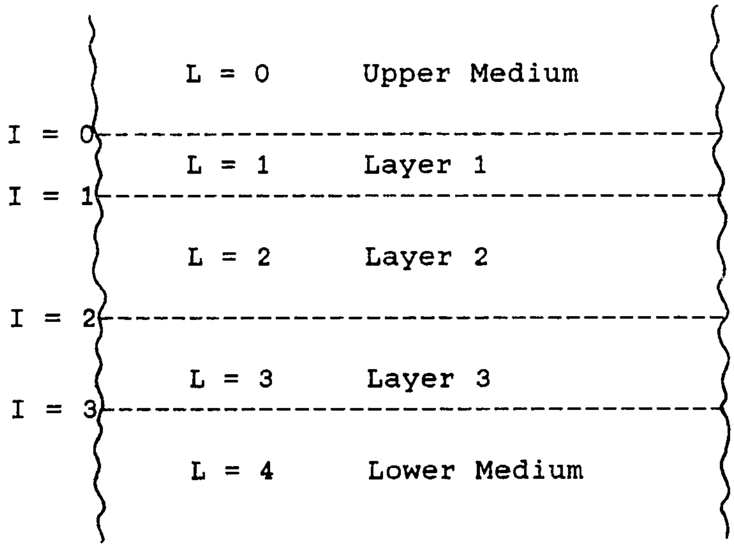

Figure A1. Notation used to identify individual layers and interfaces in arbitrary multilayer.

The matrix form of the velocity boundary conditions for this multilayer, for the first waveform to 1st order, is:

$$
\begin{array}{l}
v_n(0): \\ v_s(0): \\ v_n(1): \\ v_s(1): \\ v_n(2): \\ v_s(2): \\ v_n(3): \\ v_s(3):
\end{array}
\begin{bmatrix}
s_{00}, & s_{01}, & s_{02}, & s_{03}, & 0, & 0, & 0, & 0 \\
s_{10}, & s_{11}, & s_{12}, & s_{13}, & 0, & 0, & 0, & 0 \\
s_{20}, & s_{21}, & s_{22}, & s_{23}, & s_{24}, & s_{25}, & 0, & 0 \\
s_{30}, & s_{31}, & s_{32}, & s_{33}, & s_{34}, & s_{35}, & 0, & 0 \\
0, & 0, & s_{42}, & s_{43}, & s_{44}, & s_{45}, & s_{46}, & s_{47} \\
0, & 0, & s_{52}, & s_{53}, & s_{54}, & s_{55}, & s_{56}, & s_{57} \\
0, & 0, & 0, & 0, & s_{64}, & s_{65}, & s_{66}, & s_{67} \\
0, & 0, & 0, & 0, & s_{74}, & s_{75}, & s_{76}, & s_{77}
\end{bmatrix}
\begin{bmatrix}
\sigma(0) \\ \tau(0) \\ \sigma(1) \\ \tau(1) \\ \sigma(2) \\ \tau(2) \\ \sigma(3) \\ \tau(3)
\end{bmatrix}
=
\begin{bmatrix}
a_{00}, & a_{01}, & 0, & 0 \\
a_{10}, & a_{11}, & 0, & 0 \\
a_{20}, & a_{21}, & a_{22}, & 0 \\
a_{30}, & a_{31}, & a_{32}, & 0 \\
0, & a_{41}, & a_{42}, & a_{43} \\
0, & a_{51}, & a_{52}, & a_{53} \\
0, & 0, & a_{62}, & a_{63} \\
0, & 0, & a_{72}, & a_{73}
\end{bmatrix}
\begin{bmatrix}
A(0) \\ A(1) \\ A(2) \\ A(3)
\end{bmatrix}
\qquad (25)
$$

As before, the left subscript indicates the waveform with which the interface constants, σ and τ, and amplitude, $\underline{A}$, are associated, and the left superscript indicates the order of accuracy of the variable. Here, the right subscript refers to the layer number, $\underline{L}$, and the number in parentheses indicates the interface with which the variable is associated.

The $v_n(I)$ or $v_s(I)$ at the left of eqs. (25) indicates whether the equation represents a normal or tangential velocity boundary condition. Thus, $v_n(0)$ indicates the normal velocity boundary condition applied at the top interface, $\underline{I}$ = 0. In the notation of eq. (21a), the normal velocity boundary condition is:

$$v_n(0) = (v_n)_b - (v_n)_t = 0$$

In the notation of Fig. A1 and eq. (25), the normal velocity boundary condition becomes

$$v_n(0) = (v_n)_{L=0} - (v_n)_{L=1} = 0 \tag{26a}$$

because the top interface (I = 0) is defined by the bottom of the upper medium ($\underline{L}$ = 0) and the top of Layer 1 ($\underline{L}$ = 1).

For bonded contacts, the tangential velocity boundary condition is:

$$v_s(0) = (v_s)_{L=0} - (v_n)_{L=1} = 0 \tag{26b}$$

The boundary conditions, eqs. (26), are written in terms of the interface stress constants, σ and τ, using the expressions for the normal and tangential velocities for the layers and media, eqs. (17) and (20), respectively.

At the uppermost interface, $\underline{I}$ = 0, the velocity boundary conditions for the first waveform to 1st order accuracy and for bonded contacts are:

$$\begin{aligned} v_n(0):\quad & [(\bar{v}_z)_U \cos(\theta_U) - (\bar{v}_x)_U \sin(\theta_U) - {}^{1}_{1}\Lambda_U] \\ & - [({}^{1}_{1}\Lambda_m)_1\ ({}_{1}C^{2}_{1}) + ({}^{1}_{1}\lambda_p)_1\ (k_1) \\ & \qquad + ({}^{1}_{1}\Lambda_p)_1\ ({}_{1}S^{2}_{1}) - ({}^{1}_{1}\lambda_m)_1\ (k_1)] = 0 \end{aligned} \tag{27a}$$

$$v_s(0): \quad [(\bar{v}_z)_U \sin(\theta_U) + (\bar{v}_x)_U \cos(\theta_U) - {}^{1}_{1}\lambda_U]$$
$$- [-({}^{1}_{1}\Lambda_p)_1 \ (k_1) + ({}^{1}_{1}\lambda_m)_1 \ ({}_1C_1^2)$$
$$+ ({}^{1}_{1}\Lambda_m)_1 \ (k_1) + ({}^{1}_{1}\lambda_p)_1 \ ({}_1S_1^2)] = 0 \qquad (27b)$$

Using the values for the constants ${}^{1}_{1}\Lambda$ and ${}^{1}_{1}\lambda$ given in eqs. (16a,b) and 19(a,b), and noting that, for example, $\sigma_U = \sigma_{1t} = \sigma(0)$, I rewrite eqs. (27) as:

$$v_n(0): \quad -{}^{1}_{1}\sigma(0)$$
$$- (\mu_o/2\mu_1)[\{{}^{1}_{1}\sigma(0)-{}^{1}_{1}\sigma(1)\}({}_1C_1^2) +$$
$$\{{}^{1}_{1}\tau(0)+{}^{1}_{1}\tau(1)\}(k_1)$$
$$- 4(\mu_1)\ell\bar{D}_{xx}\{{}_1A(0)+{}_1A(1)\}(k_1)]/\{({}_1S_1)({}_1C_1)-k_1\}$$
$$- (\mu_o/2\mu_1)[\{{}^{1}_{1}\sigma(0)+{}^{1}_{1}\sigma(1)\}({}_1S_1^2) -$$
$$\{{}^{1}_{1}\tau(0)-{}^{1}_{1}\tau(1)\}(k_1)$$
$$+ 4(\mu_1)\ell\bar{D}_{xx}\{{}_1A(0)-{}_1A(1)\}(k_1)]/\{({}_1S_1)({}_1C_1)+k_1\} = 0 \qquad (28a)$$

$$v_s(0): \quad -{}^{1}_{1}\tau(0) + 2\bar{D}_{xx}\{{}_1A(0)\}$$
$$+ (\mu_o/2\mu_1)[\{{}^{1}_{1}\sigma(0)+{}^{1}_{1}\sigma(1)\}(k_1) -$$
$$\{{}^{1}_{1}\tau(0)-{}^{1}_{1}\tau(1)\}({}_1C_1^2)$$
$$+ 4(\mu_1)\ell\bar{D}_{xx}\{{}_1A(0)-{}_1A(1)\}({}_1C_1^2)]/\{({}_1S_1)({}_1C_1)+k_1\}$$
$$- (\mu_o/2\mu_1)[\{{}^{1}_{1}\sigma(0)-{}^{1}_{1}\sigma(1)\}(k_1) +$$
$$\{{}^{1}_{1}\tau(0)+{}^{1}_{1}\tau(1)\}({}_1S_1^2)$$
$$- 4(\mu_1)\ell\bar{D}_{xx}\{{}_1A(0)+{}_1A(1)\}({}_1S_1^2)]/\{({}_1S_1)({}_1C_1)-k_1\} = 0 \qquad (28b)$$

$$\{(\bar{v}_z)_o\}_0 - \{(\bar{v}_z)_o\}_1 + \bar{D}_{xx}(h_1/2) = 0 \qquad (28c)$$

in which

$_1S_1 = \sinh(k_1)$

$_1C_1 = \cosh(k_1)$

$k_1 = \pi h_1/L$, where $\underline{h}_1$ is the thickness of Layer 1 and $\underline{L}$ is the wavelength of the first waveform. The densities are assumed to be equal.

Equation (28a) is represented by the first equation in eq. (25). Thus,

$$s_{00} = -1 - (\mu_o/2\mu_1)[(_1C_1^2)/\{(_1S_1)(_1C_1)-k_1\} + (_1S_1^2)/\{(_1S_1)(_1C_1)+k_1\}] \tag{29a}$$

$$s_{01} = -(\mu_o/2\mu_1)[(k_1)/\{(_1S_1)(_1C_1)-k_1\} - (k_1)/\{(_1S_1)(_1C_1)+k_1\}] \tag{29b}$$

$$s_{02} = +(\mu_o/2\mu_1)[(_1C_1^2)/\{(_1S_1)(_1C_1)-k_1\} - (_1S_1^2)/\{(_1S_1)(_1C_1)+k_1\}] \tag{29c}$$

$$s_{03} = -(\mu_o/2\mu_1)[(k_1)/\{(_1S_1)(_1C_1)-k_1\} + (k_1)/\{(_1S_1)(_1C_1)+k_1\}] \tag{29d}$$

$$a_{00} = -2\mu_o \ell \bar{D}_{xx}(k_1)/[1/\{(_1S_1)(_1C_1)-k_1\} - 1/\{(_1S_1)(_1C_1)+k_1\}] \tag{29e}$$

$$a_{01} = -2\mu_o \ell \bar{D}_{xx}(k_1)/[1/\{(_1S_1)(_1C_1)-k_1\} + 1/\{(_1S_1)(_1C_1)+k_1\}] \tag{29f}$$

Equation (28b) is represented by the second equation in eqs. (26) and is used to define the coefficients $\underline{s}_{10}$, $\underline{s}_{11}$, $\underline{s}_{12}$, $\underline{s}_{13}$, $\underline{a}_{10}$, $\underline{a}_{11}$.

At interface 1 (I = 1), the velocity boundary conditions are:

$$(v_n)_1 - (v_n)_2 = 0 \tag{30a}$$

$$(v_s)_1 - (v_s)_2 = 0 \tag{30b}$$

The equation for the tangential velocity boundary condition, eq. (30b), written in terms of the constants Λ and λ, becomes:

$$\begin{aligned}
&-\{({}^1_1\Lambda_p)_1(k_1)-({}^1_1\Lambda_p)_2(k_2)\} \\
&+ \{({}^1_1\lambda_m)_1({}_1C^2_1)-({}^1_1\lambda_m)_2({}_1C^2_2)\} \\
&-\{({}^1_1\Lambda_m)_1(k_1)+({}^1_1\Lambda_m)_2(k_2)\} \\
&- \{({}^1_1\lambda_p)_1({}_1S^2_1)+({}^1_1\lambda_p)_2({}_1S^2_2)\} = 0
\end{aligned} \tag{31}$$

Equation (31) is used to define the coefficients $\underline{s}_{30}$, $\underline{s}_{31}$, $\underline{s}_{32}$, $\underline{s}_{33}$, $\underline{s}_{34}$, $\underline{s}_{35}$, $\underline{a}_{30}$, $\underline{a}_{31}$, $\underline{a}_{32}$. The normal velocity boundary condition for interface 1, and the normal and tangential velocity boundary conditions for the other two interfaces (I = 2, 3) in the arbitrary multilayer, Fig. A1, are used to define the other elements in the matrices of coefficients in eq. (25). The expressions for the coefficients of σ, τ, and $\underline{A}$ show that the value of an interface constant or amplitude on any one interface depends on the values of the constants and amplitudes on all the other interfaces.

The values for the interface stresses σ and τ are computed from eq. (25) by standard matrix operations.

With all of the arbitrary constants determined, we can compute the growth rates of all the waveforms in all the interfaces. To do this, we compute the rate of change in height, ζ, of an interface:

$$(\partial\zeta/\partial t) = [v_z]_\zeta - [v_x]_\zeta\ (\partial\zeta/\partial x) \qquad (32)$$

The equation for the height of the interface, eq. (2), is used in the left-hand-side of eq. (32); the 3rd order expressions for the velocities, eqs. (3) using eqs. (4) and (9), are used in the right-hand-side of eq. (32). To 3rd order, the expressions for the rate of growth of amplitudes are:

$$
\begin{aligned}
d({}_{1}A_{t,b})/d\bar{S}_x = {} & -({}_{1}A_{t,b}/\bar{S}_x) \\
& + (1/\bar{D}_{xx}\bar{S}_x)\ \Big\{\ [({}^{1}_{1}\Lambda_m+{}^{11}_{1}\Lambda_m+{}^{12}_{1}\Lambda_m+{}^{111}_{1}\Lambda_m)({}_{1}C^2) \\
& + ({}^{1}_{1}\lambda_p+{}^{11}_{1}\lambda_p+{}^{12}_{1}\lambda_p+{}^{111}_{1}\lambda_p)k \\
& \pm ({}^{1}_{1}\Lambda_p+{}^{11}_{1}\Lambda_p+{}^{12}_{1}\Lambda_p+{}^{111}_{1}\Lambda_p)({}_{1}S^2) \\
& \mp ({}^{1}_{1}\lambda_m+{}^{11}_{1}\lambda_m+{}^{12}_{1}\lambda_m+{}^{111}_{1}\lambda_m)k \\
& + ({}_{1}A_{t,b}\ell/2)[({}^{2}_{2}\Lambda_p+{}^{11}_{2}\Lambda_p)2k - ({}^{2}_{2}\lambda_m+{}^{11}_{2}\lambda_m)({}_{2}C^2) \\
& \qquad \mp ({}^{2}_{2}\Lambda_m+{}^{11}_{2}\Lambda_m)2k \mp ({}^{2}_{2}\lambda_p+{}^{11}_{2}\lambda_p)({}_{2}S^2)] \\
& - ({}_{2}A_{t,b}\ell/2)[({}^{1}_{1}\Lambda_p)k - ({}^{1}_{1}\lambda_m)({}_{1}C^2) \\
& \qquad \mp ({}^{1}_{1}\Lambda_m)k \mp ({}^{1}_{1}\lambda_p)({}_{1}S^2)] \\
& - (1/2)({}_{1}A_{t,b}\ell/2)^2[{}^{1}_{1}\Lambda_m({}_{1}C^2) + {}^{1}_{1}\lambda_p(2{}_{1}S_{1}C-k) \\
& \qquad \pm {}^{1}_{1}\Lambda_p({}_{1}S^2) \pm {}^{1}_{1}\lambda_m(2{}_{1}S_{1}C+k)]\ \Big\}
\end{aligned}
\tag{33a}
$$

$$
\begin{aligned}
d({}_{2}A_{t,b})/d\bar{S}_x = {} & -({}_{2}A_{t,b}/\bar{S}_x) \\
& + (1/\bar{D}_{xx}\bar{S}_x)\ \Big\{\ [({}^{2}_{2}\Lambda_m+{}^{11}_{2}\Lambda_m+{}^{12}_{2}\Lambda_m+{}^{111}_{2}\Lambda_m)({}_{2}C^2) \\
& + ({}^{2}_{2}\lambda_p+{}^{11}_{2}\lambda_p+{}^{12}_{2}\lambda_p+{}^{111}_{2}\lambda_p)2k \\
& \pm ({}^{2}_{2}\Lambda_p+{}^{11}_{2}\Lambda_p+{}^{12}_{2}\Lambda_p+{}^{111}_{2}\Lambda_p)({}_{2}S^2) \\
& \mp ({}^{2}_{2}\lambda_m+{}^{11}_{2}\lambda_m+{}^{12}_{2}\lambda_m+{}^{111}_{2}\lambda_m)2k \\
& + ({}_{1}A_{t,b}\ell)[({}^{1}_{1}\Lambda_p+{}^{11}_{1}\Lambda_p)k - ({}^{1}_{1}\lambda_m+{}^{11}_{1}\lambda_m)({}_{1}C^2) \\
& \qquad \mp ({}^{1}_{1}\Lambda_m+{}^{11}_{1}\Lambda_m)k \mp ({}^{1}_{1}\lambda_p+{}^{11}_{1}\lambda_p)({}_{1}S^2)] \\
& + ({}_{1}A_{t,b}\ell)[({}^{11}_{3}\Lambda_p)3k - ({}^{11}_{3}\lambda_m)({}_{3}C^2) \\
& \qquad \mp ({}^{11}_{3}\Lambda_m)3k \mp ({}^{11}_{3}\lambda_p)({}_{3}S^2)]\ \Big\}
\end{aligned}
\tag{33b}
$$

$$
\begin{aligned}
d({}_{3}A_{t,b})/d\bar{S}_x = {} & -({}_{3}A_{t,b}/\bar{S}_x) \\
& + (1/\bar{D}_{xx}\bar{S}_x)\ \Big\{\ [({}^{3}_{3}\Lambda_m+{}^{11}_{3}\Lambda_m+{}^{12}_{3}\Lambda_m+{}^{111}_{3}\Lambda_m)({}_{3}C^2) \\
& + ({}^{3}_{3}\lambda_p+{}^{11}_{3}\lambda_p+{}^{12}_{3}\lambda_p+{}^{111}_{3}\lambda_p)3k
\end{aligned}
$$

$$
\begin{aligned}
&\pm\ ({}^{3}_{3}\Lambda_p + {}^{1}{}^{1}_{3}\Lambda_p + {}^{1}{}^{2}_{3}\Lambda_p + {}^{11}{}^{1}_{3}\Lambda_p)({}_{3}S^2) \\
&\mp\ ({}^{3}_{3}\lambda_m + {}^{1}{}^{1}_{3}\lambda_m + {}^{1}{}^{2}_{3}\lambda_m + {}^{11}{}^{1}_{3}\lambda_m)3k \\
&+\ 3({}_{1}A_{t,b}\ell/2)[({}^{2}_{2}\Lambda_p + {}^{1}{}^{1}_{2}\Lambda_p)2k\ -\ ({}^{2}_{2}\lambda_m + {}^{1}{}^{1}_{2}\lambda_m)({}_{2}C^2) \\
&\qquad\qquad \mp\ ({}^{2}_{2}\Lambda_m + {}^{1}{}^{1}_{2}\Lambda_m)2k\ \mp\ ({}^{2}_{2}\lambda_p + {}^{1}{}^{1}_{2}\lambda_p)({}_{2}S^2)] \\
&+\ 3({}_{2}A_{t,b}\ell/2)[({}^{1}_{1}\Lambda_p)k\ -\ ({}^{1}_{1}\lambda_m)({}_{1}C^2) \\
&\qquad\qquad \mp\ ({}^{1}_{1}\Lambda_m)k\ \mp\ ({}^{1}_{1}\lambda_p)({}_{1}S^2)] \\
&-\ (3/2)({}_{1}A_{t,b}\ell/2)^2[{}^{1}_{1}\Lambda_m({}_{1}C^2)\ +\ {}^{1}_{1}\lambda_p(2{}_{1}S_{1}C-k) \\
&\qquad\qquad \pm\ {}^{1}_{1}\Lambda_p({}_{1}S^2)\ \pm\ {}^{1}_{1}\lambda_m(2{}_{1}S_{1}C+k)]\ \Big\}
\end{aligned}
\tag{33c}
$$

$$
\begin{aligned}
d({}_{4}A_{t,b})/d\bar{S}_x &= -({}_{4}A_{t,b}/\bar{S}_x) \\
&+\ (1/\bar{D}_{xx}\bar{S}_x)\ \Big\{\ [({}^{4}_{4}\Lambda_m + {}^{1}{}^{2}_{4}\Lambda_m + {}^{11}{}^{1}_{4}\Lambda_m)({}_{4}C^2) \\
&+\ ({}^{4}_{4}\lambda_p + {}^{1}{}^{2}_{4}\lambda_p + {}^{11}{}^{1}_{4}\lambda_p)4k \\
&\pm\ ({}^{4}_{4}\Lambda_p + {}^{1}{}^{2}_{4}\Lambda_p + {}^{11}{}^{1}_{4}\Lambda_p)({}_{4}S^2) \\
&\mp\ ({}^{4}_{4}\lambda_m + {}^{1}{}^{2}_{4}\lambda_m + {}^{11}{}^{1}_{4}\lambda_m)4k \\
&+\ 2({}_{1}A_{t,b}\ell)[({}^{1}{}^{1}_{3}\Lambda_p)3k\ -\ ({}^{1}{}^{1}_{3}\lambda_m)({}_{3}C^2) \\
&\qquad\qquad \mp\ ({}^{1}{}^{1}_{3}\Lambda_m)3k\ \mp\ ({}^{1}{}^{1}_{3}\lambda_p)({}_{3}S^2)]\ \Big\}
\end{aligned}
\tag{33d}
$$

A general equation for the growth rate of a waveform to 3rd order accuracy is cast in terms of amplification factors, $\underline{q}_{ik}$:

$$d({}_{j}A_{i})/d(-\bar{D}_{xx}dt) = (\delta_{ik} + {}^{1}_{j}q_{ik})({}_{j}A_{k})$$

$$+ {}^{11}_{j}q_{ik}({}_{1}A_{k})^{2} + {}^{111}_{j}q_{ik}({}_{1}A_{k})^{3} \qquad (34)$$

where $\underline{j}$ is the waveform: $j = 1,2,3,4$ (no summation);

$\underline{i}$ and $\underline{k}$ are the number of interfaces:

$i = 1,2, \ldots ,n$ (summation)

$k = 1,2, \ldots ,n$ (summation)

and δ_{ik} is the Kronecker delta. Not only may the growth of a waveform may be different on every interface, but it is affected by the growth of the waveforms on the other interfaces. Thus, each of the two subscripts, $\underline{i}$ and $\underline{k}$, on the amplification factors takes on values of all the interfaces in the multilayer.

Growth rate equations for the four waveforms which we use in a 3rd order solution to describe interface shape are derived from the general equation, eq. (34), by letting the subscript $\underline{j}$ take on values one through four. The resulting four equations are:

$$d({}_{1}A_{i})/d(-\bar{D}_{xx}dt) = (\delta_{ik} + {}^{1}_{1}q_{ik})({}_{1}A_{k})$$

$$+ {}^{11}_{1}q_{ik}({}_{1}A_{k})^{2} + {}^{111}_{1}q_{ik}({}_{1}A_{k})^{3} \qquad (35a)$$

$$d({}_{2}A_i)/d(-\bar{D}_{xx}dt) = (\delta_{ik} + {}^{2}_{2}q_{ik})({}_{2}A_k)$$

$$+ {}^{11}_{2}q_{ik}({}_{1}A_k)^2 + {}^{111}_{2}q_{ik}({}_{1}A_k)^3 \quad (35b)$$

$$d({}_{3}A_i)/d(-\bar{D}_{xx}dt) = (\delta_{ik} + {}^{3}_{3}q_{ik})({}_{3}A_k)$$

$$+ {}^{11}_{3}q_{ik}({}_{1}A_k)^2 + {}^{111}_{3}q_{ik}({}_{1}A_k)^3 \quad (35c)$$

$$d({}_{4}A_i)/d(-\bar{D}_{xx}dt) = (\delta_{ik} + {}^{4}_{4}q_{ik})({}_{4}A_k)$$

$$+ {}^{111}_{4}q_{ik}({}_{1}A_k)^3 \quad (35d)$$

Expressions for the amplification factors $\underline{g}_{ik}$ are found by equating eqs. (33 a,b,c,d) and eqs. (35 a,b,c,d).

Once we have the equations for the rates of growth of the component waveforms on each interface, we can compute the rate of growth of the fold with the equations for the first waveform, eq. (35a), and the shape of the interface with the equations for all four component waveforms, eqs. (35 a,b,c,d). Integration of the growth rate equations provides values, to 3rd order accuracy, for the amplitudes of the component waveforms at any stage in the deformation of the multilayer.

In practice, a computer program is used to compute the values of the interface stresses and to integrate the growth rate equations, eq. (35), for the amplitudes of the component waveforms in a multilayer with a finite number of interfaces. My computer program, "Folding3rdOrder.bas", written in Microsoft BASIC, is presented in Appendix C.

Eigenvalues and eigenvectors can be extracted from the system of growth rate equations for the first component waveform, eq. (35a). The eigenvalue of greatest absolute value contains the maximum amplification factor for the whole system; the eigenvector associated with it represents the relative amplitudes of the first waveform on each interface that together maximize growth of folds in the multilayer. My computer program, "Eigen.bas", for determining eigenvalues and eigenvectors for a multilayer is also presented in Appendix C.

APPENDIX B

If the orientation of the principal compressive stress is oblique to layering, viscous multilayers fold in response to the layer-parallel shortening and develop asymmetric interfaces in response to the layer-parallel shear. In this Appendix, I will derive equations, analogous to those derived in Appendix A for maximum compression parallel to layering, for the mean and perturbed stresses and velocities, the stress and velocity boundary conditions, and the rates of growth of amplitudes at interfaces in multilayers subjected to both layer-parallel compression and shear.

The analysis is to 2nd order accuracy in the maximum slope of the first waveform, and the interface shape is described by four component waveforms.

The multilayer consists of linear viscous layers with vertical thickness <u>h</u> and coefficient of internal viscosity μ_1 and is confined by infinitely thick, viscous media (Fig. 6, Chapter III). The model I have selected to describe contact properties relates rate of slip between layers to magnitude of shear stress applied at contacts and is explained in Chapter II. Each layer contact is represented by some specified resistance to slip described for the general case by a powerlaw relationship between the rate of slip and the contact shear stress.

The positions of points on interfaces between layers is described by ζ, the height of the interface above the local origin of coordinates. The local origin of coordinates for each layer is at middepth in that layer. The multilayer contains initial, symmetric perturbations of cosinusoidal shape and low amplitude, so the heights of the top (t) and bottom (b) interfaces of a single layer are initially:

$$\zeta_t = h/2 + {}_1A_t \cos(\ell x) \tag{1a}$$

$$\zeta_b = -h/2 + {}_1A_b \cos(\ell x) \tag{1b}$$

The mean positions of the top and bottom interfaces are $h/2$ and $-h/2$, respectively; the variation of points about the mean position is described initially by a cosinusoidal function of amplitude ${}_1A$.

Components of stress and velocity within a layer are separated into mean and perturbed values (*e.g.*, Fletcher, 1974, 1977): the mean values of stress and velocity and those that solve the problem describing the uniform deformation of a layer with planar interfaces, and the perturbed values of stress and velocity are those that must be added to the mean values to match stresses and velocities at perturbed interfaces.

The mean stresses and velocities within the layer are

$$\bar{v}_x = x\bar{D}_{xx} + 2z\bar{D}_{xz} + (\bar{v}_x)_o \tag{2a}$$

$$\bar{v}_z = z\bar{D}_{zz} + (\bar{v}_z)_o = (\bar{v}_z)_o - z\bar{D}_{xx} \tag{2b}$$

$$\bar{\sigma}_{xx} = 2\mu\bar{D}_{xx} - \bar{p} \tag{2c}$$

$$\bar{\sigma}_{zz} = -2\mu\bar{D}_{xx} - \bar{p} \tag{2d}$$

$$\bar{\sigma}_{xz} = 2\mu_{\ell}\bar{D}_{xz} \tag{2e}$$

$$\bar{p} = -(\bar{\sigma}_{xx} + \bar{\sigma}_{zz})/2 \tag{2f}$$

in which the deformation rate, $\underline{\bar{D}}$, is:

$$\bar{D}_{ij} = (1/2)(\partial\bar{v}_i/\partial x_j + \partial\bar{v}_j/\partial x_i) \tag{2g}$$

For incompressible viscous materials, the rate of horizontal shortening and the rate of vertical thickening must balance:

$$\bar{D}_{xx} = -\bar{D}_{zz} \tag{2h}$$

This analysis considers mean simple shearing parallel to layering only; vertical shearing is zero:

$$(\partial\bar{v}_z/\partial x) = 0 \tag{2i}$$

The orientation of maximum compression, $\bar{\sigma}_c$, within a stiff, viscous layer is defined by the angle $\bar{\theta}$, measured clockwise from the $\underline{x}$-direction (Fig. 6, Ch. III), which lies in the plane of the unperturbed layering. The ratio of the mean shear stress to the difference of the mean normal stresses is a function of the angle $\bar{\theta}$:

$$\bar{\sigma}_{xz}/(\bar{\sigma}_{xx} - \bar{\sigma}_{zz}) = -(1/2)\tan(2\bar{\theta}) \tag{3a}$$

Within viscous layers, therefore, the mean layer-parallel shear stress is a function of the viscosity of the layers, μ_ℓ, and the magnitude and orientation of the maximum compressive stress:

$$\bar{\sigma}_{xz} = -2\mu_\ell \bar{D}_{xx}\tan(2\bar{\theta}) \tag{3b}$$

In the boundary-value problems I solve, I have elected to specify a combination of uniform, layer-parallel normal deformation rate, $\underline{\bar{D}}_{xx}$, and uniform, layer-parallel shear stress, $\bar{\sigma}_{xz}$. The multilayer and medium are allowed to shear in a combination of mean pure shearing, as specified by $\underline{\bar{D}}_{xx} - \underline{\bar{D}}_{zz}$, and mean layer-parallel <u>simple</u> shearing, $2\underline{\bar{D}}_{xz}$. The mean velocities specified for a layer, eqs. (2a) and (2b), reflect this choice.

The mean velocities, $\underline{\bar{v}}_x$ and $\underline{\bar{v}}_z$, increase in magnitude with mean vertical distance from the global origin of coordinates for the multilayer and vary locally with vertical distance from the local origin of coordinates for the layer (Fig. B1). The layer-normal velocity, $\underline{\bar{v}}_z$, is unchanged by the shearing deformation. The layer-parallel velocity, $\underline{\bar{v}}_x$, on the other hand, increases with the mean shearing deformation within the layers and at the layer contacts. According to eqs. (2a) and (2e), the dependence of the mean layer-parallel velocity on the mean shear stress and on vertical position in the multilayer is:

$$\bar{v}_x = \bar{D}_{xx}x + (\bar{\sigma}_{xz}/\mu_\ell)(\omega_L + \zeta_{t,b})$$
$$\pm \{(\bar{\sigma}_{xz}/\beta_c)|\bar{\sigma}_{xz}/\beta_c|^{(m-1)} + \Delta(\bar{v}_x)_o\}(i) \qquad (4)$$

in which $\omega_L + \zeta_{t,b}$ is the vertical distance from the origin of global coordinates (Fig. B1) and i is the number of layer interfaces contained in the distance $\omega_L + \zeta_{t,b}$.

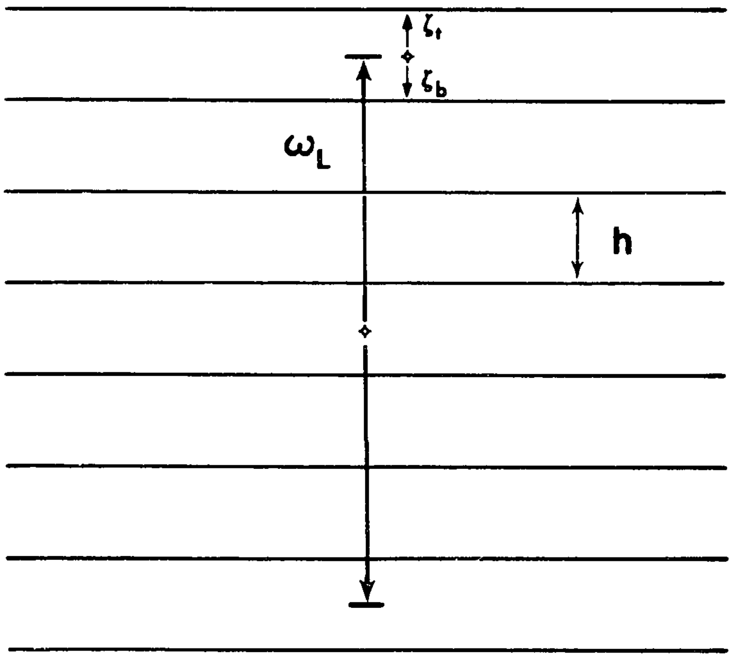

Figure B1. Global and local coordinate systems for multilayer. For the mean positions of the interfaces shown, $\zeta_{t,b} = \pm h/2$.

If the mean shear stress, $\bar{\sigma}_{xz}$, is zero, the mean layer-parallel velocity reflects only the shortening, through $\bar{D}_{xx}x$. If the mean simple shearing stress is not zero, however, a velocity gradient across the layer is produced which is inversely proportional to the viscosity of the layer, μ_{ℓ}.

At the contacts between layers, there is a velocity jump in the x-direction that depends on the rate of slip parallel to the contact. The rate of slip, in turn, is a function of the mean shear stress, $\bar{\sigma}_{xz}$, and the parameters β_c and m which describe resistance to slip at that contact. The mean part of the velocity jump in the x-direction is the difference in mean velocities at the top (t) of one layer and at the bottom (b) of the overlying layer.

To 2nd order, we write the heights of the top (t) and bottom (b) interfaces of a layer in terms of their mean position and a variation about that mean that is described in terms of four component waveforms:

$$\zeta_t = h/2 + {}_1A_t \cos(\ell x) + {}_1A_t \sin(\ell x) + {}_2A_t \cos(2\ell x) + {}_2A_t \sin(2\ell x) \tag{5a}$$

$$\zeta_b = -h/2 + {}_1A_b \cos(\ell x) + {}_1A_b \sin(\ell x) \quad {}_2A_b \cos(2\ell x) + {}_2A_b \sin(2\ell x) \tag{5b}$$

The perturbed interface shape is described by two first component waveforms with wavelength L and two second component waveforms with wavelength $\underline{L}/2$. Each pair consists of a cosinusoidal and a sinusoidal waveform.

The two cosinusoidal component waveforms, ${}_1\underline{A}\cos(\ell\underline{x})$ and ${}_2\underline{A}\cos(2\ell\underline{x})$, are the same two cosinusoidal waveforms that arise in a 2nd order analysis of layer-parallel shortening. If the maximum compressive stress were parallel to layering, the amplitudes of the cosinusoidal waveforms would reduce the corresponding ones derived in Appendix A.

The two sinusoidal component waveforms, ${}_{\mathbf{1}}\underline{A}\sin(\ell\underline{x})$ and ${}_{\mathbf{2}}\underline{A}\sin(2\ell\underline{x})$, are generated by the shearing deformation. If the maximum compressive stress were parallel to layering, the amplitudes of the sinusoidal component waveforms would be zero.

The order of approximation refers to the maximum power to which the slope of the first waveform is raised. Because the interface is described by two independent first waveforms, both first waveform amplitudes, ${}_1\underline{A}$ and ${}_{\mathbf{1}}\underline{A}$, are significant in determining the order of approximation. Thus in a 2nd order solution, terms proportional to $({}_1\underline{A}\ell)$, $({}_{\mathbf{1}}\underline{A}\ell)$, $({}_1\underline{A}\ell)^2$, $({}_{\mathbf{1}}\underline{A}\ell)^2$, and $({}_1\underline{A}\ell)({}_{\mathbf{1}}\underline{A}\ell)$ are retained. Terms proportional to 1st order in the maximum slopes of the second component waveforms -- terms proportional to $({}_2\underline{A}\ell)$ and $({}_{\mathbf{2}}\underline{A}\ell)$ -- also are retained.

The perturbed values satisfy the biharmonic equation in the stream function, ψ:

$$\nabla^4\psi = 0 \tag{6a}$$

The stream function ψ for this problem contains both sinusoidal and cosinusoidal functions:

$$\psi = (1/j\ell)\,[{}_jg(z)\,\sin(j\ell x) - {}_jh(z)\,\cos(j\ell x)];$$
$$j = 1,2 \text{ (results summed)} \tag{6b}$$

in which ℓ is the wavenumber, $\ell = 2\pi/\underline{L}$, $\underline{L}$ is the wavelength of the perturbation, and ${}_j\underline{g}$ and ${}_j\underline{h}$ are functions of $\underline{z}$.

The perturbed velocities are derivatives of the stream function:

$$\hat{v}_x = -\partial\psi/\partial z$$
$$\hat{v}_z = \partial\psi/\partial x \tag{6c}$$

The solution for the perturbed velocities and stresses consists of two sets of equations, one for the velocities and stresses generated by the layer-parallel shortening (eq. 7) and one for the stresses and velocities generated by the layer-parallel shearing (eq. 8):

$$\hat{v}_z = [\{{}_ja + {}_jb(j\ell z)\}\cosh(j\ell z)$$
$$+ \{{}_jc + {}_jd(j\ell z)\}\sinh(j\ell z)]\cos(j\ell x) \tag{7a}$$

$$\tilde{v}_x = -[\{{}_ja + {}_jd + {}_jb(j\ell z)\}\sinh(j\ell z)$$

$$+ \{{}_jb + {}_jc + {}_jd(j\ell z)\}\cosh(j\ell z)]\sin(j\ell x) \tag{7b}$$

$$\tilde{\sigma}_{zz} = 2j\mu\ell[\{{}_ja + {}_jb(j\ell z)\}\sinh(j\ell z)$$

$$+ \{{}_jc + {}_jd(j\ell z)\}\cosh(j\ell z)]\cos(j\ell x) - \tilde{p}_o \tag{7c}$$

$$\tilde{\sigma}_{xx} = -2j\mu\ell[\{{}_ja + 2{}_jd + {}_jb(j\ell z)\}\sinh(j\ell z)$$

$$+ \{{}_jc + 2{}_jb + {}_jd(j\ell z)\}\cosh(j\ell z)]\cos(j\ell x) - \tilde{p}_o \tag{7d}$$

$$\tilde{\sigma}_{xz} = -2j\mu\ell[\{{}_ja + {}_jd + {}_jb(j\ell z)\}\cosh(j\ell z)$$

$$+ \{{}_jc + {}_jb + {}_jd(j\ell z)\}\sinh(j\ell z)]\sin(j\ell x) \tag{7e}$$

$$\tilde{v}_z = [\{{}_ja + {}_jb(j\ell z)\}\cosh(j\ell z)$$

$$+ \{{}_jc + {}_jd(j\ell z)\}\sinh(j\ell z)]\sin(j\ell x) \tag{8a}$$

$$\tilde{v}_x = [\{{}_ja + {}_jd + {}_jb(j\ell z)\}\sinh(j\ell z)$$

$$+ \{{}_jb + {}_jc + {}_jd(j\ell z)\}\cosh(j\ell z)]\cos(j\ell x) \tag{8b}$$

$$\tilde{\sigma}_{zz} = 2j\mu\ell[\{{}_ja + {}_jb(j\ell z)\}\sinh(j\ell z)$$

$$+ \{{}_jc + {}_jd(j\ell z)\}\cosh(j\ell z)]\sin(j\ell x) - \tilde{p}_o \tag{8c}$$

$$\tilde{\sigma}_{xx} = -2j\mu\ell[\{{}_ja + 2{}_jd + {}_jb(j\ell z)\}\sinh(j\ell z)$$

$$+ \{{}_jc + 2{}_jb + {}_jd(j\ell z)\}\cosh(j\ell z)]\sin(j\ell x) - \tilde{p}_o \tag{8d}$$

$$\tilde{\sigma}_{xz} = 2j\mu\ell[\{{}_ja + {}_jd + {}_jb(j\ell z)\}\cosh(j\ell z)$$

$$+ \{{}_jc + {}_jb + {}_jd(j\ell z)\}\sinh(j\ell z)]\cos(j\ell x) \tag{8e}$$

in which

j is the waveform number: $j = 1$ to 2 (results summed);

ℓ is the wavenumber: $\ell = 2\pi/L$;

L is the wavelength of the first component waveform;

and ${}_j\underline{a}$, ${}_j\underline{b}$, ${}_j\underline{c}$, and ${}_j\underline{d}$ are arbitrary constants.

The leading subscript indicates the waveform with which the constant is associated.

The solution for the cosinusoidal interface (produced by layer-parallel shortening, eq. 7) can be transformed to the solution for the sinusoidal interface (produced by layer-parallel shearing, eq. 8) by using two trigonometric identities:

$$\sin(\ell x) = \sin(\ell x + 90°) = \cos(\ell x) \tag{9a}$$

$$\cos(\ell x) = \cos(\ell x + 90°) = -\sin(\ell x) \tag{9b}$$

The 2nd order expressions for the perturbed stresses and velocities at the interface are derived by substituting the 2nd order expression for the height of the interface, ζ (eq. 5), for $\underline{z}$ in the exact, general expressions for the perturbed stresses and velocities, eqs. (7) and (8). Using trigonometric identities to regroup terms according to waveform, we derive the following expressions for the perturbed stresses and velocities, to 2nd order accuracy:

$$
\begin{aligned}
[\tilde{v}_z] = & \Big\{ [\{{}^{1}_{1}a \pm {}^{1}_{1}bk\}({}_{1}C) + \{\pm {}^{1}_{1}c + {}^{1}_{1}dk\}({}_{1}S)] \\
& + [\{{}^{1}_{1}a \pm {}^{1}_{1}bk\}({}_{1}C) + \{\pm {}^{1}_{1}c + {}^{1}_{1}dk\}({}_{1}S)] \Big\} \qquad \cos(\ell x) \\
+ & \\
& \Big\{ [\{{}^{1}_{1}a \pm {}^{1}_{1}bk\}({}_{1}C) + \{\pm {}^{1}_{1}c + {}^{1}_{1}dk\}({}_{1}S)] \\
& + [\{{}^{1}_{1}a \pm {}^{1}_{1}bk\}({}_{1}C) + \{\pm {}^{1}_{1}c + {}^{1}_{1}dk\}({}_{1}S)] \Big\} \qquad \sin(\ell x) \\
+ & \\
& \Big\{ [\{{}^{2}_{2}a \pm 2{}^{2}_{2}bk\}({}_{2}C) + \{\pm {}^{2}_{2}c + 2{}^{2}_{2}dk\}({}_{2}S)] \\
& + [\{{}^{2}_{2}a \pm 2{}^{2}_{2}bk\}({}_{2}C) + \{\pm {}^{2}_{2}c + 2{}^{2}_{2}dk\}({}_{2}S)] \\
& + (1/2)[\{{}^{1}_{1}b + {}^{1}_{1}c \pm {}^{1}_{1}dk\}({}_{1}C) + \{\pm {}^{1}_{1}a \pm {}^{1}_{1}d + {}^{1}_{1}bk\}({}_{1}S)]({}_{1}A\ell) \\
& + (1/2)[\{{}^{1}_{1}b + {}^{1}_{1}c \pm {}^{1}_{1}dk\}({}_{1}C) + \{\pm {}^{1}_{1}a \pm {}^{1}_{1}d + {}^{1}_{1}bk\}({}_{1}S)]({}_{1}A\ell) \\
& - (1/2)[\{{}^{1}_{1}b + {}^{1}_{1}c \pm {}^{1}_{1}dk\}({}_{1}C) + \{\pm {}^{1}_{1}a \pm {}^{1}_{1}d + {}^{1}_{1}bk\}({}_{1}S)]({}_{1}A\ell) \\
& - (1/2)[\{{}^{1}_{1}b + {}^{1}_{1}c \pm {}^{1}_{1}dk\}({}_{1}C) + \{\pm {}^{1}_{1}a \pm {}^{1}_{1}d + {}^{1}_{1}bk\}({}_{1}S)]({}_{1}A\ell) \\
& + [\{{}^{1}{}^{1}_{2}a \pm 2{}^{1}{}^{1}_{2}bk\}({}_{2}C) + \{\pm {}^{1}{}^{1}_{2}c + 2{}^{1}{}^{1}_{2}dk\}({}_{2}S)] \\
& + [\{{}^{1}{}^{1}_{2}a \pm 2{}^{1}{}^{1}_{2}bk\}({}_{2}C) + \{\pm {}^{1}{}^{1}_{2}c + 2{}^{1}{}^{1}_{2}dk\}({}_{2}S)] \\
& + [\{{}^{1}{}^{1}_{2}a \pm 2{}^{1}{}^{1}_{2}bk\}({}_{2}C) + \{\pm {}^{1}{}^{1}_{2}c + 2{}^{1}{}^{1}_{2}dk\}({}_{2}S)] \Big\} \qquad \cos(2\ell x) \\
+ & \\
& \Big\{ [\{{}^{2}_{2}a \pm 2{}^{2}_{2}bk\}({}_{2}C) + \{\pm {}^{2}_{2}c + 2{}^{2}_{2}dk\}({}_{2}S)] \\
& + [\{{}^{2}_{2}a \pm 2{}^{2}_{2}bk\}({}_{2}C) + \{\pm {}^{2}_{2}c + 2{}^{2}_{2}dk\}({}_{2}S)] \\
& + (1/2)[\{{}^{1}_{1}b + {}^{1}_{1}c \pm {}^{1}_{1}dk\}({}_{1}C) + \{\pm {}^{1}_{1}a \pm {}^{1}_{1}d + {}^{1}_{1}bk\}({}_{1}S)]({}_{1}A\ell) \\
& + (1/2)[\{{}^{1}_{1}b + {}^{1}_{1}c \pm {}^{1}_{1}dk\}({}_{1}C) + \{\pm {}^{1}_{1}a \pm {}^{1}_{1}d + {}^{1}_{1}bk\}({}_{1}S)]({}_{1}A\ell) \\
& + (1/2)[\{{}^{1}_{1}b + {}^{1}_{1}c \pm {}^{1}_{1}dk\}({}_{1}C) + \{\pm {}^{1}_{1}a \pm {}^{1}_{1}d + {}^{1}_{1}bk\}({}_{1}S)]({}_{1}A\ell) \\
& + (1/2)[\{{}^{1}_{1}b + {}^{1}_{1}c \pm {}^{1}_{1}dk\}({}_{1}C) + \{\pm {}^{1}_{1}a \pm {}^{1}_{1}d + {}^{1}_{1}bk\}({}_{1}S)]({}_{1}A\ell)
\end{aligned}
$$

$$+ \ [\{{}^{1}{}^{1}_{2}a \pm 2\,{}^{1}{}^{1}_{2}bk\}({}_{2}C) \ + \ \{\pm {}^{1}{}^{1}_{2}c + 2\,{}^{1}{}^{1}_{2}dk\}({}_{2}S)]$$

$$+ \ [\{{}^{1}{}^{1}_{2}a \pm 2\,{}^{1}{}^{1}_{2}bk\}({}_{2}C) \ + \ \{\pm {}^{1}{}^{1}_{2}c + 2\,{}^{1}{}^{1}_{2}dk\}({}_{2}S)]$$

$$+ \ [\{{}^{1}{}^{1}_{2}a \pm 2\,{}^{1}{}^{1}_{2}bk\}({}_{2}C) \ + \ \{\pm {}^{1}{}^{1}_{2}c + 2\,{}^{1}{}^{1}_{2}dk\}({}_{2}S)] \ \Big\} \qquad \sin(2\ell x)$$

$$+$$

$$+ \ (1/2)[\{{}^{1}_{1}b + {}^{1}_{1}c \pm {}^{1}_{1}dk\}({}_{1}C) \ + \ \{\pm {}^{1}_{1}a \pm {}^{1}_{1}d + {}^{1}_{1}bk\}({}_{1}S)]({}_{1}A\ell)$$

$$+ \ (1/2)[\{{}^{1}_{1}b + {}^{1}_{1}c \pm {}^{1}_{1}dk\}({}_{1}C) \ + \ \{\pm {}^{1}_{1}a \pm {}^{1}_{1}d + {}^{1}_{1}bk\}({}_{1}S)]({}_{1}A\ell)$$

$$+ \ (1/2)[\{{}^{1}_{1}b + {}^{1}_{1}c \pm {}^{1}_{1}dk\}({}_{1}C) \ + \ \{\pm {}^{1}_{1}a \pm {}^{1}_{1}d + {}^{1}_{1}bk\}({}_{1}S)]({}_{1}A\ell)$$

$$+ \ (1/2)[\{{}^{1}_{1}b + {}^{1}_{1}c \pm {}^{1}_{1}dk\}({}_{1}C) \ + \ \{\pm {}^{1}_{1}a \pm {}^{1}_{1}d + {}^{1}_{1}bk\}({}_{1}S)]({}_{1}A\ell) \qquad (9a)$$

$$[\hat{V}_x] \ = \ \Big\{ - \ [\{{}^{1}_{1}b + {}^{1}_{1}c \pm {}^{1}_{1}dk\}({}_{1}C) \ + \ \{\pm {}^{1}_{1}a \pm {}^{1}_{1}d + {}^{1}_{1}bk\}({}_{1}S)]$$

$$- \ [\{{}^{1}_{1}b + {}^{1}_{1}c \pm {}^{1}_{1}dk\}({}_{1}C) \ + \ \{\pm {}^{1}_{1}a \pm {}^{1}_{1}d + {}^{1}_{1}bk\}({}_{1}S)] \ \Big\} \qquad \sin(\ell x)$$

$$+$$

$$\Big\{ + \ [\{{}^{1}_{1}b + {}^{1}_{1}c \pm {}^{1}_{1}dk\}({}_{1}C) \ + \ \{\pm {}^{1}_{1}a \pm {}^{1}_{1}d + {}^{1}_{1}bk\}({}_{1}S)]$$

$$+ \ [\{{}^{1}_{1}b + {}^{1}_{1}c \pm {}^{1}_{1}dk\}({}_{1}C) \ + \ \{\pm {}^{1}_{1}a \pm {}^{1}_{1}d + {}^{1}_{1}bk\}({}_{1}S)] \ \Big\} \qquad \cos(\ell x)$$

$$+$$

$$\Big\{ - \ [\{{}^{2}_{2}b + {}^{2}_{2}c \pm 2\,{}^{2}_{2}dk\}({}_{2}C) \ + \ \{\pm {}^{2}_{2}a \pm {}^{2}_{2}d + 2\,{}^{2}_{2}bk\}({}_{2}S)]$$

$$- \ [\{{}^{2}_{2}b + {}^{2}_{2}c \pm 2\,{}^{2}_{2}dk\}({}_{2}C) \ + \ \{\pm {}^{2}_{2}a \pm {}^{2}_{2}d + 2\,{}^{2}_{2}bk\}({}_{2}S)]$$

$$- \ (1/2)[\{{}^{1}_{1}a + 2\,{}^{1}_{1}d \pm {}^{1}_{1}bk\}({}_{1}C) \ + \ \{\pm {}^{1}_{1}c \pm 2\,{}^{1}_{1}b + {}^{1}_{1}dk\}({}_{1}S)]({}_{1}A\ell)$$

$$- \ (1/2)[\{{}^{1}_{1}a + 2\,{}^{1}_{1}d \pm {}^{1}_{1}bk\}({}_{1}C) \ + \ \{\pm {}^{1}_{1}c \pm 2\,{}^{1}_{1}b + {}^{1}_{1}dk\}({}_{1}S)]({}_{1}A\ell)$$

$$+ \ (1/2)[\{{}^{1}_{1}a + 2\,{}^{1}_{1}d \pm {}^{1}_{1}bk\}({}_{1}C) \ + \ \{\pm {}^{1}_{1}c \pm 2\,{}^{1}_{1}b + {}^{1}_{1}dk\}({}_{1}S)]({}_{1}A\ell)$$

$$+ \ (1/2)[\{{}^{1}_{1}a + 2\,{}^{1}_{1}d \pm {}^{1}_{1}bk\}({}_{1}C) \ + \ \{\pm {}^{1}_{1}c \pm 2\,{}^{1}_{1}b + {}^{1}_{1}dk\}({}_{1}S)]({}_{1}A\ell)$$

$$- \ [\{{}^{1}{}^{1}_{2}b + {}^{1}{}^{1}_{2}c \pm 2\,{}^{1}{}^{1}_{2}dk\}({}_{2}C) \ + \ \{\pm {}^{1}{}^{1}_{2}a \pm {}^{1}{}^{1}_{2}d + 2\,{}^{1}{}^{1}_{2}bk\}({}_{2}S)]$$

$$- \ [\{{}^{1}{}^{1}_{2}b + {}^{1}{}^{1}_{2}c \pm 2\,{}^{1}{}^{1}_{2}dk\}({}_{2}C) \ + \ \{\pm {}^{1}{}^{1}_{2}a \pm {}^{1}{}^{1}_{2}d + 2\,{}^{1}{}^{1}_{2}bk\}({}_{2}S)]$$

$$- \ [\{{}^{1}{}^{1}_{2}b + {}^{1}{}^{1}_{2}c \pm 2\,{}^{1}{}^{1}_{2}dk\}({}_{2}C)$$

$$+ \{\pm{}^{1}{}^{1}_{2}a\pm{}^{1}{}^{1}_{2}d+2{}^{1}{}^{1}_{2}bk\}({}_{2}S)] \;\Big\} \qquad \sin(2\ell x)$$

$+$

$$\Big\{ \;+ [\{{}^{2}_{2}b+{}^{2}_{2}c\pm 2{}^{2}_{2}dk\}({}_{2}C) + \{\pm{}^{2}_{2}a\pm{}^{2}_{2}d+2{}^{2}_{2}bk\}({}_{2}S)]$$

$$+ [\{{}^{2}_{2}b+{}^{2}_{2}c\pm 2{}^{2}_{2}dk\}({}_{2}C) + \{\pm{}^{2}_{2}a\pm{}^{2}_{2}d+2{}^{2}_{2}bk\}({}_{2}S)]$$

$$+ (1/2)[\{{}^{1}_{1}a+2{}^{1}_{1}d\pm{}^{1}_{1}bk\}({}_{1}C) + \{\pm{}^{1}_{1}c\pm 2{}^{1}_{1}b+{}^{1}_{1}dk\}({}_{1}S)]({}_{1}A\ell)$$

$$+ (1/2)[\{{}^{1}_{1}a+2{}^{1}_{1}d\pm{}^{1}_{1}bk\}({}_{1}C) + \{\pm{}^{1}_{1}c\pm 2{}^{1}_{1}b+{}^{1}_{1}dk\}({}_{1}S)]({}_{1}A\ell)$$

$$+ (1/2)[\{{}^{1}_{1}a+2{}^{1}_{1}d\pm{}^{1}_{1}bk\}({}_{1}C) + \{\pm{}^{1}_{1}c\pm 2{}^{1}_{1}b+{}^{1}_{1}dk\}({}_{1}S)]({}_{1}A\ell)$$

$$+ (1/2)[\{{}^{1}_{1}a+2{}^{1}_{1}d\pm{}^{1}_{1}bk\}({}_{1}C) + \{\pm{}^{1}_{1}c\pm 2{}^{1}_{1}b+{}^{1}_{1}dk\}({}_{1}S)]({}_{1}A\ell)$$

$$+ [\{{}^{1}{}^{1}_{2}b+{}^{1}{}^{1}_{2}c\pm 2{}^{1}{}^{1}_{2}dk\}({}_{2}C) + \{\pm{}^{1}{}^{1}_{2}a\pm{}^{1}{}^{1}_{2}d+2{}^{1}{}^{1}_{2}bk\}({}_{2}S)]$$

$$+ [\{{}^{1}{}^{1}_{2}b+{}^{1}{}^{1}_{2}c\pm 2{}^{1}{}^{1}_{2}dk\}({}_{2}C) + \{\pm{}^{1}{}^{1}_{2}a\pm{}^{1}{}^{1}_{2}d+2{}^{1}{}^{1}_{2}bk\}({}_{2}S)]$$

$$+ [\{{}^{1}{}^{1}_{2}b+{}^{1}{}^{1}_{2}c\pm 2{}^{1}{}^{1}_{2}dk\}({}_{2}C)$$

$$+ \{\pm{}^{1}{}^{1}_{2}a\pm{}^{1}{}^{1}_{2}d+2{}^{1}{}^{1}_{2}bk\}({}_{2}S)] \;\Big\} \qquad \cos(2\ell x)$$

$+$

$$+ (1/2)[\{{}^{1}_{1}a+2{}^{1}_{1}d\pm{}^{1}_{1}bk\}({}_{1}C) + \{\pm{}^{1}_{1}c\pm 2{}^{1}_{1}b+{}^{1}_{1}dk\}({}_{1}S)]({}_{1}A\ell)$$

$$+ (1/2)[\{{}^{1}_{1}a+2{}^{1}_{1}d\pm{}^{1}_{1}bk\}({}_{1}C) + \{\pm{}^{1}_{1}c\pm 2{}^{1}_{1}b+{}^{1}_{1}dk\}({}_{1}S)]({}_{1}A\ell)$$

$$- (1/2)[\{{}^{1}_{1}a+2{}^{1}_{1}d\pm{}^{1}_{1}bk\}({}_{1}C) + \{\pm{}^{1}_{1}c\pm 2{}^{1}_{1}b+{}^{1}_{1}dk\}({}_{1}S)]({}_{1}A\ell)$$

$$- (1/2)[\{{}^{1}_{1}a+2{}^{1}_{1}d\pm{}^{1}_{1}bk\}({}_{1}C) + \{\pm{}^{1}_{1}c\pm 2{}^{1}_{1}b+{}^{1}_{1}dk\}({}_{1}S)]({}_{1}A\ell)$$

(9b)

$$[\tilde{\sigma}_{zz}] = \Big\{ \;2\mu\ell[\{{}^{1}_{1}c\pm{}^{1}_{1}dk\}({}_{1}C) + \{\pm{}^{1}_{1}a+{}^{1}_{1}bk\}({}_{1}S)]$$

$$+ 2\mu\ell[\{{}^{1}_{1}c\pm{}^{1}_{1}dk\}({}_{1}C) + \{\pm{}^{1}_{1}a+{}^{1}_{1}bk\}({}_{1}S)] \;\Big\} \qquad \cos(\ell x)$$

$+$

$$\Big\{ \;2\mu\ell[\{{}^{1}_{1}c\pm{}^{1}_{1}dk\}({}_{1}C) + \{\pm{}^{1}_{1}a+{}^{1}_{1}bk\}({}_{1}S)]$$

$$+ 2\mu\ell[\{{}^{1}_{1}c\pm{}^{1}_{1}dk\}({}_{1}C) + \{\pm{}^{1}_{1}a+{}^{1}_{1}bk\}({}_{1}S)] \;\Big\} \qquad \sin(\ell x)$$

$+$

$$\Big\{ + 4\mu\ell[\{{}^{2}_{2}c \pm 2\,{}^{2}_{2}dk\}({}_{2}C) + \{\pm{}^{2}_{2}a + 2\,{}^{2}_{2}bk\}({}_{2}S)]$$

$$+ 4\mu\ell[\{{}^{2}_{2}c \pm 2\,{}^{2}_{2}dk\}({}_{2}C) + \{\pm{}^{2}_{2}a + 2\,{}^{2}_{2}bk\}({}_{2}S)]$$

$$+ \mu\ell[\{{}^{1}_{1}a + {}^{1}_{1}d \pm {}^{1}_{1}bk\}({}_{1}C) + \{\pm{}^{1}_{1}c \pm {}^{1}_{1}b + {}^{1}_{1}dk\}({}_{1}S)]({}_{1}A\ell)$$

$$+ \mu\ell[\{{}^{1}_{1}a + {}^{1}_{1}d \pm {}^{1}_{1}bk\}({}_{1}C) + \{\pm{}^{1}_{1}c \pm {}^{1}_{1}b + {}^{1}_{1}dk\}({}_{1}S)]({}_{1}A\ell)$$

$$- \mu\ell[\{{}^{1}_{1}a + {}^{1}_{1}d \pm {}^{1}_{1}bk\}({}_{1}C) + \{\pm{}^{1}_{1}c \pm {}^{1}_{1}b + {}^{1}_{1}dk\}({}_{1}S)]({}_{1}A\ell)$$

$$- \mu\ell[\{{}^{1}_{1}a + {}^{1}_{1}d \pm {}^{1}_{1}bk\}({}_{1}C) + \{\pm{}^{1}_{1}c \pm {}^{1}_{1}b + {}^{1}_{1}dk\}({}_{1}S)]({}_{1}A\ell)$$

$$+ 4\mu\ell[\{{}^{1\,1}_{2}c \pm 2\,{}^{1\,1}_{2}dk\}({}_{2}C) + \{\pm{}^{1\,1}_{2}a + 2\,{}^{1\,1}_{2}bk\}({}_{2}S)]$$

$$+ 4\mu\ell[\{{}^{1\,1}_{2}c \pm 2\,{}^{1\,1}_{2}dk\}({}_{2}C) + \{\pm{}^{1\,1}_{2}a + 2\,{}^{1\,1}_{2}bk\}({}_{2}S)]$$

$$+ 4\mu\ell[\{{}^{1\,1}_{2}c \pm 2\,{}^{1\,1}_{2}dk\}({}_{2}C) + \{\pm{}^{1\,1}_{2}a + 2\,{}^{1\,1}_{2}bk\}({}_{2}S)] \Big\} \qquad \cos(2\ell x)$$

$$+$$

$$\Big\{ + 4\mu\ell[\{{}^{2}_{2}c \pm 2\,{}^{2}_{2}dk\}({}_{2}C) + \{\pm{}^{2}_{2}a + 2\,{}^{2}_{2}bk\}({}_{2}S)]$$

$$+ 4\mu\ell[\{{}^{2}_{2}c \pm 2\,{}^{2}_{2}dk\}({}_{2}C) + \{\pm{}^{2}_{2}a + 2\,{}^{2}_{2}bk\}({}_{2}S)]$$

$$+ \mu\ell[\{{}^{1}_{1}a + {}^{1}_{1}d \pm {}^{1}_{1}bk\}({}_{1}C) + \{\pm{}^{1}_{1}c \pm {}^{1}_{1}b + {}^{1}_{1}dk\}({}_{1}S)]({}_{1}A\ell)$$

$$+ \mu\ell[\{{}^{1}_{1}a + {}^{1}_{1}d \pm {}^{1}_{1}bk\}({}_{1}C) + \{\pm{}^{1}_{1}c \pm {}^{1}_{1}b + {}^{1}_{1}dk\}({}_{1}S)]({}_{1}A\ell)$$

$$+ \mu\ell[\{{}^{1}_{1}a + {}^{1}_{1}d \pm {}^{1}_{1}bk\}({}_{1}C) + \{\pm{}^{1}_{1}c \pm {}^{1}_{1}b + {}^{1}_{1}dk\}({}_{1}S)]({}_{1}A\ell)$$

$$+ \mu\ell[\{{}^{1}_{1}a + {}^{1}_{1}d \pm {}^{1}_{1}bk\}({}_{1}C) + \{\pm{}^{1}_{1}c \pm {}^{1}_{1}b + {}^{1}_{1}dk\}({}_{1}S)]({}_{1}A\ell)$$

$$+ 4\mu\ell[\{{}^{1\,1}_{2}c \pm 2\,{}^{1\,1}_{2}dk\}({}_{2}C) + \{\pm{}^{1\,1}_{2}a + 2\,{}^{1\,1}_{2}bk\}({}_{2}S)]$$

$$+ 4\mu\ell[\{{}^{1\,1}_{2}c \pm 2\,{}^{1\,1}_{2}dk\}({}_{2}C) + \{\pm{}^{1\,1}_{2}a + 2\,{}^{1\,1}_{2}bk\}({}_{2}S)]$$

$$+ 4\mu\ell[\{{}^{1\,1}_{2}c \pm 2\,{}^{1\,1}_{2}dk\}({}_{2}C) + \{\pm{}^{1\,1}_{2}a + 2\,{}^{1\,1}_{2}bk\}({}_{2}S)] \Big\} \qquad \sin(2\ell x)$$

$$+$$

$$+ \mu\ell[\{{}^{1}_{1}a + {}^{1}_{1}d \pm {}^{1}_{1}bk\}({}_{1}C) + \{\pm{}^{1}_{1}c \pm {}^{1}_{1}b + {}^{1}_{1}dk\}({}_{1}S)]({}_{1}A\ell)$$

$$+ \mu\ell[\{{}^{1}_{1}a + {}^{1}_{1}d \pm {}^{1}_{1}bk\}({}_{1}C) + \{\pm{}^{1}_{1}c \pm {}^{1}_{1}b + {}^{1}_{1}dk\}({}_{1}S)]({}_{1}A\ell)$$

$$+ \mu\ell[\{{}^{1}_{1}a + {}^{1}_{1}d \pm {}^{1}_{1}bk\}({}_{1}C) + \{\pm{}^{1}_{1}c \pm {}^{1}_{1}b + {}^{1}_{1}dk\}({}_{1}S)]({}_{1}A\ell)$$

$$+ \mu\ell[\{{}^{1}_{1}a + {}^{1}_{1}d \pm {}^{1}_{1}bk\}({}_{1}C) + \{\pm{}^{1}_{1}c \pm {}^{1}_{1}b + {}^{1}_{1}dk\}({}_{1}S)]({}_{1}A\ell)$$

$$- \tilde{p}_{o} - \rho g z \tag{9c}$$

$$[\bar{\sigma}_{xx}] = \Big\{ - 2\mu\ell[\{{}^{1}_{1}c+2{}^{1}_{1}b\pm{}^{1}_{1}dk\}({}_{1}C) + \{\pm{}^{1}_{1}a\pm 2{}^{1}_{1}d+{}^{1}_{1}bk\}({}_{1}S)]$$

$$- 2\mu\ell[\{{}^{1}_{1}c+2{}^{1}_{1}b\pm{}^{1}_{1}dk\}({}_{1}C) + \{\pm{}^{1}_{1}a\pm 2{}^{1}_{1}d+{}^{1}_{1}bk\}({}_{1}S)] \Big\} \qquad \cos(\ell x)$$

$+$

$$\Big\{ - 2\mu\ell[\{{}^{1}_{1}c+2{}^{1}_{1}b\pm{}^{1}_{1}dk\}({}_{1}C) + \{\pm{}^{1}_{1}a\pm 2{}^{1}_{1}d+{}^{1}_{1}bk\}({}_{1}S)]$$

$$- 2\mu\ell[\{{}^{1}_{1}c+2{}^{1}_{1}b\pm{}^{1}_{1}dk\}({}_{1}C) + \{\pm{}^{1}_{1}a\pm 2{}^{1}_{1}d+{}^{1}_{1}bk\}({}_{1}S)] \Big\} \qquad \sin(\ell x)$$

$+$

$$\Big\{ - 4\mu\ell[\{{}^{2}_{2}c+2{}^{2}_{2}b\pm 2{}^{2}_{2}dk\}({}_{2}C) + \{\pm{}^{2}_{2}a\pm 2{}^{2}_{2}d+2{}^{2}_{2}bk\}({}_{2}S)]$$

$$- 4\mu\ell[\{{}^{2}_{2}c+2{}^{2}_{2}b\pm 2{}^{2}_{2}dk\}({}_{2}C) + \{\pm{}^{2}_{2}a\pm 2{}^{2}_{2}d+2{}^{2}_{2}bk\}({}_{2}S)]$$

$$- \mu\ell[\{{}^{1}_{1}a+3{}^{1}_{1}d\pm{}^{1}_{1}bk\}({}_{1}C) + \{\pm{}^{1}_{1}c\pm 3{}^{1}_{1}b+{}^{1}_{1}dk\}({}_{1}S)]({}_{1}A\ell)$$

$$- \mu\ell[\{{}^{1}_{1}a+3{}^{1}_{1}d\pm{}^{1}_{1}bk\}({}_{1}C) + \{\pm{}^{1}_{1}c\pm 3{}^{1}_{1}b+{}^{1}_{1}dk\}({}_{1}S)]({}_{1}A\ell)$$

$$+ \mu\ell[\{{}^{1}_{1}a+3{}^{1}_{1}d\pm{}^{1}_{1}bk\}({}_{1}C) + \{\pm{}^{1}_{1}c\pm 3{}^{1}_{1}b+{}^{1}_{1}dk\}({}_{1}S)]({}_{1}A\ell)$$

$$+ \mu\ell[\{{}^{1}_{1}a+3{}^{1}_{1}d\pm{}^{1}_{1}bk\}({}_{1}C) + \{\pm{}^{1}_{1}c\pm 3{}^{1}_{1}b+{}^{1}_{1}dk\}({}_{1}S)]({}_{1}A\ell)$$

$$- 4\mu\ell[\{{}^{1}{}^{1}_{2}c+2{}^{1}{}^{1}_{2}b\pm 2{}^{1}{}^{1}_{2}dk\}({}_{2}C) + \{\pm{}^{1}{}^{1}_{2}a\pm 2{}^{1}{}^{1}_{2}d+2{}^{1}{}^{1}_{2}bk\}({}_{2}S)]$$

$$- 4\mu\ell[\{{}^{1}{}^{1}_{2}c+2{}^{1}{}^{1}_{2}b\pm 2{}^{1}{}^{1}_{2}dk\}({}_{2}C) + \{\pm{}^{1}{}^{1}_{2}a\pm 2{}^{1}{}^{1}_{2}d+2{}^{1}{}^{1}_{2}bk\}({}_{2}S)]$$

$$- 4\mu\ell[\{{}^{1}{}^{1}_{2}c+2{}^{1}{}^{1}_{2}b\pm 2{}^{1}{}^{1}_{2}dk\}({}_{2}C) + \{\pm{}^{1}{}^{1}_{2}a\pm 2{}^{1}{}^{1}_{2}d+2{}^{1}{}^{1}_{2}bk\}({}_{2}S)] \Big\} \qquad \cos(2\ell x)$$

$+$

$$\Big\{ - 4\mu\ell[\{{}^{2}_{2}c+2{}^{2}_{2}b\pm 2{}^{2}_{2}dk\}({}_{2}C) + \{\pm{}^{2}_{2}a\pm 2{}^{2}_{2}d+2{}^{2}_{2}bk\}({}_{2}S)]$$

$$- 4\mu\ell[\{{}^{2}_{2}c+2{}^{2}_{2}b\pm 2{}^{2}_{2}dk\}({}_{2}C) + \{\pm{}^{2}_{2}a\pm 2{}^{2}_{2}d+2{}^{2}_{2}bk\}({}_{2}S)]$$

$$- \mu\ell[\{{}^{1}_{1}a+3{}^{1}_{1}d\pm{}^{1}_{1}bk\}({}_{1}C) + \{\pm{}^{1}_{1}c\pm 3{}^{1}_{1}b+{}^{1}_{1}dk\}({}_{1}S)]({}_{1}A\ell)$$

$$- \mu\ell[\{{}^{1}_{1}a+3{}^{1}_{1}d\pm{}^{1}_{1}bk\}({}_{1}C) + \{\pm{}^{1}_{1}c\pm 3{}^{1}_{1}b+{}^{1}_{1}dk\}({}_{1}S)]({}_{1}A\ell)$$

$$- \mu\ell[\{{}^{1}_{1}a+3{}^{1}_{1}d\pm{}^{1}_{1}bk\}({}_{1}C) + \{\pm{}^{1}_{1}c\pm 3{}^{1}_{1}b+{}^{1}_{1}dk\}({}_{1}S)]({}_{1}A\ell)$$

$$- \mu\ell[\{{}^{1}_{1}a+3{}^{1}_{1}d\pm{}^{1}_{1}bk\}({}_{1}C) + \{\pm{}^{1}_{1}c\pm 3{}^{1}_{1}b+{}^{1}_{1}dk\}({}_{1}S)]({}_{1}A\ell)$$

$$- 4\mu\ell[\{{}^{1}{}^{1}_{2}c+2{}^{1}{}^{1}_{2}b\pm 2{}^{1}{}^{1}_{2}dk\}({}_{2}C) + \{\pm{}^{1}{}^{1}_{2}a\pm 2{}^{1}{}^{1}_{2}d+2{}^{1}{}^{1}_{2}bk\}({}_{2}S)]$$

$$- 4\mu\ell[\{{}^{1}{}^{1}_{2}c+2\,{}^{1}{}^{1}_{2}b\pm 2\,{}^{1}{}^{1}_{2}dk\}({}_{2}C) + \{\pm{}^{1}{}^{1}_{2}a\pm 2\,{}^{1}{}^{1}_{2}d+2\,{}^{1}{}^{1}_{2}bk\}({}_{2}S)]$$

$$- 4\mu\ell[\{{}^{1}{}^{1}_{2}c+2\,{}^{1}{}^{1}_{2}b\pm 2\,{}^{1}{}^{1}_{2}dk\}({}_{2}C) + \{\pm{}^{1}{}^{1}_{2}a\pm 2\,{}^{1}{}^{1}_{2}d+2\,{}^{1}{}^{1}_{2}bk\}({}_{2}S)] \Big\} \qquad \sin(2\ell x)$$

$$- \mu\ell[\{{}^{1}_{1}a+3\,{}^{1}_{1}d\pm{}^{1}_{1}bk\}({}_{1}C) + \{\pm{}^{1}_{1}c\pm 3\,{}^{1}_{1}b+{}^{1}_{1}dk\}({}_{1}S)]({}_{1}A\ell)$$

$$- \mu\ell[\{{}^{1}_{1}a+3\,{}^{1}_{1}d\pm{}^{1}_{1}bk\}({}_{1}C) + \{\pm{}^{1}_{1}c\pm 3\,{}^{1}_{1}b+{}^{1}_{1}dk\}({}_{1}S)]({}_{1}A\ell)$$

$$- \mu\ell[\{{}^{1}_{1}a+3\,{}^{1}_{1}d\pm{}^{1}_{1}bk\}({}_{1}C) + \{\pm{}^{1}_{1}c\pm 3\,{}^{1}_{1}b+{}^{1}_{1}dk\}({}_{1}S)]({}_{1}A\ell)$$

$$- \mu\ell[\{{}^{1}_{1}a+3\,{}^{1}_{1}d\pm{}^{1}_{1}bk\}({}_{1}C) + \{\pm{}^{1}_{1}c\pm 3\,{}^{1}_{1}b+{}^{1}_{1}dk\}({}_{1}S)]({}_{1}A\ell)$$

$$- \tilde{p}_{o} - \rho g z \qquad (9d)$$

$$[\tilde{\sigma}_{xz}] = \Big\{ -2\mu\ell[\{{}^{1}_{1}a+{}^{1}_{1}d\pm{}^{1}_{1}bk\}({}_{1}C) + \{\pm{}^{1}_{1}c\pm{}^{1}_{1}b+{}^{1}_{1}dk\}({}_{1}S)]$$

$$-2\mu\ell[\{{}^{1}_{1}a+{}^{1}_{1}d\pm{}^{1}_{1}bk\}({}_{1}C) + \{\pm{}^{1}_{1}c\pm{}^{1}_{1}b+{}^{1}_{1}dk\}({}_{1}S)] \Big\} \qquad \sin(\ell x)$$

$$+$$

$$\Big\{ +2\mu\ell[\{{}^{1}_{1}a+{}^{1}_{1}d\pm{}^{1}_{1}bk\}({}_{1}C) + \{\pm{}^{1}_{1}c\pm{}^{1}_{1}b+{}^{1}_{1}dk\}({}_{1}S)]$$

$$+2\mu\ell[\{{}^{1}_{1}a+{}^{1}_{1}d\pm{}^{1}_{1}bk\}({}_{1}C) + \{\pm{}^{1}_{1}c\pm{}^{1}_{1}b+{}^{1}_{1}dk\}({}_{1}S)] \Big\} \qquad \cos(\ell x)$$

$$+$$

$$\Big\{ - 4\mu\ell[\{{}^{2}_{2}a+{}^{2}_{2}d\pm 2\,{}^{2}_{2}bk\}({}_{2}C) + \{\pm{}^{2}_{2}c\pm{}^{2}_{2}b+2\,{}^{2}_{2}dk\}({}_{2}S)]$$

$$- 4\mu\ell[\{{}^{2}_{2}a+{}^{2}_{2}d\pm 2\,{}^{2}_{2}bk\}({}_{2}C) + \{\pm{}^{2}_{2}c\pm{}^{2}_{2}b+2\,{}^{2}_{2}dk\}({}_{2}S)]$$

$$- \mu\ell[\{{}^{1}_{1}c+2\,{}^{1}_{1}b\pm{}^{1}_{1}dk\}({}_{1}C) + \{\pm{}^{1}_{1}a\pm 2\,{}^{1}_{1}d+{}^{1}_{1}bk\}({}_{1}S)]({}_{1}A\ell)$$

$$- \mu\ell[\{{}^{1}_{1}c+2\,{}^{1}_{1}b\pm{}^{1}_{1}dk\}({}_{1}C) + \{\pm{}^{1}_{1}a\pm 2\,{}^{1}_{1}d+{}^{1}_{1}bk\}({}_{1}S)]({}_{1}A\ell)$$

$$+ \mu\ell[\{{}^{1}_{1}c+2\,{}^{1}_{1}b\pm{}^{1}_{1}dk\}({}_{1}C) + \{\pm{}^{1}_{1}a\pm 2\,{}^{1}_{1}d+{}^{1}_{1}bk\}({}_{1}S)]({}_{1}A\ell)$$

$$+ \mu\ell[\{{}^{1}_{1}c+2\,{}^{1}_{1}b\pm{}^{1}_{1}dk\}({}_{1}C) + \{\pm{}^{1}_{1}a\pm 2\,{}^{1}_{1}d+{}^{1}_{1}bk\}({}_{1}S)]({}_{1}A\ell)$$

$$- 4\mu\ell[\{{}^{1}{}^{1}_{2}a+{}^{1}{}^{1}_{2}d\pm 2\,{}^{1}{}^{1}_{2}bk\}({}_{2}C) + \{\pm{}^{1}{}^{1}_{2}c\pm{}^{1}{}^{1}_{2}b+2\,{}^{1}{}^{1}_{2}dk\}({}_{2}S)]$$

$$- 4\mu\ell[\{{}^{1}{}^{1}_{2}a+{}^{1}{}^{1}_{2}d\pm 2\,{}^{1}{}^{1}_{2}bk\}({}_{2}C) + \{\pm{}^{1}{}^{1}_{2}c\pm{}^{1}{}^{1}_{2}b+2\,{}^{1}{}^{1}_{2}dk\}({}_{2}S)]$$

$$- 4\mu\ell[\{{}^{1}{}^{1}_{2}a+{}^{1}{}^{1}_{2}d\pm 2{}^{1}{}^{1}_{2}bk\}({}_{2}C)$$
$$+ \{\pm{}^{1}{}^{1}_{2}c\pm{}^{1}{}^{1}_{2}b+2{}^{1}{}^{1}_{2}dk\}({}_{2}S)] \Big\} \qquad \sin(2\ell x)$$

$$+$$

$$\Big\{ + 4\mu\ell[\{{}^{2}_{2}a+{}^{2}_{2}d\pm 2{}^{2}_{2}bk\}({}_{2}C) + \{\pm{}^{2}_{2}c\pm{}^{2}_{2}b+2{}^{2}_{2}dk\}({}_{2}S)]$$
$$+ 4\mu\ell[\{{}^{2}_{2}a+{}^{2}_{2}d\pm 2{}^{2}_{2}bk\}({}_{2}C) + \{\pm{}^{2}_{2}c\pm{}^{2}_{2}b+2{}^{2}_{2}dk\}({}_{2}S)]$$
$$+ \mu\ell[\{{}^{1}_{1}c+2{}^{1}_{1}b\pm{}^{1}_{1}dk\}({}_{1}C) + \{\pm{}^{1}_{1}a\pm 2{}^{1}_{1}d+{}^{1}_{1}bk\}({}_{1}S)]({}_{1}A\ell)$$
$$+ \mu\ell[\{{}^{1}_{1}c+2{}^{1}_{1}b\pm{}^{1}_{1}dk\}({}_{1}C) + \{\pm{}^{1}_{1}a\pm 2{}^{1}_{1}d+{}^{1}_{1}bk\}({}_{1}S)]({}_{1}A\ell)$$
$$+ \mu\ell[\{{}^{1}_{1}c+2{}^{1}_{1}b\pm{}^{1}_{1}dk\}({}_{1}C) + \{\pm{}^{1}_{1}a\pm 2{}^{1}_{1}d+{}^{1}_{1}bk\}({}_{1}S)]({}_{1}A\ell)$$
$$+ \mu\ell[\{{}^{1}_{1}c+2{}^{1}_{1}b\pm{}^{1}_{1}dk\}({}_{1}C) + \{\pm{}^{1}_{1}a\pm 2{}^{1}_{1}d+{}^{1}_{1}bk\}({}_{1}S)]({}_{1}A\ell)$$
$$+ 4\mu\ell[\{{}^{1}{}^{1}_{2}a+{}^{1}{}^{1}_{2}d\pm 2{}^{1}{}^{1}_{2}bk\}({}_{2}C) + \{\pm{}^{1}{}^{1}_{2}c\pm{}^{1}{}^{1}_{2}+2{}^{1}{}^{1}_{2}dk\}({}_{2}S)]$$
$$+ 4\mu\ell[\{{}^{1}{}^{1}_{2}a+{}^{1}{}^{1}_{2}d\pm 2{}^{1}{}^{1}_{2}bk\}({}_{2}C) + \{\pm{}^{1}{}^{1}_{2}c\pm{}^{1}{}^{1}_{2}b+2{}^{1}{}^{1}_{2}dk\}({}_{2}S)]$$
$$+ 4\mu\ell[\{{}^{1}{}^{1}_{2}a+{}^{1}{}^{1}_{2}d\pm 2{}^{1}{}^{1}_{2}bk\}({}_{2}C)$$
$$+ \{\pm{}^{1}{}^{1}_{2}c\pm{}^{1}{}^{1}_{2}b+2{}^{1}{}^{1}_{2}dk\}({}_{2}S)] \Big\} \qquad \cos(2\ell x)$$

$$+$$

$$+ \mu\ell[\{{}^{1}_{1}c+2{}^{1}_{1}b\pm{}^{1}_{1}dk\}({}_{1}C) + \{\pm{}^{1}_{1}a\pm 2{}^{1}_{1}d+{}^{1}_{1}bk\}({}_{1}S)]({}_{1}A\ell)$$
$$+ \mu\ell[\{{}^{1}_{1}c+2{}^{1}_{1}b\pm{}^{1}_{1}dk\}({}_{1}C) + \{\pm{}^{1}_{1}a\pm 2{}^{1}_{1}d+{}^{1}_{1}bk\}({}_{1}S)]({}_{1}A\ell)$$
$$- \mu\ell[\{{}^{1}_{1}c+2{}^{1}_{1}b\pm{}^{1}_{1}dk\}({}_{1}C) + \{\pm{}^{1}_{1}a\pm 2{}^{1}_{1}d+{}^{1}_{1}bk\}({}_{1}S)]({}_{1}A\ell)$$
$$- \mu\ell[\{{}^{1}_{1}c+2{}^{1}_{1}b\pm{}^{1}_{1}dk\}({}_{1}C) + \{\pm{}^{1}_{1}a\pm 2{}^{1}_{1}d+{}^{1}_{1}bk\}({}_{1}S)]({}_{1}A\ell) \qquad (9e)$$

in which

$_j\underline{C} = \cosh(j\underline{k})$ and $_j\underline{S} = \sinh(j\underline{k})$

$\underline{j}$ is the waveform number ($\underline{j}$ = 1 or 2)

$\underline{k}$ is the dimensionless wavenumber, $k = \ell(h/2)$

ℓ is the wavenumber, $\ell = 2\pi/L$

$\underline{L}$ is the wavelength of the first component waveform

$\underline{h}$ is the vertical thickness of a layer.

The "±" sign refers to the top (+) and bottom (-) of a layer. Equations (10) are analogous to eqs. (10) in Appendix A.

The complete expressions for the velocities and stresses are found by summing the individual expressions for the mean and perturbed components, eqs. (2) and (10), respectively.

On each arbitrary constant in eq. (10), the leading subscript identifies the waveform with which the constant is associated; the leading superscript indicates the product of maximum slopes that enters the expression for that constant. For example, ${}^{2}_{2}\underline{a}$ is a constant for the second cosinusoidal waveform (subscript "2") that is to 1st order in the maximum slope of the second sinusoidal waveform (superscript "**2**"). The constant ${}^{1\mathbf{1}}_{\mathbf{2}}\underline{a}$ is associated with the second sinusoidal waveform (subscript "**2**") and is to 2nd order in the slopes of the cosinusoidal and sinusoidal first waveforms (superscript "1**1**").

Expressions for the individual constants which arise here in the analysis of combined layer-parallel shortening and shearing are identical to those for individual constants with the same notation derived in the analysis of layer-parallel shortening alone, Appendix A.

In Appendix A, I outlined a method for reducing the number of constants by about half: I apply the stress boundary conditions to transform layer constants, $\underline{a}$, $\underline{b}$, $\underline{c}$, $\underline{d}$, into interface constants σ and τ. I apply the same method in this derivation, maintaining 2nd order accuracy.

The 2nd order expressions for the interface stresses, σ_{nn} and σ_{ns}, in terms of the layer constants are:

$$(\sigma_{nn})_{t,b} = \bar{\sigma}_{zz} + 2\mu\bar{D}_{xx}({}_{1}A_{t,b}\ell)^2 + 2\mu\bar{D}_{xx}({}_{\mathbf{1}}A_{t,b}\ell)^2$$

$$- \bar{p}_o - \bar{\mathbf{p}}_o \pm \rho g(h/2)$$

$$- \mu\ell[\{{}^{1}_{1}a+{}^{1}_{1}d\pm{}^{1}_{1}bk\}({}_{1}C) + \{\pm{}^{1}_{1}c\pm{}^{1}_{1}b+{}^{1}_{1}dk\}({}_{1}S)]({}_{1}A_{t,b}\ell)$$

$$- \mu\ell[\{{}^{\mathbf{1}}_{1}a+{}^{\mathbf{1}}_{1}d\pm{}^{\mathbf{1}}_{1}bk\}({}_{1}C) + \{\pm{}^{\mathbf{1}}_{1}c\pm{}^{\mathbf{1}}_{1}b+{}^{\mathbf{1}}_{1}dk\}({}_{1}S)]({}_{1}A_{t,b}\ell)$$

$$- \mu\ell[\{{}^{\mathbf{1}}_{\mathbf{1}}a+{}^{\mathbf{1}}_{\mathbf{1}}d\pm{}^{\mathbf{1}}_{\mathbf{1}}bk\}({}_{1}C) + \{\pm{}^{\mathbf{1}}_{\mathbf{1}}c\pm{}^{\mathbf{1}}_{\mathbf{1}}b+{}^{\mathbf{1}}_{\mathbf{1}}dk\}({}_{1}S)]({}_{\mathbf{1}}A_{t,b}\ell)$$

$$- \mu\ell[\{{}^{1}_{\mathbf{1}}a+{}^{1}_{\mathbf{1}}d\pm{}^{1}_{\mathbf{1}}bk\}({}_{1}C) + \{\pm{}^{1}_{\mathbf{1}}c\pm{}^{1}_{\mathbf{1}}b+{}^{1}_{\mathbf{1}}dk\}({}_{1}S)]({}_{\mathbf{1}}A_{t,b}\ell)$$

$$+$$

$$\Big\{ -2\bar{\sigma}_{xz}({}_{\mathbf{1}}A_{t,b}\ell) + \rho g({}_{1}A_{t,b})$$

$$+ 2\mu\ell[\{{}^{1}_{1}c\pm{}^{1}_{1}dk\}({}_{1}C) + \{\pm{}^{1}_{1}a+{}^{1}_{1}bk\}({}_{1}S)]$$

$$+ 2\mu\ell[\{{}^{\mathbf{1}}_{1}c\pm{}^{\mathbf{1}}_{1}dk\}({}_{1}C) + \{\pm{}^{\mathbf{1}}_{1}a+{}^{\mathbf{1}}_{1}bk\}({}_{1}S)] \Big\} \qquad \cos(\ell x)$$

$$+$$

$$\Big\{ 2\bar{\sigma}_{xz}({}_{1}A_{t,b}\ell) + \rho g({}_{\mathbf{1}}A_{t,b})$$

$$+ 2\mu\ell[\{{}^{\mathbf{1}}_{\mathbf{1}}c\pm{}^{\mathbf{1}}_{\mathbf{1}}dk\}({}_{1}C) + \{\pm{}^{\mathbf{1}}_{\mathbf{1}}a+{}^{\mathbf{1}}_{\mathbf{1}}bk\}({}_{1}S)]$$

$$+ 2\mu\ell[\{{}^{1}_{\mathbf{1}}c\pm{}^{1}_{\mathbf{1}}dk\}({}_{1}C) + \{\pm{}^{1}_{\mathbf{1}}a+{}^{1}_{\mathbf{1}}bk\}({}_{1}S)] \Big\} \qquad \sin(\ell x)$$

$$+$$

$$\Big\{ - 4\bar{\sigma}_{xz}({}_{\mathbf{2}}A_{t,b}\ell) + \rho g({}_{2}A_{t,b})$$

$$-2\mu\bar{D}_{xx}({}_{1}A_{t,b}\ell)^2 + 2\mu\bar{D}_{xx}({}_{\mathbf{1}}A_{t,b}\ell)^2$$

$$+ 4\mu\ell[\{{}^{2}_{2}c\pm 2{}^{2}_{2}dk\}({}_{2}C) + \{\pm{}^{2}_{2}a+2{}^{2}_{2}bk\}({}_{2}S)]$$

$$+ 4\mu\ell[\{{}^{\mathbf{2}}_{2}c\pm 2{}^{\mathbf{2}}_{2}dk\}({}_{2}C) + \{\pm{}^{\mathbf{2}}_{2}a+2{}^{\mathbf{2}}_{2}bk\}({}_{2}S)]$$

$$+ 3\mu\ell[\{{}^{1}_{1}a+{}^{1}_{1}d\pm{}^{1}_{1}bk\}({}_{1}C) + (\pm{}^{1}_{1}c\pm{}^{1}_{1}b+{}^{1}_{1}dk\}({}_{1}S)]({}_{1}A_{t,b}\ell)$$

$$+ 3\mu\ell[\{{}^{\mathbf{1}}_{1}a+{}^{\mathbf{1}}_{1}d\pm{}^{\mathbf{1}}_{1}bk\}({}_{1}C) + (\pm{}^{\mathbf{1}}_{1}c\pm{}^{\mathbf{1}}_{1}b+{}^{\mathbf{1}}_{1}dk\}({}_{1}S)]({}_{1}A_{t,b}\ell)$$

$$- 3\mu\ell[\{{}^{\mathbf{1}}_{\mathbf{1}}a+{}^{\mathbf{1}}_{\mathbf{1}}d\pm{}^{\mathbf{1}}_{\mathbf{1}}bk\}({}_{1}C) + (\pm{}^{\mathbf{1}}_{\mathbf{1}}c\pm{}^{\mathbf{1}}_{\mathbf{1}}b+{}^{\mathbf{1}}_{\mathbf{1}}dk\}({}_{1}S)]({}_{\mathbf{1}}A_{t,b}\ell)$$

$$- 3\mu\ell[\{{}^{1}_{\mathbf{1}}a+{}^{1}_{\mathbf{1}}d\pm{}^{1}_{\mathbf{1}}bk\}({}_{1}C) + (\pm{}^{1}_{\mathbf{1}}c\pm{}^{1}_{\mathbf{1}}b+{}^{1}_{\mathbf{1}}dk\}({}_{1}S)]({}_{\mathbf{1}}A_{t,b}\ell)$$

$$+ 4\mu\ell[\{{}^{1}{}^{1}_{2}c\pm 2{}^{1}{}^{1}_{2}dk\}({}_{2}C) + \{\pm{}^{1}{}^{1}_{2}a+2{}^{1}{}^{1}_{2}bk\}({}_{2}S)]$$

$$+ 4\mu\ell[\{{}^{1}{}^{\mathbf{1}}_{2}c\pm 2{}^{1}{}^{\mathbf{1}}_{2}dk\}({}_{2}C) + \{\pm{}^{1}{}^{\mathbf{1}}_{2}a+2{}^{1}{}^{\mathbf{1}}_{2}bk\}({}_{2}S)]$$

$$+\ 4\mu\ell[\{{}^{11}_{\ 2}c \pm 2\,{}^{11}_{\ 2}dk\}({}_2C)\ +\ \{\pm\,{}^{11}_{\ 2}a + 2\,{}^{11}_{\ 2}bk\}({}_2S)]\ \Big\} \qquad \cos(2\ell x)$$

$+$

$$\Big\{\ +\ 4\bar{\sigma}_{xz}({}_2A_{t,b}\ell)\ +\ \rho g({}_2A_{t,b})\ -4\mu\bar{D}_{xx}({}_1A_{t,b}\ell)({}_1A_{t,b}\ell)$$

$$+\ 4\mu\ell[\{{}^{2}_{2}c \pm 2\,{}^{2}_{2}dk\}({}_2C)\ +\ \{\pm\,{}^{2}_{2}a + 2\,{}^{2}_{2}bk\}({}_2S)]$$

$$+\ 4\mu\ell[\{{}^{2}_{2}c \pm 2\,{}^{2}_{2}dk\}({}_2C)\ +\ \{\pm\,{}^{2}_{2}a + 2\,{}^{2}_{2}bk\}({}_2S)]$$

$$+\ 3\mu\ell[\{{}^{1}_{1}a + {}^{1}_{1}d \pm {}^{1}_{1}bk\}({}_1C)\ +\ (\pm\,{}^{1}_{1}c \pm {}^{1}_{1}b + {}^{1}_{1}dk\}({}_1S)]({}_1A_{t,b}\ell)$$

$$+\ 3\mu\ell[\{{}^{1}_{1}a + {}^{1}_{1}d \pm {}^{1}_{1}bk\}({}_1C)\ +\ (\pm\,{}^{1}_{1}c \pm {}^{1}_{1}b + {}^{1}_{1}dk\}({}_1S)]({}_1A_{t,b}\ell)$$

$$+\ 3\mu\ell[\{{}^{1}_{1}a + {}^{1}_{1}d \pm {}^{1}_{1}bk\}({}_1C)\ +\ (\pm\,{}^{1}_{1}c \pm {}^{1}_{1}b + {}^{1}_{1}dk\}({}_1S)]({}_1A_{t,b}\ell)$$

$$+\ 3\mu\ell[\{{}^{1}_{1}a + {}^{1}_{1}d \pm {}^{1}_{1}bk\}({}_1C)\ +\ (\pm\,{}^{1}_{1}c \pm {}^{1}_{1}b + {}^{1}_{1}dk\}({}_1S)]({}_1A_{t,b}\ell)$$

$$+\ 4\mu\ell[\{{}^{11}_{\ 2}c \pm 2\,{}^{11}_{\ 2}dk\}({}_2C)\ +\ \{\pm\,{}^{11}_{\ 2}a + 2\,{}^{11}_{\ 2}bk\}({}_2S)]$$

$$+\ 4\mu\ell[\{{}^{11}_{\ 2}c \pm 2\,{}^{11}_{\ 2}dk\}({}_2C)\ +\ \{\pm\,{}^{11}_{\ 2}a + 2\,{}^{11}_{\ 2}bk\}({}_2S)]$$

$$+\ 4\mu\ell[\{{}^{11}_{\ 2}c \pm 2\,{}^{11}_{\ 2}dk\}({}_2C)\ +\ \{\pm\,{}^{11}_{\ 2}a + 2\,{}^{11}{}_{2}bk\}({}_2S)]\ \Big\} \qquad \sin(2\ell x)$$

(11a)

$$(\sigma_{ne})_{t,b}\ =\ \bar{\sigma}_{xz}[1\ -\ ({}_1A_{t,b}\ell)^2\ -\ ({}_1A_{t,b}\ell)^2]$$

$$+\ \mu\ell[\{{}^{1}_{1}c \pm {}^{1}_{1}dk\}({}_1C)\ +\ \{\pm\,{}^{1}_{1}a + {}^{1}_{1}bk\}({}_1S)]({}_1A_{t,b}\ell)$$

$$+\ \mu\ell[\{{}^{1}_{1}c \pm {}^{1}_{1}dk\}({}_1C)\ +\ \{\pm\,{}^{1}_{1}a + {}^{1}_{1}bk\}({}_1S)]({}_1A_{t,b}\ell)$$

$$-\ \mu\ell[\{{}^{1}_{1}c \pm {}^{1}_{1}dk\}({}_1C)\ +\ \{\pm\,{}^{1}_{1}a + {}^{1}_{1}bk\}({}_1S)]({}_1A_{t,b}\ell)$$

$$-\ \mu\ell[\{{}^{1}_{1}c \pm {}^{1}_{1}dk\}({}_1C)\ +\ \{\pm\,{}^{1}_{1}a + {}^{1}_{1}bk\}({}_1S)]({}_1A_{t,b}\ell)$$

$+$

$$\Big\{\ 4\mu\bar{D}_{xx}({}_1A_{t,b}\ell)$$

$$-\ 2\mu\ell[\{{}^{1}_{1}a + {}^{1}_{1}d \pm {}^{1}_{1}bk\}({}_1C)\ +\ \{\pm\,{}^{1}_{1}c \pm {}^{1}_{1}b + {}^{1}_{1}dk\}({}_1S)]$$

$$-\ 2\mu\ell[\{{}^{1}_{1}a + {}^{1}_{1}d \pm {}^{1}_{1}bk\}({}_1C)\ +\ \{\pm\,{}^{1}_{1}c \pm {}^{1}_{1}b + {}^{1}_{1}dk\}({}_1S)]\ \Big\} \qquad \sin(\ell x)$$

$$+$$

$$\Big\{ -4\mu\bar{D}_{xx}({}_{1}A_{t,b}\ell)$$

$$+\ 2\mu\ell[\{{}^{1}_{1}a+{}^{1}_{1}d\pm{}^{1}_{1}bk\}({}_{1}C)\ +\ \{\pm{}^{1}_{1}c\pm{}^{1}_{1}b+{}^{1}_{1}dk\}({}_{1}S)]$$

$$+\ 2\mu\ell[\{{}^{1}_{1}a+{}^{1}_{1}d\pm{}^{1}_{1}bk\}({}_{1}C)\ +\ \{\pm{}^{1}_{1}c\pm{}^{1}_{1}b+{}^{1}_{1}dk\}({}_{1}S)]\ \Big\} \qquad \cos(\ell x)$$

$$+$$

$$\Big\{ 4\mu\bar{D}_{xx}({}_{2}A_{t,b}2\ell)\ +\ 2\bar{\sigma}_{xz}({}_{1}A_{t,b}\ell)({}_{1}A_{t,b}\ell)$$

$$-\ 4\mu\ell[\{{}^{2}_{2}a+{}^{2}_{2}d\pm2{}^{2}_{2}bk\}({}_{2}C)\ +\ \{\pm{}^{2}_{2}c\pm{}^{2}_{2}b+2{}^{2}_{2}dk\}({}_{2}S)]$$

$$-\ 4\mu\ell[\{{}^{2}_{2}a+{}^{2}_{2}d\pm2{}^{2}_{2}bk\}({}_{2}C)\ +\ \{\pm{}^{2}_{2}c\pm{}^{2}_{2}b+2{}^{2}_{2}dk\}({}_{2}S)]$$

$$-\ \mu\ell[\{3{}^{1}_{1}c+4{}^{1}_{1}b\pm3{}^{1}_{1}dk\}({}_{1}C)$$
$$+\ \{\pm3{}^{1}_{1}a\pm4{}^{1}_{1}d+3{}^{1}_{1}bk\}({}_{1}S)]({}_{1}A_{t,b}\ell)$$

$$-\ \mu\ell[\{3{}^{1}_{1}c+4{}^{1}_{1}b\pm3{}^{1}_{1}dk\}({}_{1}C)$$
$$+\ \{\pm3{}^{1}_{1}a\pm4{}^{1}_{1}d+3{}^{1}_{1}bk\}({}_{1}S)]({}_{1}A_{t,b}\ell)$$

$$+\ \mu\ell[\{3{}^{1}_{1}c+4{}^{1}_{1}b\pm3{}^{1}_{1}dk\}({}_{1}C)$$
$$+\ \{\pm3{}^{1}_{1}a\pm4{}^{1}_{1}d+3{}^{1}_{1}bk\}({}_{1}S)]({}_{1}A_{t,b}\ell)$$

$$+\ \mu\ell[\{3{}^{1}_{1}c+4{}^{1}_{1}b\pm3{}^{1}_{1}dk\}({}_{1}C)$$
$$+\ \{\pm3{}^{1}_{1}a\pm4{}^{1}_{1}d+3{}^{1}_{1}bk\}({}_{1}S)]({}_{1}A_{t,b}\ell)$$

$$-\ 4\mu\ell[\{{}^{1}{}^{1}_{2}a+{}^{1}{}^{1}_{2}d\pm2{}^{1}{}^{1}_{2}bk\}({}_{2}C)\ +\ \{\pm{}^{1}{}^{1}_{2}c\pm{}^{1}{}^{1}_{2}b+2{}^{1}{}^{1}_{2}dk\}({}_{2}S)]$$

$$-\ 4\mu\ell[\{{}^{1}{}^{1}_{2}a+{}^{1}{}^{1}_{2}d\pm2{}^{1}{}^{1}_{2}bk\}({}_{2}C)\ +\ \{\pm{}^{1}{}^{1}_{2}c\pm{}^{1}{}^{1}_{2}b+2{}^{1}{}^{1}_{2}dk\}({}_{2}S)]$$

$$-\ 4\mu\ell[\{{}^{1}{}^{1}_{2}a+{}^{1}{}^{1}_{2}d\pm2{}^{1}{}^{1}_{2}bk\}({}_{2}C)$$
$$+\ \{\pm{}^{1}{}^{1}_{2}c\pm{}^{1}{}^{1}_{2}b+2{}^{1}{}^{1}_{2}dk\}({}_{2}S)]\ \Big\} \qquad \sin(2\ell x)$$

$$+$$

$$\Big\{ -4\mu\bar{D}_{xx}({}_{2}A_{t,b}2\ell)\ +\ \bar{\sigma}_{xz}[({}_{1}A_{t,b}\ell)^{2}\ -\ ({}_{1}A_{t,b}\ell)^{2}]$$

$$+\ 4\mu\ell[\{{}^{2}_{2}a+{}^{2}_{2}d\pm2{}^{2}_{2}bk\}({}_{2}C)\ +\ \{\pm{}^{2}_{2}c\pm{}^{2}_{2}b+2{}^{2}_{2}dk\}({}_{2}S)]$$

$$+\ 4\mu\ell[\{{}^{2}_{2}a+{}^{2}_{2}d\pm2{}^{2}_{2}bk\}({}_{2}C)\ +\ \{\pm{}^{2}_{2}c\pm{}^{2}_{2}b+2{}^{2}_{2}dk\}({}_{2}S)]$$

$$+\ \mu\ell[\{3{}^{1}_{1}c+4{}^{1}_{1}b\pm3{}^{1}_{1}dk\}({}_{1}C)$$
$$+\ \{\pm3{}^{1}_{1}a\pm4{}^{1}_{1}d+3{}^{1}_{1}bk\}({}_{1}S)]({}_{1}A_{t,b}\ell)$$

$$+\ \mu\ell[\{3{}^{1}_{1}c+4{}^{1}_{1}b\pm3{}^{1}_{1}dk\}({}_{1}C)$$
$$+\ \{\pm3{}^{1}_{1}a\pm4{}^{1}_{1}d+3{}^{1}_{1}bk\}({}_{1}S)]({}_{1}A_{t,b}\ell)$$

$$+\ \mu\ell[\{3{}^{1}_{1}c+4{}^{1}_{1}b\pm3{}^{1}_{1}dk\}({}_{1}C)$$
$$+\ \{\pm3{}^{1}_{1}a\pm4{}^{1}_{1}d+3{}^{1}_{1}bk\}({}_{1}S)]({}_{1}A_{t,b}\ell)$$

$$
\begin{aligned}
&+ \mu\ell\Big[\{3\,{}^{1}_{1}c + 4\,{}^{1}_{1}b \pm 3\,{}^{1}_{1}dk\}({}_{1}C) \\
&\qquad\qquad + \{\pm 3\,{}^{1}_{1}a \pm 4\,{}^{1}_{1}d + 3\,{}^{1}_{1}bk\}({}_{1}S)\Big]({}_{1}A_{t,b}\ell) \\
&+ 4\mu\ell\Big[\{{}^{1}_{2}a + {}^{1}_{2}d \pm 2\,{}^{1}_{2}bk\}({}_{2}C) + \{\pm {}^{1}_{2}c \pm {}^{1}_{2}b + 2\,{}^{1}_{2}dk\}({}_{2}S)\Big] \\
&+ 4\mu\ell\Big[\{{}^{1}_{2}a + {}^{1}_{2}d \pm 2\,{}^{1}_{2}bk\}({}_{2}C) + \{\pm {}^{1}_{2}c \pm {}^{1}_{2}b + 2\,{}^{1}_{2}dk\}({}_{2}S)\Big] \\
&+ 4\mu\ell\Big[\{{}^{1}_{2}a + {}^{1}_{2}d \pm 2\,{}^{1}_{2}bk\}({}_{2}C) \\
&\qquad\qquad + \{\pm {}^{1}_{2}c \pm {}^{1}_{2}b + 2\,{}^{1}_{2}dk\}({}_{2}S)\Big]\ \Big\} \qquad \cos(2\ell x)
\end{aligned}
\tag{11b}
$$

Equations (11) are analogous to eqs. (12) in Appendix A.

The 2nd order expressions for the interface stresses in terms of the interface constants, σ and τ, are:

$$
\begin{aligned}
(\sigma_{nn})_{t,b} = \sigma_o &+ ({}^{1}_{1}\sigma_{t,b}+{}^{1}_{1}\sigma_{t,b}) \cos(\ell x) \\
&+ ({}^{1}_{1}\sigma_{t,b}+{}^{1}_{1}\sigma_{t,b}) \sin(\ell x) \\
&+ ({}^{2}_{2}\sigma_{t,b}+{}^{2}_{2}\sigma_{t,b}+{}^{11}_{2}\sigma_{t,b}+{}^{11}_{2}\sigma_{t,b}+{}^{11}_{2}\sigma_{t,b}) \cos(2\ell x) \\
&+ ({}^{2}_{2}\sigma_{t,b}+{}^{2}_{2}\sigma_{t,b}+{}^{11}_{2}\sigma_{t,b}+{}^{1}_{2}\sigma_{t,b}+{}^{11}_{2}\sigma_{t,b}) \sin(2\ell x)
\end{aligned}
\tag{12a}
$$

$$
\begin{aligned}
(\sigma_{ns})_{t,b} = \tau_o &+ ({}^{1}_{1}\tau_{t,b}+{}^{1}_{1}\tau_{t,b}) \sin(\ell x) \\
&+ ({}^{1}_{1}\tau_{t,b}+{}^{1}_{1}\tau_{t,b}) \cos(\ell x) \\
&+ ({}^{2}_{2}\tau_{t,b}+{}^{2}_{2}\tau_{t,b}+{}^{11}_{2}\tau_{t,b}+{}^{11}_{2}\tau_{t,b}+{}^{11}_{2}\tau_{t,b}) \sin(2\ell x) \\
&+ ({}^{2}_{2}\tau_{t,b}+{}^{2}_{2}\tau_{t,b}+{}^{11}_{2}\tau_{t,b}+{}^{11}_{2}\tau_{t,b}+{}^{11}_{2}\tau_{t,b}) \cos(2\ell x)
\end{aligned}
\tag{12b}
$$

Equations (12) are analogous to eqs. (13) in Appendix A.

Equating the two expressions, eqs. (11a) and (12a), for the interface normal stress, σ_{nn}, provides an expression for the interface constant σ in terms of the layer constants, a, b, c, and d. Similarly, equating the two expressions, eqs. (11b) and (12b), for the interface shear stress, σ_{ns}, provides an expression for the interface constant, τ, in terms of the layer constants, a, b, c, and d (e.g., eq. 14 in Appendix A). A pair of equations, one for σ and one for

τ, can be written for each combination of waveform and amplitude dependency. By solving the pairs of σ and τ equations simultaneously, we derive expressions for the layer constants in terms of the interface constants (eq. 15 in Appendix A). In deriving these latter equations, we introduce new constants, lambda, which contain the interface constants and the interaction terms responsible for generating that particular waveform-order combination.

The constants, lambda, for a 2nd order analysis of layer-parallel shearing and shortening deformation are:

$$ {}^{1}_{1}\Lambda_{p,m}[2({}_{1}S_{1}C \pm k)] = ({}^{1}_{1}\sigma_{t} \pm {}^{1}_{1}\sigma_{b})/2\mu\ell \tag{13a} $$

$$ {}^{1}_{1}\lambda_{p,m}[2({}_{1}S_{1}C \mp k)] = ({}^{1}_{1}\tau_{t} \pm {}^{1}_{1}\tau_{b})/2\mu\ell - 2({}_{1}A_{t} \pm {}_{1}A_{b}) \tag{13b} $$

$$ {}^{1}_{1}\Lambda_{p,m}[2({}_{1}S_{1}C \pm k)] = ({}^{1}_{1}\sigma_{t} \pm {}^{1}_{1}\sigma_{b})/2\mu\ell + (\bar{\sigma}_{xz}/\mu)({}_{1}A_{t} \pm {}_{1}A_{b}) \tag{13c} $$

$$ {}^{1}_{1}\lambda_{p,m}[2({}_{1}S_{1}C \mp k)] = ({}^{1}_{1}\tau_{t} \pm {}^{1}_{1}\tau_{b})/2\mu\ell \tag{13d} $$

$$ {}^{1}_{1}\Lambda_{p,m}[2({}_{1}S_{1}C \pm k)] = ({}^{1}_{1}\sigma_{t} \pm {}^{1}_{1}\sigma_{b})/2\mu\ell \tag{13e} $$

$$ -{}^{1}_{1}\lambda_{p,m}[2({}_{1}S_{1}C \mp k)] = ({}^{1}_{1}\tau_{t} \pm {}^{1}_{1}\tau_{b})/2\mu\ell + 2({}_{1}A_{t} \pm {}_{1}A_{b}) \tag{13f} $$

$$ {}^{1}_{1}\Lambda_{p,m}[2({}_{1}S_{1}C \pm k)] = ({}^{1}_{1}\sigma_{t} \pm {}^{1}_{1}\sigma_{b})/2\mu\ell - (\bar{\sigma}_{xz}/\mu)({}_{1}A_{t} \pm {}_{1}A_{b}) \tag{13g} $$

$$ -{}^{1}_{1}\lambda_{p,m}[2({}_{1}S_{1}C \mp k)] = ({}^{1}_{1}\tau_{t} \pm {}^{1}_{1}\tau_{b})/2\mu\ell \tag{13h} $$

$$ {}^{2}_{2}\Lambda_{p,m}[2({}_{2}S_{2}C \pm 2k)] = ({}^{2}_{2}\sigma_{t} \pm {}^{2}_{2}\sigma_{b})/4\mu\ell \tag{13i} $$

$$ {}^{2}_{2}\lambda_{p,m}[2({}_{2}S_{2}C \mp 2k)] = ({}^{2}_{2}\tau_{t} \pm {}^{2}_{2}\tau_{b})/4\mu\ell - 2({}_{2}A_{t} \pm {}_{2}A_{b}) \tag{13j} $$

$$ {}^{2}_{2}\Lambda_{p,m}[2({}_{2}S_{2}C \pm 2k)] = ({}^{2}_{2}\sigma_{t} \pm {}^{2}_{2}\sigma_{b})/4\mu\ell + (\bar{\sigma}_{xz}/\mu)({}_{2}A_{t} \pm {}_{2}A_{b}) \tag{13k} $$

$$ {}^{2}_{2}\lambda_{p,m}[2({}_{2}S_{2}C \mp 2k)] = ({}^{2}_{2}\tau_{t} \pm {}^{2}_{2}\tau_{b})/4\mu\ell \tag{13ℓ} $$

$$ {}^{2}_{2}\Lambda_{p,m}[2({}_{2}S_{2}C \pm 2k)] = ({}^{2}_{2}\sigma_{t} \pm {}^{2}_{2}\sigma_{t})/4\mu\ell \tag{13m} $$

$$ -{}^{2}_{2}\lambda_{p,m}[2({}_{2}S_{2}C \mp 2k)] = ({}^{2}_{2}\tau_{t} \pm {}^{2}_{2}\tau_{b})/4\mu\ell + 2({}_{2}A_{t} \pm {}_{2}A_{b}) \tag{13n} $$

$$ {}^{2}_{2}\Lambda_{p,m}[2({}_{2}S_{2}C \pm 2k)] = ({}^{2}_{2}\sigma_{t} \pm {}^{2}_{2}\sigma_{b})/4\mu\ell $$

$$ - (\bar{\sigma}_{xz}/\mu)({}_{2}A_{t} \pm {}_{2}A_{b}) \qquad (13o) $$

$$ -{}^{2}_{2}\lambda_{p,m}[2({}_{2}S_{2}C \mp 2k)] = ({}^{2}_{2}\tau_{t} \pm {}^{2}_{2}\tau_{b})/4\mu\ell \qquad (13p) $$

$$ {}^{1}{}^{1}_{2}\Lambda_{p,m}[2({}_{2}S_{2}C \pm 2k)] = ({}^{1}{}^{1}_{2}\sigma_{t} \pm {}^{1}{}^{1}_{2}\sigma_{b})/4\mu\ell $$

$$ + (\ell/2)[({}_{1}A_{t})^{2} \pm ({}_{1}A_{b})^{2}] $$

$$ + (3\ell/4)[({}_{1}A_{t} \pm {}_{1}A_{b})({}^{1}_{1}\lambda_{p})({}_{1}S_{1}C-k) $$

$$ + ({}_{1}A_{t} \mp {}_{1}A_{b})({}^{1}_{1}\lambda_{m})({}_{1}S_{1}C+k)] \qquad (13q) $$

$$ {}^{1}{}^{1}_{2}\lambda_{p,m}[2({}_{2}S_{2}C \mp 2k)] = ({}^{1}{}^{1}_{2}\tau_{t} \pm {}^{1}{}^{1}_{2}\tau_{b})/4\mu\ell $$

$$ - (\ell/4)({}_{1}A_{t} \pm {}_{1}A_{b})[{}^{1}_{1}\Lambda_{p}({}_{1}S_{1}C-3k)+4{}^{1}_{1}\lambda_{m}({}_{1}C^{2})] $$

$$ - (\ell/4)({}_{1}A_{t} \mp {}_{1}A_{b})[{}^{1}_{1}\Lambda_{m}({}_{1}S_{1}C+3k)+4{}^{1}_{1}\lambda_{p}({}_{1}S^{2})] \qquad (13r) $$

$$ {}^{1}{}^{1}_{2}\Lambda_{p,m}[2({}_{2}S_{2}C \pm 2k)] = ({}^{1}{}^{1}_{2}\sigma_{t} \pm {}^{1}{}^{1}_{2}\sigma_{b})/4\mu\ell $$

$$ - (\ell/2)[({}_{1}A_{t})^{2} \pm ({}_{1}A_{b})^{2}] $$

$$ - (3\ell/4)[({}_{1}A_{t} \pm {}_{1}A_{b})({}^{1}_{1}\lambda_{p})({}_{1}S_{1}C-k) $$

$$ + ({}_{1}A_{t} \mp {}_{1}A_{b})({}^{1}_{1}\lambda_{m})({}_{1}S_{1}C+k)] \qquad (13s) $$

$$ {}^{1}{}^{1}_{2}\lambda_{p,m}[2({}_{2}S_{2}C \mp 2k)] = ({}^{1}{}^{1}_{2}\tau_{t} \pm {}^{1}{}^{1}_{2}\tau_{b})/4\mu\ell $$

$$ + (\ell/4)({}_{1}A_{t} \pm {}_{1}A_{b})[{}^{1}_{1}\Lambda_{p}({}_{1}S_{1}C-3k)+4{}^{1}_{1}\lambda_{m}({}_{1}C^{2})] $$

$$ + (\ell/4)({}_{1}A_{t} \mp {}_{1}A_{b})[{}^{1}_{1}\Lambda_{m}({}_{1}S_{1}C+3k)+4{}^{1}_{1}\lambda_{p}({}_{1}S^{2})] \qquad (13t) $$

$$ {}^{1}{}^{1}_{2}\Lambda_{p,m}[2({}_{2}S_{2}C \pm 2k)] = ({}^{1}{}^{1}_{2}\sigma_{t} \pm {}^{1}{}^{1}_{2}\sigma_{b})/4\mu\ell $$

$$ + (3\ell/4)[({}_{1}A_{t} \pm {}_{1}A_{b})({}^{1}_{1}\lambda_{p})({}_{1}S_{1}C-k) $$

$$ + ({}_{1}A_{t} \mp {}_{1}A_{b})({}^{1}_{1}\lambda_{m})({}_{1}S_{1}C+k)] $$

$$ - (3\ell/4)[({}_{1}A_{t} \pm {}_{1}A_{b})({}^{1}_{1}\lambda_{p})({}_{1}S_{1}C-k) $$

$$ + ({}_{1}A_{t} \mp {}_{1}A_{b})({}^{1}_{1}\lambda_{m})({}_{1}S_{1}C+k)] \qquad (13u) $$

$$
\begin{aligned}
{}^{1}_{2}\lambda_{p,m}[2({}_{2}S_{2}C \mp 2k)] = {}& ({}^{1}_{2}\tau_{t} \pm {}^{1}_{2}\tau_{b})/4\mu\ell \\
& - (\ell/2)(\bar{\sigma}_{xz}/\mu)[({}_{1}A_{t})({}_{1}A_{t}) \pm ({}_{1}A_{b})({}_{1}A_{b})] \\
& + (\ell/4)({}_{1}A_{t} \pm {}_{1}A_{b})[{}^{1}_{1}\Lambda_{p}({}_{1}S_{1}C-3k)+4{}^{1}_{1}\lambda_{m}({}_{1}C^{2})] \\
& + (\ell/4)({}_{1}A_{t} \mp {}_{1}A_{b})[{}^{1}_{1}\Lambda_{m}({}_{1}S_{1}C+3k)+4{}^{1}_{1}\lambda_{p}({}_{1}S^{2})] \\
& - (\ell/4)({}_{1}A_{t} \pm {}_{1}A_{b})[{}^{1}_{1}\Lambda_{p}({}_{1}S_{1}C-3k)+4{}^{1}_{1}\lambda_{m}({}_{1}C^{2})] \\
& - (\ell/4)({}_{1}A_{t} \mp {}_{1}A_{b})[{}^{1}_{1}\Lambda_{m}({}_{1}S_{1}C+3k)+4{}^{1}_{1}\lambda_{p}({}_{1}S^{2})] \qquad (13v)
\end{aligned}
$$

$$
\begin{aligned}
{}^{1}_{2}\Lambda_{p,m}[2({}_{2}S_{2}C \pm 2k)] = {}& ({}^{1}_{2}\sigma_{t} \pm {}^{1}_{2}\sigma_{b})/4\mu\ell \\
& + (3\ell/4)[({}_{1}A_{t} \pm {}_{1}A_{b})({}^{1}_{1}\lambda_{p})({}_{1}S_{1}C-k) \\
& \qquad + ({}_{1}A_{t} \mp {}_{1}A_{b})({}^{1}_{1}\lambda_{m})({}_{1}S_{1}C+k)] \qquad (13w)
\end{aligned}
$$

$$
\begin{aligned}
-{}^{1}_{2}\lambda_{p,m}[2({}_{2}S_{2}C \mp 2k)] = {}& ({}^{1}_{2}\tau_{t} \pm {}^{1}_{2}\tau_{b})/4\mu\ell \\
& - (\ell/4)(\bar{\sigma}_{xz}/\mu)[({}_{1}A_{t})^{2} \pm ({}_{1}A_{b})^{2}] \\
& + (\ell/4)({}_{1}A_{t} \pm {}_{1}A_{b})[{}^{1}_{1}\Lambda_{p}({}_{1}S_{1}C-3k)+4{}^{1}_{1}\lambda_{m}({}_{1}C^{2})] \\
& + (\ell/4)({}_{1}A_{t} \mp {}_{1}A_{b})[{}^{1}_{1}\Lambda_{m}({}_{1}S_{1}C+3k)+4{}^{1}_{1}\lambda_{p}({}_{1}S^{2})] \qquad (13x)
\end{aligned}
$$

$$
\begin{aligned}
{}^{1}_{2}\Lambda_{p,m}[2({}_{2}S_{2}C \pm 2k)] = {}& ({}^{1}_{2}\sigma_{t} \pm {}^{1}_{2}\sigma_{b})/4\mu\ell \\
& + (3\ell/4)[({}_{1}A_{t} \pm {}_{1}A_{b})({}^{1}_{1}\lambda_{p})({}_{1}S_{1}C-k) \\
& \qquad + ({}_{1}A_{t} \mp {}_{1}A_{b})({}^{1}_{1}\lambda_{m})({}_{1}S_{1}C+k)] \qquad (13y)
\end{aligned}
$$

$$
\begin{aligned}
-{}^{1}_{2}\lambda_{p,m}[2({}_{2}S_{2}C \mp 2k)] = {}& ({}^{1}_{2}\tau_{t} \pm {}^{1}_{2}\tau_{b})/4\mu\ell \\
& + (\ell/4)(\bar{\sigma}_{xz}/\mu)[({}_{1}A_{t})^{2} \pm ({}_{1}A_{b})^{2}] \\
& + (\ell/4)({}_{1}A_{t} \pm {}_{1}A_{b})[{}^{1}_{1}\Lambda_{p}({}_{1}S_{1}C-3k)+4{}^{1}_{1}\lambda_{m}({}_{1}C^{2})] \\
& + (\ell/4)({}_{1}A_{t} \mp {}_{1}A_{b})[{}^{1}_{1}\Lambda_{m}({}_{1}S_{1}C+3k)+4{}^{1}_{1}\lambda_{p}({}_{1}S^{2})] \qquad (13z)
\end{aligned}
$$

$$
\begin{aligned}
{}^{1}{}^{1}_{2}\Lambda_{p,m}[2({}_{2}S_{2}C \pm 2k)] = {} & ({}^{1}{}^{1}_{2}\sigma_{t} \pm {}^{1}{}^{1}_{2}\sigma_{b})/4\mu\ell \\
& + \ell[({}_{1}A_{t})({}_{1}A_{t}) \pm ({}_{1}A_{b})({}_{1}A_{b})] \\
& + (3\ell/4)[({}_{1}A_{t} \pm {}_{1}A_{b})({}^{1}_{1}\lambda_{p})({}_{1}S_{1}C-k) \\
& \qquad + ({}_{1}A_{t} \mp {}_{1}A_{b})({}^{1}_{1}\lambda_{m})({}_{1}S_{1}C+k)] \\
& + (3\ell/4)[({}_{1}A_{t} \pm {}_{1}A_{b})({}^{1}_{1}\lambda_{p})({}_{1}S_{1}C-k) \\
& \qquad + ({}_{1}A_{t} \mp {}_{1}A_{b})({}^{1}_{1}\lambda_{m})({}_{1}S_{1}C+k)]
\end{aligned}
\tag{13aa}
$$

$$
\begin{aligned}
-{}^{1}{}^{1}_{2}\lambda_{p,m}[2({}_{2}S_{2}C \mp 2k)] = {} & ({}^{1}{}^{1}_{2}\tau_{t} \pm {}^{1}{}^{1}_{2}\tau_{b})/4\mu\ell \\
& + (\ell/4)({}_{1}A_{t} \pm {}_{1}A_{b})[{}^{1}_{1}\Lambda_{p}({}_{1}S_{1}C-3k)+4{}^{1}_{1}\lambda_{m}({}_{1}C^{2})] \\
& + (\ell/4)({}_{1}A_{t} \mp {}_{1}A_{b})[{}^{1}_{1}\Lambda_{m}({}_{1}S_{1}C+3k)+4{}^{1}_{1}\lambda_{p}({}_{1}S^{2})] \\
& + (\ell/4)({}_{1}A_{t} \pm {}_{1}A_{b})[{}^{1}_{1}\Lambda_{p}({}_{1}S_{1}C-3k)+4{}^{1}_{1}\lambda_{m}({}_{1}C^{2})] \\
& + (\ell/4)({}_{1}A_{t} \mp {}_{1}A_{b})[{}^{1}_{1}\Lambda_{m}({}_{1}S_{1}C+3k)+4{}^{1}_{1}\lambda_{p}({}_{1}S^{2})]
\end{aligned}
\tag{13bb}
$$

The interface velocities can now be written in terms of the interface stress constants, σ and τ. According to the procedure outlined in Appendix A, we derive the following expressions for the interface velocities normal and tangential to the interface:

$$(v_n)_{t,b} = (\bar{v}_z)_{t,b}\cos(\theta_{t,b}) - (\bar{v}_x)_{t,b}\sin(\theta_{t,b})$$

$$+$$

$$\begin{aligned}
&+ \Big\{ ({}^{1}_{1}\Lambda_m + {}^{1}_{1}\Lambda_m)({}_{1}C^2) + ({}^{1}_{1}\lambda_p + {}^{1}_{1}\lambda_p)k \\
&\pm ({}^{1}_{1}\Lambda_p + {}^{1}_{1}\Lambda_p)({}_{1}S^2) \mp ({}^{1}_{1}\lambda_m + {}^{1}_{1}\lambda_m)k \Big\} \qquad \cos(\ell x)
\end{aligned}$$

$$+$$

$$\begin{aligned}
&+ \Big\{ ({}^{1}_{1}\Lambda_m + {}^{1}_{1}\Lambda_m)({}_{1}C^2) + ({}^{1}_{1}\lambda_p + {}^{1}_{1}\lambda_p)k \\
&\pm ({}^{1}_{1}\Lambda_p + {}^{1}_{1}\Lambda_p)({}_{1}S^2) \mp ({}^{1}_{1}\lambda_m + {}^{1}_{1}\lambda_m)k \Big\} \qquad \sin(\ell x)
\end{aligned}$$

$$+$$

$$\begin{aligned}
&+ \Big\{ ({}^{2}_{2}\Lambda_m + {}^{2}_{2}\Lambda_m + {}^{1\,1}_{\;\;2}\Lambda_m + {}^{1\,1}_{\;\;2}\Lambda_m + {}^{1\,1}_{\;\;2}\Lambda_m)({}_{2}C^2) \\
&+ ({}^{2}_{2}\lambda_p + {}^{2}_{2}\lambda_p + {}^{1\,1}_{\;\;2}\lambda_p + {}^{1\,1}_{\;\;2}\lambda_p + {}^{1\,1}_{\;\;2}\lambda_p)2k \\
&\pm ({}^{2}_{2}\Lambda_p + {}^{2}_{2}\Lambda_p + {}^{1\,1}_{\;\;2}\Lambda_p + {}^{1\,1}_{\;\;2}\Lambda_p + {}^{1\,1}_{\;\;2}\Lambda_p)({}_{2}S^2) \\
&\mp ({}^{2}_{2}\lambda_m + {}^{2}_{2}\lambda_m + {}^{1\,1}_{\;\;2}\lambda_m + {}^{1\,1}_{\;\;2}\lambda_m + {}^{1\,1}_{\;\;2}\lambda_m)2k \\
&+ ({}_{1}\bar{A}_{t,b}\bar{\ell})[{}^{1}_{1}\bar{\Lambda}_p k - {}^{1}_{1}\lambda_m({}_{1}\bar{C}^2) \mp {}^{1}_{1}\bar{\Lambda}_m k \mp {}^{1}_{1}\lambda_p({}_{1}\bar{S}^2)] \\
&+ ({}_{1}A_{t,b}\ell)[{}^{1}_{1}\Lambda_p k - {}^{1}_{1}\lambda_m({}_{1}C^2) \mp {}^{1}_{1}\Lambda_m k \mp {}^{1}_{1}\lambda_p({}_{1}S^2)] \\
&- ({}_{1}A_{t,b}\ell)[{}^{1}_{1}\Lambda_p k - {}^{1}_{1}\lambda_m({}_{1}C^2) \mp {}^{1}_{1}\Lambda_m k \mp {}^{1}_{1}\lambda_p({}_{1}S^2)] \\
&- ({}_{1}A_{t,b}\ell)[{}^{1}_{1}\Lambda_p k - {}^{1}_{1}\lambda_m({}_{1}C^2) \mp {}^{1}_{1}\Lambda_m k \mp {}^{1}_{1}\lambda_p({}_{1}S^2)] \Big\} \qquad \cos(2\ell x)
\end{aligned}$$

$$+$$

$$+ \Big\{ \ ({}^{2}_{2}\Lambda_m+{}^{2}_{2}\Lambda_m+{}^{1}{}^{1}_{2}\Lambda_m+{}^{1}{}^{1}_{2}\Lambda_m+{}^{1}{}^{1}_{2}\Lambda_m)({}_{2}C^2)$$

$$+ \ ({}^{2}_{2}\lambda_p+{}^{2}_{2}\lambda_p+{}^{1}{}^{1}_{2}\lambda_p+{}^{1}{}^{1}_{2}\lambda_p+{}^{1}{}^{1}_{2}\lambda_p)2k$$

$$\pm \ ({}^{2}_{2}\Lambda_p+{}^{2}_{2}\Lambda_p+{}^{1}{}^{1}_{2}\Lambda_p+{}^{1}{}^{1}_{2}\Lambda_p+{}^{1}{}^{1}_{2}\Lambda_p)({}_{2}S^2)$$

$$\mp \ ({}^{2}_{2}\lambda_m+{}^{2}_{2}\lambda_m+{}^{1}{}^{1}_{2}\lambda_m+{}^{1}{}^{1}_{2}\lambda_m+{}^{1}{}^{1}_{2}\lambda_m)2k$$

$$+ \ ({}_{1}A_{t,b}\ell)[{}^{1}_{1}\Lambda_p k-{}^{1}_{1}\lambda_m({}_{1}C^2)\mp{}^{1}_{1}\Lambda_m k\mp{}^{1}_{1}\lambda_p({}_{1}S^2)]$$

$$+ \ ({}_{1}A_{t,b}\ell)[{}^{1}_{1}\Lambda_p k-{}^{1}_{1}\lambda_m({}_{1}C^2)\mp{}^{1}_{1}\Lambda_m k\mp{}^{1}_{1}\lambda_p({}_{1}S^2)]$$

$$+ \ ({}_{1}A_{t,b}\ell)[{}^{1}_{1}\Lambda_p k-{}^{1}_{1}\lambda_m({}_{1}C^2)\mp{}^{1}_{1}\Lambda_m k\mp{}^{1}_{1}\lambda_p({}_{1}S^2)]$$

$$+ \ ({}_{1}A_{t,b}\ell)[{}^{1}_{1}\Lambda_p k-{}^{1}_{1}\lambda_m({}_{1}C^2)\mp{}^{1}_{1}\Lambda_m k\mp{}^{1}_{1}\lambda_p({}_{1}S^2)] \ \Big\} \qquad \sin(2\ell x)$$

(14a)

$$(v_s)_{t,b} = (\bar{v}_z)_{t,b}\ \sin(\theta_{t,b}) + (\bar{v}_x)_{t,b}\cos\ (\theta_{t,b})$$

$$- \ ({}_{1}A_{t,b}\ell)[({}^{1}_{1}\Lambda_m+{}^{1}_{1}\Lambda_m)({}_{1}C^2) \ + \ ({}^{1}_{1}\lambda_p+{}^{1}_{1}\lambda_p)({}_{1}S_{1}C)]$$

$$\mp \ ({}_{1}A_{t,b}\ell)[({}^{1}_{1}\Lambda_p+{}^{1}_{1}\Lambda_p)({}_{1}S^2) \ + \ ({}^{1}_{1}\lambda_m+{}^{1}_{1}\lambda_m)({}_{1}S_{1}C)]$$

$$+ \ ({}_{1}A_{t,b}\ell)[({}^{1}_{1}\Lambda_m+{}^{1}_{1}\Lambda_m)({}_{1}C^2) \ + \ ({}^{1}_{1}\lambda_p+{}^{1}_{1}\lambda_p)({}_{1}S_{1}C)]$$

$$\pm \ ({}_{1}A_{t,b}\ell)[({}^{1}_{1}\Lambda_p+{}^{1}_{1}\Lambda_p)({}_{1}S^2) \ + \ ({}^{1}_{1}\lambda_m+{}^{1}_{1}\lambda_m)({}_{1}S_{1}C)]$$

$$+$$

$$\Big\{ \ - \ ({}^{1}_{1}\Lambda_p+{}^{1}_{1}\Lambda_p)k \ + \ ({}^{1}_{1}\lambda_m+{}^{1}_{1}\lambda_m)({}_{1}C^2)$$

$$\pm \ ({}^{1}_{1}\Lambda_m+{}^{1}_{1}\Lambda_m)k \ \pm \ ({}^{1}_{1}\lambda_p+{}^{1}_{1}\lambda_p)({}_{1}S^2) \ \Big\} \qquad \sin(\ell x)$$

$$+$$

$$\Big\{ \ + \ ({}^{1}_{1}\Lambda_p+{}^{1}_{1}\Lambda_p)k \ - \ ({}^{1}_{1}\lambda_m+{}^{1}_{1}\lambda_m)({}_{1}C^2)$$

$$\mp \ ({}^{1}_{1}\Lambda_m+{}^{1}_{1}\Lambda_m)k \ \mp \ ({}^{1}_{1}\lambda_p+{}^{1}_{1}\lambda_p)({}_{1}S^2) \ \Big\} \qquad \cos(\ell x)$$

$$
\begin{aligned}
+ \\
& \Big\{ - \left({}^{2}_{2}\Lambda_p + {}^{3}_{2}\Lambda_p + {}^{11}_{2}\Lambda_p + {}^{12}_{2}\Lambda_p + {}^{13}_{2}\Lambda_p\right) 2k \\
& + \left({}^{2}_{2}\lambda_m + {}^{3}_{2}\lambda_m + {}^{11}_{2}\lambda_m + {}^{12}_{2}\lambda_m + {}^{13}_{2}\lambda_m\right) \left({}_{2}C^{2}\right) \\
& \pm \left({}^{2}_{2}\Lambda_m + {}^{3}_{2}\Lambda_m + {}^{11}_{2}\Lambda_m + {}^{12}_{2}\Lambda_m + {}^{13}_{2}\Lambda_m\right) 2k \\
& \pm \left({}^{2}_{2}\lambda_p + {}^{3}_{2}\lambda_p + {}^{11}_{2}\lambda_p + {}^{12}_{2}\lambda_p + {}^{13}_{2}\lambda_p\right) \left({}_{2}S^{2}\right) \\
& + \left({}_{1}A_{t,b}\ell\right) \Big[\left({}^{1}_{1}\lambda_p + {}^{2}_{1}\lambda_p\right) \left({}_{1}S_{1}C - k\right) \\
& \qquad \pm \left({}^{1}_{1}\lambda_m + {}^{2}_{1}\lambda_m\right) \left({}_{1}S_{1}C + k\right) \Big] \\
& - \left({}_{1}A_{t,b}\ell\right) \Big[\left({}^{2}_{1}\lambda_p + {}^{1}_{1}\lambda_p\right) \left({}_{1}S_{1}C - k\right) \\
& \qquad \pm \left({}^{2}_{1}\lambda_m + {}^{1}_{1}\lambda_m\right) \left({}_{1}S_{1}C + k\right) \Big] \Big\} \qquad \sin(2\ell x) \\
+ \\
& \Big\{ + \left({}^{3}_{2}\Lambda_p + {}^{2}_{2}\Lambda_p + {}^{11}_{2}\Lambda_p + {}^{12}_{2}\Lambda_p + {}^{13}_{2}\Lambda_p\right) 2k \\
& - \left({}^{3}_{2}\lambda_m + {}^{2}_{2}\lambda_m + {}^{11}_{2}\lambda_m + {}^{12}_{2}\lambda_m + {}^{13}_{2}\lambda_m\right) \left({}_{2}C^{2}\right) \\
& \mp \left({}^{3}_{2}\Lambda_m + {}^{2}_{2}\Lambda_m + {}^{11}_{2}\Lambda_m + {}^{12}_{2}\Lambda_m + {}^{13}_{2}\Lambda_m\right) 2k \\
& \mp \left({}^{3}_{2}\lambda_p + {}^{2}_{2}\lambda_p + {}^{11}_{2}\lambda_p + {}^{12}_{2}\lambda_p + {}^{13}_{2}\lambda_p\right) \left({}_{2}S^{2}\right) \\
& - \left({}_{1}A_{t,b}\ell\right) \Big[\left({}^{2}_{1}\lambda_p + {}^{1}_{1}\lambda_p\right) \left({}_{1}S_{1}C - k\right) \\
& \qquad \pm \left({}^{2}_{1}\lambda_m + {}^{1}_{1}\lambda_m\right) \left({}_{1}S_{1}C + k\right) \Big] \\
& - \left({}_{1}A_{t,b}\ell\right) \Big[\left({}^{1}_{1}\lambda_p + {}^{2}_{1}\lambda_p\right) \left({}_{1}S_{1}C - k\right) \\
& \qquad \pm \left({}^{1}_{1}\lambda_m + {}^{2}_{1}\lambda_m\right) \left({}_{1}S_{1}C + k\right) \Big] \Big\} \qquad \cos(2\ell x)
\end{aligned}
\tag{14b}
$$

Equations (14) are analogous to eqs. (17) in Appendix A.

Expressions for the perturbed stresses and velocities in the upper and lower confining media are derived according to the procedure outlined in Appendix A.

The lambda constants for the upper (U̲) and lower (L̲) media are:

$${}^{1}_{1}\Lambda_{U,L} = {}^{1}_{1}\sigma_{U,L}/2\mu\ell \tag{15a}$$

$${}^{1}_{1}\lambda_{U,L} = {}^{1}_{1}\tau_{U,L}/2\mu\ell - 2({}_{1}\mathbf{A}_{U,L}) \tag{15b}$$

$${}^{1}_{1}\Lambda_{U,L} = {}^{1}_{1}\sigma_{U,L}/2\mu\ell + (\bar{\sigma}_{xz}/\mu_{o})({}_{1}\mathbf{A}_{U,L}) \tag{15c}$$

$${}^{1}_{1}\lambda_{U,L} = {}^{1}_{1}\tau_{U,L}/2\mu\ell \tag{15d}$$

$${}^{1}_{1}\Lambda_{U,L} = {}^{1}_{1}\sigma_{U,L}/2\mu\ell \tag{15e}$$

$$-{}^{1}_{1}\lambda_{U,L} = {}^{1}_{1}\tau_{U,L}/2\mu\ell + 2({}_{1}\mathbf{A}_{U,L}) \tag{15f}$$

$${}^{1}_{1}\Lambda_{U,L} = {}^{1}_{1}\sigma_{U,L}/2\mu\ell - (\bar{\sigma}_{xz}/\mu_{o})({}_{1}\mathbf{A}_{U,L}) \tag{15g}$$

$$-{}^{1}_{1}\lambda_{U,L} = {}^{1}_{1}\tau_{U,L}/2\mu\ell \tag{15h}$$

$${}^{2}_{2}\Lambda_{U,L} = {}^{2}_{2}\sigma_{U,L}/4\mu\ell \tag{15i}$$

$${}^{2}_{2}\lambda_{U,L} = {}^{2}_{2}\tau_{U,L}/4\mu\ell - 2({}_{2}\mathbf{A}_{U,L}) \tag{15j}$$

$${}^{2}_{2}\Lambda_{U,L} = {}^{2}_{2}\sigma_{U,L}/4\mu\ell + (\bar{\sigma}_{xz}/\mu_{o})({}_{2}\mathbf{A}_{U,L}) \tag{15k}$$

$${}^{2}_{2}\lambda_{U,L} = {}^{2}_{2}\tau_{U,L}/4\mu\ell \tag{15ℓ}$$

$${}^{2}_{2}\Lambda_{U,L} = {}^{2}_{2}\sigma_{U,L}/4\mu\ell \tag{15m}$$

$$-{}^{2}_{2}\lambda_{U,L} = {}^{2}_{2}\tau_{U,L}/4\mu\ell + 2({}_{2}\mathbf{A}_{U,L}) \tag{15n}$$

$${}^{2}_{2}\Lambda_{U,L} = {}^{2}_{2}\sigma_{U,L}/4\mu\ell - (\bar{\sigma}_{xz}/\mu_{o})({}_{2}\mathbf{A}_{U,L}) \tag{15o}$$

$$-{}^{2}_{2}\lambda_{U,L} = {}^{2}_{2}\tau_{U,L}/4\mu\ell \tag{15p}$$

$${}^{1}{}^{1}_{2}\Lambda_{U,L} = {}^{1}{}^{1}_{2}\sigma_{U,L}/4\mu\ell + (\dot{\ell}/2)({}_{1}\mathbf{A}_{U,L})^{2} + (3/4)({}_{1}\mathbf{A}_{U,L}\ell)({}^{1}_{1}\lambda_{U,L}) \tag{15q}$$

$$
\begin{aligned}
{}^{1}{}^{1}_{2}\lambda_{U,L} &= {}^{1}{}^{1}_{2}\tau_{U,L}/4\mu\ell \\
&\quad - ({}_{1}A_{U,L}\ell/4)({}^{1}_{1}\Lambda_{U,L} \mp 4\,{}^{1}_{1}\lambda_{U,L}) && (15r) \\
{}^{1}{}^{1}_{2}\Lambda_{U,L} &= {}^{1}{}^{1}_{2}\sigma_{U,L}/4\mu\ell - (\ell/2)({}_{1}A_{U,L})^{2} \\
&\quad - (3/4)({}_{1}A_{U,L}\ell)({}^{1}_{1}\lambda_{U,L}) && (15s) \\
{}^{1}{}^{1}_{2}\lambda_{U,L} &= {}^{1}{}^{1}_{2}\tau_{U,L}/4\mu\ell \\
&\quad + ({}_{1}A_{U,L}\ell/4)({}^{1}_{1}\Lambda_{U,L} \mp 4\,{}^{1}_{1}\lambda_{U,L}) && (15t) \\
{}^{1}{}^{1}_{2}\Lambda_{U,L} &= {}^{1}{}^{1}_{2}\sigma_{U,L}/4\mu\ell \\
&\quad + (3/4)[({}_{1}A_{U,L}\ell)({}^{1}_{1}\lambda_{U,L}) - ({}_{1}A_{U,L}\ell)({}^{1}_{1}\lambda_{U,L})] && (15u) \\
{}^{1}{}^{1}_{2}\lambda_{U,L} &= {}^{1}{}^{1}_{2}\tau_{U,L}/4\mu\ell - (\ell/2)(\bar{\sigma}_{xz}/\mu_{o})({}_{1}A_{U,L})({}_{1}A_{U,L}) \\
&\quad + ({}_{1}A_{U,L}\ell/4)({}^{1}_{1}\Lambda_{U,L} \mp 4\,{}^{1}_{1}\lambda_{U,L}) \\
&\quad - ({}_{1}A_{U,L}\ell/4)({}^{1}_{1}\Lambda_{U,L} \mp 4\,{}^{1}_{1}\lambda_{U,L}) && (15v) \\
{}^{1}{}^{1}_{2}\Lambda_{U,L} &= {}^{1}{}^{1}_{2}\sigma_{U,L}/4\mu\ell \\
&\quad + (3/4)({}_{1}A_{U,L}\ell)({}^{1}_{1}\lambda_{U,L}) && (15w) \\
-{}^{1}{}^{1}_{2}\lambda_{U,L} &= {}^{1}{}^{1}_{2}\tau_{U,L}/4\mu\ell - (\ell/4)(\bar{\sigma}_{xz}/\mu_{o})({}_{1}A_{U,L})^{2} \\
&\quad + ({}_{1}A_{U,L}\ell/4)({}^{1}_{1}\Lambda_{U,L} \mp 4\,{}^{1}_{1}\lambda_{U,L}) && (15x) \\
{}^{1}{}^{1}_{2}\Lambda_{U,L} &= {}^{1}{}^{1}_{2}\sigma_{U,L}/4\mu\ell \\
&\quad + (3/4)({}_{1}A_{U,L}\ell)({}^{1}_{1}\lambda_{U,L}) && (15y) \\
-{}^{1}{}^{1}_{2}\lambda_{U,L} &= {}^{1}{}^{1}_{2}\tau_{U,L}/4\mu\ell + (\ell/4)(\bar{\sigma}_{xz}/\mu_{o})({}_{1}A_{U,L})^{2} \\
&\quad + ({}_{1}A_{U,L}\ell/4)({}^{1}_{1}\Lambda_{U,L} \mp 4\,{}^{1}_{1}\lambda_{U,L}) && (15z) \\
{}^{1}{}^{1}_{2}\Lambda_{U,L} &= {}^{1}{}^{1}_{2}\sigma_{U,L}/4\mu\ell + \ell({}_{1}A_{U,L})({}_{1}A_{U,L}) \\
&\quad + (3/4)[({}_{1}A_{U,L}\ell)({}^{1}_{1}\lambda_{U,L}) + ({}_{1}A_{U,L}\ell)({}^{1}_{1}\lambda_{U,L})] && (15aa) \\
-{}^{1}{}^{1}_{2}\lambda_{U,L} &= {}^{1}{}^{1}_{2}\tau_{U,L}/4\mu\ell \\
&\quad + ({}_{1}A_{U,L}\ell/4)({}^{1}_{1}\Lambda_{U,L} \mp 4\,{}^{1}_{1}\lambda_{U,L}) \\
&\quad + ({}_{1}A_{U,L}\ell/4)({}^{1}_{1}\Lambda_{U,L} \mp 4\,{}^{1}_{1}\lambda_{U,L}) && (15bb)
\end{aligned}
$$

Equations (15) are analogous to eqs. (19) in Appendix A.

The expressions for the velocities normal and tangential to the interface for the upper (U) and lower (L) media are:

$$(v_n)_{U,L} = (\bar{v}_z)_{U,L} \cos(\theta_{U,L}) - (\bar{v}_x)_{U,L} \sin(\theta_{U,L})$$

$+$

$$\mp \; ({}^{1}_{1}\Lambda_{U,L} + {}^{1}_{1}\Lambda_{U,L}) \quad \cos(\ell x)$$

$+$

$$\mp \; ({}^{1}_{1}\Lambda_{U,L} + {}^{1}_{1}\Lambda_{U,L}) \quad \sin(\ell x)$$

$+$

$$\mp \; [{}^{2}_{2}\Lambda_{U,L} + {}^{2}_{2}\Lambda_{U,L} + {}^{1}{}^{1}_{2}\Lambda_{U,L} + {}^{1}{}^{1}_{2}\Lambda_{U,L} + {}^{1}{}^{1}_{2}\Lambda_{U,L}$$
$$- ({}_{1}\bar{A}_{U,L}\hat{\ell})({}^{1}_{1}\lambda_{U,L} + {}^{1}_{1}\lambda_{U,L})$$
$$+ ({}_{1}A_{U,L}\ell)({}^{1}_{1}\lambda_{U,L} + {}^{1}_{1}\lambda_{U,L})] \; \cos(2\ell x)$$

$+$

$$\mp \; [{}^{2}_{2}\Lambda_{U,L} + {}^{2}_{2}\Lambda_{U,L} + {}^{1}{}^{1}_{2}\Lambda_{U,L} + {}^{1}{}^{1}_{2}\Lambda_{U,L} + {}^{1}{}^{1}_{2}\Lambda_{U,L}$$
$$- ({}_{1}A_{U,L}\ell)({}^{1}_{1}\lambda_{U,L} + {}^{1}_{1}\lambda_{U,L})$$
$$- ({}_{1}A_{U,L}\ell)({}^{1}_{1}\lambda_{U,L} + {}^{1}_{1}\lambda_{U,L})] \; \sin(2\ell x) \qquad (16a)$$

$$(v_{s})_{U,L} = (\bar{v}_{z})_{U,L} \sin(\theta_{U,L}) + (\bar{v}_{x})_{U,L} \cos(\theta_{U,L})$$

$$\pm ({}_{1}A_{U,L}\ell)[({}^{1}_{1}\Lambda_{U,L} + {}^{1}_{1}\Lambda_{U,L}) \mp ({}^{1}_{1}\lambda_{U,L} + {}^{1}_{1}\lambda_{U,L})]$$

$$\mp ({}_{1}A_{U,L}\ell)[({}^{1}_{1}\Lambda_{U,L} + {}^{1}_{1}\Lambda_{U,L}) \mp ({}^{1}_{1}\lambda_{U,L} + {}^{1}_{1}\lambda_{U,L})]$$

$+$

$$\mp ({}^{1}_{1}\lambda_{U,L} + {}^{1}_{1}\lambda_{U,L}) \quad \sin(\ell x)$$

$+$

$$\pm ({}^{1}_{1}\lambda_{U,L} + {}^{1}_{1}\lambda_{U,L}) \quad \cos(\ell x)$$

$+$

$$\mp [{}^{2}_{2}\lambda_{U,L} + {}^{2}_{2}\lambda_{U,L} + {}^{1\,1}_{\;\;2}\lambda_{U,L} + {}^{1\,1}_{\;\;2}\lambda_{U,L} + {}^{1\,1}_{\;\;2}\lambda_{U,L}$$

$$\mp ({}_{1}A_{U,L}\ell)({}^{1}_{1}\lambda_{U,L} + {}^{1}_{1}\lambda_{U,L})$$

$$\pm ({}_{1}A_{U,L}\ell)({}^{1}_{1}\lambda_{U,L} + {}^{1}_{1}\lambda_{U,L}) \;] \sin(2\ell x)$$

$+$

$$\pm [{}^{2}_{2}\lambda_{U,L} + {}^{2}_{2}\lambda_{U,L} + {}^{1\,1}_{\;\;2}\lambda_{U,L} + {}^{1\,1}_{\;\;2}\lambda_{U,L} + {}^{1\,1}_{\;\;2}\lambda_{U,L}$$

$$\mp ({}_{1}A_{U,L}\ell)({}^{1}_{1}\lambda_{U,L} + {}^{1}_{1}\lambda_{U,L})$$

$$\mp ({}_{1}A_{U,L}\ell)({}^{1}_{1}\lambda_{U,L} + {}^{1}_{1}\lambda_{U,L}) \;] \cos(2\ell x) \qquad (16b)$$

Equations (16) are analogous to eqs. (20) in Appendix A.

The velocity boundary conditions are used to determine values for the interface constants σ and τ.

The velocity boundary conditions we apply to a multilayer subjected to principal compressive stress oblique to layering are the same as those applied for principal compressive stress parallel to layering. In both situations, the normal velocity components must match at the interface. In both cases, the difference in tangential velocities on either side of the interface is controlled by the resistance to slip at that interface. Resistance to slip is modeled theoretically by a powerlaw relationship between the rate of slip, $\delta \underline{v}_s$, and the interface shear stress, σ_{ns}, at the contact, as explained in Appendix A and Chapter II.

The velocity boundary conditions are:

$$(v_n)_b = (v_n)_t \tag{17a}$$

$$(v_s)_b - (v_s)_t = (\sigma_{ns}/\beta_c)|\sigma_{ns}/\beta_c|^{(m-1)} \tag{17b}$$

in which β_c and $\underline{m}$ are parameters describing the resistance to slip.

The presence of a mean layer-parallel shear stress, $\bar{\sigma}_{xz}$, in the theoretical analysis removes the restrictions on the values that the powerlaw exponent $\underline{m}$ can assume. We write the tangential velocity boundary condition, eq. (17b), to 2nd order accuracy by substituting the 2nd order expression for the interface shear stress, eq. (13b), for σ_{ns} and then expanding σ_{ns} to the <u>m</u>th power with the binomial series approximation. The leading term, $\bar{\sigma}_{xz}$, in the expression for the shear stress, σ_{ns}, is a 0th order constant which can be raised to the <u>m</u>th power without exceeding the limitations of 2nd order accuracy. The series expansion is limited, however, by the power to which the perturbed stress constants, τ, can be raised.

The expanded tangential velocity boundary condition, accurate to 2nd order, is:

$$
\begin{aligned}
(v_s)_b - (v_s)_t = (1/\beta_c)^m \Big\{ & (\bar{\sigma}_{xz})^m \\
& + [m(m-1)/4](\bar{\sigma}_{xz})^{(m-2)}({}^1_1\tau+{}^{\mathbf{1}}_1\tau)^2 \\
& + [m(m-1)/4](\bar{\sigma}_{xz})^{(m-2)}({}^{\mathbf{1}}_{\mathbf{1}}\tau+{}^1_{\mathbf{1}}\tau)^2 \\
& + m(\bar{\sigma}_{xz})^{(m-1)}({}^{11}\tau_o+{}^{\mathbf{11}}\tau_o+{}^{\mathbf{11}}\tau_o) \\
& + \{m(\bar{\sigma}_{xz})^{(m-1)}({}^1_1\tau+{}^{\mathbf{1}}_1\tau)\} \sin(\ell x) \\
& + \{m(\bar{\sigma}_{xz})^{(m-1)}({}^{\mathbf{1}}_{\mathbf{1}}\tau+{}^1_{\mathbf{1}}\tau)\} \cos(\ell x) \\
& + \{ [m(m-1)/2](\bar{\sigma}_{xz})^{(m-2)}({}^1_1\tau+{}^{\mathbf{1}}_1\tau)({}^{\mathbf{1}}_{\mathbf{1}}\tau+{}^1_{\mathbf{1}}\tau) \\
& \quad + m(\bar{\sigma}_{xz})^{(m-1)}({}^2_2\tau+{}^{\mathbf{2}}_2\tau+{}^{1}{}^1_2\tau+{}^{1}{}^{\mathbf{1}}_2\tau+{}^{\mathbf{1}}{}^1_2\tau) \} \sin(2\ell x) \\
& + \{ [m(m-1)/4](\bar{\sigma}_{xz})^{(m-2)}[({}^1_1\tau+{}^{\mathbf{1}}_1\tau)^2 - ({}^{\mathbf{1}}_{\mathbf{1}}\tau+{}^1_{\mathbf{1}}\tau)^2] \\
& \quad + m(\bar{\sigma}_{xz})^{(m-1)}({}^{\mathbf{2}}_{\mathbf{2}}\tau+{}^2_{\mathbf{2}}\tau+{}^1{}^1_{\mathbf{2}}\tau+{}^1{}^{\mathbf{1}}_{\mathbf{2}}\tau+{}^{\mathbf{1}}{}^{\mathbf{1}}_{\mathbf{2}}\tau) \} \cos(2\ell x) \Big\}
\end{aligned}
\tag{18}
$$

Because I choose to specify a uniform, layer-parallel shear stress, $\bar{\sigma}_{xz}$, I add a constant term, $(\bar{\underline{v}}_x)_o$, to the mean layer-parallel velocity, eq. (2a). The constant $(\bar{\underline{v}}_x)_o$ is determined by the $\underline{x}$-independent terms in the velocity boundary conditions.

Once the constants have been determined, the growth rates of the component waveforms can be computed. The method is outlined in Appendix A. The computer program I use to calculate the values of the interface stresses and to integrate the growth rate equations for finite multilayers subjected to a combination of layer-parallel shear and shortening is presented in Appendix C ("Shear.bas")

APPENDIX C

COMPUTER PROGRAMS

1. Folding3rdOrder.bas: layer-parallel shortening of finite multilayers.
2. Infmult.bas: layer-parallel shortening of infinitely thick multilayers.
3. Shear.bas: layer-parallel shortening and shear of finite multilayers.
4. Infshear.bas: layer-parallel shortening and shear of infinitely thick multilayers.
5. Eigen.bas: eigenvectors and eigenvalues for 3rd order analysis.

```
1 REM LAYER-PARALLEL SHORTENING
2 REM 3RD ORDER ANALYSIS
3 REM POWERLAW EXPONENT M = 1, 2, OR 3
5 WIDTH LPRINT 80
10 LPRINT "<Folding3rdOrder.bas>":GOTO 300
99 REM
100 REM *********** CALCULATION OF TRIG FUNCTIONS **********************
105 T5=1/(2*WN*WF*MU(LL)):K1=WF*K(LL)
110 EM=1/(E^K1):EP=E^K1:CH=(EP+EM)/2:SH=(EP-EM)/2
115 TM1=CH*SH-K1:TP1=CH*SH+K1
120 N1=(CH^2)/TM1:N2=K1/TM1:N3=(SH^2)/TP1:N4=K1/TP1
125 S1=(CH^2)/TP1:S2=K1/TP1:S3=(SH^2)/TM1:S4=K1/TM1
130 N6=SH*CH/TM1:N7=SH*CH/TP1:S6=SH*CH/TP1:S7=SH*CH/TM1
135 NP1=(N1+N3)*T5:NM1=(N1-N3)*T5:NP2=(N2+N4)*T5:NM2=(N2-N4)*T5
140 SP1=(S1+S3)*T5:SM1=(S1-S3)*T5:SP2=(S2+S4)*T5:SM2=(S2-S4)*T5
150 AM=0:AP=0
155 IF IW>3 AND IW<9 THEN 160
156 IF IW=9 THEN IW=4
157 AM=A(I,IW)-A(I+1,IW):AP=A(I,IW)+A(I+1,IW)
158 IF IW=4 THEN IW=9
160 RETURN
165 REM ************* END CALCULATIONS *****************
166 REM
200 REM **************** CLEAR MATRIX ****************************
205 FOR I=0 TO ILAST*2+1:FOR J=0 TO 6:Y(I,J)=0:NEXT:NEXT
206 FOR L=1 TO LB:CLP(L)=0:CLM(L)=0:SLP(L)=0:SLM(L)=0:NEXT:RETURN
300 GOSUB 5350:SX=1:IN=0:IMAX=-1:IIMAX=0:IISL=10
302 REM
303 REM ********** INCREASE AMOUNT OF STRETCH *************
305 TP=(SZ-1/(SX+DS+ABS(DS/10)))
310 IF TP<0 THEN LPRINT "SX>SXF":GOTO 9999
315 SX=SX+DS:IN=IN+1
317 FOR L=1 TO LB:K(L)=PI*T(L)/(WL*SX^2):NEXT
320 TT=0:FOR L=1 TO LB:TT=TT+T(L)/SX:NEXT
325 WN=2*PI/(WL*SX)
335 FOR I=0 TO LLAST:FOR IW=1 TO 4:B(I,IW)=0:NEXT:NEXT
338 REM
339 REM *********** FIRST AND SECOND WAVEFORMS, 1ST ORDER *****************
340 IW=1:WF=1
350 WF=IW:GOSUB 205
351 IF A(INT(ILAST/2),IW)=0 THEN 375 ELSE AP=A(0,IW):AM=A(ILAST,IW):GOSUB 405
353 PRINT WF;"-";IW;:GOSUB 5790
360 FOR L=1 TO LLAST:II=L-1:LL=L:SN=1:IF L=LLAST THEN LL=LB:SN=-1
365 I=LL-1:GOSUB 105:GOSUB 610:GOSUB 750
370 B(II,IW)=(1/2)*(CM*N1+SP*N2+SN*(CP*N3-SM*N4)):NEXT
375 IF IW=1 THEN IW=2:GOTO 350
385 IF IW=2 THEN 810
402 REM
403 REM ******* FILL COLUMNS 0-5 OF MATRIX, SOLVE MATRIX ******************
404 REM *** MEDIA ***
```

```
405 L=0:I=0:T5=1/(2*WN*WF*MU(0))
410 Y(0,2)=Y(0,2)-2*T5:Y(1,3)=Y(1,3)-2*T5-2*ULMUC:Y(1,6)=Y(1,6)-4*AP
415 L=LLAST:I=L-1:T5=1/(2*WN*WF*MU(LLAST)):II=2*I
420 Y(II,2)=Y(II,2)-2*T5
425 Y(II+1,3)=Y(II+1,3)-2*T5-2*ULMUC:Y(II+1,6)=Y(II+1,6)-4*AM
430 FOR L=1 TO LB:I=L-1:LL=L:GOSUB 105:IT=I:IB=L:I=2*IT
431 J=1:IF L=LB THEN J=0
433 REM *** VN FOR TOP OF LAYER ***
435 Y(I,2)=Y(I,2)-NP1:Y(I,3)=Y(I,3)-NM2:Y(I,4)=Y(I,4)+NM1
440 Y(I,5)=Y(I,5)-NP2:Y(I,6)=Y(I,6)-2*(AP*N2-AM*N4):I=I+1
443 REM *** VS FOR TOP OF LAYER ***
445 Y(I,2)=Y(I,2)+SM2:Y(I,3)=Y(I,3)-SP1:Y(I,4)=Y(I,4)+SP2
450 Y(I,5)=Y(I,5)+SM1:Y(I,6)=Y(I,6)-2*(AM*S1+AP*S3):I=IB*2
453 REM *** VN FOR BOTTOM OF LAYER ***
455 Y(I,0)=Y(I,0)+NM1:Y(I,1)=Y(I,1)+NP2:Y(I,2)=Y(I,2)-NP1
460 Y(I,3)=Y(I,3)+NM2:Y(I,6)=Y(I,6)+2*(AP*N2+AM*N4):I=I+1
463 REM *** VS FOR BOTTOM OF LAYER ***
465 Y(I,0)=Y(I,0)-SP2:Y(I,1)=Y(I,1)+SM1:Y(I,2)=Y(I,2)-SM2
470 Y(I,3)=Y(I,3)-SP1-J*2*MUC:Y(I,6)=Y(I,6)+2*(AM*S1-AP*S3)
475 NEXT
476 REM ***** MATRIX FILLED -- SOLVE FOR CONSTANTS *****
477 REM ******************** MATRIX-SOLVER *****************
478 REM ** IP IS PIVOT ROW (SEE DIAGRAM FOLLOWING PROGRAM)
480 FOR L=1 TO LLAST:IT=L-1:IB=L:IP=2*IT:YY=1/(Y(IP,2)):I=IP
485 FOR J=2 TO 6:Y(I,J)=Y(I,J)*YY:NEXT:IP1=I+1:IP2=I+2:IP3=I+3
490 FOR J=3 TO 6:Y(IP1,J)=Y(IP1,J)-Y(IP1,2)*Y(I,J):NEXT:Y(IP1,2)=0
495 IF L=LLAST THEN Y(IP1,6)=Y(IP1,6)/Y(IP1,3):Y(IP1,3)=1:GOTO 545
500 FOR IJ=IP2 TO IP3:FOR J=1 TO 3:Y(IJ,J)=Y(IJ,J)-Y(IJ,0)*Y(IP,J+2):NEXT
505 Y(IJ,6)=Y(IJ,6)-Y(IJ,0)*Y(IP,6)
510 Y(IJ,0)=0:NEXT
512 REM ** MOVE TO PIVOT BELOW
515 IP=IP+1:YY=1/Y(IP,3):I=IP
520 FOR J=3 TO 6:Y(I,J)=Y(I,J)*YY:NEXT
525 IP1=I+1:IP2=I+2:FOR IJ=IP1 TO IP2:FOR J=2 TO 3
530 Y(IJ,J)=Y(IJ,J)-Y(IJ,1)*Y(IP,J+2):NEXT
535 Y(IJ,6)=Y(IJ,6)-Y(IJ,1)*Y(IP,6):Y(IJ,1)=0
540 NEXT
545 NEXT
546 REM ** COMPUTE CONSTANTS AND PUT THEM IN LAST COLUMN
550 IP=2*LB:Y(IP,6)=Y(IP,6)-Y(IP+1,6)*Y(IP,3):Y(IP,3)=0
555 FOR L=LB-1 TO 0 STEP -1:IP=2*L+1
560 Y(IP,6)=Y(IP,6)-Y(IP,4)*Y(IP+1,6)-Y(IP,5)*Y(IP+2,6)
565 Y(IP,4)=0:Y(IP,5)=0:IP=IP-1
570 Y(IP,6)=Y(IP,6)-Y(IP,3)*Y(IP+1,6)-Y(IP,4)*Y(IP+2,6)-Y(IP,5)*Y(IP+3,6)
575 FOR IK=3 TO 5:Y(IP,IK)=0:NEXT:NEXT
577 REM ** STORE CONSTANTS
580 FOR I=0 TO ILAST:J=2*I:JP1=J+1
585 SIG(I,IW)=Y(J,6):TAU(I,IW)=Y(JP1,6)
590 NEXT
595 RETURN
```

```
596 REM ********************END MATRIX *******************
597 REM
600 REM ***** COMPUTE LAYER LAMBDA PAIRS (AS CP, ETC.) *****
610 ITT=LL-1
615 CP=(SIG(ITT,IW)+SIG(LL,IW))*T5+CLP(LL)
620 CM=(SIG(ITT,IW)-SIG(LL,IW))*T5+CLM(LL)
625 SP=(TAU(ITT,IW)+TAU(LL,IW))*T5+SLP(LL)-2*AP
630 SM=(TAU(ITT,IW)-TAU(LL,IW))*T5+SLM(LL)-2*AM
635 RETURN
700 REM ** RETRIEVE LAMBDA PAIRS (CLAMP), STORE TEMPORARILY AS CP OR CPT **
705 CP=CLAMP(LL,IW):CM=CLAMM(LL,IW):SP=SLAMP(LL,IW):SM=SLAMM(LL,IW):RETURN
725 CPT=CLAMP(LL,IW):CMT=CLAMM(LL,IW):SPT=SLAMP(LL,IW):SMT=SLAMM(LL,IW):RETURN
740 REM ***** STORE LAMBDA PAIRS (CP) AS CLAMP *****
750 CLAMP(LL,IW)=CP:CLAMM(LL,IW)=CM:SLAMP(LL,IW)=SP:SLAMM(LL,IW)=SM:RETURN
770 REM ***** COMPUTE MEDIA LAMBDAS ******
775 T5=1/(2*WF*MU(0)*WN)
777 SLAM(0,IW)=TAU(0,IW)*T5:CLAM(0,IW)=SIG(0,IW)*T5
778 T5=1/(2*WF*MU(LLAST)*WN)
779 SLAM(LLAST,IW)=TAU(ILAST,IW)*T5:CLAM(LLAST,IW)=SIG(ILAST,IW)*T5
780 RETURN
800 REM
805 REM ************ SECOND WAVEFORM, 2ND ORDER *********************
810 IW=4:GOSUB 205
820 Y(0,6)=Y(0,6)-A(0,1)*(TAU(0,1)/(4*MU(0))-2*A(0,1)*WN)
822 Y(1,6)=Y(1,6)-A(0,1)*SIG(0,1)/(4*MU(0))
825 L=LLAST:I=ILAST:J=I*2
830 Y(J,6)=Y(J,6)-A(I,1)*(TAU(I,1)/(4*MU(L))-2*A(I,1)*WN)
840 Y(J+1,6)=Y(J+1,6)-A(I,1)*SIG(I,1)/(4*MU(L))
845 FOR L=1 TO LB:I=L-1:LL=L:IP=I+1:IT=I*2
850 IW=1:WF=1:GOSUB 105:GOSUB 705
860 CLP(L)=(2*(AP^2+AM^2)+3*(AP*SP+AM*SM))*WN/8
865 CLM(L)=(4*(AP*AM)+3*(AM*SP+AP*SM))*WN/8
870 T1=(CP*(S6-3*S2)+SM*4*S1)*WN/8
875 T2=(CM*(S7+3*S4)+SP*4*S3)*WN/8
880 SLP(L)=-AP*T1-AM*T2:SLM(L)=-AM*T1-AP*T2
885 TV5(L)=CP*S2-SM*S1:TV6(L)=-CM*S4-SP*S3
890 WF=2:IW=4:GOSUB 105
895 T3=CLM(L)*N1+SLP(L)*N2:T4=CLP(L)*N3-SLM(L)*N4
900 Y(IT,6)=Y(IT,6)+T3+T4+A(I,1)*WN*(TV5(L)+TV6(L))
905 Y(IT+2,6)=Y(IT+2,6)-T3+T4-A(IP,1)*WN*(TV5(L)-TV6(L))
910 T3=-CLP(L)*S2+SLM(L)*S1:T4=CLM(L)*S4+SLP(L)*S3
915 Y(IT+1,6)=Y(IT+1,6)+T3+T4+A(I,1)*WN*(SP+SM)
920 Y(IT+3,6)=Y(IT+3,6)-T3+T4-A(IP,1)*WN*(SP-SM)
925 NEXT
930 IW=4:WF=2:AM=0:AP=0:GOSUB 405
931 PRINT " 2-11";:GOSUB 5790
935 FOR L=1 TO LLAST:II=L-1:LL=L:AA=A(II,1)*WN/2:SN=1
937 IF L=LLAST THEN SN=-1:LL=LB
945 T5=1/(4*MU(LL)*WN):IW=4:AP=0:AM=0:GOSUB 610:GOSUB 750
955 I=LL-1:IW=2:WF=2:GOSUB 105
```

```
960 TP=(1/2)*(CM*N1+SP*N2+SN*(CP*N3-SM*N4))
970 Q(II,2)=Q(II,2)+TP+AA*(TV5(LL)+SN*TV6(LL))
975 NEXT
980 REM
990 REM ************ FIRST WAVEFORM, 3RD ORDER ***********************
1005 IW=5:GOSUB 205
1010 T5=1/(2*MU(0)*WN):AA=A(0,1)*WN/2:S6=SIG(0,1)*T5:TA=TAU(0,1)*T5
1015 VNT=A(0,2)*(-4*AA-2*TA*WN)-AA*TAU(0,2)*T5
1020 T1=2*(AA^2)*(S6-2*(TA-2*A(0,1))):TP=(M-2)*(M-1)/2*(3/2)*(TAU(0,1)^3)/BHAT
1025 Y(0,6)=Y(0,6)-T1-AA*TAU(0,4)*T5+VNT
1027 VST=A(0,2)*(4*TA*WN-16*AA-2*S6*WN)-AA*T5*SIG(0,2)
1030 Y(1,6)=Y(1,6)+4*(AA^2)*S6-AA*SIG(0,4)*T5+10*(AA^2)*A(0,1)+VST+TP
1035 L=LLAST:I=ILAST:J=2*I
1040 T5=1/(2*MU(L)*WN):AA=A(I,1)*WN/2:S6=SIG(I,1)*T5:TA=TAU(I,1)*T5
1045 T1=2*(AA^2)*(S6+2*(TA-2*A(I,1)))
1047 VNB=A(I,2)*(-4*AA-2*TA*WN)-AA*T5*TAU(I,2)
1050 Y(J,6)=Y(J,6)-T1-AA*TAU(I,4)*T5+VNB
1053 VSB=A(I,2)*(16*AA-4*WN*TA-2*WN*S6)-AA*T5*SIG(I,2)
1055 Y(J+1,6)=Y(J+1,6)-4*(AA^2)*S6-AA*SIG(I,4)*T5+10*(AA^2)*A(I,1)+VSB
1060 FOR L=1 TO LB:I=L-1:LL=L:IP=I+1:IT=I*2
1063 IW=1:WF=1:GOSUB 105:GOSUB 705
1065 AAP=(AP^2+AM^2)*(WN^2)/32:AAM=(AP*AM)*(WN^2)/16
1066 AP1=AP:AM1=AM:TSP=SP:TSM=SM
1075 T1=CP*(S6-5*S2)+SM*6*S1:T2=CM*(S7+5*S4)+SP*6*S3
1076 H1=CP*(S6+3*S2)-SM*2*S1:H2=CM*(S7-3*S4)-SP*2*S3
1080 CLP(L)=-AAP*T1-AAM*T2:CLM(L)=-AAM*T1-AAP*T2
1085 T1=CM*6*N1-SP*(N6-7*N2):T2=CP*6*N3-SM*(N7+7*N4)
1087 TVN1(L)=CP*S2-SM*S1:TVN2(L)=-CM*S4-SP*S3
1090 IW=2:WF=2:GOSUB 105:IW=4:GOSUB 705:IW=2:GOSUB 725
1095 CLP(L)=CLP(L)-4*WN*(A(I,1)*A(I,2)+A(IP,1)*A(IP,2))-(3*WN/4)*(AP*TSP+AM*TSM)
1096 CLM(L)=CLM(L)-4*WN*(A(I,1)*A(I,2)-A(IP,1)*A(IP,2))-(3*WN/4)*(AM*TSP+AP*TSM)
1100 T3=CP*S6+SM*S1:T4=CM*S7+SP*S3
1101 H3=CPT*S6+SMT*S1:H4=CMT*S7+SPT*S3
1105 TP=(3/2)*(A(I,1)^3+A(IP,1)^3)*WN^2-AAP*T1-AAM*T2-AP1*WN*T3-AM1*WN*T4
1115 TM=(3/2)*(A(I,1)^3-A(IP,1)^3)*WN^2-AAM*T1-AAP*T2-AM1*WN*T3-AP1*WN*T4
1117 TPTP=(WN/4)*(AP*H1+AM*H2)-WN*(AP1*H3+AM1*H4)
1118 TMTM=(WN/4)*(AM*H1+AP*H2)-WN*(AM1*H3+AP1*H4)
1120 SLP(L)=TP+TPTP:SLM(L)=TM+TMTM
1125 TV1(L)=CP*S2-SM*S1:TV2(L)=-CM*S4-SP*S3
1127 TVN3(L)=CPT*S2-SMT*S1:TVN4(L)=-CMT*S4-SPT*S3
1130 IW=1:WF=1:GOSUB 105:GOSUB 705
1135 TV3=-SP*N6-CM*N1:TV4=-SM*N7-CP*N3
1140 T1=CLM(L)*N1+SLP(L)*N2:T2=CLP(L)*N3-SLM(L)*N4
1145 AA=A(I,1)*WN/2:AB=A(IP,1)*WN/2:AAAA=A(I,2)*WN/2:ABAB=A(IP,2)*WN/2
1149 XX=-AAAA*(TVN1(L)+TVN2(L))+AA*(TVN3(L)+TVN4(L))
1150 Y(IT,6)=Y(IT,6)+T1+T2+AA*(TV1(L)+TV2(L))+(AA^2)*(TV3+TV4)+XX
1154 XX=ABAB*(TVN1(L)-TVN2(L))-AB*(TVN3(L)-TVN4(L))
1155 Y(IT+2,6)=Y(IT+2,6)-T1+T2-AB*(TV1(L)-TV2(L))-(AB^2)*(TV3-TV4)+XX
1165 T1=-CLP(L)*S2+SLM(L)*S1:T2=CLM(L)*S4+SLP(L)*S3
1170 T9=CP*S6+SM*S1:T6=CM*S7+SP*S3
```

```
1171 H6=CM*3*N1+SP*(2*N6+N2):H7=CP*3*N3+SM*(2*N7-N4)
1175 WF=2:GOSUB 105:IW=4:GOSUB 705
1180 T3=3*CM*N1+SP*(4*N6-N2):T4=3*CP*N3+SM*(4*N7+N4)
1181 H8=CMT*3*N1+SPT*(4*N6-N2):H9=CPT*3*N3+SMT*(4*N7+N4)
1189 XX=-AAAA*(H6+H7)+AA*(H8+H9)
1190 Y(IT+1,6)=Y(IT+1,6)+T1+T2+AA*(T3+T4)+(AA^2)*(T9+T6)+XX
1195 TP=(M-2)*(M-1)/2*(3/2)*(TAU(IP,1)^3)/BHAT
1199 XX=ABAB*(H6-H7)-AB*(H8-H9)
1200 Y(IT+3,6)=Y(IT+3,6)-T1+T2-AB*(T3-T4)-(AB^2)*(T9-T6)+XX+TP
1205 NEXT
1210 IW=5:WF=1:AM=0:AP=0:GOSUB 405
1211 PRINT " 1-12-111";:GOSUB 5790
1215 FOR L=1 TO LLAST:II=L-1:LL=L:AA=A(II,1)*WN/4:SN=1
1220 IF L=LLAST THEN LL=LB:SN=-1
1225 T5=1/(2*MU(LL)*WN):IW=5:AM=0:AP=0:GOSUB 610
1230 I=LL-1:IW=1:WF=1:GOSUB 105
1235 TP=(1/2)*(CM*N1+SP*N2+SN*(CP*N3-SM*N4))
1240 IW=1:GOSUB 705
1250 TV3(LL)=CM*N1+SP*(2*N6-N2):TV4(LL)=CP*N3+SM*(2*N7+N4)
1255 PT=AA*(TV1(LL)+TVN3(LL)+SN*(TV2(LL)+TVN4(LL)))
1257 TPPT=-(A(II,2)*WN/4)*(TVN1(LL)+SN*TVN2(LL))
1260 Q(II,1)=Q(II,1)+TP+PT+TPPT-(AA^2)*(TV3(LL)+SN*TV4(LL))
1265 NEXT
1290 REM
1300 REM *********** THIRD WAVEFORM, 1ST AND 3RD ORDERS ***********
1305 IW=3:GOSUB 205
1307 T5=1/(2*MU(0)*WN):AA=A(0,1)*WN/2:TP=-(1/2)*(M-2)*(M-1)/2*(TAU(0,1)^3)/BHAT
1308 VNT=(A(0,2)/3)*(36*AA-4*WN*TAU(0,1)*T5)-(AA/3)*TAU(0,2)*T5
1309 VST=-A(0,2)*WN*(4/3)*SIG(0,1)*T5-(AA/3)*T5*SIG(0,2)
1310 Y(0,6)=Y(0,6)-(1/3)*AA*TAU(0,4)*T5+VNT
1315 Y(1,6)=Y(1,6)-(1/3)*AA*SIG(0,4)*T5-4*(AA^3)/WN+VST+TP
1320 L=LLAST:I=ILAST:J=2*I:T5=1/(2*MU(L)*WN):AA=A(I,1)*WN/2
1322 VNB=(A(I,2)/3)*(36*AA-4*WN*TAU(I,1)*T5)-(AA/3)*TAU(I,2)*T5
1323 VSB=-A(I,2)*WN*(4/3)*T5*SIG(I,1)-(AA/3)*T5*SIG(I,2)
1325 Y(J,6)=Y(J,6)-(1/3)*AA*TAU(I,4)*T5+VNB
1330 Y(J+1,6)=Y(J+1,6)-(1/3)*AA*SIG(I,4)*T5-4*(AA^3)/WN+VSB
1335 FOR L=1 TO LB:I=L-1:IP=I+1:IT=I*2:LL=L
1340 WF=1:IW=1:GOSUB 105:GOSUB 705
1341 AP1=AP:AM1=AM
1345 TV5=-CM*N1-SP*(3*N6-2*N2):TV6=-CP*N3-SM*(3*N7+2*N4)
1350 AAP=(AP^2+AM^2)*(WN^2)/96:AAM=(AP*AM)*(WN^2)/48
1355 T1=CP*(5*S6-9*S2)+SM*14*S1:T2=CM*(5*S7+9*S4)+SP*14*S3
1356 H1=(5*WN/12)*SP:H2=(5*WN/12)*SM
1357 H6=CP*(S6-5*S2)+SM*6*S1:H7=CM*(S7+5*S4)+SP*6*S3
1358 T11=CM*2*N1+SP*(5*N6-3*N2):T22=CP*2*N3+SM*(5*N7+3*N4)
1360 WF=2:IW=2:GOSUB 105:GOSUB 725:IW=4:GOSUB 705
1361 H3=(2*WN/3)*SPT:H4=(2*WN/3)*SMT
1364 CPCP=AP*H1+AM*H2+AP1*H3+AM1*H4+(4*WN/3)*(A(I,1)*A(I,2)+A(IP,1)*A(IP,2))
1365 CLP(L)=(2/3)*WN*(AP1*SP+AM1*SM)+AAP*T1+AAM*T2+CPCP
1369 CMCM=AM*H1+AP*H2+AM1*H3+AP1*H4+(4*WN/3)*(A(I,1)*A(I,2)-A(IP,1)*A(IP,2))
```

```
1370 CLM(L)=(2/3)*WN*(AM1*SP+AP1*SM)+AAM*T1+AAP*T2+CMCM
1372 H8=CPT*(S6-2*S2)+SMT*3*S1:H9=CMT*(S7+2*S4)+SPT*3*S3
1373 SPSP=-(WN/12)*(AP*H6+AM*H7)-(WN/3)*(AP1*H8+AM1*H9)
1374 SMSM=-(WN/12)*(AM*H6+AP*H7)-(WN/3)*(AM1*H8+AP1*H9)
1390 T3=CP*(S6-2*S2)+SM*3*S1:T4=CM*(S7+2*S4)+SP*3*S3
1391 APP=AAP*3:AMM=AAM*3
1392 AP3=A(I,1)^3+A(IP,1)^3:AM3=A(I,1)^3-A(IP,1)^3
1395 SLP(L)=-(1/6)*(WN^2)*AP3-APP*T11-AMM*T22-(AP1*T3+AM1*T4)*WN/3+SPSP
1400 SLM(L)=-(1/6)*(WN^2)*AM3-AMM*T11-APP*T22-(AM1*T3+AP1*T4)*WN/3+SMSM
1405 IW=1:WF=3:GOSUB 105
1406 T1=CLM(L)*N1+SLP(L)*N2:T2=CLP(L)*N3-SLM(L)*N4
1408 T7=-CLP(L)*S2+SLM(L)*S1:T8=CLM(L)*S4+SLP(L)*S3
1410 AA=A(I,1)*WN/2:AB=A(IP,1)*WN/2:AAAA=A(I,2)*WN/2:ABAB=A(IP,2)*WN/2
1419 XX=3*AAAA*(TVN1(L)+TVN2(L))+3*AA*(TVN3(L)+TVN4(L))
1420 Y(IT,6)=Y(IT,6)+T1+T2+3*AA*(TV1(L)+TV2(L))+(AA^2)*(TV5+TV6)+XX
1429 XX=-3*ABAB*(TVN1(L)-TVN2(L))-3*AB*(TVN3(L)-TVN4(L))
1430 Y(IT+2,6)=Y(IT+2,6)-T1+T2-3*AB*(TV1(L)-TV2(L))-(AB^2)*(TV5-TV6)+XX
1435 WF=2:GOSUB 105
1440 T3=CM*N1+SP*(4*N6-3*N2):T4=CP*N3+SM*(4*N7+3*N4)
1441 T88=CMT*N1+SPT*(4*N6-3*N2):T99=CPT*N3+SMT*(4*N7+3*N4)
1445 WF=1:GOSUB 105:IW=1:GOSUB 705:TP=-(1/2)*(M-2)*(M-1)/2*(TAU(IP,1)^3)/BHAT
1450 T9=CP*(S6-2*S2)+SM*3*S1:T6=CM*(S7+2*S4)+SP*3*S3
1451 T66=CM*N1-SP*(2*N6-3*N2):T77=CP*N3-SM*(2*N7+3*N4)
1454 XX=-AAAA*(T66+T77)+AA*(T88+T99)
1455 Y(IT+1,6)=Y(IT+1,6)+T7+T8+AA*(T3+T4)+(AA^2)*(T9+T6)+XX
1459 XX=ABAB*(T66-T77)-AB*(T88-T99)
1460 Y(IT+3,6)=Y(IT+3,6)-T7+T8-AB*(T3-T4)-(AB^2)*(T9-T6)+XX+TP
1465 NEXT
1470 IW=3:WF=3:AM=A(ILAST,3):AP=A(0,3):GOSUB 405
1471 PRINT " 3-3-12-111";:GOSUB 5790
1475 FOR L=1 TO LLAST:II=L-1:LL=L:SN=1:AA=A(II,1)*WN/4
1480 IF L=LLAST THEN LL=LB:SN=-1
1490 I=LL-1:IW=3:WF=3:GOSUB 105:GOSUB 610
1495 TP=(1/2)*(CM*N1+SP*N2+SN*(CP*N3-SM*N4))
1500 PT=3*AA*(TV1(LL)+TVN3(LL)+SN*(TV2(LL)+TVN4(LL)))
1510 TPPT=3*(A(II,2)*WN/4)*(TVN1(LL)+SN*TVN2(LL))
1520 Q(II,3)=TP+PT+TPPT-3*(AA^2)*(TV3(LL)+SN*TV4(LL))
1530 NEXT
1540 IF M=1 THEN 5000
1990 REM
1995 REM ************** FIRST WAVEFORM, 2ND ORDER ********************
2000 IW=6:GOSUB 205
2010 Y(1,6)=Y(1,6)+(3-M)*(M-1)*2*ABS(TAU(0,1))*TAU(0,1)*5*SQR(2)/(BHAT*8)
2020 FOR L=1 TO LB:I=L-1:LL=L:IP=I+1:IT=I*2
2030 TP=(3-M)*(M-1)*2*ABS(TAU(IP,1))*TAU(IP,1)*5*SQR(2)/(BHAT*8)
2040 Y(IT+3,6)=Y(IT+3,6)+TP
2050 NEXT
2060 IW=6:WF=1:AM=0:AP=0:GOSUB 405
2070 PRINT " 1-11";:GOSUB 5790
2075 IW=6:WF=1:GOSUB 775
```

```
2080 FOR L=1 TO LLAST:II=L-1:LL=L:SN=1
2090 IF L=LLAST THEN SN=-1:LL=LB
2100 T5=1/(2*MU(LL)*WN):IW=6:AP=0:AM=0:GOSUB 610:GOSUB 750
2110 I=LL-1:IW=6:WF=1:GOSUB 105
2120 TP=(1/2)*(CM*N1+SP*N2+SN*(CP*N3-SM*N4))
2130 Q(II,1)=Q(II,1)+TP
2140 NEXT
2290 REM
2295 REM *************** THIRD WAVEFORM, 2ND ORDER ****************************
2300 IW=7:GOSUB 205
2310 Y(1,6)=Y(1,6)-(3-M)*(M-1)*2*ABS(TAU(0,1))*TAU(0,1)*SQR(2)/(BHAT*8)
2320 FOR L=1 TO LB:I=L-1:LL=L:IP=I+1:IT=I*2
2330 TP=-(3-M)*(M-1)*2*ABS(TAU(IP,1))*TAU(IP,1)*SQR(2)/(BHAT*8)
2340 Y(IT+3,6)=Y(IT+3,6)+TP
2350 NEXT
2360 IW=7:WF=3:AM=0:AP=0:GOSUB 405
2370 PRINT " 3-11";:GOSUB 5790
2375 IW=7:WF=3:GOSUB 775
2380 FOR L=1 TO LLAST:II=L-1:LL=L:SN=1
2390 IF L=LLAST THEN SN=-1:LL=LB
2400 T5=1/(6*MU(LL)*WN):IW=7:AP=0:AM=0:GOSUB 610:GOSUB 750
2410 I=LL-1:IW=7:WF=3:GOSUB 105
2420 TP=(1/2)*(CM*N1+SP*N2+SN*(CP*N3-SM*N4))
2430 Q(II,3)=Q(II,3)+TP
2440 NEXT
2490 REM
2495 REM ***************** SECOND WAVEFORM, 3RD ORDER ***************
2500 IW=8:GOSUB 205
2510 AA=A(0,1)*WN/2
2530 Y(0,6)=Y(0,6)-AA*(SLAM(0,6)+SLAM(0,7))
2550 TP=(3-M)*(M-1)*2*ABS(TAU(0,1))*(TAU(0,2)+TAU(0,4))*8*SQR(2)/(BHAT*8)
2560 Y(1,6)=Y(1,6)-AA*(CLAM(0,6)+CLAM(0,7))+TP
2570 L=LLAST:I=ILAST:J=2*I
2580 AA=A(I,1)*WN/2
2600 Y(J,6)=Y(J,6)-AA*(SLAM(L,6)+SLAM(L,7))
2620 Y(J+1,6)=Y(J+1,6)-AA*(CLAM(L,6)+CLAM(L,7))
2630 FOR L=1 TO LB:I=L-1:LL=L:IP=I+1:IT=I*2
2640 IW=6:GOSUB 705:IW=7:GOSUB 725
2650 T1=SP+SPT:T2=SM+SMT
2660 IW=1:WF=1:GOSUB 105
2670 CLP(L)=(3*WN/8)*(AP*T1+AM*T2)
2680 CLM(L)=(3*WN/8)*(AM*T1+AP*T2)
2690 T1=-(WN/8)*(CP*(S6-3*S2)+SM*4*S1)
2700 T2=-(WN/8)*(CM*(S7+3*S4)+SP*4*S3)
2705 TVN5(LL)=CP*S2-SM*S1:TVN6(LL)=-CM*S4-SP*S3
2710 IW=1:WF=3:GOSUB 105
2720 T3=-(3*WN/8)*(CPT*(3*S6-S2)+SMT*4*S1)
2730 T4=-(3*WN/8)*(CMT*(3*S7+S4)+SPT*4*S3)
2740 SLP(L)=AP*(T1+T3)+AM*(T2+T4)
2750 SLM(L)=AM*(T1+T3)+AP*(T2+T4)
```

```
2760 TVN7(LL)=CPT*S2-SMT*S1:TVN8(LL)=-CMT*S4-SPT*S3
2765 T8=CMT*2*N1+SPT*(3*N6-N2):T9=CPT*2*N3+SMT*(3*N7+N4)
2770 IW=8:WF=2:GOSUB 105
2780 AA=A(I,1)*WN:AB=A(IP,1)*WN
2790 T1=CLM(L)*N1+SLP(L)*N2:T2=CLP(L)*N3-SLM(L)*N4
2800 T3=TVN5(LL)+TVN7(LL):T4=TVN6(LL)+TVN8(LL)
2810 Y(IT,6)=Y(IT,6)+T1+T2+AA*(T3+T4)
2820 Y(IT+2,6)=Y(IT+2,6)-T1+T2-AB*(T3-T4)
2830 T1=-CLP(L)*S2+SLM(L)*S1:T2=CLM(L)*S4+SLP(L)*S3
2835 TP=(3-M)*(M-1)*2*ABS(TAU(IP,1))*(TAU(IP,2)+TAU(IP,4))*8*SQR(2)/(BHAT*8)
2840 Y(IT+1,6)=Y(IT+1,6)+T1+T2+AA*(SP+SM+T8+T9)
2850 Y(IT+3,6)=Y(IT+3,6)-T1+T2-AB*(SP-SM+T8-T9)+TP
2860 NEXT
2870 IW=8:WF=2:AM=0:AP=0:GOSUB 405
2880 PRINT " 2-12-111";:GOSUB 5790
2890 FOR L=1 TO LLAST:II=L-1:LL=L:AA=A(II,1)*WN/2:SN=1
2900 IF L=LLAST THEN LL=LB:SN=-1
2910 T5=1/(4*MU(LL)*WN):IW=8:AM=0:AP=0:GOSUB 610
2920 I=LL-1:IW=8:WF=2:GOSUB 105
2930 TP=(1/2)*(CM*N1+SP*N2+SN*(CP*N3-SM*N4))
2940 TM=AA*(TVN5(LL)+TVN7(LL)+SN*(TVN6(LL)+TVN8(LL)))
2950 Q(II,2)=Q(II,2)+TP+TM
2960 NEXT
3190 REM
3195 REM ************* FOURTH WAVEFORM, 1ST AND 3RD ORDERS ***********
3200 IW=9:GOSUB 205
3210 AA=A(0,1)*WN/4
3220 TP=-(3-M)*(M-1)*2*ABS(TAU(0,1))*(TAU(0,2)+TAU(0,4))*3*SQR(2)/(BHAT*8)
3230 Y(0,6)=Y(0,6)-AA*SLAM(0,7)
3240 Y(1,6)=Y(1,6)-AA*CLAM(0,7)+TP
3250 L=LLAST:I=ILAST:J=2*I:AA=A(I,1)*WN/4
3260 Y(J,6)=Y(J,6)-AA*SLAM(L,7)
3270 Y(J+1,6)=Y(J+1,6)-AA*CLAM(L,7)
3280 FOR L=1 TO LB:I=L-1:IP=I+1:IT=I*2:LL=L
3290 IW=7:GOSUB 705
3300 IW=1:GOSUB 150
3310 CLP(L)=(15*WN/16)*(AP*SP+AM*SM)
3320 CLM(L)=(15*WN/16)*(AM*SP+AP*SM)
3330 IW=1:WF=3:GOSUB 105
3340 T1=CP*(3*S6-5*S2)+SM*8*S1:T2=CM*(3*S7+5*S4)+SP*8*S3
3350 SLP(L)=-(3*WN/16)*(AP*T1+AM*T2)
3360 SLM(L)=-(3*WN/16)*(AM*T1+AP*T2)
3361 T8=CM*N1+SP*(3*N6-2*N2):T9=CP*N3+SM*(3*N7+2*N4)
3365 IW=1:WF=4:GOSUB 105
3370 T1=CLM(L)*N1+SLP(L)*N2:T2=CLP(L)*N3-SLM(L)*N4
3380 Y(IT,6)=Y(IT,6)+T1+T2+(AP+AM)*WN*(TVN7(LL)+TVN8(LL))
3390 Y(IT+2,6)=Y(IT+2,6)-T1+T2-(AP-AM)*WN*(TVN7(LL)-TVN8(LL))
3400 T1=-CLP(L)*S2+SLM(L)*S1:T2=CLM(L)*S4+SLP(L)*S3
3410 Y(IT+1,6)=Y(IT+1,6)+T1+T2+((AP+AM)/2)*WN*(T8+T9)
3420 TP=-(3-M)*(M-1)*2*ABS(TAU(IP,1))*(TAU(IP,2)+TAU(IP,4))*3*SQR(2)/(BHAT*8)
```

```
3430 Y(IT+3,6)=Y(IT+3,6)-T1+T2-((AP-AM)/2)*WN*(T8-T9)+TP
3440 NEXT
3450 IW=9:WF=4:AP=A(0,4):AM=A(ILAST,4):GOSUB 405
3460 PRINT " 4-4-12-111";:GOSUB 5790
3470 FOR L=1 TO LLAST:II=L-1:LL=L:SN=1:AA=A(II,1)*WN
3480 IF L=LLAST THEN LL=LB:SN=-1
3490 I=LL-1:IW=9:WF=4:GOSUB 105:GOSUB 610
3500 TP=(1/2)*(CM*N1+SP*N2+SN*(CP*N3-SM*N4))
3510 Q(II,4)=TP+AA*(TVN7(LL)+SN*TVN8(LL))
3520 NEXT
4999 REM
5000 REM ***************** CALCULATE AMPLITUDES ******************
5050 I=INT(ILAST/2):J=1:IF IN=1 THEN J=0
5100 TM=(1/SX)*(A(I,1)-Q(I,1))
5102 ATEST=A(I,1)-DS*TM+J*(DS/2)*(TM-DAO(I,1)):ALTEST=ATEST*WN
5110 IF ABS(ALTEST)>1 THEN LPRINT:LPRINT "SLOPE TOO LARGE":SX=SX-DS:GOTO 9999
5115 IF (ATEST/AINIT)-AMPLIF<0 THEN SX=SX-DS:GOTO 9999
5116 AMPLIF=ATEST/AINIT
5120 FOR I=0 TO ILAST:FOR IW=1 TO 4:DADSX(I,IW)=(1/SX)*(A(I,IW)-Q(I,IW))
5130 A(I,IW)=A(I,IW)-DS*DADSX(I,IW)+J*(DS/2)*(DADSX(I,IW)-DAO(I,IW))
5140 DAO(I,IW)=DADSX(I,IW):NEXT:NEXT
5150 GOSUB 8301
5160 IF INT(IN/10)>IMAX THEN GOSUB 8000
5170 IF INT((ATN(ALTEST)*180/PI)/IISL)>IIMAX THEN GOSUB 8001:IISL=IISL+2.5
5171 IF IISL>35 THEN 10500
5270 DS=(SX^2)*DSS*AINIT/ATEST
5275 REM *** INCREASE STRETCH OR EXIT PROGRAM ************
5280 IF IN>=NN THEN 5290 ELSE 305
5290 PRINT:PRINT "STEPS FINISHED."
5300 PRINT "TO QUIT, TYPE <Q>. TO CONTINUE, TYPE <C> AND ENTER NO. OF STEPS"
5310 A$=INKEY$:IF A$="" THEN 5310
5320 IF A$="Q" THEN 10500
5330 IF A$="C" THEN PRINT:PRINT "NN=";NN:INPUT "NEW NN";NN:IF NN>IN THEN 305
5340 PRINT "NEW NN<IN--QUIT":GOTO 9999
5345 REM
5346 REM *************** READ IN DATA FOR MULTILAYER ************
5350 DEFINT I,J,L:DEFDBL Y,E
5360 I=0:J=0
5370 INPUT "LAYS=";LAYS:LLAST=LAYS-1:ILAST=LLAST-1:LB=LLAST-1
5380 L=LLAST
5385 DIM T(L),TAU(L,10),MU(L),A(L,4),K(L),SIG(L,10),Q(L,4),IZ(L),DAO(L,4)
5390 DIM Y(2*L-1,6),CLAMP(L,10),CLAMM(L,10),SLAMP(L,10),SLAMM(L,10),DADSX(L,4)
5395 DIM CLAM(L,9),SLAM(L,9)
5400 DIM CLP(L),CLM(L),SLP(L),SLM(L),TV1(L),TV2(L),TV3(L),TV4(L),TV5(L),TV6(L)
5410 DIM TVN1(L),TVN2(L),TVN3(L),TVN4(L)
5415 DIM TVN5(L),TVN6(L),TVN7(L),TVN8(L)
5420 PI=3.141592653589793#:E=2.718281828459045#
5430 INPUT "MAXIMUM THICKENING(T/TO)";SZ
5440 INPUT "MAX. INITIAL SLOPE (DEGS.)";DEGSLOPE
5450 SLOPE=TAN(DEGSLOPE*PI/180)
```

```
5460 INPUT "T(1)/T(2) LAYERS=";T2
5470 INPUT "MU(1)/MU(2) LAYERS=";MU2
5480 INPUT "MU(U.M.)/MU(2)=";MU(0)
5490 INPUT "MU(L.M.)/MU(2)=";MU(LLAST)
5500 FOR I=2 TO LB STEP 2:T(I)=1:MU(I)=1:NEXT
5510 FOR I=1 TO LB STEP 2:T(I)=T2:MU(I)=MU2:NEXT
5520 SCALE=T(1):TT=0:FOR L=1 TO LB:T(L)=T(L)/(SZ*SCALE):TT=TT+T(L):NEXT
5530 LPRINT:LPRINT "LENGTH SCALE=";SCALE
5540 MMU=MU(1):FOR L=0 TO LLAST:MU(L)=MU(L)/MMU:NEXT
5550 LPRINT:LPRINT "LAY NO","MU(L)/MU(1)","T(L)/SCALE","T(L) INITIAL"
5560 FOR L=0 TO LLAST:LPRINT L,MU(L),T(L),T(L)*SCALE:NEXT
5570 INPUT "ANISO";ANISO:LPRINT "ANISOTROPY (ETA N/ETA S)=";ANISO
5580 ULMUC=10000000#:INPUT "MUC";MUC
5590 INPUT "POWERLAW EXP M (1, 2, OR 3)=";M
5595 LPRINT "POWERLAW EXPONENT M =";M
5600 BHAT=M*(4*SLOPE)^(M-1)/(ANISO-1)
5610 LPRINT "MUC=";MUC,"BHAT=";BHAT
5620 INPUT "NO. DEF. STEPS";NN:LPRINT "ORIG. NO. DEF. STEPS=";NN
5630 DSFACT=60:DS=(1/SZ-1)/DSFACT:DSS=DS:LPRINT "DS=(1/SZ-1)/";DSFACT
5640 LPRINT "FINAL TOTAL THICK";TT*SZ*SCALE,"INIT TOTAL THICK=";TT*SCALE
5650 INPUT "INIT WL-TO-SINGLE-THICK=";WLINIT
5655 LPRINT "INIT WL-TO-SINGLE-THICK=";WLINIT
5660 WL=WLINIT*TT/(LAYS-2):LPRINT "INITIAL WL=";WL*SCALE
5670 LPRINT "FINAL WL=";WL*SCALE/SZ
5680 LPRINT "FINAL WL/TT=";WL/(TT*SZ^2),"INITIAL WL/TT=";WL/(TT)
5690 LPRINT:LPRINT "SZZ",SZ
5700 LPRINT "MAX. INITIAL SLOPE";DEGSLOPE;"DEGS."
5705 INPUT "(L/T) RATIO AT WHICH EIGEN IS CALCULATED=";EIGENWL
5710 FOR I=0 TO INT(ILAST/2):PRINT "I=";I;:INPUT "A(I,1)=";A(I,1)
5720 A(ILAST-I,1)=A(I,1):NEXT
5730 FOR I=0 TO ILAST:A(I,1)=(A(I,1)/(SZ*SCALE))*(WLINIT/EIGENWL):LPRINT I,A(I,1)*SCALE:NEXT
5740 AINIT=SLOPE*WL/(2*PI):REM I=INT(ILAST/2):A(I,1)=AINIT
5750 REM FOR I=0 TO ILAST:A(I,1)=AINIT:LPRINT "I,A(I,1)";I,A(I,1)*SCALE:NEXT
5760 LPRINT "INITIAL AMPLITUDE";AINIT*SCALE
5770 AMPLIF=0
5780 RETURN
5782 REM ************************************************
5783 REM ******** SUBROUTINE TO LPRINT ARRAYS **************
5790 RETURN:FOR IK=0 TO 2*ILAST+1:LPRINT:FOR IL=0 TO 6
5800 U=Y(IK,IL):LPRINT U;
5810 NEXT:NEXT
5820 LPRINT
5830 RETURN
7900 REM ******* END SUB ************
7950 REM ********************* LPRINT AMPLITUDES ********************
8000 IMAX=INT(IN/10)
8001 LPRINT:LPRINT "AMPLITUDES**DEF. STEP=" IN;"D SX=";DS;"SX=";SX;"SZ=";1/SX
8002 LPRINT "CURR. WL=";WL*SX*SCALE;"CURR. WL/T=";WL*SX^2/T(1)
8004 LPRINT "CURR. WN=";WN/SCALE;"CURR. T(1)=";T(1)*SCALE/SX:LPRINT
8005 FOR I=0 TO INT(ILAST/2):LPRINT TAB(0) I;:FOR IW=1 TO 4
```

```
8006 LPRINT TAB(5+18*(IW-1)) A(I,IW)*SCALE;:NEXT:NEXT
8010 I=INT(ILAST/2):ALZ=A(I,1)*WN
8030 ANEFF=(M*(4*ALZ)^(M-1)/BHAT)+1
8040 LPRINT:LPRINT:LPRINT "ANEFF=";ANEFF,"SLOPE(1ST WF,MID)=";ALZ
8050 A1MID=A(I,1)
8060 LPRINT "AMPLIF. 1ST WF=";A1MID/AINIT
8070 LPRINT "A2(0)/A1(MID)=";A(0,2)/A1MID;"A3(MID)/A1(MID)=";A(I,3)/A1MID
8075 LPRINT "A4(0)/A1(MID)=";A(0,4)/A1MID
8080 RETURN
8095 REM
8096 REM ***************** PRINT AMPLITUDES *************
8301 PRINT:PRINT "AMPLITUDES**DEF. STEP=" IN;"D SX=";DS;"SX=";SX;"SZ=";1/SX
8302 PRINT "CURR. WL=";WL*SX*SCALE;"CURR. WL/T=";WL*SX^2/T(1)
8304 PRINT "CURR. WN=";WN/SCALE;"CURR. T(1)=";T(1)*SCALE/SX:PRINT
8305 FOR I=0 TO INT(ILAST/2):PRINT TAB(0) I;:FOR IW=1 TO 4
8306 PRINT TAB(5+18*(IW-1)) A(I,IW)*SCALE;:NEXT:NEXT
8310 I=INT(ILAST/2):ALZ=A(I,1)*WN
8330 ANEFF=(M*(4*ALZ)^(M-1)/BHAT)+1
8340 PRINT:PRINT:PRINT "ANEFF=";ANEFF,"SLOPE(1ST WF,MID)=";ALZ
8350 A1MID=A(I,1)
8360 PRINT "AMPLIF. 1ST WF=";A1MID/AINIT
8370 PRINT "A2(0)/A1(MID)=";A(0,2)/A1MID;"A3(MID)/A1(MID)=";A(I,3)/A1MID
8375 PRINT "A4(0)/A1(MID)=";A(0,4)/A1MID
8380 RETURN
9999 GOSUB 8001
10500 END
```

```
REM
REM
REM **********DEFINITIONS OF L AND I NUMBERS********
REM
REM                     THICK OVERBURDEN  L=0
REM
REM --------I = 0 ----------------------------------------
REM                      L = 1
REM --------I = 1 ----------------------------------------
REM                      L = 2
REM --------I = 2 ----------------------------------------
REM                      L = 3     L = LB
REM --------I = 3   I = ILAST-----------------------------
REM
REM       L=4        L=LLAST    THICK SUBSTRATUM
REM
REM
REM ****************DEFINITION OF MATRIX*******************
REM   THE STANDARD MATRIX WOULD BE AS FOLLOWS:
REM
REM            SIG  TAU  SIG  TAU  SIG  TAU  SIG  TAU  DRIVING
REM
REM            J=0  J=1  J=2  J=3  J=4  J=5  J=6  J=7  J=8
REM II=0:VN    IP   XX   X    X    0    0    0    0    XX
REM II=1:VS    XX   IP   X    X    0    0    0    0    XX
REM II=2:VN    X    X    IP   XX   X    X    0    0    XX
REM II=3:VS    X    X    XX   IP   X    X    0    0    XX
REM II=4 VN    0    0    X    X    IP   XX   X    X    XX
REM II=5 VS    0    0    X    X    XX   IP   X    X    XX
REM II=6 VN    0    0    0    0    X    X    IP   XX   XX
REM II=7 VS    0    0    0    0    X    X    XX   IP   XX
REM
REM   NOTE:IP IS PIVOT
REM
REM
REM THE CONDENSED MATRIX USED IN THIS PROGRAM IS AS FOLLOWS:
REM
REM                                           DRIVING
REM            J=0  J=1  J=2  J=3  J=4  J=5  J=6
REM II=0:VN    NULL NULL IP   XX   X    X    XX
REM II=1:VS    NULL NULL XX   IP   X    X    XX
REM II=2:VN    X    X    IP   XX   X    X    XX
REM II=3:VS    X    X    XX   IP   X    X    XX
REM II=4:VN    X    X    IP   XX   X    X    XX
REM II=5:VS    X    X    XX   IP   X    X    XX
REM II=6:VN    X    X    IP   XX   NULL NULL XX
REM II=7:VS    X    X    XX   IP   NULL NULL XX
REM
REM ********************END**************************
```

```
1 REM LAYER-PARALLEL SHORTENING OF INFINITELY THICK MULTILAYER
2 REM 3RD ORDER ANALYSIS
2 DEFINT I:DEFDBL E,P
5 WIDTH LPRINT 80
10 LPRINT "<INFMULT.BAS>"
11 PI=3.141592653589793#:E=2.718281828459045#
20 INPUT "NN";NN:LPRINT "NUMBER OF STEPS";NN
25 JK=0:KJ=0
30 DIM SX(NN),A1(NN),A3(NN),AA(NN),AB(NN),AC(NN)
33 INPUT "MAX. SLOPE=";AL:LPRINT "INITIAL SLOPE=";AL
35 INPUT "ANISO=";ANISO:LPRINT "ANISOTROPY (ETA N/ETA S)=";ANISO
37 BHAT=12*(AL^2)/(ANISO-1):LPRINT "BHAT=";BHAT
38 BHATAL=(AL^2)/BHAT:LPRINT "(AL^2)/BHAT=";BHATAL
39 INPUT "SXF";SXF:LPRINT "SXF=";SXF
40 TF=1:SCALE=TF:T0=TF*SXF/SCALE
42 FOR WLT=1 TO 10:LPRINT:LPRINT "INITIAL L/T=";WLT
43 AINIT=WLT*AL*T0*SCALE/(2*PI):LPRINT "INIT AMP=";AINIT
60 K1=PI/WLT:K2=2*K1:K3=3*K1
61 E1=E^K1:E2=1/(E^K1):E3=E^K3:E4=1/(E^K3):E5=E^K2:E6=1/(E^K2)
62 S1=(E1-E2)/2:S3=(E3-E4)/2:S2=(E5-E6)/2
63 CH1=(E1+E2)/2:CH3=(E3+E4)/2:CH2=(E5+E6)/2
64 SC1=S1*CH1:SKM=SC1-K1:SKP=SC1+K1
67 T1=SXF^2+(48*BHATAL*K1^2/S1^2)*(SXF^2-1)
68 IF T1<0 THEN LPRINT "T1<0":GOTO 72
69 W1=1/SQR(T1):W3=((S1^2)/(S3^2))*((1/SXF)-W1)
70 LPRINT "T1=";T1 TAB(20) "W1=";W1 TAB(40) "W3=";W3
72 T2=2*(1+2*K1/SKM):T3=(AL^2)/(2*SKM*SKP)
73 T4=4*SC1^2+SC1*K1+K1^2-2*S1^2*(CH2/S2)*SKM
75 T6=((SXF^T2)+T3*T4*(1-(SXF^T2)))
76 V1=1/SQR(T6)
77 LPRINT "T6=";T6 TAB(20) "V1=";V1
78 LPRINT:LPRINT "STEP" TAB(6) "SX" TAB(18) "SZ" TAB(30) "WLTC" TAB(42) "WL"
79 LPRINT "TYPE" TAB(6) "CURR AL" TAB(18) "1A/1A0";
80 LPRINT TAB(32) "2A/1A0" TAB(39) "3A/1A0" TAB(52) "Q11" TAB(66) "Q13"
81 LPRINT TAB(39) "FS:     Q1,Q31,Q33"
82 LPRINT TAB(18) "A1" TAB(32) "A2" TAB(39) "A3" TAB(53) "A2/A1" TAB(60) "A3/A1"
83 SX(0)=1:A1(0)=1:A3(0)=0:AA(0)=1:AB(0)=0:AC(0)=0
84 IMAX=-1
85 H=(SXF-1)/NN
87 FOR I=0 TO NN-1
88 IF JK=1 AND KJ=1 THEN GOTO 999
89 SX(I)=SX(0)+I*H
90 SXC=SX(I):SXB=SXC:A1C=A1(I):A3C=A3(I):GOSUB 500:GOSUB 600
91 AAC=AA(I):ABC=AB(I):ACC=AC(I):GOSUB 700
95 WLT1=WLTC:GOSUB 800
100 C1=DA1DSX*H:Z1=DA3DSX*H:F1=DA1*H:G1=DA2*H:J1=DA3*H
110 SXC=SX(I)+H/2:A1C=A1(I)+C1/2:A3C=A3(I)+Z1/2:GOSUB 500:GOSUB 600
111 AAC=AA(I)+F1/2:ABC=AB(I)+G1/2:ACC=AC(I)+J1/2:GOSUB 700
120 C2=DA1DSX*H:Z2=DA3DSX*H:F2=DA1*H:G2=DA2*H:J2=DA3*H
130 A1C=A1(I)+C2/2:A3C=A3(I)+Z2/2:GOSUB 600
```

```
131 AAC=AA(I)+F2/2:ABC=AB(I)+G2/2:ACC=AC(I)+J2/2:GOSUB 700
140 C3=DA1DSX*H:Z3=DA3DSX*H:F3=DA1*H:G3=DA2*H:J3=DA3*H
150 SXC=SX(I)+H:A1C=A1(I)+C3:A3C=A3(I)+Z3:GOSUB 500:GOSUB 600
151 AAC=AA(I)+F3:ABC=AB(I)+G3:ACC=AC(I)+J3:GOSUB 700
160 C4=DA1DSX*H:Z4=DA3DSX*H:F4=DA1*H:G4=DA2*H:J4=DA3*H
170 A1(I+1)=A1(I)+(1/6)*(C1+2*C2+2*C3+C4)
175 A3(I+1)=A3(I)+(1/6)*(Z1+2*Z2+2*Z3+Z4)
177 IF A1(I+1)>1000000! THEN LPRINT:LPRINT "POWER OVERFLOW AT SX=";SXB:A1(I+1)=1:A3(I+1)=0:JK=1
180 AA(I+1)=AA(I)+(1/6)*(F1+2*F2+2*F3+F4)
182 AB(I+1)=AB(I)+(1/6)*(G1+2*G2+2*G3+G4)
184 AC(I+1)=AC(I)+(1/6)*(J1+2*J2+2*J3+J4)
185 IF AA(I+1)>1000000! THEN LPRINT:LPRINT "FREE OVERFLOW AT SX=";SXB:AA(I+1)=1:AB(I+1)=0:AC(I+1)=0:KJ=1
186 IF Q1FS<0 THEN LPRINT:LPRINT "Q1FS < 0 AT SX=";SXB:AA(I+1)=1:AB(I+1)=0:AC(I+1)=0:KJ=1
188 IF I=NN-1 THEN GOTO 205
189 IF JK=1 AND KJ=1 THEN GOTO 205
190 IF INT(I/40)<=IMAX THEN 216
191 IMAX=INT(I/40)
200 PRINT I;
205 LPRINT:LPRINT I TAB(6) SXB TAB(18) 1/SXB TAB(30) WLTI TAB(42) CURRWL
206 IF KJ=1 AND JK=1 THEN GOTO 209
207 IF KJ=1 THEN GOTO 212
209 LPRINT "FS" TAB(4) ALC TAB(18) AA(I) TAB(32) AB(I) TAB(38) AC(I) TAB(52) Q11FS TAB(66) Q13FS
210 LPRINT TAB(39) Q1FS TAB(53) Q31FS TAB(67) Q33FS
211 LPRINT TAB(18) AA(I)*AINIT TAB(32) AB(I)*AINIT TAB(39) AC(I)*AINIT TAB(53) AB(I)/AA(I) TAB(60) AC(I)/AA(I)
212 IF KJ=1 AND JK=1 THEN GOTO 214
213 IF JK=1 THEN GOTO 216
214 LPRINT:LPRINT "PL" TAB(4) ALD TAB(18) A1(I) TAB(32) "---" TAB(38) A3(I) TAB(52) Q1PL TAB(66) Q3PL
215 LPRINT TAB(18) A1(I)*AINIT TAB(32) "---" TAB(39) A3(I)*AINIT TAB(53) "---" TAB(60) A3(I)/A1(I)
216 NEXT I
217 REM LPRINT:LPRINT I TAB(6) SXB TAB(18) WLTI
218 REM LPRINT "FS" TAB(4) ALC TAB(18) AA(I) TAB(32) AB(I) TAB(38) AC(I) TAB(52) Q11FS TAB(66) Q13FS
219 REM LPRINT TAB(39) Q1FS TAB(53) Q31FS TAB(67) Q33FS
220 REM LPRINT "PL" TAB(4) ALD TAB(18) A1(I) TAB(32) "---" TAB(38) A3(I) TAB(52) Q1PL TAB(66) Q3PL
230 REM LPRINT:LPRINT "POWER A3/A1=";A3(I)/A1(I),"FREE AC/AA=";AC(I)/AA(I)
235 REM LPRINT "W1=";W1,"W3=";W3
449 NEXT
450 GOTO 999
500 WLTC=WLT*SXC^2:K1=PI/WLTC:K2=2*K1:K3=3*K1
505 E1=E^K1:E2=1/(E^K1):E3=E^K3:E4=1/(E^K3):E5=E^K2:E6=1/(E^K2)
510 S1=(E1-E2)/2:S2=(E5-E6)/2:S3=(E3-E4)/2
511 CH1=(E1+E2)/2:CH2=(E5+E6)/2:CH3=(E3+E4)/2:RETURN
600 IF JK=1 THEN DA1DSX=0:DA3DSX=0:RETURN
605 DA1DSX=-(A1C/SXC)*(1+(48/SXC^2)*((A1C*K1/S1)^2)*BHATAL)
610 DA3DSX=(1/SXC)*(-A3C+(48/SXC^2)*(A1C^3)*((K1/S3)^2)*BHATAL)
620 RETURN
700 IF KJ=1 THEN DA1=0:DA2=0:DA3=0:RETURN
701 SC1=S1*CH1:SC3=S3*CH3:SK1=SC1-K1:SK3=SC3-K3
705 TP=(4*(SC1^2)+SC1*K1+(K1^2)-2*(S1^2)*(CH2/S2)*SK1)/(2*(SK1^2))
710 DA1=-(AAC/SXC)*(1+(2*K1/SK1)-((AAC^2)*(AL^2)/(SXC^2))*TP)
720 DA2=-(ABC/SXC)*(1+(2*K2/(S2*CH2-K2)))
```

```
725 TP=4*S1^2*CH2/S2*(3*SC3-K1)+5*SC1*K1-2*K1^2+SC3*K3-6*CH3*S1*(CH3*S1+CH1*S3)
730 TX=((AAC^3)*(AL^2)/((SXC^3)*4*SK3*SK1))*TP
740 DA3=-(ACC/SXC)*(1+2*K3/SK3)-TX
750 RETURN
800 ALC=AA(I)*AL/SXC:ALD=A1(I)*AL/SXC
801 CURRWL=WLT*TO*SXC
805 Q11FS=2*K1/SK1
810 TP=(4*(SC1^2)+SC1*K1+(K1^2)-2*(S1^2)*(CH2/S2)*SK1)/(2*(SK1^2))
815 Q13FS=-(ALC^2)*TP
820 Q1FS=Q11FS+Q13FS
825 Q31FS=2*K3/SK3
830 TM=4*(S1^2)*(CH2/S2)*(3*SC3-K1)+5*SC1*K1-2*(K1^2)+SC3*K3-6*S1*CH3*(CH1*S3+CH3*S1)
835 Q33FS=(ALC^2)*TM/(4*SK1*SK3)
840 Q1PL=((ALD^2)/BHAT)*48*(K1/S1)^2
845 Q3PL=-((ALD^2)/BHAT)*48*(K1/S3)^2
850 RETURN
999 END
```

```
1 REM LAYER-PARALLEL SHORTENING AND SHEAR
2 REM 2ND ORDER ANALYSIS
5 WIDTH LPRINT 80
6 WIDTH 80
10 LPRINT "<SHEAR.BAS>":GOTO 3000
100 REM ***************CALCULATION OF TRIG FUNCTIONS *******************
105 T5=1/(2*WN*WF*MU(LL)):K1=WF*K(LL)
110 EM=1/(E^K1):EP=E^K1:CH=(EP+EM)/2:SH=(EP-EM)/2
115 TM1=CH*SH-K1:TP1=CH*SH+K1
120 N1=(CH^2)/(2*TM1):N2=K1/(2*TM1):N3=(SH^2)/(2*TP1):N4=K1/(2*TP1)
125 S1=(CH^2)/(2*TP1):S2=K1/(2*TP1):S3=(SH^2)/(2*TM1):S4=K1/(2*TM1)
130 N6=SH*CH/(2*TM1):N7=SH*CH/(2*TP1):S6=SH*CH/(2*TP1):S7=SH*CH/(2*TM1)
135 NP1=(N1+N3)*T5:NM1=(N1-N3)*T5:NP2=(N2+N4)*T5:NM2=(N2-N4)*T5
140 SP1=(S1+S3)*T5:SM1=(S1-S3)*T5:SP2=(S2+S4)*T5:SM2=(S2-S4)*T5
150 RETURN
200 REM ****************CLEAR MATRIX; SET SG*********************************
205 FOR I=0 TO ILAST*2+1:FOR J=0 TO 6:Y(I,J)=0:NEXT:NEXT
210 SG=1:IF NS=2 THEN SG=-1
211 RETURN
400 REM ***************FILL COLUMNS 0-5 OF MATRIX, SOLVE MATRIX ***************
405 L=0:I=0:T5=1/(2*WN*WF*MU(0))
410 Y(0,2)=Y(0,2)-T5:Y(1,3)=Y(1,3)-T5-RPRIME*T(LN)/(SX*MU(LN))
415 L=LLAST:I=L-1:T5=1/(2*WN*WF*MU(LLAST)):II=2*I
420 Y(II,2)=Y(II,2)-T5:Y(II+1,3)=Y(II+1,3)-T5
425 FOR L=1 TO LB:I=L-1:LL=L:GOSUB 105:IT=I:IB=L:I=2*IT
435 Y(I,2)=Y(I,2)-NP1:Y(I,3)=Y(I,3)-SG*NM2:Y(I,4)=Y(I,4)+NM1
440 Y(I,5)=Y(I,5)-SG*NP2:I=I+1
445 Y(I,2)=Y(I,2)+SG*SM2:Y(I,3)=Y(I,3)-SP1:Y(I,4)=Y(I,4)+SG*SP2
450 Y(I,5)=Y(I,5)+SM1:I=IB*2
455 Y(I,0)=Y(I,0)+NM1:Y(I,1)=Y(I,1)+SG*NP2:Y(I,2)=Y(I,2)-NP1
460 Y(I,3)=Y(I,3)+SG*NM2:I=I+1
465 Y(I,0)=Y(I,0)-SG*SP2:Y(I,1)=Y(I,1)+SM1:Y(I,2)=Y(I,2)-SG*SM2
470 Y(I,3)=Y(I,3)-SP1-RPRIME*T(LN)/(SX*MU(LN))
475 NEXT
480 FOR L=1 TO LLAST:IT=L-1:IB=L:IP=2*IT:YY=1/(Y(IP,2)):I=IP
485 FOR J=2 TO 6:Y(I,J)=Y(I,J)*YY:NEXT:IP1=I+1:IP2=I+2:IP3=I+3
490 FOR J=3 TO 6:Y(IP1,J)=Y(IP1,J)-Y(IP1,2)*Y(I,J):NEXT:Y(IP1,2)=0
495 IF L=LLAST THEN Y(IP1,6)=Y(IP1,6)/Y(IP1,3):Y(IP1,3)=1:GOTO 545
500 FOR IJ=IP2 TO IP3:FOR J=1 TO 3:Y(IJ,J)=Y(IJ,J)-Y(IJ,0)*Y(IP,J+2):NEXT
505 Y(IJ,6)=Y(IJ,6)-Y(IJ,0)*Y(IP,6)
510 Y(IJ,0)=0:NEXT
515 IP=IP+1:YY=1/Y(IP,3):I=IP
520 FOR J=3 TO 6:Y(I,J)=Y(I,J)*YY:NEXT
525 IP1=I+1:IP2=I+2:FOR IJ=IP1 TO IP2:FOR J=2 TO 3
530 Y(IJ,J)=Y(IJ,J)-Y(IJ,1)*Y(IP,J+2):NEXT
535 Y(IJ,6)=Y(IJ,6)-Y(IJ,1)*Y(IP,6):Y(IJ,1)=0
540 NEXT
545 NEXT
550 IP=2*LB:Y(IP,6)=Y(IP,6)-Y(IP+1,6)*Y(IP,3):Y(IP,3)=0
555 FOR L=LB-1 TO 0 STEP -1:IP=2*L+1
560 Y(IP,6)=Y(IP,6)-Y(IP,4)*Y(IP+1,6)-Y(IP,5)*Y(IP+2,6)
565 Y(IP,4)=0:Y(IP,5)=0:IP=IP-1
```

```
570 Y(IP,6)=Y(IP,6)-Y(IP,3)*Y(IP+1,6)-Y(IP,4)*Y(IP+2,6)-Y(IP,5)*Y(IP+3,6)
575 FOR IK=3 TO 5:Y(IP,IK)=0:NEXT:NEXT
580 FOR I=0 TO ILAST:J=2*I:JP1=J+1
585 SIG(I,WF,NS,OA)=Y(J,6):TAU(I,WF,NS,OA)=Y(JP1,6)
590 NEXT
595 RETURN
599 REM ***** CALCULATE MEDIA LAMBDAS (AS CLAMP, ETC.)************************
600 L=LLAST:I=ILAST
601 T50=1/(2*WN*WF*MU(0)):T5L=1/(2*WN*WF*MU(L))
603 CLAMP(0,WF,NS,OA)=SIG(0,WF,NS,OA)*T50+SG*MNSH*A(0,WF,NS+SG)/MU(0)
605 SLAMP(0,WF,NS,OA)=SG*TAU(0,WF,NS,OA)*T50-2*A(0,WF,NS)
610 CLAMM(0,WF,NS,OA)=CLAMP(0,WF,NS,OA):SLAMM(0,WF,NS,OA)=SLAMP(0,WF,NS,OA)
615 CLAMP(L,WF,NS,OA)=SIG(I,WF,NS,OA)*T5L+SG*MNSH*A(I,WF,NS+SG)/MU(L)
620 SLAMP(L,WF,NS,OA)=SG*TAU(I,WF,NS,OA)*T5L-2*A(I,WF,NS)
625 CLAMM(L,WF,NS,OA)=CLAMP(L,WF,NS,OA):SLAMM(L,WF,NS,OA)=SLAMP(L,WF,NS,OA)
630 RETURN
634 REM ************ CALCULATE LAYER LAMBDA PAIRS (AS CP, ETC.) *************
635 ITT=LL-1
639 TP=SG*MNSH*APO/MU(LL):TM=SG*MNSH*AMO/MU(LL)
640 CP=(SIG(ITT,WF,NS,OA)+SIG(LL,WF,NS,OA))*T5+CLP(LL,WF,NS,OA)+TP
645 CM=(SIG(ITT,WF,NS,OA)-SIG(LL,WF,NS,OA))*T5+CLM(LL,WF,NS,OA)+TM
650 SP=SG*(TAU(ITT,WF,NS,OA)+TAU(LL,WF,NS,OA))*T5+SLP(LL,WF,NS,OA)-2*APS
655 SM=SG*(TAU(ITT,WF,NS,OA)-TAU(LL,WF,NS,OA))*T5+SLM(LL,WF,NS,OA)-2*AMS
660 RETURN
700 REM ********** RETRIEVE CLAMP'S FOR SPECIFIC LAYER IN CP SHORTHAND *******
705 CP(NS)=CLAMP(LL,WF,NS,OA):CM(NS)=CLAMM(LL,WF,NS,OA)
710 SP(NS)=SLAMP(LL,WF,NS,OA):SM(NS)=SLAMM(LL,WF,NS,OA)
715 RETURN
745 REM ************* STORE LAYER LAMBDA PAIRS (CP, ETC.) AS CLAMP'S **********
750 CLAMP(LL,WF,NS,OA)=CP:CLAMM(LL,WF,NS,OA)=CM
755 SLAMP(LL,WF,NS,OA)=SP:SLAMM(LL,WF,NS,OA)=SM
760 RETURN
947 REM **************************CALCULATE Q ********************************
950 FOR L=1 TO LLAST:II=L-1:LL=L:SN=1:IF L=LLAST THEN LL=LB:SN=-1
952 IT=LL-1:IB=LL:AS1=A(II,1,NS):AO1=A(II,1,NS+SG)
954 AST=A(IT,WF,NS):ASB=A(IB,WF,NS):AOT=A(IT,WF,NS+SG):AOB=A(IB,WF,NS+SG)
956 APS=(AST+ASB)*(2-OA):AMS=(AST-ASB)*(2-OA)
958 APO=(AOT+AOB)*(2-OA):AMO=(AOT-AOB)*(2-OA)
960 AP1=AS1*AO1*(OA-1):AD1=(AS1^2-AO1^2)*(OA-1)
962 GOSUB 105:GOSUB 635:IF WF=1 AND OA=1 THEN GOSUB 750
964 FLMS=(RPRIME*2*K(LN)/(M*MU(LN)))*(ILMID-LL+(1/2)*(-(LAYS MOD 2)+1))
966 TF=(MNSH*(KMU(LL)+SN*(K(LL)/MU(LL))+FLMS)+DELV(LL)*WN)
967 TM=-SG*WF*A(II,WF,NS+SG)*TF
968 TS=-SG*(MNSH*WN/(MU(LL)*NS))*((1+SG)*AP1/2-(1-SG)*AD1/2)
970 TP=WN*(SG*AO1*(TV3(LL)+SN*TV4(LL))-AS1*(TV1(LL)+SN*TV2(LL)))
971 TQ=CM*N1+SP*N2+SN*(CP*N3-SM*N4)
972 Q(II,WF,NS)=Q(II,WF,NS)+TQ+TP+TS+TM*(2-OA)
973 REM LPRINT TQ;Q(II,WF,NS)
974 NEXT
976 RETURN
999 REM **************FILL COLUMN 6 FOR MEDIA AND LAYERS, 1ST ORDER *********
1000 AUS=A(0,WF,NS):ALS=A(ILAST,WF,NS)
```

```
1002 AUO=A(0,WF,NS+S6):ALO=A(ILAST,WF,NS+S6)
1005 TM=S6*((MNSH*RPRIME*2*K(LN)/(M*MU(LN)))+DELTAVO(0)*WN)*AUO*WF
1006 Y(0,6)=Y(0,6)+S6*MNSH*AUO/MU(0)+TM
1010 Y(1,6)=Y(1,6)-S6*2*AUS-(MNSH/MU(0))*AUO
1015 I=ILAST:II=2*I
1020 Y(II,6)=Y(II,6)+S6*MNSH*ALO/MU(LLAST)
1025 Y(II+1,6)=Y(II+1,6)-S6*2*ALS+(MNSH/MU(LLAST))*ALO
1030 FOR L=1 TO LB:I=L-1:LL=L:GOSUB 105:IT=I:IB=L
1032 APS=A(IT,WF,NS)+A(IB,WF,NS):AMS=A(IT,WF,NS)-A(IB,WF,NS)
1034 APO=A(IT,WF,NS+S6)+A(IB,WF,NS+S6):AMO=A(IT,WF,NS+S6)-A(IB,WF,NS+S6)
1036 J=2*IT:SC=1:GOSUB 1050
1038 J=2*IB:SC=-1:GOSUB 1050
1039 TM=S6*((MNSH*RPRIME*2*K(LN)/(M*MU(LN)))+DELTAVO(IB)*WN)*WF*A(IB,WF,NS+S6)
1040 Y(J,6)=Y(J,6)+TM
1043 NEXT
1045 RETURN
1050 TP=SC*S6*MNSH*(AMO*N1+SC*APO*N3)/MU(LL)
1052 Y(J,6)=Y(J,6)-SC*2*(APS*N2-SC*AMS*N4)+TP
1055 TP=-SC*MNSH*(APO*S2-SC*AMO*S4)/MU(LL)
1056 TS=SC*(MNSH/(2*MU(LL)))*(APO+SC*AMO)
1057 Y(J+1,6)=Y(J+1,6)-SC*S6*2*(AMS*S1+SC*APS*S3)+TP+TS
1060 RETURN
1099 REM *********************FILL COLUMN 6 FOR MEDIA, 2ND ORDER ***************
1100 AAS=A(I,WF,NS):AO=A(I,WF,NS+S6)
1110 AD=AAS^2-AO^2:AP=AAS*AO
1115 TY=-(WN/4)*(AAS*SP(1)-S6*AO*SP(2))
1117 TP=SC*(MNSH*WN/(2*NS*MU(0)))*((1+S6)*AP+(1-S6)*AD)
1120 Y(J,6)=Y(J,6)+(NS*WN/2)*((1+S6)*AD/2+(1-S6)*AP/2)+TY+TP
1125 TY=-S6*(WN/4)*(AAS*CP(1)-S6*AO*CP(2))
1130 Y(J+1,6)=Y(J+1,6)-S6*(MNSH*WN/(MU(LL)*2*NS))*((1+S6)*AP/2+(1-S6)*AD/2)+TY
1140 RETURN
1146 REM ******************CALCULATE CLAMPS FOR LAYERS, 2ND ORDER **************
1150 AST=A(I,WF,NS):ASB=A(IP,WF,NS):AOT=A(I,WF,NS+S6):AOB=A(IP,WF,NS+S6)
1155 AD=AST^2+SC*ASB^2-(AOT^2+SC*AOB^2):AP=AST*AOT+SC*ASB*AOB
1160 T1=(3*WN/8)*((AST+SC*ASB)*SP(1)+(AST-SC*ASB)*SM(1))
1165 T2=-S6*(3*WN/8)*((AOT+SC*AOB)*SP(2)+(AOT-SC*AOB)*SM(2))
1170 T3=-(WN/4)*(AST+SC*ASB)*(CP(1)*(S6-3*S2)+SM(1)*4*S1)
1175 T4=-(WN/4)*(AST-SC*ASB)*(CM(1)*(S7+3*S4)+SP(1)*4*S3)
1180 T6=S6*(WN/4)*(AOT+SC*AOB)*(CP(2)*(S6-3*S2)+SM(2)*4*S1)
1185 T7=S6*(WN/4)*(AOT-SC*AOB)*(CM(2)*(S7+3*S4)+SP(2)*4*S3)
1190 TC=(WN*NS/2)*((1+S6)*AD/2+(1-S6)*AP/2)+T1+T2
1195 TS=-(MNSH*WN/(MU(LL)*2*NS))*((1+S6)*AP/2+(1-S6)*AD/2)+T3+T4+T6+T7
1200 RETURN
1240 REM ******************FILL COLUMN 6 FOR LAYERS, 2ND ORDER ****************
1250 GOSUB 105
1251 T3=CLM(LL,WF,NS,OA)*N1+SLP(LL,WF,NS,OA)*N2
1252 T4=CLP(LL,WF,NS,OA)*N3-SLM(LL,WF,NS,OA)*N4
1253 T6=WN*(S6*AOT*(TV3(LL)+TV4(LL))-AST*(TV1(LL)+TV2(LL)))
1254 T7=-(MNSH*WN/(MU(LL)*2*NS))*((1+S6)*AST*AOT+(1-S6)*(AST^2-AOT^2))
1255 Y(IT,6)=Y(IT,6)+T3+T4+T6+T7
1257 T6=WN*(S6*AOB*(TV3(LL)-TV4(LL))-ASB*(TV1(LL)-TV2(LL)))
1258 T7=(MNSH*WN/(2*MU(LL)*NS))*((1+S6)*ASB*AOB+(1-S6)*(ASB^2-AOB^2))
```

```
1260 Y(IT+2,6)=Y(IT+2,6)-T3+T4-T6+T7
1265 T3=-CLP(LL,WF,NS,OA)*S2+SLM(LL,WF,NS,OA)*S1
1266 T4=CLM(LL,WF,NS,OA)*S4+SLP(LL,WF,NS,OA)*S3
1267 T12=(MNSH*RPRIME*2*K(LN)*WN/(M*MU(LN)*4*NS)+DELTAVO(IP)*WN^2/(4*NS))
1268 T7=-T12*((1+S6)*ASB*AOB-(1-S6)*(ASB^2-AOB^2))
1269 T1=TAU(IP,1,1,1):T2=TAU(IP,1,2,1)
1270 T8=((1+S6)*T1*T2+(1-S6)*(T2^2-T1^2))
1271 T9=(RPRIME*(M-1)*T(LN)/(SX*MU(LN)*MNSH*4*NS))*T8
1272 T10=(WN/2)*(S6*AST*(SP(1)+SM(1))-AOT*(SP(2)+SM(2)))
1273 T11=(WN/2)*(S6*ASB*(SP(1)-SM(1))-AOB*(SP(2)-SM(2)))
1275 Y(IT+1,6)=Y(IT+1,6)+S6*T3+S6*T4+T10
1279 Y(IT+3,6)=Y(IT+3,6)-S6*T3+S6*T4-T11+T7+T9
1280 RETURN
1399 REM ******** CALCULATION OF DELTA VO **************
1400 FOR I=0 TO ILAST
1402 LL=I+1:IF I<>ILAST THEN 1405
1403 GOSUB 1525:T1=TP:T2=TM
1404 GOTO 1411
1405 GOSUB 105:FOR NS=1 TO 2:GOSUB 705:NEXT
1410 GOSUB 1500:T1=TP:T2=TM
1411 LL=I:IF I<>0 THEN 1415
1412 GOSUB 1525:TC2=CLAMP(0,1,2,1):TC1=CLAMP(0,1,1,1)
1413 GOTO 1425
1415 GOSUB 105:FOR NS=1 TO 2:GOSUB 705:NEXT
1420 GOSUB 1500:TC2=(CP(2)-CM(2))/2:TC1=(CP(1)-CM(1))/2
1425 T3=WN*(A(I,1,1)*(TP-T1)-A(I,2,1)*(TM-T2))
1430 T4=-(MU(LL)*WN^2)*(A(I,1,1)*TC2-A(I,2,1)*TC1)
1435 T5=((M-1)/(4*MNSH))*(TAU(I,1,1,1)^2+TAU(I,1,2,1)^2)
1440 T6=(MNSH/M)*((1/4)-M)*WN^2*(A(I,1,1)^2+A(I,2,1)^2)
1445 T7=1-(WN^2/4)*(A(I,1,1)^2+A(I,2,1)^2)
1450 DELTAVO(I)=((RPRIME*T(LN)/(SX*MU(LN)))*(T6+T5+T4)+T3)/T7
1475 NEXT
1480 RETURN
1500 SN=1:IF LL=I THEN SN=-1
1504 TP=SP(2)*N6+CM(2)*N1+SN*(SM(2)*N7+CP(2)*N3)
1505 TM=SP(1)*N6+CM(1)*N1+SN*(SM(1)*N7+CP(1)*N3)
1510 RETURN
1525 SN=1:IF LL=0 THEN SN=-1
1528 TP=SLAMP(LL,1,2,1)+SN*CLAMP(LL,1,2,1)
1529 TM=SLAMP(LL,1,1,1)+SN*CLAMP(LL,1,1,1)
1530 RETURN
2006 REM ********* END OF SUBROUTINES **** BEGINNING OF MAIN PROGRAM **********
3000 GOSUB 6020
3002 FOR M=MLOW TO MUP STEP MSTEP:LPRINT:LPRINT "POWERLAW EXP M=";M
3005 R=(ANISO-1)/(TAN(2*THETA*PI/180))^(M-1):RPRIME=ANISO-1
3006 LPRINT "R=";R,"RPRIME=";RPRIME
3007 THETAPR=ATN(ANISO*TAN(2*THETA*PI/180))*90/PI
3008 LPRINT "ANGLE (DEG.) BETW. PRINC. DEF. RATE AND X=";THETAPR
3010 DS=DSS
3012 FOR I=0 TO ILAST:FOR WF=1 TO WFT:FOR NS=1 TO NST
3013 A(I,WF,NS)=0:NEXT:NEXT:NEXT
3014 FOR I=0 TO ILAST:A(I,1,1)=AAA(I,1,1):NEXT
```

```
3015 FOR L=1 TO LB:T(L)=TINIT(L):NEXT:WL=WLINIT*T(LN)
3020 AMPLIF=0:SX=1:IN=0:IMAX=-1:IIMAX=0
3030 TP=((1/SXF)-1/(SX+DS+ABS(DS/10)))
3035 IF TP<0 THEN LPRINT "SX=SXF":GOTO 5552
3040 SX=SX+DS:IN=IN+1
3045 FOR L=1 TO LB:K(L)=PI*T(L)/(WL*SX^2):NEXT
3050 TT=0:FOR L=1 TO LB:TT=TT+T(L)/SX:NEXT
3055 WN=2*PI/(WL*SX)
3060 FOR L=1 TO LB:TV1(L)=0:TV2(L)=0:TV3(L)=0:TV4(L)=0:KMU(L)=0:DELV(L)=0:NEXT
3061 FOR I=0 TO ILAST:ACK(I)=0:NEXT
3062 FOR L=1 TO LB:FOR WF=1 TO WFT:FOR NS=1 TO NST:FOR OA=1 TO OAT
3065 CLP(L,WF,NS,OA)=0:CLM(L,WF,NS,OA)=0:SLP(L,WF,NS,OA)=0:SLM(L,WF,NS,OA)=0
3066 NEXT:NEXT:NEXT:NEXT
3070 FOR I=0 TO ILAST:FOR WF=1 TO WFT:FOR NS=1 TO NST
3071 Q(I,WF,NS)=0:NEXT:NEXT:NEXT
3100 ON -(LAYS MOD 2)+2 GOTO 3105,3150
3105 LMID=(LLAST/2):KMU(LMID)=0:DELV(LMID)=0
3107 ACK(LMID-1)=K(LMID):ACK(LMID)=-K(LMID)
3110 FOR L=1 TO LMID-1
3113 I=L-1
3115 KMU(L)=K(LMID)/MU(LMID)+K(L)/MU(L)
3120 ACK(I)=K(LMID)+2*K(L)
3122 DELV(L)=DELTAVO(L)
3125 LK=LLAST-L
3127 IK=ILAST-I
3130 KMU(LK)=-K(LMID)/MU(LMID)-K(LK)/MU(LK)
3131 ACK(IK)=-K(LMID)-2*K(LK)
3132 DELV(LK)=-DELTAVO(LMID)
3133 IF L=LMID-1 THEN 3148
3135 FOR J=L+1 TO LMID-1
3140 T1=2*K(J)/MU(J):T2=-2*K(LLAST-J)/MU(LLAST-J)
3142 T3=2*K(J):T4=-2*K(LLAST-J)
3143 T5=DELTAVO(J):T6=-DELTAVO(LLAST-J)
3144 KMU(L)=KMU(L)+T1:KMU(LK)=KMU(LK)+T2
3145 ACK(I)=ACK(I)+T3:ACK(IK)=ACK(IK)+T4
3146 DELV(L)=DELV(L)+T5:DELV(LK)=DELV(LK)+T6
3147 NEXT
3148 NEXT
3149 GOTO 3200
3150 IMID=ILAST/2
3152 ACK(IMID)=0
3155 FOR I=0 TO IMID-1
3157 L=I+1:KMU(L)=K(L)/MU(L)
3158 ACK(I)=2*K(L)
3160 LK=LLAST-L:KMU(LK)=-K(LK)/MU(LK)
3161 IK=ILAST-I
3162 ACK(IK)=-2*K(LK)
3165 IF I=IMID-1 THEN 3190
3170 FOR J=L+1 TO IMID
3172 T1=2*K(J)/MU(J):T2=-2*K(LLAST-J)/MU(LLAST-J)
3173 T3=2*K(J):T4=-2*K(LLAST-J)
3175 KMU(L)=KMU(L)+T1:KMU(LK)=KMU(LK)+T2
```

```
3180 ACK(I)=ACK(I)+T3:ACK(IK)=ACK(IK)+T4
3185 NEXT
3190 NEXT
3195 REM ****************CALCULATION OF 1ST ORDER CONTRIBUTIONS ***************
3200 WF=1:NS=1:OA=1
3205 GOSUB 205
3210 GOSUB 1000:GOSUB 405
3215 PRINT WF;"-";NS;"-";OA;:GOSUB 9005
3220 IF WF=1 THEN GOSUB 600
3225 GOSUB 950
3230 IF NS=1 THEN NS=2:GOTO 3205
3235 IF WF=1 THEN WF=2:NS=1:GOTO 3205
3240 WF=1:NS=1:OA=1:GOSUB 1400
3250 IF OAT=1 THEN 5050
3390 REM **************CALCULATION OF 2ND ORDER CONTRIBUTION ******************
3500 NSNS=1
3501 WFWF=2:OAOA=2
3502 WF=WFWF:NS=NSNS:OA=OAOA:GOSUB 205
3505 WF=1:OA=1:LL=0:FOR NS=1 TO 2:GOSUB 705:NEXT
3508 NS=NSNS:SC=1:I=0:J=0:GOSUB 1100
3510 TDV=DELTAVO(0)*WN^2/(4*NS)
3511 TX=-((MNSH*RPRIME*2*K(LN)*WN/(M*MU(LN)*4*NS))+TDV)*((1+SG)*AP-(1-SG)*AD)
3512 T1=TAU(0,1,1,1):T2=TAU(0,1,2,1)
3513 TY=((1+SG)/2)*T1*T2+((1-SG)/2)*(T2^2-T1^2)
3514 TZ=(RPRIME*(M-1)*T(LN)/(SX*MU(LN)*MNSH*2*NS))*TY
3515 Y(1,6)=Y(1,6)+TX+TZ
3517 LL=LLAST:FOR NS=1 TO 2:GOSUB 705:NEXT
3520 NS=NSNS:SC=-1:I=ILAST:J=I*2:GOSUB 1100
3525 FOR L=1 TO LB:I=L-1:LL=L:WF=1:OA=1:GOSUB 105:IP=I+1:IT=I*2
3530 FOR NS=1 TO 2:GOSUB 705:NEXT
3535 NS=NSNS:SC=1:GOSUB 1150
3540 CLP(LL,WFWF,NSNS,OAOA)=TC:SLP(LL,WFWF,NSNS,OAOA)=TS
3542 IF NS=2 THEN 3550
3545 TV3(LL)=-CP(2)*S2+SM(2)*S1:TV4(LL)=CM(2)*S4+SP(2)*S3
3546 TV1(LL)=-CP(1)*S2+SM(1)*S1:TV2(LL)=CM(1)*S4+SP(1)*S3
3550 NS=NSNS:SC=-1:GOSUB 1150
3555 CLM(LL,WFWF,NSNS,OAOA)=TC:SLM(LL,WFWF,NSNS,OAOA)=TS
3560 WF=WFWF:OA=OAOA:NS=NSNS:GOSUB 1250
3565 NEXT
3570 WF=WFWF:NS=NSNS:OA=OAOA:GOSUB 405
3575 PRINT " 2-";NSNS;"-11";:GOSUB 9005
3580 GOSUB 950
3585 IF NSNS=1 THEN NSNS=2:GOTO 3501
5499 REM *************** CALCULATE AND LPRINT DA/DSX, ETC. ********************
5500 I=INT(ILAST/2):J=1:IF IN=1 THEN J=0
5502 TM=(1/SX)*(A(I,1,1)-B(I,1,1))
5504 ATEST=A(I,1,1)-DS*TM+J*(DS/2)*(TM-DAO(I,1,1)):ALTEST=ATEST*WN*SCALE
5506 IF ABS(ALTEST)>1 THEN LPRINT:LPRINT "SLOPE WILL BE TOO LARGE":SX=SX-DS:GOTO 9999
5508 IF (ATEST/AINIT)-AMPLIF<0 THEN LPRINT "AMPLIF. DECREASING":SX=SX-DS:GOTO 9999
5510 AMPLIF=ATEST/AINIT
5512 FOR I=0 TO ILAST:FOR WF=1 TO WFT:FOR NS=1 TO NST
5514 DADSX(I,WF,NS)=(1/SX)*(A(I,WF,NS)-B(I,WF,NS))
```

```
5516 TP=J*(DS/2)*(DADSX(I,WF,NS)-DAO(I,WF,NS))
5518 A(I,WF,NS)=A(I,WF,NS)-DS*DADSX(I,WF,NS)+TP
5520 DAO(I,WF,NS)=DADSX(I,WF,NS)
5522 NEXT:NEXT:NEXT
5524 GOSUB 8301
5525 IF INT(IN/10)>IMAX THEN GOSUB 8000
5535 IF INT((ATN(ALTEST)*180/PI)/15)>IIMAX THEN GOSUB 8001:GOTO 5552
5545 DS=(SX^2)*DSS*AINIT/ATEST
5550 IF IN>=NN THEN 5552 ELSE 3030
5552 NEXT:REM NEXT M
5553 GOTO 10500
5555 PRINT:PRINT "STEPS FINISHED. TO LIST AMPLITUDES & PHI'S, TYPE <A>"
5566 PRINT "TO QUIT, TYPE <Q>. TO CONTINUE, TYPE <C> AND ENTER NO. OF STEPS"
5567 A$=INKEY$:IF A$="" THEN 5567
5568 IF A$="A" THEN 9999
5569 IF A$="Q" THEN 10500
5571 IF A$="C" THEN PRINT:PRINT "NN=";NN:INPUT "NEW NN";NN:IF NN>IN THEN 3030
5573 PRINT "NEW NN<IN--QUIT":GOTO 10500
6010 REM **************** READ IN DATA FOR SPECIFIC PROBLEM *******************
6020 DEFINT I,J,L:DEFDBL Y,E
6022 I=0:J=0:L=0
6024 INPUT "LAYS (INCL. MEDIA)=";LAYS
6028 LLAST=LAYS-1:ILAST=LLAST-1:LB=LLAST-1
6029 ILMID=INT(LLAST/2)
6030 INPUT "TOTAL NO. WF, NS, OA=";WFT,NST,OAT
6031 LPRINT "WFT,NST,OAT=";WFT;NST;OAT
6032 L=LLAST::WF=WFT:NS=NST:OA=OAT
6035 DIM T(L),MU(L),K(L),IZ(L),KMU(L),ACK(L),PHI1(L),TINIT(L)
6037 DIM A(L,WF,NS),DAO(L,WF,NS),Q(L,WF,NS),DADSX(L,WF,NS),AAA(L,1,1)
6038 DIM Y(2*L-1,6),TAU(L,WF,NS,OA),SIG(L,WF,NS,OA),DELTAVO(L),DELV(L)
6040 DIM CLAMP(L,WF,NS,OA),CLAMM(L,WF,NS,OA),CLP(L,WF,NS,OA),CLM(L,WF,NS,OA)
6041 DIM SLAMP(L,WF,NS,OA),SLAMM(L,WF,NS,OA),SLP(L,WF,NS,OA),SLM(L,WF,NS,OA)
6042 DIM CP(NS),CM(NS),SP(NS),SM(NS)
6045 DIM TV1(L),TV2(L),TV3(L),TV4(L)
6050 PI=3.141592653589793#:E=2.718281828459045#
6055 INPUT "MAXIMUM SHORTENING(L/LO)";SXF
6056 LPRINT:LPRINT "SXF=";SXF
6057 INPUT "MAX. INITIAL SLOPE (DEGREES)";DEGSLOPE
6058 SLOPE=TAN(DEGSLOPE*PI/180)
6060 INPUT "T(1)/T(2) LAYERS=";T2
6061 INPUT "MU(1)/MU(2) LAYERS=";MU2
6062 INPUT "MU(U.M.)/MU(2)=";MU(0)
6063 INPUT "MU(L.M.)/MU(2)=";MU(LLAST)
6064 FOR I=2 TO LB STEP 2:T(I)=1:MU(I)=1:NEXT
6065 FOR I=1 TO LB STEP 2:T(I)=T2:MU(I)=MU2:NEXT
6070 LN=2:REM INPUT "LAYER NO. OF STIFF LAYER (U.M.=0)=";LN
6071 LPRINT "LAYER NO. OF STIFF LAYER=";LN
6075 SCALE=T(LN):TT=0:FOR L=1 TO LB:T(L)=T(L)*SXF/SCALE:TT=TT+T(L):TINIT(L)=T(L):NEXT
6077 LPRINT "LENGTH SCALE=";SCALE
6085 MMU=MU(LN):FOR L=0 TO LLAST:MU(L)=MU(L)/MMU:NEXT
6095 LPRINT:LPRINT "LAY NO","MU(L)/MU(LN)","T(L)/SCALE","T(L) INITIAL"
6100 FOR L=0 TO LLAST:LPRINT L,MU(L),T(L),T(L)*SCALE:NEXT
```

```
6102 INPUT "ANGLE (DEGREES) BETW. COMPR. AND STIFF LAYER=";THETA
6103 LPRINT "THETA (ANGLE BETW. COMPR. AND STIFF LAYER)=";THETA
6104 MNSH=-2*TAN(2*PI*THETA/180)
6105 LPRINT "MEAN SHEAR SIGMA BAR XZ STAR=";MNSH
6107 INPUT "ANISO=";ANISO
6108 LPRINT "ANISOTROPY (ETA N/ETA S)=";ANISO
6110 INPUT "LOWER M LIMIT=";MLOW
6111 INPUT "UPPER M LIMIT=";MUP
6112 INPUT "M STEP=";MSTEP
6117 INPUT "NO. DEF. STEPS";NN
6120 DSFACT=50:DS=(SXF-1)/DSFACT:DSS=DS:LPRINT "DS=(SXF-1)/";DSFACT
6125 LPRINT "FINAL TOTAL THICK";TT*SCALE/SXF,"INIT TOTAL THICK=";TT*SCALE
6129 INPUT "INIT WL-TO-SINGLE-STIFF-LAYER-(LN)-THICK=";WLINIT
6130 LPRINT "INIT WL-TO-SINGLE-STIFF-LAYER-(LN)-THICK=";WLINIT
6131 WL=WLINIT*T(LN):LPRINT "INITIAL WL=";WL*SCALE
6132 LPRINT "FINAL WL=";WL*SCALE*SXF
6135 LPRINT "FINAL WL/TT=";WL*SXF^2/TT,"INITIAL WL/TT=";WL/TT
6140 LPRINT "MAX. INITIAL SLOPE (DEGREES)";DEGSLOPE
6142 FOR I=0 TO ILAST:DELTAVO(I)=0
6143 FOR WF=1 TO WFT:FOR NS=1 TO NST
6144 A(I,WF,NS)=0:NEXT:NEXT:NEXT
6145 FOR I=0 TO ILAST/2
6146 PRINT I;:INPUT "A(I,1,1)";AAA(I,1,1)
6147 AAA(ILAST-I,1,1)=AAA(I,1,1):NEXT
6148 FOR I=0 TO ILAST:AAA(I,1,1)=AAA(I,1,1)*SXF/SCALE
6149 LPRINT "I,A(I,1,1)";I,AAA(I,1,1)*SCALE:NEXT
6150 AINIT=SLOPE*WL/(2*PI):
6151 REM FOR I=0 TO ILAST:A(I,1,1)=AINIT
6152 REM LPRINT "I,A(I,1,1)";I,A(I,1,1)*SCALE:NEXT
6153 LPRINT "INITIAL AMPLITUDE";AINIT*SCALE
6155 RETURN
7999 REM ********* LPRINT CURRENT AMPLITUDES AND PHI'S ****************
8000 IMAX=INT(IN/10)
8001 LPRINT:LPRINT "DEF. STEP=";IN,"DSX=";DS,"SX=";SX
8002 LPRINT "CURR.WL=";WL*SX*SCALE;"CURR.WL/T=";WL*SX^2/T(LN)
8004 LPRINT "CURR.WN=";WN/SCALE;"CURR. T(1)=";T(1)*SCALE/SX
8006 LPRINT "AMPLITUDES" TAB(13) "WF=1" TAB(28) "WF=2";
8007 LPRINT TAB(53) "WF=1" TAB(68) "WF=2"
8008 FOR I=0 TO INT(ILAST/2):LPRINT TAB(0) I;:LPRINT "NS=1";:FOR WF=1 TO WFT
8010 LPRINT TAB(WF*9+(WF-1)*5) A(I,WF,1)*SCALE;:NEXT:LPRINT TAB(43) "NS=2";:FOR WF=1 TO WFT
8012 LPRINT TAB(40+WF*9+(WF-1)*5) A(I,WF,2)*SCALE;:NEXT:NEXT
8014 I=INT(ILAST/2):ALZ=A(I,1,1)*WN
8016 LPRINT:LPRINT "SLOPE(I=MID,1,1)=";ALZ
8018 LPRINT "DADSX(I,1,1)=";DADSX(I,1,1),"AMPLIF.A(I,1,1)=";A(I,1,1)/AINIT
8058 LPRINT TAB(0) "I" TAB(4) "A(COS LX)" TAB(20) "B(COS 2LX)" TAB(37) "C(SIN 2LX)";
8060 LPRINT TAB(53) "PHI1 (DEG)" TAB(68) "CAPPHI1"
8062 FOR I=0 TO INT(ILAST/2):LPRINT TAB(0) I;
8064 PHI1(I)=ATN(-A(I,1,2)/A(I,1,1))
8068 CAPPHI1=INT(100*(180/PI)*ATN(-PHI1(I)/ACK(I)))/100
8070 A1=A(I,1,1)/COS(PHI1(I))
8072 B2=A(I,2,1)*COS(2*PHI1(I))-A(I,2,2)*SIN(2*PHI1(I))
8074 C2=A(I,2,1)*SIN(2*PHI1(I))+A(I,2,2)*COS(2*PHI1(I))
```

```
8076 LPRINT TAB(4) A1*SCALE TAB(20) B2*SCALE TAB(37) C2*SCALE;
8078 LPRINT TAB(53) PHI1(I)*180/PI TAB(68) CAPPHI1
8080 NEXT
8082 PSI=(ATN(-(SX^2-1)*TAN(2*THETA*PI/180)))*(180/PI)
8084 LPRINT "PSI (DEG)=";PSI
8090 LPRINT "DELTAVO'S ---":FOR I=0 TO ILAST:LPRINT I;DELTAVO(I),:NEXT:LPRINT
8100 RETURN
8299 REM ********* PRINT CURRENT AMPLITUDES AND PHI'S ****************
8301 PRINT:PRINT "DEF. STEP=";IN,"DSX=";DS,"SX=";SX
8302 PRINT "CURR.WL=";WL*SX*SCALE;"CURR.WL/T=";WL*SX^2/T(LN)
8304 PRINT "CURR.WN=";WN/SCALE;"CURR.T(1)=";T(1)*SCALE/SX
8314 I=INT(ILAST/2):ALZ=A(I,1,1)*WN
8316 PRINT:PRINT "SLOPE(I=MID,1,1)=";ALZ
8318 PRINT "DADSX(I,1,1)=";DADSX(I,1,1),"AMPLIF.A(I,1,1)=";A(I,1,1)/AINIT
8358 PRINT TAB(1) "I" TAB(5) "A(COS LX)" TAB(22) "B(COS 2LX)" TAB(39) "C(SIN 2LX)";
8360 PRINT TAB(54) "PHI1 (DEG)" TAB(68) "CAPPHI1"
8362 FOR I=0 TO ILAST:PRINT TAB(0) I;
8364 PHI1(I)=ATN(-A(I,1,2)/A(I,1,1))
8368 CAPPHI1=INT(100*(180/PI)*ATN(-PHI1(I)/ACK(I)))/100
8370 A1=A(I,1,1)/COS(PHI1(I))
8372 B2=A(I,2,1)*COS(2*PHI1(I))-A(I,2,2)*SIN(2*PHI1(I))
8374 C2=A(I,2,1)*SIN(2*PHI1(I))+A(I,2,2)*COS(2*PHI1(I))
8376 PRINT TAB(5) A1*SCALE TAB(22) B2*SCALE TAB(39) C2*SCALE;
8378 PRINT TAB(54) PHI1(I)*180/PI TAB(68) CAPPHI1
8380 NEXT
8382 PSI=(ATN(-(SX^2-1)*TAN(2*THETA*PI/180)))*(180/PI)
8384 PRINT "PSI (DEG)=";PSI
8385 PRINT
8390 PRINT "DELTAVO'S ---":FOR I=0 TO ILAST:PRINT I;DELTAVO(I),:NEXT:PRINT
8400 RETURN
9002 REM **************** LPRINT ELEMENTS OF MATRIX ****************************
9005 RETURN:FOR IK=0 TO 2*ILAST+1:LPRINT:FOR IL=0 TO 6
9010 U=Y(IK,IL):LPRINT U;
9015 NEXT:NEXT
9020 LPRINT
9025 RETURN
9050 REM ***********************************************************************
9999 GOSUB 8000
10500 END
```

```
1 REM LAYER-PARALLEL SHEAR AND SHORTENING IN INFINITELY THICK MULTILAYER
2 REM 2ND ORDER ANALYSIS
10 DEFINT I:DEFDBL E
15 WIDTH LPRINT 80
20 LPRINT "<INFSHEAR.BAS>"
25 EPI=3.141592653589793#:E=2.718281828459045#
30 INPUT "NN";NN:LPRINT "NUMBER OF STEPS";NN
35 DIM SX(NN),A(NN),C(NN),PHI(NN)
45 INPUT "MAX. INIT. SLOPE (IN DEGREES)=":SLOPE
60 INPUT "SXF=";SXF:LPRINT "SXF=";SXF
75 LPRINT "INITIAL SLOPE=";SLOPE;"DEGS."
76 FOR ANISO=1.5 TO 5.5
78 FOR M=1 TO 9 STEP 2
80 FOR THETA=7 TO 15 STEP 4
81 IF ANISO=1.5 THEN WLT=114.3
82 IF ANISO=2.5 THEN WLT=39.7
83 IF ANISO=3.5 THEN WLT=27!
84 IF ANISO=4.5 THEN WLT=25.1
85 IF ANISO=5.5 THEN WLT=24.6
87 LPRINT:LPRINT "INITIAL L/T=";WLT
88 LPRINT:LPRINT "POWERLAW EXPONENT M=";M
90 LPRINT "THETA=";THETA;"DEGS."
95 TF=1:SCALE=TF:TF=TF/SCALE:TO=TF*SXF:MU=1:MUREF=MU:MU=MU/MUREF
97 AL=TAN(EPI*SLOPE/180):CURRAL=AL
100 MNSH=-2*TAN(2*EPI*THETA/180)
106 R=(ANISO-1)/(TAN(2*THETA*EPI/180)^(M-1))
107 LPRINT "ANISOTROPY=";ANISO
108 LPRINT "R=";R
110 AINIT=WLT*AL*TO/(2*EPI)
112 LPRINT "INIT AMP=";AINIT*SCALE
115 LPRINT:LPRINT "STEP" TAB(9) "SX" TAB(22) "WLTC" TAB(33) "WL" TAB(40) "LAYER THICK." TAB(57) "CURR AL(DEG)"
120 LPRINT TAB(8) "A" TAB(22) "C" TAB(36) "C/A" TAB(50) "PHI(DEG)" TAB(62) "CAP PHI (DEG)"
130 SX(0)=1:A(0)=AINIT:C(0)=0:PHI(0)=0
135 IMAX=-1
140 H=(SXF-1)/NN
145 FOR I = 0 TO NN-1
146 J=I
150 SX(I)=SX(0)+I*H
155 SXC=SX(I):AC=A(I):CC=C(I)
165 GOSUB 1000:GOSUB 2000
175 V1=DADSX*H:Y1=DCDSX*H:Z1=DPHIDSX*H
180 SXC=SX(I)+H/2:AC=A(I)+V1/2:CC=C(I)+Y1/2
190 GOSUB 1000:GOSUB 2000
195 V2=DADSX*H:Y2=DCDSX*H:Z2=DPHIDSX*H
200 AC=A(I)+V2/2:CC=C(I)+Y2/2
206 GOSUB 2000
210 V3=DADSX*H:Y3=DCDSX*H:Z3=DPHIDSX*H
215 SXC=SX(I)+H:AC=A(I)+V3:CC=C(I)+Y3
221 GOSUB 1000:GOSUB 2000
225 V4=DADSX*H:Y4=DCDSX*H:Z4=DPHIDSX*H
230 A(I+1)=A(I)+(1/6)*(V1+2*V2+2*V3+V4)
245 C(I+1)=C(I)+(1/6)*(Y1+2*Y2+2*Y3+Y4)
```

```
250 PHI(I+1)=PHI(I)+(1/6)*(Z1+2*Z2+2*Z3+Z4)
256 PHIDEG=PHI(I+1)*180/EPI
257 CURRAL=A(I+1)*WN:ALCURR=(180/EPI)*ATN(CURRAL)
258 CAPPHI=INT(100*(180/EPI)*ATN(-PHI(I+1)/K1))/100
260 IF A(I+1)>1000000! THEN LPRINT:LPRINT "A OVERFLOW AT SX=";SXC:I=NN
265 IF I=NN-1 THEN J=NN:GOTO 280
267 IF ALCURR>20 THEN 280
270 IF INT(ALCURR/2.5)<=IMAX THEN 300
275 IMAX=INT(ALCURR/2.5)
280 PRINT J
285 LPRINT:LPRINT J TAB(6) SXC TAB(18) WLTC TAB(30) CURRWL*SCALE TAB(43) THC*SCALE TAB(60) ALCURR
290 LPRINT TAB(2) A(I+1)*SCALE TAB(17) C(I+1)*SCALE TAB(32) C(I+1)/A(I+1) TAB(48) PHIDEG TAB(64) CAPPHI
295 IF ALCURR>20 THEN I=NN
300 NEXT
304 NEXT:NEXT:NEXT
305 GOTO 9999
1000 WLTC=WLT*SXC^2:THC=T0/SXC:CURRWL=WLTC*THC:WN=2*EPI/CURRWL
1005 K1=EPI/WLTC:K2=2*K1
1010 E1=E^K1:E2=1/(E^K1):E3=E^K2:E4=1/(E^K2)
1015 S1=(E1-E2)/2:S2=(E3-E4)/2
1020 C1=(E1+E2)/2:C2=(E3+E4)/2
1025 SC1=S1*C1:SC2=S2*C2:SM1=SC1-K1:SP1=SC1+K1:SM2=SC2-K2:SP2=SC2+K2
1030 N12=K1/(2*SM1):N13=S1^2/(2*SP1):S12=K1/(2*SP1):S13=S1^2/(2*SM1)
1035 N22=K2/(2*SM2):S23=S2^2/(2*SM2):S16=SC1/(2*SP1)
1040 RETURN
2000 DENOM=(ANISO-1)*2*K1
2010 F1=S13/(S13+DENOM/2)
2020 F2=S23/(S23+DENOM)
2030 TAU11HAT=4*F1
2035 T1=M*(M-1)*N13*(TAU11HAT/MNSH)^2
2040 QVZERO=((4*M+3)*N13+DENOM-T1)/(((4/CURRAL^2)+3)*N13+DENOM)
2050 QSTAR=(MNSH*K1/MU)*(1+((ANISO-1)/M)*(1-QVZERO))
2055 TMM1=(ANISO-1)*(M-1)*TAU11HAT^2*2*K1*WN*MU/MNSH
2060 TMNM=((ANISO-1)*2*K1*WN*MNSH/(M*MU))*(1-QVZERO)
2065 Q11=4*N12*(1-F1)
2070 QBB=4*N22*(1-F2)
2080 T1=(WN*MNSH/(2*MU))*(1+N22*(1-F2))
2085 TP=(1/N13)*(S12-(N22/2)*(S16-3*S12)*(1-F2))
2090 T2=(TMNM/2)*(TP-N22/(4*(S23+DENOM)))
2105 T3=-(TMM1/8)*N22/(S23+DENOM)
2110 QB11=T1+T2+T3
2120 DADSX=-(AC/SXC)*(1+Q11)
2135 DCDSX=-(CC/SXC)*(1+QBB)+(1/SXC)*AC^2*QB11
2175 DPHIDSX=(1/SXC)*(-QSTAR)
2200 RETURN
9999 END
```

```
1 REM EIGENVALUES, EIGENVECTORS, AND AMPLIFICATION FACTORS
2 REM FOR 3RD ORDER ANALYSIS OF LAYER-PARALLEL SHORTENING
3 REM POWERLAW EXPONENT N = 1, 2, OR 3
5 WIDTH LPRINT 80
10 LPRINT "<EIGEN.BAS>":GOTO 185
100 T5=1/(2*WN*MU(LL)*WF):K1=WF*K(LL)
105 EM=1/(E^K1):EP=E^K1:CH=(EP+EM)/2:SH=(EP-EM)/2
110 TM1=2*(CH*SH-K1):TP1=2*(CH*SH+K1)
115 N1=(CH^2)/TM1:N2=K1/TM1:N3=(SH^2)/TP1:N4=K1/TP1
120 S1=(CH^2)/TP1:S2=K1/TP1:S3=(SH^2)/TM1:S4=K1/TM1
125 N6=SH*CH/TM1:N7=SH*CH/TP1:S6=SH*CH/TP1:S7=SH*CH/TM1
130 NP1=(N1+N3)*T5:NM1=(N1-N3)*T5:NP2=(N2+N4)*T5:NM2=(N2-N4)*T5
135 SP1=(S1+S3)*T5:SM1=(S1-S3)*T5:SP2=(S2+S4)*T5:SM2=(S2-S4)*T5
140 RETURN
175 FOR I=0 TO ILAST*2+1:FOR J=0 TO I6:Y(I,J)=0:NEXT:NEXT
180 FOR I=1 TO LB:FOR J=0 TO ILAST:CLP(I,J)=0:CLM(I,J)=0
181 SLP(I,J)=0:SLM(I,J)=0:NEXT:NEXT:RETURN
185 GOSUB 5010
203 INPUT "MIN. WL/T(1)";WMIN:INPUT "MAX. WL/T(1)";WMAX:INPUT "DENOM.";WD
204 WINT=(WMAX-WMIN)/WD:WT=WMAX+WINT:WNP=1
205 WT=WT-WINT:WL=WT*T(1):IF WT<WMIN THEN 9999
207 IF WT=0 THEN 9999 ELSE LPRINT:LPRINT "WAVELENGTH/T(1)";WT;"  WL";WL*SCALE
210 FOR L=1 TO LB:K(L)=PI*T(L)/WL:NEXT
215 WN=2*PI/WL
220 FOR I=0 TO ILAST:A(I,0)=A(I,0)*WNP/WN:NEXT
221 WNP=WN
222 TD1=0:TD5=0
230 FOR I=0 TO 4*LLAST-1:FOR J=0 TO 2*ILAST+1:YLP(I,J)=0:NEXT:NEXT
231 FOR I=0 TO 4*LLAST-1:FOR J=0 TO ILAST:YLP1(I,J)=0:YLP3(I,J)=0:NEXT:NEXT
232 FOR I=0 TO ILAST:FOR J=0 TO ILAST:Y0(I,J)=0:Y01(I,J)=0:Y02(I,J)=0
233 Y03(I,J)=0:Y04(I,J)=0:Y05(I,J)=0:Y06(I,J)=0:Y07(I,J)=0:NEXT:NEXT
240 WF=1:GOSUB 175
242 Y(1,6)=-2:Y(2*LLAST-1,I6)=-2
243 FOR L=1 TO LB:I=L-1:II6=I+6:LL=L:GOSUB 100:IT=I*2
244 Y(IT,II6)=Y(IT,II6)-2*(N2-N4):Y(IT,II6+1)=Y(IT,II6+1)-2*(N2+N4)
245 Y(IT+1,II6)=Y(IT+1,II6)-2*(S1+S3):Y(IT+1,II6+1)=Y(IT+1,II6+1)+2*(S1-S3)
246 Y(IT+2,II6)=Y(IT+2,II6)+2*(N2+N4):Y(IT+2,II6+1)=Y(IT+2,II6+1)+2*(N2-N4)
247 Y(IT+3,II6)=Y(IT+3,II6)+2*(S1-S3):Y(IT+3,II6+1)=Y(IT+3,II6+1)-2*(S1+S3)
248 NEXT
250 GOSUB 300:GOSUB 505
255 FOR L=1 TO LLAST:I=L-1
256 IF L<LLAST THEN LL=L:GOSUB 100:IK=I:IL=4*(L-1)+2:S6=1
257 IF L=LLAST THEN S6=-1
259 FOR J=0 TO ILAST
260 Y0(I,J)=-N1*YLP(IL+1,J)-N2*YLP(IL+2,J)-S6*(N3*YLP(IL,J)-N4*YLP(IL+3,J))
261 NEXT
262 Y0(I,IK)=Y0(I,IK)+(1+S6)/2:Y0(I.IK+1)=Y0(I,IK+1)+(1-S6)/2
264 NEXT
275 GOTO 1040
300 L=0:I=0:T5=1/(2*WN*MU(0)*WF)
```

```
305 Y(0,2)=Y(0,2)-T5:Y(1,3)=Y(1,3)-T5-ULMUC
310 L=LLAST:I=L-1:T5=1/(2*WN*MU(LLAST)*WF):II=2*I
320 Y(II,2)=Y(II,2)-T5:Y(II+1,3)=Y(II+1,3)-T5-ULMUC
325 FOR L=1 TO LB:I=L-1:LL=L:GOSUB 100:IT=I:IB=L:I=2*IT
330 J=1:IF L=LB THEN J=0
335 Y(I,2)=Y(I,2)-NP1:Y(I,3)=Y(I,3)-NM2:Y(I,4)=Y(I,4)+NM1
345 Y(I,5)=Y(I,5)-NP2:I=I+1
350 Y(I,2)=Y(I,2)+SM2:Y(I,3)=Y(I,3)-SP1:Y(I,4)=Y(I,4)+SP2
360 Y(I,5)=Y(I,5)+SM1:I=IB*2
365 Y(I,0)=Y(I,0)+NM1:Y(I,1)=Y(I,1)+NP2:Y(I,2)=Y(I,2)-NP1
375 Y(I,3)=Y(I,3)+NM2:I=I+1
380 Y(I,0)=Y(I,0)-SP2:Y(I,1)=Y(I,1)+SM1:Y(I,2)=Y(I,2)-SM2
390 Y(I,3)=Y(I,3)-SP1-J*MUC
395 NEXT
396 PRINT "MATRIX FULL"
400 REM ***INVERT MATRIX***
405 FOR L=1 TO LLAST:IT=L-1:IB=L:IP=2*IT:YY=1/(Y(IP,2)):I=IP
410 FOR J=2 TO I6:Y(I,J)=Y(I,J)*YY:NEXT:IP1=I+1:IP2=I+2:IP3=I+3
415 FOR J=3 TO I6:Y(IP1,J)=Y(IP1,J)-Y(IP1,2)*Y(I,J):NEXT:Y(IP1,2)=0
420 IF L<>LLAST THEN 425
421 FOR J=6 TO I6:Y(IP1,J)=Y(IP1,J)/Y(IP1,3):NEXT:Y(IP1,3)=1:GOTO 470
425 FOR IJ=IP2 TO IP3:FOR J=1 TO 3:Y(IJ,J)=Y(IJ,J)-Y(IJ,0)*Y(IP,J+2):NEXT
430 FOR J=6 TO I6:Y(IJ,J)=Y(IJ,J)-Y(IJ,0)*Y(IP,J):NEXT
435 Y(IJ,0)=0:NEXT
440 IP=IP+1:YY=1/Y(IP,3):I=IP
445 FOR J=3 TO I6:Y(I,J)=Y(I,J)*YY:NEXT
450 IP1=I+1:IP2=I+2:FOR IJ=IP1 TO IP2:FOR J=2 TO 3
455 Y(IJ,J)=Y(IJ,J)-Y(IJ,1)*Y(IP,J+2):NEXT
460 FOR J=6 TO I6:Y(IJ,J)=Y(IJ,J)-Y(IJ,1)*Y(IP,J):NEXT:Y(IJ,1)=0
465 NEXT
470 NEXT
475 IP=2*LB:FOR J=6 TO I6:Y(IP,J)=Y(IP,J)-Y(IP+1,J)*Y(IP,3):NEXT:Y(IP,3)=0
480 FOR L=LB-1 TO 0 STEP -1:IP=2*L+1
485 FOR J=6 TO I6:Y(IP,J)=Y(IP,J)-Y(IP,4)*Y(IP+1,J)-Y(IP,5)*Y(IP+2,J):NEXT
490 Y(IP,4)=0:Y(IP,5)=0:IP=IP-1
494 FOR J=6 TO I6
495 Y(IP,J)=Y(IP,J)-Y(IP,3)*Y(IP+1,J)-Y(IP,4)*Y(IP+2,J)-Y(IP,5)*Y(IP+3,J)
496 NEXT
497 FOR J=3 TO 5:Y(IP,J)=0:NEXT:NEXT
498 PRINT "MATRIX INVERTED"
499 FOR I=0 TO 2*LLAST-1:FOR J=0 TO ILAST:Y(I,J)=Y(I,J+6):NEXT
500 FOR J=ILAST+1 TO I6:Y(I,J)=0:NEXT:NEXT:RETURN
505 FOR I=1 TO 2*LLAST-1 STEP 2:FOR J=0 TO ILAST
507 TAU((I-1)/2,J)=Y(I,J):NEXT:NEXT
511 FOR J=0 TO ILAST
512 YLP(0,J)=Y(0,J)*(1/(2*MU(0)*WN)):YLP(1,J)=Y(1,J)*(1/(2*MU(0)*WN))
514 YLP(4*LLAST-2,J)=Y(2*LLAST-2,J)*(1/(2*MU(LLAST)*WN))
516 YLP(4*LLAST-1,J)=Y(2*LLAST-1,J)*(1/(2*MU(LLAST)*WN))
518 NEXT
520 YLP(1,0)=YLP(1,0)-2:YLP(4*LLAST-1,ILAST)=YLP(4*LLAST-1,ILAST)-2
```

```
522 FOR L=1 TO LB:IT=2*(L-1):IL=IT+(2*L):T5=1/(2*MU(L)*WN)
524 FOR J=0 TO ILAST
526 YLP(IL,J)=(Y(IT,J)+Y(IT+2,J))*T5
529 YLP(IL+1,J)=(Y(IT,J)-Y(IT+2,J))*T5
532 YLP(IL+2,J)=(Y(IT+1,J)+Y(IT+3,J))*T5
535 YLP(IL+3,J)=(Y(IT+1,J)-Y(IT+3,J))*T5
540 NEXT
542 YLP(IL+2,L-1)=YLP(IL+2,L-1)-2:YLP(IL+2,L)=YLP(IL+2,L)-2
544 YLP(IL+3,L-1)=YLP(IL+3,L-1)-2:YLP(IL+3,L)=YLP(IL+3,L)+2
545 NEXT:RETURN
547 FOR I=1 TO 2*LLAST-1 STEP 2:FOR J=0 TO ILAST
548 TAU2((I-1)/2,J)=Y(I,J):NEXT:NEXT
550 FOR J=ILAST+1 TO ILAST*2+1
551 JK=J-(ILAST+1):L4=4*LLAST:L2=2*LLAST:T5=1/(4*MU(LLAST)*WN)
552 YLP(0,J)=Y(0,JK)*(1/(4*MU(0)*WN))+(3*WN*A(0,0)/4)*(YLP(1,JK))
554 YLP(1,J)=Y(1,JK)*(1/(4*MU(0)*WN))+(A(0,0)*WN/4)*(4*YLP(1,JK)-YLP(0,JK))
555 YLP(L4-2,J)=Y(L2-2,JK)*T5+(3*WN*A(ILAST,0)/4)*(YLP(L4-1,JK))
556 YLP(L4-1,J)=Y(L2-1,JK)*T5-(A(ILAST,0)*WN/4)*(4*YLP(L4-1,JK)+YLP(L4-2,JK))
557 NEXT
558 YLP(0,ILAST+1)=YLP(0,ILAST+1)+A(0,0)*WN/2
559 YLP(4*LLAST-2,2*ILAST+1)=YLP(4*LLAST-2,2*ILAST+1)+A(ILAST,0)*WN/2
560 FOR L=1 TO LB:IT=2*(L-1):IL=IT+(L*2):T5=1/(4*MU(L)*WN)
562 FOR J=ILAST+1 TO ILAST*2+1
563 JK=J-(ILAST+1)
565 YLP(IL,J)=(Y(IT,JK)+Y(IT+2,JK))*T5+CLP(L,JK)
567 YLP(IL+1,J)=(Y(IT,JK)-Y(IT+2,JK))*T5+CLM(L,JK)
570 YLP(IL+2,J)=(Y(IT+1,JK)+Y(IT+3,JK))*T5+SLP(L,JK)
573 YLP(IL+3,J)=(Y(IT+1,JK)-Y(IT+3,JK))*T5+SLM(L,JK)
575 NEXT
580 NEXT:RETURN
700 REM ******SOLVE FOR MAX. EIGENVALUE AND EIGENVECTOR******
705 LPRINT:FOR I=0 TO ILAST:PRINT A(I,0):NEXT
708 IT=0
710 IT=IT+1:ERRMAX=0:PRINT:FOR I=0 TO ILAST:A(I,1)=0:FOR J=0 TO ILAST
715 A(I,1)=A(I,1)+(YQ(I,J)+YQ1(I,J)+YQ3(I,J))*A(J,0):NEXT:NEXT
716 PRINT "NUMBER OF ITERATIONS";IT:IF IT>ITMAX THEN 734
725 TP=0:FOR J=0 TO ILAST:TP=TP+A(J,1)^2:NEXT
726 TP=SQR(TP):FOR J=0 TO ILAST:TEMP=A(J,0):A(J,0)=A(J,1)/TP
727 XERR=ABS(TEMP-A(J,0)):PRINT INT(100000!*A(J,0))/100000!;
728 IF XERR>ERRMAX THEN ERRMAX=XERR
729 NEXT:IF ERRMAX<.000009999999# THEN 734
730 GOTO 710
734 LPRINT:LPRINT TAB(0) "INTERFACE" TAB(15) "EIGENVALUE";
735 LPRINT TAB(29) "AMPLIF. FACT." TAB(44) "EIGENVECTOR" TAB(60) "NORMALIZED"
736 FOR J=0 TO ILAST:Q(J)=A(J,1)/A(J,0):NEXT
738 TPTP=A(0,0):FOR J=1 TO ILAST:IF A(J,0)-TPTP>0 THEN TPTP=A(J,0)
739 NEXT
740 IF TPTP=A(0,0) THEN LPRINT "NO MAXIMUM FOUND":GOTO 744
742 TP=TPTP*WN/SLOPE:FOR J=0 TO ILAST:A(J,0)=A(J,0)/TP:NEXT
744 FOR J=0 TO ILAST
```

```
746 LPRINT TAB(5) J TAB(15) Q(J) TAB(30) Q(J)-1 TAB(43) A(J,0);
748 LPRINT TAB(62) INT(10000*A(J,0)*WN/SLOPE)/10000:NEXT
750 TQ1=A(1,0):TQ5=A(5,0):RETURN
755 REM ************END COMPUTATION OF EIGENVALUES********
760 REM ****************************************************
1040 WF=2:GOSUB 175
1050 FOR J=0 TO ILAST
1055 Y(0,J+6)=-(A(0,0)*WN/4)*YLP(1,J)
1060 Y(1,J+6)=-(A(0,0)*WN/4)*YLP(0,J)
1065 Y(2*LLAST-2,J+6)=-(A(ILAST,0)*WN/4)*YLP(4*LLAST-1,J)
1070 Y(2*LLAST-1,J+6)=-(A(ILAST,0)*WN/4)*YLP(4*LLAST-2,J)
1075 NEXT
1080 Y(0,6)=Y(0,6)+(A(0,0)*WN/2)
1081 Y(2*LLAST-2,I6)=Y(2*LLAST-2,I6)+(A(ILAST,0)*WN/2)
1100 FOR L=1 TO LB:I=L-1:LL=L:IL=4*L-2:IT=2*I:IP=I+1
1105 AP=A(I,0)+A(IP,0):AM=A(I,0)-A(IP,0):ALT=A(I,0)*WN:ALB=A(IP,0)*WN
1110 WF=1:GOSUB 100
1112 FOR J=0 TO ILAST
1115 T1=(WN/4)*((S6-3*S2)*YLP(IL,J)+4*S1*YLP(IL+3,J))
1116 T2=(WN/4)*((S7+3*S4)*YLP(IL+1,J)+4*S3*YLP(IL+2,J))
1120 SLP(L,J)=-AP*T1-AM*T2:SLM(L,J)=-AM*T1-AP*T2
1121 CLP(L,J)=(3*WN/8)*(AP*YLP(IL+2,J)+AM*YLP(IL+3,J))
1122 CLM(L,J)=(3*WN/8)*(AM*YLP(IL+2,J)+AP*YLP(IL+3,J))
1124 T3(L,J)=YLP(IL,J)*S2-YLP(IL+3,J)*S1:T4(L,J)=-YLP(IL+1,J)*S4-YLP(IL+2,J)*S3
1125 NEXT
1130 CLP(L,I)=CLP(L,I)+ALT/2:CLP(L,L)=CLP(L,L)+ALB/2
1135 CLM(L,I)=CLM(L,I)+ALT/2:CLM(L,L)=CLM(L,L)-ALB/2
1140 WF=2:GOSUB 100
1145 FOR J=0 TO ILAST
1150 TNT=CLM(L,J)*N1+SLP(L,J)*N2+CLP(L,J)*N3-SLM(L,J)*N4
1155 Y(IT,J+6)=Y(IT,J+6)+TNT+ALT*(T3(L,J)+T4(L,J))
1160 TNB=-CLM(L,J)*N1-SLP(L,J)*N2+CLP(L,J)*N3-SLM(L,J)*N4
1165 Y(IT+2,J+6)=Y(IT+2,J+6)+TNB-ALB*(T3(L,J)-T4(L,J))
1170 TST=-CLP(L,J)*S2+SLM(L,J)*S1+CLM(L,J)*S4+SLP(L,J)*S3
1175 Y(IT+1,J+6)=Y(IT+1,J+6)+TST+(ALT/2)*(YLP(IL+2,J)+YLP(IL+3,J))
1180 TSB=CLP(L,J)*S2-SLM(L,J)*S1+CLM(L,J)*S4+SLP(L,J)*S3
1185 Y(IT+3,J+6)=Y(IT+3,J+6)+TSB-(ALB/2)*(YLP(IL+2,J)-YLP(IL+3,J))
1190 NEXT
1195 NEXT
1200 WF=2:GOSUB 300:GOSUB 547
1300 WF=1:GOSUB 175
1304 AA=A(0,0)*WN/2:AB=A(ILAST,0)*WN/2:L2=2*LLAST:L4=4*LLAST
1305 FOR J=0 TO ILAST:K=J+ILAST+1
1306 TP=(M-2)*((M-1)/2)*(3/4)*(A(J,0)^2)*(TAU(0,J)^3)/BHAT
1310 Y(0,J+6)=-AA*YLP(1,K)+((AA^2)/2)*(8*YLP(1,J)-3*YLP(0,J))
1315 Y(1,J+6)=-AA*YLP(0,K)+((AA^2)/2)*(3*YLP(1,J)+4*YLP(0,J))+TP
1320 Y(L2-2,J+6)=-AB*YLP(L4-1,K)-((AB^2)/2)*(8*YLP(L4-1,J)+3*YLP(L4-2,J))
1325 Y(L2-1,J+6)=-AB*YLP(L4-2,K)+((AB^2)/2)*(3*YLP(L4-1,J)-4*YLP(L4-2,J))
1330 NEXT
1340 Y(1,6)=Y(1,6)+6*(AA^2)
```

```
1345 Y(2*LLAST-1,I6)=Y(2*LLAST-1,I6)+6*(AB^2)
1350 FOR L=1 TO LB:I=L-1:LL=L:IL=4*L-2:IT=2*I:IP=I+1
1352 ALT=A(I,0)*WN/2:ALB=A(IP,0)*WN/2
1355 AP=WN*(A(I,0)+A(IP,0)):AM=WN*(A(I,0)-A(IP,0))
1357 APP=(AP^2+AM^2)/16:AMM=(AP*AM)/8
1360 WF=1:GOSUB 100
1362 FOR J=0 TO ILAST
1365 T1=(S6-5*S2)*YLP(IL,J)+6*S1*YLP(IL+3,J)
1370 T2=(S7+5*S4)*YLP(IL+1,J)+6*S3*YLP(IL+2,J)
1375 CLP(L,J)=-APP*T1-AMM*T2:CLM(L,J)=-AMM*T1-APP*T2
1380 T6(L,J)=6*N1*YLP(IL+1,J)-(N6-7*N2)*YLP(IL+2,J)
1385 T7(L,J)=6*N3*YLP(IL,J)-(N7+7*N4)*YLP(IL+3,J)
1390 NEXT
1395 WF=2:GOSUB 100
1400 FOR J=0 TO ILAST:K=J+ILAST+1
1405 T1=S6*YLP(IL,K)+S1*YLP(IL+3,K):T2=S7*YLP(IL+1,K)+S3*YLP(IL+2,K)
1410 SLP(L,J)=-APP*T6(L,J)-AMM*T7(L,J)-2*(AP*T1+AM*T2)
1415 SLM(L,J)=-AMM*T6(L,J)-APP*T7(L,J)-2*(AM*T1+AP*T2)
1417 TVN1(L,J)=S2*YLP(IL,K)-S1*YLP(IL+3,K)
1418 TVN2(L,J)=-S4*YLP(IL+1,K)-S3*YLP(IL+2,K)
1420 T8(L,J)=3*N1*YLP(IL+1,K)+(4*N6-N2)*YLP(IL+2,K)
1421 T9(L,J)=3*N3*YLP(IL,K)+(4*N7+N4)*YLP(IL+3,K)
1423 NEXT
1425 SLP(L,I)=SLP(L,I)+(3/2)*((AP+AM)/2)^2
1427 SLP(L,L)=SLP(L,L)+(3/2)*((AP-AM)/2)^2
1430 SLM(L,I)=SLM(L,I)+(3/2)*((AP+AM)/2)^2
1432 SLM(L,L)=SLM(L,L)-(3/2)*((AP-AM)/2)^2
1435 WF=1:GOSUB 100
1440 FOR J=0 TO ILAST
1445 T8=-N1*YLP(IL+1,J)-N6*YLP(IL+2,J):T9=-N3*YLP(IL,J)-N7*YLP(IL+3,J)
1448 TNT=N1*CLM(L,J)+N2*SLP(L,J)+N3*CLP(L,J)-N4*SLM(L,J)
1450 Y(IT,J+6)=Y(IT,J+6)+TNT+ALT*(TVN1(L,J)+TVN2(L,J))+(ALT^2)*(T8+T9)
1452 TNB=-N1*CLM(L,J)-N2*SLP(L,J)+N3*CLP(L,J)-N4*SLM(L,J)
1455 Y(IT+2,J+6)=Y(IT+2,J+6)+TNB-ALB*(TVN1(L,J)-TVN2(L,J))-(ALB^2)*(T8-T9)
1456 TP=(M-2)*((M-1)/2)*(3/4)*(A(J,0)^2)*(TAU(IP,J)^3)/BHAT
1458 T1=S6*YLP(IL,J)+S1*YLP(IL+3,J):T2=S7*YLP(IL+1,J)+S3*YLP(IL+2,J)
1459 TST=-S2*CLP(L,J)+S1*SLM(L,J)+S4*CLM(L,J)+S3*SLP(L,J)
1460 Y(IT+1,J+6)=Y(IT+1,J+6)+TST+ALT*(T8(L,J)+T9(L,J))+(ALT^2)*(T1+T2)
1463 TSB=S2*CLP(L,J)-S1*SLM(L,J)+S4*CLM(L,J)+S3*SLP(L,J)
1465 Y(IT+3,J+6)=Y(IT+3,J+6)+TSB-ALB*(T8(L,J)-T9(L,J))-(ALB^2)*(T1-T2)+TP
1470 NEXT:NEXT
1475 WF=1:GOSUB 300
1500 WF=1:FOR L=1 TO LLAST:I=L-1:AA=A(I,0)*WN/2
1505 IF L<LLAST THEN LL=L:GOSUB 100:IT=2*(L-1):IL=4*(L-1)+2:S6=1
1508 IF L=LLAST THEN S6=-1
1509 FOR J=0 TO ILAST
1510 TDA1(LL,J)=N1*YLP(IL+1,J)+(2*N6-N2)*YLP(IL+2,J)
1515 TDA2(LL,J)=N3*YLP(IL,J)+(2*N7+N4)*YLP(IL+3,J)
1520 T3=N1*((Y(IT,J)-Y(IT+2,J))*T5+CLM(LL,J))
1522 T4=N2*((Y(IT+1,J)+Y(IT+3,J))*T5+SLP(LL,J))
```

```
1524 T6=N3*((Y(IT,J)+Y(IT+2,J))*T5+CLP(LL,J))
1526 T7=N4*((Y(IT+1,J)-Y(IT+3,J))*T5+SLM(LL,J))
1529 T8=-AA*(TVN1(LL,J)+S6*TVN2(LL,J))
1530 YQ3(I,J)=-T3-T4-S6*(T6-T7)+T8+(AA^2/2)*(TDA1(LL,J)+S6*TDA2(LL,J))
1535 NEXT:NEXT
1550 WF=1:GOSUB 175
1552 FOR J=0 TO ILAST
1554 Y(1,J+6)=(3-M)*(M-1)*ABS(TAU(0,J))*TAU(0,J)*A(J,0)*5*SQR(2)/(BHAT*8)
1556 NEXT
1557 FOR L=1 TO LB:I=L-1:IT=2*I:IP=I+1
1558 FOR J=0 TO ILAST
1560 Y(IT+3,J+6)=(3-M)*(M-1)*ABS(TAU(IP,J))*TAU(IP,J)*A(J,0)*5*SQR(2)/(BHAT*8)
1564 NEXT:NEXT
1566 GOSUB 300
1568 FOR J=0 TO ILAST
1570 YLP1(0,J)=Y(0,J)*(1/(2*MU(0)*WN)):YLP1(1,J)=Y(1,J)*(1/(2*MU(0)*WN))
1572 YLP1(4*LLAST-2,J)=Y(2*LLAST-2,J)*(1/(2*MU(LLAST)*WN))
1574 YLP1(4*LLAST-1,J)=Y(2*LLAST-1,J)*(1/(2*MU(LLAST)*WN))
1576 NEXT
1580 FOR L=1 TO LB:IT=2*(L-1):IL=IT+(2*L):T5=1/(2*MU(L)*WN)
1582 FOR J=0 TO ILAST
1584 YLP1(IL,J)=(Y(IT,J)+Y(IT+2,J))*T5
1586 YLP1(IL+1,J)=(Y(IT,J)-Y(IT+2,J))*T5
1588 YLP1(IL+2,J)=(Y(IT+1,J)+Y(IT+3,J))*T5
1590 YLP1(IL+3,J)=(Y(IT+1,J)-Y(IT+3,J))*T5
1592 NEXT
1598 NEXT
1600 FOR L=1 TO LLAST:I=L-1
1602 IF L<LLAST THEN LL=L:GOSUB 100:IL=4*(L-1)+2:S6=1
1604 IF L=LLAST THEN S6=-1
1606 FOR J=0 TO ILAST
1607 TP=-N1*YLP1(IL+1,J)-N2*YLP1(IL+2,J)-S6*(N3*YLP1(IL,J)-N4*YLP1(IL+3,J))
1608 YQ1(I,J)=TP
1610 NEXT:NEXT
1625 GOSUB 705
1630 IJIJ=2:IF ABS(TQ1-TD1)>.0001 THEN IJIJ=1
1635 JIJI=2:IF ABS(TQ5-TD5)>.0001 THEN JIJI=1
1640 TD1=TQ1:TD5=TQ5:IF IJIJ=1 OR JIJI=1 THEN GOTO 1040
1650 WF=3:GOSUB 175
1652 AA=A(0,0)*WN/2:AB=A(ILAST,0)*WN/2:L2=2*LLAST:L4=4*LLAST
1654 FOR J=0 TO ILAST:K=J+ILAST+1
1656 TP=-(M-2)*((M-1)/2)*(1/4)*(A(J,0)^2)*(TAU(0,J)^3)/BHAT
1658 Y(0,J+6)=-(AA/3)*YLP(1,K)+((AA^2)/6)*(4*YLP(1,J)-YLP(0,J))
1660 Y(1,J+6)=-(AA/3)*YLP(0,K)+((AA^2)/2)*YLP(1,J)+TP
1662 Y(L2-2,J+6)=-(AB/3)*YLP(L4-1,K)-((AB^2)/6)*(4*YLP(L4-1,J)+YLP(L4-2,J))
1664 Y(L2-1,J+6)=-(AB/3)*YLP(L4-2,K)+((AB^2)/2)*YLP(L4-1,J)
1665 NEXT
1666 Y(1,6)=Y(1,6)-2*(AA^2)/3:Y(2*LLAST-1,I6)=Y(2*LLAST-1,I6)-2*(AB^2)/3
1668 FOR L=1 TO LB:I=L-1:LL=L:IL=4*L-2:IT=2*I:IP=I+1
1670 ALT=A(I,0)*WN/2:ALB=A(IP,0)*WN/2
```

```
1671 AP=WN*(A(I,0)+A(IP,0)):AM=WN*(A(I,0)-A(IP,0))
1672 APP=(AP^2+AM^2)/48:AMM=(AP*AM)/24
1673 WF=1:GOSUB 100
1674 FOR J=0 TO ILAST:K=J+ILAST+1
1675 T1=2*N1*YLP(IL+1,J)+(5*N6-3*N2)*YLP(IL+2,J)
1676 T2=2*N3*YLP(IL,J)+(5*N7+3*N4)*YLP(IL+3,J)
1677 T6=YLP(IL,J)*(5*S6-9*S2)+YLP(IL+3,J)*14*S1
1678 T7=YLP(IL+1,J)*(5*S7+9*S4)+YLP(IL+2,J)*14*S3
1679 T8(L,J)=YLP(IL,J)*(S6-2*S2)+YLP(IL+3,J)*3*S1
1680 T9(L,J)=YLP(IL+1,J)*(S7+2*S4)+YLP(IL+2,J)*3*S3
1681 T10(L,J)=-N1*YLP(IL+1,J)-(3*N6-2*N2)*YLP(IL+2,J)
1682 T11(L,J)=-N3*YLP(IL,J)-(3*N7+2*N4)*YLP(IL+3,J)
1685 CLP(L,J)=(2/3)*(AP*YLP(IL+2,K)+AM*YLP(IL+3,K))+APP*T6+AMM*T7
1687 CLM(L,J)=(2/3)*(AM*YLP(IL+2,K)+AP*YLP(IL+3,K))+AMM*T6+APP*T7
1689 SLP(L,J)=-3*(APP*T1+AMM*T2):SLM(L,J)=-3*(AMM*T1+APP*T2)
1690 NEXT
1692 WF=2:GOSUB 100
1693 FOR J=0 TO ILAST:K=J+ILAST+1
1694 T6(L,J)=N1*YLP(IL+1,K)+(4*N6-3*N2)*YLP(IL+2,K)
1695 T7(L,J)=N3*YLP(IL,K)+(4*N7+3*N4)*YLP(IL+3,K)
1696 T3=YLP(IL,K)*(S6-2*S2)+YLP(IL+3,K)*3*S1
1697 T4=YLP(IL+1,K)*(S7+2*S4)+YLP(IL+2,K)*3*S3
1699 SLP(L,J)=SLP(L,J)-(2/3)*(AP*T3+AM*T4)
1700 SLM(L,J)=SLM(L,J)-(2/3)*(AM*T3+AP*T4)
1702 NEXT
1704 SLP(L,I)=SLP(L,I)-(1/6)*((AP+AM)/2)^2
1705 SLP(L,L)=SLP(L,L)-(1/6)*((AP-AM)/2)^2
1706 SLM(L,I)=SLM(L,I)-(1/6)*((AP+AM)/2)^2
1707 SLM(L,L)=SLM(L,L)+(1/6)*((AP-AM)/2)^2
1710 WF=3:GOSUB 100
1712 FOR J=0 TO ILAST
1714 TNT=N1*CLM(L,J)+N2*SLP(L,J)+N3*CLP(L,J)-N4*SLM(L,J)
1715 TM=3*ALT*(TVN1(L,J)+TVN2(L,J))
1716 Y(IT,J+6)=Y(IT,J+6)+TNT+TM+(ALT^2)*(T10(L,J)+T11(L,J))
1718 TST=-S2*CLP(L,J)+S1*SLM(L,J)+S4*CLM(L,J)+S3*SLP(L,J)
1720 Y(IT+1,J+6)=Y(IT+1,J+6)+TST+ALT*(T6(L,J)+T7(L,J))+ALT^2*(T8(L,J)+T9(L,J))
1722 TP=-(M-2)*((M-1)/2)*(1/4)*(A(J,0)^2)*(TAU(IP,J)^3)/BHAT
1724 TNB=-N1*CLM(L,J)-N2*SLP(L,J)+N3*CLP(L,J)-N4*SLM(L,J)
1725 TM=-3*ALB*(TVN1(L,J)-TVN2(L,J))
1726 Y(IT+2,J+6)=Y(IT+2,J+6)+TNB+TM-(ALB^2)*(T10(L,J)-T11(L,J))
1728 TSB=S2*CLP(L,J)-S1*SLM(L,J)+S4*CLM(L,J)+S3*SLP(L,J)
1729 TM=-ALB*(T6(L,J)-T7(L,J))
1730 Y(IT+3,J+6)=Y(IT+3,J+6)+TSB+TM-(ALB^2)*(T8(L,J)-T9(L,J))+TP
1731 NEXT:NEXT
1732 WF=3:GOSUB 300
1740 WF=3:FOR L=1 TO LLAST:I=L-1:AA=A(I,0)*WN/2
1741 IF L<LLAST THEN LL=L:GOSUB 100:IT=2*(L-1):IL=4*(L-1)+2:S6=1
1742 IF L=LLAST THEN S6=-1
1744 FOR J=0 TO ILAST
1745 T3=N3*((Y(IT,J)+Y(IT+2,J))*T5+CLP(LL,J))
```

```
1746 T1=N1*((Y(IT,J)-Y(IT+2,J))*T5+CLM(LL,J))
1747 T2=N2*((Y(IT+1,J)+Y(IT+3,J))*T5+SLP(LL,J))
1748 T4=-N4*((Y(IT+1,J)-Y(IT+3,J))*T5+SLM(LL,J))
1750 T8=-3*AA*(TVN1(LL,J)+S6*TVN2(LL,J))
1752 YQ6(I,J)=-T1-T2-S6*(T3+T4)+(3/2)*(AA^2)*(TDA1(LL,J)+S6*TDA2(LL,J))+T8
1755 NEXT:NEXT
1760 WF=2:FOR L=1 TO LLAST:I=L-1:AA=A(I,0)*WN
1765 IF L<LLAST THEN LL=L:GOSUB 100:IL=4*(L-1)+2:IT=2*(L-1):S6=1
1767 IF L=LLAST THEN S6=-1
1770 FOR J=0 TO ILAST:K=J+ILAST+1
1772 TP=-N1*YLP(IL+1,K)-N2*YLP(IL+2,K)-S6*(N3*YLP(IL,K)-N4*YLP(IL+3,K))
1775 YQ2(I,J)=TP-AA*(T3(LL,J)+S6*T4(LL,J))
1777 NEXT:NEXT
2000 WF=3:GOSUB 175
2010 FOR J=0 TO ILAST
2020 Y(1,J+6)=-(3-M)*(M-1)*ABS(TAU(0,J))*TAU(0,J)*A(J,0)*SQR(2)/(BHAT*8)
2030 NEXT
2035 FOR L=1 TO LB:I=L-1:IT=2*I:IP=I+1
2040 FOR J=0 TO ILAST
2050 Y(IT+3,J+6)=-(3-M)*(M-1)*ABS(TAU(IP,J))*TAU(IP,J)*A(J,0)*SQR(2)/(BHAT*8)
2060 NEXT:NEXT
2070 GOSUB 300
2080 FOR J=0 TO ILAST
2090 YLP3(0,J)=Y(0,J)*(1/(6*MU(0)*WN)):YLP3(1,J)=Y(1,J)*(1/(6*MU(0)*WN))
2100 YLP3(4*LLAST-2,J)=Y(2*LLAST-2,J)*(1/(6*MU(LLAST)*WN))
2110 YLP3(4*LLAST-1,J)=Y(2*LLAST-1,J)*(1/(6*MU(LLAST)*WN))
2120 NEXT
2130 FOR L=1 TO LB:IT=2*(L-1):IL=IT+(2*L):T5=1/(6*MU(L)*WN)
2140 FOR J=0 TO ILAST
2150 YLP3(IL,J)=(Y(IT,J)+Y(IT+2,J))*T5
2160 YLP3(IL+1,J)=(Y(IT,J)-Y(IT+2,J))*T5
2170 YLP3(IL+2,J)=(Y(IT+1,J)+Y(IT+3,J))*T5
2180 YLP3(IL+3,J)=(Y(IT+1,J)-Y(IT+3,J))*T5
2190 NEXT
2200 NEXT
2210 FOR L=1 TO LLAST:I=L-1
2220 IF L<LLAST THEN LL=L:GOSUB 100:IL=4*(L-1)+2:S6=1
2230 IF L=LLAST THEN S6=-1
2240 FOR J=0 TO ILAST
2250 TP=-N1*YLP3(IL+1,J)-N2*YLP3(IL+2,J)-S6*(N3*YLP3(IL,J)-N4*YLP3(IL+3,J))
2260 YQ5(I,J)=TP
2270 NEXT:NEXT
2500 WF=2:GOSUB 175
2510 AA=A(0,0)*WN/4:AB=A(ILAST,0)*WN/4:L2=2*LLAST:L4=4*LLAST
2520 FOR J=0 TO ILAST
2530 TP=(3-M)*(M-1)*ABS(TAU(0,J))*TAU2(0,J)*A(J,0)*8*SQR(2)/(BHAT*8)
2540 Y(0,J+6)=-AA*(YLP1(1,J)+YLP3(1,J))
2550 Y(1,J+6)=-AA*(YLP1(0,J)+YLP3(0,J))+TP
2560 Y(L2-2,J+6)=-AB*(YLP1(L4-1,J)+YLP3(L4-1,J))
2570 Y(L2-1,J+6)=-AB*(YLP1(L4-2,J)+YLP3(L4-2,J))
```

```
2580 NEXT
2590 FOR L=1 TO LB:I=L-1:LL=L:IL=4*L-2:IT=2*I:IP=I+1
2600 AP=A(I,0)+A(IP,0):AM=A(I,0)-A(IP,0)
2610 WF=1:GOSUB 100
2620 FOR J=0 TO ILAST
2630 T1=YLP1(IL+2,J)+YLP3(IL+2,J):T2=YLP1(IL+3,J)+YLP3(IL+3,J)
2640 CLP(L,J)=(3*WN/8)*(AP*T1+AM*T2)
2650 CLM(L,J)=(3*WN/8)*(AM*T1+AP*T2)
2660 T6(L,J)=-(WN/4)*(YLP1(IL,J)*(S6-3*S2)+YLP1(IL+3,J)*4*S1)
2670 T7(L,J)=-(WN/4)*(YLP1(IL+1,J)*(S7+3*S4)+YLP1(IL+2,J)*4*S3)
2680 TVN1(L,J)=YLP1(IL,J)*S2-YLP1(IL+3,J)*S1
2690 TVN2(L,J)=-YLP1(IL+1,J)*S4-YLP1(IL+2,J)*S3
2700 NEXT
2710 WF=3:GOSUB 100
2720 FOR J=0 TO ILAST
2730 T3=-(3*WN/4)*(YLP3(IL,J)*(3*S6-S2)+YLP3(IL+3,J)*4*S1)
2740 T4=-(3*WN/4)*(YLP3(IL+1,J)*(3*S7+S4)+YLP3(IL+2,J)*4*S3)
2750 SLP(L,J)=AP*(T6(L,J)+T3)+AM*(T7(L,J)+T4)
2760 SLM(L,J)=AM*(T6(L,J)+T3)+AP*(T7(L,J)+T4)
2770 TVN7(L,J)=YLP3(IL,J)*S2-YLP3(IL+3,J)*S1
2780 TVN8(L,J)=-YLP3(IL+1,J)*S4-YLP3(IL+2,J)*S3
2790 T8(L,J)=YLP3(IL+1,J)*2*N1+YLP3(IL+2,J)*(3*N6-N2)
2800 T9(L,J)=YLP3(IL,J)*2*N3+YLP3(IL+3,J)*(3*N7+N4)
2810 NEXT
2820 WF=2:GOSUB 100
2830 AA=A(I,0)*WN:AB=A(IP,0)*WN
2840 FOR J=0 TO ILAST
2850 T1=CLM(L,J)*N1+SLP(L,J)*N2:T2=CLP(L,J)*N3-SLM(L,J)*N4
2860 T3=TVN1(L,J)+TVN7(L,J):T4=TVN2(L,J)+TVN8(L,J)
2870 Y(IT,J+6)=Y(IT,J+6)+T1+T2+AA*(T3+T4)
2880 Y(IT+2,J+6)=Y(IT+2,J+6)-T1+T2-AB*(T3-T4)
2890 T1=-CLP(L,J)*S2+SLM(L,J)*S1:T2=CLM(L,J)*S4+SLP(L,J)*S3
2900 TP=(3-M)*(M-1)*ABS(TAU(IP,J))*TAU2(IP,J)*A(J,0)*B*SQR(2)/(BHAT*B)
2910 TM=AA*(((YLP1(IL+2,J)+YLP1(IL+3,J))/2)+T8(L,J)+T9(L,J))
2920 Y(IT+1,J+6)=Y(IT+1,J+6)+T1+T2+TM
2930 TM=-AB*(((YLP1(IL+2,J)-YLP1(IL+3,J))/2)+T8(L,J)-T9(L,J))
2940 Y(IT+3,J+6)=Y(IT+3,J+6)-T1+T2+TM+TP
2950 NEXT:NEXT
2960 WF=2:GOSUB 300
2970 FOR L=1 TO LLAST:I=L-1:AA=A(I,0)*WN
2980 IF L<LLAST THEN LL=L:GOSUB 100:IT=2*(L-1):IL=4*(L-1)+2:S6=1
2990 IF L=LLAST THEN S6=-1
3000 FOR J=0 TO ILAST
3010 T3=N1*((Y(IT,J)-Y(IT+2,J))*T5+CLM(LL,J))
3020 T4=N2*((Y(IT+1,J)+Y(IT+3,J))*T5+SLP(LL,J))
3030 T6=N3*((Y(IT,J)+Y(IT+2,J))*T5+CLP(LL,J))
3040 T7=N4*((Y(IT+1,J)-Y(IT+3,J))*T5+SLM(LL,J))
3050 T8=AA*(TVN1(LL,J)+TVN7(LL,J)+S6*(TVN2(LL,J)+TVN8(LL,J)))
3060 YB7(I,J)=-T3-T4-S6*(T6-T7)-T8
3070 NEXT:NEXT
```

```
3200 WF=4:GOSUB 175
3210 AA=A(0,0)*WN/8:AB=A(ILAST,0)*WN/8:L2=2*LLAST:L4=4*LLAST
3215 FOR J=0 TO ILAST
3220 TP=-(3-M)*(M-1)*ABS(TAU(0,J))*TAU2(0,J)*A(J,0)*3*SQR(2)/(BHAT*8)
3230 Y(0,J+6)=-AA*YLP3(1,J)
3240 Y(1,J+6)=-AA*YLP3(0,J)+TP
3250 Y(L2-2,J+6)=-AB*YLP3(L4-1,J)
3260 Y(L2-1,J+6)=-AB*YLP3(L4-2,J)
3270 NEXT
3280 FOR L=1 TO LB:I=L-1:LL=L:IL=4*L-2:IT=2*I:IP=I+1
3290 AP=A(I,0)+A(IP,0):AM=A(I,0)-A(IP,0)
3300 WF=3:GOSUB 100
3310 FOR J=0 TO ILAST
3320 CLP(L,J)=(15*WN/16)*(AP*YLP3(IL+2,J)+AM*YLP3(IL+3,J))
3330 CLM(L,J)=(15*WN/16)*(AM*YLP3(IL+2,J)+AP*YLP3(IL+3,J))
3340 T1=YLP3(IL,J)*(3*S6-5*S2)+YLP3(IL+3,J)*8*S1
3350 T2=YLP3(IL+1,J)*(3*S7+5*S4)+YLP3(IL+2,J)*8*S3
3360 SLP(L,J)=-(3*WN/8)*(AP*T1+AM*T2)
3370 SLM(L,J)=-(3*WN/8)*(AM*T1+AP*T2)
3380 T8(L,J)=YLP3(IL+1,J)*N1+YLP3(IL+2,J)*(3*N6-2*N2)
3390 T9(L,J)=YLP3(IL,J)*N3+YLP3(IL+3,J)*(3*N7+2*N4)
3400 NEXT
3410 WF=4:GOSUB 100
3420 FOR J=0 TO ILAST
3430 T1=CLM(L,J)*N1+SLP(L,J)*N2:T2=CLP(L,J)*N3-SLM(L,J)*N4
3440 Y(IT,J+6)=Y(IT,J+6)+T1+T2+(AP+AM)*WN*(TVN7(L,J)+TVN8(L,J))
3450 Y(IT+2,J+6)=Y(IT+2,J+6)-T1+T2-(AP-AM)*WN*(TVN7(L,J)-TVN8(L,J))
3460 T1=-CLP(L,J)*S2+SLM(L,J)*S1:T2=CLM(L,J)*S4+SLP(L,J)*S3
3470 TP=-(3-M)*(M-1)*ABS(TAU(IP,J))*TAU2(IP,J)*A(J,0)*3*SQR(2)/(BHAT*8)
3480 Y(IT+1,J+6)=Y(IT+1,J+6)+T1+T2+((AP+AM)/2)*WN*(T8(L,J)+T9(L,J))
3490 Y(IT+3,J+6)=Y(IT+3,J+6)-T1+T2-((AP-AM)/2)*WN*(T8(L,J)-T9(L,J))+TP
3500 NEXT:NEXT
3510 WF=4:GOSUB 300
3520 FOR L=1 TO LLAST:I=L-1:AA=A(I,0)*WN*2
3530 IF L<LLAST THEN LL=L:GOSUB 100:IT=2*(L-1):IL=4*(L-1)+2:S6=1
3540 IF L=LLAST THEN S6=-1
3550 FOR J=0 TO ILAST
3560 T3=N1*((Y(IT,J)-Y(IT+2,J))*T5+CLM(LL,J))
3570 T4=N2*((Y(IT+1,J)+Y(IT+3,J))*T5+SLP(LL,J))
3580 T6=N3*((Y(IT,J)+Y(IT+2,J))*T5+CLP(LL,J))
3590 T7=N4*((Y(IT+1,J)-Y(IT+3,J))*T5+SLM(LL,J))
3600 T8=AA*(TVN7(LL,J)+S6*TVN8(LL,J))
3610 Y84(I,J)=-T3-T4-S6*(T6-T7)-T8
3620 NEXT:NEXT
4500 LPRINT:LPRINT "INT." TAB(7) "Y8(1-1)" TAB(21) "Y81(1-11)" TAB(35) "Y83(1-111)" TAB(50) "Y8(1-1-111)"
4510 FOR I=0 TO ILAST:U=0:V=0:X=0:Z=0:FOR J=0 TO ILAST
4520 U=U+Y8(I,J)*A(J,0):V=V+Y81(I,J)*A(J,0):X=X+Y83(I,J)*A(J,0):NEXT
4530 LPRINT I TAB(5) (U/A(I,0))-1 TAB(20) V/A(I,0) TAB(35) X/A(I,0) TAB(50) ((U+X+V)/A(I,0))-1
4540 NEXT
```

```
4550 LPRINT
4551 LPRINT "INT." TAB(7) "Y02(2-11)" TAB(20) "Y07(2-111)" TAB(34);
4552 LPRINT  "Y05(3-11)" TAB(49) "Y06(3-111)" TAB(64) "Y04(4-111)"
4560 FOR I=0 TO ILAST:U=0:V=0:W=0:X=0:Z=0:FOR J=0 TO ILAST
4570 U=U+Y02(I,J)*A(J,0):V=V+Y07(I,J)*A(J,0):W=W+Y05(I,J)*A(J,0):X=X+Y06(I,J)*A(J,0):Z=Z+Y04(I,J)*A(J,0):NEXT
4580 LPRINT TAB(0) I TAB(4) U/A(I,0) TAB(19) V/A(I,0) TAB(33) W/A(I,0) TAB(48) X/A(I,0) TAB(63) Z/A(I,0)
4590 NEXT
4600 GOTO 205
5000 REM ********************INITIALIZE*****************
5010 DEFINT I,J,L:DEFDBL Y,E
5020 I=0:J=0
5030 INPUT "NUMBER OF LAYERS (INCL. MEDIA)";LAYS
5040 LLAST=LAYS-1:ILAST=LLAST-1:LB=LLAST-1:I6=ILAST+6:ITX=ILAST*2:ITMAX=20
5050 L=LLAST
5060 DIM T(L),MU(L),A(L,1),K(L),Q(L-1),Y(2*L-1,I6),YLP(4*L-1,2*L-1)
5065 DIM YLP1(4*L-1,L-1),YLP3(4*L-1,L-1)
5070 DIM Y0(L-1,L-1),Y01(L-1,L-1),Y02(L-1,L-1),Y03(L-1,L-1),Y04(L-1,L-1)
5080 DIM Y05(L-1,L-1),Y06(L-1,L-1),Y07(L-1,L-1)
5090 DIM CLP(L,L-1),CLM(L,L-1),SLP(L,L-1),SLM(L,L-1)
5120 DIM TVN1(L,L-1),TVN2(L,L-1),TVN7(L,L-1),TVN8(L,L-1)
5130 DIM TDA1(L,L),TDA2(L,L)
5140 DIM T3(L,L-1),T4(L,L-1),T6(L,L-1),T7(L,L-1)
5150 DIM T8(L,L-1),T9(L,L-1),T10(L,L-1),T11(L,L-1)
5160 DIM TAU(L,L-1),TAU2(L,L-1)
5170 PI=3.141592653589793#:E=2.718281828459045#
5180 INPUT "T(1)/T(2) LAYERS =";T2
5190 INPUT "MU(1)/MU(2) LAYERS =";MU2
5200 INPUT "MU(U.M.)/MU(2)=";MU(0)
5210 INPUT "MU(L.M.)/MU(2)=";MU(LLAST)
5220 FOR I=2 TO LB STEP 2:T(I)=1:MU(I)=1:NEXT
5230 FOR I=1 TO LB STEP 2:T(I)=T2:MU(I)=MU2:NEXT
5240 SCALE=T(1):TT=0:FOR L=1 TO LB:T(L)=T(L)/SCALE:TT=TT+T(L):NEXT
5250 LPRINT "LENGTH SCALE=";SCALE
5260 MMU=MU(1):FOR L=0 TO LLAST:MU(L)=MU(L)/MMU:NEXT
5270 LPRINT:LPRINT "LAY NO","MU(L)/MU(1)","T(L)/SCALE","T(L)"
5280 FOR L=0 TO LLAST:LPRINT L,MU(L),T(L),T(L)*SCALE:NEXT
5290 PRINT "THE FOLLOWING RANGE FROM 0 (BONDED) TO VERY LARGE (FREE SLIP)"
5300 ULMUC=10000000#:REM INPUT "MU(LAYER)/MU(CONTACTS AT UPPER AND LOWER CONTACTS)";ULMUC
5310 INPUT "MU(LAYER)/MU(CONTACTS BETWEEN LAYERS)";MUC
5320 LPRINT "ULMUC=";ULMUC,"MUC=";MUC
5330 INPUT "POWERLAW EXP M (1, 2, OR 3)";M
5340 LPRINT "POWERLAW EXP M=";M
5350 INPUT "MAX. SLOPE (DEGS.)";DEGSLOPE:LPRINT "MAX. SLOPE=";DEGSLOPE;"DEGS."
5360 SLOPE=TAN(DEGSLOPE*PI/180)
5370 INPUT "ANISO=";ANISO:LPRINT "ANISOTROPY (ETA N/ETA S)=";ANISO
5380 BHAT=(M*(4*SLOPE)^(M-1))/(ANISO-1):LPRINT "BHAT=";BHAT
5390 LPRINT "TOTAL THICKNESS",TT*SCALE
5400 LPRINT "AL^(M-1)/BHAT=";(SLOPE^(M-1))/BHAT
5410 FOR I=0 TO ILAST:A(I,0)=SLOPE:NEXT
5420 RETURN
```